AD-A144 227 PROCEEDINGS OF THE GENERAL MEETING OF THE AMERICAN TOWING TANK CONFERENCE..(U) STEVENS INST OF TECH HOBOKEN NJ DAVIDSON LAB D SAVITSKY ET AL. AUG 83 1/8

UNCLASSIFIED SIT-DL-TR-13029-VOL-2 N00167-83-M-4062 F/G 20/4 NL

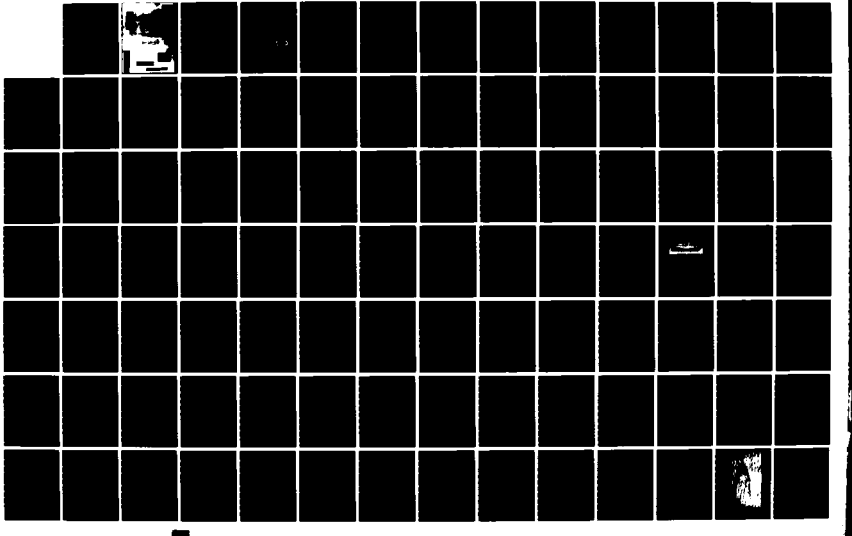

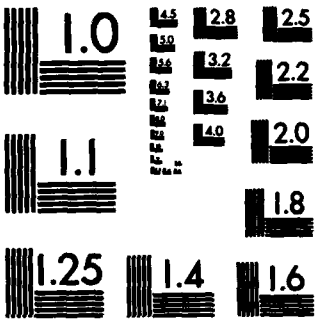

MICROCOPY RESOLUTION TEST CHART
NATIONAL BUREAU OF STANDARDS-1963-A

AD-A144 227

PROCEEDINGS OF THE

TWENTIETH GENERAL MEETING OF THE

AMERICAN TOWING TANK CONFERENCE

VOLUME II

DAVIDSON LABORATORY
STEVENS INSTITUTE OF TECHNOLOGY
HOBOKEN, NEW JERSEY

2-4 AUGUST 1983

DISTRIBUTION STATEMENT A
Approved for public release;
Distribution Unlimited

UNCLASSIFIED

SECURITY CLASSIFICATION OF THIS PAGE (When Data Entered)

REPORT DOCUMENTATION PAGE	READ INSTRUCTIONS BEFORE COMPLETING FORM
1. REPORT NUMBER: TR-13029	2. GOVT ACCESSION NO.: AD-A144 227
	3. RECIPIENT'S CATALOG NUMBER:
4. TITLE (and Subtitle): PROCEEDINGS OF THE TWENTIETH GENERAL MEETING OF THE AMERICAN TOWING TANK CONFERENCE	5. TYPE OF REPORT & PERIOD COVERED: Final Report August 1983
	6. PERFORMING ORG. REPORT NUMBER:
7. AUTHOR(s): Edited by: Daniel Savitsky, John F. Dalzell and Mary Palazzo	8. CONTRACT OR GRANT NUMBER(s): NSF Grant MEA-8311237; ONR Grant N00014-83-G-0089; NSRDC Contract N00167-83-M-4062
9. PERFORMING ORGANIZATION NAME AND ADDRESS: Davidson Laboratory, Stevens Institute of Technology, Hoboken, NJ 07030	10. PROGRAM ELEMENT, PROJECT, TASK AREA & WORK UNIT NUMBERS:
11. CONTROLLING OFFICE NAME AND ADDRESS: David W. Taylor Naval Ship Research and Develop. Center, Bethesda, MD; National Science Foundation, Wash. DC; ONR, Arlington, VA	12. REPORT DATE: August 1983
	13. NUMBER OF PAGES:
14. MONITORING AGENCY NAME & ADDRESS (if different from Controlling Office):	15. SECURITY CLASS. (of this report): UNCLASSIFIED
	15a. DECLASSIFICATION/DOWNGRADING SCHEDULE:

16. DISTRIBUTION STATEMENT (of this Report)

APPROVED FOR PUBLIC RELEASE: DISTRIBUTION UNLIMITED

17. DISTRIBUTION STATEMENT (of the abstract entered in Block 20, if different from Report)

18. SUPPLEMENTARY NOTES

19. KEY WORDS (Continue on reverse side if necessary and identify by block number)

Cavitation	High Speed Vehicles
Ice Testing	Propulsion
Seakeeping	Systems and Techniques
Steering and Maneuvering	Resistance and Flow

20. ABSTRACT (Continue on reverse side if necessary and identify by block number)

Collection of contributions for the Proceedings of the 20th American Towing Tank Conference contained in a two (2) volume set.

DD FORM 1 JAN 73 1473 EDITION OF 1 NOV 65 IS OBSOLETE S/N 0102-014-6601

UNCLASSIFIED

PROCEEDINGS OF THE

TWENTIETH GENERAL MEETING OF THE

AMERICAN TOWING TANK CONFERENCE

DAVIDSON LABORATORY
STEVENS INSTITUTE OF TECHNOLOGY
HOBOKEN, NEW JERSEY

2-4 AUGUST 1983

VOLUME II

DTIC
ELECTE
JUN 8 1984
S D
B

EDITED BY:

Daniel Savitsky
John F. Dalzell
Mary Palazzo

SPONSORED BY:

Stevens Institute of Technology
National Science Foundation
Office of Naval Research
David W. Taylor Naval Ship Research and Development Center
Society of Naval Architects and Marine Engineers
Maritime Industry Sponsors

COMPONENT PART NOTICE

THIS PAPER IS A COMPONENT PART OF THE FOLLOWING COMPILATION REPORT:

(TITLE): Proceedings of the General Meeting of the American Towing Tank Conference (20th) Held at Hoboken, New Jersey on 2-4 August 1983. Volume 2.

(SOURCE): Stevens Inst. of Tech., Hoboken, NJ. Davidson Lab.

TO ORDER THE COMPLETE COMPILATION REPORT USE AD-A144 227.

THE COMPONENT PART IS PROVIDED HERE TO ALLOW USERS ACCESS TO INDIVIDUALLY AUTHORED SECTIONS OF PROCEEDINGS, ANNALS, SYMPOSIA, ETC. HOWEVER, THE COMPONENT SHOULD BE CONSIDERED WITHIN THE CONTEXT OF THE OVERALL COMPILATION REPORT AND NOT AS A STAND-ALONE TECHNICAL REPORT.

THE FOLLOWING COMPONENT PART NUMBERS COMPRISE THE COMPILATION REPORT:

AD#:	TITLE:
AD-P003 818	Major Scaling Problems with Ice Model Testing of Ships.
AD-P003 819	Model Testing of Structures in Ice: Consideration of Scale Effects.
AD-P003 820	Ice Reseistance Tests on Two Models of the WTGB Icebreaker.
AD-P003 821	Manoeuvring of Swath Ships.
AD-P003 822	A Catalog of Existing Mathematical Models for Maneuvering.
AD-P003 823	A Proposed Basis for Evaluating Ship Maneuvering Performance.
AD-P003 824	Application of Microcomputer Technology to Physical and Numerical.
AD-P003 825	Air-Path Acoustic Tracking System.
AD-P003 826	Advances in Evironment Specification for Seakeeping Analyses.
AD-P003 827	A Transient Wave Generation Technique and Some Engineering Applications.
AD-P003 828	Deck Wetness Experiments.
AD-P003 829	Comparison of Theoretical Seakeeping Predictions with Model Test Results for a Wide Beam Fishing Vessel.
AD-P003 830	Roll Damping at Forward Speed.
AD-P003 831	New Towing Facilities at Memorial University of Newfoundland.
AD-P003 832	New Model Testing Facilities of the NRC (National Research Council) Arctic Vessel and Marine Research Institute.
AD-P003 833	A Modernized Control System for the David Taylor Naval Ship R & D Center's 36 Inch Variable Pressure Water Tunnel.

COMPONENT PART NOTICE (CON'T)

AD#:	TITLE:
AD-P003 834	High Precision Differential Force Balance and Experimental Method to Measure Small Fluid-Dynamic Forces Due to small Geometry Changes.
AD-P003 835	An Inexpensive Two-Component Force Balance for Towing Tanks and Flumes.
AD-P003 836	Data Analysis Techniques in Model Testing.
AD-P003 837	Design of a Dynamometer for Testing Yacht Models.
AD-P003 838	University of Michigan - Ship Model Towing Tank Speed Control Upgrade.

DTIC
S ELECTE D
AUG 2 2 1984
A

Accession For
NTIS GRA&I ☑
DTIC TAB ☐
Unannounced ☐
Justification
By
Distribution/
Availability Codes
Dist | Avail and/or Special
A-1

This document has been approved for public release and sale; its distribution is unlimited.

TABLE OF CONTENTS

VOLUME II

PROGRAM:

Ice Testing - Chaired by Dr. A. Keinonen

1. "Major Scaling Problems with Ice Model Testing of Ships,"
   A. Keinonen, Dome Petroleum Ltd.....595

2. "Model Testing of Structures in Ice: Consideration of Scale Effects,"
   G.W. Timco, National Research Council.....613

3. "Ice Resistance Tests on Two Models of the WTGB Icebreaker,"
   J.C. Tatinclaux, U.S. Army Cold Regions Research and Engineering Laboratory and
   D.H Humphreys, U.S. Coast Guard.....627

Steering and Maneuvering - Chaired by Mr. F.W. DeBord

1. "Steering and Maneuvering State-of-the-Art Report,"
   Committee Report.....641

2. "Manoeuvring of SWATH Ships,"
   W.C.E. Nethercote, Defence Research Establishment Atlantic, M.D. Miles and W.D. Molyneux,
   National Research Council.....657

3. "A Catalog of Existing Mathematical Models for Maneuvering,"
   G.R. Hagen, Designers and Planners.....673

4. "A Proposed Basis for Evaluating Ship Maneuvering Performance,"
   R.A. Barr and E.R. Miller, Jr., Tracor Hydronautics.....811

5. "Application of Microcomputer Technology to Physical and Numerical Analysis of Ship Maneuvering,"
   F.W. DeBord, Jr., Offshore Technology Corp.....839

6. "Air-Path Acoustic Tracking System,"
   L.E. Motter and D. Huminik, David W. Taylor Naval Ship Research and Development Center.....869

Seakeeping - Chaired by Prof. R.F. Beck

1. "Report of the Seakeeping Committee".....887

2. "Advances in Environment Specification for Seakeeping Analysis,"
S.L. Bales, W.E. Cummins and W.T. Lee,
David W. Taylor Naval Ship Research and
Development Center.....929

3. "A Transient Wave Generation Technique and Some Engineering Applications,"
J.O. Salsich, B. Johnson and C. Holton,
U.S. Naval Academy.....949

4. "Deck Wetness Experiments,"
A.R.J.M. Lloyd, U.S. Naval Academy.....969

5. "Absolute and Relative Motion Measurements on a Model of a High Speed Containership,"
J.F. O'Dea and H.D. Jones, David W. Taylor
Naval Ship Research and Development Center.....1001

6. "Extension of the Bales Seakeeping Rank Factor Concept,"
D.A. Walden, David W. Taylor Naval Ship
Research and Development Center.....1037

7. "Comparison of Theoretical Seakeeping Predictions with Model Test Results for a Wide Beam Fishing Vessel,"
T.O. Karppinen, National Research Council.....1047

8. "Roll Damping at Forward Speed,"
M.A. Abkowitz, Massachusetts Institute
of Technology.....1065

Systems and Techniques - Chaired by Prof. B. Johnson

1. "Report of the Committee on Systems and Techniques,".....1081

2. "New Towing Facilities at Memorial University of Newfoundland,"
C.C. Hsiung, D. Friis, W. Milne, G.R. Peters,
Memorial University of Newfoundland and
H.W. Weber, Kempf and Remmers GmbH.....1085

3. "New Model Testing Facilities of the NRC Arctic Vessel and Marine Research Institute,"
D. Gospodnetic and M.D. Miles, National
Research Council.....1107

4. "A Modernized Control System for the David Taylor Naval Ship R&D Center's 36 Inch Variable Pressure Water Tunnel,"
H.D. Harper, David W. Taylor Naval Ship Research and Development Center.....1117

5. "A High Precision Differential Force Balance and Experimental Method to Measure Small Fluid-Dynamic Forces due to Small Geometry Changes,"
D.W. Coder, B.B. Wisler, Jr. and M.F. Jeffers, David W. Taylor Naval Ship Research and Development Center.....1189

6. "An Inexpensive Two-Component Force Balance for Towing Tanks and Flumes,"
T. Kowalski, University of Rhode Island and D. Brown, Naval Underwater Systems Center.....1207

7. "Data Analysis Techniques in Model Testing,"
J.T. Dillingham and J.H. Hoste, Offshore Technology Corporation.....1219

8. "Design of a Dynamometer for Testing Yacht Models,"
C.M.J. Gommers and P. van Oossanen, Netherlands Ship Model Basin.....1267

9. "University of Michigan - Ship Model Towing Tank Speed Control Upgrade,"
A.W. Troesch and F.G. Phelps, University of Michigan.....1285

10. "Particulars: Davidson Laboratory Tank 3 Wave Machine,"
J.F. Dalzell, Davidson Laboratory.....1297

GENERAL REPORT:

Business Session.....1307

Aims and Organization of The American Towing Tank Conference.....1309

Past Meetings of The American Towing Tank Conference.....1311

REPORTS OF THE

ICE TESTING

COMMITTEE

Accession For	
NTIS GRA&I	☑
DTIC TAB	☐
Unannounced	☐
Justification	
By	
Distribution/	
Availability Codes	
Dist	Avail and/or Special
A-1	

AD-P003 818

MAJOR SCALING PROBLEMS WITH ICE MODEL TESTING OF SHIPS

For the 20th ATTC

Prepared by
Arno J. Keinonen
Dome Petroleum Ltd.
May, 1983

INTRODUCTION

In North America there is a considerable amount of pressure to develop its Arctic for the extraction of natural resources such as oil, gas, and various mining products and also, to demonstrate and maintain operational sovereignity there. Any such developments require major steps towards the improvement of operational capability and safety in the Arctic offshore areas through advances in Arctic technology. These developments involve major government and industrial projects and large amounts of dollars. Thus the decision-makers have to feel confident in the appropriate technical development related to Arctic operational capability. There is an increasing pressure to develop the methodologies related to technical progress such as ice model testing.

Ice model testing is still a young science. The first actual ice model basin was built in USSR, in 1955 and the first in the western world was built in Finland, 1969. Since that time, several facilities have been built in USA, Canada, Germany, and Japan for ice model testing purposes. The development of ice modelling and scaling techniques for interpreting the results of ice model tests have experienced a rapid progress during the last decade. These methodologies vary quite considerably between different ice model basins and it is expected to take several years, may be tens of years before a set of standard internationally accepted techniques will be established.

It is imperative that ice model testing and scaling techniques be developed continually to promote a growing confidence in them as they develop. At any point in time, we have to know how best to use ice model testing for the benefit of Arctic development and how accurate and useful our model test results are.

During the seventies, the early days of ice model testing in the western world, good full scale data was scarce for use in calibrating ice model testing. Still, there is only a limited number of actual full scale ship test programs in ice which have given data in year-round Arctic operational conditions both in ship and offshore structure-related areas. Dome Petroleum/Canadian Marine Drilling has had several major developments taking place in the Arctic, offshore-related operations. Rapid development in offshore structures technology and design as well as in icebreaker technology

and design has taken place especially during the last four years. Two new generations of icebreakers and Arctic offshore drilling structures were developed during this time period. The operational full scale experience and data from both icebreakers and artificial islands has put Dome in a position to evaluate the design methodologies, both analytical and model testing, and the quality of results of same.

In this paper, a short review provides of the major problems of practical importance seen in ice model tests and interpretation of them for the CANMAR Kigoriak. The specific problems related to quality of model ice material and scaling techniques are addressed.

The main questions the user of ice model tests has to address when using such tests are:

(a) what kinds of ice model tests should be done?
(b) how accurate are the ice mode tests in predicting full scale results for a particular design? and do the model tests show the right direction for optimizing designs?

In the case of the Kigoriak, the ice model tests were performed after the ship had been designed and actually took place during ship construction. Thus, the role of ice model tests in this case has not been in design but in calibration of the scaling methodologies based on full scale model scale test correlation for future extrapolations for larger size ships. The lessons learned related to the behaviour of the propulsion of this ship as well as those related to scaling methodologies were addressed. The key phenomenon that effects the scaling is the fracturing behaviour of model ice and how it scales to natural ice. The key parameters in the scaling of resistance are the breaking component and frictional component of the ice resistance.

The criticism in this paper is meant to encourage a hard look at ice model testing and thus benefit all those involved to give a better picture of what really has happened with ice model testing. On the other hand, we have to realize that the ice model testing facilities have been mainly operated for practical applications orientated work during their short lifetime. The development of ice model testing techniques as well as that of scaling techniques virtually from scratch has been very rapid and encouraging. The

assistance coming from academic side and governments in the area of basic developments in ice model testing has not been able to catch up on the urgent needs in applications oriented work. Only quite recently has the needed basic development received adequate attention so that meaningful development, orientated communication and co-operation between ice scientists, government and commercial ice facilities and users of ice model tests can start.

THE KIGORIAK

The Kigoriak is a Canadian Arctic Class 3 Icebreaker built in St. John Shipyard 1979, with principle particulars (main dimensions and features) as shown in Fig. I. It departs quite radically from a so called conventional icebreaker design having for example: sharp corners to the bow, a vertical sided parallel middle body, and direct drive single CP propeller housed within a nozzle.

From an ice model testing point of view, this introduces a departure from the known area of validity of based on ice model tests predictions. Previous designs are based on more conventional approaches and generally not to ice conditions in the Arctic for year-round confirmation of full scale performance.

FULL SCALE AND MODEL SCALE TESTS IN ICE

The Kigoriak is one of the world's most extensively tested icebreakers. The ship has been operated and it's performance and resistance has been tested in virtually all first-year ice conditions one can find in the Southern Beaufort Sea. Model tests in ice were performed in Arctec Canada's ice model basin in Kanata in saline model ice and in Wärtsilä's old ice model basin in saline model ice as well. In these tests, the model was tested with and without propeller at one ice-hull friction level. Arctec used a friction factor of 0.126 and Wärtsilä one of 0.16. The model was to the 22.5th scale. References Arctec '79 and Wärtsilä '79.

If all the conditions of all the model and full scale tests with the Kigoriak were described it would be a very extensive paper. Further, for confidentiality reasons that information cannot be made available.

It is conceived that it is most important at this stage to tell what the present problem areas are in ice model tests from the users point of view, based on the Kigoriak experience.

Essentially attention is drawn to two areas:

1. The behaviour of ice around the propulsion which has become a major input into design decision; and,

2. The unknowns related to the scaling of ice resistance which have become a major factor influencing the confidence of the predicted values of performance.

PROPELLER ICE INTERACTION

The ice model tests showed propeller ice interaction results such as shown in Fig. 2 and 3. Figure 2 displays a typical model test result from torque measurement on the shaft of the propeller of the Kigoriak from Wärtsilä ice model basin. Figure 3 shows the estimated average drop of propeller thrust due to propeller-ice interaction. Both model tests and figures results in Fig.'s 2 and 3 basically produce compatible results. Model test results are clearly discouraging, suggesting that the propulsion of the Kigoriak would be poor in ice - the nozzle being blocked by ice a big part of the time and at least propeller milling ice virtually continuously. In the past, icebreaker propulsion systems featuring nozzles have been discarded and discredited largely, I believe, based on similar types of ice model test results, even though the potential benefit from a nozzle in the form of added thrust and protection is quite important.

The full scale test results in similar ice show virtually no propeller ice interaction and no blocking of the nozzle. It can be claimed that in heaviest ice conditions such as ridges, ice goes through the nozzle in any case, but even that propeller-ice interaction in full scale does not amount nearly to what was seen in model scale. Also, the fact that the Kigoriak has been able to operate year-round in heavily ridged southern Beaufort Sea confirms the fact that the nozzle must have worked efficiently in ice. This indicates that ice model tests are in the most important part straightforward misleading.

The example shows that good innovations could be killed by ice model tests for practical purposes of the designer.

The answer to why there is an important difference between model and full scale with respect to propeller-ice interaction is found in the properties of model ice. The breaking pattern is radically different in these two scales. In the model tests, the ice is broken into large cusps, the typical size of ice blocks anywhere between 3 - 6 times the ice thickness. In full scale, the typical blocks are radically smaller being in the range of 0.5 - 2 times the ice thickness. This is not only due to what is called the breaking pattern for breaking initial ice cusps, which can be scaled reasonably well based on existing experiences, but is probably mainly due to the fact that natural ice is so brittle that it contains dense cracks which have propogated during local ice edge crushing. Consequently, the original cusps fall apart when being pushed down. Model ice cusps tend not to contain such internal cracks. Two things follow: the ice flow around the hull change due to block size changes and also any ice that may enter the nozzle appears in smaller blocks in full scale causing lesser disturbances in propulsion.

This kind of difference in behaviour between model ice and natural ice has other consequences as well. The effects of various small features like corners in hull or appendage design for icebreaking ships becomes difficult to study by using model tests because the ice flow and the sizes of ice blocks must have an important effect in the energy losses due to these features. For examples, the effects of reamers has not been detected in ice model tests.

SCALING OF ICE RESISTANCE

The scaling approaches taken in interpretation of Kigoriak's ice model tests by Arctec Canada and by Wärtsilä are radically different.

Arctec's Method

Arctec basically assumes that the model ice scales correctly both in elastic strength and in frictional behaviour and that this is sufficient for a nondimensional expression for ice resistance which essentially scales the ice resistance to a third power of scale. They run the model in level ice and use that type of data as input to their model. One weak point in this method is

that ice properties are not scaled correctly. In the previous section, it was pointed out how different the fracturing of model and natural ice is. Also, taking into account other components of strength than just the regularly used bending or tensile strength, is important. NOT taking the crushing, shearing and flaking into account means that right phenomena have not been included. Also, one has to know the right actual friction factor between the ship's hull and ice/snow before a nondimensional approach can be counted on. Another weak point is that there is no empirical confirmation from full scale tests guaranteeing that all existing experience confirms the possibility of prediction from ice model tests being approximately right.

One peculiarity hiding unknowns in Arctec's methodology is the fact that when performing ice model tests in different thicknesses of ice the strength of thicker model ice is higher than that of the thinner. Consequently, one cannot perceive the separate effects of the thickness on resistance and that of the strength. A large selection of combinations of thickness and strength exponents is available for the analyst starting from eliminating either one of these parameters fully from equations. As a matter of fact, the effect of ice strength has been totally eliminated from Kigoriak's prediction equation, which takes the form:

$$\frac{R}{\rho_w g B h^2} = C_1 + C_2 \cdot \frac{v^2}{gh} \qquad (1)$$

where:
- R = ice resistance in level ice
- ρ_w = density of water
- B = ship beam
- h = ice thickness
- v = ship speed
- $C_1 C_2$ = empirical coefficients

The practical importance of the unknown thickness/strength exponent is in scaling. In natural ice for practical purposes a good assumption is that, for practical purposes a good assumption is that the strength does not vary with thickness. If in model tests a low strength exponent is chosen, the thickness exponent is too high and thus conservative. That will especially lead to conservations for thickest ice where least full scale data exists.

Wärtsila's Method

Wärtsilä does not believe in ice properties scaling properly in saline model ice concluding based on testing and scaling procedures chosen for ice resistance predictions and has introduced two important departures from the approach of Arctec Canada.

In order to separate the effect of thickness and strength Wärtsilä performs 0-strength tests additional to the level ice tests by precutting the ice sheet to eliminate icebreaking resistance.

The resistance scaling equation takes the form of:

$$R = \lambda^3 C_\mu \cdot (R_s + k_{ice} R_b + R_v) \qquad (2)$$

where:
- R = ice resistance in level ice
- λ = scale factor
- C_μ = semi-empirical correction factor
- R_s = submersion component of ice
- k_{ice} = correction factor for difference in elastic and strength properties of ice (~ 0.1)
- R_b = breaking component of ice resistance
- R_v = velocity component of ice resistance

A correction (k_{ice}) is made taking into account the non-scaling elastic properties of ice. A second correction (C_μ), is made to cover all unknowns. It is an empirical coefficient introduced to calibrate the ice model test results with a wide variety of existing full scale data from icebreaking tests with ships. C_μ, according to Wärtsilä, takes into account the influence of the ship's size and shape.

One weak link in this method is that it virtually eliminates the breaking component from the ice resistance (when k_{ice} is a number around 0.1). The total resistance will then be compensated for this underestimate by multiplying with a number higher than one (=C_μ), If the design of a ship effects the icebreaking component differently from the submersion component this will automatically lead to an unknown bias in the method, unless Wärtsilä has included any such correction in the determination of C_μ.

One, maybe the key parameter to model testing, is the friction factor. It is known from the Kigoriak experience that the ice resistance from the model tests scale using considerably lower friction factor than was used by either one of the two ice model basins (0.126-0.16) showing that ice model tests and scaling methods are conservative in Kigoriak's case. Also, in different ice thicknesses it seems that different friction factors produce the best match between full scale and model scale results. This could be due to a real change in friction but more likely due to a wrong icebreaking component resulting from the model testing and scaling methodologies.

DISCUSSION

General

The examples shown reflect the state of the art in two facilities about four years ago. It is known that improvements have or are just about to take place in both those facilities.

Arctec has gone over to garbamide doped ice which based on the best available information scales ice block sizes somewhat better than saline ice. In this medium scaling of crack propagation is not known. Related to Arctec's methodology the controversy over the mixing of strength and thickness effects does not disappear by changing ice material. The principle of dimension less scaling, if still in use, looks somewhat premature as well.

Wärtsilä has publicly announced (ENKVIST '83) that the breaking component has been underestimated radically. Enkvist has also announced that Wärtsilä is applying for a patent for a new improved model ice material. Also, Wärtsilä is keeping the exclusive right to the contents of its own secret factor (C) to produce the best full scale predictions. This makes it difficult for users to appreciate how the prediction is made and why.

Users Viewpoints

As a wrap up of what the lessons from Kigoriak's experiences are referring to the highest priorities of a general user of ice model tests.

Ice Resistance Model Tests (Level Ice)

Using existing methodologies an estimate of what actual ice resistance in full ship scale is, is fairly accurate if not departing from conventional hull designs and ice thickness range beyond existing full scale range of ice thicknesses for icebreaker tests. Any corners or extra appendages around the hull cast uncertainty over any of the results maybe even when it has been confirmed that the ice block size scales. Departing from conventional shapes causes yet another key uncertainty in not knowing the right friction coefficient. This suggests conservative results based on Kigoriak lessons, i.e. producing too high resistance predictions.

Propulsion Effectiveness Ice Model Tests (Level Ice)

Tests to test efficiency of a propulsion system in ice should only be conducted once the proper ice block size distribution is confirmed for model tests, as well as all the strength parameters being right or at least known for the model ice.

Optimization Tests

For design optimization, ice model tests should be chosen very selectively as long as the ice block pattern, breaking component and friction factor are still major parameters not scaling right or when they are not even satisfactorily known. Any optimization attempts should include skillfull analytical interpretation of model test results, not only routine scaling. In case of propulsion design related hull line variations or studies on appendages, I would discourage any optimization attempts by means of ice model tests for the time being. Only very general guidelines can be received and even then the results can drastically mislead the user, like in the case of poor behaviour of Kigoriak's propulsion in model tests.

REFERENCES

Arctec Canada, Final Report AML-X4 Model Test Program, May '79 (Unpublished).

Enkvist, G., A Survey of Experimental Indications of the Relation Between the Submersion and Breaking Components of Level Ice Resistance to Ships. Proceedings of POAC '83, Helsinki.

Keinonen, A.; "Canmar Kigoriak" - Demonstration of Arctic Capability. Proceedings of POAC '83, Helsinki.

Wärtsilä, Model Tests in Ice With the Anchor-Handling Tug "Canmar Kigoriak", September '79 (Unpublished).

PRINCIPAL PARTICULARS

FEATURE	MEASUREMENT
LENGTH (OVERALL)	90.0 m
LENGTH (AT WATERLINE)	84.2 m
BREADTH (MOULDED)	17.25 m
BREADTH (OVER REAMERS)	19.25 m
DEPTH	10.0 m
DRAFT (MAXIMUM)	8.5 m
SHAFT POWER (HULL LUBE OFF)	12.2 MW
SHAFT POWER (HULL LUBE ON)	11.8 MW

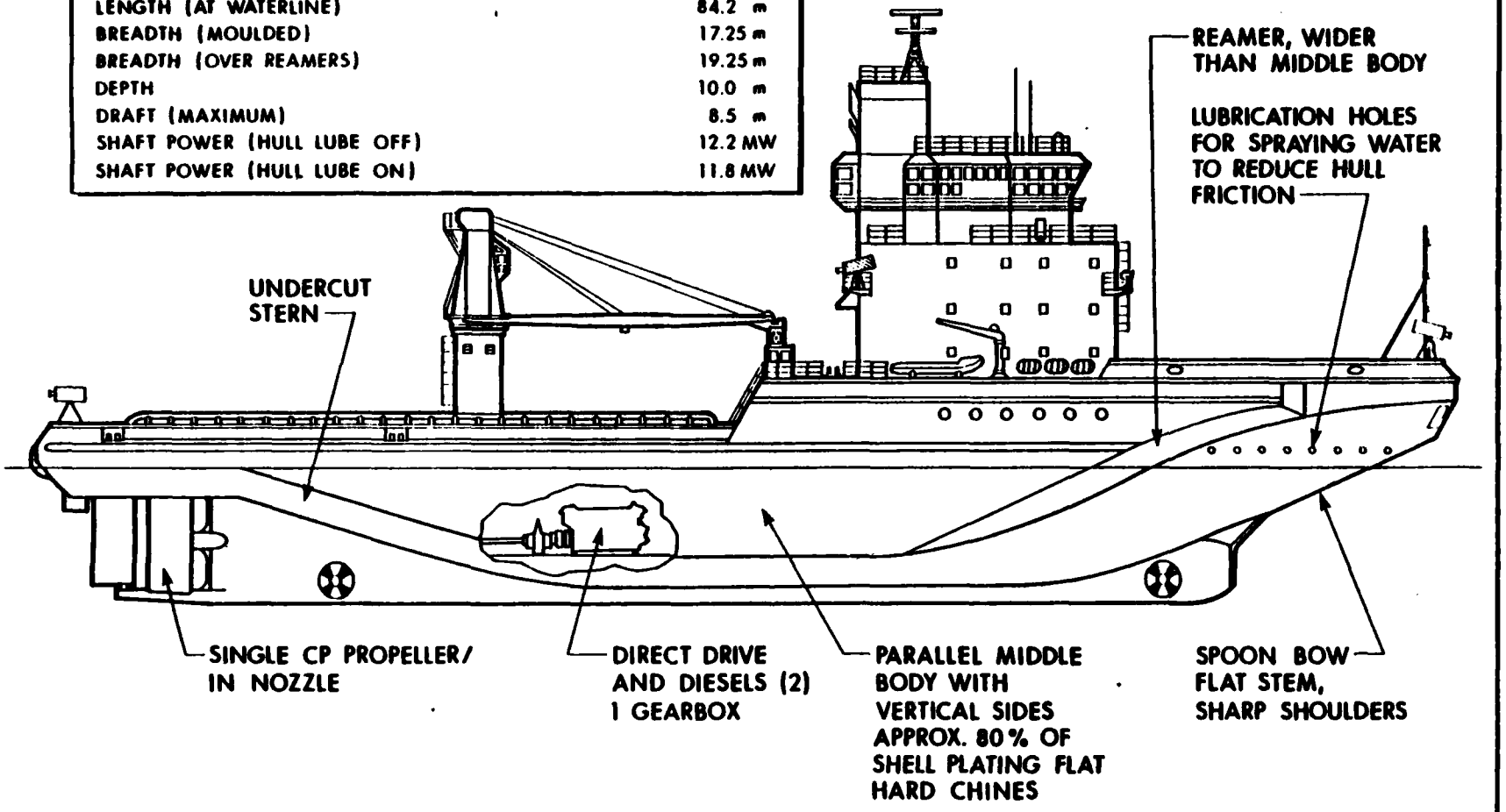

FIG. 1: KIGORIAK GENERAL ARRANGEMENT

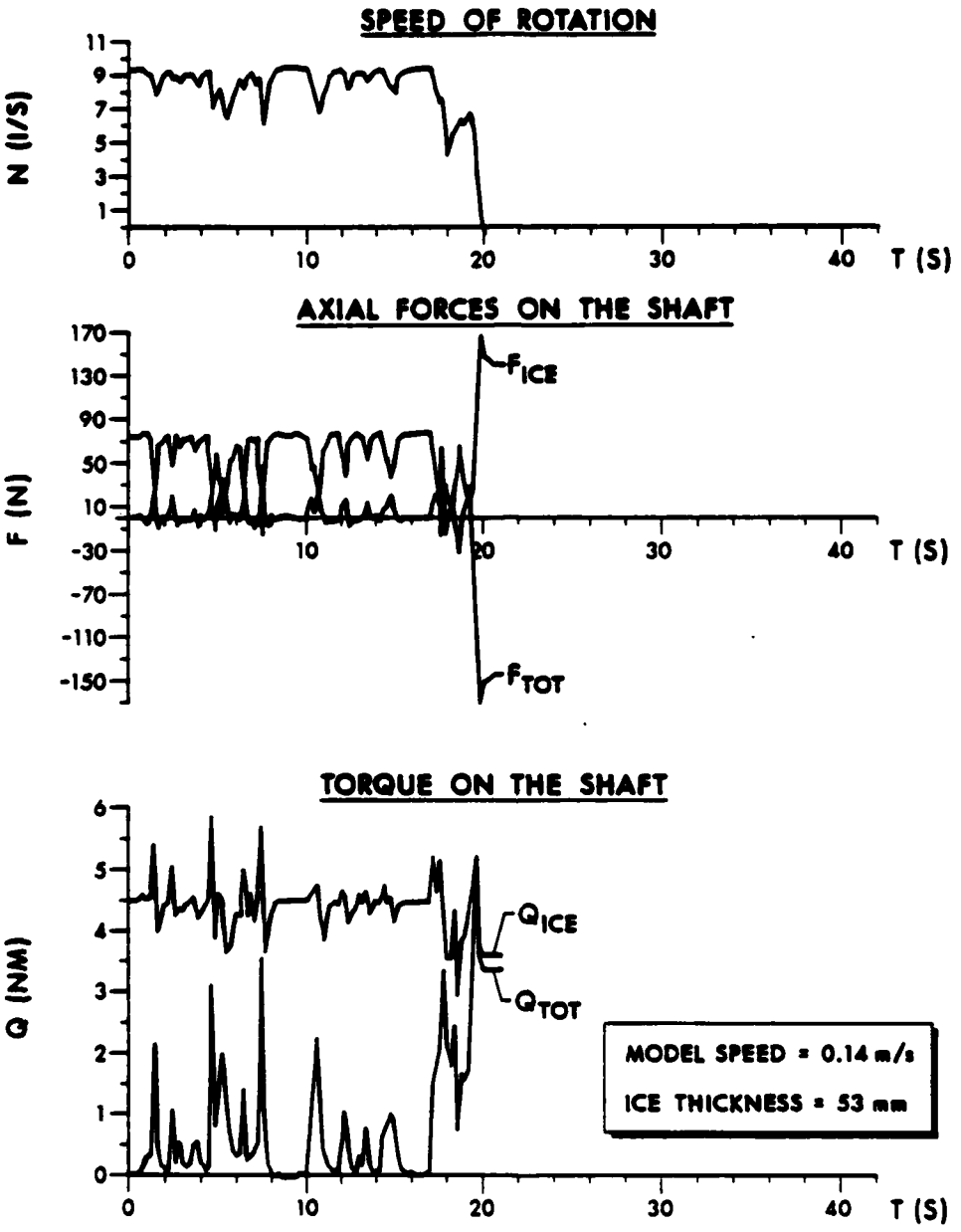

FIGURE 2 KIGORIAK MODEL TESTS IN LEVEL ICE, MEASUREMENTS ON THE PROPELLER SHAFT. (WÄRTSILÄ - 79)

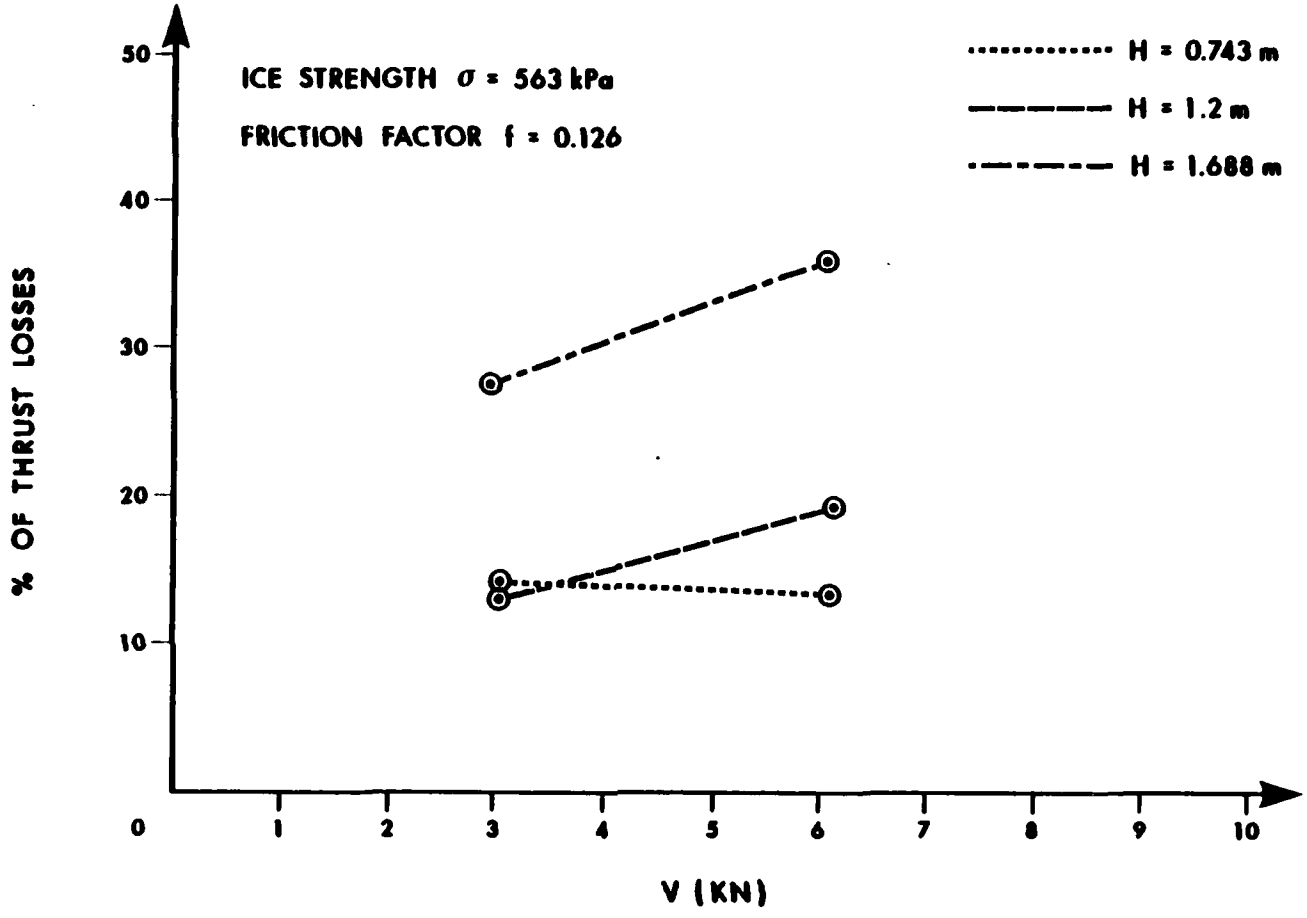

FIGURE 3 ACTUAL DATA PLOT OF PROPELLER THRUST LOSSES IN % OF EXPECTED DELIVERED THRUST VERSUS VELOCITY FOR VARIOUS ICE THICKNESSES FOR AML X-4. (ARCTEC-79)

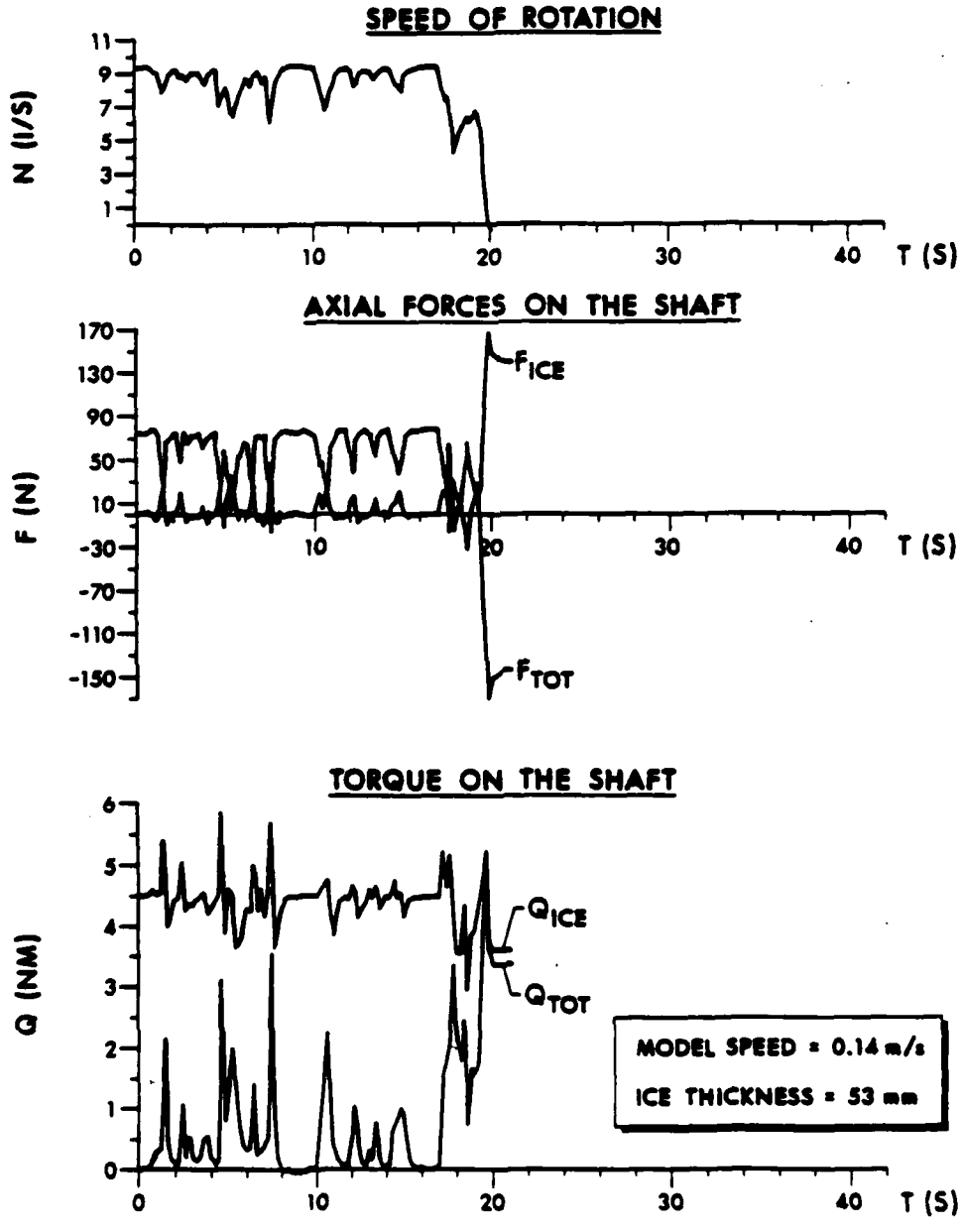

FIGURE 2 KIGORIAK MODEL TESTS IN LEVEL ICE, MEASUREMENTS ON THE PROPELLER SHAFT. (WÄRTSILÄ - 79)

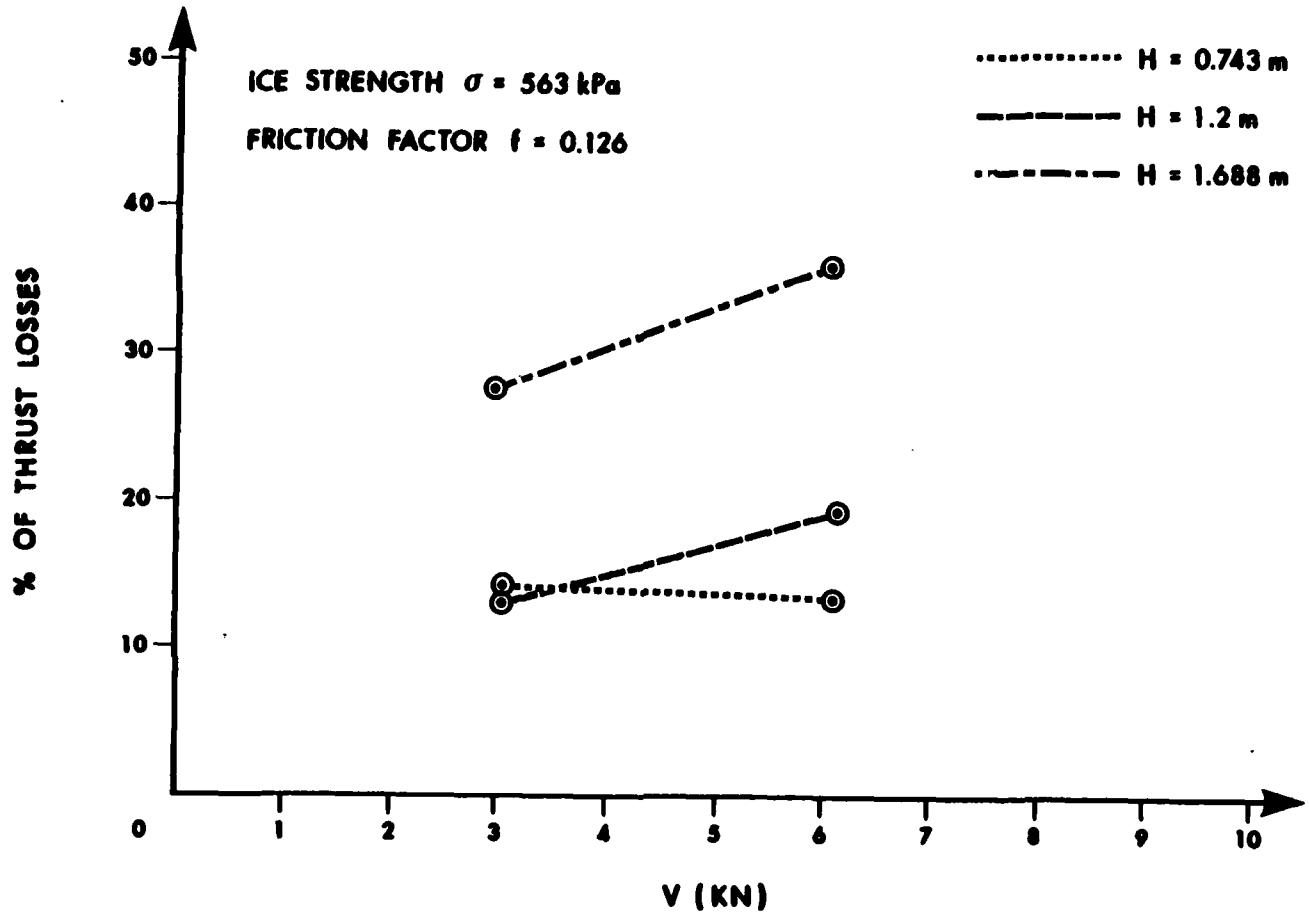

FIGURE 3 ACTUAL DATA PLOT OF PROPELLER THRUST LOSSES IN % OF EXPECTED DELIVERED THRUST VERSUS VELOCITY FOR VARIOUS ICE THICKNESSES FOR AML X-4. (ARCTEC-79)

DISCUSSION

I.F. Glen
Arctec Canada Limited

The author has made some very bold statements in order to attract attention and action to the problem under discussion. We look forward to tackling these problems in our subcommittee.

It should, however, be stated that numerous model tests of various hull forms and bow forms in particular were carried out in the process of final selection of the bow form of KIGORIAK and I believe that the experience of this program was that, in some aspects, the model tests were a significant contribution to the design development.

Comparison of full scale results with model tests in a continual process in model basins, limited only by the quality and availability of good full scale data. A number of such comparisons have been made, some published, for example Reference 1.

The number of parameters to be recorded in a full scale level ice resistance test is considerable. Among these which can significantly effect results are snow cover, ice strength, ship speed and friction.

In a recent review of over a score of full scale trials data on ships from a tug to the SS MANHATTAN, about 25 percent had sufficient quantity and quality of data to be considered as highly reliable full scale data (Reference 2). In the case of KIGORIAK, a further complication in assessing full scale resistance from measurement of thrust, etc. is introduced by the contribution of the duct around the propeller.

It is my understanding that model tests for the AMLX-4 were carried out completely independently at Wartsila and Arctec and that results were reasonably close. We must surely attach some credibility to results from two independent sources acquired under reasonably controlled conditions.

The question of ice geometry (broken piece size) must be addressed as this has not been well modeled traditionally. We therefore approach the work of this subcommittee with enthusiasm and intent to advance the state-of-the-art in this area.

1. Lewis, J.W., "Recent Developments in Physical Ice Modeling," 14th Offshore Technology Conference, May 1982.

2. Lewis, J.W., DeBord, F., and Bulat, V., "Resistance and Propulsion of Ice Worthy Ships," SNAME Annual Meeting, 1982.

AD-P003 819

MODEL TESTING OF STRUCTURES IN ICE: CONSIDERATION OF SCALE EFFECTS

G. W. Timco
Hydraulics Laboratory
National Research Council Canada
Ottawa, Ontario K1A 0R6
Canada

PREAMBLE

The American Towing Tank Conference has established an ice testing committee under the chairmanship of Dr. A. Keinonen of Dome Petroleum Ltd., Canada. For this 20th ATTC meeting, members of the committee were invited to submit papers on any aspect of model testing in ice. The present paper is intended as a very general overview of model testing of structures in ice, with an emphasis on the ability of model tank operators to scale the properties of both the prototype structure and ice in model tests. The paper is meant as a starting point for future discussions in this area. It is presented in a relatively straightforward, non-technical manner with attendant citations to the appropriate technical references.

1.0 INTRODUCTION

With increasing frequency, model tests of stationary structures are being performed in model test basins. There has been an interest in the use of physical modelling techniques for predicting the ice loads on stationary structures such as lighthouses, piers, caissons, monocone, etc. In these types of tests, the ice can fail in several ways through either flexural failures of the ice (either up or down), compressive or crushing failures, buckling, tensile cracking of the ice or any combination of the above. In these tests the loading rate is relatively low, especially in comparison to the loading rates of an icebreaking ship in ice. Model tests of a stationary structure in ice are usually characterized by high ice loads at low loading rates. All of these factors impose severe conditions on both the properties of the model ice which is used in the test, and on the model test facility. The model ice must have certain mechanical properties of flexural and compressive strength, strain modulus, fracture toughness and friction. The model test facility must have the capability of generating high loads at low, steady speeds. All of these factors are directly influenced by the scale factor (λ) which is chosen for the test. In this paper, a number of the factors which influence the results of an ice-structure interaction test will be considered, and their variation with scale factor will be discussed. How they affect the degree of confidence with which the results of ice model tests can be extrapolated to full scale will also be addressed.

In order to discuss these questions, it is necessary to briefly look at the process of physical modelling. In theory for model tests, the ratio of the forces involved in both model and prototype are considered constant so as to satisfy the Froude No. (inertial forces/gravitational forces), Reynolds No. (inertial forces/viscous forces) and Cauchy No. (inertial forces/elastic forces). In practice this cannot be completely accomplished and so a compromise is made and scaling is by the Froude number. In these tests a model of the prototype is usually instrumented through load cells to a carriage and then pushed or pulled through a sheet of model ice. In this case, the standard practice is to model a structure such that its geometric dimensions are reduced by the scaling factor (λ) of the test, whereas the mass of the structure is reduced by λ^3. With regard to the ice, the properties of the ice necessary for proper scaling are that the thickness (h), strength (including flexural strength σ_f, compressive strength σ_c and tensile strength σ_t) and strain modulus (E) should be reduced from the prototype by the scale factor of the tests, the fracture toughness (K_{1c}) should be scaled by $\lambda^{3/2}$, whereas the friction coefficient, Poisson's ratio and density should be the same as in the prototype. In order to have a high degree of confidence in the test results, accurate representation of these quantities are required in the model regime. Thus, to answer the question of the degree of confidence in model tests, it is necessary to examine the confidence with which both the structure and ice can be modelled and their limitation in terms of scale factor.

2.0 SCALE FACTOR EFFECTS OF THE STRUCTURE

There are several different types of structures which can be studied using physical techniques such as moored drilling platforms, artificial islands, rubble-mound breakwaters, lighthouses, monocones, etc. For these structures, proper scaling of linear dimensions, mass and friction over a wide range of scale factors is not usually a problem. From an economic point of view, it is usually better to use as high a scale factor as possible in order to make the structure as small as possible. Depending upon the structure under test, there are different modelling techniques which are used to determine the ice loads on the structure. For example, in testing of artificial islands or breakwaters, it is usually advantageous to build the structure on the basin floor and push the ice sheet past it. In other cases, the structure can be mounted through load cells to the carriage and pushed through the ice sheet. In either case, the relative motion between the structure and the ice should be constant. This necessitates the use of a high capacity carriage with a smooth operation to either push the ice sheet past the structure or push the structure through the ice sheet. Since the loads on the structure (and carriage) decrease with increasing scale factor for the same test configuration, it is clear that for a given carriage, the smoothest operation will be at high scale factors. Because the ice loads can be high, it is necessary to use a stiff, high capacity carriage which has a smooth drive system in order to minimize these effects.

In certain types of tests, one must look at the dynamic response of the structure (including resonance frequencies) and compare this to the prototype. For these types of tests, it is possible to use, for example, Fourier techniques with an appropriate transfer function in order to determine the ice driving force (see e.g. Maattanen, 1979). Part of the structure response will depend upon the relative stiffness of the load cells or force blocks. This influence can be minimized by using very stiff, rigid units mounted to a corresponding stiff carriage. With low scale factors, the size, capacity and cost of this type of system may be substantial. From this point of view, to minimize this influence, tests at high scale factors are desirable.

In tests in which the ice loads on a lighthouse or bridge pier are being investigated, proper scaling of the foundation of the structure in the soil-bed is of utmost importance since it will directly influence the dynamic behaviour of the structure. This is very difficult to do. Also, tests on large, moored structures in which the response of the structure as a whole is important must also be properly simulated dynamically. This is also difficult since there are no ice model basins large enough to allow full extension of the mooring lines, and as such, some form of mooring-line simulator must be used. If the structure itself dynamically responds to the ice loading, it must be scaled using a hydroelastic model. This has not been done to date.

From this discussion, it is clear that in modelling the structure, several precautions must be taken and scale-effects must be considered. The structure and test system of load cells and carriage must be designed and chosen so that the structure behaves dynamically in the same fashion as the structure in the prototype, with minimal interference from the test system. The degree of similarity in the dynamic behaviour of the model with that of the prototype should be evaluated in every model test.

3.0 SCALE FACTOR EFFECTS OF THE ICE

With regard to the proper scaling of the ice, this is of great importance for reliable results of model tests. Since many types of structures involve mixed-mode failure conditions (for example, both flexural and compressive failure), it is necessary to evaluate the degree of accuracy of scaling each of the physical properties. This must be known not only for structures testing, but also for testing and determining pressure ridge and rubble field building forces using modelling techniques. As such, each of the mechanical properties of model ice must be considered to check their accuracy of scaling and their limitations due to scale factor.

In model testing, there are two types of model ice which are used: refrigerated ice and synthetic ice. The refrigerated ice is grown from aqueous solutions containing specific dopants (either carbamide (urea) or sodium chloride) which are trapped as impurity pockets in the ice during growth. By warming up the ice sheet, these chemical

impurities internally melt the ice, thereby providing a mechanism for reducing the strength of the ice. Synthetic ice is manufactured using a number of compounds in various amounts in order to control the properties of the ice. There are two different types of synthetic model ice - one based on a plaster and salt matrix (Tryde, 1977) and the other is a proprietary mix (MOD-ICE) developed by B. Michel and used by Arctec Inc. and Arctec Canada Ltd. (Kotras et al, 1977). Since the properties of the synthetic ice have not been published in detail in the open literature, and since refrigerated ice is the much more commonly used type of model ice, all discussions in this paper will be directed towards the properties of refrigerated ice.

Ice Thickness - The ice thickness, which is scaled by λ, is easily scaled for any scale factor by simply altering the freezing time. With increasing scale factor, the freezing time decreases but the time necessary to reduce the strength of the ice (the "warm'up" time) increases.

Flexural Strength - The scaling of the flexural strength together with the geometric scaling of the structure usually defines the scale factor for the test. Depending upon the dopant concentration in the solution and the warm-up time, the flexural strength can be varied over a wide range of scale factors. In the tank at NRCC (Pratte and Timco, 1981) at a dopant concentration of 0.5% urea, the flexural strength of the ice is ≈130 kPa after a freeze and decreases to 20 kPa with a 10-12 hr warm-up at +1.5°C (see Figure 1). This figure shows the variation of both the flexural strength and strain modulus with warm-up time for two different concentrations of urea-dopant in the Hydraulics Laboratory, NRCC tank. From this figure it is evident that by simply altering the warm-up time, any desired flexural ice strength can be obtained. As such, scaling of the flexural strength over a wide range of scale factors is not usually a problem. Note from the figure the excellent consistency from sheet to sheet which can be obtained for this model ice if care is taken in the growth procedure of the ice.

Although the flexural strength can be properly simulated over a range of scale factors, there are limits to the amount in which the energy similarity of ice breaking can be properly scaled. This is shown in Figure 2. This figure shows the load versus time curves for tests on cantilever beams of model ice at scale factors of 10, 15, 20 and 40 (based on a prototype flexural strength of 800 kPa). In allcases the load increases rapidly until failure and then drops off and eventually levels to the buoyancy load of the beam. In contrast to the prototype system where the load decreases rapidly to the buoyancy level after the break, for model ice there is a "remnant" load which gradually decreases to the buoyancy load. The amount of the remnant load appears to be independent of the strength of the ice. This represents an extra energy required to break the ice which is not seen in the prototype system. The reason for this is not known, but it could be that it is the energy required to peel apart the interlocking

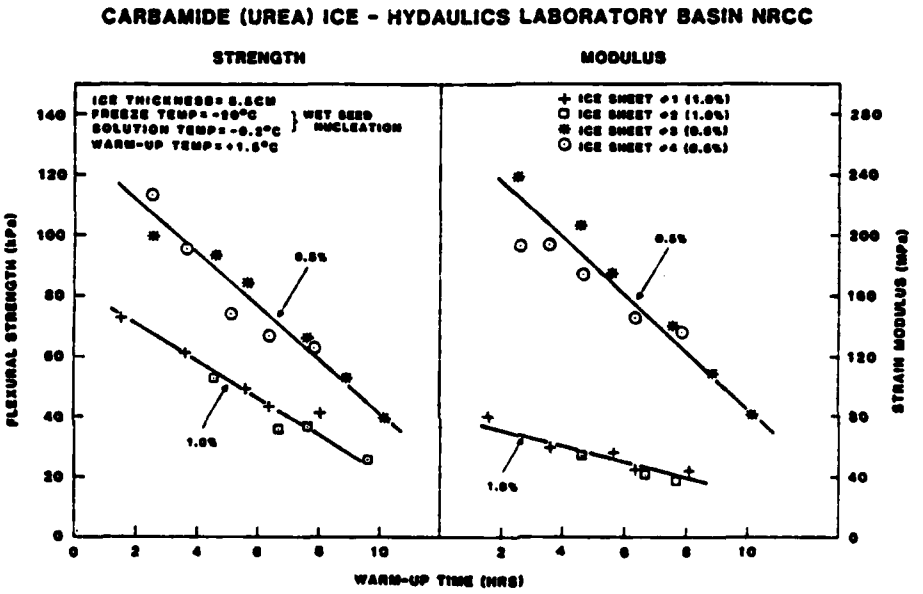

Figure 1 Flexural strength and strain modulus versus warm-up time for urea model ice at two different concentrations.

crystals of the ice. In any event, it is clear that this extra energy becomes increasingly significant for increasing scale factors. This effectively limits the scaling of the flexural strength. For example, for ice of less than 20 kPa flexural strength, there is no apparent break or fracture of the ice - it just peels apart when a load is applied. From this point of view, the best scaling of this property occurs for low scale factors.

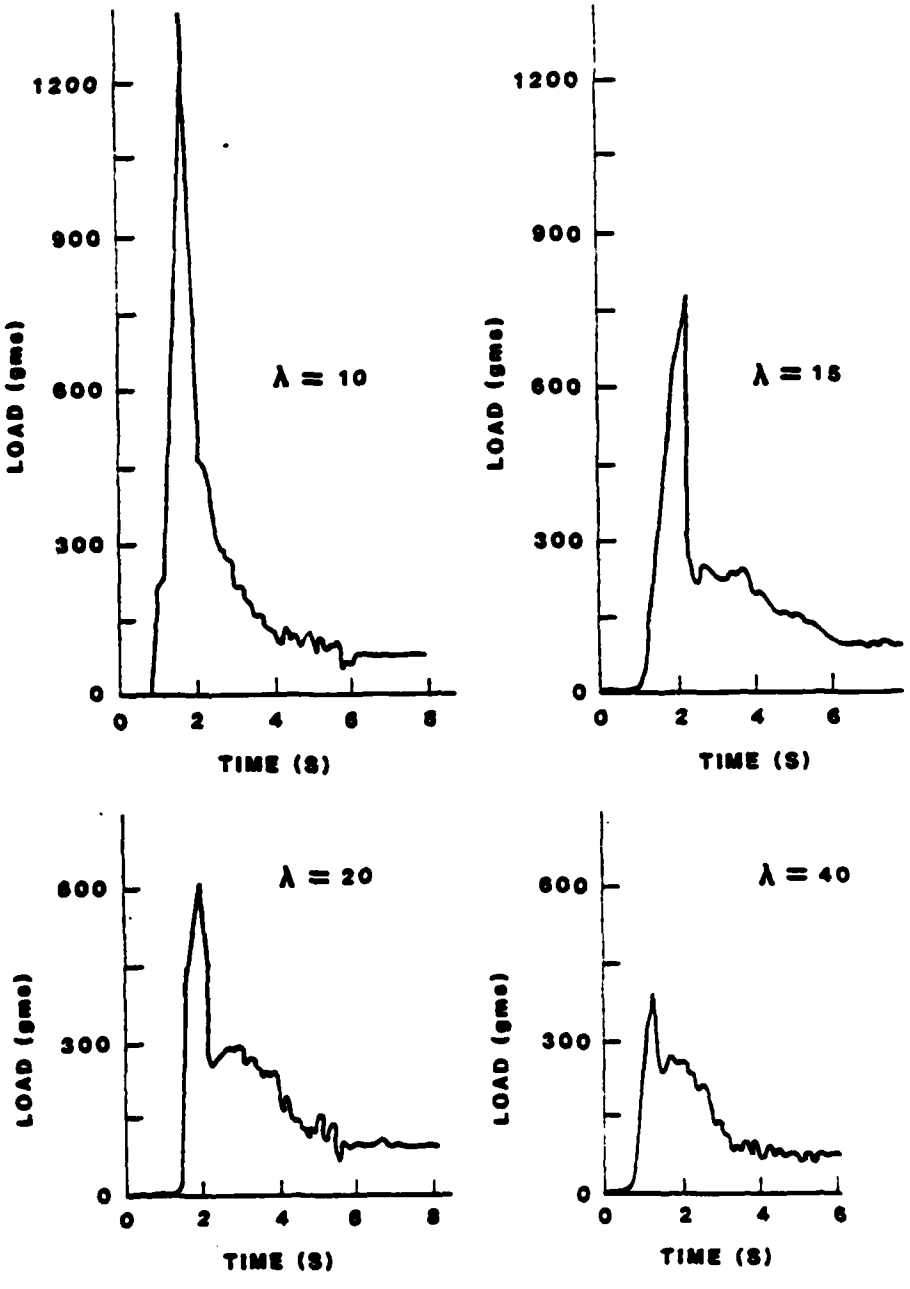

Figure 2 Load-time curves for flexural failures of model ice at various scale factors.

Tensile Strength - Measurement of the true tensile strength of the ice is virtually impossible since machining a sample into an appropriate shape for a tensile test is not possible (see Timco, 1981b). Because of this, indirect test techniques have been employed. Using a ring tensile test (which does not measure the true tensile strength, Mellor and Hawkes, 1971), the results would suggest that model ice scales reasonably well in tension (Timco, 1981a). Because of its importance, more effort should be spent in looking at this property of model ice.

Compressive Strength - The compressive or crushing behaviour of the ice is also very important in model testing of structures since ice fails in this fashion around several types of structures. The compressive strength for model ice is shown in Figure 3 as a function of scale factor for both vertical and horizontal loading directions (Timco, 1982). In both cases, the compressive strength decreases with increasing scale factor (based on the flexural strength), such that the horizontally loaded compressive strength is approximately twice the flexural strength, whereas the vertically loaded compressive strength is four-and-a-half times the flexural strength. Thus, the vertical compressive strength is ≈2-3 times the horizontal compressive strength. This relationship between the vertically and horizontally loaded compressive strength is the same as that found for sea ice (Frederking and Timco, 1984). However, in contrast to the behaviour of "real" ice, the horizontally loaded compressive strength of model ice is strain-rate independent in the range of strain rates studied in model tests (Timco, 1982). Therefore, the confidence with which the compressive strength is properly scaled depends upon the type of test being performed. For example, if the loads on an artificial island in a slowly moving ice field were being studied, the prototype strain rate ($\dot{\varepsilon}$) would be:

$$\dot{\varepsilon} = \frac{v}{2D}$$

where v is the ice movement rate and D is the diameter of the island. For v = 2.4 m/hr and D=150 m, the strain rate would be $\dot{\varepsilon}=2\times10^{-6}$ sec^{-1}. From uni-axial tests of the horizontally loaded compressive strength of freshwater ice using a high capacity, closed-loop test machine, the strength (σ) is related to the strain rate by

$$\sigma = 210\ (\dot{\varepsilon})^{0.34}$$

where σ is in MPa and $\dot{\varepsilon}$ is in sec^{-1} (Sinha, 1981). Thus for $\dot{\varepsilon}=2\times10^{-6}$ sec^{-1}, freshwater ice strength is 2.4 MPa. For a model test at λ=30 (say), the model ice strength should be 80 kPa which is in good agreement with the experimentally measured value for compressive strength at this scale factor (Figure 3). As such, in a test of this type, both

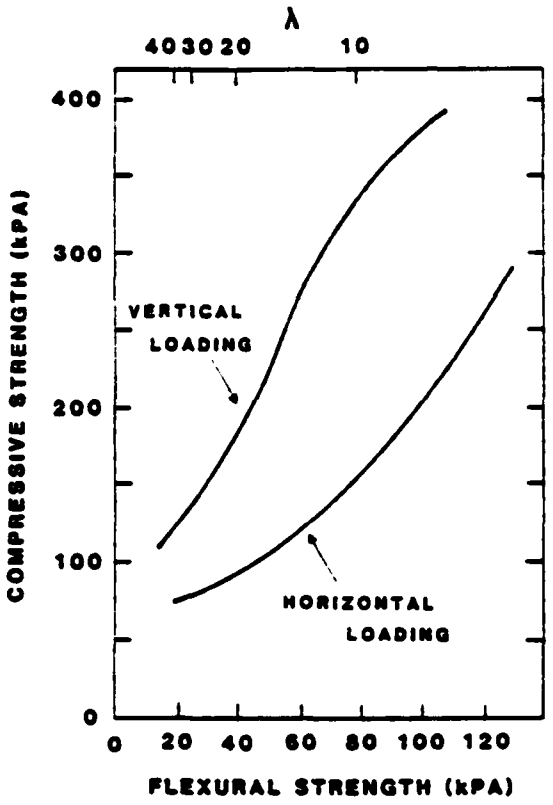

Figure 3 Graph of the vertically and horizontally loaded compressive strength of model ice as a function of flexural strength and scale factor.

the flexural and compressive strengths would be scaled correctly. However, it should be borne in mind that since the strength is strain rate dependent for "real" ice, but strain-rate independent for model ice, this correct scaling of both strengths will not always be possible. Therefore, an analysis such as this is required to check on the accuracy of compressive strength scaling. In many cases such an analysis will define a unique λ at which both the flexural and compressive strengths are properly scaled. Therefore, for structures testing (where both strengths should be properly scaled), the capability of performing tests at any scale factor is highly desirable.

Confined Compressive Strength - In most cases when an ice sheet interacts with a structure, the stress field in the ice is not uni-axial. There can be a complex stress field with a resulting complex failure mode of the ice. Because of this, it is necessary that the 3-dimensional failure envelope of model ice be similar to that of the prototype ice. Columnar sea ice and freshwater ice are anisotropic materials with pressure sensitive mechanical properties which are dif-

ferent for compression and tension. Because of this, the failure envelope for columnar ice cannot be described by the classical von Mises or Tresca-type yield behaviour (see Ralston, 1978 for detail). As an example, Figure 4 shows the yield surfaces in the plane of the ice cover for plane-stress conditions (the third principle stress is zero) for granular and columnar sea ice at a temperature of -11°C and nominal strain rate of 2×10^{-4} sec^{-1} (Timco and Frederking, 1983). In this figure, σ is the yield stress and C is the uni-axial compressive strength of the ice. Note that for granular ice (i.e. the upper part of the ice cover), the yield stress never exceeds 1.3 times the uni-axial compressive strength, even for confined loading conditions. On the other hand, for columnar ice (i.e. the lower part and majority of the ice cover), the yield stress for confined conditions can become four times as large as the unconfined uni-axial strength of the ice. This can create much higher loads by an ice sheet on a structure. For a complete ice cover, the failure envelope will be a combination of these functions for granular and columnar ice at different temperatures. It should be noted that these failure envelopes are both temperature and strain rate dependent.

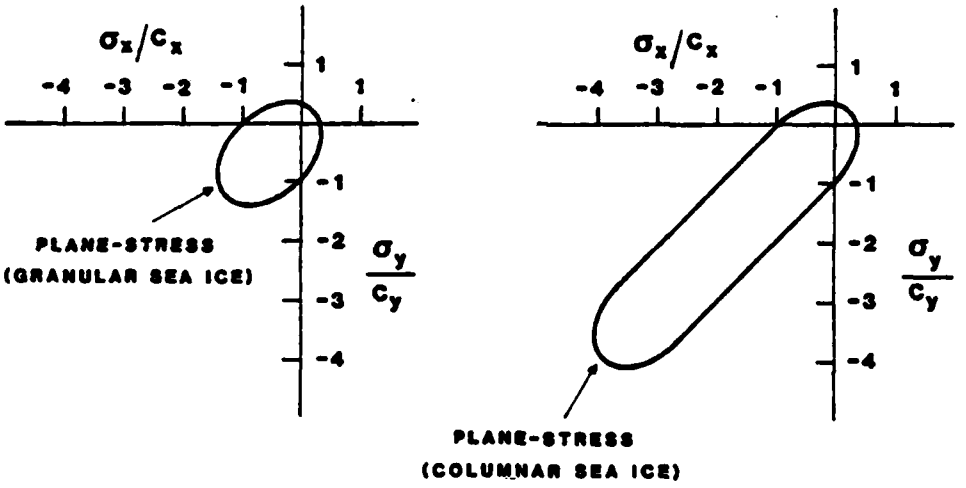

Figure 4 Plane-stress failure envelopes for granular and columnar sea ice at T=-11°C and $\dot{\varepsilon}=2\times10^{-4}$ s^{-1}.

For refrigerated model ice, the ice is also an anisotropic material with pressure sensitive mechanical properties which are different for compression and tension. Figure 5 shows the corresponding failure envelopes to those of sea ice (Figure 4) for model ice at scale factors of λ=10, 15, 20 and 40 as derived from the confined compression tests of Timco (1982). In this case, for low scale factors, the fail-

ure envelope is similar to that for columnar sea ice. With increasing scale factor, the shape of the failure envelope approaches that of granular sea ice. The shape and size of the failure envelope is a function of the scale factor of the ice. In general, it is a good representation of the failure behaviour of prototype ice. At this time, it is not possible to compare quantitatively the full failure behaviour of model ice to prototype ice. Much more work is required in this area, especially to determine the failure surfaces for prototype ice representing a full ice sheet (i.e. a mixture of granular and columnar ice with an appropriate temperature gradient). When this is done, it will be possible to compare more rigorously the scale factor effects of this aspect of ice behaviour.

Strain Modulus - Proper scaling of the strain modulus (E) is important since the modulus defines the characteristic length which influences the size of ice pieces, crack lengths, etc. Analysis of prototype data has indicated that the range of modulus to flexural strength ratio should be 2000-5000 (Schwarz, 1975). For saline model ice, it is known from the work of Enkvist (1972) and Schwarz (1975) that the E/σ_f ratio is too low for proper similitude. Because of its importance, the National Research Council of Canada developed a model ice which more correctly scales the E/σ_f ratio over a wide range of scale factors. This model ice uses carbamide (urea) as a chemical dopant instead of sodium chloride (Timco, 1979, 1981c). By altering the conentration of urea in the freezing solution, the properties of this ice can be adjusted such that $E/\sigma_f \geq 2000$. As shown in Figure 1, the urea concentration required to obtain this E/σ_f ratio is 0.5% for the tank at NRCC. At this time, the majority of refrigerated model ice basins are using this ice. Using urea ice, the E/σ_f ratio is scaled well for scale factors up to λ=40.

Fracture Toughness - The fracture toughness (K_{1c}) of model ice is a parameter which has not been measured but should be considered in defining the scale factor for model tests. At this time, however, there is only limited information on the fracture toughness of sea ice (Urabe and Yoshitake, 1981; Timco and Frederking, 1983). More work is required in the prototype system to define K_{1c} before estimates as to the accuracy of scaling the toughness can be determined.

Frictional Coefficients - Correct scaling of the frictional coefficients of the model ice is extremely important since it can significantly influence the test results. The static and dynamic ice-ice and ice-structure coefficients should be properly simulated and should scale reasonably well for all scale factors (as long as care is taken in matching the finish of the structure under test to that of the prototype).

Poisson's Ratio - Poisson's ratio has not been measured for model ice. It is usually assumed to be the same as that for prototype ice.

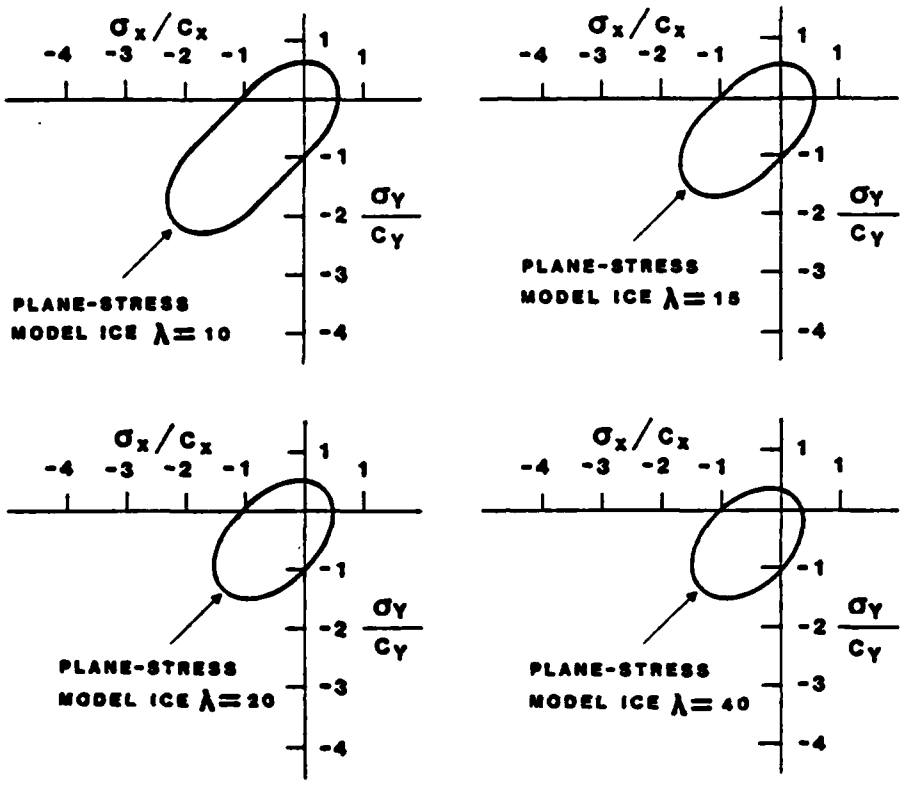

Figure 5 Plane-stress failure envelopes for model ice at various scale factors (λ).

Density - The density should be the same for both model and prototype. Based on freeboard observations and direct density measurements, the density of model ice scales well from that of the prototype for all scale factors (Timco, 1981a).

4.0 SUMMARY

Based on the foregoing discussion, it is evident that the question posed of the confidence and scale factor effects of model tests is extremely complex. Modelling of the structure is not always straightforward, but in most cases a good representation of the prototype structure can be built. The properties of refrigerated model ice all scale very well, especially if care is taken in choosing the scale factor based on the crushing strength of the ice. It would seem, therefore, that the results of structure testing in model ice should

give very good estimates of the forces to be encountered in the prototype situation for scale factors up to at least λ=30.

With regard to the question of the most appropriate scale factor for model tests again the answer is not clear-cut. On the one hand, performing tests at high scale factors has the advantages that the structures are smaller and therefore easier to build and handle, the carriage and load cells can be more easily made comparatively rigid, and the freezing time for an ice sheet is relatively shortened. On the other hand, performing tests at low scale factors has the advantage that the warm-up time is decreased, the energy similarity involved in breaking the ice in flexure is more accurately scaled, the tests tend to appear more realistic and the inaccuracies involved in scaling up model test results by the scale factor are decreased. The question of the confidence with which model tests can be extrapolated to full scale very much depends on these scale factor effects. The most suitable scale factor for a test will vary depending upon the type of test being done.

5.0 REFERENCES

Enkvist, E., 1972, "On the Ice Resistance Encountered by Ships Operating in the Continuous Mode of Icebreaking", Swedish Acad. of Eng. Sci. in Finland, Report No. 24, Helsinki.

Frederking, R. and Timco, G.W., 1984, "Compressive Behaviour of Beaufort Sea Ice Under Vertical and Horizontal Loading", to be presented at 3rd Int. Symp. on Offshore Mechanics and Arctic Engineering, New Orleans, February 12-16, 1984.

Kotras, T., Lewis, J. and Etzel, R., 1977, "Hydraulic Modelling of Ice-Covered Waters", Proc. POAC 77, Vol. I, pp. 453-463, St. John's, Nfld., Canada.

Maattanen, M., 1979, "Laboratory Tests for Dynamic Ice-Structure Interactions", Proc. POAC 79, Vol. II, pp. 1139-1153, Trondheim, Norway.

Mellor, M. and Hawkes, I., 1971, "Measurement of Tensile Strength by Diametral Compression of Discs and Annuli", Eng. Geol. 5, pp. 173-225.

Pratte, B.D. and Timco, G.W., 1981, "A New Model Basin for the Testing of Ice-Structure Interactions", Proc. POAC 81, Vol. II, pp. 857-866, Quebec City, Canada.

Ralston, T.D., 1978, "An Analysis of Ice Sheet Indentation", Proc. IAHR Symp. on Ice Problems, Vol. I, pp. 13-31, Lulea, Sweden.

Schwarz, J., 1975, "On the Flexural Strength and Elasticity of Saline Ice", Proc. IAHR Symp. on Ice Problems, pp. 373-386, Hanover, N.H., U.S.A.

Sinha, N.K., 1981, "Comparative Study of Ice Strength Data", Proc. IAHR Symp. on Ice Problems, Vol. II, pp. 581-595, Quebec City, Canada.

Timco, G.W., 1979, "The Mechanical and Morphological Properties of Doped Ice", Proc. POAC 79, Vol. I, pp. 719-739, Trondheim, Norway.

Timco, G.W., 1981a, "The Mechanical Properties of Saline-Doped and Carbamide (Urea)-Doped Model Ice", Cold Reg. Sci. and Tech. 3, pp. 45-56.

Timco, G.W., 1981b, "Invited Commentary: On the Test Methods for Model Ice", Cold Reg. Sci. and Tech. 4, pp. 269-274.

Timco, G.W., 1981c, "A Comparison of Several Chemically-Doped Types of Model Ice", Proc. IAHR Symp. on Ice, Vol. II, pp. 489-502, Quebec City, Canada.

Timco, G.W., 1982, "Uni-axial and Plane-strain Compressive Strength of Model Ice", Annals of Glaciology 4, (in press).

Timco, G.W. and Frederking, R., 1983, "Confined Compressive Strength of Sea Ice", Proc. POAC 83, Vol. I, pp. 243-253, Helsinki, Finland.

Timco, G.W. and Frederking, R., 1983, "Flexural Strength and Fracture Toughness of Sea Ice", Cold Reg. Sci. and Tech. (in press).

Tryde, P., 1977, "Intermittent Ice Forces Acting on Inclined Wedges", U.S.A. CRREL Report 77-26, Hanover, N.H., U.S.A.

Urabe, N. and Yoshitake, A., 1981, "Fracture Toughness of Sea Ice - in situ Measurement and its Application", Proc. POAC 81, Vol. I, pp. 356-365, Quebec City, Canada.

AD-P003 820

20th AMERICAN TOWING TANK CONFERENCE
August 2-4, 1983
Davidson Laboratory - Stevens Institute of Technology
Hoboken, N.J.

ICE RESISTANCE TESTS ON TWO MODELS OF THE WTGB ICEBREAKER[1]

by
Jean-Claude Tatinclaux[2] and LCDR David H. Humphreys[3]

I. Introduction

The "Katmai Bay" class of icebreaking tug (WTGB) has proved successful in the ice on the great Lakes. During the winter months these vessels provide icebreaking assistance in areas that would otherwise be impassable much of the time. The United States Coast Guard with the United States Army Cold Regions Research and Engineering Laboratory (CRREL) has performed full scale icebreaking resistance tests [1][4] on these ships. Model icebreaking resistance tests [2] were conducted during design as were conventional ice free model tests [3]. Recent tests were performed at CRREL to compare large and small scale model icebreaking resistance results. This report describes these tests and their results. Future efforts are anticipated that will compare different scale model icebreaking results for other icebreaker designs. It is hoped that the results of this program will lead to more economical design procedures for icebreakers.

Model testing in ice is an important, but very expensive, element of the icebreaker design process. Analytical and empirical methods exist for predicting icebreaking power requirements, but these methods suffer from limitations and inaccuracies that can only be overcome by model testing. Testing with large models is commonly carried out in an attempt to reduce scale effects in ice. These tests prove expensive since only a few speeds can be achieved per sheet of ice in our relatively small ice tanks. Significant savings can result if small

---

[1] This study was performed under U.S. Coast Guard MIPR #270099-206490. The opinions expressed herein are those of the authors and should not be interpreted as those of the U.S. Army or U.S. Coast Guard.

[2] Hydraulic Research Engineer, Ice Engineering Research Branch, U.S. Army Cold Regions Research and Engineering Laboratory, Hanover, N.H.
[3] Chief, Icebreaker Technology Section, Naval Engineering Division, U.S. Coast Guard, Washington, D.C.

[4] Numbers within brackets correspond to references listed at the end of the paper.

scale model tests can achieve reasonably accurate results during early design efforts. The use of a small model allows more speed runs per ice sheet providing more data in an efficient, less costly and more timely manner. The savings in time and expense allow model tests to be conducted and completed during conceptual or preliminary design efforts. This allows time for parametric studies to be carried out to assess the effects of slight form variations on resistnace. On the other hand, the time to build and test large scale models is too long for early design decisions and designers are reluctant to run any but the most essential large scale model tests.

II. Ship Description

The Coast Guard Katmai Bay Class WTGB (tug, icebreaker) is 42.7 m (140 feet) long. These cutters were built by Tacoma Boat Building Company, Inc. of Tacoma, WA. All Coast Guard cutters are designed for multi-mission capabilities. The Katmai Bay class are tasked with search and rescue, towing and law enforcement, but are primarily designed to serve as icebreakers on the Great Lakes and Atlantic Coast. The cutters are built with an ice strengthened hull, an air bubbler system for hull lubrication, and a low friction (Inerta 160) bottom coating. Principal characteristics are shown in Table I. An abbreviated lines plan is shown in Figure 1. Figures 2 and 3 are outboard and inboard profiles respectively.

Table I. Principal characteristics of the Katmai Bay class WTGB [1].

Length overall	42.7 m (140 ft)
Maximum beam	11.4 m (37 ft 6 in)
Maximum beam at DWL	10.4 m (34 ft 2 in)
Mean draft	3.7 m (12 ft)
Maximum displacement (winter)	660 metric tons (650 long tons)
Shaft horsepower	1864 Kw (2500 SHP)
Maximum speed (ice-free water)	7.6 m/sec (14.7 kts)

Propulsion - Twin Fairbanks Morse 38D8-1/8 diesel driving Westinghouse 1000 KW, 900 volt D.C. generators which in turn power a single Westinghouse D.C. motor coupled directly to the single propeller shaft.

Auxiliaries - Two 175 KW Kato generators driven by Murphy MP24T diesels (6 cylinder, 252 H.P.).

Crew - 17 (3 officers, 14 enlisted)

Bow slope	28°
Entrance half angle at DWL	28.5°
Transverse spread angle complement	41.4°
Flare angle	48.6°

III. Purpose of Tests

The purpose of the tests described by this paper is to determine the feasibility of model testing in ice using small models during preliminary icebreaker design. Large scale model, small scale model and full scale ice trial results are compared to determine model size effects in icebreaking model tests results.

IV. Ship Models and Test Conditions

Two models of the WTGB icebreaker were available: one at a scale of 1:9.273 (herein called the 1:10 model) and the other at a scale of 1:24. The ice characteristics in the CRREL towing basin were scaled down to correspond to full scale conditions of 18 in (46 cm) in thickness and 800-1000 kPa in bending strength. The friction factors between ice and ship-model hulls were measured at 0.132±0.010 for the 1:10 model, and at 0.148±0.016 for the 1:24 model. With both models, the resistance tests were conducted at five different towing velocities corresponding to full scale speeds of 1, 2, 3, 4 and 5 kts. With the 1:10 model only two speeds were tested per ice sheet with a total of 14 tests conducted in seven ice sheets. With the smaller 1:24 model, all five speeds could be tested in one ice sheet and a total of fifteen tests were conducted in three ice sheets.

In addition to resistance tests in level ice, tests were also conducted in broken ice filling the channels cut by the ship models in the level ice sheets. In particular, because of its relatively small size and weight, the 1:24 model could be lifted out of the test basin, and returned to the trim tank without disturbing the ice in the channel created during the just completed test in level ice. These "brash-ice" tests were conducted in an attempt to separate the total ice resistance into its various components.

It should be mentioned that in all the tests the models were free to heave, pitch and roll, were limited in sway, and totally restricted in surge.

V. Test Results and Analysis

A detailed description of the test results and of various analyses performed on the results will be available shortly [4]. Only the highlights of these results will be presented here.

1. Comparison of test results in level ice for the two models: the model level ice resistance, R_i, was calculated as $R_i = R_{it} - R_{ow}$, when R_{it} was the total resistance measured during the EHP tests in level ice and R_{ow} was the ice-free resistance estimated from the data in [3]. This ice resistance was adimensionalized by $\gamma B h_i^2$, where γ was the specific weight of water (taken equal to 9810 N/m^3), B was the ship model maximum beam at the waterline and h_i was the ice thickness. The independent variables considered in the

analysis were the Froude number based on ice thickness $F_n = V/\sqrt{gh_i}$, where V was the ship speed and g the acceleration of gravity, and the Cauchy number $C_n = \sigma/\gamma h_i$, where σ was the ice bending strength.

The dimensionless ice resistance in level ice is plotted versus the product ($C_n \times F_n$) on Figure 4. It can be seen that the results obtained with both models are in remarkable agreement, which indicates that there is no measurable scale effect between the two models, at least for the range of parameters, velocity, ice thickness and especially ice strength, investigated. Figure 4 also shows the results of the previous model study conducted on the 1:24 model by ARCTEC, Inc. [2], which can be seen to be in agreement with the results of the current test program.

2. Resistance tests in broken channel: As stated previously, resistance tests in the undisturbed broken channel were possible with the 1:24 model, but not with the larger 1:10 model. During the level ice tests with both models, it was observed that the broken floes re-emerged into the ship track to almost reoccupy their initial location. The resistance measured in the tests through the undisturbed broken channel could then be interpreted as the submergence and inertia components, R_{is}, of the level ice resistance.

The dimensionless resistance in broken channel is plotted against F_n on Figure 5 for the three ice sheets tested, and shows good repeatability. Regression analysis of the data in Figure 5 yielded the equation

$$\frac{R_{is}}{\gamma B h_i^2} = 2.28 + 0.784 \left(\frac{V}{\sqrt{gh_i}}\right)^2 \qquad (1)$$

with a correlation coefficient of 0.79.

3. Analysis of ice-breaking resistance

The ice breaking component of the level ice resistance was then defined as

$$R_{bk} = R_i - R_{is} \qquad (2)$$

with R_{is} calculated by Eq. 1.

Under the assumption that ice failure occurs primarily in bending, the breaking resistance should be proportional to σh_i, that is the dimensionless quantity $R_{bk}/\sigma B h_i$ should be independent of C_n and either a constant or a function of F_n only. This dimensionless form of the ice-breaking component is plotted against F_n on Figure 6. It is apparent that $R_{bk}/\sigma B h_i$ initially increases rapidly with Froude number, reaches a maximum and drops rapidly to an almost constant value. In view of the scatter in the data points, it was considered sufficient to divide the data into three zones for

which the following linear relationships were obtained.

$$\frac{R_{bk}}{\sigma B h_i} = 0.01 + 0.115\ F_n \qquad F_n < 0.4 \qquad (3a)$$

$$\frac{R_{bh}}{\sigma B h_i} = 0.1 - 0.11\ F_n \qquad 0.4 < F_n < 0.5 \qquad (3b)$$

$$\frac{R_{bk}}{\sigma B h_i} = 0.042 + 0.0063\ F_n \qquad F_n > 0.5 \qquad (3b)$$

The transition Froude number range $F_n = 0.4 - 0.5$ corresponds for a full-scale ice thickness of 18 in (46 cm) to a full scale speed range of 1.7 - 2.1 knots. It is to be noted that during the model tests it was observed that the amplitude of the pitching motion was relatively high for speedsof 1, 1.5 and 2 knots (full scale equivalent) and decreased rapidly at higher speeds, so much so that, at the nominal full-scale speeds of 4 and 5 knots, the ship model took a practically constant trim angle. The loss of energy due to these pitching and heaving motions would result in an additional resistance. As the ship speed increases the additional resistance due to pitching decreases so that the total ice resistance may actually decrease over a narrow range of speed or Froude number before the monotically increasing inertia component of the resistance overcomes this effect. Such a reversal in the ice resistance curve has been observed before [5] and predicted theoretically by Milano [6]. It is sometimes called the "Milano hump." It would be useful to perform additional tests in the range of Froude number 0.1-0.75 to confirm the observed hump and to better define the behavior of the breaking resistance with Froude number in this range.

Combination of Eqs 1 and 3 then leads to the following expression for the total resistance in level ice

$$R_{it} = R_{ow} + \gamma B h_i^2 \left[2.28 + 0.784\ F_n^2 + C_n\ (a - b\ F_n)\right] \qquad (4)$$

with $a = 0.01$, $b = 0.115$ for $F_n < 0.4$; $a = 0.1$, $b = -0.11$ for $0.4 < F_n < 0.5$ and $a = 0.042$, $b = 0.0063$ for $F_n > 0.5$.

Since it is based on model test data, Eq. 4 should be applied only for the range of parameters tested namely

$$75 < C_n < 300$$

$$0.23 < F_n < 1.2$$

4. Comparison of Model and Full Scale Data

The model data and the full-scale trial values of resistance in level ice reported by Vance et al. [1] are plotted in Figure 7 for comparison. In Figure 8, the dimensionless form of the resistance measured during the trials is plotted against the resistance calculated by Eq. 4 for the trial conditions of ice thickness, ice strength and ship speed. From both Figures 7 and 8 it is evident that the model tests gave significantly higher resistance than measured in the full scale trials. However it is worth noting that the trial data in Figure 8 can be divided into two groups, one where the measured resistance is of the order of 60 percent of the predicted values, the other where it is 75 percent or more of the predicted values. These two groups of data correspond to two series of trial tests conducted on two different days at two different locations. Also, the full-scale trials resistance data were estimated from thrust measurements T as

$$R = (1 - t)\ T$$

with the thrust deduction factor, t, taken equal to 0.2. Finally, very large variations in the friction factor was reported by Vance [1], from as low as 0.02 for "Inerta 160" coated steel plate to 0.165 for snow covered ice against steel plate, so that the actual full scale ice-hull friction coefficient could not be readily evaluated and may have been smaller than for the models.

VI. Conclusions

For the particular full-scale conditions modelled in the tests, the dimensionless level ice resistance obtained with the two models of the 140-foot WTGB was essentially independent of the model scale. The fact that no scale effects were identified in the present tests can be interpreted in two ways: one is that icebreakers of size and operating conditions in ice similar to those of the WTGB can be confidently model tested at a scale of at least 1:24. The second interpretation is that model tests of icebreakers may be conducted in model ice 2 cm thick or thicker and/or with a bending strength of 30 kPa or more, since these values were the test conditions for the smaller WTGB model; these tests conditions would then specify a limiting model scale so that they correspond to the desired operating conditions of an icebreaker under design.

By conducting model tests not only in level ice but also through broken ice channels, it was possible to separate the level ice resistance into two main components. According to this analysis, it was shown that the "ice-breaking" component is primarily a function of the Cauchy number but also of the Froude number, especially at speed low enough for the ship to experience significant pitching and heaving motions when riding on the level ice and falling back as the ice sheet fails. The contribution of these heaving and pitching motions to the

overall resistance would not have been recognized, had the test data been analyzed purely on the basis of non-linear regression analyses according to any of the various forms of the ice resistance equation available in the literature.

References

[1] Vance, G.P., Goodwin, M.J., and Gracewski, A.S. (1982) Full Scale Icebreaking Test of the Katmai Bay, Proceedings, SNAME Sixth Ship Technology and Research Symposium (Ice Tech '81).

[2] Lecourt, E.J. (1975) Icebreaking Model Tests of the 140-foot WYTM, Arctec, Inc. Report 202C-2.

[3] West, E.E. (1975) Powering predictions for the U.S. Coast Guard 140-ft WYTM represented by model 5336, DTNSRDC Report SPD-223-16.

[4] Tatinclaux, J.C. (in press) Ice Resistance Tests on Two Models of the USCG 140-foot WTGB, CRREL Report.

[5] Schwarz, J. (1977) New developments in modeling ice problems. Proceedings, POAC 77, St. John's, Newfoundland.

[6] Milano, V.R. (1975) Ship resistance to continuous motion in ice. Ice Tech 75, SNAME Symposium, Montreal, Quebec.

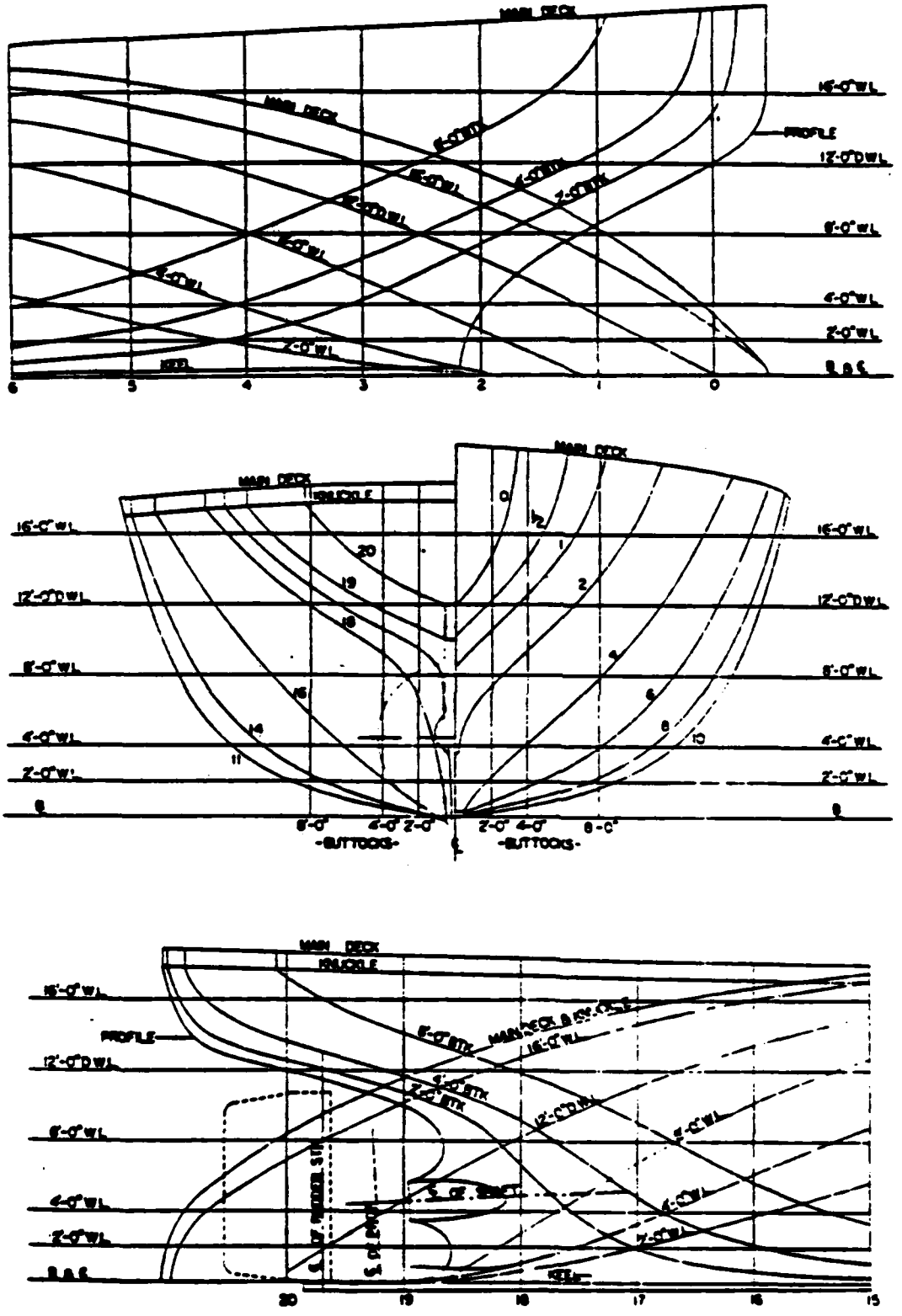

Fig. 1: Abbreviated lines and body plan of United States Coast Guard 140-foot WTGB [3].

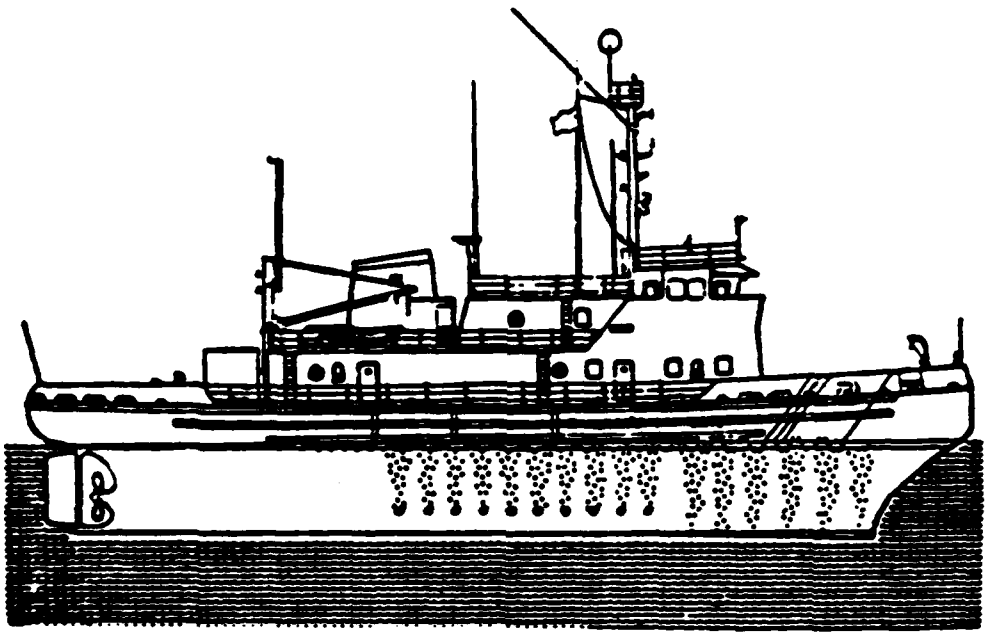

Note: Starboard view showing the action of the hull air lubrication system.

Fig. 2: Profile of the WTGB class icebreaker [1].

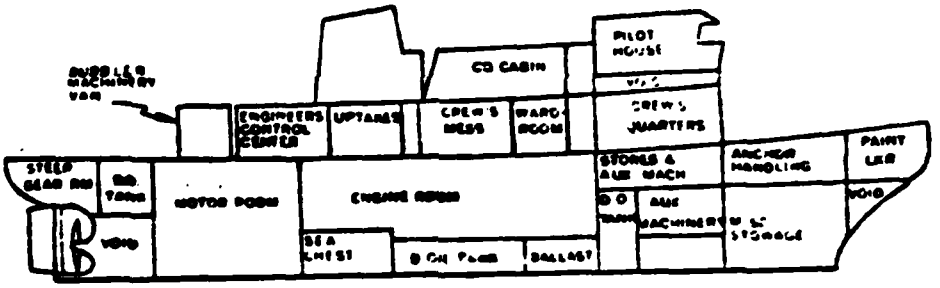

Fig. 3: Inboard profile of 140-foot WTGB [1].

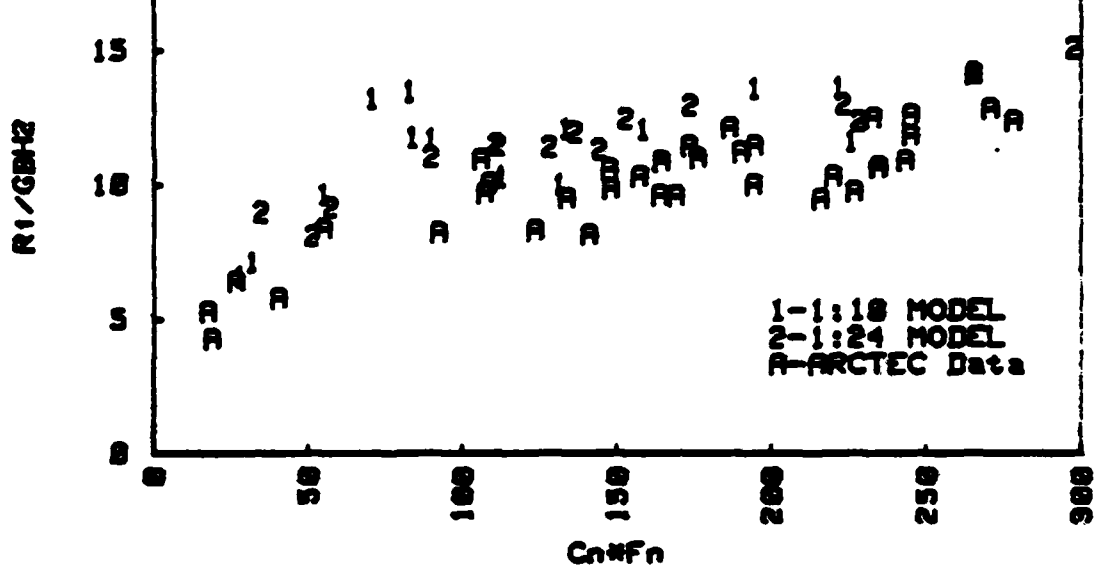

Fig. 4: Level ice resistance vs C_n F_n.

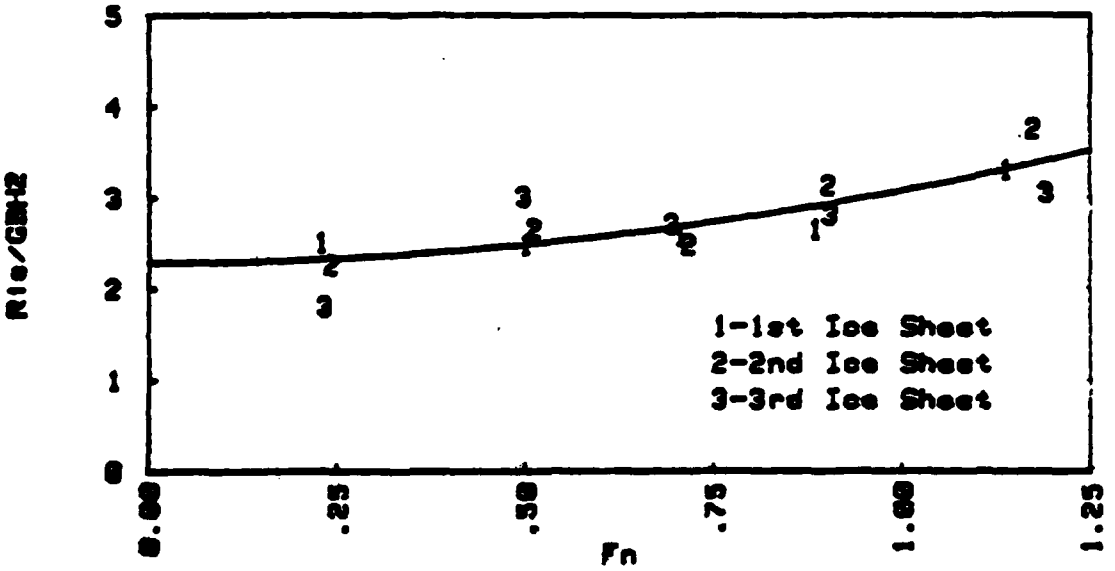

Fig. 5: Resistance in broken channel (1:10 model).

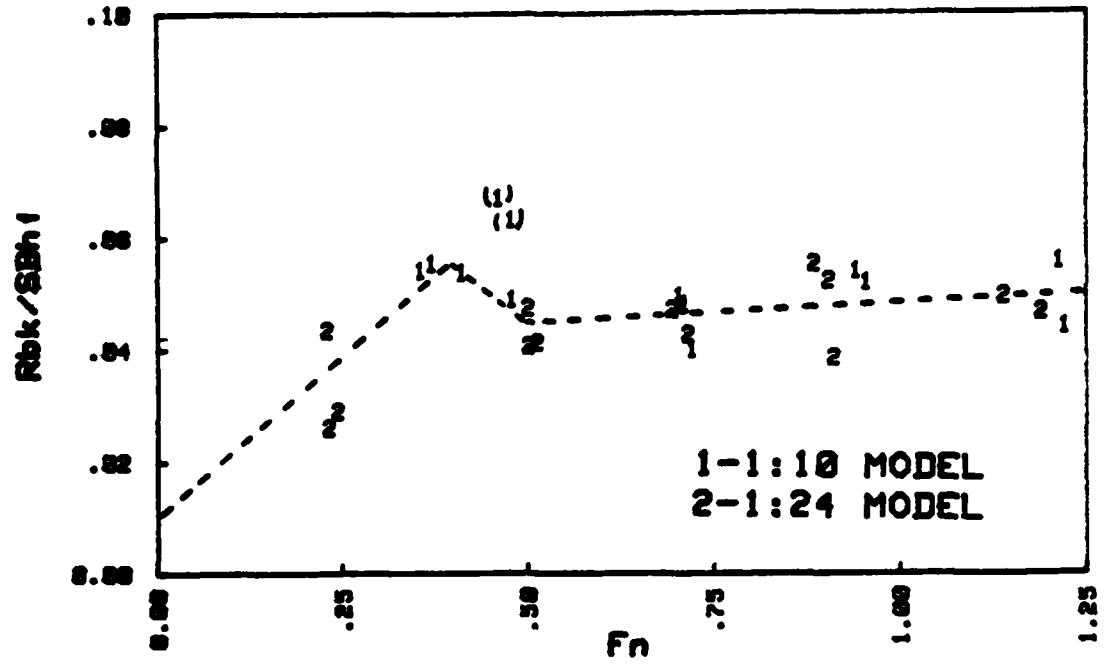

Fig. 6: Ice breaking resistance vs F_n.

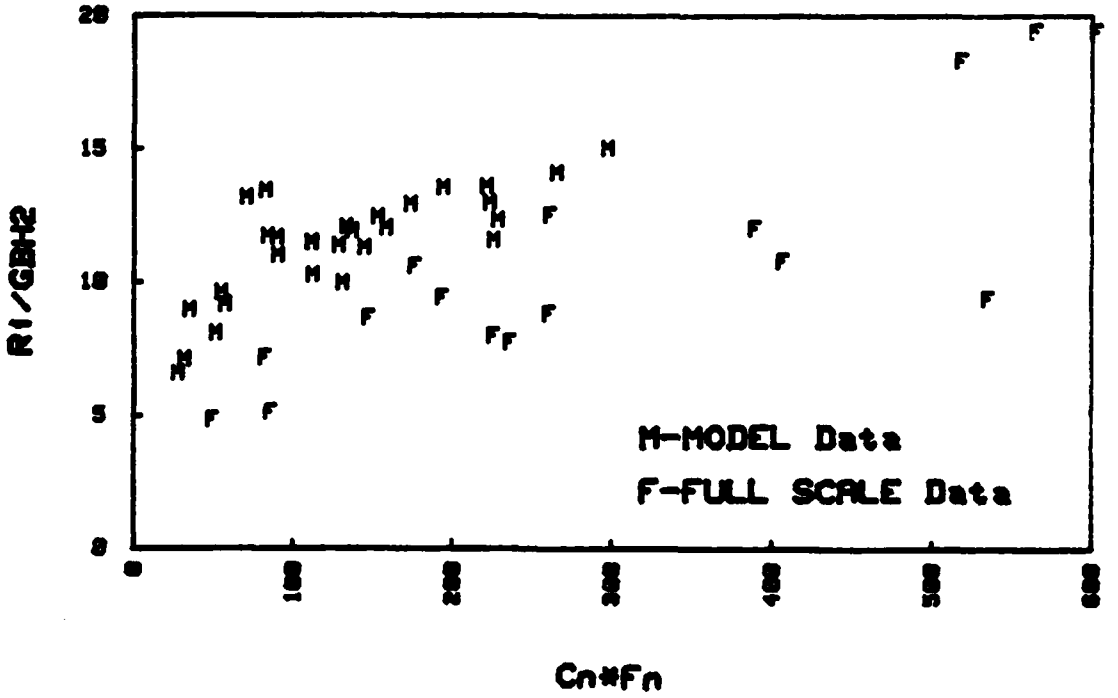

Fig. 7: Comparison of model data with full-scale data.

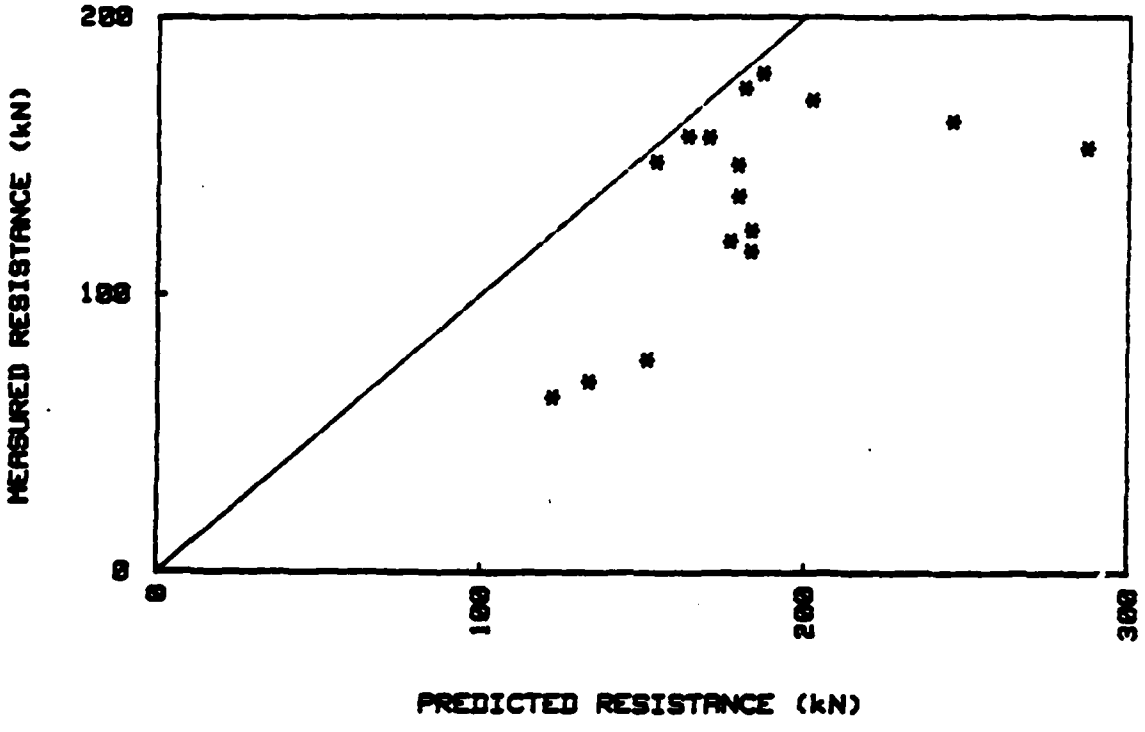

Fig. 8: Comparison of full-scale data with predictions.

REPORTS OF THE

STEERING AND MANEUVERING

COMMITTEE

STEERING AND MANEUVERING

STATE-OF-THE-ART REPORT

In the three years since the nineteenth American Towing Tank Conference there has been a gratifying continuation of the substantial research reported in the proceedings of that conference. Concurrent with this orderly development, there has been an accelerating trend on the part of governmental agencies and international bodies to begin regulation of the steering and maneuvering of ships. It is sensible to consider setting standards in this area since the safety of a ship (and of any object around it) is certainly affected by its ability to steer and maneuver. In fact it is surprising that some form of regulation has taken such a long time to appear on the scene. At any rate, the specter of **quantitative** requirements for the steering and maneuvering capabilities of a ship adds a certain direction and, to a degree a sense of urgency to research in this often neglected area. The Committee felt that this new dimension to steering and maneuvering will become increasingly important to the towing tanks, since the standards which are being discussed pose unique challenges to the art of tankery. We therefore are breaking somewhat from tradition to present the background of two of these "political" activities, since they do set the stage for much of the research which is being performed today. Some of the current research relevant to these activities is also discussed.

Maneuvering Standards

The thrust of the recent regulatory activity is aimed at the inherent characteristics of the ship. That is, the characteristics which do not depend on the pilot, the automatic steering control system, the steering machinery and the like. A detailed review of the events which led to this situation and a proposed design procedure will be presented in a paper at the annual SNAME meetings in the Fall[1]. The following discussion is a summary of some of the material in that paper.

In the late 60's and early 70's there was a considerable concern in the general public about the safety of the then new very large

---

[1] "Design and Verification for Adequate Ship Maneuverability", prepared by the SNAME H-10 Panel, to be presented at the 1983 SNAME Annual Meeting.

tankers. The governing bodies were concerned for two reasons: first, they perceived that the larger ships were not as maneuverable as the smaller ones, and many believed that the accident rate was already too large. Subsequent studies showed that collision, ramming and grounding made up more than 70% of all vessel accidents. As a result of action by the Intergovernmental Maritime Consultative Organization (IMCO), now called the International Maritime Organization (IMO), and by the U. S. Government, work towards improvement proceeded on many fronts. New and better navigation equipment was developed and incorporated into regulations; traffic separation schemes were developed and implemented; the rules of the road were revised; and improvements in vessel design were studied.

Early efforts by IMO and the Coast Guard to reduce accidents produced only marginal improvements. Recognizing that navigation and ship handling is a complex process involving many factors, both governing bodies choose to approach regulation gradually. As a first step, it was required to provide maneuvering information to the ship handler. One aspect of this was the requirement that a chart with such quantities as turning circles and stopping distances was to be prominently displayed on the bridge. In spite of these efforts, the accident of the AMOCO CADIZ and the discovery that several new and highly sophisticated vessels have extremely poor maneuvering characteristics pointed out that much more was still needed. For instance, it has been reported that certain loaded LNG ships operating at 22 knots occasionally make 360 degree turns without warning! Clearly such poor performance is a reflection of the lack of any definitive maneuvering standards to guide the design.

As a result of all this, the Coast Guard and IMO suggest and encourage that from now on all new vessels should be designed with some level of inherent maneuvering performance in mind. Incorporated in this belief is the proposition that the shiphandler should not be required to compensate for poor vessel design. Since ship operators have to integrate so much information when navigating a ship, they should not be additionally burdened by trying to handle a ship which is unreliable, unpredictable or is, for lack of a better word, a "maverick". In order to translate this philosophy into practical maneuvering standards the following two part approach was adopted by the United States and IMO.

Part 1 -

Task 1. Assemble and evaluate available inherent controllability information from full-scale trials, model tests and computer simulations.

Task 2. Obtain evaluations from pilots and masters on what they consider to be good and poor ship handling characteristics of existing ships.

Task 3. Analyze various available numerical expressions which have been developed to evaluate inherent controllability including characteristics of turning circles, stopping tests, z maneuvers, and other course change results, and coursekeeping indicators. Such expressions include advance, transfer, stopping distance, head reach, side reach, overshoot angles, K and T numbers, Norrbin's "P" number, and spiral test loop width and height, when existant,

Task 4. Compare existing vessel inherent controllability information described by the numerical expressions and the subjective evaluations from the pilots (Task 2).

Task 5. Determine which expressions best describe inherent controllability.

Task 6. Define standardized trials which are best for developing the expressions determined in Task 5.

Task 7. Evaluate special maneuvering scenarios to see if other numerical expressions of inherent controllability and trials are needed for special cases, i.e. for "accelerating turns".

Part 2 -

Task 8. Present available maneuvering information in terms of numerical expressions determined best for describing inherent controllability. Separate these indicators of existing vessel's inherent controllability according to general categories of vessels, possibly by broad classes of size and design speed.

This systematic approach has been pursued by the U. S. Coast Guard and IMO on very parallel courses. The intention is to arrive at maneuvering criteria for new ships which is based on demonstrated maneuvering performance from good existing ships. These criteria would encompass turning, stopping, coursekeeping, course changing and the ability to operate at an acceptably slow speed (the latter is a problem for many diesel powered ships). The international governing bodies would require owners, shipyards and designers to plan for maneuverability in the design process and to submit documentation of such planning to the Home Administration (presumably the Coast Guard in the U. S.). Also required will be full-scale trails of completed ships and a comparison of the trial results to the maneuvering performance of existing ships. Thus each new design will be required to be compared to existing designs, and to what the naval architect had predicted for it. In this way, the owner, the shipbuilder and the government will know the relative maneuverability of each new ship. Just by requiring all parties to be aware of this comparison should lead to improved maneuvering designs and eliminate the occasional "mavericks".

Considerable progress has been already made in many of these tasks. The paper by R. Barr and E. Miller to be presented in this session will outline the results of a comprehensive study corresponding to tasks 1 through 6 above. Definitions of standard full-scale trials appropriate to determine inherent controllability have also been formulated by several agencies, such as SNAME and ITTC (task 6). What is lacking, and what concerns us here, is the question of tankery. When regulations do become a fact, it will not make sense to wait for the full-scale trials in order to confirm that the ship meets the standards.

Any setting of steering and maneuvering standards will require that careful scrutiny be given to the choice of model tests required to validate this aspect of the design, and to the question of scale effects. For instance, in the last meeting of the ATTC it was reported that a good comparison exists between the measured full-scale response of the Esso Osaka and the predicted response derived from captive test results of a 25' long self-propelled model. These tests were conducted at Hydronautics using a large amplitude PMM. If it is necessary to conduct tests on models this large in order to determine accurately enough sufficient coefficients to model the steering and maneuvering properties of each new ship design, then it is fair to say that the coming maneuvering standards will have a tremendous impact on both the ship designers and the towing tanks as well.

On the other hand, a different approach, using free-running, radio controlled models and systems identifications methods, has continued to be developed and refined. Although this method may not lead to experimental procedures which are less complicated or costly than captive model tests, they can be used for both the model tests as well as for the full scale trials. A review of this research is presented under the heading of Systems Identification Research below.

With either technique it is apparent that an owner wishing to verify that his prospective new ship has steering and maneuvering characteristics which fall within the standards is likely to find the required model tests to be both costly and time consuming.

Ship-Bridge Collisions

A second type of regulatory pressure exists which, although related to the inherent stability of the ship discussed above, is broader in scope. The collision of a cargo ship with the Sunshine Skyway Bridge in Tampa Bay on May 9, 1980 caused that bridge to collapse with a loss of 35 lives. This accident, together with many other ship-bridge collisions led the National Academy of Sciences' Marine Board to review the causes and to make recommendations for their prevention. A report resulting from this study[2] has been issued and several of their findings are relevant to this committee's interests. Further there has been an international colloquium [3] on this subject. From these sources the following facts emerged:

a. Catastrophic collisions with bridges occur about once every three years someplace around the world.

b. When Collisions occur, often as not the ship collides with a side bridge pier, not a main pier. That is, at the time of the collision the ship is often well outside the normal shipping lane.

---

[2] "Ship Collisions with Bridges: The Nature of the Accidents, Their Prevention and Mitigation", Committee on Ship-Bridge Collisions, Marine Board, National Academy of Sciences, July 1983.

[3] "Ship Collision with Bridges and Offshore Structures", IABSE Colloquium, Copenhagen, May 1983.

c. Typically the major cost of the accident (not including the human lives lost) is neither the repair of the bridge or ship, but the cost to the local economy caused by the disruption of the land-based traffic which depends on the bridge.

d. A large number of bridges are vulnerable to ship collision and it would be extremely expensive to provide sufficient protection around the bridge piers to survive a direct ship collision. It some cases it is simply not possible to provide any significant protection.

e. Most of the waterways which the endangered bridges cross are of restricted draft and these waterways are regularly plied by ships with less than one foot of clearance under the keel.

Because of (c) many communities are extremely concerned about the possible effects of bridge collisions. Some have given consideration to enactment of local regulation of shipping and of ship's operating personnel. The experience indicated by (b) indicates that these collisions are often not the result of a slight miscalculation, but rather are ones in which a significant failure or a serious misjudgement in seamanship took place. The result is that our profession can expect to see increased pressure for understanding and predicting of the steering capabilities of ships in these kinds of restricted waterways, and increased pressure for the training the ship's operating personnel using simulators and the like.

Fortunately, with respect to the latter issue, a considerable amount of progress has taken place in the development of simulations in the last few years. Simulation models for various specific ships have been developed and tested. Most of these mathematical models are based on infinite depth of water. A few, such as the previously mentioned Esso Osaka model, do have shallow water corrections. A catalog of these models will be presented by G. Hagen as a paper in this session.

On the other hand, the steering and maneuvering behavior of ships in extreme shallow water with only the slightest amount of water under the keel is not well understood. Conduct of experiments in extreme shallow draft has many difficulties[4], and performance of standard full-scale maneuvering trials with such a low underkeel clearance is

probably out of the question. Measurements presented by D. Ball[5] show that a 100% reduction in lateral added mass occurs when the underkeel clearance is reduced from 4% to 2% of the draft. Potential theory indicates that there should be a 100% increase for this change. This effect is even more marked in the presence of a wall in the channel. Although these experiments were conducted at zero forward speed, it seems likely that similar unexpected effects would be observed for maneuvering ships with low underkeel clearance. It is also likely that viscous effects play a great role in these effects and, thus, the question of scaling becomes a serious one. Perhaps the application of systems identification methods on actual ships as they ply these inland waterways will be the only means of obtaining good mathematical models of their performance.

It is important to note that considerable progress has been made in the theoretical analysis of the hydrodynamics of steering and maneuvering in those shallow water situations where the underkeel clearance is not as small as mentioned above. A good review of this research can be found in a recent paper by Beck[6].

Related Problems

One aspect of the general ship-bridge collision problem which was omitted from the National Academy's considerations for purely procedural reasons was the problem of barge traffic in the inland waterway system. The difficulty of steering and maneuvering these tows (which may comprise fifteen or more barges lashed together) is well known. Since there are many more bridges over the inland waterways than over the seagoing shipping lanes, one can imagine that the problem of barge collision with these fixed obstacles is also very important. In addition, there are significant economic pressures to reduce the frequency or extent of channel dredging in inportant waterways such as the upper

---

[4] "A Phenomenon Observed in Transient Testing", Sibul, O. J., Webster, W. C. and Wehausen, J. V., Schiffstechnik, Nov. 1979.

[5] "Maximum Added Mass for a Berthing Tanker in Very Shallow Water", Ball, D. J. and Markham, A., The Dock & Harbor Authority, Vol. 63, NØ. 743, October 1982.

[6] "Hydrodynamic Forces Caused by a Ship in Confined Water", Beck, R. F., Journal of Engineering Mechanics Division, ASCE. Vol. 107, No. EM3, June 1981.

Mississippi River. The impact of reduced dredging on tow maneuverability and safety is a significant concern and is at present poorly understood. In response to these needs, there has been an ongoing program at Hydronautics involving the simulation of these barge steering and maneuvering problems. This work is supported jointly by the U. S. Coast Guard and the Corps of Engineers.

In addition, a number of recent accidents has led to an interest in an improved understanding of the behavior and stability of a vessel towing a barge or a disabled vessel. Work began this summer at the University of Michigan on a two year research program entitled "A Rational Method of Upgrading Towed Vessel Safety" under sponsorhip ot the Department of Transportation University Research Program. Related work has also recently begun at MIT under sponsorship of the U. S. Navy. In these problems the steering and maneuvering of both vessels as well as the seaway-induced motions and the towing cable dynamics are all interrelated.

Systems Identification Research

At the last ATTC conference considerable attention was given to the technique of systems identification which was then just beginning to be applied to ship maneuvering problems. In the intervening time considerable progress in this area has occured. A review of some of the recent developments follows.

A considerable amount of research using systems identification techniques has been performed at the David Taylor NSRDC. A paper describing the results of a systems identification study on a Mariner model will be presented at this session by T. Moran, A. Wemple and W. Smith. Their study shows that the use of a free running model and systems identification yields more information than can be obtained from traditional captive tests. The expense in terms of the model sophistication and in terms of the accuracy of tracking is steep. The committee also understands that an effort is underway at DTNSRDC to instrument a full-scale Mariner to obtain time histories for a systems identification analysis.

In a similar effort, T. Trankle and his associates at Systems Control Inc. have developed a sensor and computer package to do real-time systems identification on board a ship. An early version of this system was used on the MARAD research vessel, the Kings Pointer. A more refined version of this equipment is scheduled to be used on

board a Coast Guard Cutter this Fall. THis research is sponsored by MARAD and the Coast Guard.

In addition to the systems identification research on surface ships mentioned above, there is a far more substantial effort concerning the systems identification of submarine motions taking place at DTNSRDC. Unfortunately, much of this work is of a classified natured and can not be dicussed in detail in this forum.

In a related piece of research Prof. Abkowitz at MIT has been involved in a reanalysis of the full-scale data obtained from the Esso Osaka trials using systems identification techniques. His particular concern is in determining just what sensing equipment is absolutely necessary to identify the mathematical model for steering and maneuvering. In the original trials, time histories of the forward velocity, U, the transverse velocity, V, the heading angle, Ψ, and the yaw rate, r were all measured. Not many ships have the capability to measure and record all of these quantities simultaneously. The question is: Is all of this information necessary? In a systematic approach, Prof. Abkowitz is eliminating various of these time histories from the systems identification procedure. Preliminary results indicate that discarding the yaw rate time history did not seriously affect the identified model of maneuvering. Further research may indicate that one can get away with even less information. The important result from this research will be the determination of the minimum instrumentation required to perform systems identification.

Other Research in Steering and Maneuvering

In the last three years there has been several important pieces of research that deserve mention. We will present four here as a group, although they are not particularly related to one another.

The Spring of 1983 saw the publication of a revised version of the Notes on Ship Contollability[7] by SNAME. The original version of this very useful document was published in 1966. H. Eda of Stevens Institute edited this revised version, brought this material up-to-date and included much new material and an extensive set of references to recent literature. This SNAME T&R Bulletin will clearly become a

---

[7] "Notes on Ship Controllability (Revised)", H. Eda, Editor, SNAME Technical & Research Bulletin No. 1-41, April, 1983.

standard reference in this field.

One of the more interesting outcomes from the development of steering and maneuvering simulators has been the use of these simulators, together with experienced pilots, to analyze the adequacy of the design of navigation aids and of the design of the waterways themselves. A series of reports prepared for the U. S. Coast Guard by W. Bertsche and others[8] have investigated the effect of placement of buoys, of electronic radio aids to navigation displays, and of the width and configuration of waterway channels on the navigability of waterways. The concept of using simulators for design should eliminate development hazardous new waterways. Related studies have also been conducted by the personnel at CAORF. Recently released reports have concerned, for instance, piloted stability and the usage of tugs. The report on piloted stability[9] concludes that ships with less inherent stability are, in fact, harder to navigate, even for very experienced pilots. This study gives foundation to the premise that inherent stability should be regulated.

An interesting refinement to the classical approach to the mathematical modelling of steering and maneuvering has been developed by Prof. Abkowitz at MIT. He has included a representation of the flow field over the rudder induced by the propeller race. This representation has been derived by an analysis of the fluid flow induced by a propeller disk and includes both the situation when the propellor is rotating in the forward direction and when the propeller is backing. In the latter case, the blanketting effect of the propeller on the rudder and the resulting directional instability of the ship is modelled. It is hoped that the the results of this project will be available soon.

Another interesting development has been the advent of microcomputers with sufficient speed, capacity and graphics ability that is is feasible to use them as very low cost simulators. In fact, one such simulator system (based on the British BBC microcomputer) costing less

---

[8] "Aids to Navigation Principal Findings Report on the Ship Variables Experiment: The Effect of Ship Characteristics and Related Variables on Piloting Performance", Bertsche, W. R. et al., Eclectech Associates, Inc., Nov. 1981.

[9] "Maneuvering Response", Aranow, P. I., CAORF Report 42-8106-02, Kings Point, New York, Feb. 1983.

than $2000.00 is already on the market. The impact of this new technology on more traditional simulators which use older computer hardware (such as CAORF) is not clear.

Conclusions and Recommendations

Based on this review of both the current research in steering and maneuvering, and on the "political" pressures which are pressing certain issues, such as inherent stability and simulation, the Committee sees the following problems as needing further research and increased attention:

a. What are appropriate model tests which can be performed to confirm that a design when built will meet any inherent stability standards that may be imposed? Are current facilities adequate to perform these tests or will new equipment be required? What size model will be required in order to reduce scale effects to an acceptable level?

b. How can the steering and maneuvering characteristics of a ship plying a waterway with almost no underkeel clearance be determined, tested or modelled? If, as it appears, that viscosity plays a major role in the physics of this flow, what will the scale effects be in any model test?

c. What type of instrumentation will be required to conduct systems identification analyses on full-scale ships? Will the microcomputer revolution make it feasible to place such instrumentation on a large number of ships?

d. Will the new low-cost, microcomputer-based simulators be adequate for training of pilots and for other jobs such as the design of waterways?

DISCUSSION

Albert Strumpf
Davidson Laboratory

Captive model tests of a 6-foot long model of a destroyer were made at Davidson Laboratory (1). The four force and moment coefficient components obtained at David W. Taylor Naval Ship Research and Development Center in tests of a 21.4 foot model of the same destroyer were compared with the Davidson Laboratory 6-foot model results. Examples of these comparisons are shown on the plates. The good agreement between the two sets of results indicates that the methods used for treating 6-foot model force and moment data reduce the "scale effects" on the coefficients to acceptable levels.

---

1. Strumpf, Albert, "Analysis and Correlation of Captive Model, Rotating Arm Tests of a Destroyer," Davidson Laboratory, Stevens Institute of Technology Report 2264, February 1982.

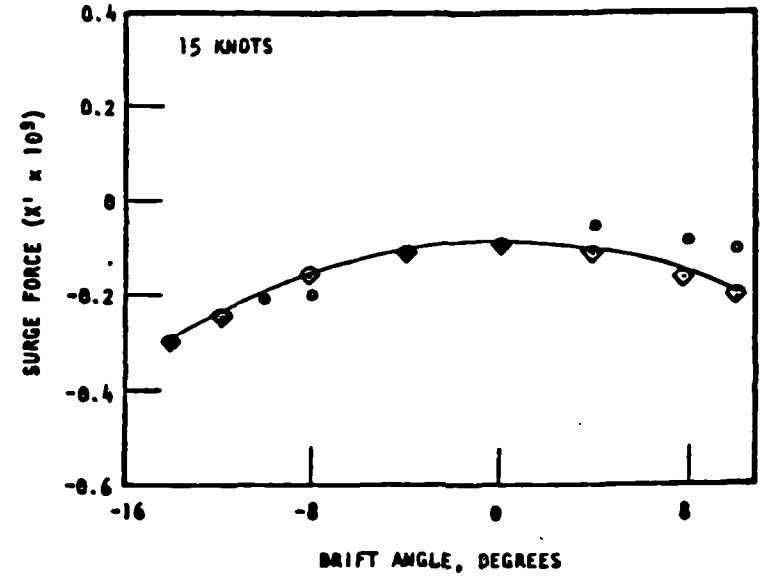

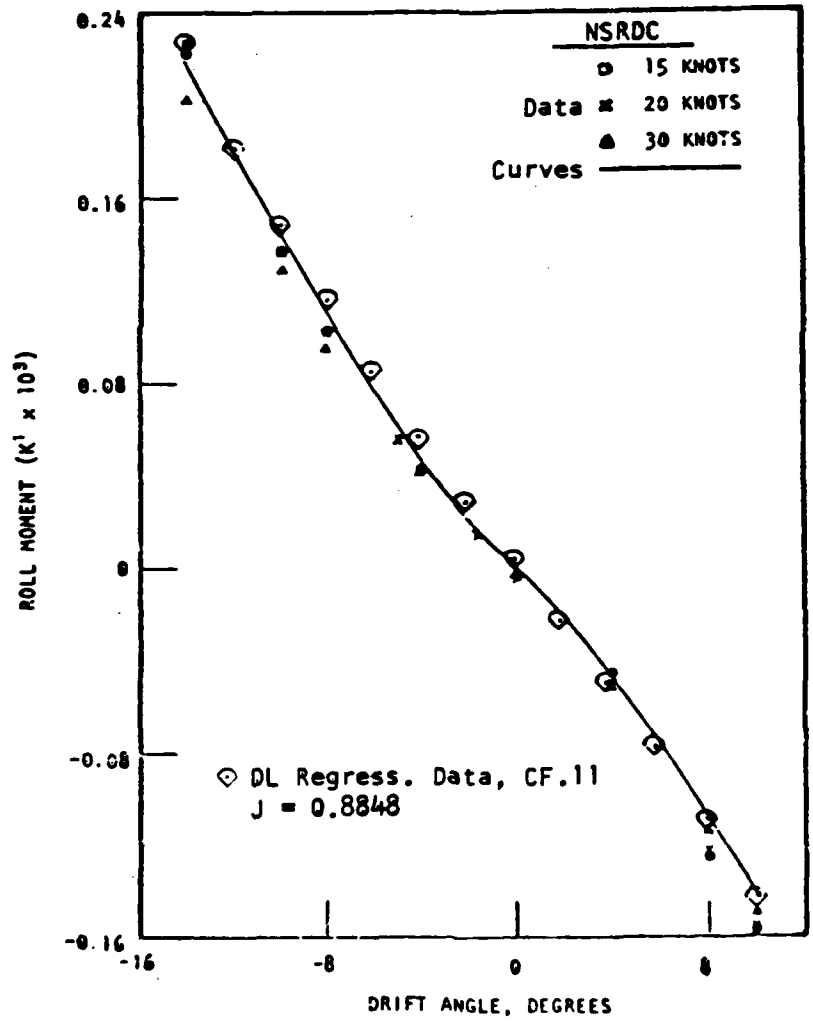

PLATE 20. COMPARISON OF NSRDC AND DL MODEL DATA FOR X' AND K' VS. β.
($\dot{v}'=\delta_r=\varphi=\theta=0$, h/b = 0.3627)

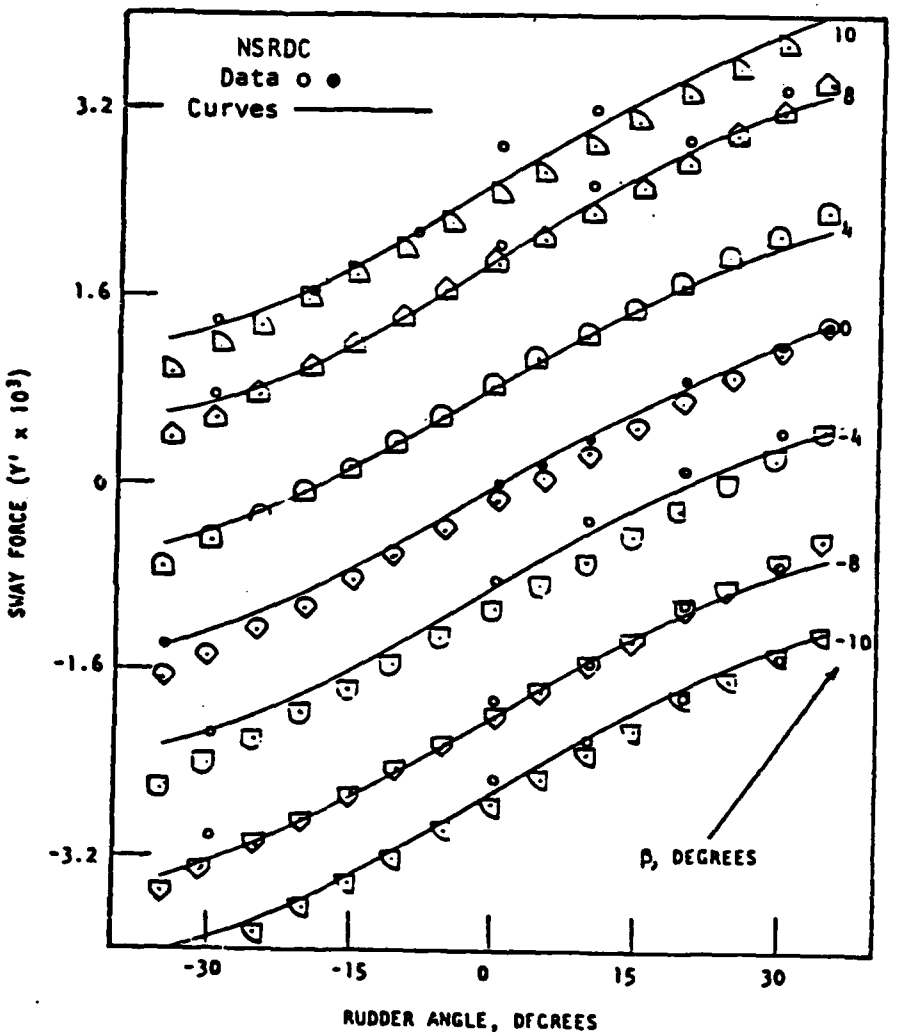

DL Regr. Data, CF.11, J=0.8848, U_p=15 kt

β, deg	10	8	4	0	-4	-8	-10	-14
Symbol								

PLATE 23. COMPARISON OF NSRDC AND DL DATA FOR Y' VS. δ_r WITH β AS PARAMETER. ($\psi'=\varphi=\theta=0$, h/b = 0.3627)

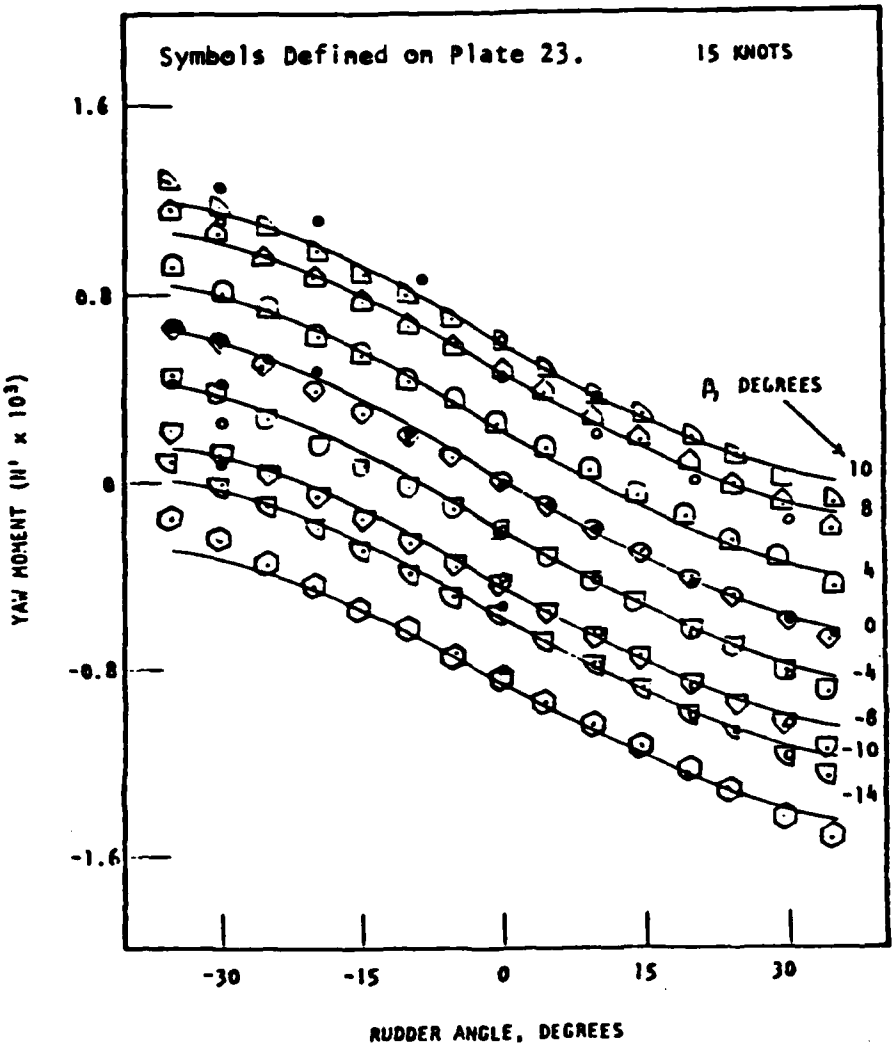

PLATE 25. COMPARISON OF NSRDC AND DL DATA FOR N' VS δ_r WITH β AS PARAMETER. ($\dot{\psi}'=\varphi=\theta=0$, h/b = 0.3627)

AD-P003 821

MANOEUVRING OF SWATH SHIPS

W.C.E. Nethercote*, M.D. Miles† and W.D. Molyneux†

ABSTRACT

SWATH ship model manoeuvring experiments were performed to investigate the effects of rudder configuration on turning performance and to provide free-running model data to test the accuracy of numerical simulations. Both aft of strut and aft of propeller rudders were tested. The model results indicate that the turning performance of the two types of rudders is similar at low Froude numbers, whereas the aft of propeller rudders offer superior performance at Froude numbers greater than 0.35. Correlation studies indicate broad agreement between the experiments and numerical simulation and show that trim can influence SWATH ship manoeuvring performance significantly.

NOMENCLATURE

ADV	Advance
D	Turning circle diameter
DWL	Design waterline length
Fn	Froude number
Fn_I	Initial Froude number
GM	Metacentric height
GM_L	Longitudinal metacentric height
GM_T	Transverse metacentric height
K'	Nondimensional Nomoto steering index
L	Demi-hull length
T'	Nondimensional Nomoto steering index
T_ϕ	Roll period
T_θ	Pitch period
TD	Tactical diameter
$\delta Fn/Fn_I$	Speed loss ratio

*Defence Research Establishment Atlantic, Dartmouth, Nova Scotia
†Arctic Vessel and Marine Research Institute, National Research Council, Ottawa, Ontario

1. INTRODUCTION

Manoeuvrability of SWATH ships is an aspect of their performance that has seen little investigation. Only Fein and Waters have reported any systematic work, first describing rotating arm experiments[1], and then reporting on numerical simulations[2] using the results of the rotating arm experiments. This paper extends the scope of Reference 2.

The Defence Research Establishment Atlantic (DREA) sponsored radio-controlled SWATH manoeuvring experiments at the Arctic Vessel and Marine Research Institute (AVMRI) of the National Research Council of Canada to investigate the effects of variation of rudder configuration. The basis form was that of SWATH 6A to allow comparison with Reference 2. The variant form was a rudder aft of propeller design, now known as a 'long-' or 'extended-strut' design. Outboard profiles are shown in Figure 1 and principal particulars in Table 1. Hereafter the basis form will be known as SWATH $6A_1$, the variant as $6A_2$.

The $6A_2$ configuration has broad correspondence to the aft of propeller rudder described in Reference 2 (see Figure 2 from Reference 2), so it was possible to compare the AVMRI test results for the $6A_2$ configuration
to those from Reference 2 as well to as those for $6A_1$.

2. EXPERIMENTS AT AVMRI

The experiments were carried out in AVMRI's outdoor manoeuvring basin, which is 122 m long, 61 m wide and 3 m deep, using free-running radio-controlled models.

The basis model, $6A_1$, was subsequently converted to $6A_2$ configuration by adding strut extensions. Both configurations had the same draft, transverse GM and rudder area (see Table 1). A DC propulsion motor was installed in each demi-hull and shaft speeds were synchronized electronically. Five-bladed stock propellers were fitted. Each model was also fitted with fore and aft pitch control fins. The aft fins were fixed at zero angle of attack but the forward fins were adjusted manually for zero running trim at the approach speed and held constant during each manoeuvre.

2.1 Test Procedures

The model was fitted with a high intensity lamp as an aiming point, which was tracked using two automatic photosensitive telescopes. Model velocity and trajectory were established by triangulation. A yaw gyro and telemetry system were not fitted to the model as the model size, the same as for Reference 1, severely constrained payload.

Turning circles were measured for eight Froude numbers ranging from 0.1 to 0.54 (based on demi-hull length) at a range of rudder angles from 10 to 35 degrees. Some tests at high speeds and small rudder angles could not be done for the $6A_1$ configuration within the dimensions of the basin.

Zigzag tests were also done at rudder angles of 10, 15 and 20 degrees by fitting a yaw rate gyro and telemetry package in place of one propulsion battery, a substitution which limited maximum model Froude number to 0.38.

The test data were analysed by first fitting splines to the measured X and Y coordinates of the model trajectory as individual functions of time using a least-squares technique. These splines thus served to define both position and velocity as continuous functions of time. A first-order wind drift correction was then applied by subtracting a constant wind drift velocity vector from the measured model velocity. Since tests were only conducted when the wind was light, this correction was always small.

2.2 Discussion of Results

The nondimensional turning circle test results are summarized in Tables 2 and 3. Both configurations have similar performance when Froude number is less than 0.35, but $6A_1$ is greatly inferior to $6A_2$ at higher speeds with its tactical diameter becoming twice as large as $6A_2$'s at a Froude number of 0.54.

The zigzag tests were analysed using Nomoto's method[3]. The validity of this procedure was confirmed by simulating experimental conditions. Figure 3 shows a typical comparison of measured heading and simulated heading, calculated using the method. Nomoto's nondimensional steering quality indices, K' and T', are plotted as averages over all rudder angles to a base of Froude number in Figure 4. The results suggest that $6A_1$ has somewhat greater turning ability at Froude numbers less than 0.35, but the trend of K' suggests that $6A_2$ will be superior at higher Froude numbers, as was indeed found for the turning circles.

Since it appeared that the surface piercing rudders of $6A_1$ were ventilating at the higher speeds, it was decided to conduct some further tests to investigate the importance of this factor. Three alternative fence designs were fitted on the $6A_1$ rudders and the turning circle tests were repeated for the higher Froude numbers. The three designs were:

(a) single fence with approximately 50% chord length;
(b) single fence completely surrounding the rudder;
(c) both (a) and (b) fitted to the rudder.

The resulting tactical diameters for all rudder arrangements tested are summarized in Figures 5 and 6 for rudder angles of 25 and 35 degrees. It is clear that $6A_2$ with fully submerged rudders remains the superior configuration, at high Froude numbers. The use of rudder fences does reduce the tactical diameter of $6A_1$ and also delays the transition point somewhat, but even the best $6A_1$ design does not approach the performance of $6A_2$ at high speeds.

Considering the limited influence of the rudder fences, other factors must have caused the high speed turning performance disparity. The $6A_1$ and $6A_2$ rudders were of equal area at zero speed, but geometric restrictions forced a lower aspect ratio to be adopted for $6A_1$: 0.73 vs 1.48 for $6A_2$. The $6A_2$ rudder also benefitted from accelerated flow from the propeller discharge current. At high speeds, $6A_1$'s rudder capability was degraded by bow down trim associated with speed loss in turning and by wave profile, both of which caused a relative depression of the free surface at the rudder, thus reducing effective rudder area. The former was a consequence of the test procedure since weight constraint prohibited use of an active fin attitude control system. The model tests were carried out at Froude scaled speeds so surface depression due to wave profile must be accurately modelled. Of course, ambient pressure cannot be scaled in an atmospheric basin, but the minor effect of ventilation on performance has already been shown by the small effect of the addition of fences. A last possibility is that of rudder stall. Were the struts to act as flow straighteners, and it seems a reasonable assumption, the $6A_1$ rudders could experience stall before those on the $6A_2$ design, which benefit from operation in the accelerated discharge current of the propeller.

3. CORRELATION

The AVMRI experimental results have been compared with the Waters and Fein rotating arm-based simulations[2] in two ways.

Figure 7 and 8 show the effect of Froude number on tactical diameter, with fixed rudder angles of 25 and 35 degrees. The experimental and simulation results are only of broadly similar character, with differences in tactical diameter of up to 50 percent. In the $6A_1$ case, the simulation does not suggest the tactical diameter jump which is so apparent in Figures 5, 6 and 8, although one can only speculate whether simulations at more intermediate speeds would have identified this feature. For $6A_2$, measured and simulated rate of change of tactical diameters with Froude number differ significantly.

Figure 9 shows the effect of rudder angle on both tactical diameter and speed loss in turns at a 0.384 initial Froude number. The correlation of the experimental and simulated diameters for $6A_2$ is very good. For $6A_1$ the correlation is good only for low rudder angles, becoming progressively worse as rudder angles increase beyond 25 degrees. For both $6A_1$ and $6A_2$ the experimental speed loss is consistently higher than the simulation value. This could be expected due to the additional trim induced drag of the free running model.

There are a number of possible reasons for the poor correlations. The AVMRI model was free to trim in response to speed loss during a turn, whereas the simulations were based on fixed trim rotating arm experiments. Section 2.2 noted that trim would lead to relative surface depression around $6A_1$'s rudders, in excess of that due to wave profile alone. This is consistent with a better simulation-experiment correlation for the $6A_2$ model because its fully submerged rudder will be affected less by trim, trim that will be less in any case for $6A_2$ due to its increased GM_L relative to $6A_1$. Of course, the fully submerged $6A_2$ rudder should be free of any ventilation effects.

Propeller loading may also affect the correlations, for whereas the rotating arm experiments were performed with propeller revolutions corresponding to an ITTC+0.0004 ship propulsion point, the AVMRI experiments were of necessity run at the model self-propulsion point. As a result, the NRC model propellers rotate about seven percent faster than those in the rotating arm tests, possibly biasing the NRC $6A_2$ results towards smaller tactical diameter than those predicted by Waters' and Fein's simulations.

Contrary to the expected effect of operation at difference propulsion points, Figures 7 and 8 show low speed simulated tactical diameters for $6A_2$ to be smaller than AVMRI's experimental ones. The difference in aspect ratio between aft of propeller rudders used in rotating arm and free-running model experiments may account for this discrepancy. The low aspect ratio rudder used in rotating arm tests may act more as a flow deflector than a hydrofoil.

4. CONCLUDING REMARKS

The correlations reported in Section 3 are in some respects disappointing, even though the two designs are similarly ranked by both the simulations and AVMRI experiments. Measured and simulated tactical diameters differ by over 50 percent in some cases, and a similar comparison for speed loss in turns shows even larger differences. The speed loss difference is easily explainable by considering the trim induced added drag of the free-running model, because speed loss correlations are good at low rudder angles where speed loss and trim change are both small. Trim is less useful for explaining tactical diameter differences. For $6A_1$, trim change can be used to explain the tactical diameter jump, but cannot explain why free-running model tactical diameters are otherwise smaller than simulation values. $6A_2$, with fully submerged rudders, should have tactical diameters affected less by trim, and indeed the correlation is good above Froude number 0.3. Different geometric details, particularly rudder aspect ratio, may be responsible for the much poorer correlation at lower speed.

$6A_1$ and $6A_2$ have similar manoeuvrability at Froude numbers below 0.35, but the $6A_2$ configuration with fully submerged rudders has better performance at higher speeds and is far superior if the craft are not dynamically stabilized in heel or trim. The manoeuvrability of the $6A_2$ configuration is comparable to that of conventional modern frigates.

Nomoto's method[3] for analysis of zigzag tests gave excellent agreement with experiment for both the $6A_1$ and $6A_2$ configurations. The K' and T' steering quality indices are therefore at least as valid for SWATH ships as they are for more conventional craft.

REFERENCES

1. Fein, J.A. and Waters, R.T.: Rotating Arm Experiments for SWATH-6A Manoeuvring Predictions. DTNSRDC SPD698-01, July 1976

2. Waters, R.T. and Fein, J.A.: Manoeuvrability of SWATH Ships. Proc. 19th ATTC, Ann Arbor, 1980.

3. Nomoto, K.: Analysis of Kempf's Standard Manoeuver Test and Proposed Steering Quality Indices. First Symposium on Ship Manoeuvrability, DTMB Report 1461, Oct 1960.

TABLE 1: PRINCIPAL PARTICULARS

AVMRI Model 329 λ = 1/22.5

Configuration	$6A_1$	$6A_2$
Hull length, m	3.25	3.25
Maximum breadth, m	1.22	1.22
Reference point, m abaft bow	1.56	1.56
Displacement, kg	252	266
Draft, m	0.365	0.365
GM_T, m	0.149	0.149
GM_L, m	0.281	0.869
T_ϕ, sec	3.58	3.70
T_θ, sec	4.15	2.53
Rudder Details		
Chord, m	0.241	0.171
Span at leading edge, m	0.330	0.252
Span to D.W.L. at leading edge, m	0.171	-
Area to D.W.L., m^2	0.043	0.043
Thickness/chord	0.150	0.150
Aft Control Fin Details		
Chord, m	0.200	
Span at leading edge, m	0.222	
Thickness/chord	0.150	
Distance 1/4 chord abaft bow, m	2.749	
Forward Control Fin Details		
Chord, m	0.116	
Span at leading edge, m	0.129	
Thickness/chord	0.150	
Distance 1/4 chord abaft bow, m	0.743	

TABLE 2: SWATH $6A_1$ TURNING CIRCLE TEST RESULTS

FROUDE NUMBER	RUDDER ANGLE	$\frac{ADV}{L}$	$\frac{TD}{L}$	$\frac{D}{L}$	SPEED LOSS RATIO
0.096	10.0	5.94	10.52	10.71	0.09
	15.0	4.86	7.12	7.34	0.14
	20.0	3.47	5.02	5.59	0.14
	25.0	3.60	4.99	4.96	0.22
	30.0	3.45	4.17	4.92	0.27
	35.0	3.42	4.40	4.98	0.26
0.135	10.0	5.96	10.41	10.69	0.10
	15.0	4.72	6.61	7.12	0.12
	20.0	3.82	5.46	5.65	0.16
	30.0	2.76	4.10	4.29	0.24
	35.0	2.78	3.77	3.99	0.30
0.192	10.0	6.02	11.32	11.04	0.04
	15.0	4.85	7.14	6.95	0.09
	20.0	4.05	5.32	5.22	0.12
	30.0	3.08	3.94	3.94	0.22
	35.0	3.10	3.62	3.61	0.26
0.288	15.0	5.73	9.05	8.59	0.07
	20.0	4.24	6.65	6.54	0.08
	30.0	3.69	4.21	4.17	0.16
	35.0	3.04	3.66	3.66	0.21
0.384	20.0	8.14	10.48	10.53	0.08
	30.0	4.80	4.90	4.57	0.23
	35.0	5.03	4.27	4.23	0.28
0.432	30.0	5.28	7.56	6.52	0.20
	35.0	6.21	7.74	6.39	0.23
0.480	25.0	7.89	13.29	13.14	0.05
	30.0	6.47	11.73	11.41	0.08
	35.0	6.44	9.55	9.79	0.08
0.538	25.0	8.77	13.17	13.78	0.07
	30.0	7.07	10.53	10.89	0.10
	35.0	7.63	9.83	10.00	0.12

TABLE 3: SWATH $6A_2$ TURNING CIRCLE TEST RESULTS

FROUDE NUMBER	RUDDER ANGLE	ADV / L	TD / L	D / L	SPEED LOSS RATIO
0.096	10.0	6.40	11.16	11.16	0.01
	15.0	5.14	7.48	6.93	0.09
	20.0	3.56	5.28	5.57	0.10
	30.0	2.83	4.08	4.14	0.26
	35.0	2.93	3.88	3.75	0.31
0.135	10.0	6.24	10.80	I0.76	0.05
	15.0	4.57	6.88	6.70	0.12
	20.0	3.73	5.39	5.37	0.15
	30.0	2.98	4.21	4.09	0.27
	35.0	3.12	3.91	3.80	0.33
0.192	10.0	5.44	11.43	11.17	0.05
	15.0	4.27	7.48	7.49	0.10
	20.0	3.45	6.91	5.73	0.13
	30.0	2.69	4.35	4.10	0.28
	35.0	2.42	3.92	3.79	0.33
0.288	15.0	15.01	7.82	7.92	0.02
	20.0	4.16	5.99	6.10	0.05
	30.0	3.64	4.62	4.53	0.16
	35.0	3.36	4.20	4.18	0.23
0.384	10.0	6.91	11.77	11.72	0.04
	15.0	5.25	8.21	8.10	0.14
	20.0	4.20	6.44	6.33	0.23
	30.0	3.54	4.92	4.80	0.27
	35.0	3.12	4.38	4.36	0.30
0.432	10.0	8.21	13.81	13.87	0.03
	15.0	6.06	9.91	9.79	0.05
	20.0	4.87	7.30	7.18	0.09
	30.0	3.66	5.21	4.75	0.28
	35.0	3.17	4.50	4.35	0.32
0.480	15.0	5.69	10.06	9.90	0.07
	20.0	4.28	7.69	7.63	0.11
	30.0	3.77	5.85	5.81	0.16
	35.0	3.19	5.14	5.13	0.20
0.538	15.0	5.95	10.50	10.45	0.09
	20.0	4.88	8.11	7.97	0.15
	30.0	3.65	6.10	6.00	0.21
	35.0	3.57	5.31	5.44	0.22

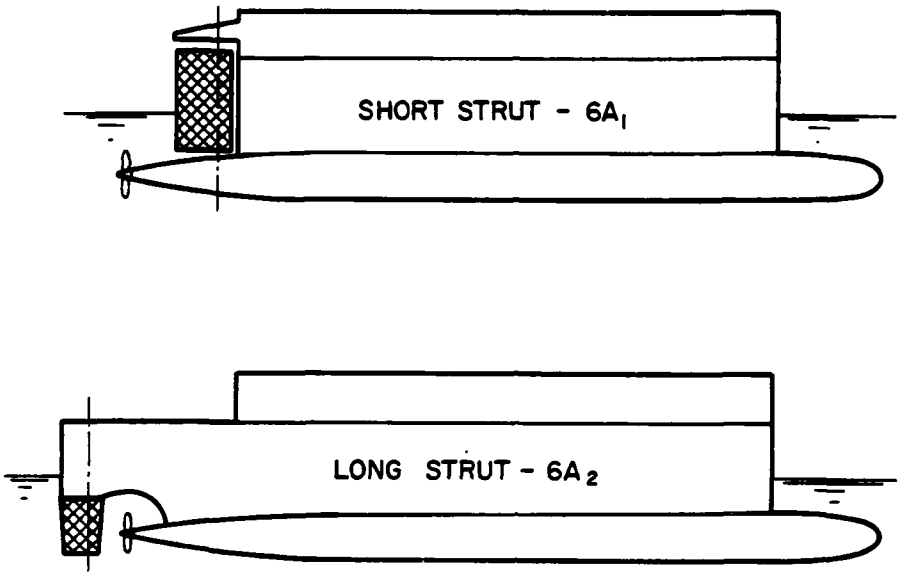

FIG. 1 OUTBOARD PROFILES

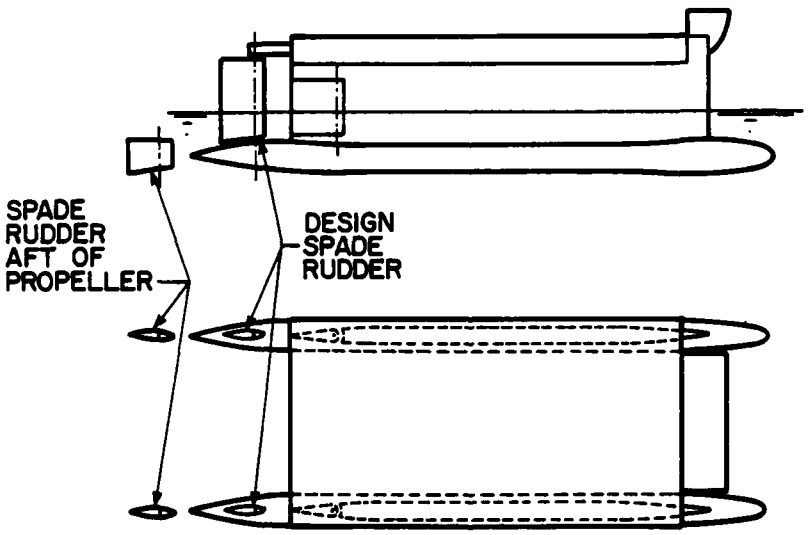

FIG. 2 FEIN AND WATERS RUDDER ARRANGEMENTS

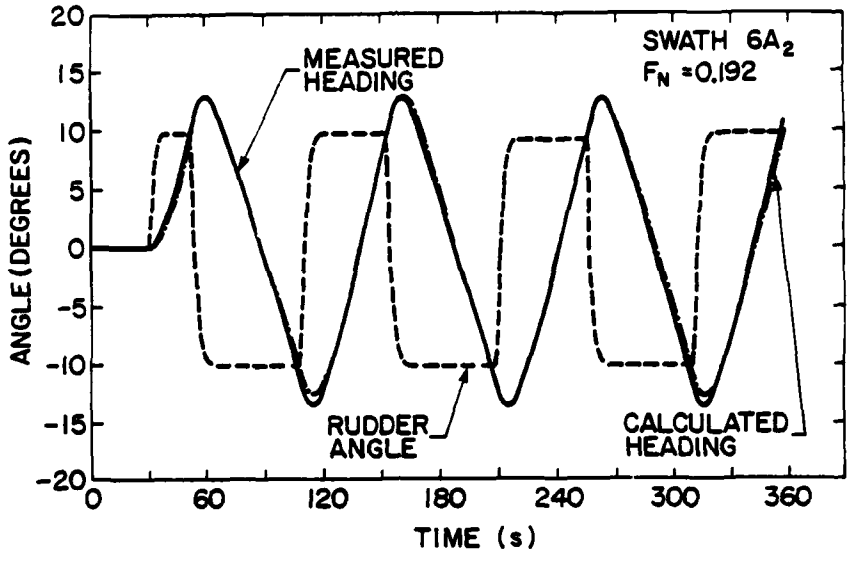

FIG. 3 COMPARISON OF TYPICAL ZIG-ZAG TEST HEADING CALCULATED USING NOMOTO'S METHOD (REF. 3)

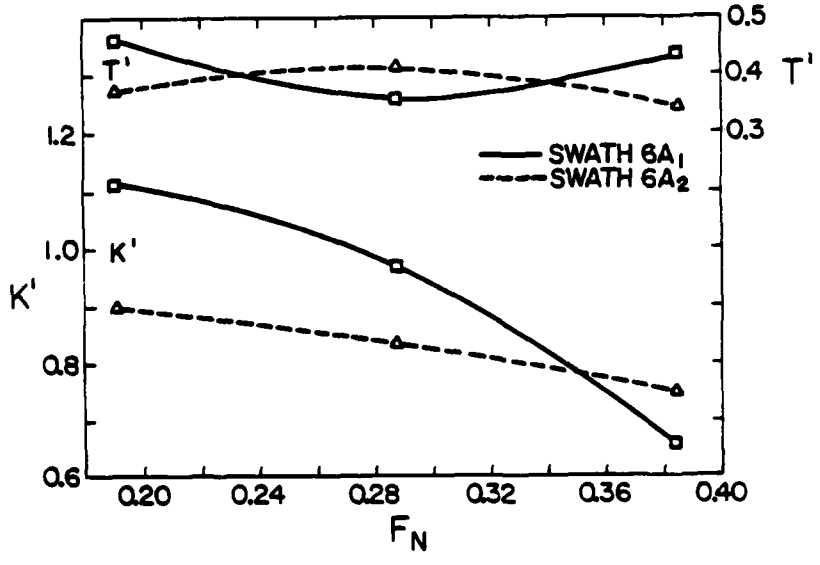

FIG. 4 NON-DIMENSIONAL NOMOTO STEERING QUALITY INDICES

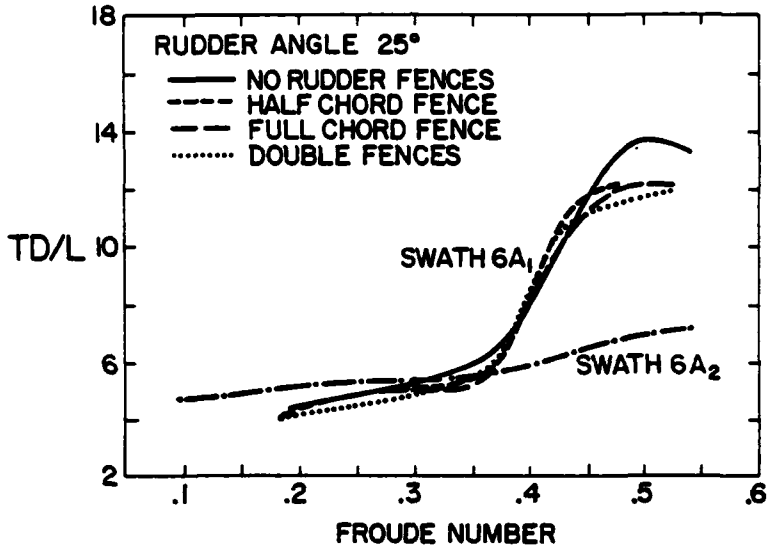

FIG. 5 TACTICAL DIAMETER AT 25 DEGREE RUDDER ANGLE

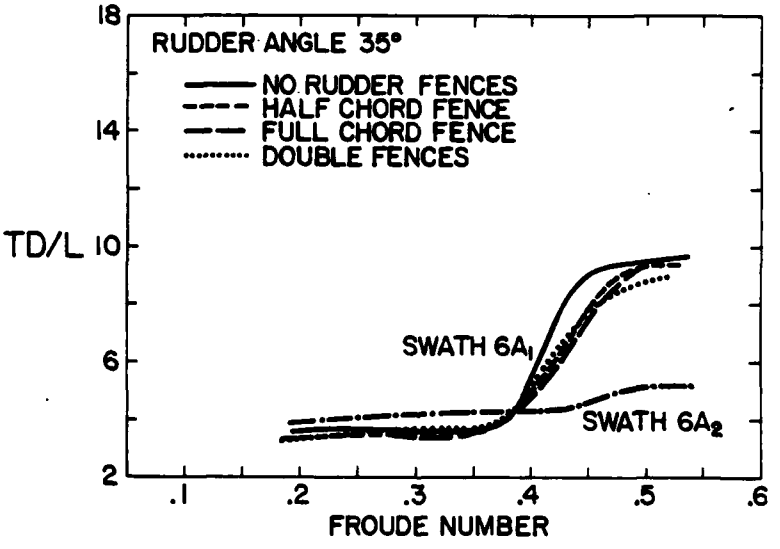

FIG. 6 TACTICAL DIAMETER AT 35 DEGREE RUDDER ANGLE

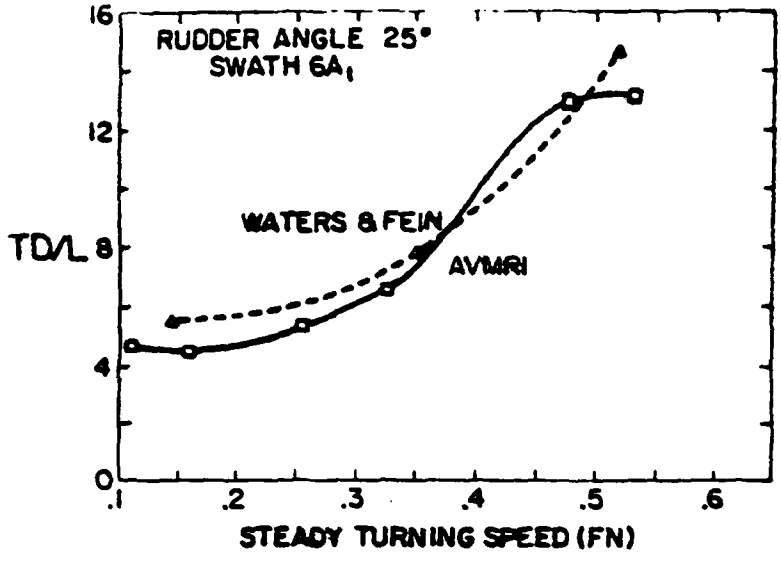

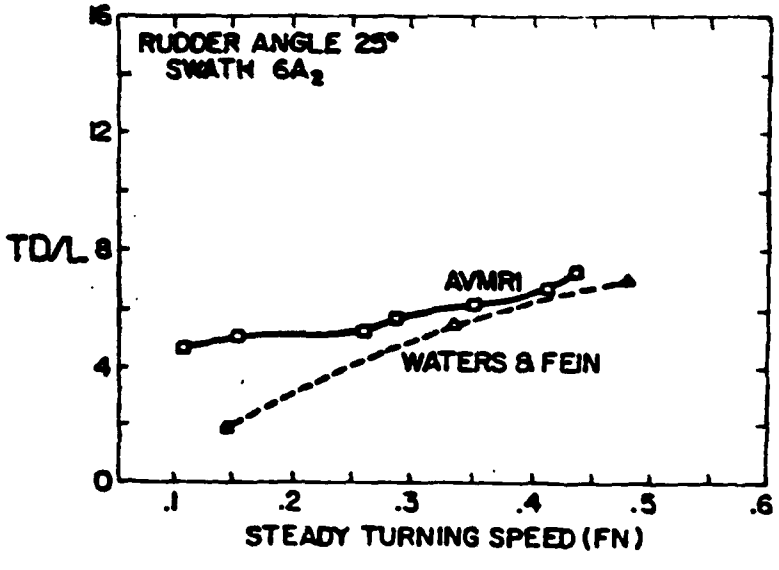

FIG. 7 EFFECT OF SPEED ON TURNING, 25 DEGREE RUDDER ANGLE

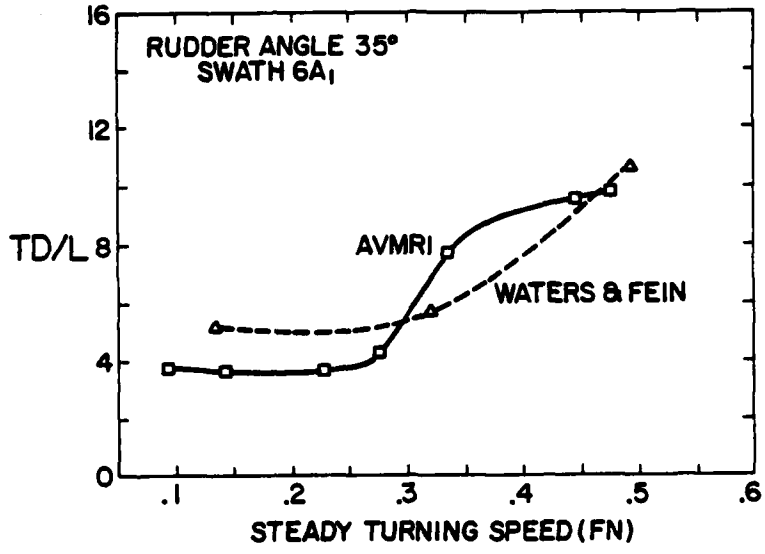

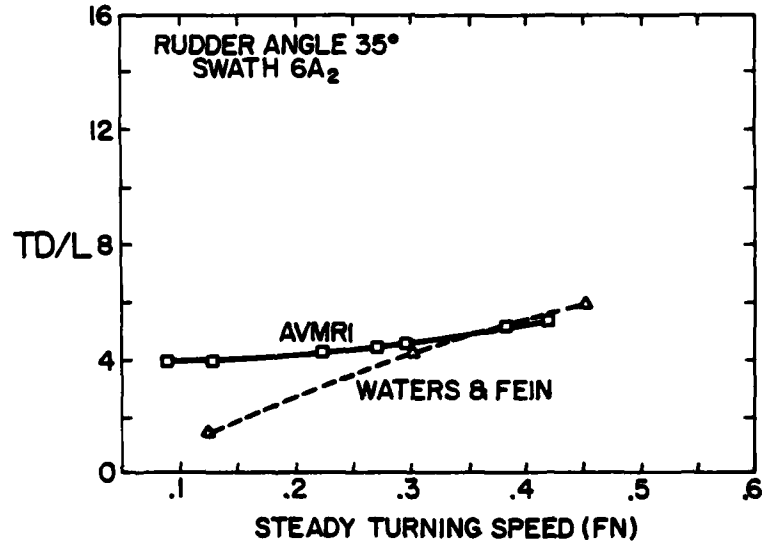

FIG. 8 EFFECT OF SPEED ON TURNING, 35 DEGREE RUDDER ANGLE

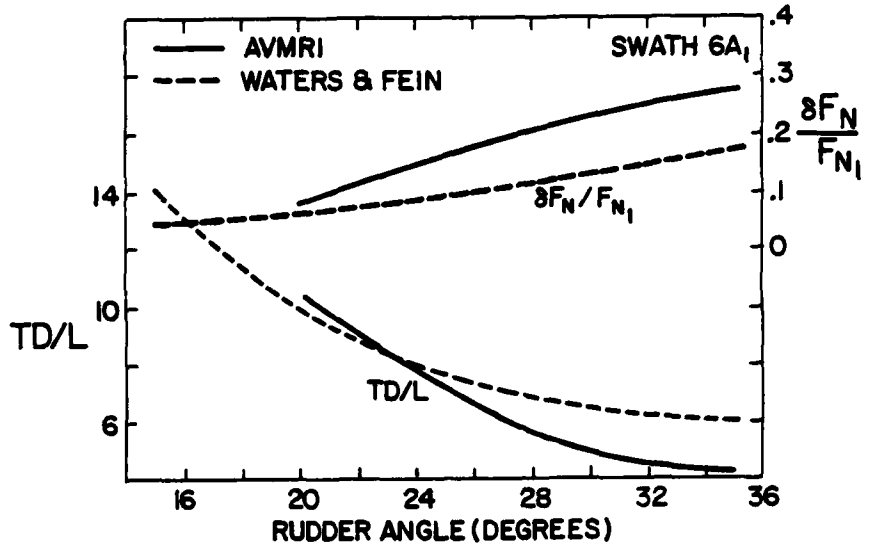

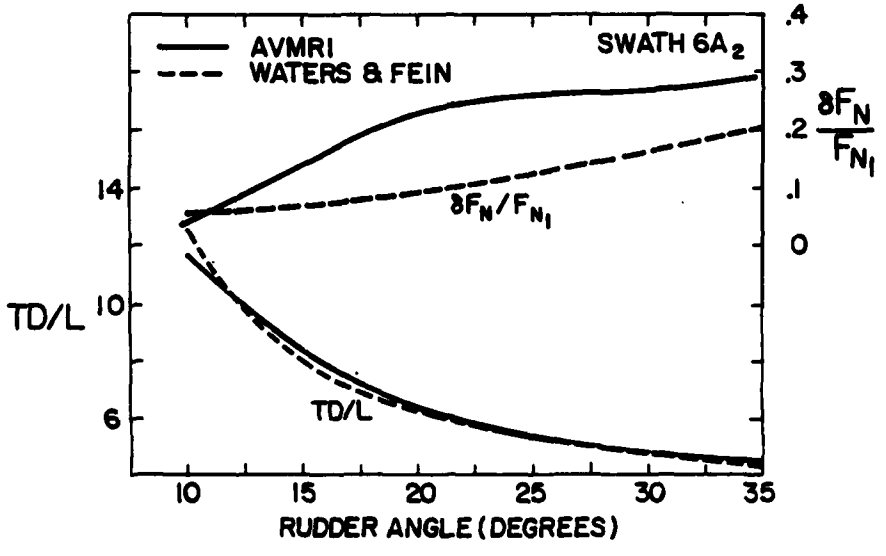

FIG. 9 EFFECT OF RUDDER ANGLE ON TURNING, INITIAL F_N = 0.384

AD-P003 822

A Catalog of Existing Mathematical Models for Maneuvering. G. R. Hagen

MATHEMATICAL SHIP MANEUVERING MODELS AND THE SOCIETY COEFFICIENT DATA SHEETS (A PRIMER)

1.0 INTRODUCTION

1.1 PURPOSE OF MANUAL

This manual is intended to be a primer with a twofold purpose. First, it provides an introduction to the concept of mathematical ship maneuvering models and their roles in solving a variety of problems confronting designers, operators, and others concerned with ship maneuverability and safety. Secondly, it serves as a guide to, and complements the use of, the Society of Naval Architects and Marine Engineers (SNAME) "Standardized Data Sheets" which contain such mathematical maneuvering models and other associated data for specific ships.

In satisfying the first part of this objective, the scope of the manual is that of a primer, and no attempt is made to treat the derivation and historical development of mathematical ship-maneuvering models in depth. Therefore, those interested in more detailed treatments of this subject should refer to Reference 1 and other primary sources cited in subsequent sections of this manual.

The need for the second part of the objective follows from the nature of the SNAME "Mathematical Manuevering Model Standardized Data Sheets". As can be seen from Section 7, these data sheets were designed to provide a means for presenting mathematical maneuvering model data pertaining to individual ships in concise and compact form. Accordingly, items such as the voluminous notations, definitions, and other generalized information considered pertinent, particularly to the uninitiated, are properly relegated to this manual.

It should be mentioned at this point that the "Standardized Data Sheets" were developed with the hope of providing the medium for increased exchange of information within the community that possesses or uses mathematical maneuvering models of various ship types. Therefore, the data sheets do not constrain a modeler to a specific reporting system. Instead, they offer a convenient format that permits a consistency of reported data among different experimenters and modelers. It is intended that the Society will publish a continuing series of these sheets as such data become available in the standard format.

1.2 DEFINITION OF MATHEMATICAL MODELING

The typical mathematical ship maneuvering model[1] is comprised of a set of equations of motion (of the form: Force = Mass x Acceleration) in which the hydrostatic and hydrodynamic forces (due to the hull, maneuvering system, and propulsion system) are represented. The equations may also include environmental forces such as those which arise due to wind, waves, or current. These equations of motion are integrated through small time steps to solve for the motions of the vessel which occur as a result of the forces acting on it.

Specific ships are described by specific sets of constants (hydrodynamic coefficients) used in the equations of motion. These coefficients are predominately determined by experimental means and depend on the pertinent geometrical characteristics of the ship. The precise composition of some of the mathematical ship maneuvering models presently in use is given in Appendix C.

The resultant mathematical model is a powerful tool for use in predicting the path and associated data of a given ship in response to the action of its controls in various specified environments. As an example of its use, consider a MARINER Class ship operating at a steady speed and course. At some specified time, the rudder is ordered hardover, with the throttle setting remaining fixed. The mathematical model can predict a

---

[1] To avoid confusion in the remainder of this manual, the type of ship maneuvering model defined above will be denoted simply as the mathematical model. This is in contrast to the term model which alone generally applies to the physical model of a ship such as is used in captive or free running model tests.

time history of the ship's speed, rate of turn, heading, and position. (Heel angle is generally not included in the models.) Depending upon the sophistication of the mathematical model, this can be done for calm water or rough seas, for deep water or shallow water, and for various ship loading conditions and other variations in environment such as wind and current.

In practice, the validity and extent to which maneuvering predictions can be made depends on the ability to determine the numerous hydrodynamic coefficients involved in the mathematical model for the specific ship and environment being represented. Fortunately, fairly advanced captive model test techniques for supplying the needed information have been developed in recent years. The application of these techniques has resulted in the acquisition of a relatively large body of hydrodynamic coefficient data for a variety of ships in the calm, deep-water case.

Similarly, hydrodynamic coefficient have been produced for a few ships in the case of calm water at various shallow-water depths. Also, theoretically-based methods and system/parameter identification methods based on free-running model and full-scale trajectory data have contributed to determining the structure of mathematical models. Brief description of these various techniques, along with references which provide more detailed treatment of the subject, are given in Section 4.

In summary, the mathematical model always contains some representations or assumptions regarding:

a. The ship, control surfaces, main propulsion, and thrusters (if any).

b. The waterway, whether open seas, harbor approaches, or restricted channels.

c. The environment, such as specific wind conditions, currents, and wave spectra.

The presentation of a complete mathematical model can cover several pages of equations, particularly if all of the above elements are involved. Modern practice is to program the equations for solution by digital computers, and then insert inputs which vary depending upon the ship or case being represented. The computer output is then typically either a numerical prediction of the ship's path at selected time intervals (Table 1-1), or a scaled plot of the ship's path (Figure 1-1). To a lesser extent, analog computers are still used, particularly in some of the ship maneuvering simulations. The outputs in this case are usually given as continuous time histories on a strip-chart recorder.

1.3 USERS OF STANDARDIZED DATA SHEETS

There is a growing variety of practitioners who are engaged either in the development or use of mathematical ship maneuvering models. Each can be identified with one of the following four types:

a. The "General Mathematical Modeler" (including training simulator technicians) who may not have specific knowledge in the field of ship hydrodynamics.

b. The "Design Naval Architect" who is concerned with maneuverability characteristics primarily to the extent that they may affect the design of ship hull, propulsion, and control system.

c. The "Waterway Designer or Regulator" who must ensure safe operations in waterways that may be congested, shallow, or restricted.

d. The "Ship Maneuvering Specialist" who is an expert in the field of ship dynamics and is usually connected with a model testing tank research facility which is a major source of inputs to the various mathematical models.

Some practical instances which mathematical models and the standardized data sheets can be utilized by the above types of practitioners include the following:

a. Development of simulators to provide realistic accuracy for instruction on techniques of ship handling or for research into the behavior of bridge personnel in various situations.

b. Prediction of controllability characteristics for existing ships in existing waterways, and establishment of safe operating limits.

c. Prediction of the maneuverability characteristics for new ships so that design features can be incorporated as

appropriate to the waterways in which they will operate.

d. Investigation of the control logic of an autopilot in a seaway and the determination the logic that provides best course control or speed-made-good.

The above applications are discussed in more detail in Section 2 which deals with the growing need for mathematical maneuvering models.

1.4 DESCRIPTION OF MANUAL CONTENTS

In addition to introducing notations in the Appendices which are essential adjuncts to the SNAME Mathematical Maneuvering Model Standardized Data Sheets, this manual contains the following information:

Section 2 addresses the variety of needs for mathematical maneuvering models which have been greatly expanded due to the increase in ship traffic, the trend toward large or unusual vessel types, and the increased concern for safety and for the preservation of the environment. Section 3 discusses the basic approaches to the mathematical modeling of ship trajectories, including the equations of motion, the nature of the hydrodynamic coefficients, other inputs required, and the limitations restricting the various applications. Section 4 describes the various techniques used to evaluate numerically the hydrodynamic coefficients required for the mathematical models. Section 5 treats the special case of linearized mathematical models including the directional stability indices and control effectiveness parameters which are useful as Preliminary Design criteria. Section 6 describes typical computer simulation studies involving the use of mathematical models including evaluations based on definitive maneuvers, comparisons of predicted with corresponding full-scale data, and the development of maneuvering criteria. Finally, Section 7 describes the standardized data sheets and explains their use.

Appendices A and B presents common notation required for some of the models. Appendix C presents the basic equations of motion of representative mathematical models in current use. Appendix D provides a blank copy of the standardized data sheet and Appendices E, F, and G show examples of completed data sheets.

TABLE 1-1 Typical Computer Printout for a Predicted Turning Maneuver

TIME	DELDEG	PSIDEG	XP	YP	PSIDOT	V KT	U KT
0.000E+00	0.000E+00	0.000E+00	0.000E+00	0.000E+00	0.000E+00	0.000E+00	1.500E+01
2.002E+01	-3.500E+01	7.159E+00	0.449E-03	0.731E-01	9.798E-01	-9.349E-01	1.449E+01
4.004E+01	-3.500E+01	3.849E+01	1.776E-01	1.661E+00	1.182E+00	-1.931E+00	1.281E+01
6.006E+01	-3.500E+01	5.256E+01	5.565E-01	2.208E+00	1.859E+00	-2.839E+00	1.119E+01
8.008E+01	-3.500E+01	7.343E+01	1.055E+00	2.642E+00	9.948E-01	-1.947E+00	9.993E+00
1.001E+02	-3.500E+01	9.259E+01	1.595E+00	2.818E+00	9.547E-01	-1.831E+00	9.142E+00
1.201E+02	-3.500E+01	1.117E+02	2.122E+00	2.889E+00	9.278E-01	-1.731E+00	8.552E+00
1.401E+02	-3.500E+01	1.318E+02	2.591E+00	2.944E+00	9.079E-01	-1.652E+00	8.149E+00
1.601E+02	-3.500E+01	1.488E+02	2.960E+00	2.952E+00	8.951E-01	-1.594E+00	7.876E+00
1.800E+02	-3.500E+01	1.659E+02	3.231E+00	1.969E+00	8.868E-01	-1.551E+00	7.692E+00
2.000E+02	-3.500E+01	1.829E+02	3.361E+00	1.532E+00	8.814E-01	-1.521E+00	7.569E+00
2.200E+02	-3.500E+01	2.011E+02	3.393E+00	1.084E+00	8.788E-01	-1.501E+00	7.487E+00
2.400E+02	-3.500E+01	2.187E+02	3.211E+00	6.419E-01	8.788E-01	-1.486E+00	7.432E+00
2.600E+02	-3.500E+01	2.362E+02	2.969E+00	3.048E-01	8.744E-01	-1.477E+00	7.396E+00
2.800E+02	-3.500E+01	2.516E+02	2.594E+00	4.489E-02	8.735E-01	-1.470E+00	7.372E+00
3.000E+02	-3.500E+01	2.711E+02	2.178E+00	-0.750E-02	8.729E-01	-1.466E+00	7.356E+00
3.200E+02	-3.500E+01	2.886E+02	1.768E+00	-1.879E-01	8.726E-01	-1.463E+00	7.346E+00
3.400E+02	-3.500E+01	3.060E+02	1.319E+00	1.371E-02	8.723E-01	-1.461E+00	7.339E+00
3.600E+02	-3.500E+01	3.235E+02	9.543E-01	2.597E-01	8.722E-01	-1.459E+00	7.334E+00
3.800E+02	-3.500E+01	3.409E+02	6.798E-01	5.958E-01	8.721E-01	-1.459E+00	7.331E+00

Time	Rudder Angle	Heading Angle	Lateral Distance	Longitudinal Distance	Rate of Swing	Side Slip Speed	Longitudinal Speed
sec.	deg.	deg.	$y' = y/L$	$x' = x_0/L$	deg/sec	knot	knot

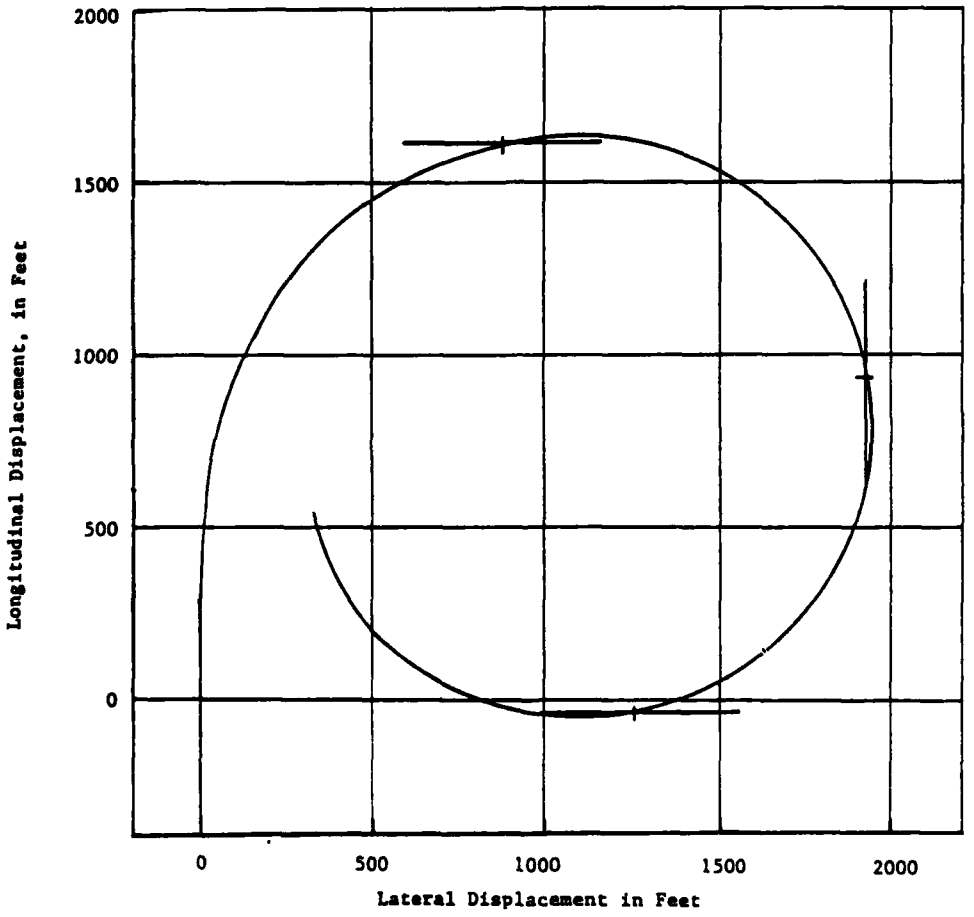

Figure 1-1 Graphical Presentation of Turning Maneuver Corresponding to Data in Table 1-1

2.0 THE NEED FOR MATHEMATICAL MANEUVERING MODELS

The need for reliable mathematical models which can be used to perform a variety of studies associated with ship maneuverability has been long understood by specialists in the field. However, it has been only within the last 15 to 20 years that such mathematical models have become available. This is due to the relatively recent developments in modern experimental and analytical techniques described in subsequent sections of this manual.

Currently, mathematical maneuvering models are used in a variety of situations for many different purposes. Undoubtedly, the applications will become expanded as more good maneuvering model data become available. Typical needs and uses are discussed in the following paragraphs under the following three categories:

a. Ship Maneuverability Analysis

b. Training and Research Simulators

c. Shipboard Maneuvering Predictors

2.1 SHIP MANEUVERABILITY ANALYSIS

Ship maneuverability analysis, involving the use of mathematical models, can play an important role in the design of the ship itself (including subsystems); the design and improvement of the waterways and port facilities in which the ship must operate; and the simulation of casualties and establishment of safety regulations imposed by regulatory authorities. These applications, though closely interrelated, are discussed separately in the following subsections.

2.1.1 Ship Design

Ship design is an area where maneuverability has long been a concern. Historically, the first opportunity that a naval architect had to evaluate a design from the standpoint of maneuverability was on the basis of free-running model tests. These were performed on most new naval ship designs but were seldom conducted for new merchant ship designs. The data were useful to the extent that they provided a direct measure of overall open-loop characteristics such as turning circles and (rudder fixed) directional stability. They provided little guidance to the separate effects of proposed changes in the design of hull, rudder, and other appendages.

The present trend in the ship design process is toward the use of mathematical models to achieve desired ship maneuverability characteristics. This approach permits determination of the effect of items such as rudder size, rudder deflection rate, and hull shape necessary for good maneuverability characteristics, in the early design stage. Moreover, it enables early evaluation of other control system requirements such as those used in the design of the ship's autopilot.

There have been few specific requirements for manuevering performance of merchant ships. Naval vessels, however, often have had very stringent requirements set on performance, requiring a great deal of analysis to ensure meeting the specified standards. The high degree of maneuverability of a cruiser which was recently added to the U.S. Fleet is depicted in Figure 2-1. In the future, the design naval architect will have an increasing need to ensure designs with good maneuverability for both merchant and naval vessels. Vessel trajectory predictions in the very early stages of design will be needed and probably done by the naval architectural firm itself. Later, model tests an studies by maneuvering specialists will be needed as the vessel design progresses. The naval architect will have a basic understanding of what can be done with maneuvering prediction analyses but will have little time to study the field in depth.

The standardized data sheets will make mathematical models and other hydrodynamic data for representative ship types more easily usable to the design naval architect. This can provide a major step toward fulfilling his early design needs in the maneuvering area. As additional data sheets

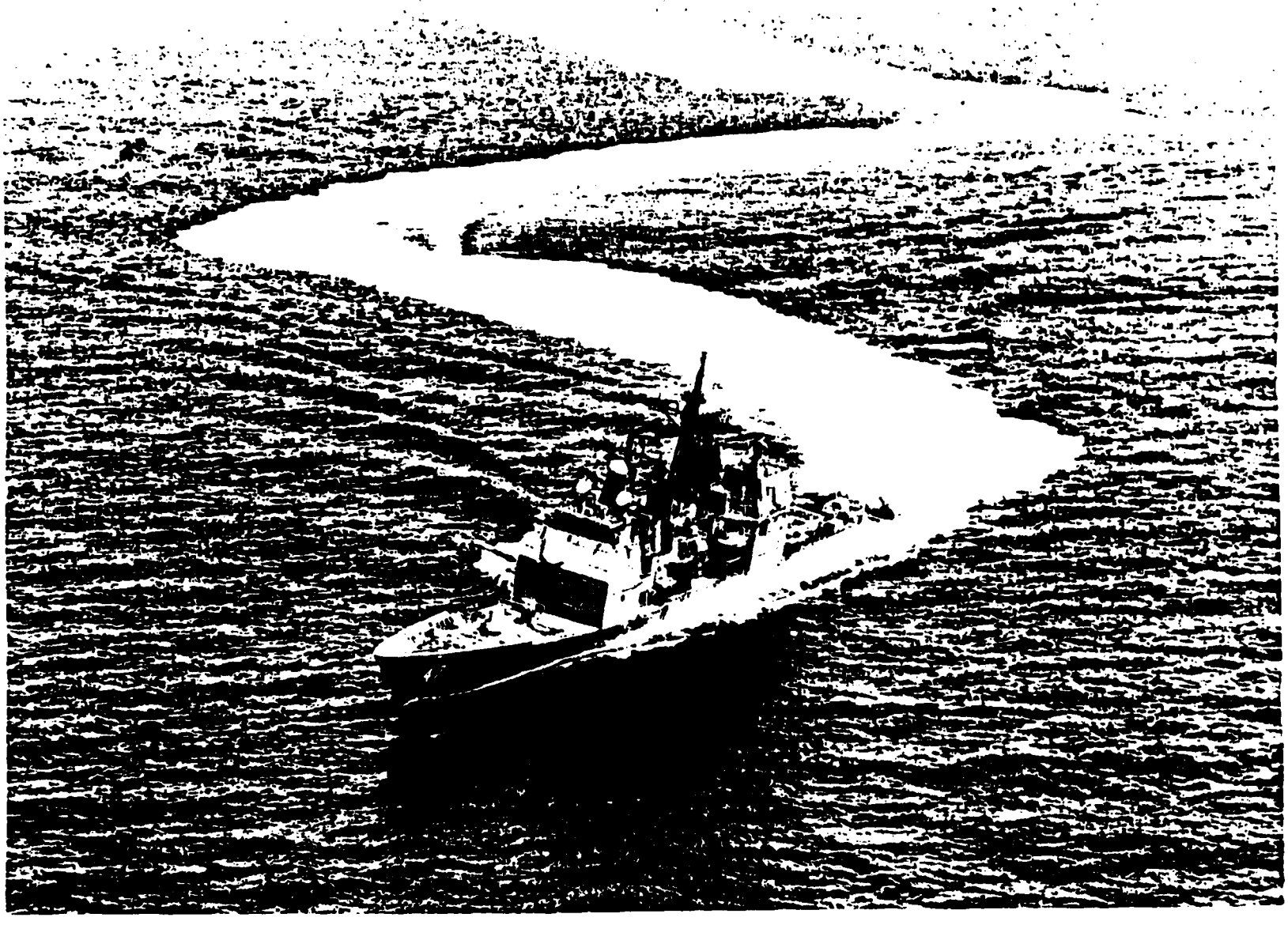

Figure 2-1 The U.S. Navy's AEGIS Cruiser (CG 47) Maneuvering Sharply During Trials

covering a wider range of ship proportions are accumulated, they will combine to form a data base which should be of considerable usefulness in the Preliminary Design stage.

2.1.2 Waterway Improvement and Port Facilities

Recently, ship owners, port authorities, and regulatory bodies have become involved with the use of mathematical models in planning the design of port facilities and waterway improvements for increased safety. A ship owner, for instance, may question the ability of a ship to navigate safely into a harbor or may want to determine what the limiting characteristics are for safe control. In order to use a facility, he may also need to demonstrate the ability of his ships to perform a maneuver in a particular port/waterway situation.

A port authority may similarly question the suitability of a waterway to handle future anticipated ship traffic. In planning improvements he may utilize mathematical models to project the impact of that traffic on safety in the waterway.

A regulatory body also must determine the conditions under which vessels will be allowed to transit waterways. Various conditions of weather, tide, current, visibility, and traffic can be tried on a simulator incorporating mathematical models. The effects on safety can thus be studied.

The design and improvement of canals requires that critical tradeoffs be made between the large costs involved in excavation and considerations of efficient and safe handling of ships in transit. The problem is particularly acute in the case of the modern large bulk carriers. In the past, canal cross sectional dimensions were determined principally on basis of steady state criteria. The existence of mathematical models now offers the potential for such determinations to be made more precisely on the basis of dynamic situations involving representative vessels either singly or in combination. Furthermore, such mathematical models can be used in conjunction with simulators as an assist to training of canal pilots.

2.1.3 Safety Regulations and Casualty Studies

Regulatory authorities are turning more frequently to analytical maneuverability analysis to establish safety regulations governing ship traffic. Mathematical models exercised on high-speed computers provide a very effective tool to quickly review the "rules of the road" under numerous situations of traffic and ship encounters. Study results can be later refined by real-time simulator studies taking human responses into account.

The same techniques can be used to determine the consequences, the best action to be taken, and the need for backup devices in the event of casualties to machinery or control system components. For example, the effects of casualties such as mechanical failure of the rudder or loss of propulsion can be quickly examined.

The importance of employing mathematical models, which predict ship motions correctly in those studies which are relied on by regulatory agencies, can be readily appreciated.

2.2 TRAINING AND RESEARCH SIMULATORS

A number of ship maneuvering simulators have been developed in recent years. They are used in training of shipboard personnel or for conducting research applicable to a wide variety of problems facing the shipbuilding industry and regulatory authorities. The heart of nearly all modern ship maneuvering simulators is the mathematical model. Consequently, their efficiency in training and the scope of problems they can investigate depend to a large extent on the accuracy and realism achieved, and on the range of maneuvers, environmental factors, and types of waterways that can be represented by available mathematical models. Most existing simulators can be readily reprogrammed to represent the maneuvers of ships of various designs and proportions. This again stresses the need for using the standardized data sheets as a means for making more mathematical maneuvering models available.

Modern training simulators have reached a fairly high degree of sophistication. In addition to mathematically modeling trajectories, they often achieve a high degree of realism by reproducing the entire ship's bridge. Visual displays may also be of a very high quality with changing scenery as seen from the bridge of the moving ship. The latter is achieved either by use of television cameras or by means of computer generated pictorial displays. Although such training simulators are very expensive, the value of today's ships and cargoes, as well as the potential danger of pollution that could result from collision or grounding has made computer simulator training of ship's officers a common event.

AD-A144 227 PROCEEDINGS OF THE GENERAL MEETING OF THE AMERICAN TOWING TANK CONFERENCE.. (U) STEVENS INST OF TECH HOBOKEN NJ DAVIDSON LAB D SAVITSKY ET AL. AUG 83 SIT-DL-TR-13029-VOL-2 N00167-83-M-4062 F/G 20/4 NL

UNCLASSIFIED

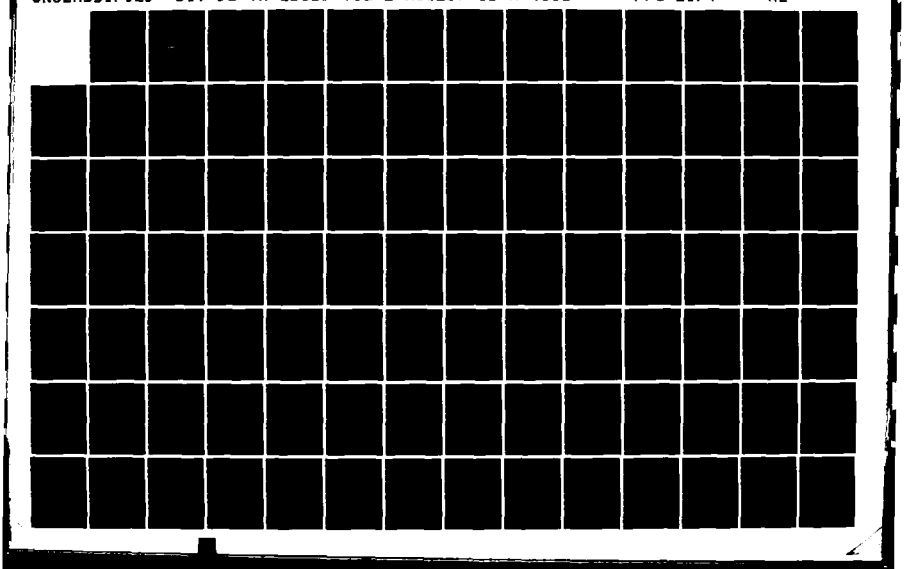

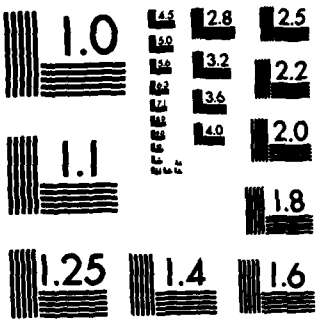

MICROCOPY RESOLUTION TEST CHART
NATIONAL BUREAU OF STANDARDS-1963-A

Research simulators range from the relatively simple to the highly complex depending upon the types of problems to be investigated. For example, the Maritime Administration Computer Aided Operations Research Facility (CAORF) contains all of the features of the most sophisticated training simulator including the realistic bridge and visual representations. In addition, it has a host of other ancillary equipment needed to make and document statistical studies. The layout of this facility is depicted in Figure 2-2. At the other extreme, a research simulator can consist simply of the computer elements necessary to make either open-loop trajectory studies or those involving the use of automatic course-keeping or coursechanging controls.

2.3 SHIPBOARD MANEUVERING PREDICTORS

Automatic Radar Plotting Aids (ARPA) or Collision Avoidance Radar Systems (CAS) are being utilized aboard an increasing number of vessels. Interest and utility has spurred the development of "shipboard maneuvering predictors". These devices utilize a fare more sophisticated mathematical predictor than the CAS. They promise to provide assistance to the navigator in making turns and otherwise planning the trajectory of the vessel so that mishaps do not occur. The predictor also doubles as an onboard training tool that is more akin to a computer game for entertainment.

The mathematical model data contained in the standardized data sheets are directly applicable to the development of shipboard maneuvering predictors. Obviously, the quality of the predictor will improve as such data become available for ship types or designs which more nearly approximate the ship on which it is installed. It should be noted, in this respect, that the maneuvering characteristics of a given ship in deep water differ considerably from those in shallow water or from those in confined waterways where bank suction and traffic interaction influences are strong. The predictor must take this difference into account, particularly in those situations where ships tend to operate in close quarters with each other. This further emphasizes the need for making reliable mathematical model data available for the shallow-water case on future standardized data sheets.

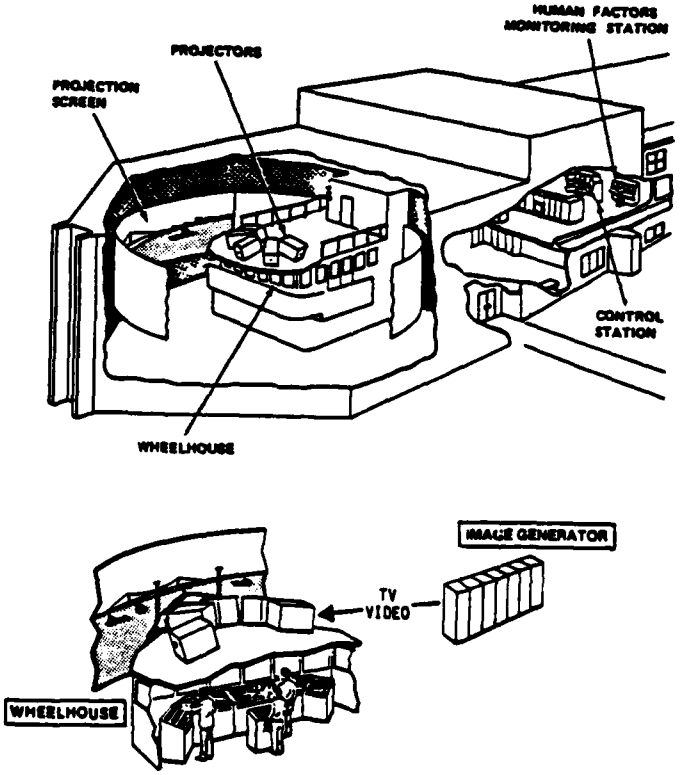

Figure 2-2 Depiction of the CAORF Simulation Facility

3.0 PRINCIPLES OF MATHEMATICAL MODELING OF SHIP MANEUVERS

The purpose of this section is to provide an overview and some insight into the fundamental principles which govern mathematical modeling of ship maneuvers, without the technical detail that is of interest to the expert. The emphasis is placed on the information and data needed to develop the kind of mathematical models which are generally in demand.

The advent of modern high-speed computers has rapidly advanced the state of the art in mathematical modeling techniques covering a wide range of applications in many scientific fields extending from space technology to medical research. The term mathematical models, for those unfamiliar with the concepts, is generally applied to a case where a mathematical expression is taken to represent the characteristics or actions of given real-world physical counterpart. The mathematical expression employed is usually based on some fundamental law or theory, although fairly arbitrary expressions have been used occasionally in some problem areas. It should be observed that a mathematical model may be fairly simple and represent only a single individual component or it may become highly complex and describe an entire system consisting of many component parts.

The role of mathematical models in the field of surface ship maneuverability can best be understood by reference to the block or flow diagrams in Figures 3-1 and 3-2. Figure 3-1 depicts the different approaches currently being used to solve a variety of problems concerned with the maneuverability of surface ships. The most direct approach from the standpoint of acquiring trajectory data is by means of maneuvering trials with the actual full-scale ship. As a practical matter, however, specially instrumented maneuvering trials of the type required to produce data for detailed analyses are extremely expensive and difficult to conduct, and are therefore rarely performed for commercial ships. Furthermore, the data obtained from even these trials, in a strict sense, are limited to the specific ship system being evaluated. Nevertheless, it is important to conduct such extensive full-scale trials, at least on several different representative ship types, to fully validate and establish the confidence level in the various alternative prediction techniques being used.

Two alternative predictive methods for obtaining ship trajectory data are shown by Figure 3-1. The one which utilizes mathematical models (with inputs derived principally from captive-model tests) in conjunction with computer simulation is of primary interest because of its versatility and importance to the development of real-time shiphandling simulators (see Section 2.0). The free-running model approach which produces trajectory data directly is not discussed any further in this manual except to the extent that the data are used to validate or provide inputs to the mathematical model. This application, along with other experimental and analytical methods for providing inputs to the mathematical model, is discussed in Section 4.0.

Figure 3-2 schematically shows the physical components involved in a typical ship maneuvering system. For purposes of illustration, the overall system is considered to be subdivided into two main parts: one called "external dynamics" which deals with responses due to hydrodynamic and other forces applied externally to the ship's hull; and the other called "internal dynamics" which deals with the responses of the helmsman rudder machinery or actuator system, main propulsion machinery system, and instrumentation including sensors, indicators, and displays.

Ship maneuvers based on consideration of the external dynamics alone can be defined as "open-loop" maneuvers or responses. Such maneuvers are typified by definitive maneuvers such as the spirals, zigzags, and steady turns described in Section 6.0. Those maneuvers which involve an interplay between the internal and external dynamics are known as "closed-loop" maneuvers. These maneuvers are typified by coursekeeping or coursechanging maneuvers which require continuous activated control action to overcome the effects of environmental disturbances or directional instability.

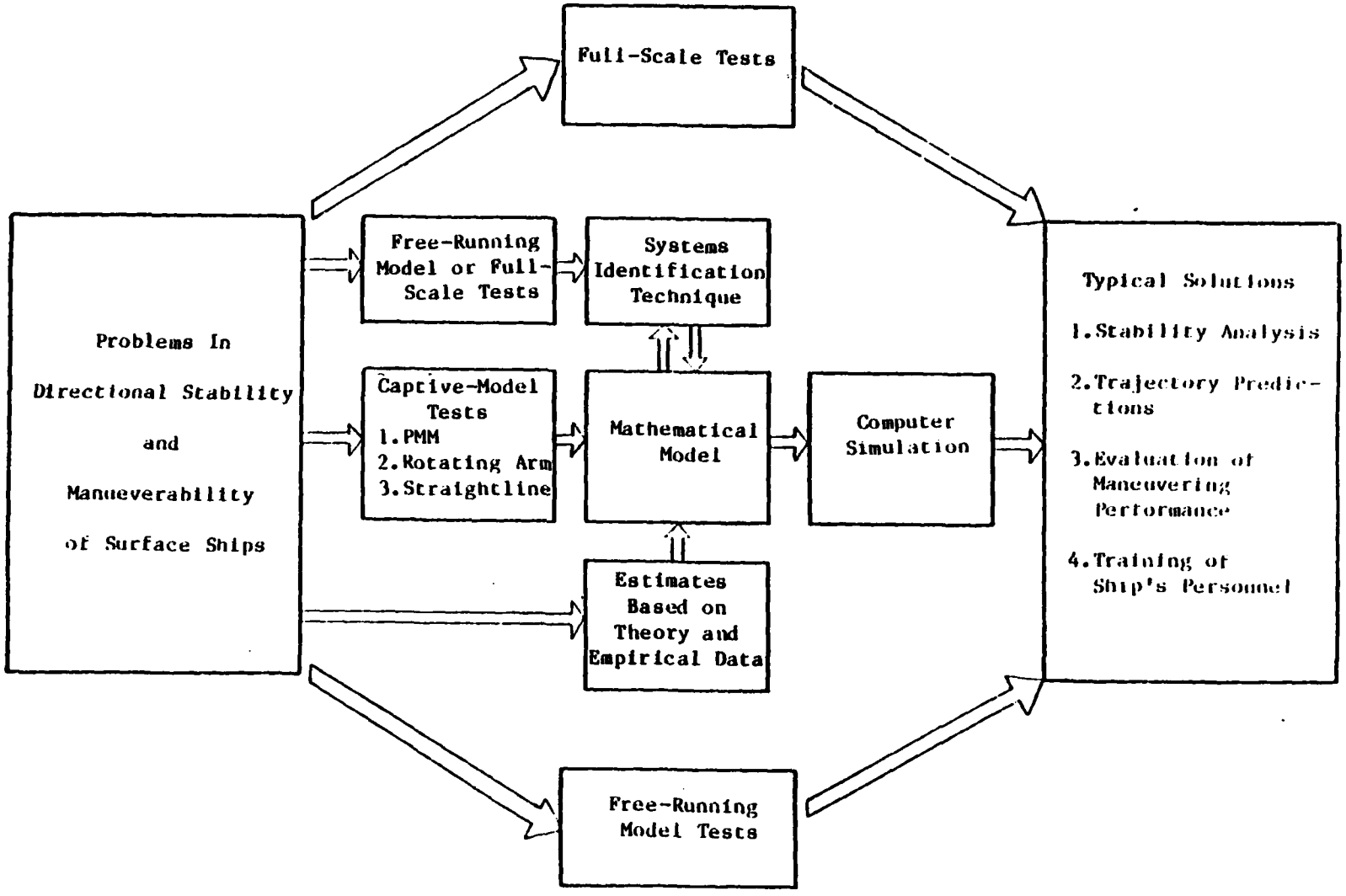

Figure 3-1 Alternative Approaches to Solutions of Surface-Ship Directional Stability and Maneuverability Problems

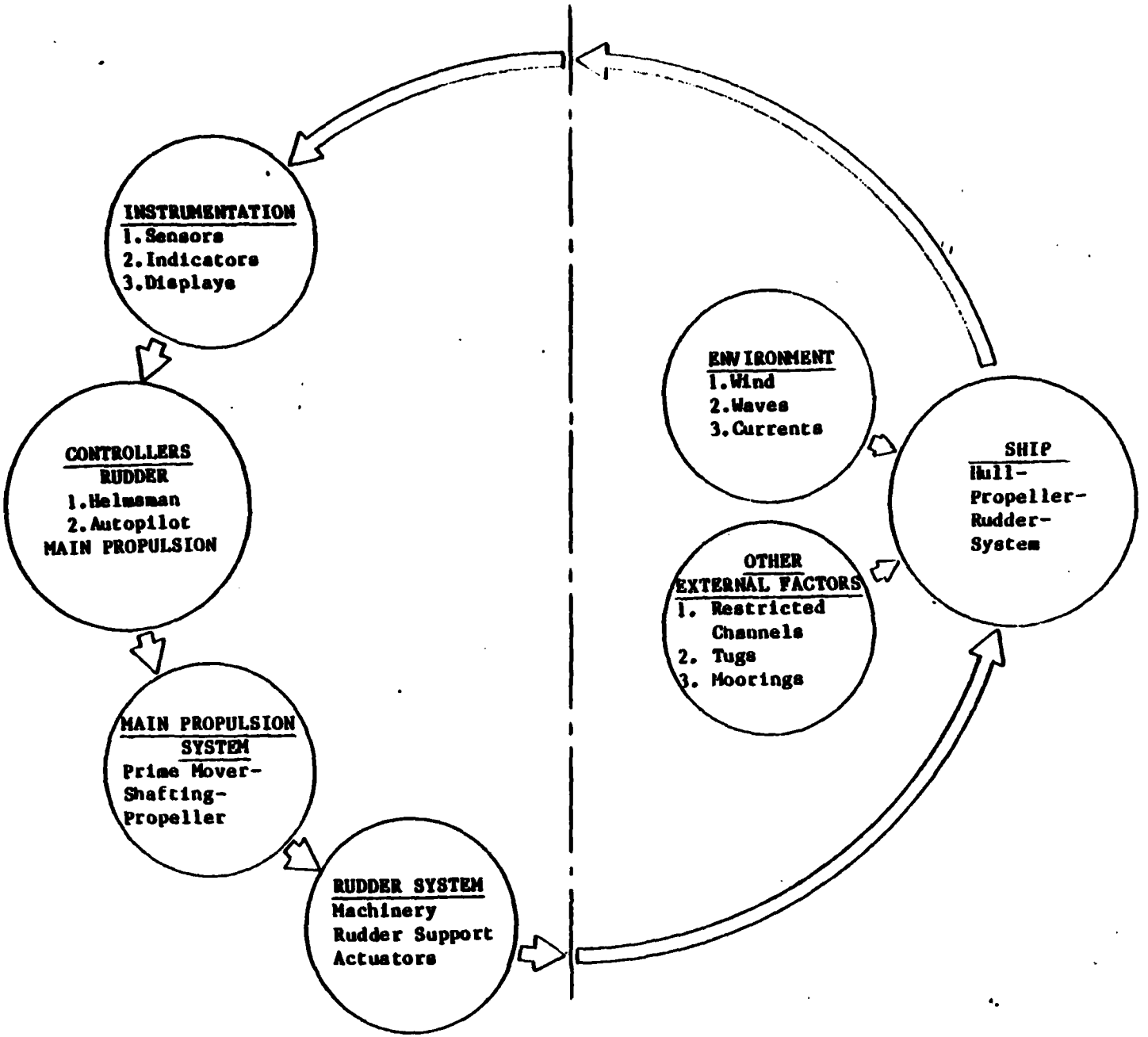

Figure 3-2 Schematic of Typical Ship Maneuvering System

In general, all of the components of both parts of the system shown by Figure 3-2, with possible exception of the human operator, are being represented by mathematical models. Some research facilities have even made several studies in an attempt to mathmatically represent human operator responses.

Primary emphasis in this manual will be on the "basic" mathematical model, related to external ship dynamics, needed to obtain computed trajectories of ship maneuvers in response to various control and other inputs. It should be understood, however, that auxiliary mathematical models representing internal dynamics associated with autopilot, control linkages, and propulsion machinery are also very important, particularly for closed-loop maneuvering studies which are the mainstay of most training and research simulators. Accordingly, provision is made on the standardized data sheets for including the various auxiliary types of mathematical models.

The basic model can consist of any mathematical expression whose terms are numerically adjusted to represent various types of maneuvers of a given ship. Some of the earliest mathematical models consisted of transfer functions derived from backfits to trajectories of specific manuevers obtained either from free-running model tests or full-scale ship trials. However, most modern mathematical models utilize various sets of equations, all of which are based on Newton's laws of motion. This more fundamental approach provides much greater versatility in that it allows prediction of a wide variety of maneuvers of a given ship from a prescribed set of equations of motion along with a fixed set of numerically evaluated coefficients. Furthermore, such mathematical models can be readily changed from representing the maneuvers of one ship design to those of another merely by substituting a new set of coefficient values.

3.1 EQUATIONS OF MOTION

Most modern mathematical-maneuvering models are based on the Newtonian law of motion: force equals mass times acceleration. The various quasi steady-state equations of motion derived from this law have been used successfully to solve diverse problems in the field of rigid body mechanics ranging in complexity from studies of passive motions of freely falling bodies to actively controlled maneuvers of aircraft, submarines, and surface ships.

The purpose of this section is to briefly discuss the principles and nature of the equations of motion as currently applied to surface ship maneuvering studies with emphasis on those feature pertinent to the SNAME Standardized Data Sheets. For those who are interested in more detailed treatment, mathematical derivations and solutions of the general equations of motion for marine vehicles can be found in References 1, 2, and 3. These include the cases of submarines (6 degrees of freedom) and surface ships (3 or 4 degrees of freedom).

The motions of primary interest for steering and maneuvering surface ships take place in the horizontal plane. Vertical plane motions such as pitching, heaving, and rolling can usually be neglected. In the interest of simplification, the following discussion is limited to equations involving only 3 degrees of freedom: surge, sway, and yaw. Such equations are typical of those used for slow and intermediate speed merchant ship types such as tankers and cargo ships. For high-speed ship types, it may be advisable to add the fourth degree of freedom or roll equation, since a relatively large roll could interact to influence horizontal plane trajectories, even in calm water maneuvers.

Before proceeding with the discussion in this section, the reader should become familiar with the standard notation of Appendix A which presents symbols and definitions for all of the quantities involved in the equations of motion. Some of the general features of the SNAME system, which will become apparent upon examination of Appendix A, are as follows:

a. "Dot" Notation

A dot above the symbol for a quantity such as the linear velocity components u or v signifies the first derivative of that quantity with respect to time. Thus, u and v become linear acceleration components. Similarly, a double dot above the symbol denotes the second derivative of the quantity with respect to time. For example, for the heading angle ψ, $\dot{\psi} = r$, the angular velocity component about the z axis; and $\ddot{\psi} = \dot{r}$, the angular acceleration component about the z axis.

b. Functional Derivatives

Subscripts are used in the hydrodynamic or other coefficients involved in the equations to indicate the functional relationships between the quantities (such as forces) and various parameters (such as velocities). For example,

Y_v denotes the first order coefficient (or derivative) used to represent the variation of the hydrodynamic lateral force component Y with the linear velocity component v, or $\frac{\partial Y}{\partial v}$.

c. Prime Notation

Prime notation is used to indicate that a given quantity is nondimensional in accordance with the standard SNAME system which is based on mass density (ρ), length (L), and velocity (U). For example, Y'_v denotes the nondimensional equivalent of Y_v, where

$$Y'_v = \frac{Y_v}{1/2\rho L^2 U}.$$

A right hand orthogonal system of reference axes, which are fixed in and move with the body, is the usual practice for most hydrodynamic applications, such as ship maneuvering, which involve motions in the time domain. The standard system adopted by SNAME, along with the sign conventions indicating positive direction of path, angles, velocities, forces, and moments for the 3-degree of freedom case, is shown by the sketch at the end of Appendix A. Normally, the origin of this system is taken at the ship's center of gravity. This has the advantage of either eliminating or simplifying some of the terms in the equations. The advantage is particularly true for the case of large displacement ships where there may be little or no shift in center of gravity from that for the initial loading condition over an extended period of time. On the other hand, some investigators have elected to locate the origin of the axis system at midships, presumably on the bases that both the hydrodynamic and the hydrostatic forces and moments are functions of a ship's geometry, and not on the mass distribution; and that determination of the hydrodynamic forces can be simplified by taking advantage of geometrical symmetries.

For the purposes of the standardized data sheets, it is urged that the center of gravity location for the origin be used wherever possible. This will enable more direct comparison of the mathematical models and individual hydrodynamic coefficient values. To avoid possible confusion on the standardized data sheets, the exact location of the origin should be specified both with respect to the particular set of equations used and to the tables listing the values of the various hydrodynamic coefficients.

Keeping the definitions and conventions in mind, the quasi, steady-state differential equations of motion applicable to surface ship maneuvers can be expressed as:

$$X = m(\dot{u} - rv - x_G r^2)$$
$$Y = m(\dot{v} + ur + x_G \dot{r})$$
$$N = I_z \dot{r} + m x_G(\dot{v} + ur)$$

where:

X is the total hydrodynamic force component directed along the x axis (longitudinal force),

Y is the total hydrodynamic force component directed along the y axis (lateral forces),

N is the total hydrodynamic moment component about the z axis (yawing moment), and x_G is the x coordinate of the center of gravity, equal to zero when the origin is at the ship center of gravity.

For the case of a specific ship maneuvering in a calm seaway of unrestricted depth and width, X, Y, and N, for most practical purposes, can be considered to be functions only of the pertinent motion parameters and rudder deflection, or

$$\left.\begin{matrix} X \\ Y \\ N \end{matrix}\right\} = f(u, v, r, \dot{u}, \dot{v}, \dot{r}, \delta)$$

Thus, the basic set of equations of motion can be given symbolically using these functional relationships as follows:

$$X(u, v, r, \dot{u}, \dot{v}, \dot{r}, \delta) =$$
$$m(\dot{u} - rv - x_G r^2) \qquad (1)$$

$$Y(u, v, r, \dot{u}, \dot{v}, \dot{r}, \delta) =$$
$$m(\dot{v} + ur + x_G \dot{r}) \qquad (2)$$

$$N(u, v, r, \dot{u}, \dot{v}, \dot{r}, \delta) =$$
$$I_z \dot{r} + m x_G(\dot{v} + ur) \qquad (3)$$

The usual practice is to develop the equations of motion involving the functional relationships shown in Equations (1), (2), and (3) in terms of hydrodynamic coefficients of the types described in Section 3.2. The number and kinds of hydrodynamic coefficients involved will vary depending upon whether or not a function is nonlinear as well as upon the kinds of motion for which the resulting equations are intended. Also, the usual practice is to use nondimenisonal hydrodynamic coefficients in the various terms of the equations even though the overall equations are dimensional and are

intended for use in real-time simulators. The reasons and advantages of using nondimensional hydrodynamic coefficients are discussed further in Section 3.2.

In recent years, a number of different formats have evolved for equations of motion written in terms of nondimensional hydrodynamic coefficients. To avoid redundancy or indication of preference, specific equations of motion are not presented in this section. Rather, the reader is referred to Appendix C which presents such equations of the type and format actually being used by practitioners to perform computer simulation studies of ship maneuvers. A brief discussion of some of the general charcteristics that distinguish the various formats is given in the following paragraphs.

Most equations of motion for surface ship maneuvering studies fall into two major categories:

a. General Nonlinear Equations

These are usually written for 3 degrees of freedom (surge, sway, and yaw) and contain numerous coefficients needed to define the higher order and coupling terms. Such equations are sufficiently comprehensive to enable reasonably accurate predictions to be made of trajectories of ships undergoing a complete range of maneuvers including large amplitude zigzags, tight turns, and other maneuvers involving substantial speed changes.

b. Linearized Equations

These are usually written on the assumption that the ship is proceeding at some initial steady straightline speed which remains constant throughout the maneuver. Consequently, the surge equation can be neglected and only the sway and yaw equations (composed of derivatives) are considered. Such equations are used primarily to perform various types of analyses such as those used to determine inherent dynamic stability and control effectiveness, and also closed-loop autopilot characteristics, during the early design stages of a ship system. However, they are frequently used to effectively perform computer simulation studies involving coursekeeping (or other small scale maneuvers) with either the human operator or an automatic control system system as an integral part of the control loop. (See Section 5.0 for a discussion of linearized equations and their uses.)

Models of the first category are most pertinent to the overall objectives of the SNAME Standardized Data Sheet program. Two forms of the general nonlinear equations of motion have received wide usage and achieved a measure of acceptance for computer simulation studies of surface ship maneuvers. The first is based on a Taylor expansion with terms of progressively higher order to represent the nonlinear functional relationships which exist between forces and moments on the one hand and motion parameters on the other. The most common practice in this regard is to eliminate terms higher than the third order (see References 1, 4, and 5). This is because experience has shown that there is no significant improvement in accuracy by inclusion of higher than third order terms. Furthermore, practical measurement techniques as well as the state of the art of present hydrodynamic theory does not appear to justify the increased complexity that would be caused by adding these higher order items. One should note in these third order equations, that only the second order coefficients appear for even functions such as $X(v)$ since the first and third order terms must be zero. For odd functions such as $Y(v)$, the coefficients of the first and third order terms appear in the equations, but the coefficients of the second order terms are zero. It is noted also that functions such as $Y(v)$ also require zero order terms (such as Y_* in Appendix A) for asymmetrical, e.g., single-screw, ships.

The second form of the general nonlinear equations of motion that is widely used involves the so-called "square-absolute" method of coefficient representation (see References 6 and 7). Such equations are patterned after the Standard Equations of Reference 3 which have been used extensively for a number of years to perform simulation studies of submarines undergoing complex maneuvers in 6 degrees of freedom. The surface ship case (3 degrees of freedom) is obtained by deleting the coupling terms due to pitch, heave, and roll motions from the surge, sway, and yaw equations. In the square-absolute form, the nonlinear functional relationships in the equations are represented by obtaining least square fits to the polynomials used which are carried out only up to second order coefficients. In making such fits, absolute values of the appropriate kinematic variables are employed with the coefficients, and this ensures that the proper sign occurs with a given function in the computer

representation (usually for odd functions). It is also used in some cases where a function happens to be asymmetrical.

Presently, there is no overwhelming evidence as to which of the two foregoing forms of the general nonlinear equations of motion is better. Proponents of the third order Taylor expansion approach claim it is mathematically more rigorous and provides better fits to the force and moment data obtained from captive model tests. On the other hand, although the square-absolute method was devised, at least in part, as a convenience for use in simulation studies employing analog computers, some of its proponents claim that it has a better foundation in hydrodynamic theory. This is based on the premise (about which differences in thought exist) that many of the nonlinearities in the lateral force and yawing moment coefficients are related to crossflow drag which tends to be a second order function. In fact, crossflow drag theory has been used successfully to analytically predict some of the nonlinearities in cases where only the first order coefficient was obtained experimentally (for example, in some tests using a small amplitude planar motion mechanism).

Regarding the form of representation used, it is interesting to note that some of the most ardent proponents of the third order Taylor expansion method are now using the square-absolute method, at least to a partial extent, and on a case by case basis. In the final analysis, of course, the major criteria regarding the form of the equations to be used is the goodness of fit with the experimental data over the range of the pertinent variables encountered in the maneuver to be simulated.

It should be mentioned at this point that, even within the same overall format, there are other major differences between the general nonlinear equations of motion used by various establishments. Among the most important of these is the manner in which the hydrodynamic effects due to the actions of main ship propulsion, including effects of propeller slipstream on rudder, are represented for various modes of motion. It is beyond the scope of this section to consider all of these various differences, even as they pertain to the basic mathematical model. However, these differences should become apparent from the presentations and discussions given for the various typical ship maneuvering mathematical models in Appendix C.

For the reasons stated, the preceding discussion has been concerned only with the so-called basic equations of motion which apply to maneuvering in calm water of unrestricted depth and width. In practice, these equations can be expanded to include terms which represent hydrodynamic forces and moments pertinent to maneuvering in shallow water of varying depth, restricted channels, and rough seas; and also nonhydrodynamic forces and moments due to tugs, mooring lines, etc. Such effects can be treated in computer simulation studies either as an integral part of the basic equations or as auxiliary equations and subroutines, as discussed further in Sections 3.2 and 3.3.

3.2 HYDRODYNAMIC COEFFICIENTS

A ship moving through the water is subjected to various hydrodynamic forces and moments which govern its motions and ability to perform certain types of maneuvers. The most effective way of analytically treating these forces and moments in the field of ship maneuverability is through the use of the so-called hydrodynamic coefficients. The purpose of this section is to provide some insight into the nature and variety of the hydrodynamic coefficients that appear on the SNAME Standardized Data Sheets, and simultaneously provide a basis for understanding the techniques required for their numerical evaluation which are given in Section 4.0.

The hydrodynamic coefficients referred to throughout this text are defined as those coefficients (usually nondimensional) which are associated with the various terms of the equations of motion. This is to distinguish them from the nondimensional hydrodynamic forces and moments which are also often called hydrodynamic coefficients. (For example, X' and Y' are called longitudinal and lateral force coefficients, respectively.) Among other advantages, of nondimensionalizing the hydrodynamic coefficients for the equations of motion, it provides a means for presenting a single set of numerical values for any given mathematical model that can be readily used internationally. (For example, see Table III-C of the sample data sheets in the appendices.)

The hydrodynamic coefficients required in the equations of motion of a body moving through a fluid are usually classified into three general categories: static, rotary, and acceleration. The static coefficients are due to the components of linear velocity of the body relative to the fluid; the rotary coefficients are due to the components of angular velocity; and the acceleration coefficients are due to either linear or angular acceleration components.

For very moderate drift angles and turning maneuvers, force coefficients are essentially linear with respect to the appropriate variables, and thus the hydrodynamic coefficients, as defined above, may be utilized as static, rotary, and acceleration derivatives in linearized equations of motion. It may be noted at this point that the acceleration coefficients, commonly known as the "added mass" coefficients or derivatives, can always be considered as being linear. This is in agreement with theory and has been confirmed experimentally over a range beyond the capability of most ships (see Reference 7).

The number and kinds of hydrodynamic coefficients required will vary depending upon the scope of the problem being investigated, the format adopted for the equations of motion, and the extent to which various hydrodynamic effects, are included in the representation. For example, Table III-C of Appendix E presents what is considered to be a complete set of nondimensional coefficient values for basic equations of motion using the "square-absolute" format. The values given apply only to the case of ship maneuvers in water of unrestricted depth and width. Included, however, are coefficients representing variations with propeller effects necessary to accurately predict all ahead maneuvers within the ship capability including tight turns and other maneuvers involving large speed losses. It may be seen that even this calm-deep-water case involves almost 50 nondimensional hydrodynamic coefficients.

For ship systems for which hydrodynamic forces and moments cannot be adequately represented by a third order Taylor series expansion, or a "square-absolute" method, an alternative method of representing these forces is available. Discrete forces and moments obtained from model experiments (usually rotating arm) are recorded in a matrix as discrete functions of static, rotary, and acceleration parameters. As an example, in a five-dimensional matrix of yaw rate, sway veloity, speed, pitch angle, and roll angle, each discrete combination of the five parameters is associated with the six forces and moments which would occur for that condition. For values of the parameters not recorded in the matrix, the forces and moments are obtained by interpolating between known points in the matrix. These calculated forces are then used directly in the equations of motion in lieu of computing them by use of hydrodynamic coefficients.

The discussion up to this point has been concerned mainly with those hydrodynamic coefficients associated with prediction of ship trajectories in open sea. There is, of course, a strong interest in shallow water maneuverability and a concentrated effort is being made to acquire more extensive data which can be used to support mathematical models representing the shallow water case. Experimental techniques developed in recent years should result in better and more abundant hydrodynamic coefficient data applicable to the shallow water case. (For example, see Reference 8.)

There are two general approaches to setting up the mathematical models and processing the hydrodynamic coefficients for the shallow water case. The first approach assumes that the ship is operating in shallow water of constant depth and unrestricted width. Thus, the same set of basic equations of motion having the same number and types of nondimensional coefficients as those of the deep water case can be used, but with a new set of numerical coefficient values representing each constant shallow water depth of interest (see Reference 8). The second approach consists of setting up the mathematics so that it represents the ship maneuvering from deep to shallow water of continuously varying depth. This has been accomplished by use of supplementary terms to the basic deep water equations which reflect the incremented changes to the basic coefficient values as functions of shallow water depth.

Supplementary terms are included only for those coefficients which are considered to be significantly affected by shallow water depth. The methods used to develop the nondimensional hydrodynamic coefficients for shallow water effects are explained in Reference 9. Typical applications of this approach are given in Reference 10 and in Standardized Data Sheet Tables III-A and III-C of Appendix F. The second approach to representing shallow water maneuvers is more complex than the first and involves a number of additional types of coefficients.

For the case of ships moving through restricted channels or canals, it is necessary to include hydrodynamic coefficients to represent displacement of the ship from the channel centerline and proximity to the wall or bank. Even with the assumption of constant water depth, representation of restricted channel effects, if treated separately, would add a considerable number of hydrodynamic coefficients to the basic mathematical model. On the other hand, due to the small scale maneuvers normally performed in a channel or canal, many of the nonlinear coefficients in the basic equations of motion may become less significant and can possibly be omitted (see References 11 and 12).

One of the original goals sought for the SNAME Standardized Data Sheets was to achieve some measure of uniformity in mathematical modeling, at least in method of data presentation. Although some progress has been made in this respect, efforts should continue toward achieving this goal as usage of the data sheets becomes more prevalent. In the case of the hydrodynamic coefficients, it is urged that, to the extent possible, all contributors use the same methods of nondimensionalization and notation, as well as the same origin for the principal axes, namely at the ship center of gravity, as are given in Appendix A. The advantages of uniformity are great. Even though coefficient types may differ according to equation format used, there will always be some nondimensional coefficient types whose numerical values can be directly compared. This is especially true for the coefficients (or derivatives) of the types listed in Table IV-A of the Standardized Data Sheets.

The "Bis" systems is an alternative method of nondimensionalizing the hydrodynamic coefficients, and is used for the sample data sheet in Appendix F. In this system, the coefficients are made nondimensional by use of units of mass m, length L, and acceleration of gravity g in lieu of mass density ρ, length L, and linear velocity U used in the standard SNAME system. The "Bis" system concept is developed, and reasons for its use are explained, in Reference 9. Proponents of the "Bis" system involved in computer simulation feel that it has merit, particularly for use in simulating near-zero speed maneuvers where inertial characteristics predominantly influence the motions.

To accommodate the use of the "Bis" system, a supplementary notation which individually defines each of the nondimensional hydrodynamic coefficients and other quantities involved is given in Appendix B. Also, a provision has been made in Table IV-A of Appendix F for comparing some numerical values for the hydrodynamic derivatives of the "Bis" system with those of the SNAME system.

3.3 OTHER INPUTS

Input data in addition to the numerical values of the nondimensional coefficients must be provided to complete the model before its use in real-time simulators. Pertinent geometrical characteristics of the full-scale ship are required such as length, displacement, location of ship center of gravity, and moments of inertia or radii of gyration. Also, certain supplementary mathematical models or subroutines are required to perform a complete maneuvering simulation.

Typical subroutines used in simulation of ship maneuvers are as follows:

a. Time history of rudder movement in degrees including the scenarios required for the conduct of various definitive maneuvers.

b. Time history of change in propeller RPM from full ahead to full astern including appropriate lags due to communication, human reaction, and prime mover response.

c. Autopilot equations for coursekeeping and coursechanging including numerical values of the sensitivities when simulating an existing system.

The time histories of rudder movement can be constructed based on an average rudder deflection rate or by fitting the rudder traces recorded during maneuvers of a representative full scale ship. A more sophisticated method, if required, would actually mathematically model the dynamics of the rudder machinery and actuator system indicated in Figure 3-2.

The time histories of change of propeller RPM are usually obtained from fits of data recorded on a representative full-scale ship during the course of acceleration and deceleration trials. These fits are usually linearized and certain assumptions are made concerning the lags. Sophisticated representations of RPM time histories are often made through the use of mathematical models of the dynamics of the propulsion machinery-shafting-propeller system (see Figure 3-2). An example of such a mathematical model is given in Tables III-B and III-C of Appendix F.

For simulations which go beyond the case of maneuvering in calm deep water, it is necessary to provide additional mathematical models or subroutines. Typical of these are:

a. Supplementary mathematical models representing variation of the static, rotary, and acceleration coefficients with shallow water depth (see Section 3.2).

b. Forcing functions due to wind and waves.

c. Forcing functions due to asymmetrical forces and moments due to proximity to a bank in a canal, or channel, or due to proximity to another passing or overtaking ship in parallel.

d. Forcing functions due to tugs or mooring lines.

All of the above types of input data are pertinent to the standardized data sheets and should be furnished whenever they are available.

4.0 DETERMINATION OF HYDRODYNAMIC COEFFICIENTS

The purpose of this section is to introduce the reader to various methodologies currently in use for obtaining numerical values for the hydrodynamic coefficients discussed in Section 3.0. No attempt is made to describe the detailed analyses by which the values of the coefficients are obtained by experimental or theoretical processes. Those readers with further interest can find ample treatment of the subject in the literature.

4.1 COEFFICIENT DETERMINATION BY EXPERIMENTS

The determination of the coefficients by experimental methods generally is accomplished by using a model of the ship. In principle, the model can be either captive (constrained) or free running. In the latter case, the "model" can actually by the full-scale ship. It is probably safe to assert that nearly all of the coefficients which have been determined and used up to this time have been obtained by the use of captive models, although a considerable amount of effort is being devoted to developing processes of coefficient determination by use of free running models or ships.

In the case of the captive model, the model is attached to a towing device (carriage) through a system of gages which measure the forces and moments which are required to impose various states of motion on the model by the towing device. In general, the motions may be in a straight line, in a circular path, or oscillatory, both in translation and heading. The measured forces and moments are equal (except for known inertia forces) to the hydrodynamic forces and moments which act on the model during the forced motions. Thus, this process provides a direct determination of the functional relationships between hydrodynamic forces and motion variables, and is particularly useful (in contrast with the free-running model) in that it can provide insight concerning the physical processes which relate geometry, motion variables, and hydrodynamic forces.

4.1.1 Planar Motion Mechanism Tests

The Planar Motion Mechanism (PMM) system is a device for performing captive model tests, both static (steady state) and dynamic. The use of the word "planar" denotes that the forced motions of the model occur in a plane which can be taken to be the plane defined by the undisturbed free water surface. Figure 4-1 depicts the three distinct modes of motion which can be imparted to the model by the PMM.

Steady State ("Static")

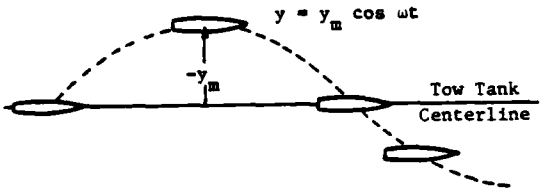

Pure Sway Oscillation

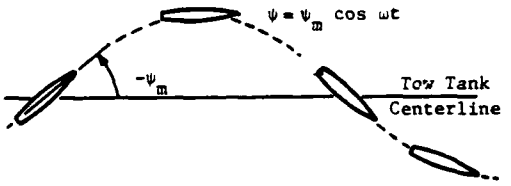

Pure Yaw Oscillation

Figure 4-1 Three Test Modes of a PMM

In the static tests, the towed model is constrained to a straight course, but the tests are carried out for combinations of towing speed, drift angle, rudder angle, and propeller revolutions. For any given combination of these test parameters, the measured forces are constant (thus, the term "static tests"). In actual fact, slight variations in towing speed or propeller revolutions generally prevent the realization of truly constant forces, but this presents no serious problem. In some cases, however, flow instabilities may occur, and this gives rise to relatively large variations in the measured forces.

A unique capability of the PMM is that it can be used for dynamic, as well as static, testing. For the dynamic testing, the PMM is able to force the model to follow a sinusoidal path as it is being towed in the towing tank. The lateral and angular displacements of the model vary harmonically with time, as do the measured forces which are required to impart the sinusoidal motion. By suitable adjustments of the driving mechanism of the PMM, the model can be forced to undergo "pure swaying" motion or "pure yawing" motion. This feature of the PMM enables the separate determination of the hydrodynamic forces and moments due to sway (or drift) velocity v and those due to angular velocity r. The PMM dynamic tests also enable the determination of linear and angular acceleration derivatives.

4.1.2 Rotating Arm Tests

A rotating arm facility, shown in Figure 4-2, is also used for captive model tests and is ideal for measuring steady state forces as functions of the angular velocity r. In this facility, the model is towed in a circular path while attached at a fixed radial location on an arm which rotates about a vertical axis fixed in the tank. When the model is oriented with its centerline normal to the radial towing arm, the model experiences only a rotation velocity r and its longitudinal velocity component is identical to its linear speed. With linear speed maintained constant, as is usually desirable, the only way to vary the magnitude of rotation velocity r is to change the radius of the model attachment point on the arm. Drift velocity v can be changed by changing the drift angle of the model, and the rudder angle can be set at discrete values. Thus, the rotating arm provides information on the cross coupling between r, v, and δ as well as on the effects of r alone. Despite the substantial advantages of a rotating arm, it cannot be used to provide the usual added mass terms (acceleration derivatives).

4.1.3 Special Tests (Shallow Water, Maneuvering Devices, etc.)

It is evident from the presentation of various mathematical models in Appendix C of this primer that it is not feasible to give a general formulation of the mathematical model of a maneuvering ship. For each specific case, the most appropriate formulation of the mathematical model will depend on the circumstances which must be accounted for, and the formulation must allow for the proper representation of the hydrodynamic forces as found from measurements or other means.

Some ships may have single propellers while others may have multiple propellers which can be operated independently; some may have thrusters for maneuvering; many ships must maneuver in both deep water and shallow water; some must sail near banks in canals and must also pass close by other vessels which are underway. In general, it is to be expected that ships will be required to maneuver in wind, current, and waves. Thus, it is evident that a mathematical model which is suitable for representing a given ship in deep, open water may not be suitable for another ship or even for the same ship maneuvering in a harbor.

The experimental determination of the hydrodynamic forces which enter into the special situations which have been referred to is in general very costly. Few, if any, mathematical models of specific ships have been formulated on the basis of experimentally determined information required for the representation of these situations. Maneuvering experiments in shallow water are straightforward in principle, but not all towing tanks are designed and constructed for such experiments. Experiments to measure bank suction and interaction forces between passing vessels require complicated test setups, and the required testing is both extensive and expensive.

For ships with control thrusters, special experiments are sometimes performed to obtain the hydrodynamic information necessary to incorporate the thruster effects in the mathematical model. Scale effects for small models also result in boundary layer differences which must be considered.

To summarize, special tests such as have been discussed are costly, and few are performed for specific ships. It becomes a matter of judgment whether special situations require the investment of funds and time to perform such tests for the enhancement of the mathematical model.

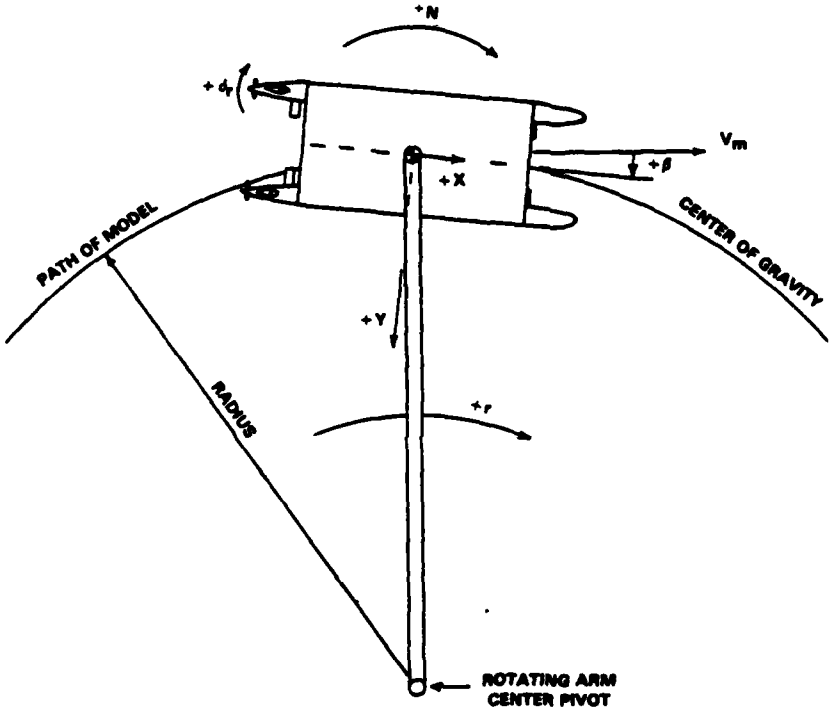

Figure 4-2 Schematic of a Rotating Arm Test Facility

4.1.4 Wind Tunnel Tests

As has been indicated in Section 3.0, wind forces as well as hydrodynamic forces need to be taken into account for some ships. For example, LNG carriers and containerships have large above-water areas which are exposed to the wind, and the wind forces (and moments) can have a very significant effect on the maneuvering of such ships. Their magnitudes depend on the geometry of the exposed area and on the velocity (magnitude and direction) of the wind relative to the ship. The effects of the wind can be accounted for by providing additional terms to the mathematical model.

The determination of the wind forces is best accomplished by means of wind tunnel tests. For this purpose, only the above-water portion of the ship model is required. The model is usually mounted in very close proximity to a large "ground board" which represents the water surface, and force measurements on the model are made for a range of ship headings which would usually embrace the range from zero through 360 degrees. Even in this relatively straightforward test, screens (or grids) should be placed in the flow to enable the simulation of the velocity gradient of the wind between the surface of the water and the uppermost parts of the ship.

4.1.5 System/Parameter Identification Methods

It was indicated earlier that, in principle, the hydrodynamic coefficients could be determined by experiments with a free running model or even from maneuvering trials on an actual ship. The methodology or process by which this is accomplished is termed "parameter identification". It did not have its origin in ship applications, but in recent years substantial efforts have been made to apply the process to ships. One more often encounters the term "system identification" than the term "parameter identification", and some clarification of this specialized terminology may be helpful.

The general idea behind system identification is that if all of the inputs and the associated outputs of, say, a dynamic, physical system are known, then the system can be "identified", i.e., a mathematical model of the system can be established. In the case of a maneuvering ship, for example, if the inputs (rudder actions and other control actions) are known and the ensuing outputs (the ship's motion responses) are known, the equations of motion and the numerical values of the coefficients can be determined. On the other hand, the idea of parameter identification is comparable to that of coefficient determination by use of captive models. The process depends on the measurement of input and output with a very high degree of accuracy, and the acquisition of adequate data is a formidable obstacle to the practicability of the process.

4.2 REDUCTION AND ANALYSIS OF EXPERIMENTAL DATA

Data which is acquired during captive-model experiments consists for the most part of measured hydrodynamic forces and moments as functions of motion parameters and other independent variables (drift/sideslip angle, rudder angle, propeller speed, components of linear and angular velocities and accelerations, etc., and combinations of some of the parameters). Since the objective of the captive-model experiments is to enable evaluation of the performance of the full-scale ship, it is necessary to "reduce" the data to nondimensional form which is applicable to a geometrically similar vessel of any size. The nondimensional quantities which result from the data reduction are the hydrodynamic coefficients which have been discussed in Section 3.2.

Data from free-running experiments with models or ships does not consist of forces and moments, of course. Only input actions and measured motion responses are obtained, and these data must be processes to yield the required coefficients.

4.2.1 Captive-Model Data

The process of nondimensionalizing forces measured during captive-model tests is usually accomplished by dividing the force by the quantity $\rho L^2U^2/2$, where

- ρ is the mass density of water in the towing tank,
- L is the length of the model (or some other characteristics linear dimension), and
- U is the model speed in the towing tank.

The resulting quantity is a nondimensional force, and in general, it is considered to be applicable to a geometrically similar model or ship of any size undergoing a similar test (i.e., same relative draft, trim, rudder angle, motion parameter, etc.). Moments are nondimensionalized in a similar manner. As observed in Section 3.2, the nondimensional quantities obtained by the foregoing process are commonly referred to as force coefficients, and they should be distinguished from the hydrodynamic coefficients which appear in

the equations of motion. An extensive test with a model will result in many plots of nondimensional forces and moments as functions of variables such as drift angle, rudder angle, and nondimensional turning rate. Figure 4-3 is a typical plot of side force as a function of nondimensional sway velocity (or drift angle) based on static tests of a model of a MARINER ship.

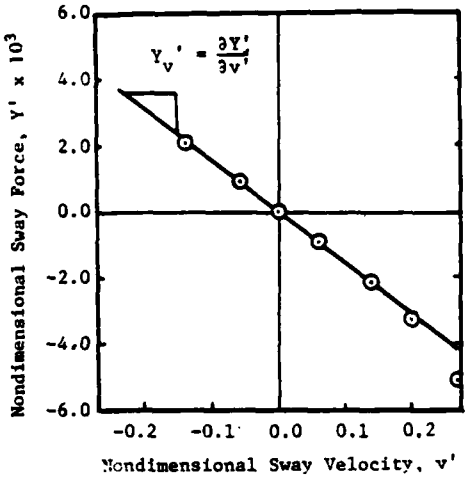

Figure 4-3 Typical Plot of Data from a Static Test, Illustrating Method of Determining the Derivative Y_v'

These plots form the basis for determining the coefficients which appear in the equations. In general, the plots are curves, and curve fitting used to produce the hydrodynamic coefficients which enable the mathematical description of the curves. These coefficients are the ones which appear in the equations of motion, and clearly are not simply nondimensional forces and moments. In some cases (as in linearized equations), the only part of the plot which is of interest can be represented by a straight line, and the slope of the line is termed a "derivative", even though it has every appearance of being a coefficient in the linearized equations.

The foregoing discussion on reduction of captive-model data is intended only to introduce the subject. The details of the process of reduction and analysis of experimental data to provide the many coefficients required in the equations of motion are far beyond the scope of this primer. An extensive treatment of the reduction and analysis of experimental data, particularly as it applies to investigations using the PMM, can be found in the Reference 7.

4.2.2 Free-Running Model Data

The use of free-running model data for the determination of hydrodynamic coefficients depends on the methodology of system/parameter identification. Different investigators have approached parameter identification in different ways and with various degrees of mathematical sophistication. The methodology is still under development, and it does not seem that one can neatly identify a portion of the process as "data reduction" as is the case with data obtained from tests with captive models.

4.3 COEFFICIENT DETERMINATION BY THEORY

Although many highly competent individuals have addressed themselves to the development of theoretical models for determining hydrodynamic coefficients for ships, they have had only limited success. In general, the theoretical developments have been concerned with only the linear terms in the equations of motion, and even for these coefficients (or derivatives), the agreement with experiment is less satisfactory than is desired. The qualitative agreement is reasonable in many cases, but in general, the quantitative agreement is not good enough to encourage the use of theoretically determined coefficients alone in the prediction of ship maneuvers. Of course, the mathematical model contains nonlinear, as well as linear, terms and the determination of nonlinear coefficients by theoretical methods is not within the present state of the art. Nonetheless, where the qualitative agreement between theory and experiment is reasonable, the theoretical methods can be useful in interpolating between isolated bits of experimental data.

Probably the most significant use of theoretical methods is in estimating the effects of shallow and restricted water. Considerable progress in these areas has been made in recent years, and it appears reasonable to use theoretical methods for some situations for which the cost of experiments is prohibitive.

4.4 COEFFICIENT DETERMINATION USING HISTORICAL DATA

A number of ship model basins throughout the world have accumulated a considerable amount of hydrodynamic data over the years as a result of their experiments on specific ship designs and also from experiments where systematic changes to geometric parameters have been made. Such data can be used in attempts to identify empirical relationships between hydrodynamic

coefficients and geometric parameters. For example, one may construct a plot showing a particular coefficient as a function of a selected geometric parameter or a combination of parameters. If a large body of data is available and judicious choices of parameters are made, the data can often be made to "collapse", i.e., the plotted data points will tend to define a unique curve which exhibits the relationship which is being sought. If sufficient data is available, this process can be used to relate many of the coefficients to ship geometry, and the plots serve as a data base for estimating the coefficients for a given ship design whose geometric parameters are within the boundaries of the plots. The process is entirely empirical, and the validity of the coefficients is subject to the limitations of such an approach.

It seems evident that, at best, the empirical approach as described is limited to the case of a ship sailing in deep, unrestricted waters. Even for this case it is not likely that all of the required coefficients can be obtained. However, for some investigations of limited scope it may provide enough coefficients to enable a reasonable computer simulation to be performed.

5.0 ANALYSES BASED ON LINEARIZED EQUATIONS

The equations of motion which have been formulated for use in computing the general motions of ships in maneuvers, and which are the subject matter of Section 3.1, are rather complex. However, not all analytical investigations into maneuvering performance require the use of these equations in their entirety. In particular, investigations of straight-line stability and of relatively moderate turning maneuvers for "straight-line" stable ships can be accomplished satisfactorily with "linearized" equations which are far simpler than those which have been presented in Appendix C. The linearized equations are those in which the hydrodynamic forces and moments are taken to be linear functions of velocity components v and r and control inputs (e.g., rudder angle δ), and in which terms involving the products of motion variables such as vr, the product of lateral velocity and turning rate, are excluded.

5.1 DERIVATIVES

In the linearized equations of motion the coefficients of the various terms are referred to as "derivatives". For example, in the term $Y_v v$, the coefficient Y_v is the slope of the curve which exhibits the relationship between the force component Y and the velocity component v which gives rise to the force. In general, such relationships are not linear over the whole range of values of the variable (e.g., velocity component v). They may, however, be taken to be linear over ranges which are of interest. As has been indicated in Section 4.2.1, captive model experiments result in many plots (curves) of forces and moments as functions of motion variables. The slopes of the curves, taken usually at the points where the motion variables are zero, are the coefficients (derivatives) used in the linearized equations. It is worth noting that when the coefficients for the full nonlinear equations are determined by curve fitting the experimental data, the coefficients of the linear terms in the fits may not agree exactly with the derivatives which are the coefficients of those same terms in the linearized equations. The slopes, which are determined graphically, and which relate only to the portions of the curves which are of interest, are usually taken to be the derivatives for use in the linearized equations.

5.2 INHERENT DIRECTIONAL STABILITY INDICES

It was indicated earlier that one of the uses of linearized equations was in investigations of straight-line stability. Such stability is to be distinguished from "directional" stability which implies that the ship would return to its original heading. However, the term "directional stability" is commonly, but loosely, used to denote straight-line stability. Figure 5-1 depicts graphically the distinction between the two types of stability.

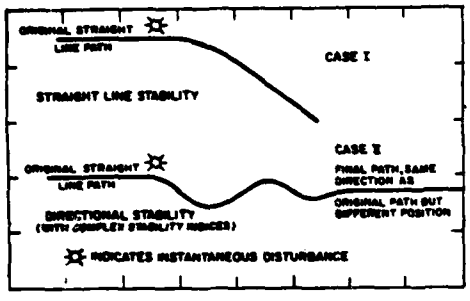

Figure 5-1 Illustration of the Distinction between Straight-Line Stability and Directional Stability

Inherent stability refers to the response of a ship to a distrubance without use of controls, and it is an important consideration in the evaluation of a ship's steering and maneuvering performance.

Since the notion of stability has to do with the ship's response to small, momentary disturbances, it is appropriate to consider that the forward speed remains unchanged, and to examine the ship's response using only the linearized sway and yaw equations. More precisely, these are two simultaneous differential equations of the first order in two unknowns, the horizontal-velocity component v and the yaw angular-velocity component r. (It is usual to work with nondimensional equations in which the nondimensional forms are indicated as

v' and r'.) The solutions for v' and r' take the form:

$$v' = v_2 e^{\sigma_1 t} + v_3 e^{\sigma_2 t}$$

$$r' = r_2 e^{\sigma_1 t} + r_3 e^{\sigma_2 t}$$

In these solutions, v_2, v_3, r_2, and r_3 are constants of integration, σ_1 and σ_2 are the roots of the governing equations (commonly referred to as "stability indexes"), and t is time. It is clear that if both indexes are negative, v' and r' will approach zero as time increases, which is to say that the ship will resume motion in a straight line, and thus it possesses straight-line stability. On the other hand, if either σ_1 or σ_2 is positive, v' and r' will increase with increasing time. The ship is then said to be unstable, and with increasing time it will not end up in a straight line, even with zero rudder angle.

The indexes σ_1 and σ_2 are simple functions of the derivatives and inertial properties of the ship, and their values can be computed readily. Thus, the question of stability can be answered very simply once the derivatives are known.

5.3 CONTROL EFFECTIVENESS PARAMETERS

The usefulness of linearized equations is not limited to investigations of stability. For computing moderate maneuvers of stable ships the side force Y and turning moment N can be taken to be linear functions of v, r, and δ with a reasonable degree of accuracy. Also, the speed change induced by steering is not pronounced, and speed can be assumed to be constant.

Based on a consideration of linearized equations, Nomoto has developed a highly simplified approach to investigations of maneuvering through mathematical modeling (Reference 13). Beginning with the two linearized equations in sway and yaw, Nomoto derives the following simple equation:

$$T\ddot{\Psi} + \dot{\Psi} = K\delta$$

where $\dot{\Psi} = r$, and T and K are determined from the hydrodynamic coefficients and inertial terms which appear in the linearized equations. If a rudder deflection δ_o is suddenly applied at time zero (t = 0), the induced ship motion is:

$$\dot{\Psi} = K\,\delta_o(1 - e^{-t/T})$$

$$\Psi = K\,\delta_o(t - T + Te^{-t/T})$$

As time increases, the yaw rate reaches a final steady value of $K\,\delta_o$, and the response time is governed by the time constant T, faster response time being associated with smaller values of T.

The "K - T" formulation of the equations of motion can also be used to examine course stability. Smaller values of T are associated with quicker decays of disturbed motion and consequently with smaller deviation in course. A negative value of T corresponds to instability on course. In this case yaw rate does not decay with time following a disturbance. Rather it can increase even with zero rudder angle.

K and T are referred to as "steering quality indices". K defines the turning ability; T defines the quickness of response to the rudder, and also is a measure of stability on course. The physical interpretations K and T can be shown to be:

$$K = \frac{\text{turning moment per rudder angle}}{\text{viscous damping per yaw rate}}$$

$\sim$ turning ability

$$T = \frac{\text{inertia of ship}}{\text{viscous damping per yaw rate}}$$

$\sim$ quickness of rudder response

Although the values of K and T can be determined from the inertial terms and the hydrodynamic derivatives which appear in the linearized equations of motion, Nomoto suggests that a more practical way of assessing them is to analyze zig-zag steering tests, whether model or full scale. He presents a table of values of K and T derived from such tests on actual ships, and they cover a fairly wide spectrum of ship types.

A fairly extensive treatment of the use of linearized equations can be found in Reference 14.

6.0 COMPUTER PREDICTION AND SIMULATION OF SHIP MANEUVERING CHARACTERISTICS

This section provides some limited examples of correlations between computer predictions and full-scale trials results, and uses of mathematical ship-trajectory-prediction models.

6.1 CORRELATION OF COMPUTER PREDICTIONS WITH FULL-SCALE TRIAL DATA

The usefulness of computer predictions of ship maneuvers depends on the fidelity of the predicted maneuvers to actual ship maneuvers. The predicted maneuvers are typically used to evaluate ship or harbor design features prior to construction and for ship operator training, as will be discussed in subsequent paragraphs.

A limited number of carefully instrumented ship trials have been performed, which provide the data base for comparison with computer predictions. The trials of the MARINER Class ship USS COMPASS ISLAND, Reference 15, formed the basis of the ITTC Cooperative Captive-Model Test Program, Reference 16. Among the correlation studies performed to duplicate the MARINER ship trials with generally good results are those reported in Reference 4, 7, and 17. Another study of large tanker maneuver-

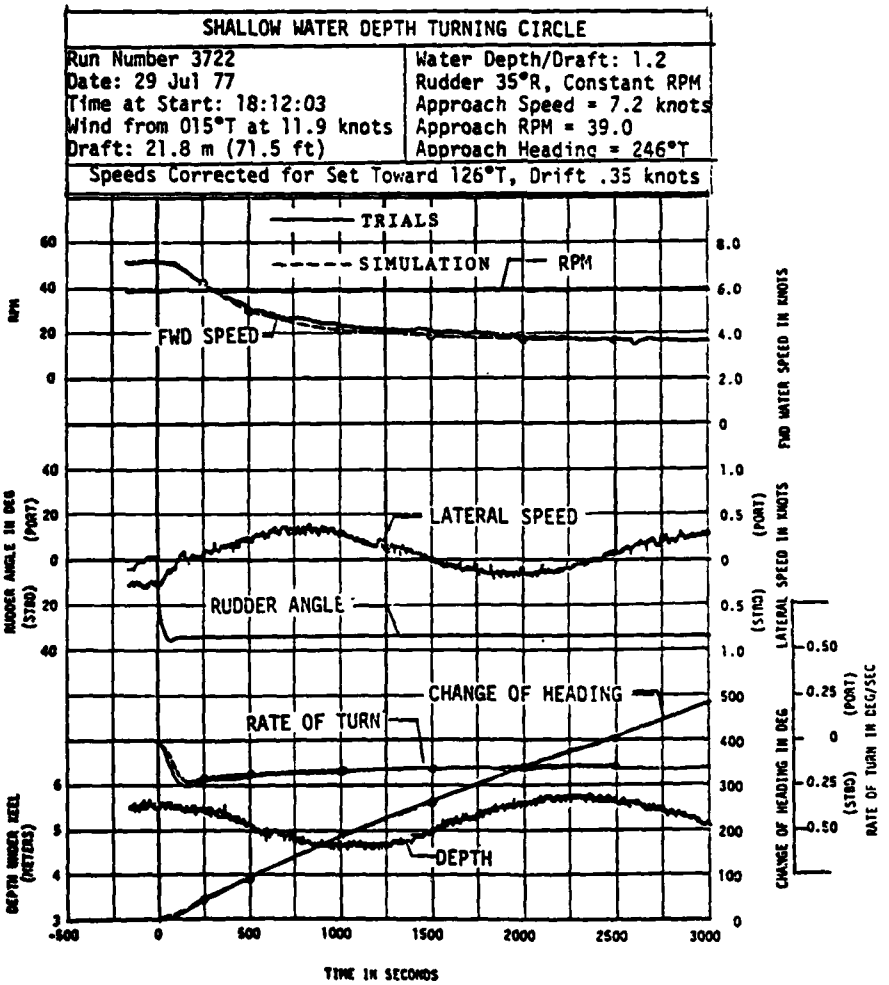

Figure 6-1 Comparison of Predicted and Measured Turning Characteristics of ESSO OSAKA in Shallow Water

ability, presented in Reference 10, indicated good correlation of the simulation with a maneuver of the ESSO BERNICIA during sea trials.

The most recent and extensive ship trials were performed on the ESSO OSAKA in shallow and deep water, Reference 18. Several model testing facilities have performed model tests and simulations of the ship trial maneuvers, References 19 and 20. The trials data has also been used to obtain the mathematical model coefficients using system identification methods, Reference 21. These correlation studies indicate that model testing and system identification methods produce results which are in acceptable to very good agreement with actual ship maneuvers. This correlation is illustrated for a shallow-water-depth turning circle in Figure 6-1 and for a medium-water-depth stopping maneuver in Figure 6-2.

6.2 EVALUATIONS BASED ON DEFINITIVE MANEUVERS

The most common use of mathematical models over the years has been to predict the track of a vessel when it executes standardized definitive maneuvers. The maneuvers are selected to demonstrate certain inherent capabilities of the vessel and offer a basis of comparison with other vessels where tests of full-scale results are available. The commonly used definitive maneuvers are steady turns, slowing or stopping, zig zags, and spirals, which are described in detail in the literature, including Reference 7.

The steady turn maneuver is performed by moving the rudder to the maximum angle (or one of a range of angles) and holding rudder angle and propulsion constant while the ship turns 540 degrees. The measures of performance are the advance, transfer, tactical diameter, steady turn diameter, time to turn 90 degrees and 180 degrees, and steady turn speed as defined in Figure 6-3. This maneuver defines the maximum turning capability of the ship which can be compared to a large historical data base.

The slowing or stopping maneuver is performed by ordering maximum astern power until the ship stops. The rudder may be left centered, used to control

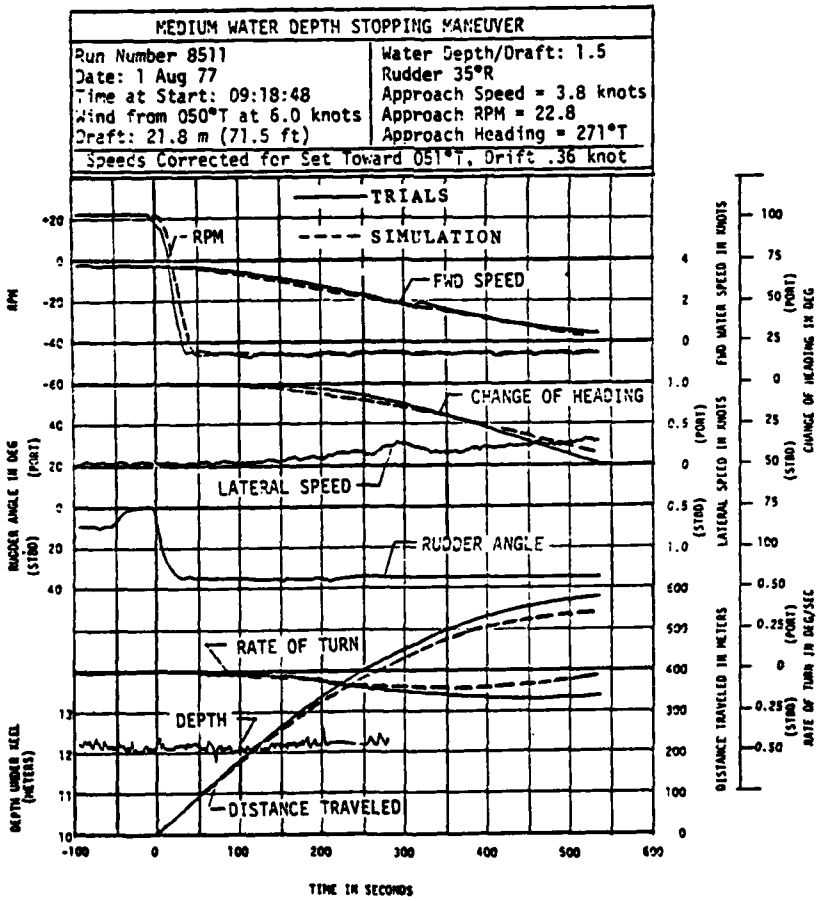

Figure 6-2 Comparison of Predicted and Measured Stopping Characteristics of ESSO OSAKA in Medium-Depth Water

heading, or shifted from side to side to aid stopping. Measures of performance include head reach(distance traveled), side reach, time to stop, and final heading, as illustrated in Figures 6-2 and 6-4.

A zig-zag maneuver is accomplished by moving the rudder to an angle (typically 10 degrees or 20 degrees) which is held until the ship has changed heading by the same amount. The rudder is shifted to the opposite angle and held until the ship has turned beyond the base course by the same amount. The shifting of the rudder is repeated up to five times. The performance measures are the angle of overshoot (beyond the heading that the rudder was shifted), the time to reach the heading where the rudder is first shifted, and overshoot width of path, as shown in Figure 6-5. The zig-zag maneuver demonstrates how quickly and precisely the ship can start and stop a change of course.

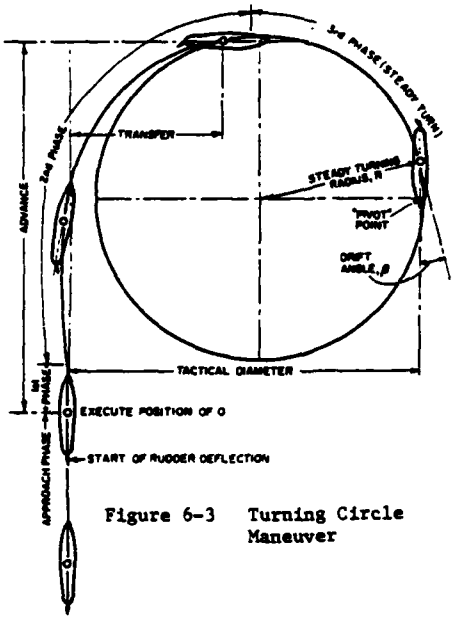

Figure 6-3 Turning Circle Maneuver

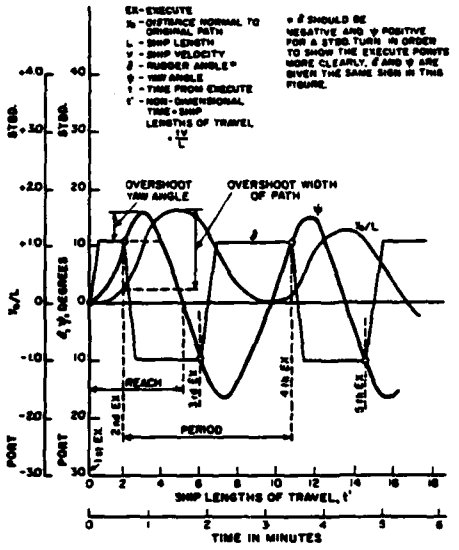

Figure 6-5 Zigzag Maneuver

The spiral maneuver is performed by moving the rudder to a small angle and holding it steady until the turn rate becomes steady. The rudder angle is

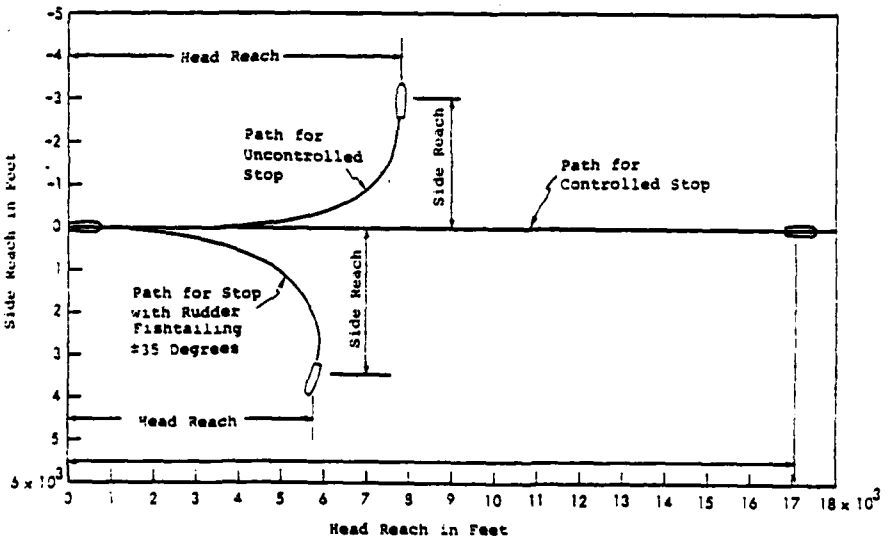

Figure 6-4 Computer Predictions of a Slowing/Stopping Maneuver

increased in small steps, which are held until the turn rate is steady, to a moderate angle (10 to 15 degrees), and then decreased in steps to amidship and on to repeat for the opposite rudder angles. The measure of performance is the relationship of the turn rate to rudder angle. The ship has straight-line stability if the plot of turn rate versus rudder angle is a single continuous curve with negative slope as shown in Figure 6-6. If the ship is unstable, that fact is evidenced by the need for continual corrective rudder angles, near zero, and the "spiral" curve takes the form shown for an unstable ship in Figure 6-6.

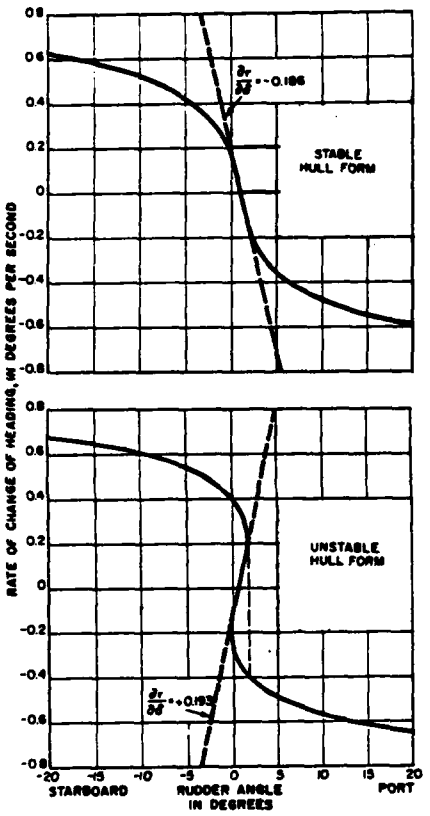

Figure 6-6 Results of a Spiral Maneuver

6.3 EVALUATIONS AND TRAINING USING SHIPHANDLING SIMULATORS

As has been observed in Section 3.0, mathematical ship motion prediction models are now used extensively in shiphandling simulators. These simulators are used to evaluate ship maneuverability, the suitability of the ship bridge design, and the adequacy of harbors and channels. Training of deck officers and the study groundings and collision avoidance factors are also now performed on these simulators.

An example of the utility of simulators was a study in which a ship maneuvering simulator was used to evaluate the maneuverability of a Navy rescue salvage ship design as reported in Reference 22. The ship maneuvering mathematical model used data from pmm model tests. A simplified ship bridge provided the deck officers with similar types of controls and information to that available on the ship. The Navy deck officers performed simulated approaches to a stranded ship in shallow water and approach and towing operations on a drifting ship. The results demonstrated that the ship design had adequate maneuverability, that the bow thruster was useful and necessary, and that the engine order schedule needed to provide more power at its lower settings.

The Computer-Aided Operations Research Facility (CAORF), Reference 23, was used to determine the extent of dredging required for safe operation of coal handling facilities at Norfolk, Virginia. Simulated maneuvers of typical ships into and out of berths performed by qualified pilots indicated the required areas for dredging around the terminals. Simulated transits of the access channel demonstrated the need for additional aids to navigation to permit reduction of dredged channel width.

CAORF was employed to train tug/barge deck officers, Reference 23, and to study the effects of work schedules and fatigue on watchkeeping performance.

7.0 STANDARD FORMAT FOR FINAL DATA PRESENTATION

The format finally adopted for the SNAME Mathematical Maneuvering Model Standardized Data Sheets is described in this section along with supplementary information, instructions, and reasons for their use. The Standardized Data Sheet forms were developed by SNAME Panel H-10 (Ship Controllability). They incorporate the results of comments and suggestions from various organizations involved in the field of ship maneuverability throughout the world which were surveyed by the Panel during the past several years.

The current data sheet forms are designed to provide a degree of standardization compatible with existing state of the art. However, they are intended to be flexible enough to facilitate the reporting of mathematical models and related data from all likely sources. For example, the data sheets do not constrain the user to a specific reporting system. Rather they are arranged to accommodate a variety of formulations and types of coefficients that may be forthcoming from various establishments throughout the world.

It is hoped that both the standardization and flexibility aspects will promote the adoption and widespread use of the SNAME Mathematical Maneuvering Model Standardized Data Sheets. As more such data sheet sets are accumulated, common grounds may be found for further standardization and improvements resulting in better international communication and efficacy.

7.1 Standardized Formats

The format currently adopted for the SNAME Mathematical Maneuvering Model Standardized Data Sheets is illustrated by the blank forms presented in Appendix D. It may be noted that each set of data sheets consists of four major sections held together with a cover sheet. These sections and their significant subdivisions are summarized as follows:

I. Data Source and Acquisition Techniques
   - A. Hydrodynamic Coefficient Data
   - B. Ship Maneuvering Predictions
   - C. Full-Scale Maneuvering Trials and Correlation Data

II. Ship Geometry
   - A. Table II-A - Principal Geometric Characteristics
   - B. Lines (Sketch)
   - C. Rudder Details (Sketch)

III. Mathematical Model
   - A. Basic Equations
   - B. Supplementary Equations
   - C. Coefficient Values

IV. Ship Maneuvering Characteristics
   - A. Stability and Control Derivatives and Indices
   - B. Numerical Measures from Definitive Maneuvers

The SNAME Standardized Data Sheets were designed to provide fairly complete data in concise and compact form, the primary emphasis being on the types of mathematical-maneuvering model data used for modern computer simulation studies. Accordingly, it was necessary to resort to mathematical and other symbols within the context of the data sheets, and to provide a separate means for the necessary definitions and amplification. The latter is accomplished by the extensive notation presented in Appendix A and supplemented by Appendix B.

The notations of Appendices A and B are intended to anticipate the requirements of, and serve as a common denominator for, all completed data sheet sets including those that may be received in the future. Obviously, to accomplish this objective within reasonable bounds, it has been necessary to standardize to the extent practicable. In doing so, the standard notations already developed by SNAME, ATTC, and

ITTC have been generally adopted and extended to cover the requirements of the present state of the art. Considerable effort has gone into the preparation and consolidation of Appendices A and B directed toward achieving at least a practical degree of universality. Nevertheless, it is reasonable to assume that periodic revisions including extension of the notations may be required to accommodate future contributions.

In view of the foregoing, it is felt that a set of blank data sheets together with the notations of Appendices A and B should enable contributors who are at least familiar with the field to participate in the program. The blank data forms will be furnished by SNAME to potential contributors upon request. These blank forms are designed oversized to accept pica or 12-point type for ease in preparation. They can be readily reproduced to provide a readable standard 8-1/2 by 11-inch page size. Separate copies of the standard notation also may be furnished upon request in advance of publication of the Primer.

It is urged that future contributors to the program follow the format and standards established for the data sheets insofar as is reasonably possible. This includes items such as the use of the standard notation particularly for the nondimensional hydrodynamic coefficients, and the use of the metric system for the numerical values of all the dimensional quantities. Following these basic guidelines will tend to expedite the processing of future data sheet sets which should result in their early publication and dissemination in accordance with the overall objectives of the program.

7.2 Purpose and Use

The major purpose of the Standard Data Sheet Program is to advance the state of the art of mathematical modeling as applied primarily to computer simulation techniques involved in the field of ship maneuverability. This goal is pursued by promoting the sharing of hydrodynamic coefficient and related ship maneuverability data that either exist or may be developed in the future by researchers and various other potential contributors. Thus, the success of the program will depend upon the timeliness and the extent to which substantially completed data sheet sets can be generated by potential contributors. As each such data sheet is received, it will be promptly processed, printed, and be made available for distribution by SNAME.

The three sample data sheet sets presented in Appendices E, F, and G can be used to illustrate how future data sheets may be filled out. The sample sheets were prepared by SNAME using existing data obtained from published and other reasonably accessible sources. These data were presented in a variety of different formats usually directed toward specialized or limited purposes. As the result, some of the sample sheets are not quite as complete as would have been desired. However, they do demonstrate how most of the standards outlined in Section 7.1 can be met and yet allow for the flexibility required by various contributors based on their current practices.

The four major sections of the sample data sheets are discussed separately in detail in the following paragraphs along with other matters relevant to the preparation of future data sheet sets. It should be emphasized again at this point that the discussion is concerned mainly with the degree of standardization that can be achieved without undue restraints on potential contributors. No attempt is made to alter or pass judgment on the relative merit, technical content, or basic philosophy of the various mathematical models and associated data submitted. It is urged, however, that all four major sections be filled out as completely as possible by contributors closest to the source of the information. This will help users to understand the given mathematical model including its purpose, accuracy, and range of validity, and to determine the degree of confidence to be placed in maneuvering predictions based on its use.

7.2.1 Data Source and Acquisition Techniques

Among the three sample data sheets, Appendix E serves as the best example of how Section I should be filled out. This is understandable since the information presented therein is well documented as the result of participation in the ITTC cooperative program described by References 16, 24, and 25. The ITTC program was directed toward standardization of techniques used for captive-model tests, computer simulation predictions, and data presentation methods in the field of ship maneuverability. Accordingly, fairly stringent information requirements considered pertinent to these objectives were established by ITTC in advance of the program. Furthermore, the representative ship deliberately selected for purposes of the ITTC program was one for which extensive data from specially conducted research maneuvering trials were available in published form. Consequently, all of the information needed to completely fill out Section I of the data sheets, including published

references to provide additional detail, was previously available.

Appendices F and G adequately fulfill most of the requirements of Section I of the data sheets. However, important information on the particulars of the full-scale maneuvering trials were not available at the time of preparation, and therefore was omitted.

7.2.2 Ship Geometry

Section II of the blank data sheet forms (Appendix D) is self explanatory and therefore requires very little comment in terms of the sample sheets. The role of this section will become increasingly important as more data on different ships are accumulated which will permit analyses to be made of the relationship of ship geometry to directional stability and maneuverability characteristics. Future contributors are therefore urged to completely fill out Section II including: all of the geometric quantities listed in Table II-A; a lines sketch of hull-rudder-propeller arrangement as illustrated by Appendices E and G; and a profile sketch showing rudder details. It may be noted that detailed rudder and propeller characteristics were omitted from Table II-A of Appendix F. It is assumed that this information is available and eventually could be provided along with the missing sketches unless prevented for proprietary reasons.

7.2.3 Mathematical Model

Section III is the heart of the SNAME Standardized Data Sheets and therefore an attempt should be made to comply with all of its elements. A complete mathematical model for any prescribed case consists of suitable equations of motion taken in conjunction with the numerical values of its coefficients such as those listed in Table III-C. In general, the equations of motion can be subdivided into basic equations and supplementary equations (including items such as autopilot, effects of wind, waves, and other forcing functions, and various subroutines). In view of the overall objectives of the SNAME program, the mathematical model should be presented primarily in a format suitable for direct use in real-time ship maneuvering simulators. Accordingly, a dimensional format is recommended wherein each of the various terms of the equations consists of a nondimensional coefficient and a dimensional multiplier. Such a representation has all of the advantages attendant with the use of nondimensional coefficients mentioned in Section 3.2 of the Primer without the need for frequent reference to the notation to determine their composition. Finally, it should be emphasized that any other information needed to accurately define the equations and the numerical values of their coefficients should be contained in notes on the page to which it applies. Typical examples of such notes are the specification of axis system and origin location with respect to ship center of gravity, as shown on all three data sheet sets.

Section III of Appendix E is an example of a case where the mathematical model as received was already in a format which essentially follows the standards recommended by SNAME. Consequently, it was readily transferrable to the Standardized Data Sheets and is completely defined by the SNAME Standard Notation of Appendix A. In this case, the contributing organization had already developed its own standard mathematical model format and methods used for surface ship maneuvering predictions (see Reference 6). Therefore, these standard equations and the symbols of Table III-C (without numerical values) can be incorporated in the blank forms of Section III and used by this organization to facilitate future submittals. Although these standard equations were set up initially for the calm, deep-water case, they can be used to simulate maneuvers in shallow water of constant depth. This can be accomplished by substituting a new set of coefficient values in Table III-C for each of the water depths considered. Thus, the time and effort saved by having the required forms printed in advance becomes very attractive.

Section III of Appendix F represents a variation from SNAME standards in that the nondimensional data constituting the mathematical model were presented in the so-called "bis" system format. To accommodate this format, the SNAME Standard Notation was followed for the dimensional quantities and the supplementary notation of Appendix B was prepared to define the nondimensional "bis" coefficients. Therefore, the complete definition of the terms in the mathematical model of Appendix F depends upon the combined use of the notations of Appendices A and B.

Another variation in Section III of Appendix F is due to the system used to mathematically model continuous maneuvers in which the ship passes from deep to shallow water of varying depth. To provide for this system, the basic equations (expressed in dimensional format similar to that given in Section III of Appendix E) are divided into two columns. The first column contains the separate terms of the basic equations for the case of maneuvering in deep water only. The second column contains the corresponding supplementary terms needed to represent the case of the ship maneuvering in shallow water of

continuously varying depth. The numerical values of the nondimensional coefficients needed to complete the mathematical model for the specific ship are similarly divided and arranged in two columns in Table III-C. Thus, if the above format proves to be satisfactory, oversized Section III data forms containing all of the required information except for numerical values could be prepared in advance for future contributors who prefer the "bis" system.

Section III of Appendix G represents a case where the mathematical model was submitted in a nondimensional format using the contributing organization's own notation system. In interest of standardization and to avoid the need for further expansion of the notation, it was decided to present the set of basic equations of motion in two separate formats as shown by two versions of Tables III-A and III-B of Appendix G. The first uses the recommended dimensional format parallel to that of Appendix E and conforms to the SNAME Standard Notation. The second uses the nondimensional format and notation originally submitted. Thus, the basic equations of the first type are completely defined by the notation of Appendix A which now includes those coefficients that were previously not listed. The nondimensional coefficients in the original notation are defined through Appendix A by equating them with the corresponding SNAME notation, as shown by Table III-C of Appendix G.

7.2.4 Ship Maneuvering Characteristics

7.2.4.1 Stability and Control Derivatives and Indices

Table IV-A of the data sheets is designed to provide fundamental data which can be used to determine the inherent directional stability and control characteristics of various ship types in the early design stages. Accordingly, this is definitely one area of the data sheets where strict adherence of prescribed standards will produce maximum benefits. The standards proposed in Table IV-A are in accordance with ITTC recommendations (Reference 16), namely that these nondimensional quantities are to be presented in the SNAME Standard (Prime System) Notation and referred to an axis system with an origin at the ship center of gravity. The ITTC Standards set out in Reference 16 also require that hydro- from these standards should be carefully noted on Table IV-A.

In addition to the standardized data for the fully appended ship, Table IV-A provides a column for the bare-hull case. Such data are desirable since they can be used to more accurately determine the separate effects of the appendages, particularly the rudder. In turn, they can be used in design studies to investigate the effect of rudder size or shape on inherent directional stability and control effectiveness as applied to new or existing ships. Unfortunately, such bare-hull data are rarely obtained in captive-model tests of specific ship designs, but are more likely to be found in sources containing the results of systematic series tests such as Reference 26.

The data presented in Table IV-A of Appendices E and G follow the desired standards including the notation and origin location used. However, the data received for Appendix F were in the "bis" system based on an origin located at midships and therefore are not easily convertible to the corresponding standard values. Consequently, the "bis" values are included in a separate column with hopes that they eventually can be replaced by standard Prime System values. It is known that the original model test data were processed in the Prime System and perhaps will be forthcoming in the future.

7.2.4.2 Numerical Measures from Definitive Maneuvers

Table IV-B consists mainly of tabulations of numerical measures obtained from simulated or full-scale definitive maneuvers of the types described by Section 7.1 of Reference 27. From the standpoint of the SNAME Standardized Data Sheets, these definitive maneuvers and associated numerical measures are intended to serve the following objectives or functions:

a. Provide a means for setting up, exercising, and checking computer programming of a given mathematical model on various training or research simulators prerequisite to conduct of more detailed maneuvering studies such as those involving the human operator in the control loop.

b. Provide a basis for establishing correlation between computer simulation predictions of maneuvering characteristics of various ship types with aim toward development of improved mathematical modeling techniques and enhancement of con- confidence levels in their use.

c. Provide a fundamental data base which eventually can lead to the development of handling quality criteria for various ship types.

The following comments and suggestions concerning how the Table IV-B data sheets should be filled out are made with view toward satisfying these three major objectives.

The definitive maneuvers selected for Table IV-B include the so-called spirals, zigzags, and steady turns. These three basic types of maneuvers were chosen because of their prevalent use in computer simulation studies as well as full-scale maneuvering trials, especially those research trials conducted for correlation purposes. Additional definitive maneuvers may be included on future data sheets, if desirable, particularly if the data derived therefrom contribute toward Objectives b. and c.

As may be seen from the blank forms in Appendix D, the definitive-maneuver data are set up as tables of numerical measures supplemented by graphs or typical time-history plots. The tables provide for dimensional data (in metric units) primarily to appeal to users such as ship operators and other non-research oriented types. Each table consists of a set of two columns to facilitate direct comparison between computer simulator predictions with full-scale values for each of two ship speeds. The 8 and 16-knot speeds are included on the blank forms merely because they are typical of speeds at which studies are conducted on most full-form commercial ship types. Obviously, these speeds should be changed where required for other ship types and to conform to existing full-scale trial data. Other items typed on the data forms such as rudder angles, are also merely recommended values to be used in absence of other considerations. It may be noted in this respect that provision is made for 45-degree rudder steady turns whereas the rudder machinery systems on most existing commercial ship types do not permit rudder angles beyond 35 degrees. However, the mathematical model is not necessarily so limited, and computer predictions from large rudder-angle turning maneuvers may be of interest for several reasons. For example, they may provide design data which indicates the trade offs between improved maneuverability and increased capacity of rudder machinery system for new or perhaps even some existing ships. Further, such data may provide additional insight into the validity of a given mathematical model in the range of extreme maneuvers.

In filling out the Table IV-B data sheets, future contributors should make an effort to provide numerical measures determined from the original or most accurate sources. Typical of such sources are tabulated output data from digital computers and large-scale plots of the original data from full-scale trials. Most of the numbers provided in the sample data sheets were read from small-scale graphs in the form of either numerical-measure crossplots or time-history plots. This process is not only time-consuming but is easily subject to error.

Table IV-B of Appendix E is representative of a case where fairly extensive computer predictions and corresponding full-scale definitive-maneuver data were available. It may be noted that the two comparative speeds given in the tables were changed to correspond to the average approach speeds measured from each set of full-scale definitive maneuvers. Unfortunately, computer simulation predictions corresponding to the full-scale 35-degree-left rudder steady turns were not available from the published source used to prepare the data sheets. It is hoped that direct digital computer readout data can be made available in the future to update and complete Table IV-B of Appendix E.

The tabulated values in Table IV-B of Appendix F are fairly sparse since the data available from published sources were rather limited. Only deep-water predictions and corresponding full-scale data are presented. It is hoped that the shallow-water mathematical model presented in Section III of Appendix F, together with any full-scale data that can be made available, will be used to prepare Table IV-B type data sheets for selected shallow-water cases. It may be noted for the deep-water case that the full-scale data for steady turns at an approach speed of 16 knots are subdivided into two columns. This is done to demonstrate the disparity that can be obtained from full-scale measurements of the same steady-turning maneuver conducted on two sister ships.

Table IV-B of Appendix G contains only a relatively small amount of definitive maneuver data based on availability from published sources at time of preparation. The only comparative full-scale trial data presented are shown by the graph of a 35-degree rudder steady turn which is too small to permit accurate reading of numerical measures. Again, it is hoped that Table IV-B of Appendix G can be more completely filled out in the future based on digital computer prediction readouts and correlative full-scale measurements.

REFERENCES

1. Mandel, Philip, "Ship Maneuvering and Control," Principles of Naval Architecture, Chapter VIII, SNAME, 1967.

2. Abkowitz, M.A., "Lectures on Ship Hydrodynamics-Steering and Maneuverability," Hydro and Aerodynamics Laboratory Report HyA-5, May 1964.

3. Gertler, Morton and Hagen, Grant R., "Standard Equations of Motion for Submarine Simulation," NSRDC Report 2510, June 1967.

4. Chislett, M.S. and Strom-Tejsen, J., "Planar Motion Mechanism Tests and Full-Scale Steering and Maneuvering Predictions for a Mariner Class Vessel," Hydro and Aerodynamics Laboratory Report HyA-6, April 1965.

5. Strom-Tejsen, J., "A Digital Computer Technique for Prediction of Standard Maneuvers of Surface Ships," David Taylor Model Basin Report 2130, December 1965.

6. Goodman, Alex and Gertler, Morton, "Analytical and Experimental Techniques used at HSMB for Surface-Ship Directional Stability and Control Studies," Presented at the Meeting of the Chesapeake Chapter of SNAME on 24 April 1975, HYDRONAUTICS, Incorporated Technical Report 7500-1, April 1965.

7. Goodman, Alex, Gertler, Morton and Kohl, Robert, "Experimental Techniques and Methods of Analysis used at HYDRONAUTICS, for Surface-Ship Maneuvering Predictions," Proceedings of Eleventh ONR Symposium on Naval Hydrodynamics, April 1976, HYDRONAUTICS, Incorporated Technical Report 7600-1, June 1976.

8. Gertler, Morton, Miller, Eugene R., and Ankudinov, Vladimir, "Shallow-Water Maneuverability Characteristics of MARAD Systematic Series for Large Full-Form Merchant Ships," HYDRONAUTICS, Incorporated Technical Report 7568-1, August 1977.

9. Norrbin, Nils H., "Theory and Observations of the Use of a Mathematical Model for Ship Maneuvering in Deep and Confined Waters," Proceedings of the Eighth Symposium on Naval Hydrodynamics, August 1970, Swedish State Shipbuilding Experimental Tank Publication Nr68, 1971.

10. van Berlekom, Willem B. and Goddard, Thomas A., "Maneuvering of Large Tankers," Trans. SNAME, Vol. 80, 1972.

11. Fujino, Masataka, "Experimental Studies on Ship Maneuverability in Restricted Waters, Parts I and II," International Shipbuilding Progress, No. 168, 1968 and No. 186, 1970.

12. Eda, H., "Directional Stability and Control of Ships in Restricted Channels," Trans. SNAME, Vol. 79, 1971.

13. Nomoto, K., et al, "On the Steering Qualities of Ships," International Shipbuilding Progress, Vol. 4, No. 35, July 1957.

14. Clarke, D., et al, "The Application of Manoeuvring Criteria in Hull Design Using Linear Theory," The Naval Architect, March 1983, pp. 45-68.

15. Morse, R.V., and D. Price, "Maneuvering Characteristics of the MARINER Type Ship (USS COMPASS ISLAND) in Calm Seas," Sperry Gyroscope Publication G7-2233-1019, prepared for David Taylor Model Basin under Contract No. NOnr-3061(00), 1961.

16. Gertler, M., "Final Analysis of First Phase of ITTC Standard Captive-Model-Test Program," Appendix 3, Part 2 of Maneuverability Committee Report, Proceedings of the 12th ITTC, 1969.

17. Smitt, L.W. and M.S. Chislett, "Large Amplitude PMM Tests and

APPENDIX A

NOTATION

FOR

SNAME MATHEMATICAL-MANEUVERING MODEL STANDARDIZED DATA SHEET

The following pages provide the nomeclature for ship geometry (hull, rudder, and propeller); resistance and propulsion; and maneuverability (directional stability and control) for use with the Standardized Data Sheets. the resistance and propulsion notation generally conforms to ATTC and ITTC standards. The notation for directional stability and control conforms to DTMB Report 1319 and NSRDC Report 2510, to the extent applicable, which are extensions of the standard SNAME notation established by T&R Bulletin 1-5. Incuded is a sketch showing the positive direction of principal axes, angles, forces, moments, and velocities.

HULL GEOMETRY

Symbol	Definition
A	Area of midship section to design full-load waterline
B	Maximum beam at design full-load waterline
L	Characteristic length; length between perpendiculars
L_E	Length of entrance measured from forward perpendicular FP
L_M	Length of parallel midbody
L_R	Length of run measured from after perpendicular AP
LCB	Longitudinal center of buoyancy position
S	Wetted surface area
T	Draft at design full-load condition
∇	Volume of displacement at design full-load condition
B/T	Beam-draft ratio
C_B	Block coefficient; ∇/LBT
C_{BE}	Block coefficient of entrance; ∇_E/L_EBT
C_{BR}	Block coefficient of run; ∇_R/L_RBT
C_M	Midship section coefficient; A/BT
LCB/L	Nondimensional LCB position expressed as percentage of L forward of midships
L_E/L	Nondimensional entrance length
L_M/L	Nondimensional parallel midbody length
L_R/L	Nondimensional run length
L_R/B	Length-beam ratio of run
$S/\nabla^{2/3}$	Wetted-surface coefficient
C_s	Wetted-surface coefficient; $S/(VL)^{\frac{1}{2}}$
C_∇	Volumetric coefficient; ∇/L^3

RUDDER GEOMETRY

Symbol	Definition
A_T	Total planform area
A_F	Fixed area
A_M	Movable area
$\bar{b}$	Mean span
c_r	Root chord
c_t	Tip chord
a	Aspect ratio (geometric; $\bar{b}^2/A_T$
λ	Taper ratio

PROPELLER GEOMETRY

c	Blade chord at 0.7 radius
D	Diameter
P	Pitch at 0.7 radius
D/T	Diameter-draft ratio
P/D	Pitch-diameter ratio

RESISTANCE AND PROPULSION

Symbol	Definition
EHP	Effective horsepower
n	Propeller revolutions per unit time
Q	Propeller torque
R_A	Added resistance
R_F	Frictional resistance
R_I	Ideal resistance; model resistance for ship propulsion point
R_R	Residual resistance
R_T	Total resistance
T	Propeller thrust
SHP	Shaft horsepower
v	Speed
v_a	Propeller speed of advance
ρ	Mass density
ν	Kinematic viscosity
C_A	Model-ship correlation allowance coefficient; $R_A/\frac{1}{2}\rho Sv^2$
C_F	Frictional-resistance coefficient; $R_F/\frac{1}{2}\rho Sv^2$; C_{Fm} in model range, C_{Fs} in ship range
C_R	Residual-resistance coefficient; $R_R/\frac{1}{2}\rho Sv^2$
C_T	Total-resistance coefficient; $R_T/\frac{1}{2}\rho Sv^2$
C_{Ti}'	Loading coefficient; $C_{Ti}' = C_{Ti}$ at ship propulsion point
e_p	Propeller efficiency
e_h	Hull efficiency; 1-t/1-w
e_{rr}	Relative rotative efficiency
F_N	Froude number; $v/\sqrt{gL}$
J	Propeller advance coefficient; v_a/nD
J_a	Apparent advance coefficient
J_{tQ}	True advance coefficient-torque identity
J_{tT}	True advance coefficient-thrust identity
K_Q	Propeller torque coefficient; $Q/\rho n^2D^5$
K_T	Propeller thrust coefficient; $T/\rho n^2D^4$
PC	Propulsive coefficient; EHP/SHP = $R_I v/2\pi Qn$
R_N	Reynolds number; vL/ν
t	Thrust deduction fraction; $1 - \frac{R_I}{T}$
w	Taylor wake fraction; $1 - \frac{v_a}{v}$
w_Q	Taylor wake fraction-tirque identity; $1 - \frac{J_{tQ}}{J_a}$
w_T	Taylor wake fraction-thrust identity; $1 - \frac{J_{tT}}{J_a}$

DIRECTIONAL STABILITY AND CONTROL

The following nomenclature conforms to DTMB Report 1319 and NSRDC Report 2510 where applicable. The positive direction of axes, angles, forces, moments, and velocities are shown by the accompanying sketch.

Symbol	Nondimensional Form	Definition
a_i		Constant in quadratic fit to axial force equation $X'_{\beta=\delta_r=0} = f(\eta)$ for each of i^{th} segments where i = 1,2,3,4; $a_i = X_{uu}'$ at $\eta = 0$ in appropriate segement
b_i		First order coefficient in quadratic fit to axial propeller force equation $X'_{\beta=\delta_r=0} = f(\eta)$ for each of i^{th} segments where i = 1,2,3,4
c_i		Second order coefficient in quadratic fit to axial propeller force equation $X'_{\beta=\delta_r=0} = f(\eta)$ for each of i^{th} segments where i = 1,2,3,4
AD	$AD' = \frac{AD}{L}$	Advance
CB		Center of buoyancy
CG		Center of mass of ship
D		Propeller diameter
D_s	$D_s' = \frac{D_s}{L}$	Steady-turning diameter
I_x	$I_x' = \frac{I_x}{\frac{1}{2}\rho L^5}$	Moment of inertia of ship about x axis
I_y	$I_y' = \frac{I_y}{\frac{1}{2}\rho L^5}$	Moment of inertia of ship about y axis
I_z	$I_z' = \frac{I_z}{\frac{1}{2}\rho L^5}$	Moment of inertia of ship about z axis
J	$J = \frac{u}{nD}$	Propeller advance coefficient based on ship speed u
J_c	$J_c' = \frac{u_c}{n_c D}$	Propeller advance coefficient at steady ship command speed u_c
k_x	$k_x' = \frac{k_x}{L}$	Radius of gyration of ship about x axis
k_y	$k_y' = \frac{k_y}{L}$	Radius of gyration of ship about y axis
k_z	$k_z' = \frac{k_z}{L}$	Radius of gyration of ship about z axis
L	$L' = 1$	Characteristic length; length between perpendiculars for commercial ships
ℓ_d	$\ell_d' = \frac{\ell_d}{L} = \frac{\ell_r - \ell_v}{L}$	Dynamic stability lever
ℓ_r	$\ell_r' = \frac{\ell_r}{L} = \frac{N_r'}{Y_r' - m'}$	Damping lever
ℓ_v	$\ell_v' = \frac{\ell_v}{L} = \frac{N_v'}{Y_v'}$	Static stability lever
m	$m' = \frac{m}{\frac{1}{2}\rho L^3}$	Mass of ship

N	$N' = \frac{N}{\frac{1}{2}\rho L^3 U^2}$	Hydrodynamic moment component about z axis (yawing moment)
$N_\star$	$N_\star' = \frac{N_\star}{\frac{1}{2}\rho L^3 U^2}$	Yawing moment when $\beta = \delta_r = 0$
$N_{(a)}$	$N_{(a)}' = \frac{N_{(a)}}{\frac{1}{2}\rho L^3 U^2}$	Aerodynamic yawing moment due to wind
$N_{(A)}$	$N_{(A)}' = \frac{N_{(A)}}{\frac{1}{2}\rho L^3 U^2}$	Yawing moment due to anchors
$N_{(b)}$	$N_{(b)}' = \frac{N_{(b)}}{\frac{1}{2}\rho L^3 U^2}$	Yawing moment generated by bow thruster
$N_{(c)}$	$N_{(c)}' = \frac{N_{(c)}}{\frac{1}{2}\rho L^3 U^2}$	Yawing moment due to cross-flow current
$N_{(f)}$	$N_{(f)}' = \frac{N_{(c)}}{\frac{1}{2}\rho L^3 U^2}$	Yawing moment due to other forcing functions
$N_{(m)}$	$N_{(m)}' = \frac{N_{(m)}}{\frac{1}{2}\rho L^3 U^2}$	Yawing moment due to mooring
$N_{(p)}$	$N_{(p)}' = \frac{N_{(p)}}{\frac{1}{2}\rho L^3 U^2}$	Yawing moment due to propeller
$N_{(t)}$	$N_{(t)}' = \frac{N_{(t)}}{\frac{1}{2}\rho L^3 U^2}$	Yawing moment due to tugs
N_r	$N_r' = \frac{N_r}{\frac{1}{2}\rho L^4 U}$	First order coefficient used in representing N as a function of r
N_{rrr}	$N_{rrr}' = \frac{N_{rrr}}{\frac{1}{2}\rho L^6 U^{-1}}$	Third order coefficient used in representing N as a function of r. Second order coefficient is zero
$N_{r\eta}$	$N_{r\eta}' = \frac{N_{r\eta}}{\frac{1}{2}\rho L^4 U}$	First order coefficient used in representing N_r as a function of $(\eta-1)$
$N_{\dot{r}}$	$N_{\dot{r}}' = \frac{N_{\dot{r}}}{\frac{1}{2}\rho L^5}$	Coefficient used in representing N as a function of $\dot{r}$
$N_{r\|r\|}$	$N_{r\|r\|}' = \frac{N_{r\|r\|}}{\frac{1}{2}\rho L^5}$	Second order coefficient used in representing N as a function of r
$N_{\|r\|\delta r}$	$N_{\|r\|\delta r}' = \frac{N_{\|r\|\delta r}}{\frac{1}{2}\rho L^4 U}$	Coefficient used in representing $N_{\delta r}$ as a function of r
N_v	$N_v' = \frac{N_v}{\frac{1}{2}\rho L^3 U}$	First order coefficient used in representing N as a function of v
$N_{v\eta}$	$N_{v\eta}' = \frac{N_{v\eta}}{\frac{1}{2}\rho L^3 U}$	First order coefficient used in representing N_v as a function of $(\eta-1)$
$N_{\dot{v}}$	$N_{\dot{v}}' = \frac{N_{\dot{v}}}{\frac{1}{2}\rho L^4}$	Coefficient used in representing N as a function of $\dot{v}$
$N_{\|v\|r}$	$N_{\|v\|r}' = \frac{N_{\|v\|r}}{\frac{1}{2}\rho L^4}$	Coefficient used in representing N_r as a function of v
N_{vrr}	$N_{vrr}' = \frac{N_{vrr}}{\frac{1}{2}\rho L^3 U^{-1}}$	Coefficient used in representing N_v as a function of r^2
N_{vvr}	$N_{vvr}' = \frac{N_{vvr}}{\frac{1}{2}\rho L^4 U^{-1}}$	Coefficient used in representing N_v as a function of the product vr
$N_{v\|v\|}$	$N_{v\|v\|}' = \frac{N_{v\|v\|}}{\frac{1}{2}\rho L^5}$	Second order coefficient used in representing N as a function of v

N_{vvv}	$N_{vvv}' = \frac{N_{vvv}}{\frac{1}{2}\rho L^2 U^{-1}}$	Third order coefficient used in representing N as a function of v. Second order coefficient is zero
$N_{v\|v\|n}$	$N_{v\|v\|n}' = \frac{N_{v\|v\|n}}{\frac{1}{2}\rho L^3}$	First order coefficient used in representing $N_{v\|v\|}$ as a function of (n-1)
N_{y_o}	$N_{y_o}' = \frac{N_{y_o}}{\frac{1}{2}\rho L^2 U^2}$	First order coefficient used in representing N as a function of lateral distance of ship C.G. from channel centerline
$N_{y_o y_o y_o}$	$N_{y_o y_o y_o}' = \frac{N_{y_o y_o y_o}}{\frac{1}{2}\rho U^2}$	Third order coefficient used in representing N as a function of lateral distance of ship C.G. from channel centerline. Second order coefficient is zero
$N_{\delta r}$	$N_{\delta r}' = \frac{N_{\delta r}}{\frac{1}{2}\rho L^2 U^2}$	First order coefficient used in representing N as a function of δr
$N_{\delta r \delta r \delta r}$	$N_{\delta r \delta r \delta r}' = \frac{N_{\delta r \delta r \delta r}}{\frac{1}{2}\rho L^3 U^2}$	Third order coefficient used in representing N as a function of δr. Second order coefficient
$N_{\delta r n}$	$N_{\delta r n}' = \frac{N_{\delta r n}}{\frac{1}{2}\rho L^3 U^2}$	First order coefficient used in representing $N_{\delta r}$ as a function of (n-1)
n		Propeller revolution rate
n_c		Propeller revolution rate at steady command speed
n_o		Ordered propeller revolution rate
o_y	$o_y = \frac{o_y}{L}$	Overshoot width of path
o_ψ		Overshoot heading angle; measured from value at second execute
R	$R' = \frac{R}{L}$	Steady-turning radius
r	$r' = \frac{rL}{U}$	Angular velocity component about z axis relative to fluid (yaw)
$\dot{r}$	$\dot{r} = \frac{rL^2}{U^2}$	Angular acceleration component about z axis relative to fluid
T	$T' = \frac{T}{\frac{1}{2}\rho L^2 U^2}$	Propeller thrust (directed along x axis); $T'(1-t) = -X_{uu}'$ at ship-propulsion point
TD	$TD' = \frac{TD}{L}$	Tactical diameter
TR	$TR' = \frac{TR}{L}$	Transfer
t	$t' = \frac{tU}{L}$	Time
t_i	$t_i' = \frac{t_i U}{L}$	Time in i^{th} execute in an overshoot or zigzag maneuver
t_o	$t_o' = \frac{t_o U}{L}$	Time at initiation of a maneuver
t_{90}	$t_{90}' = \frac{t_{90} U}{L}$	Time to reach 90-degree change of heading in a turn
t_{180}	$t_{180}' = \frac{t_{180} U}{L}$	Time to reach 180-degree change of heading in a turn
U	$U' = \frac{U}{U}$	Linear velocity of origin of body axes relative to fluid

u	$u' = \frac{u}{U}$	Component of U in direction of the x axis
$\dot{u}$	$\dot{u}' = \frac{\dot{u}L}{U^2}$	Time rate of change of u in direction of the x axis
u_c	$u_c' = \frac{u_c}{U}$	Command speed: steady value of ahead speed component u for a given propeller rpm for $\delta = \delta r = 0$; sign changes with propeller reversal
V		Absolute speed in knots
V_o		Steady approach speed in knots
V_{90}		Speed in knots at 90-degree heading change in turn
V_{180}		Speed in knots at 180-degree heading change in a turn
v	$v' = \frac{v}{U}$	Component of U in direction of the y axis
$\dot{v}$	$\dot{v}' = \frac{\dot{v}L}{U^2}$	Time rate of change of v in direction of the y axis
x	$x' = \frac{x}{L}$	Longitudinal body axis; also the coordinate of a point relative to the origin of body axes
x_B	$x_B' = \frac{x_B}{L}$	The x coordinate of CB
x_G	$x_G' = \frac{x_G}{L}$	The x coordinate of CG
x_o	$x_o' = \frac{x_o}{L}$	A coordinate of the displacement of CG relative to the origin of a set of fixed axes
X	$X' = \frac{X}{\frac{1}{2}\rho L^2 U^2}$	Hydrodynamic force component along x axis (longitudinal, or axial force)
$X_{(a)}$	$X_{(a)}' = \frac{X_{(a)}}{\frac{1}{2}\rho L^2 U^2}$	Aerodynamic longitudinal force due to wind
$X_{(A)}$	$X_{(A)}' = \frac{X_{(A)}}{\frac{1}{2}\rho L^2 U^2}$	Longitudinal force due to anchors
$X_{(f)}$	$X_{(f)}' = \frac{X_{(f)}}{\frac{1}{2}\rho L^2 U^2}$	Longitudinal force due to other forcing functions
$X_{(m)}$	$X_{(m)}' = \frac{X_{(m)}}{\frac{1}{2}\rho L^2 U^2}$	Longitudinal force due to mooring
$X_{(p)}$	$X_{(p)}' = \frac{X_{(p)}}{\frac{1}{2}\rho L^2 U^2}$	Longitudinal delivered propeller force equal to -T(1-t)
$X_{(t)}$	$X_{(t)}' = \frac{X_{(t)}}{\frac{1}{2}\rho L^2 U^2}$	Longitudinal force due to tugs
X_{rr}	$X_{rr}' = \frac{X_{rr}}{\frac{1}{2}\rho L^4}$	Second order coefficient used in representing X as a function of r. First order coefficient is zero
$X_{\dot{u}}$	$X_{\dot{u}}' = \frac{X_{\dot{u}}}{\frac{1}{2}\rho L^3}$	Coefficient used in representing X as a function of $\dot{u}$
X_{uu}	$X_{uu}' = \frac{X_{uu}}{\frac{1}{2}\rho L^2}$	Second order coefficient used in representing X as a function of u in the non-propelled case. First order coefficient is zero

X_{vr}	$X_{vr}' = \frac{X_{vr}}{\frac{1}{2}\rho L^3}$	Coefficient used in representing X as a function of the product vr
X_{vv}	$X_{vv}' = \frac{X_{vv}}{\frac{1}{2}\rho L^2}$	Second order coefficient used in representing X as a function of v. First order coefficient is zero
$X_{vv\eta}$	$X_{vv\eta}' = \frac{X_{vv\eta}}{\frac{1}{2}\rho L^2}$	First order coefficient used in representing X_{vv} as a function of (n-1)
$X_{\delta r\delta r}$	$X_{\delta r\delta r}' = \frac{X_{\delta r\delta r}}{\frac{1}{2}\rho L^2U^2}$	Second order coefficient used in representing X as a function of δr at $\eta = 0$. First order coefficient is zero
$X_{\delta r\delta r\eta\eta}$	$X_{\delta r\delta\eta\eta}' = \frac{X_{\delta r\delta\eta\eta}}{\frac{1}{2}\rho L^2U^2}$	Second order coefficient used in representing $X_{\delta r\delta r}$ as a function of η
$Y_{\|r\|\delta r}$	$Y_{\|r\|\delta r}' = \frac{Y_{\|r\|\delta r}}{\frac{1}{2}\rho L^3U}$	Coefficient used in representing $Y_{\delta r}$ as a function of r
Y_v	$Y_v' = \frac{Y_v}{\frac{1}{2}\rho L^2U}$	First order coefficient used in representing Y as a function of v
$Y_{v\eta}$	$Y_{v\eta}' = \frac{Y_{v\eta}}{\frac{1}{2}\rho L^2U}$	First order coefficient used in representing Y_v as a function of (n-1)
$Y_{\dot{v}}$	$Y_{\dot{v}}' = \frac{Y_{\dot{v}}}{\frac{1}{2}\rho L^3}$	Coefficient used in representing Y as a function of $\dot{v}$
$Y_{v\|r\|}$	$Y_{v\|r\|}' = \frac{Y_{v\|r\|}}{\frac{1}{2}\rho L^3}$	Coefficient used in representing Y_v as a function of r
Y_{vrr}	$Y_{vrr}' = \frac{Y_{vrr}}{\frac{1}{2}\rho L^4U^{-1}}$	Coefficient used in representing Y_v as a function of r^2
Y_{vvr}	$Y_{vvr}' = \frac{Y_{vvr}}{\frac{1}{2}\rho L^3U^{-1}}$	Coefficient used in representing Y_v as a function of the produce vr
$Y_{v\|v\|}$	$Y_{v\|v\|}' = \frac{Y_{v\|v\|}}{\frac{1}{2}\rho L^2}$	Second order coefficient used in representing Y as a function of v
Y_{vvv}	$Y_{vvv} = \frac{Y_{vvv}}{\frac{1}{2}\rho L^2U^{-1}}$	Third order coefficient used in representing Y as a function of v. Second order coefficient is zero
$Y_{v\|v\|\eta}$	$Y_{v\|v\|\eta}' = \frac{Y_{v\|v\|\eta}}{\frac{1}{2}\rho L^2}$	First order coefficient used in representating $Y_{v\|v\|}$ as a function of (n-1)
Y_{yo}	$Y_{yo}' = \frac{Y_{yo}}{\frac{1}{2}\rho LU^2}$	First order coefficient used in representing Y as a function of lateral distance of ship C.G. from channel centerline
Y_{yoyoyo}	$Y_{yoyoyo}' = \frac{Y_{yoyoyo}}{\frac{1}{2}\rho L^{-1}U^2}$	Third order coefficient used in representing Y as a function of lateral distance of ship C.G. from channel centerline. Second order coefficient is zero
$Y_{\delta r}$	$Y_{\delta r}' = \frac{Y_{\delta r}}{\frac{1}{2}\rho L^2U^2}$	First order coefficient used in representing Y as a function of δr
$Y_{\delta r\delta r\delta r}$	$Y_{\delta r\delta r\delta r}' = \frac{Y_{\delta r\delta r\delta r}}{\frac{1}{2}\rho L^2U^2}$	Third order coefficient used in representing Y as a function of δr. Second order coefficient is zero
$Y_{\delta r\eta}'$	$Y_{\delta r\eta}' = \frac{Y_{\delta r\eta}}{\frac{1}{2}\rho L^2U^2}$	First order coefficient used in representing $Y_{\delta r}$ as a function of (n-1)
β		Angle of drift
δr		Deflection of rudder
δr_i		Steady rudder angle at i^{th} execute in an overshoot of zigzag maneuver; i = 1,2,3.....

$\dot{\delta}_r$	$\dot{\delta}_r' = \frac{\dot{\delta}_r L}{U}$	Rudder deflection rate
n	$n = \frac{J_c}{J}$	Ship propulsion ratio; $\frac{u_c}{u}$ or $\frac{n_o}{n}$
y	$y' = \frac{Y}{L}$	Lateral body axis; also the coordinate of a point relative to the origina of body axes
y_B	$y_B' = \frac{y_B}{L}$	The y coordinate of CB
y_G	$y_G' = \frac{y_G}{L}$	The y coordinate of CG
y_o	$y_o' = \frac{y_o}{L}$	A coordinate of the displacement of CG relative to the origin of a set of fixed axes (also lateral distance of ship C.G. to channel centerline).
Y	$Y' = \frac{Y}{\frac{1}{2}\rho L^2 U^2}$	Hydrodynamic force component along y axis (lateral force)
Y_*	$Y_*' = \frac{Y}{\frac{1}{2}\rho L^2 U^2}$	Lateral force when $\beta = \delta_r = 0$
$Y_{(a)}$	$Y_{(a)}' = \frac{Y_{(a)}}{\frac{1}{2}\rho L^2 U^2}$	Aerodynamic lateral force due to wind
$Y_{(A)}$	$Y_{(A)}' = \frac{Y_{(A)}}{\frac{1}{2}\rho L^2 U^2}$	Lateral force due to anchors
$Y_{(f)}$	$Y_{(f)}' = \frac{Y_{(f)}}{\frac{1}{2}\rho L^2 U^2}$	Lateral force due to other forcing functions
$Y_{(m)}$	$Y_{(m)}' = \frac{Y_{(m)}}{\frac{1}{2}\rho L^2 U^2}$	Lateral force due to moorings
$Y_{(p)}$	$Y_{(p)}' = \frac{Y_{(p)}}{\frac{1}{2}\rho L^2 U^2}$	Lateral force due to propeller
$Y_{(t)}$	$Y_{(t)}' = \frac{Y_{(t)}}{\frac{1}{2}\rho L^2 U^2}$	Lateral force due to tugs
Y_r	$Y_r' = \frac{Y_r}{\frac{1}{2}\rho L^3 U}$	First order coefficient used in representing Y as a function of r
$Y_{r\eta}$	$Y_{r\eta}' = \frac{Y_{r\eta}}{\rho L^3 U}$	First order coefficient used in representing Y_r as a function of (n-1)
$Y_{\dot{r}}$	$Y_{\dot{r}}' = \frac{Y_{\dot{r}}}{\frac{1}{2}\rho L^4}$	Coefficient used in representing Y as a function of $\dot{r}$
$Y_{r\|r\|}$	$Y_{r\|r\|}' = \frac{Y_{r\|r\|}}{\frac{1}{2}\rho L^4}$	Second order coefficient used in representing Y as a function of r
Y_{rrr}	$Y_{rrr}' = \frac{Y_{rrr}}{\frac{1}{2}\rho L^5 U^{-1}}$	Third order coefficient used in representing Y as a function of r. Second order coefficient is zero.
σ_{ih}	$\sigma_{ih}' = \sigma_{ih}\frac{L}{U}$ $\sigma_{ih}'' = \sigma_{ih}'\sqrt[3]{\frac{m}{\forall}}$	Roots of characteristic stability equation for horizontal plane motions, i = 1 or 2
ϕ		Roll angle
ϕ_m		Maximum roll angle in a maneuver
ψ		Heading or yaw angle

ψ_i		Heading angle at i^{th} execute in an overshoot or zigzag maneuver, measured from value at first execute; i = 2,3....
$\dot{\psi}$	$\dot{\psi}' = \dot{\psi}\frac{L}{U}$	Rate of change of heading
$\dot{\psi}_h$	$\dot{\psi}_h' = \dot{\psi}_h\frac{L}{U}$	Height of loop at neutral rudder angle from spiral maneuver
$\dot{\psi}_i$	$\dot{\psi}_i' = \dot{\psi}_i\frac{L}{U}$	Rate of change of heading at i^{th} execute in an overshoot or zigzag maneuver; i = 2,3.....
ω	$\omega' = \frac{\omega L}{U}$	Frequency of oscillation

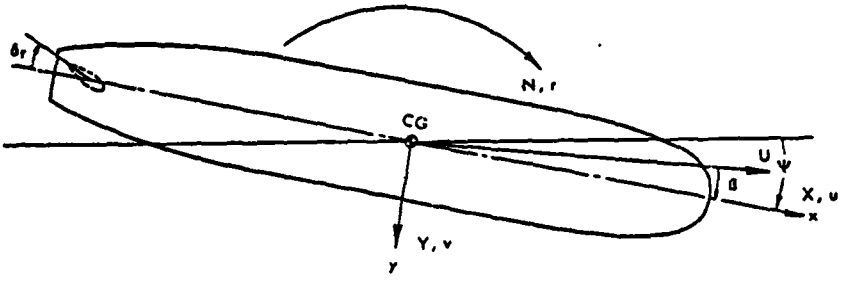

SKETCH SHOWING POSITIVE DIRECTIONS OF AXES, ANGLES, VELOCITIES, FORCES, AND MOMENTS

Note: Origin is normally taken at ship C.G.

APPENDIX B

SUPPLEMENTARY NOTATION FOR "BIS" SYSTEM

The following nomenclature is provided to facilitate the use of mathematical models presented in the so-called "bis" system format. In the "bis" system, the modes of motion, forces, and moments involved are made nondimensional by use of units of mass m, length L, and acceleration of gravity g as opposed to mass density ρ, length L, and velocity U used with the Standard SNAME system. To the extent applicable, the dimensional symbols and definitions follow those of the SNAME notation given in the preceding pages. The symbols for the nondimensional form of the various "bis" system quantities are identified by double prime (") to distinguish them from the corresponding SNAME (single prime) coefficients.

Symbol	Nondimensional Form	Definition
c	$c'' = \frac{c}{L^{1/2} g^{1/2}}$	Flow velocity past rudder
c_{nn}	$c_{nn}'' = \frac{c_{nn}}{L^{1/2} g^{-1/2}}$	Coefficient representing c as a function of propeller revolution rate n squared
$c_{\|n\|n}$	$c_{\|n\|n}'' = \frac{c_{\|n\|n}}{L^{1/2} g^{-1/2}}$	Coefficient representing c as a function of $\|n\|n$
c_{un}	$c_{un}'' = \frac{c_{un}}{L^{1/2} g^{-1/2}}$	Coefficient representing c as a function of the product of velocity component u and n
c_{uu}	$c_{uu}'' = \frac{c_{uu}}{L^{-1/2} g^{-1/2}}$	Coefficient representing c as a function u^2
I_z	$I_z'' = \frac{I_z}{mL^2}$	Moment of inertia of ship about z axis
k_p	$k_p'' = \frac{k_p}{L^2}$	Radius of gyration of propulsion system about shaft centerline
k_z	$k_z'' = \frac{k_z}{L^2}$	Radius of gyration of ship about z axis
m	$m'' = \frac{m}{\rho V} = 1$	Mass of ship
n	$n'' = \frac{n}{L^{-1/2} g^{1/2}}$	Propeller revolution rate
N	$N'' = \frac{N}{mgL}$	Hydrodynamic moment component about z axis (yawing moment)
$N_{c\|c\|\delta}$	$N_{c\|c\|\delta}'' = \frac{N_{c\|c\|\delta}}{m}$	Coefficient used in representing N as a function of $c\|c\|$ and rudder angle δ
$N_{c\|c\|\beta\|\beta\|\|\delta}$	$N_{c\|c\|\beta\|\beta\|\|\delta}'' = \frac{N_{c\|c\|\beta\|\beta\|\|\delta}}{m}$	Coefficient used in representing N as a function of $c\|c\|\beta\|\beta\|\|\delta\|$
$N_{c\|c\|\beta\|\beta\|\|\delta\|\zeta}$	$N_{c\|c\|\beta\|\beta\|\|\delta\|\zeta}'' = \frac{N_{c\|c\|\beta\|\beta\|\|\delta\|\zeta}}{m}$	Supplementary coefficient used in representing $N_{c\|c\|\beta\|\beta\|\|\delta\|}$ as a function of shallow-water depth parameter ζ (where $\zeta \neq 0$)
$N_{\dot{r}}$	$N_{\dot{r}}'' = \frac{N_{\dot{r}}}{mL^2}$	Coefficient used in representing N as a function of $\dot{r}$
$N_{r\zeta}$	$N_{r\zeta}'' = \frac{N_{r\zeta}}{mL^2}$	Supplementary coefficient used in representing $N_{\dot{r}}$ as a function of ζ (where $\zeta \neq 0$)
$N_{\|r\|r}$	$N_{\|r\|r}'' = \frac{N_{\|r\|r}}{mL^2}$	Second order coefficient used in representing N as a function of r
N_T	$N_T'' = \frac{N_T}{mgL}$	Yawing moment due to propeller force
N_{ur}	$N_{ur}'' = \frac{N_{ur}}{mL}$	First order coefficient used in representing N as a function of ur
$N_{ur\zeta}$	$N_{ur\zeta}'' = \frac{N_{ur\zeta}}{mL}$	Supplementary coefficient used in representing N_{ur} as a function of ζ (where $\zeta \neq 0$)

N_{uur}	$N_{uur}'' = \frac{N_{uur}}{mL^{\frac{1}{2}}g^{-\frac{1}{2}}}$	Coefficient used in representing N as a function of the product u^2r
N_{uv}	$N_{uv}'' = \frac{N_{uv}}{m}$	First order coefficient used in representing N as a function of uv
$N_{uv\zeta}$	$N_{uv\zeta}'' = \frac{N_{uv\zeta}}{m}$	Supplementary coefficient used in representing N_{uv} as a function of ζ (where $\zeta \neq 0$)
N_{uuv}	$N_{uuv}'' = \frac{N_{uuv}}{mL^{-\frac{1}{2}}g^{-\frac{1}{2}}}$	Coefficient used in representing N as a function of the product u^2v
$N_{\dot{v}}$	$N_{\dot{v}}'' = \frac{N_{\dot{v}}}{mL}$	Coefficient used in representing N as a function of $\dot{v}$
$N_{\|v\|r}$	$N_{\|v\|r}'' = \frac{N_{\|v\|r}}{mL}$	Coefficient used in representing N as a function of $\|v\|r$
$N_{v\|r\|}$	$N_{v\|r\|}'' = \frac{N_{v\|r\|}}{mL}$	Coefficient used in representing N as a function of $v\|r\|$
$N_{\|v\|r\zeta}$	$N_{\|v\|r\zeta}'' = \frac{N_{\|v\|r\zeta}}{mL}$	Supplementary coefficient used in representing $N_{\|v\|r}$ as a function of ζ (where $\zeta \neq 0$)
$N_{v\|v\|}$	$N_{v\|v\|}'' = \frac{N_{v\|v\|}}{m}$	Second order coefficient used in representing N as a function of v
Q	$Q'' = \frac{Q}{mgL}$	Torque about propeller shaft
Q^F	$Q^{F''} = \frac{Q^F}{mgL}$	Torque about propeller shaft due to mechanical friction
Q_n^E	$Q_n^{E''} = \frac{Q_n^E}{mg^{\frac{1}{2}}L^{\frac{1}{2}}}$	Coefficient used in representing engine torque as a function of n
$Q_{\dot{n}}$	$Q_{\dot{n}}'' = \frac{Q_{\dot{n}}}{mL^2}$	Coefficient used in representing propeller torque as a function of $\dot{n}$
Q_{nn}	$Q_{nn}'' = \frac{Q_{nn}}{mL^2}$	Coefficient used in representing propeller torque as a function of n^2
$Q_{\|n\|n}$	$Q_{\|n\|n}'' = \frac{Q_{\|n\|n}}{mL^2}$	Coefficient used in representing propeller torque as a function of $\|n\|n$
Q_{un}	$Q_{un}'' = \frac{Q_{un}}{mL}$	Coefficient used in representing propeller torque as a function of un
Q_{uu}	$Q_{uu}'' = \frac{Q_{uu}}{m}$	Coefficient used in representing propeller torque as a function of u^2
Q_k^E	$Q_k^{E''} = \frac{Q_k^E}{mgL}$	Engine torque due to output torque ratio
r	$r'' = \frac{r}{L^{-\frac{1}{2}}g^{\frac{1}{2}}}$	Angular velocity component about z axis relative to fluid (yaw)
$\dot{r}$	$\dot{r}'' = \frac{\dot{r}}{L^{-1}g}$	Angular acceleration component about z axis relative to fluid

T	$T' = \frac{T}{mg}$	Propeller thrust
T_{nn}	$T_{nn}' = \frac{T_{nn}}{mL}$	Coefficient used in representing propeller thrust as a function of n^2
$T_{\|n\|n}$	$T_{\|n\|n}' = \frac{T_{\|n\|n}}{mL}$	Coefficient used in representing propeller thrust as a function of $\|n\|n$
T_{un}	$T_{un}' = \frac{T_{un}}{m}$	Coefficient used in representing propeller thrust as a function of un
T_{uu}	$T_{uu}' = \frac{T_{uu}}{mL^{-1}}$	Coefficient used in representing propeller thrust as a function of u^2
U	$U' = \frac{U}{L^{1/2}\, g^{1/2}}$	Linear velocity of origin of body axis relative to fluid
u	$u' = \frac{u}{L^{1/2}\, g^{1/2}}$	Component of U in direction of x axis
$\dot{u}$	$\dot{u}' = \frac{\dot{u}}{g}$	Time rate of change of u in direction of x axis
v	$v' = \frac{v}{L^{1/2}\, g^{1/2}}$	Component of U in direction of y axis
$\dot{v}$	$\dot{v}' = \frac{\dot{v}}{g}$	Time rate of change of v in direction of y axis
X	$X' = \frac{X}{mg}$	Hydrodynamic force component along x axis (longitudinal or axial force)
$X_{c\|c\|\delta\delta}$	$X_{c\|c\|\delta\delta}' = \frac{X_{c\|c\|\delta\delta}}{mL^{-1}}$	Coefficient used in representing X as a function of $c\|c\|\delta^2$
$X_{c\|c\|\beta\delta}$	$X_{c\|c\|\beta\delta}' = \frac{X_{c\|c\|\beta\delta}}{mL^{-1}}$	Coefficient used in representing X as a function of $c\|c\|\beta\delta$
X_{rr}	$X_{rr}' = \frac{X_{rr}}{mL}$	Second order coefficient used in representing X as a function of r. First order coefficient is zero.
$X_{\dot{u}}$	$X_{\dot{u}}' = \frac{X_{\dot{u}}}{m}$	Coefficient used in representing X as a function of $\dot{u}$
$X_{\dot{u}\zeta}$	$X_{\dot{u}\zeta}' = \frac{X_{\dot{u}\zeta}}{m}$	Supplementary coefficient used in representing $X_{\dot{u}}$ as a function of ζ (where $\zeta \neq 0$)
X_{uu}	$X_{uu}' = \frac{X_{uu}}{mL^{-1}}$	Second order coefficient used in representing X as a function of u in the nonpropelled case. First order coefficient is zero
$X_{uu\zeta}$	$X_{uu\zeta}' = \frac{X_{uu\zeta}}{mL^{-1}}$	Supplementary coefficient used in representing X_{uu} as a function of ζ (where $\zeta \neq 0$)
X_{uuuu}	$X_{uuuu}' = \frac{X_{uuuu}}{mL^{-2}\, g^{-1}}$	Coefficient used in representing X as a function of u^4
$X_{u\|v\|vv}$	$X_{u\|v\|vv}' = \frac{X_{u\|v\|vv}}{mL^{-2}\, g^{-1}}$	Coefficient used in representing X as a function of $u\|v\|v^2$

X_{vr}	$X_{vr}'' = \frac{X_{vr}}{m}$	Coefficient used in representing X as a function of the product vr
$X_{vr\zeta}$	$X_{vr\zeta}'' = \frac{X_{vr\zeta}}{m}$	Supplementary coefficient used in representing X_{vr} as a function of ζ (where $\zeta \neq 0$)
X_{vv}	$X_{vv}'' = \frac{X_{vv}}{mL^{-1}}$	Second order coefficient used in representing X as a function of v. First order coefficient is zero.
$X_{vv\zeta\zeta}$	$X_{vv\zeta\zeta}'' = \frac{X_{vv\zeta\zeta}}{mL^{-1}}$	Supplementary coefficient used in representing X_{vv} as a function of ζ^2 (where $\neq 0$)
Y	$Y'' = \frac{Y}{mg}$	Hydrodynamic force component along x axis (lateral force)
$Y_{c\|c\|\delta}$	$Y_{c\|c\|\delta}'' = \frac{Y_{c\|c\|\zeta}}{mL^{-1}}$	Coefficient used in representing Y as a function of c|c| and rudder angle δ
$Y_{c\|c\|\beta\|\beta\|\|\delta\|}$	$Y_{c\|c\|\beta\|\beta\|\|\delta}'' = \frac{Y_{c\|c\|\beta\|\beta\|\|\delta}}{mL^{-1}}$	Coefficient used in representing Y as a function of $c\|c\|\beta\|\beta\|\|\delta\|$
$Y_{c\|c\|\beta\|\beta\|\|\delta\|\zeta}$	$Y_{c\|c\|\beta\|\beta\|\|\delta\|\zeta}'' = \frac{Y_{c\|c\|\beta\|\beta\|\|\delta\|\zeta}}{mL^{-1}}$	Supplementary coefficient used in representing $Y_{c\|c\|\beta\|\beta\|\|\delta\|}$ as a function of shallow water depth parameter ζ (where $\zeta \neq 0$)
Y_r	$Y_r'' = \frac{Y_r}{mL}$	Coefficient used in representing Y as a function of r
$Y_{\|r\|r}$	$Y_{\|r\|r}'' = \frac{Y_{\|r\|r}}{mL}$	Second order coefficient representing Y as a function of r
Y_T	$Y_T'' = \frac{Y_T}{mg}$	Lateral force due to propeller thrust
Y_{ur}	$Y_{ur}'' = \frac{Y_{ur}}{m}$	First order coefficient used in representing Y as a function of ur
$Y_{ur\zeta}$	$Y_{ur\zeta}'' = \frac{Y_{ur\zeta}}{m}$	Supplementary coefficient used in representing Y_{ur} as a function of ζ (where $\zeta \neq 0$)
Y_{uur}	$Y_{uur}'' = \frac{Y_{uur}}{mL^{-\frac{1}{2}}g^{-\frac{1}{2}}}$	Coefficient used in representing Y as a function of u^2r
Y_{uv}	$Y_{uv}'' = \frac{Y_{uv}}{mL^{-1}}$	First order coefficient used in representing Y as a function of uv
$Y_{uv\zeta}$	$Y_{uv\zeta}'' = \frac{Y_{uv\zeta}}{mL^{-1}}$	Supplementary coefficient used in representing Y_{uv} as a function of ζ (where $\zeta \neq 0$)
Y_{uuv}	$Y_{uuv}'' = \frac{Y_{uuv}}{mL^{-\frac{1}{2}}g^{-\frac{1}{2}}}$	Coefficient used in representing Y as a function of u^2v
$Y_{\dot{v}}$	$Y_{\dot{v}}'' = \frac{Y_{\dot{v}}}{m}$	Coefficient used in representing Y as a function of $\dot{v}$

$Y_{\dot{v}\zeta}$	$Y_{\dot{v}\zeta}'' = \frac{Y_{\dot{v}\zeta}}{m}$	Supplementary coefficient used in representing $Y_{\dot{v}}$ as a function of ζ (where $\zeta \neq 0$)
$Y_{v\|r\|}$	$Y_{v\|r\|}'' = \frac{Y_{v\|r\|}}{m}$	Coefficient used in representing Y as a function of $v\|r\|$
$Y_{\|v\|r}$	$Y_{\|v\|r}'' = \frac{Y_{\|v\|r}}{m}$	Coefficient used in representing Y as a function of $\|v\|r$
$Y_{v\|v\|}$	$Y_{v\|v\|}'' = \frac{Y_{v\|v\|}}{mL^{-1}}$	Second order coefficient used in representing Y as a function of v
$Y_{v\|v\|\zeta}$	$Y_{v\|v\|\zeta}'' = \frac{Y_{v\|v\|}}{mL^{-1}}$	Supplementary coefficient used in representing $Y_{v\|v\|}$ as a function of ζ (where $\zeta \neq 0$)
γ		Constant of proportionality in autopilot system
δ^*		Rudder deflection
δ^*		Rudder angle ordered by autopilot
σ		Constant of proportionality in autopilot system
1	$\zeta = \frac{T}{H - T}$	Shallow-water depth (under-keel clearance) parameter
$\dot{\psi}$	$\dot{\psi}'' = \frac{\dot{\psi}}{L^{-\frac{1}{2}}g^{\frac{1}{2}}}$	Rate of change of heading
$\ddot{\psi}$	$\ddot{\psi}'' = \frac{\ddot{\psi}}{L^{-1}g}$	Rate of change of $\dot{\psi}$

APPENDIX C

PRESENTATION OF A NUMBER OF REPRESENTATIVE SHIP MANEUVERING MATHEMATICAL MODELS CURRENTLY IN USE

The mathematical models are presented as received from contributors.

MATHEMATICAL SHIP MANEUVERING MODEL RECENTLY DEVELOPED AT THE MASSACHUSETTS INSTITUTE OF TECHNOLOGY

The form of the equations of motion used at MIT to simulate ship maneuvering responses to rudder and propeller actions were developed from sound hydrodynamic principles and further refined based on the system identification analysis of the data obtained from the Esso Osaka maneuvering trials.

As a result of the ship losing so much speed in a turn at the same time that the propeller maintained the original RPM, the speed loss could no longer be considered as a variable which could be validly expanded through the cubic term. Hence, the X equation is of the form of propeller effective thrust minus the total effective drag in its functional non-linear relationship. In addition, all rudder forces are expressed in terms of the effective velocity over the rudder, c, (includes race effect of propeller) and the effective angle of attack on the rudder, e. This represents the true hydrodynamic picture and eliminates many non-linear terms which appear purely from the mathematical concept of a Taylor expansion. The use of the cubic term $\overline{r^2 v_r}$ to represent all the cubic terms in r and v results from the basic response of ships which show a direct relationship between r and v when r and v are large (tight turns). This eliminates three of the cubic terms in the equations. Otherwise, the terms of rv^2, v^3, and r^3 would normally appear.

Figures 1a, 1b, and 1c describe the equations used in the simulation model, the solution of the equations, and the definition of the terms used in the equations. The hydrodynamic forces are expressed in terms of u_r and v_r, where the subscript r refers to speed relative to the water. Without the subscript r, the u and v refer to speed over the ground (the speed measured during the trials).

$$\dot{u} = \dot{u}_r - u_c \cdot r \cdot \sin(\psi - \alpha)$$

$$\dot{u}_r = \frac{f_1}{m - X_{\dot{u}_r}}$$

$$\dot{v} = \dot{v}_r - u_c \cdot r \cdot \cos(\psi - \alpha)$$

$$\dot{v}_r = \frac{1}{f_4}\left[(I_z - N_{\dot{r}})f_2 - (mx_G - Y_{\dot{r}})f_3\right]$$

$$\dot{r} = \frac{1}{f_4}\left[(m - Y_{\dot{v}_r})\, f_3 - (mx_G - N_{\dot{v}_r})f_2\right]$$

where

$$f_1 = \eta_1'\left[\frac{\rho}{2}L^2\right]u_r^2 + \eta_2'\left[\frac{\rho}{2}L^3\right]nu_r + \eta_3'\left[\frac{\rho}{2}L^4\right]n^2 - C_R'\left[\frac{\rho}{2}Su_r^2\right] + X_{v_r^2}'\left[\frac{\rho}{2}L^2\right]v_r^2$$

$$+ X_{e^2}'\left[\frac{\rho}{2}L^2c^2\right]e^2 + (X_{r^2}' + m')x_G'\left[\frac{\rho}{2}L^4\right]r^2 + (X_{v_r r} + m')\left[\frac{\rho}{2}L^3\right]v_r r$$

$$+ X_{v_r^2 r^2}'\left[\frac{\rho}{2}L^4 U_r^{-2}\right]v_r^2 r^2$$

u_r = surge speed relative to water
v_r = sway speed relative to water
} similarly for $\dot{u}_r$ and $\dot{v}_r$

e = effective rudder angle = $\delta\frac{v_c}{c} + \frac{rL}{2c}$

c = weighted average flow speed over rudder

$$= \sqrt{\frac{A_D}{A_R}\left[(1-w)u_r + ku_{A_\infty}\right]^2 + \frac{A_R - A_D}{A_R}(1-w)^2 u_r^2}$$

c_0 is the equilibrium condition of c for the speed u, when $K_T = K_{T_0}$, the propeller thrust coefficient to produce an equilibrium with drag at forward speed u_r. $\left(\frac{u_r}{nD} = \frac{u_{r_0}}{n_0 D}\right)$

$$U_r = \sqrt{u_r^2 + v_r^2}$$

$$u_{A_\infty} \quad -(1-w)u_r + \sqrt{(1-w)^2 u_r^2 + \frac{8K_T}{\pi}(nD)^2}$$

$$\rho n^2 D^4 K_T(1-t) = \eta_1 u_r^2 + \eta_2 n u_r + \eta_3 n^2$$

t = thrust deduction factor
w = wake fraction

Figure 1a. Derived form and solution of the simulation equations.

$$f_2 = Y'_{\dot{v}}\left[\frac{\rho}{2} L^2 \left(\frac{U_{Am}}{2}\right)^2\right] + \{Y'_{v_r}\left[\frac{\rho}{2} L^2 U_r\right] v_r - Y'_{\delta}(c-c_0)\frac{\rho}{2} L^2 v_r\}$$

$$+\{(Y'_r - m'u'_r)\left[\frac{\rho}{2} L^3 U_r\right] r + \frac{Y'_{\delta}}{2}(c-c_0)\frac{\rho}{2} L^3 r\} + Y'_{\delta}\left[\frac{\rho}{2} L^2 c^2\right]\delta$$

$$+\overline{Y'_{r^2 v_r}}\left[\frac{\rho}{2} L^4 U_r^{-1}\right] r^2 v_r \quad + Y'_{e^3}\left[\frac{\rho}{2} L^2 c^2\right] e^3$$

$$f_3 = N'_{\dot{v}}\left[\frac{\rho}{2} L^3 \left(\frac{U_{Am}}{2}\right)^2\right] + \{N'_{v_r}\left[\frac{\rho}{2} L^3 U_r\right] v_r - N'_{\delta}(c-c_0)\frac{\rho}{2} L^3 v_r\}$$

$$+\{(N'_r - m'x'_G u'_r)\left[\frac{\rho}{2} L^4 U_r\right] r + \frac{1}{2} N'_{\delta}(c-c_0)\frac{\rho}{2} L^4 r\} + N'_{\delta}\left[\frac{\rho}{2} L^3 c^2\right]\delta$$

$$+\overline{N'_{r^2 v_r}}\left[\frac{\rho}{2} L^5 U_r^{-1}\right] r^2 v_r \quad + N'_{e^3}\left[\frac{\rho}{2} L^3 c^2\right] e^3$$

$$f_4 = (m' - Y'_{\dot{v}_r})\left[\frac{\rho}{2} L^3\right]\left(I'_z - N'_{\dot{r}}\right)\left[\frac{\rho}{2} L^5\right] - \left(m' x'_G - N'_{\dot{v}_r}\right)\left[\frac{\rho}{2} L^4\right]\left(m' x'_G - Y'_{\dot{r}}\right)\left[\frac{\rho}{2} L^4\right]$$

$u_r = u - u_c \cos(\psi - \alpha)$

$v_r = v + u_c \sin(\psi - \alpha)$

u and v refer to speed over the ground.

Figure 1b. Derived form and solution of the simulation equations.

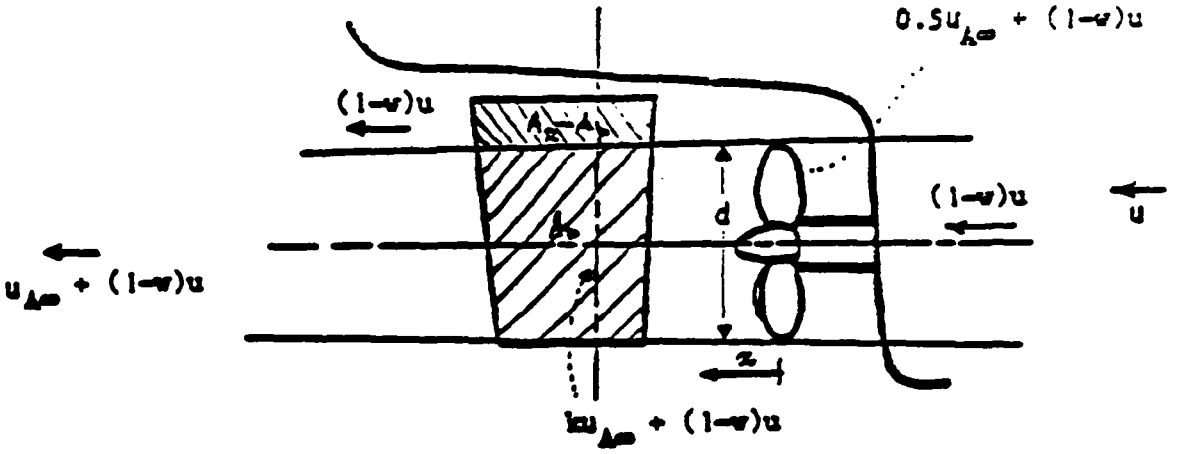

Geometrical relationship between the propeller and the rudder. Propeller race according to momentum theory.

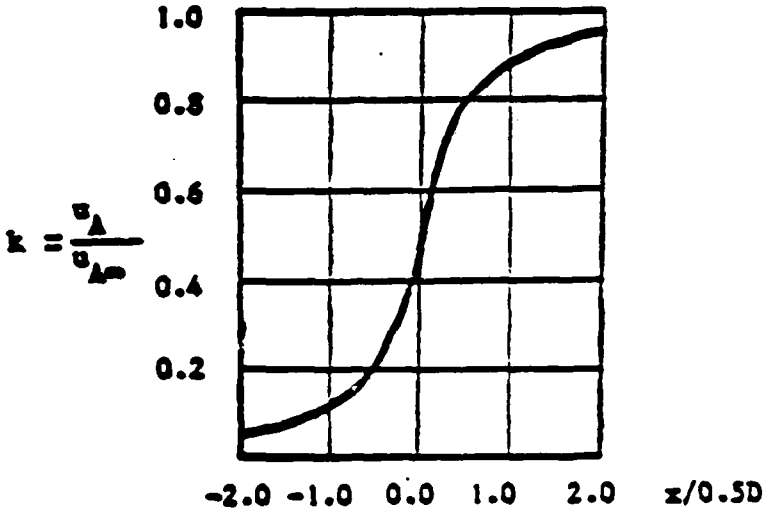

The mean axial velocity induced by a semi-infinite tube of ring vortices determined by the Law of Biot-Savart. (ref. Smitt & Chislett[1974])

Figure 1c. Description of the terms in the formulation of the velocity c (inflow velocity over the rudder).

DESCRIPTION OF MATHEMATICAL MODELING FOR SHIP MANEUVERING AS DEVELOPED AT THE NETHERLANDS SHIP MODEL BASIN

General set-up of N.S.M.B.'s mathematical model for simulating the ship's manoeuvrability.

1. The manoeuvres of the ship in the horizontal plane are described by the differential equations in a system of co-ordinates fixed to the ship

$$\begin{aligned} m\frac{du}{dt} - mrv &= X \\ m\frac{dv}{dt} + mru &= Y \\ I\frac{dr}{dt} &= M \end{aligned} \qquad (1)$$

in which:

m = mass of the ship (kg)
I = moment of inertia around the vertical axis through the centre of gravity ($kg.m^2$)
u = ship's velocity in the longitudinal direction (m/sec.)
v = ship's lateral velocity (m/sec.)
s = absolute velocity of the ship = $\sqrt{u^2+v^2}$
r = $\frac{d\psi}{dt}$ = rotational velocity (rad./sec.)

The generalized force F ≡ (X, Y, M)
is described by:

$$F = F_s + F_e \qquad (2)$$

in which:

F_s = the hydrodynamic forces inherent to the ship.

$$F_s = F\ (\dot{u},\dot{v},\dot{r},u,v,r,n_m,\delta) \qquad (3)$$

with n_m = revolutions per minute for each of the m-propellers for instance n_1 and n_2 for two main propellers and n_3 for one thruster.
δ = rudder angle.

In equation (2):

F_e = the external force due to environmental factors: wind waves, current, bank suction, tugboats, passing ships, etc.
(It is to be noted that F_e often is effected by the interaction with the ship's state variables $\dot{u},\dot{v},\dot{r},u,v,r$, etc.).

All factors in the complete description from the combination of equation (1) and (2) are considered to be quasi-stationary.

2. The force F_s is further reduced to:

$$F_s = F(\dot{u},\dot{v},\dot{r}) + F(u,v,r,n,\delta) \qquad (4)$$

in wnich $F(\dot{u},\dot{v},\dot{r})$ correspond to the added mass forces.

The force $F(u,v,r,n,\delta)$ in equation (4) is described by the summation of

$$F(u,v,r,n,\delta) = F_1(\delta) + F_2(v) + F_3(r) \qquad (5)$$

in which:

$F_1(\delta) = F(u,v=0,r=0,n,\delta)$ for the straight ahead condition thus that $F_1(\delta)$ depends on u and n in addition to δ.
$F_2(v) = F(u,v,r=0,n,\delta)$ for the condition at a straight track thus that $F_2(v)$ depends on the combined effect of u and n in addition to v and the interaction with δ ($-180^\circ < \text{arctg}\frac{v}{u} \leq +180^\circ$) and the interaction with δ
$F_3(r) = F(u,v,r,n,\delta)$ for the turning condition thus that $F_3(r)$ depends on the combined effect of u and n in addition to r and the interaction with v and δ.

3. The environmental effects are taken into account in the following way: Due to restriction of the waterdepth all information presented in 2. is described for the waterdepth considered.

Due to restrictions of the channel width all relevant factors mentioned in 2 are described for the waterwidth concerned while additional bank suction forces are introduced.
The influence of current is introduced by forces which in combination with the information in 2 are based on the relative motion concept.
Windforces, tugboats forces, forces due to passing ships are added separately to the forces in equation 2.

MATHEMATICAL MODEL FOR SHIP MANEUVERING
CONTRIBUTED BY KYUSHU UNIVERSITY, JAPAN

Appendix D

OUTLINE OF BASIC MATHEMATICAL MODEL*

by S. INOUE

A set of coordinate axes with origin fixed at the center of gravity of the ship (denoted with G hereinafter), as shown in Fig. 1, is used to describe the ship maneuvering motion. Longitudinal and transverse horizontal axes are represented by the x and y-axes respectively, and the z-axis is chosen so as to be perpendicular to the xy-plane (downward positive). By reference to this coordinate system G-xyz, the basic equations of the ship maneuvering motion can be written in the following form taking the coupling effects due to roll and propeller revolution on the horizontal motions into consideration.

$$\begin{aligned}
&\text{Surge} : m(\dot{u} - vr) = X_H + X_P + X_R \\
&\text{Sway} : m(\dot{v} + ur) = Y_H + Y_R \\
&\text{Yaw} : I_{zz}\dot{r} = N_H + N_R \\
&\text{Roll} : I_{xx}\ddot{\phi} = K_H + K_R \\
&\text{Propeller Revolution} : 2\pi I_{pp}\dot{n} = Q_E + Q_P
\end{aligned} \tag{1}$$

where the subscripts H, P, R and E denote Hull, Propeller, Rudder and Engine respectively.

---

* Inoue, S and others : A Practical Calculation Method of ship Maneuvering Motion, International Shipbuilding Progress, Vol. 28, No. 325, 1981.

The hydrodynamic forces acting on ship hull (without propeller and rudder) can be written in the form

$$
\begin{aligned}
X_H &= -m_x\dot{u} + C_m m_y vr + X(u) \\
Y_H &= -m_y\dot{v} - m_x ur + \tfrac{1}{2}\rho L d V^2 [Y'_v v' + Y'_r r' + Y'_{v|v|} v'|v'| \\
&\quad + Y'_{v|r|} v'|r'| + Y'_{r|r|} r'|r'| + Y'_\phi \phi + Y'_{v|\phi|} v'|\phi| \\
&\quad + Y'_{r|\phi|} r'|\phi|] \\
N_H &= -J_{zz}\dot{r} + \tfrac{1}{2}\rho L^2 d V^2 [N'_v v' + N'_r r' + N'_{vvr} v'^2 r' \\
&\quad + N'_{vrr} v' r'^2 + N'_{r|r|} r'|r'| + N'_\phi \phi + N'_{v|\phi|} v'|\phi| \\
&\quad + N'_{r|\phi|} r'|\phi|] + Y_H \cdot x_m \\
K_H &= -J_{xx}\ddot{\phi} - N(\dot{\phi}) - W \cdot GZ(\phi) - Y_H \cdot z_H .
\end{aligned}
\tag{2}
$$

The hydrodynamic coefficients in Eq. (2) are determined by estimate formulae or estimate charts. For example, the estimate formulae for the linear derivatives of the lateral force and the yaw moment can be written in the form

$$
\begin{aligned}
Y'_v &= [a_1 k + f(C_B B/L)](1 + b_1 \tau') \\
Y'_r &= a_2 k (1 + b_2 \tau') \\
Y'_\phi &= Y'_{v|\phi|} = Y'_{r|\phi|} = 0 \\
N'_v &= a_3 k (1 + b_3 \tau') \\
N'_r &= (a_4 k + a_5 k^2)(1 + b_4 \tau') \\
N'_\phi &= c_1 \\
N'_{v|\phi|} &= c_2 N'_v \\
N'_{r|\phi|} &= c_3 N'_r
\end{aligned}
\tag{3}
$$

$$
\text{where } k = 2d/L,\ \tau' = \tau/d \tag{4}
$$

and a_1, a_2, ---, b_1, ---, c_1, --- etc. are the constant.

X_P and Q_P are the propeller thrust and the propeller torque respectively, and they can be writen in the form

$$X_P = (1 - t_{PO}) \cdot \rho n^2 D^4 K_T(J_P)$$
$$Q_P = -2\pi J_{PP}\dot{n} - \rho n^2 D^5 K_Q(J_P). \tag{5}$$

The thrust coefficient $K_T(J_P)$ and the torque coefficient $K_Q(J_P)$ are obtained with the propeller characteristics curves as functions of the advance constant J_P, which is expressed as

$$J_P = u(1 - w_P)/(nD). \tag{6}$$

The effective propeller wake fraction in the maneuvering motion, w_P, is computed by

$$w_P = w_{PO} \exp(K_1 \beta_P{}^2) \tag{7}$$

where K_1 is the constant and β_P is defined as $\beta_P = \beta - x'_P r'$.

The rudder forces can be written in the form

$$X_R = -F_N \sin \delta$$
$$Y_R = -(1 + a_H) F_N \cos \delta$$
$$N_R = -(1 + a_H) x_R F_N \cos \delta \tag{8}$$
$$K_R = (1 + a_H) z_R F_N \cos \delta.$$

The hydrodynamic forces induced on ship hull by rudder action are inculded in Eq. (8), and for instance Y-force is described in the form of $a_H F_N \cos \delta$. The rudder normal force F_N is expressed in the following form with the concepts of the effective rudder inflow speed V_R and the effective rudder inflow angle α_R.

$$F_N = \frac{1}{2}\rho \frac{6.13\Lambda}{\Lambda + 2.25} A_R V_R{}^2 \sin \alpha_R. \tag{9}$$

The effective rudder inflow speed V_R can be expressed in the form

$$V_R = (1 - w_R)[1 + K_2 g(s)]^{1/2}. \tag{10}$$

The term $K_2 g(s)$, where K_2 is the constant and s is the slip ratio, represents the effect of the propeller slip-stream on V_R, and the effective rudder wake fraction in the maneuvering, w_R, is computed in the same manner as the effective propeller wake fraction, namely by

$$w_R/w_{RO} = w_P/w_{PO} = \exp(K_1 \beta_P^2). \tag{11}$$

The effective rudder inflow angle α_R can be expressed in the form

$$\alpha_R = \delta + \delta_O - \gamma \beta'_R. \tag{12}$$

The flow-rectification coefficient γ can be written

$$\gamma = C_P \cdot C_S \tag{13}$$

and β'_R is defined as $\beta'_R = \beta - 2x'_R r'$.

Appendix : Nomenclature

A_R = rudder area

a_H = ratio of hydrodynamic force, induced on ship hull by rudder action, to rudder force

B : breadth of ship

C_B : block coefficient

C_P : propeller flow-rectification coefficient

C_S : ship hull flow-rectification coefficient

D = propeller diameter

d = draft of ship (mean draft)

F_N = rudder normal force

$GZ(\phi)$ = restoring moment lever of roll

I_{xx}, I_{zz} = moment of inertia of ship with respect to x and z-axes respectively

I_{pp} = moment of rotary inertia of propeller-shafting system

J_P = advance constant

J_{xx}, J_{zz} = added moment of inertia of ship with respect to x and z-axes respectively

J_{pp} = added moment of rotary inertia of propeller

L = length of ship (between perpendiculars)

m = mass of ship

m_x, m_y = added mass of ship in x and y- axes direction respectively

$N(\dot{\phi})$ = roll damping moment

n = number of propeller revolution

r = turning rate

r' = dimensionless turning rate (= rL/V)

t_{PO} = thrust deduction coefficient in straight running condition

u = ship speed in x-axis direction

V = ship speed (= $(u^2 + v^2)^{1/2}$)

V_R = effective rudder inflow speed

v = ship speed in y-axis direction

v' = dimensionless ship speed in y-axis direction (= v/V)

W = displacement of ship

w_P = effective propeller wake fraction

w_{PO} = effective propeller wake fraction in straight running condition

w_R = effective rudder wake fraction

w_{RO} = effective rudder wake fraction in straight running condition

x_P = x-coordinate of propeller position

x'_P = dimensionless form of x_P (= x_P/L)

x_R = x-coordinate of point on which rudder force Y_R acts

x'_R = dimensionless form of x_R (= x_R/L)

x_m = x-coordinate of midship

z_H = z-coordinate of point on which lateral force Y_H acts

z_R = z-coordinate of point on which rudder force Y_R acts

α_R = effective rudder inflow angle

β = drift angle (= $-\sin^{-1}v'$)

γ = flow-rectification coefficient

δ = rudder angle

Λ = aspect ratio of rudder

ρ = density of water

τ = trim quantity

ϕ = roll angle

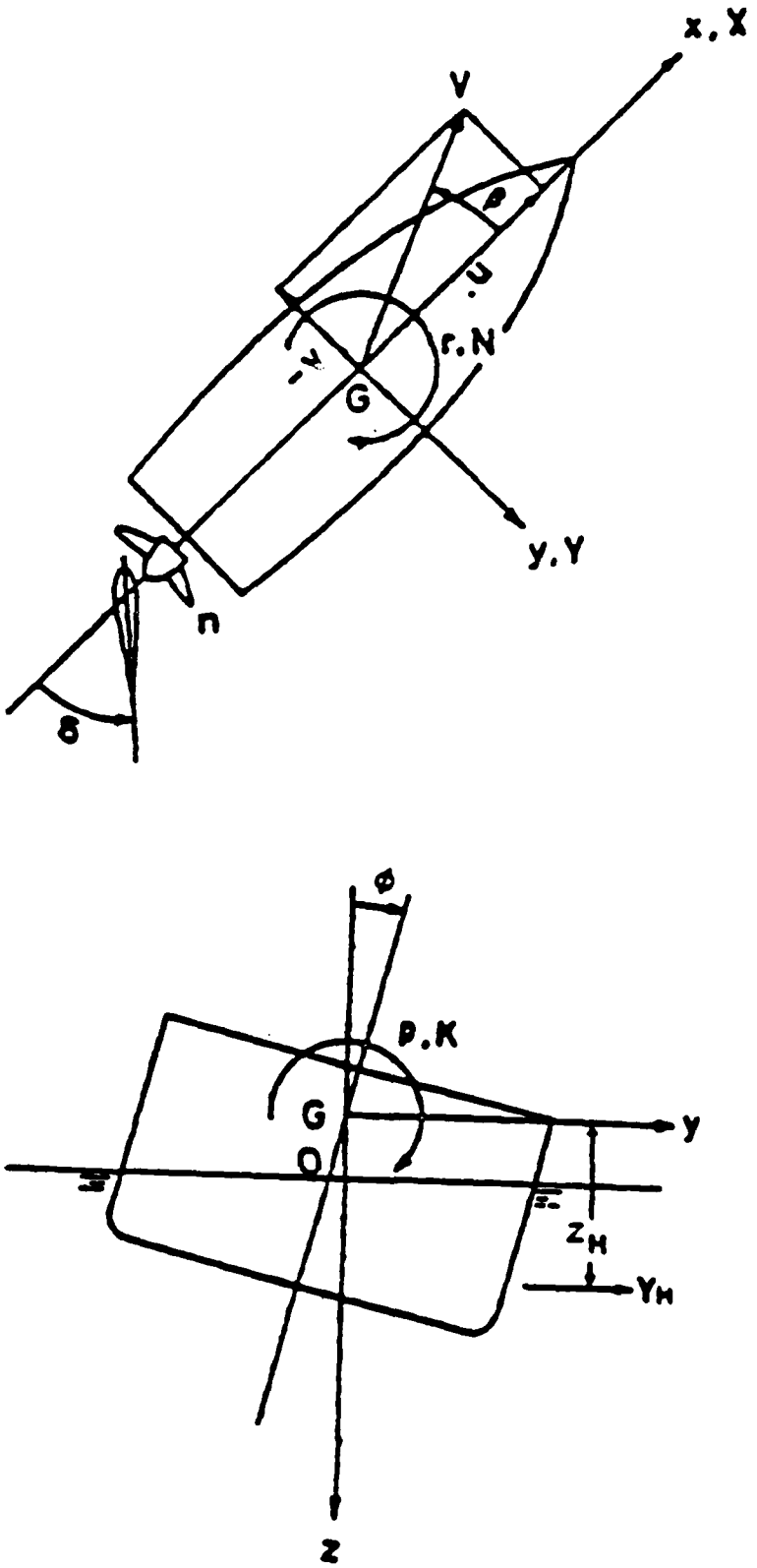

Fig. 1 Co-ordinate system G-xyz

MATHEMATICAL SHIP MANEUVERING MODEL IN RECENT USE AT THE DAVID W. TAYLOR NAVAL SHIP RESEARCH AND DEVELOPMENT CENTER

SHIP MANEUVERING EQUATIONS

The calm water ship maneuvering equations, specified with respect to a right-handed coordinate system fixed in the ship, can be written as

$$m(\dot{u} - vr - x_G r^2) = X,$$

$$m(\dot{v} + ur + x_G \dot{r}) = Y,$$

$$\dot{r} I_z + m x_G (\dot{v} + ur) = N,$$

ignoring roll motion. The origin of the coordinate system is taken at the midship, midbeam position. The nomenclature and coordinate system used is standard and described in References 1, 2 and 3. The determination of the hydrodynamic forces X and Y and moment N is basically from data obtained using the horizontal planar motion mechanism (HPMM), i.e., straight line static and oscillation experiments, supplemented by propulsion analysis work to determine the effects of speed loss, $\underline{u} = u - U_o$, on the X force.

X, Y and N are represented by coefficients, associated with the relevant variables, which are derived by a combination of least square fit curve matching procedures to the experimental data. Guidance as to the type of coefficients to use, along with the general approach to the problem, follows the method specified in Reference 4.

In nondimensional form the equations of motion are specified as:

$$(m' - X'_{\dot{u}})\dot{u}' = F_1(\underline{u}', v', r', \delta) ,$$

$$(m' - Y'_{\dot{v}})\dot{v}' + (m'x'_G - Y'_{\dot{r}})\dot{r}' = F_2(\underline{u}', v', r', \delta) ,$$

$$(m'x'_G - N'_{\dot{v}})\dot{v}' + (I'_z - N'_{\dot{r}})\dot{r}' = F_3(\underline{u}', v', r', \delta) ,$$

where

$$F_1(\underline{u}', v', r', \delta) = X'_o + X'_{\underline{u}}\underline{u}' + X'_{\underline{uu}}\underline{u}'^2 + X'_{\underline{uuu}}\underline{u}'^3 + X'_\delta \delta + X'_{\delta\delta}\delta^2 + X'_{\delta\delta\underline{u}}\delta^2\underline{u}'$$

$$+ X'_{\delta|v|}\delta|v'| + X'_v v' + X'_{vv}v'^2 + X'_{\delta\delta v}\delta^2 v' + X'_{|\delta|v}|\delta|v'$$

$$+ (X'_{rr} + m'x'_G)r'^2 + X'_{rr\underline{u}}r'^2\underline{u}' + (X'_{vr} + m')v'r' + X'_{r\delta}r'\delta + X'_{v\delta}v'\delta ;$$

$$F_2(\underline{u}',v',r',\delta) = Y'_o + Y'_{o\underline{u}}\underline{u}' + Y'_\delta\delta + Y'_{\delta\delta}\delta^2 + Y'_{\delta\delta\delta}\delta^3 + Y'_{\delta v}\delta v' + Y'_{\delta rr}\delta r'^2 + Y'_{\delta|v|}\delta|v'|$$

$$+ Y'_{\delta\underline{u}}\delta\underline{u}' + Y'_{\delta\delta\underline{u}}\delta^2\underline{u}' + Y'_{\delta\delta\delta\underline{u}}\delta^3\underline{u}' + Y'_v v' + Y'_{vv}v' + Y'_{v|v|}v'|v'| + Y'_{vrr}v'r'^2$$

$$+ Y'_{v|r|}v'|r'| + Y'_{v|\delta|}v'|\delta| + Y'_{v\underline{u}}v'\underline{u}' + (Y'_r - m'u')r' + Y'_{rrr}r'^3 + Y'_{rvv}r'v'^2$$

$$+ Y'_{r|v|}r'|v'| + Y'_{r\sqrt{|v|}}r'\sqrt{|v'|} + Y'_{r\underline{u}}r'\underline{u}' + Y'_{\delta vr}\delta v'r' \ ;$$

$$F_3(\underline{u}', v', r', \delta) = N'_o + N'_{o\underline{u}}\underline{u}' + N'_\delta\delta + N'_{\delta\delta}\delta^2 + N'_{\delta\delta\delta}\delta^3 + N'_{\delta v}\delta v' + N'_{\delta rr}\delta r'^2$$

$$+ N'_{\delta|v|}\delta|v'| + N'_{\delta\underline{u}}\delta\underline{u}' + N'_{\delta\delta\underline{u}}\delta^2\underline{u}' + N'_{\delta\delta\delta\underline{u}}\delta^3\underline{u}' + N'_v v' + N'_{vv}v'^2 + N'_{v|v|}v'|v'|$$

$$+ N'_{vrr}v'r'^2 + N'_{v|r|}v'r' + N'_{v|\delta|}v'|\delta| + N'_{v\underline{u}}v'\underline{u}' + (N'_r - m'x'_G u')r' + N'_{rrr}r'^3$$

$$+ N'_{rvv}r'v'^2 + N'_{r|v|}r'|v'| + N'_{r\sqrt{|v|}}r'\sqrt{|v'|} + N'_{r\underline{u}}r'\underline{u}' + N'_{\delta vr}\delta v'r' \ .$$

Not all of the above coefficients will be found necessary for any specific case and only those should be used which enable a good fit to the experimental and propulsion analysis data. Also the limitations of the HPMM, availability of time, etc., will preclude the experimental determination of all the possible coefficients. In this case it is necessary to estimate, or derive by other methods, a coefficient value for important coefficients.

REFERENCES

1. "Principles of Naval Architecture," edited by J.P. Comstock, published by The Society of Naval Architects and Marine Engineers, 1967.

2. Abkowitz, M.A., "Lectures on Ship Hydronamics - Steering and Manoeuvrability," Hydro-Og-Aerodynamisk Laboratory, Lyngby, Denmark, Report No. HY-5, May 1964.

3. "Nomenclature for Treating the Motion of a Submerged Body through a Fluid," SNAME Technical and Research Bulletin No. 1-5, 1952.

4. Smitt, L.W. and M.S. Chislett, "Large Amplitude PMM Tests and Maneuvering Predictions for a Mariner Class Vessel," 10th ONR Symposium on Naval Hydromechanics, Massachusetts Institute of Technology, Boston, June 1974.

MATHEMATICAL MANEUVERING MODEL DEVELOPED AT THE DAVIDSON LABORATORY AND USED IN MANEUVERING SIMULATIONS AT THE MARITIME ADMINISTRATIONS COMPUTER-AIDED OPERATIONS RESEARCH FACILITY (CAORF)

BASIC MATHEMATICAL MODEL

Figure 1 shows the coordinate system used to define ship motions in calm water. Longitudinal and transverse horizontal axes of the ship are represented by the x- and y-axes with origin fixed at the center of gravity. By reference to these body axes, the equations of motion of a ship in the horizontal plane can be written in the form

$$\begin{aligned} I_z \dot{r} &= N && \text{(Yaw)} \\ m(\dot{v} + ur) &= Y && \text{(Sway)} \\ m(\dot{u} - vr) &= X && \text{(Surge)} \end{aligned} \tag{1}$$

where N, Y and X represent total hydrodynamic terms generated by ship motions, rudder, propeller and effects of banks and bottom of narrow waterways.

Hydrodynamic forces are expressed in terms of dimensionless quantities N', Y' and X' based on nondimensionalizing parameters ρ (water density), U (resultant ship velocity relative to the water) and A (reference area = ℓH, ℓ^2 or BH), i.e.,

$$N' = \frac{N}{\frac{\rho}{2} U^2 A \ell}$$

$$Y' = \frac{Y}{\frac{\rho}{2} U^2 A} \tag{2}$$

$$X' = \frac{X}{\frac{\rho}{2} U^2 A}$$

Hydrodynamic coefficients vary with position, attitude, rudder angle, propeller revolution and velocity of the ship. For example, in the case of hydrodynamic yaw moment coefficient

$$N' = N'(v', r'; \delta, y_o', \dot{v}', \dot{r}', n', u') \tag{3}$$

where

$$v' = \frac{v}{U},\ r' = r\frac{\ell}{U},\ y_o' = \frac{Y_o}{\ell},\ n' = \frac{n}{n_e},\ u' = \frac{u}{u_e}$$

$$\dot{v}' = \dot{v}\ell/U^2,\ \dot{r}' = \dot{r}\ell^2/U^2$$

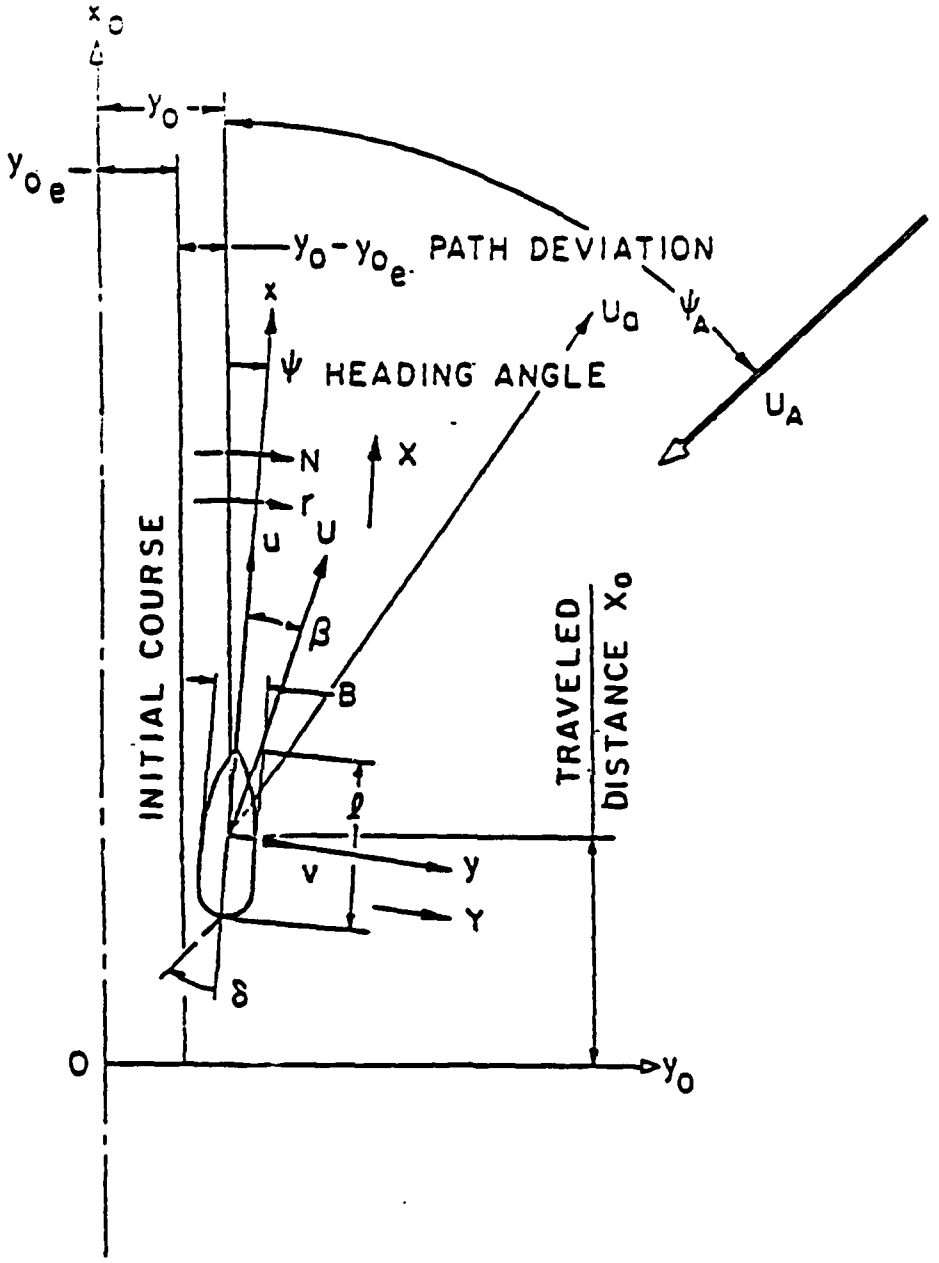

FIG. 1. COORDINATE AXES

THE FIGURE SHOWS THE POSITIVE DIRECTION OF VARIOUS QUANTITIES EXCEPT FOR β

A Taylor series expansion can be made with respect to the point

$$(v' = r' = \delta = y_o' = \dot{v}' = \dot{r}' = 0,\ n = n_e,\ u = u_e)$$

where u_e and n_e are forward speed and propeller revolutions at the equilibrium conditions. The final forms of hydrodynamic terms, such as in Eq. (3), are determined on the basis of the following factors:

(1) *Theoretical considerations of the nature of hydrodynamic forces and moments acting on ships under various conditions (e.g., in canals, in shallow waters and in open deep seas).*

(2) *Examination of captive model test results.*

Finally, the following forms of polynomials were chosen to represent the hydrodynamic forces and moments acting on a ship under straight course equilibrium conditions:

$$\begin{aligned}
N' &= a_o + a_1 v' + a_2 r' + a_3 \delta + a_4 y_o' + a_5 v'^2 r' + a_6 v' r'^2 + a_7 v'^3 + a_8 r'^3 + a_9 \delta^3 \\
&\quad + a_{10} y_o'^3 + a_{11} \dot{r}' + a_{12} \dot{v}' + N_p' + N_a' + N_b' + N_t' + N_m' + N_n' + N_f' + N_c' \\
Y' &= b_o + b_1 v' + b_2 r' + b_3 \delta + b_4 y_o' + b_5 v'^2 r' + b_6 v' r'^2 + b_7 v'^3 + b_8 r'^3 + b_9 \delta^3 \\
&\quad + b_{10} y_o'^3 + b_{11} \dot{r}' + b_{12} \dot{v}' + Y_p' + Y_a' + Y_b' + Y_t' + Y_m' + Y_n' + Y_f' \\
X' &= c_o + c_1 v' r' + c_2 v'^2 + c_3 \delta^2 + c_4 \dot{u}' + X_p' + X_a' + X_t' + X_m' + X_n' + X_f'
\end{aligned} \tag{4}$$

where a_o = initial asymmetry, usually small

$a_1 = N_v'$

$a_2 = N_r'$

$a_3 = N_\delta'$

$a_4 = N_\eta'$

.

.

.

.

.

.

.

X'_p = propeller thrust

X'_a = aerodynamic longitudinal force due to wind

X'_t = longitudinal force due to tugs

X'_m = longitudinal force due to mooring

X'_n = longitudinal force due to anchors

X'_f = longitudinal force due to other forcing functions

Subscripts p,a,b,t,m and n indicate those hydrodynamic terms due to propeller, wind, bow thruster, tugs, mooring and anchors, respectively. These terms are described in detail in later sections.

It should be noted that the above representation of hydrodynamic moment and forces include restricted water effects (bottom and side effects) as described in a later section.

The same form of equation will be valid for the dredged channel in shallow water which can be frequently encountered in the actual operation of recently-built large ships. Since hydrodynamic coefficients are not presently available under these conditions, they will be determined by the proposed captive model testing. Before the completion of captive model tests in dredged channels in shallow waters, a rough estimation of hydrodynamic coefficients will be made for the purpose of simulator development.

Furthermore, the same form of equation will be valid also for backing (although hydrodynamic coefficients are not presently available and will be determined by captive model testing).

The important effects of propeller slip on rudder coefficients are as follows:

$$a_3 = \frac{(1 + k\,s^{1.5})}{(1 + k s_e^{1.5})}\, a_{3_e}$$

$$a_9 = \frac{(1 + k\,s^{1.5})}{(1 + k s_e^{1.5})}\, a_{9_e} \quad , \text{ etc.} \tag{5}$$

and s = propeller slip = $1 - u/pn$

p = propeller pitch

n = propeller revolutions per second

k = semi-empirical constant

subscript e indicates the value at the straight course equilibrium conditions

The hydrodynamic force coefficients of X' differ in form from the lateral force coefficients Y' in Eq.(4), e.g.,

$c_o = X'_o$

$c_1 = X'_{vr}$, etc.

X'_p = propeller thrust

The following rudder control characteristics are employed:

$$\delta_d = a(\psi - \psi_d) + b'\dot{\psi}' + c'(\text{sign})p'_\ell + d'\dot{p}_\ell + \delta_e \qquad (6)$$

where

δ = rudder angle

a = yaw gain constant

b' = yaw-rate gain constant

c' = path-deviation gain constant

d' = path-deviation-rate gain constant

p'_ℓ = length of the perpendicular from the LCG of the ship to the channel centerline, non-dimensionalized in terms of ship length

sign = positive when the ship is proceeding at the righthand side of the channel; negative when the ship is proceeding at the lefthand side of the channel

subscript d indicates the desired value

subscript e indicates the value at the equilibrium condition (i.e., steady straight course condition)

$\dot{\delta}$ = rudder angular velocity (e.g., 2.33 deg/sec)

$|\delta| \leq 35$ degrees

The value with ' (prime) indicates the non-dimensional value based on the ship length used as the reference length. For example, the non-dimensional time t' is equal to tU/ℓ , which is traveled distance in terms of ship length.

$a_{11} = N'_{\dot{r}}$

$a_{12} = N'_{\dot{v}}$

N'_p = moment due to propeller

N'_a = aerodynamic moment due to wind

N'_b = moment generated by bow thruster

N'_t = moment due to tugs

N'_c = moment due to cross flow current

N'_m = moment due to mooring

N'_n = moment due to anchors

N'_f = moment due to other forcing functions

b_o = initial asymmetry, usually small

$b_1 = Y'_v$

$b_2 = Y'_r$

$b_3 = Y'_\delta$

$b_4 = Y'_n$

.

.

.

.

.

.

$b_{11} = Y'_{\dot{r}}$

$b_{12} = Y'_{\dot{v}}$

Y'_p = lateral force due to propeller

Y'_a = aerodynamic side force due to wind

Y'_b = side force generated by bow thruster

Y'_t = side force due to tugs

Y'_m = side force due to mooring

Y'_n = side force due to anchors

Y'_f = side force due to other forcing functions

c_o = resistance coefficient

$c_1 = X'_{vr}$

$c_2 = 1/2\ X'_{vv}$

$c_3 = 1/2\ X'_{\delta\delta}$

$c_4 = X'_{\dot{u}}$

STANDARDIZED DATA SHEET NO.

APPENDIX D

SNAME MATHEMATICAL-MANEUVERING MODEL STANDARDIZED DATA SHEET

FOR

PREPARED BY

The following pages describe the sources and present values for the hydrodynamic coefficients and other data required with the specified equations of motion to perform computer simulation predictions of various maneuvering characteristics of the above ship type. The results of such simulations are also presented, and compared with corresponding full-scale trial data, whenever such data exist and are readily available.

I. DATA SOURCE AND ACQUISITION TECHNIQUE

A. MODEL TEST PROGRAM

SPONSOR:

LABORATORY:

TEST FACILITY:
- SIZE -
- DESCRIPTION -

TEST APPARATUS:

SHIP MODEL PARTICULARS:
- DESIGNATION -
- CONSTRUCTION MATERIAL -
- TURBULENCE STIMULATION DEVICE -

TEST DATE:

TEST CONDITIONS:

TEST PARAMETER RANGE:

η	$\dot{r}'$	ϕ
β	$\dot{v}'$	θ
r'	$v' \mid r' \mid$	Δ
δ_r		

DATA REDUCTION AND ANALYSIS METHODS:

PUBLISHED SOURCES:

I. DATA SOURCE AND ACQUISITION TECHNIQUE (CONTINUED)

B. SHIP MANEUVERING PREDICTIONS

SPONSOR:

SIMULATION FACILITY:

MATHEMATICAL MODEL:

SIMULATED DEFINITIVE MANEUVERS:

PUBLISHED RESULTS:

C. FULL-SCALE MANEUVERING TRIALS AND CORRELATION

SHIP:

TRIALS DATES:

TYPE OF TRIALS:

TRIALS INSTRUMENTATION:

I. DATA SOURCE AND ACQUISITION TECHNIQUE (CONTINUED)

TRIALS CONDITION:

MANEUVERS PERFORMED:

DATA REDUCTION AND ANALYSIS:

PUBLISHED RESULTS:

D. REFERENCES

I. DATA SOURCES AND ACQUISITION TECHNIQUES (CONCLUDED)

D. REFERENCES

II. SHIP GEOMETRY

A. PRINCIPAL GEOMETRIC CHARACTERISTICS

Hull	Ship	Model	Rudder	Ship	Model
L, ft			$\bar{b}$, ft		
B, ft			c_r, ft		
T, ft			c_t, ft		
Trim, ft by stern			A_T, ft^2		
A, tons, lbs			A_F, ft^2		
V, ft^3			A_M, ft^2		
S, ft^2			$\lambda = \bar{b}^2/A_T$		
LCG, ft fwd of AP			Balance, percent		
VCG, ft above			$A_T/L \bullet T$		
L/B			δ_r, deg max.		
B/T			$\dot{\delta}_r$, deg/sec		
C_B					
$C_V(1000)$			Propeller (Rotation -)		
LCG/L			No. of Blades		
Bilge Keels			D, ft		
b, ft			P(0.7 R), ft		
c, ft			P/D		
			D/T		

B. LINES

C. RUDDER DETAILS

III. MATHEMATICAL MODEL

SUMMARY OF EQUATIONS OF MOTION

A. BASIC EQUATIONS	B. SUPPLEMENTARY EQUATIONS
Axial Force	Autopilot
	Wind and wave effects
Lateral Force	
	Other
Yaw Moment	

III. MATHEMATICAL MODEL (CONCLUDED)

NONDIMENSIONAL HYDRODYNAMIC COEFFICIENTS

C. COEFFICIENT VALUES

X - Equation		Y - Equation		N - Equation	
Nomdimensional Coefficient	Value	Nondimensional Coefficient	Value	Nondimensional Coefficient	Value
X'_{u}		Y'_{*}		N'_{*}	
X'_{vr}		Y'_{v}		N'_{v}	
X'_{vv}		Y'_{v}		N'_{v}	
$X'_{\delta r \delta r}$ (η=0)		$Y'_{v\|v\|}$		$N'_{v\|v\|}$	
X'_{rr}		Y'_{r}		N'_{r}	
$X'_{vv\eta}$		$Y'_{r\|r\|}$		$N'_{r\|r\|}$	
$X'_{\delta r \delta r \eta\eta}$		$Y'_{v\|r\|}$		$N'_{v\|r\|}$	
a_1		$Y'_{r\delta r}$		$N'_{r\delta r}$	
b_1		Y'_{r}		N'_{r}	
c_1		$Y'_{\delta r}$		$N'_{\delta r}$	
a_2		$Y'_{\delta r \eta}$		$N'_{\delta r \eta}$	
b_2		$Y'_{r\eta}$		$N'_{r\eta}$	
c_2		$Y'_{v\eta}$		$N'_{v\eta}$	
a_3		$Y'_{*\eta}$		$N'_{*\eta}$	
b_3		m'		I'_{z}	
c_3					
a_4					
b_4					
c_4					

IV. SHIP MANEUVERING CHARACTERISTICS

A. STABILITY AND CONTROL DERIVATIVES AND INDICES

Derivative or Index	Value	
	Fully Appended, $n = 1$	Bare Hull
Y_v'		
N_v'		
Y_r'		
N_r'		
$Y_{\dot{v}}'$		
$N_{\dot{v}}'$		
$Y_{\dot{r}}'$		
$N_{\dot{r}}'$		
$Y_{\delta r}'$		
$N_{\delta r}'$		
m'		
I_z'		
$-Y_{\dot{v}}'/m'$		
σ_{1h}'		
σ_{2h}'		
σ_{1h}''		
ℓ_v'		
ℓ_r'		
ℓ_d'		
$N_{\delta r}'/Y_{\delta r}'$		
$N_{\delta r}'/(N_{\dot{r}}'-I_z')$		

IV. SHIP MANEUVERING CHARACTERISTICS (CONTINUED)

B. NUMERICAL MEASURES FROM DEFINITIVE MANEUVERS

SPIRALS	8-Knot Approach Speed		16-Knot Approach Speed	
	Simulated	Full Scale	Simulated	Full Scale
Loop height, deg/sec				
Loop width, deg				
Neutral rudder angle, deg				
Steady-turning rate, deg/sec @:				
δ_r = 20 deg R				
δ_r = 10 deg R				
δ_r = 0 deg				
δ_r = 10 deg L				
δ_r = 20 deg L				

5-5 ZIGZAGS	8-Knot Approach Speed		16-Knot Approach Speed	
	Simulated	Full Scale	Simulated	Full Scale
First Overshoot				
Time to reach execute heading change, sec				
Overshoot heading angle, deg				
Total heading angle change, deg				
Path width at execute, ft				
Overshoot path width, ft				
Total path width, ft				
Second overshoot heading angle, deg				
Third overshoot heading angle, deg				
Period, sec				

IV. SHIP MANEUVERING CHARACTERISTIC (CONTINUED)

B. NUMERICAL MEASURES FROM DEFINITIVE MANEUVERS

10-10 ZIGZAGS	8-Knot Approach Speed		16-Knot Approach Speed	
	Simulated	Full Scale	Simulated	Full Scale
First Overshoot				
Time to reach execute heading change, sec				
Overshoot heading angle, deg				
Total heading angle change, deg				
Path width at execute, ft				
Overshoot path width, ft				
Total path width, ft				
Second overshoot heading angle, deg				
Third overshoot heading angle, deg				
Period, sec				
20-20 ZIGZAGS				
First Overshoot				
Time to reach execute heading change, sec				
Overshoot heading angle, deg				
Total heading angle change, deg				
Path width at execute, ft				
Overshoot path width, ft				
Total path width, ft				
Second overshoot heading angle, deg				
Third overshoot heading angle, deg				
Period, sec				

IV. SHIP MANEUVERING CHARACTERISTICS (CONTINUED)

B. NUMERICAL MEASURES FROM DEFINITIVE MANEUVERS

STEADY TURNS (20-DEG L RUDDER)	8-Knot Approach Speed		16-Knot Approach Speed	
	Simulated	Full Scale	Simulated	Full Scale
Time to change heading 90 deg, sec				
Time to change heading 180 deg, sec				
Speed after 90 deg heading change, knots				
Speed after 180 deg heading change, knots				
Speed loss in steady turn, percent				
Advance, ft				
Transfer, ft				
Tactical diameter, ft				
Steady-turning diameter, ft				
Steady-turning rate, deg/sec				
STEADY TURNS (20-DEG R RUDDER)				
Time to change heading 90 deg, sec				
Time to change heading 180 deg, sec				
Speed after 90 deg heading change, knots				
Speed after 180 deg heading change, knots				
Speed loss in steady turn, percent				
Advance, ft				
Transfer, ft				
Tactical diameter, ft				
Steady-turning diameter, ft				
Steady-turning rate, deg/sec				
STEADY TURNS (35-DEG R RUDDER)				
Time to change heading 90 deg, sec				
Time to change heading 180 deg, sec				
Speed after 90 deg heading change, knots				
Speed after 180 deg heading change, knots				
Speed loss in steady turn, percent				
Advance, ft				
Transfer, ft				
Tactical diameter, ft				
Steady-turning diameter, ft				
Steady-turning rate, deg/sec				

IV. SHIP MANEUVERING CHARACTERISTICS (CONCLUDED)

B. NUMERICAL MEASURES FROM DEFINITIVE MANEUVERS

STEADY TURNS (35-DEG L RUDDER)	8-Knot Approach Speed		16-Knot Approach Speed	
	Simulated	Full Scale	Simulated	Full Scale
Time to change heading 90 deg, sec				
Time to change heading 180 deg, sec				
Speed after 90 deg heading change, knots				
Speed after 180 deg heading change, knots				
Speed loss in steady turn, percent				
Advance, ft				
Transfer, ft				
Tactical diameter, ft				
Steady-turning diameter, ft				
Steady-turning rate, deg/sec				
STEADY TURNS (45-DEG R RUDDER)				
Time to change heading 90 deg, sec				
Time to change heading 180 deg, sec				
Speed after 90 deg heading change, knots				
Speed after 180 deg heading change, knots				
Speed loss in steady turn, percent				
Advance, ft				
Transfer, ft				
Tactical diameter, ft				
Steady-turning diameter, ft				
Steady-turning rate, deg/sec				
STEADY TURNS (45-DEG L RUDDER)				
Time to change heading 90 deg, sec				
Time to change heading 180 deg, sec				
Speed after 90 deg heading change, knots				
Speed after 180 deg heading change, knots				
Speed loss in steady turn, percent				
Advance, ft				
Transfer, ft				
Tactical diameter, ft				
Steady-turning diameter, ft				
Steady-turning rate, deg/sec				

STANDARDIZED DATA SHEET NO. 1

APPENDIX E

SNAME MATHEMATICAL-MANEUVERING MODEL STANDARDIZED DATA SHEET

FOR

USS COMPASS ISLAND (MARINER TYPE SHIP)

PREPARED BY

Morton Gertler

Revised October 1980

The following pages describe the sources and present values for the hydrodynamic coefficients and other data required with the specified equations of motion to perform computer simulation predictions of various maneuvering characteristics of the above ship type. The results of such simulations are also presented, and compared with corresponding full-scale trial data, whenever such data exist and are readily available.

I. DATA SOURCE AND ACQUISITION TECHNIQUE

A. MODEL TEST PROGRAM

SPONSOR: HYDRONAUTICS, Incorporated, Laurel, Maryland

LABORATORY: HYDRONAUTICS, Incorporated

TECHNIQUE USED: Planar-motion-mechanism tests

TEST FACILITY: HYDRONAUTICS Ship Model Basin (HSMB)
SIZE - 127.4 meters long, 7.62 meters wide, 3.962 meters deep (full)
DESCRIPTION - See References 1 and 2

TEST APPARATUS: HSMB Large-Amplitude-Horizontal-Planar-Motion Mechanism (LAHPMM) System (Description given in Refs. 1 and 2)

SHIP MODEL PARTICULARS:
DESIGNATION - DTNSRDC Model 4414 (Prop. 3249), 6.66m LBP x 0.96m B x 0.31m T
CONSTRUCTION MATERIAL - Wood with smooth painted surface
TURBULENCE STIMULATION DEVICE - None

TEST DATE: January, 1976

TEST CONDITIONS: Full load condition in calm deep water. Model free to trim with reference tests conducted at ship propulsion point for steady straight-line motion ($n = 1$) in accordance with ITTC recommendations (Refs. 3). PMM oscillation frequency = 0.08 Hz.

TEST PARAMETER RANGE:

n	1.0,1.5,1.6	$\dot{r}'$	0.0 to 0.9	ϕ	
β	-8 to +18 deg	$\dot{v}'$	0.0 to0.3	θ	
r'	0.0 to 0.70	$v' \lvert r' \rvert$	0.0 to 0.14	Δ	
δ_r	+10 to -35 deg				

DATA REDUCTION AND ANALYSIS METHODS: Standard methods described in Reference 2.

PUBLISHED SOURCES: Hydrodynamic coefficients are published in Reference 2.

I. DATA SOURCE AND ACQUISITION TECHNIQUE (CONTINUED)

B. SHIP MANEUVERING PREDICTIONS

SPONSOR: HYDRONAUTICS, Incorporated

SIMULATION FACILITY: HYDRONAUTICS META-4 Digital Computer System

MATHEMATICAL MODEL: Standard Equations of Motion for Surface Ships with hydrodynamic coefficients derived from LAHPMM tests. (Refs. 2)

SIMULATED DEFINITIVE MANEUVERS: Spirals; 5-5, 10-10, and 20-20 zigzags; and steady turns with 10, 20, 35 deg R and 35 deg L rudder at approach speeds of 8 and 16 knots.

PUBLISHED RESULTS: Numerical measures and trajectory data from selected definitive maneuvers simulated to correspond to the actual full-scale trials conditions are presented graphically in Reference 2, and are correlated with corresponding full-scale data from Reference 4.

C. FULL-SCALE MANEUVERING TRIALS AND CORRELATION

SHIP: USS COMPASS ISLAND (Mariner Type Ship)

TRIALS DATES: 23 and 24 August 1961

TYPE OF TRIALS: Special trials conducted under the sponsorship of NAVSHIPS GHR program specifically to provide correlation data for maneuvering predictions based on the results of model tests.

TRIALS INSTRUMENTATION: Fully instrumented (including SINS) to obtain precision measurement of the trajectory data (both path and angular). See Reference 4 for a catalog of the instrumentation.

I. DATA SOURCES AND ACQUISITION TECHNIQUE (CONCLUDED)

TRIALS CONDITION: Sea state was about 1 to 2 with no significant swell. Winds averaged less than 10 knots.

MANEUVERS PERFORMED: Spirals at nominal approach speeds of 5 and 15 knots; 20-20 zigzags at nominal approach speeds of 10, 15, and 20 knots; steady turns with nominal rudder angles of 35L, 10L, 5R, 10R, 20R, and 35R at nominal approach speeds of 10,15, and 20 knots; and deceleration/acceleration maneuvers initiated at nominal approach speeds of 10 and 20 knots.

DATA REDUCTION AND ANALYSIS: Data reduction methods including an error analysis are described in detail in Reference 4.

PUBLISHED RESULTS: Complete trajectory data as well as plots and tables of the numerical measures for the various maneuvers are given in Reference 4.

D. REFERENCES

1. "A Manual for SNAME Mathematical Maneuvering Model Standardized Data Sheets", Prepared by SNAME Panel H-10

2. Goodman, Alex, Gertler, Morton, and Kohl, Robert, "Experimental Techniques and Methods of Analysis Used at HYDRONAUTICS for Surface-Ship Maneuvering Predictions", HYDRONAUTICS, Incorporated Technical Report 7600-1, June 1976.

3. Gertler, Morton, "Final Analysis of the First Phase of ITTC Standard Captive-Model-Test Program",Appendix 3, Part 2 of Maneuverability Committee Report, Proceedings of the 12th ITTC, 1969.

4. Morse, R.V. and Price, D., "Maneuvering Characteristics of the Mariner Type Ship (USS COMPASS ISLAND) in Calm Seas", Sperry Gyroscope Publication G7-2233-1019, Prepared for the David Taylor Model Basin under Contract NOnr 3061(00), December 1961.

II. SHIP GEOMETRY

A. PRINCIPAL GEOMETRIC CHARACTERISTICS

Hull	Ship	Model	Rudder	Ship	Model
L, m	160.93	6.6569	$\bar{b}$, m	7.315	0.3026
B, m	23.17	0.9584	c_r, m	3.987	0.1649
T, m	7.467	0.3089	c_t, m		
Trim, m by stern	1.219	0.0504	A_T, m^2	29.172	0.0499
Δ, tons,	16800.00	1.1567	A_F, m^2	3.917	0.0067
∇, m^3	16650.3	1.1784	A_M, m^2	25.255	0.0432
S, m^2			$a = \bar{b}^2/A_T$	1.834	1.834
LCG, m fwd of AP	78.36	3.2414	Balance, percent	20.91	20.91
VCG, m above	7.742	0.3202	A_T/L_{BT}	0.0224	0.0224
L/B	6.947	6.947	δ_r, deg max.	40.0	
B/T	3.102	3.102	$\dot{\delta}_r$, deg/sec	2.5 - 2.7	
C_B	0.613	0.613			
C_V(1000)	3.994	3.994	Propeller (Rotation - RH)		
LCG/L	0.487	0.487	No. of Blades	4	4
Bilge Keels			D, m	6.706	
b, m	0.305	0.0126	P(0.7 R), m	6.959	
c, m	33.528	1.3869	P/D	1.038	1.038
			D/T	0.898	0.898

B. LINES

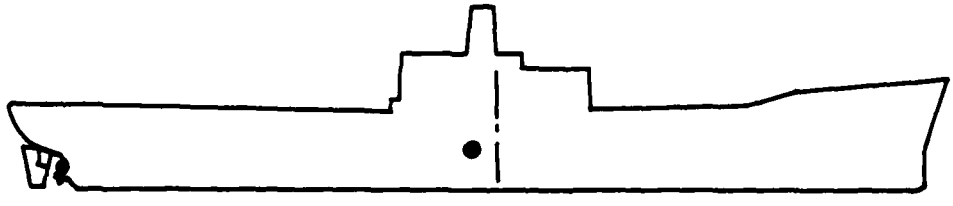

C. RUDDER DETAILS

III. MATHEMATICAL MODEL

SUMMARY OF EQUATIONS OF MOTION

A. BASIC EQUATIONS

Axial Force

$$m[\dot{u} - vr - x_G r^2] =$$
$$+\frac{\rho}{2} L^4 [X_{rr}\, r^2]$$
$$+\frac{\rho}{2} L^3 [X_{\dot{u}}\, \dot{u} + X_{vr}\, vr]$$
$$+\frac{\rho}{2} L^2 \{X_{vv}\, v^2 + [X_{vvn}\, v^2](n-1)\}$$
$$+\frac{\rho}{2} L^2 u^2 [a_1 + b_1 n + c_1 n^2]$$
$$+\frac{\rho}{2} L^2 u^2 [X_{\delta r \delta r}\, \delta r^2 + X_{\delta r \delta r n n}\, \delta r^2 n^2]$$

Lateral Force

$$m[\dot{v} + ur + x_G \dot{r}] =$$
$$+\frac{\rho}{2} L^4 [Y_{\dot{r}}\, \dot{r} + Y_{r|r|}\, r|r|]$$
$$+\frac{\rho}{2} L^3 [Y_{\dot{v}}\, \dot{v}]$$
$$+\frac{\rho}{2} L^3 [Y_r\, ur + Y_{|r|\delta r}\, u|r|\delta r + Y_{v|r|}\, v|r|]$$
$$+\frac{\rho}{2} L^2 [Y_*\, u^2 + Y_v\, uv + Y_{v|v|}\, v|v|]$$
$$+\frac{\rho}{2} L^2 [Y_{\delta r}\, u^2 \delta r]$$
$$+\frac{\rho}{2} L^3 Y_{rn}\, ur(n-1)$$
$$+\frac{\rho}{2} L^2 [Y_{*n}\, u^2 + Y_{vn}\, uv + Y_{v|v|n}\, v|v| + Y_{\delta rn}\, u^2 \delta r](n-1)$$

Yaw Moment

$$I_z \dot{r} + mx_G(\dot{v} + ur) =$$
$$+\frac{\rho}{2} L^5 [N_{\dot{r}}\, \dot{r} + N_{r|r|}\, r|r|]$$
$$+\frac{\rho}{2} L^4 [N_{\dot{v}}\, \dot{v}]$$
$$+\frac{\rho}{2} L^4 [N_r\, ur + N_{|r|\delta r}\, u|r|\delta r + N_{|v|r}\, |v|r]$$
$$+\frac{\rho}{2} L^3 [N_*\, u^2 + N_v\, uv + N_{v|v|}\, v|v|]$$
$$+\frac{\rho}{2} L^3 [N_{\delta r}\, u^2 \delta r]$$
$$+\frac{\rho}{2} L^4 [N_{rn}\, ur](n-1)$$
$$+\frac{\rho}{2} L^3 [N_{*n}\, u^2 + N_{vn}\, uv + N_{v|v|n}\, v|v| + N_{\delta rn}\, u^2 \delta r](n-1)$$

B. SUPPLEMENTARY EQUATIONS

Autopilot

Note:

The above equations are referred to a right-hand orthogonal system of moving axes, fixed in the ship, with its origin normally located at the ship center of mass ($x_G = 0$). Equations can be used to simulate maneuvers in either deep or constant-depth shallow water by substituting the appropriate coefficient values.

III. MATHEMATICAL MODEL (CONCLUDED)

NONDIMENSIONAL HYDRODYNAMIC COEFFICIENTS

C. COEFFICIENT VALUES

X - Equation		Y - Equation		N - Equation	
Nomdimensional Coefficient	Value x 10^5	Nondimensional Coefficient	Value x 10^5	Nondimensional Coefficient	Value x 10^5
X_{u}'	-36.3	Y_{*}'	3.6	N_{*}'	-1.8
X_{vr}'	480.0	Y_{v}'	-749.0	N_{v}'	-4.8
X_{vv}'	-355.6	Y_{v}'	-1142.6	N_{v}'	-394.1
$X_{\delta r\delta r}'$ (n=0)	-8.0	$Y_{v\|v\|}'$	-2380.4	$N_{v\|v\|}'$	438.0
X_{rr}'	12.5	Y_{r}'	269.6	N_{r}'	-188.7
$X_{vv\eta}'$	0.0	$Y_{r\|r\|}'$	207.6	$N_{r\|r\|}'$	-47.5
$X_{\delta r\delta r\eta\eta}'$	-10.4	$Y_{v\|r\|}'$	-720.0	$N_{v\|r\|}'$	-647.0
a_1	-34.46	$Y_{r\delta r}'$	0.0	$N_{r\delta r}'$	0.0
b_1	-110.02	Y_{r}'	-12.5	N_{r}'	-48.2
c_1	141.17	$Y_{\delta r}'$	263.6	$N_{\delta r}'$	-128.4
a_2	-82.00	$Y_{\delta r\eta}'$	340.0	$N_{\delta r\eta}'$	-162.0
b_2	-23.30	$Y_{r\eta}'$	107.0	$N_{r\eta}'$	-51.4
c_2	105.30	$Y_{v\eta}'$	-123.6	$N_{v\eta}'$	60.2
a_3	-85.40	$Y_{*\eta}'$	3.6	$N_{*\eta}'$	-1.8
b_3	32.00	m'	797.67	I_{z}'	42.8
c_3	-107.90				
a_4	-84.32				
b_4	39.39				
c_4	-98.60				

Note:

The above nondimensional coefficients are referred to a set of moving axes, fixed in the body, with its origin located at the body center of gravity ($x_G = 0$).

AD-A144 227 PROCEEDINGS OF THE GENERAL MEETING OF THE AMERICAN TOWING TANK CONFERENCE.. (U) STEVENS INST OF TECH HOBOKEN NJ DAVIDSON LAB D SAVITSKY ET AL. AUG 83 3/8

UNCLASSIFIED SIT-DL-TR-13029-VOL-2 N00167-83-M-4062 F/G 20/4 NL

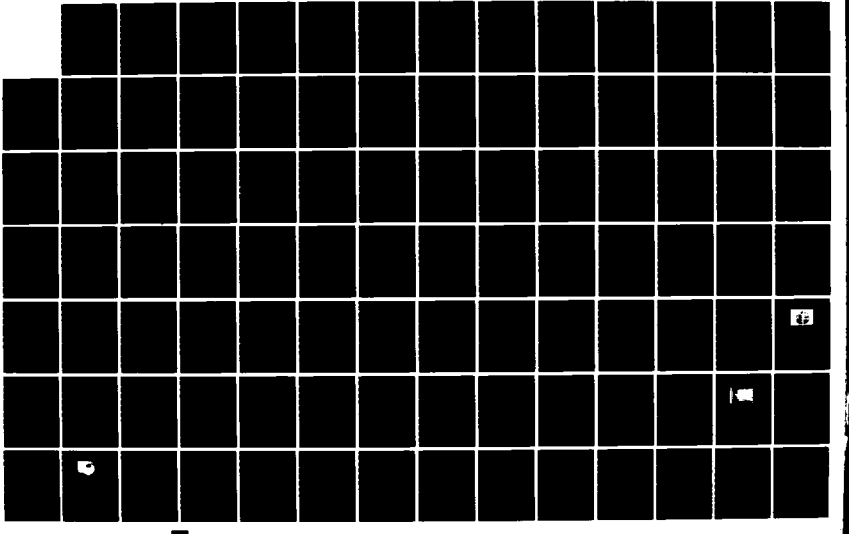

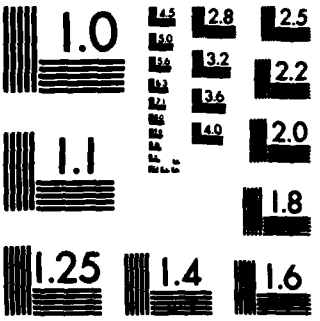

MICROCOPY RESOLUTION TEST CHART
NATIONAL BUREAU OF STANDARDS-1963-A

IV. SHIP MANEUVERING CHARACTERISTICS

A. STABILITY AND CONTROL DERIVATIVES AND INDICES

Derivative or Index	Value	
	Fully Appended, $\eta = 1$	Bare Hull
Y_v'	-0.011426	
N_v'	-0.003941	
Y_r'	0.002696	
N_r'	-0.001887	
$Y_{\dot{v}}'$	-0.007490	
$N_{\dot{v}}'$	-0.000048	
$Y_{\dot{r}}'$	-0.000125	
$N_{\dot{r}}'$	-0.000482	
$Y_{\delta r}'$	0.002636	
$N_{\delta r}'$	-0.001284	
m'	0.0079767	
I_z'	0.000428	
$-Y_{\dot{v}}'/m'$	0.93898	
σ_{1h}'	-0.01940	
σ_{2h}'	-2.84001	
σ_{1h}''	-0.003077	
ℓ_v'	0.34492	
ℓ_r'	0.35734	
ℓ_d'	0.01241	
$N_{\delta r}'/Y_{\delta r}'$	-0.48710	
$N_{\delta r}'/(N_{\dot{r}}'-I_z')$	1.41099	

Note: Nondimensional derivatives and indices are referred to an origin at the body C.G. ($x_G=0$)

IV. SHIP MANEUVERING CHARACTERISTICS (CONTINUED)

B. NUMERICAL MEASURES FROM DEFINITIVE MANEUVERS

SPIRALS	15 Kts Approach Speed		20 Kts Approach Speed	
	Simulated	Full Scale	Simulated	Full Scale
Loop height, deg/sec				
Loop width, deg				
Neutral rudder angle, deg	1.5 R	1.0		
Steady-turning rate, deg/sec @:				
δ_r = 20 deg R	0.69	0.73		
δ_r = 10 deg R	0.52	0.54		
δ_r = 0 deg	-0.16	-0.18		
δ_r = 10 deg L	-0.59	-0.68		
δ_r = 20 deg L	-0.75	-0.83		

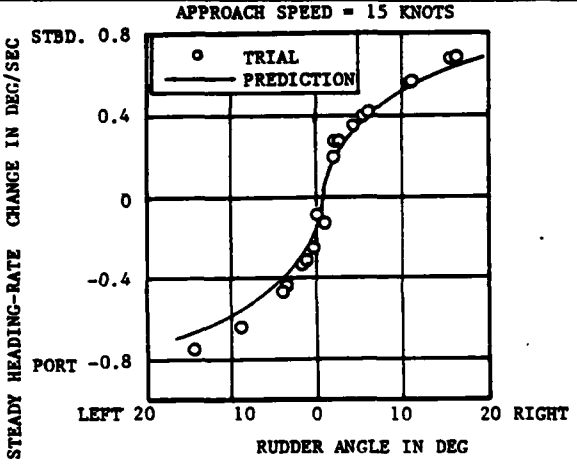

RESULTS OF SPIRAL MANEUVER FOR MARINER TYPE SHIP

Original interpretation of data in Ref. 4 suggests a loop of approximately 1 to 2 degrees width.

5-5 ZIGZAGS	Knot Approach Speed		Knot Approach Speed	
	Simulated	Full Scale	Simulated	Full Scale
First Overshoot				
Time to reach execute heading change, sec				
Overshoot heading angle, deg				
Total heading angle change, deg				
Path width at execute, meter				
Overshoot path width, meter				
Total path width, meter				
Second overshoot heading angle, deg				
Third overshoot heading angle, deg				
Period, sec				

IV. SHIP MANEUVERING CHARACTERISTICS (CONTINUED)

B. NUMERICAL MEASURES FROM DEFINITIVE MANEUVERS

10-10 ZIGZAGS	15 Kts Approach Speed		20 Kts Approach Speed	
	Simulated	Full Scale	Simulated	Full Scale
First Overshoot				
Time to reach execute heading change, sec				
Overshoot heading angle, deg				
Total heading angle change, deg				
Path width at execute, m				
Overshoot path width, m				
Total path width, m				
Second overshoot heading angle, deg				
Third overshoot heading angle, deg				
Period, sec				
20-20 ZIGZAGS				
First Overshoot				
Time to reach execute heading change, sec	35.3	36.0		36.0
Overshoot heading angle, deg	8.1	7.7		10.3
Total heading angle change, deg	28.1	27.2*		30.3*
Path width at execute, m		118.9		182.9
Overshoot path width, m		73.1		73.1
Total path width, m		192.0		256.0
Second overshoot heading angle, deg	10.1	10.7		13.3
Third overshoot heading angle, deg	9.1	7.7		8.8
Period, sec	204.7	193.8		169.2

* Corrected to 20-deg executed heading change.

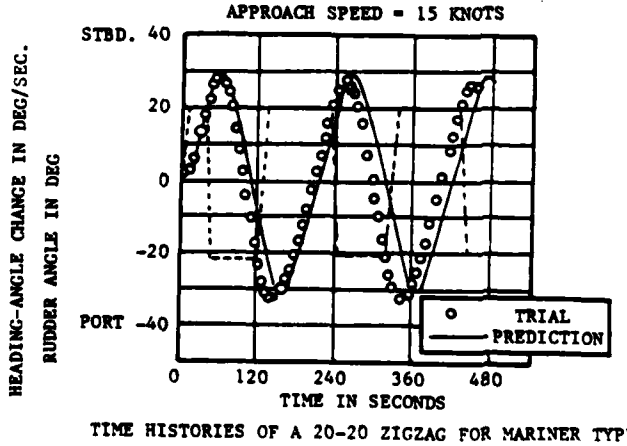

TIME HISTORIES OF A 20-20 ZIGZAG FOR MARINER TYPE SHIP

IV. SHIP MANEUVERING CHARACTERISTICS (CONTINUED)

B. NUMERICAL MEASURES FROM DEFINITIVE MANEUVERS

STEADY TURNS (20-DEG R RUDDER)	15.4 Kts Approach Speed		20.0 Kts Approach Speed	
	Simulated	Full Scale	Simulated	Full Scale
Time to change heading 90 deg, sec		131.0		104.0
Time to change heading 180 deg, sec		252.		186.
Speed after 90 deg heading change, knots		12.78		16.3
Speed after 180 deg heading change, knots		11.80		15.8
Speed loss in steady turn, percent	27.1	24.7		22.0
Advance, m	700.4	672.1		640.1
Transfer, m	448.1	521.2		548.6
Tactical diameter, m	1019.6	1024.1		1024.1
Steady-turning diameter, m	983.8	966.5		996.7
Steady-turning rate, deg/sec	0.69	0.72		0.90
STEADY TURNS (30-DEG R RUDDER)				
Time to change heading 90 deg, sec		91.		113.
Time to change heading 180 deg, sec		225.		171.
Speed after 90 deg heading change, knots		11.55		14.4
Speed after 180 deg heading change, knots		9.95		13.70
Speed loss in steady turn, percent	35.1	38.2		34.8
Advance, m	598.0	539.5		571.5
Transfer, m	329.2	466.9		429.8
Tactical diameter, m	795.5	777.2		804.7
Steady-turning diameter, m	738.8	722.4		740.7
Steady-turning rate, deg/sec	0.79	0.82		1.03

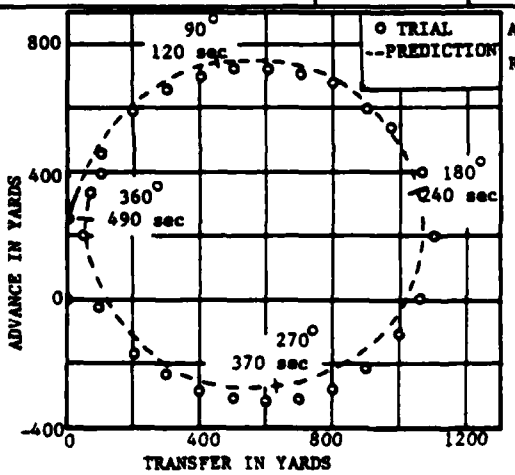

PATH IN STEADY-TURNING MANEUVER FOR MARINER TYPE SHIP

IV. SHIP MANEUVERING CHARACTERISTICS (CONTINUED)

B. NUMERICAL MEASURES FROM DEFINITIVE MANEUVERS

STEADY TURNS (35-DEG R RUDDER)	15.4 Kt Approach Speed		20.0 Kt Approach Speed	
	Simulated	Full Scale	Simulated	Full Scale
Time to change heading 90 deg, sec		112.		90.
Time to change heading 180 deg, sec		219.		168.
Speed after 90 deg heading change, knots		10.95		13.4
Speed after 180 deg heading change, knots		9.05		12.6
Speed loss in steady turn, percent		44.2		40.0
Advance, m		493.8		562.4
Transfer, m		365.8		384.0
Tactical diameter, m		713.2		726.9
Steady-turning diameter, m		621.8		640.0
Steady-turning rate, deg/sec		0.85		1.08
STEADY TURNS (20-DEG L RUDDER)				
Time to change heading 90 deg, sec		120.		
Time to change heading 180 deg, sec		228.		
Speed after 90 deg heading change, knots		11.75		
Speed after 180 deg heading change, knots		10.66		
Speed loss in steady turn, percent	28.6	34.4		
Advance, m	667.5	589.8		
Transfer, m	422.5	457.2		
Tactical diameter, m	960.1	850.4		
Steady-turning diameter, m	887.0	731.5		
Steady-turning rate, deg/sec	-0.75	-0.83		

IV. SHIP MANEUVERING CHARACTERISTICS (CONCLUDED)

B. NUMERICAL MEASURES FROM DEFINITIVE MANEUVERS

STEADY TURNS (30-DEG L RUDDER)	15.4 Kt Approach Speed		20.0 Kt Approach Speed	
	Simulated	Full Scale	Simulated	Full Scale
Time to change heading 90 deg, sec				
Time to change heading 180 deg, sec				
Speed after 90 deg heading change, knots				
Speed after 180 deg heading change, knots				
Speed loss in steady turn, percent	37.7			
Advance, m	562.4			
Transfer, m	320.0			
Tactical diameter, m	773.6			
Steady-turning diameter, m	708.7			
Steady-turning rate, deg/sec	-0.80			
STEADY TURNS (35-DEG L RUDDER)				
Time to change heading 90 deg, sec				184.
Time to change heading 180 deg, sec				168.
Speed after 90 deg heading change, knots				13.40
Speed after 180 deg heading change, knots				12.60
Speed loss in steady turn, percent				42.1
Advance, m				466.3
Transfer, m				347.5
Tactical diameter, m				667.5
Steady-turning diameter, m				539.5
Steady-turning rate, deg/sec				-1.16

STANDARDIZED DATA SHEET NO. 2

APPENDIX F

SNAME MATHEMATICAL-MANEUVERING MODEL STANDARDIZED DATA SHEET

FOR

ESSO 190,000 DWT TANKER

PREPARED BY

Morton Gertler

September 1980

The following pages describe the sources and present values for the hydrodynamic coefficients and other data required with the specified equations of motion to perform computer simulation predictions of various maneuvering characteristics of the above ship type. The results of such simulations are also presented, and compared with corresponding full-scale trial data, whenever such data exist and are readily available.

ESSO 190,000-DWT TANKER

I. DATA SOURCE AND ACQUISITION TECHNIQUE

A. MODEL TEST PROGRAM

SPONSOR: ESSO International Division, EXXON Corporation, New York, NY

LABORATORY: Hydro-og Aerodynamisk Laboratum (HyA), Lyngby, Denmark

TECHNIQUE USED: Planar-motion-mechanism tests

TEST FACILITY: HyA Ship Model Basin
SIZE - 240m long, 12m wide, 5.5m deep (full)
DESCRIPTION - Conventional towing tank with removable false bottom for shallow-waters tests.

TEST APPARATUS: Original HyA Planar Motions Mechanism (Small Amplitude) designed for surface ship model tests. Description given in Ref. 1

SHIP MODEL PARTICULARS:
DESIGNATION - HyA Model, 7.0m L x 1.08m B x 0.424m T (Approximate)
CONSTRUCTION MATERIAL - Wood with smooth painted surface
TURBULENCE STIMULATION DEVICE - None

TEST DATE:

TEST CONDITIONS: Full load condition in calm deep water, model free to trim and self-propelled at ship propulsion point(Corresponding to a speed of 16 knots at 80 rpm). A limited series of PMM tests were conducted at several shallow water depths using the false-bottom technique.

TEST PARAMETER RANGE:

η	$\dot{r}'$	ϕ
β	$\dot{v}'$	θ
r'	$v' \lvert r' \rvert$	Δ
δ_r		

DATA REDUCTION AND ANALYSIS METHODS: Values of hydrodynamic coefficients were obtained originally at HyA by the method of Ref. 1 (Cubic fits of test data nondimensionalized by standard SNAME-ITTC System). These "faired" values were recalculated at SSPA to obtain second order fits and convert to the BIS system of Ref. 2.

PUBLISHED SOURCES: Set of hydrodynamic coefficient values for equations of motion (quadratic BIS system form for calm-deep water case and for variations with shallow water depth are published in Ref. 3.

I. DATA SOURCE AND ACQUISITION TECHNIQUE (CONTINUED)

B. SHIP MANEUVERING PREDICTIONS

SPONSOR: ESSO International Division, EXXON Corporation, New York, NY

SIMULATION FACILITY: The SSPA Steering and Maneuvering Simulator, Goteborg, Sweden (Described in Ref. 4)

MATHEMATICAL MODEL: SSPA Equations of Motion(Square-absolute format with BIS coefficients with added terms representing variation with shallow-water depth, see Ref. 1); hydrodynamic coefficient values derived originally from HyA PMM tests.

SIMULATED DEFINITIVE MANEUVERS: Spirals; 20-20 zigzags; steady turns with 20, 30 deg both R and L rudder; and step responses with 5, 20, and 35 deg rudder angles were conducted at an approach speed of 16 knots in deep water and 8 knots at various fixed shallow-water depths.

PUBLISHED RESULTS: Numerical measures and a few trajectories from the simulated definitive maneuvers conducted (both deep and shallow water) are presented graphically in Ref. 3 and selected data are correlated with corresponding data from Ref. 5 and other unpublished sources for the deep-water case.

C. FULL-SCALE MANEUVERING TRIALS AND CORRELATION

SHIP: ESSO BERNICIA

TRIALS DATES:

TYPE OF TRIALS: Special maneuvering trials carried out with participation of the British Shipbuilding Research Association (BSRA)

TRIALS INSTRUMENTATION:

I. DATA SOURCE AND ACQUISITION TECHNIQUE (CONCLUDED)

TRIALS CONDITION:

MANEUVERS PERFORMED:

DATA REDUCTION AND ANALYSIS:

PUBLISHED RESULTS:

D. REFERENCES

1. Strom-Tejsen, J. and Chislett, M.S., "A Model Testing Technique and Method of Analysis for the Prediction of Steering and Maneuvering Qualities of Surface Vessels," Proceedings of 6th Symposium on Naval Hydrodynamics, 1966 (Also HyA Report Hy-7, September 1966)

2. Norrbin, Nils H., "Theory and Observations on the Use of a Mathematical Model for Ship Maneuvering in Deep and Confined Waters," Proceedings of the 8th ONR Symposium on Naval Hydrodynamics, (Also SSPA Publication No. 68, 1971)

3. van Berlekom, Willem B., and Goddard, Thomas A., "Maneuvering of Large Tankers," Trans. SNAME, Vol. 80, 1972

4. Norrbin, N.H., and Goransson, S., "The SSPA Steering and Maneuvering Simulator," (in Sweden), SSPA Report No. 28, April 1969 (English translation available). Also brief description given in Ref. 3.

5. Clarke, D., Patterson, D., and Wooderson, R., "Maneuvering Trials with the 193,000-DWT Tanker ESSO BERNICIA," Proceedings of RINA Spring Meeting, April 1972.

ESSO 190,000-DWT TANKER

II. SHIP GEOMETRY

A. PRINCIPAL GEOMETRIC CHARACTERISTICS

Hull	Ship	Model	Rudder	Ship	Model
L, m	304.8	7.00	$\bar{b}$, m		
B, m	47.17	1.083	c_r, m		
T, m	18.46	0.424	c_t, m		
Trim, m by stern			A_T, m^2		
Δ, tons			A_F, m^2		
∇, m^3	220,000.		A_M, m^2		
S, m^2			$a = \bar{b}^2/A_T$		
LCG, m fwd of AP			Balance, percent		
VCG, m			$A_T/L \bullet T$		
L/B	6.46	6.46	δ_r, deg max.	35.0	35.0
B/T	2.56	2.56	$\dot{\delta}_r$, deg/sec	2.33	2.33
C_B	0.83	0.83			
C_∇(1000)	7.77	7.77	Propeller (Rotation -)		
LCG/L			No. of Blades		
Bilge Keels			D, m		
b, m			P(0.7 R), m		
c, m			P/D		
			D/T		

Model dimensions are based on a length between perpendiculars of approximately 7.0m.

B. LINES

C. RUDDER DETAILS

III. MATHEMATICAL MODEL

SUMMARY OF EQUATIONS OF MOTION

A. BASIC EQUATIONS

B. SUPPLEMENTARY EQUATIONS

Axial Force

$$
\begin{aligned}
&[(1 - X_{\dot{u}}')\dot{u}] \\
= &+ \frac{1}{2} L^{-1} [X_{uu}' u^2] \\
&+ \frac{1}{24} L^{-1} g^{-1} [X_{uuuu}' u^4] \\
&+ g[T'(1 - t)] \\
&+ [(1 + X_{vr}')v\dot{\psi}] \\
&+ L[x_G' + \tfrac{1}{2} X_{rr}' \dot{\psi}^2] \\
&+ \frac{1}{6} L^{-2} g^{-1} [X_{u|v|vv}' u|v|v^2] \\
&+ \frac{1}{2} L^{-1} [X_{vv}' v^2] \\
&+ \frac{1}{4} L^{-1} [X_{c|c|\delta\delta}' c|c|\delta_e^2] \\
&+ \frac{1}{4} L^{-1} [X_{c|c|\beta\delta}' c|c|\beta\delta_e]
\end{aligned}
$$

Lateral Force

$$
\begin{aligned}
&[(1 - Y_{\dot{v}}')\dot{v}] \\
= &+ L[(Y_r' - x_G')\dot{\psi}] \\
&+ \frac{1}{2} L^{-1/2} g^{-1/2} [Y_{uur}' u^2 \psi]^{\cdot} \\
&+ L[Y_{uv}' uv] \\
&+ \frac{1}{2} L^{-3/2} g^{-1/2} [Y_{uuv}' u^2 v] \\
&+ \frac{1}{2} L^{-1} [Y_{v|v|}' v|v|] \\
&+ \frac{1}{2} L[Y_{|r|r}' |\dot{\psi}|\dot{\psi}] \\
&+ [Y_{|v|r}' |v|\dot{\psi}] \\
&+ [Y_{v|r|}' v|\dot{\psi}|] \\
&+ \frac{1}{2} L^{-1} [Y_{c|c|\delta}' c|c|\delta_e] \\
&+ \frac{1}{2} L^{-1} [Y_{c|c|\beta|\beta|\delta|}' c|c|\beta|\beta|\delta_e|] \\
&+ [Y_T' T']
\end{aligned}
$$

Added Terms for Shallow Water

$$
\begin{aligned}
&-[X_{u\zeta}' \dot{u}\zeta] \\
&+ \frac{1}{2} L^{-1} [X_{uu\zeta}' u\zeta] \\
&+ [X_{vr\zeta}' v\dot{\psi}\zeta] \\
&+ \frac{1}{2} L^{-1} [X_{vv\zeta\zeta}' v^2\zeta^2]
\end{aligned}
$$

$$
\begin{aligned}
&-[Y_{v\zeta}' \dot{v}\zeta] \\
&+ [y_{ur\zeta}' u\dot{\psi}\zeta] \\
&+ L[Y_{uv\zeta}' uv\zeta] \\
&+ \frac{1}{2} L^{-1} [Y_{v|v|\zeta}' v|v|\zeta] \\
&+ \frac{1}{2} L^{-1} [Y_{c|c|\beta|\beta|\delta|\zeta}' c|c|\beta|\beta|\delta_e|\zeta]
\end{aligned}
$$

III. MATHEMATICAL MODEL (CONTINUED)

SUMMARY OF EQUATIONS OF MOTION

A. BASIC EQUATIONS Continued

Yaw Moment:

$$
\begin{aligned}
&[(k_z^2 - N_{\dot{r}}")\dot{\bar{r}}] \\
&= + L^{-1}[(N_{\dot{v}}" - x_G")\dot{u}\psi] \\
&\quad + L^{-1}[(N_{\dot{u}r}" - x_G")\dot{u}\psi] \\
&\quad + \frac{1}{2} L^{-3/2} g^{-1/2} [N_{\dot{u}ur}" u^2 \dot{\psi}] \\
&\quad + L^{2}[N_{\dot{u}v}" uv] \\
&\quad + \frac{1}{2} L^{-3/2} g^{-1/2} [N_{\dot{u}uv}" u^2 v] \\
&\quad + \frac{1}{2} L^{-2}[N_{|v|v}" |v|v] \\
&\quad + \frac{1}{2} [N_{|r|r}" |r|r] \\
&\quad + L^{-1}[N_{|v|r}" |v|r] \\
&\quad + L^{-1}[N_{v|r|}" v|r|] \\
&\quad + \frac{1}{2} L^{-2}[N_{c|c|\delta}" c|c|\delta_e] \\
&\quad + \frac{1}{2} L^{-2}[N_{c|c|\beta|\beta|\delta}" c|c|\beta|\beta|\delta_e|] \\
&\quad + L^{-1} g[N_T" T]
\end{aligned}
$$

Added Terms for Shallow Water

$$
\begin{aligned}
&-[N_{\dot{r}\zeta}" \dot{\bar{r}}\zeta] \\
&\quad + L^{-1}[N_{\dot{u}r\zeta}" u\dot{\psi}\zeta] \\
&\quad + L^{-2}[N_{uv\zeta}" uv\zeta] \\
&\quad + L^{-1}[N_{|v|r\zeta}" |v|\dot{\psi}\zeta] \\
&\quad + \frac{1}{2} L^{-2}[N_{c|c|\beta|\beta|\delta|\zeta}" c|c|\beta|\beta|\delta_e|\zeta]
\end{aligned}
$$

B. AUXILIARY EQUATIONS

Rudder Advance Velocity Equation:

$$c^2 = \frac{1}{2}(c_{uu})^2 u^2 + c_{un} un + \frac{1}{2}(c_{|n|n})^2 |n|n + \frac{1}{2}(c_{nn})^2 n^2$$

Propeller Thrust Equation:

$$T" = g^{-1}[\frac{1}{2} L^{-1}(T_{uu}" u^2) + (T_{un}" un) + \frac{1}{2} L(T_{|n|n}" |n|n) + \frac{1}{2} L(T_{nn}" n^2)]$$

Propeller Shaft Torque Equation:

$$
\begin{aligned}
(k_p - Q_{\dot{n}}")\dot{n} &= gL^{-1}(Q_k^E")k + g^{1/2}L^{-1/2}(Q_n^E" n) + gL^{-1}(Q^F")n/|n| + \frac{1}{2} L^{-2}(Q_{uu}" u^2) + L^{-1}(Q_{un}" un) \\
&\quad + (Q_{|n|n}" |n|n) + \frac{1}{2}(Q_{nn}" n^2)
\end{aligned}
$$

Autopilot Equation:

$$\delta^* = \gamma(\psi - \psi_o) + \sigma\dot{\psi}$$

where: δ^* is ordered rudder angle
γ and σ are constants of proportionality
ψ is the desired heading

III. MATHEMATICAL MODEL (CONTINUED)

NONDIMENSIONAL HYDRODYNAMIC COEFFICIENTS

C. COEFFICIENT VALUES

X - Equation		Y - Equation		N - Equation	
Nondimensional Coefficient	Value	Nondimensional Coefficient	Value	Nondimensional Coefficient	Value
		DEEP WATER			
$1-X_u'$	1.05	$1-Y_v'$	2.020	$k_z^2-N_r'$	0.1232
X_{uu}'	-0.0377	Y_{uv}'	-1.205	N_v'	0.0
X_{uuuu}'	0.0	Y_{uuv}'	0.0	N_{uv}'	-0.451
$1-X_{vr}'$	2.020	$Y_{v\|v\|}'$	-2.400	N_{uuv}'	0.0
X_{vv}'	0.300	$Y_{ur}'-1$	-0.752	$N_{v\|v\|}'$	0.0
X_{rr}'	0.0	$Y_{r\|r\|}'$	0.0	$N_{r\|r\|}'$	0.0
$X_{u\|v\|vv}'$	0.0	$Y_{v\|r\|}'$	0.0	$N_{v\|r\|}'$	-0.300
$X_{c\|c\|\beta\delta}'$	0.152	Y_{uur}'	0.0	$N_{\|v\|r}'$	0.0
$X_{c\|c\|\delta\delta}'$	-0.093	Y_r'	0.0	$N_{ur}'-x_G'$	-0.231
t	0.22	$Y_{c\|c\|\delta}'$	0.208	$N_{c\|c\|\delta}'$	-0.098
		$Y_{c\|c\|\beta\|\beta\|\delta\|}'$	-2.16	$N_{c\|c\|\beta\|\beta\|\delta\|}'$	0.688
		Y_T'	0.04	N_T'	-0.02
		SHALLOW WATER			
$X_{u\zeta}'$	-0.05	$Y_{v\zeta}'$	-0.387	$N_{r\zeta}'$	-0.0045
$X_{uu\zeta}'$	-0.0061	$Y_{v\|v\|\zeta}'$	-1.50	$N_{uv\zeta}'$	-0.241
$X_{vr\zeta}'$	0.387	$Y_{ur\zeta}'$	0.182	$N_{ur\zeta}'$	-0.047
$X_{vv\zeta\zeta}'$	0.0125	$Y_{c\|c\|\beta\|\beta\|\delta\|\zeta}'$	-0.191	$N_{\|v\|r\zeta}'$	-0.120
				$N_{c\|c\|\beta\|\beta\|\delta\|\zeta}'$	0.344

III. MATHEMATICAL MODEL (CONCLUDED)

NONDIMENSIONAL HYDRODYNAMIC COEFFICIENTS

C. COEFFICIENT VALUES

Coefficient Values for Auxiliary Equations

Rudder Advance Velocity(c) Equation		Propeller Thrust (T) Equation		Propeller Torque (Q) Equation	
Nondimensional Coefficient	Value	Nondimensional Coefficient	Value	Nondimensional Coefficient	Value
c_{uu}''	0.0	T_{uu}''	-0.00695	$k_p^2 - Q_n'$	0.077×10^{-6}
c_{un}''	0.605	T_{un}''	-0.00063	$Q^{F}{}''$	-0.102
$c_{\|n\|n}''$	38.2	$T_{\|n\|n}''$	0.0000354	Q_{uu}''	22.2
c_{nn}''	0.0	T_{nn}''	0.0	Q_{un}''	1.67
Note: Coefficient values apply only when $n \geq 0$; $c = 0$ when $n \leq 0$.				$Q_{\|n\|n}''$	-0.1155
				Q_n''	-0.553
				$Q_k^{E}{}''$	8.22

Notes: (1) Double prime (") denotes that the coefficients are nondimensionalized in accordance with the "Bis" system of Ref. 2 and are referred to a set of fixed-body axis with the origin at midships. According to this system: $m'' = 1$; $I_z'' = k_z^2 m'' = k_z^2$; and $x_G'' = 0.024$.

(2) Simulation of deep water maneuvers requires soley the use of the coefficient values necessary for the deep water terms in the equations.

(3) Simulation of shallow water maneuvers ($\zeta \neq 0$) requires the use of both the deep water and the shallow water coefficients. The added coefficient $Y_{uv\zeta}'' = -0.83 \left(1 - \frac{0.8}{\zeta}\right)$ where $\zeta > 0.8$ and; $= 0$ wh e $\zeta \leq 0.8$.

ESSO 190,000-DWT TANKER

IV. SHIP MANEUVERING CHARACTERISTICS

A. STABILITY AND CONTROL DERIVATIVES AND INDICES

Derivative or Index	Value	
	Fully Appended, n = 1	Bare Hull
Y_{uv}'' Y_v'	-1.205	
N_{uv}'' N_v'		
Y_{ur}'' Y_r'	0.248	
N_{ur}'' N_r'	-0.207	
Y_v'' Y_v'	-1.020	
N_v'' N_v'		
Y_r'' Y_r'		
$k_2 - N_r''$ N_r'	0.1232	
$Y_{\delta r}''$ $Y_{\delta r}'$		
$N_{\delta r}''$ $N_{\delta r}'$		
m'' m'	1.000	
I_z'' I_z'		
$-Y_v''/m''$ $-Y_v'/m'$	1.020	
σ_{1h}''		
σ_{2h}''		
σ_{1h}''		
ℓ_v''	0.374	
ℓ_r''	0.306	
$\ell_r'' - l_v''$ l_d'	-0.068	
$N_{\delta r}''/Y_{\delta r}''$		
$N_{\delta r}''/(N_r''-I_z'')$		

$x_G'' = 0.024$

Note:

Values of nondimensional derivatives given in both the "BIS" system and SNAME standard system to facilitate comparison with other similar ship types.

ESSO 190,000-DWT TANKER

IV. SHIP MANEUVERING CHARACTERISTICS (CONTINUED)

B. NUMERICAL MEASURES FROM DEFINITIVE MANEUVERS

SPIRALS	8 Knot Approach Speed		16 Knot Approach Speed	
	Simulated	Full Scale	Simulated	Full Scale
Loop height, deg/sec	0.2		0.2	
Loop width, deg	0.8		0.8	
Neutral rudder angle, deg	0.4		0.4	
Steady-turning rate, deg/sec @:				
δ_r = 20 deg R	0.19			
δ_r = 10 deg R	0.17			
δ_r = 0 deg				
δ_r = 10 deg L	0.16			
δ_r = 20 deg L				

5-5 ZIGZAGS	Knot Approach Speed		Knot Approach Speed	
	Simulated	Full Scale	Simulated	Full Scale
First Overshoot				
Time to reach execute heading change, sec				
Overshoot heading angle, deg				
Total heading angle change, deg				
Path width at execute, m				
Overshoot path width, m				
Total path width, m				
Second overshoot heading angle, deg				
Third overshoot heading angle, deg				
Period, sec				

IV. SHIP MANEUVERING CHARACTERISTICS (CONTINUED

B. NUMERICAL MEASURES FROM DEFINITIVE MANEUVERS

10-10 ZIGZAGS	8 Knot Approach Speed		16 Knot Approach Speed	
	Simulated	Full Scale	Simulated	Full Scale
First Overshoot				
Time to reach execute heading change, sec				
Overshoot heading angle, deg				
Total heading angle change, deg				
Path width at execute, m				
Overshoot path width, m				
Total path width, m				
Second overshoot heading angle, deg				
Third overshoot heading angle, deg				
Period, sec				
20-20 ZIGZAGS				
First Overshoot				
Time to reach execute heading change, sec			77	63
Overshoot heading angle, deg	13.0		13.5	17.4
Total heading angle change, deg	33.0		33.5	37.4
Path width at execute, m				
Overshoot path width, m				
Total path width, m				
Second overshoot heading angle, deg			14.7	17.5
Third overshoot heading angle, deg				
Period, sec			470.	476.

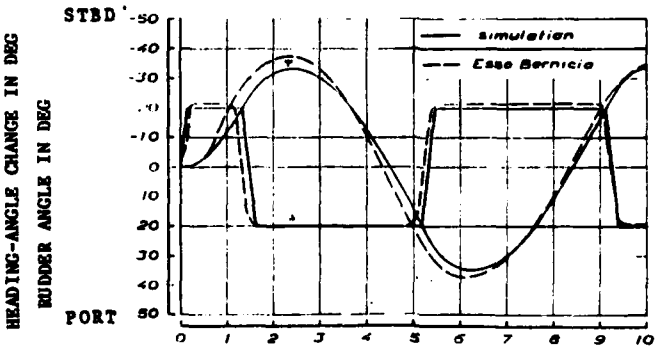

PREDICTED AND FULL-SCALE TRIALS TRAJECTORIES
OF A 20-20 ZIGZAG FOR ESSO 190,000 DWT TANKER

ESSO 190,000-DWT TANKER

IV. SHIP MANEUVERING CHARACTERISTICS (CONTINUED)

B. NUMERICAL MEASURES FROM DEFINITIVE MANEUVERS

STEADY TURNS (20-DEG L RUDDER)	8 Knot Approach Speed		16 Knot Approach Speed	
	Simulated	Full Scale	Simulated	Full Scale
				(1) (2)
Time to change heading 90 deg, sec				
Time to change heading 180 deg, sec				
Speed after 90 deg heading change, knots				
Speed after 180 deg heading change, knots				
Speed loss in steady turn, percent				
Advance, m			1260	
Transfer, m				
Tactical diameter, m			1260	
Steady-turning diameter, m			900	
Steady-turning rate, deg/sec				
STEADY TURNS (35-DEG L RUDDER)				
Time to change heading 90 deg, sec				
Time to change heading 180 deg, sec				
Speed after 90 deg heading change, knots				
Speed after 180 deg heading change, knots				
Speed loss in steady turn, percent				
Advance, m			1010	1245 1130
Transfer, m				
Tactical diameter, m			900	938 1020
Steady-turning diameter, m			600	704 844
Steady-turning rate, deg/sec				
STEADY TURNS (45-DEG L RUDDER)				
Time to change heading 90 deg, sec				
Time to change heading 180 deg, sec				
Speed after 90 deg heading change, knots				
Speed after 180 deg heading change, knots				
Speed loss in steady turn, percent				
Advance, m				
Transfer, m				
Tactical diameter, m				
Steady-turning diameter, m				
Steady-turning rate, deg/sec				

ESSO 190,000-DWT TANKER

IV. SHIP MANEUVERING CHARACTERISTICS (CONCLUDED)

B. NUMERICAL MEASURES FROM DEFINITIVE MANEUVERS

STEADY TURNS (20-DEG R RUDDER)	8 Knot Approach Speed		16 Knot Approach Speed		
	Simulated	Full Scale	Simulated	Full Scale	
Time to change heading 90 deg, sec			218	(1)	(2)
Time to change heading 180 deg, sec			313		
Speed after 90 deg heading change, knots			10.7		
Speed after 180 deg heading change, knots			9.0		
Speed loss in steady turn, percent			53		
Advance, m	1260		1290		
Transfer, m					
Tactical diameter, m	1540		1300		
Steady-turning diameter, m	900		900		
Steady-turning rate, deg/sec	0.19		0.3		
STEADY TURNS (35-DEG R RUDDER)					
Time to change heading 90 deg, sec					
Time to change heading 180 deg, sec					
Speed after 90 deg heading change, knots					
Speed after 180 deg heading change, knots					
Speed loss in steady turn, percent					
Advance, m	970		1020	1263	1060
Transfer, m					
Tactical diameter, m	1010		1010	981	950
Steady-turning diameter, m	600		600	680	844
Steady-turning rate, deg/sec	0.20				

Column (1) - Full-scale Trials of ESSO Norway (Calm deep water at full-load)

(2) - Full-scale Trials of ESSO Malaysia (Calm deep water at full-load)

STANDARDIZED DATA SHEET NO. 3

APPENDIX G

SNAME MATHEMATICAL-MANEUVERING MODEL STANDARDIZED DATA SHEET

FOR

80,000 DWT TANKER

PREPARED BY

Morton Gertler

The following pages describe the sources and present values for the hydrodynamic coefficients and other data required with the specified equations of motion to perform computer simulation predictions of various maneuvering characteristics of the above ship type. The results of such simulations are also presented, and compared with corresponding full-scale trial data, whenever such data exist and are readily available.

I. DATA SOURCE AND ACQUISITION TECHNIQUE

A. MODEL TEST PROGRAM

SPONSOR: USCG, MARAD, COE, and NSF

LABORATORY: Davidson Laboratory(DL), Stevens Institute of Technology, Hoboken, N.J.

TECHNIQUE USED: Rotating-arm tests(Supplemented by estimates based other experimental and theoretical data).

TEST FACILITY: DL Rotating-Arm Facility

SIZE - Rectangular basin-22.6 m long,22.6 m wide, and 1.524 m deep (full)

DESCRIPTION - 19.5 m long rotating arm girder is mounted on a central pivot post and its free ends are counter balanced. (See Ref. 1 and 2)

TEST APPARATUS: Electronic strain gage balances mounted above tanker model were used to measure longitudinal force, side force, and yawing moment; transducer signals transmitted by overhead cables calibrated standard recording equipment on shore. (Ref. 2)

SHIP MODEL PARTICULARS:

DESIGNATION - DL Tanker 80 Model SIZE: 155.0 cm LBP x 25.4 cm B x 8.11 T

CONSTRUCTION MATERIAL - Wood with smooth painted surface

TURBULENCE STIMULATION DEVICE -

TEST DATE:

TEST CONDITIONS: Full-load and ballast conditions in calm deep water. Also shallow tests at both conditions at various depth-to-draft ratios (H/T). Model free to trim and self propelled aver a range of overloads and underloads including the standard reference ship-propulsion point (n=1.0) recommended by ITTC (Ref. 3). See Ref. 2

TEST PARAMETER RANGE: F_N = 0.04,0.08,0.16,0.30 H/T = ∞,1.5,1.2,1.1

n Range including n=1.0 and model propulsion point.	$\dot{r}'$	ϕ
β -25 to+25 degrees	$\dot{v}'$	θ
r'-0.80 to +0.80	$v' \lvert r' \rvert$	Δ
δ_r -40 to +40 degrees		

DATA REDUCTION AND ANALYSIS METHODS: Hydrodynamic coefficient values (nondimensionalized by standard SNAME-ITTC sytem) were obtained predominantly by least squares fits to third order, of plotted rotating-arm test data (Ref. 2). Missing values such as "added mass" derivatives were estimated based on theory and/or empirical data from PMM tests for similar ships.

PUBLISHED SOURCES: Numerical values of hydrodynamic coefficients were not previously published. Values presented in the accompanying data sheets apply only to the calm, deep-water, open sea case. Numerical values of hydrodynamic coefficients required to simulate maneuvering in shallow and restricted water are not yet available.

I. DATA SOURCE AND ACQUISITION TECHNIQUE (CONTINUED)

B. SHIP MANEUVERING PREDICTIONS

SPONSOR: USCG, ONR, MARAD, COE, AND NSF

SIMULATION FACILITY: DL Simulator Facility (Combination of digital computer terminal and plotter). (See Ref. 4, 5, and 6 for description and examples)

MATHEMATICAL MODEL: DL standard equations of motion (third order Taylor expansion-second order coefficients only for even functions; first and third order coefficients for odd functions. With coefficient values supplied mainly from rotating-arm tests. The equations, rewritten with dimensional terms compatible with standard SNAME notation and format, are presented later. The original standard equations (nondimensionalized using DL notation) are given also.

SIMULATED DEFINITIVE MANEUVERS: Spirals; 20-20 zig-zags and steady turns with 15, 25, and 35 degrees rudder (assuming zero neutral rudder angle) were conducted for the calm deep-water case. Also, spirals and 35 degree rudder turns were conducted to show differences between deep- and shallow-water operations (full-load and ballast conditions) but the results are not included in the data sheets.

PUBLISHED RESULTS: Some numerical measures from simulated spirals and steady-turning maneuvers for the 80,000 DWT Tanker in deep-water and in shallow-water of depth-to-draft ratios of 1.5 and 1.2 are presented graphically for both full-load and ballast conditions in Ref. 6. Simulated trajectories for the 35 degree rudder turning maneuver at the deep- and shallow-water conditions are also presented.

C. FULL-SCALE MANEUVERING TRIALS AND CORRELATION

SHIP: 80,00 DWT Tanker

TRIALS DATES: 14 April 1968 (Deep Water)

TYPE OF TRIALS:

TRIALS INSTRUMENTATION:

I. DATA SOURCE AND ACQUISITION TECHNIQUE (CONCLUDED)

TRIALS CONDITION:

MANEUVERS PERFORMED:

DATA REDUCTION AND ANALYSIS:

PUBLISHED RESULTS: No specific published trials report. Trajectories showing correlation between simulated predictions and full-scale trial measurements for a 35 degree rudder deep-water steady-turning maneuver are given in Ref. 6.

D. REFERENCES

1. Suarez, A.,"The Davidson Laboratory Rotating-Arm Facility," DL Note 597, June 1966.

2. Eda, Haruzo,"Ship Maneuvering Characteristics in Deep and Shallow Water - Applications of Captive Model Test Results," Written in contribution to 18th ATTC, August, 1977.

3. Gertler, Morton, "Final Analysis of First Phase ITTC Standard-Model-Test Program," Appendix 3, Part 2 of Maneuverability Committee Report, Proceedings of the 12th ITTC, 1969.

4. Eda, H. and Crane, C.L.,Jr.,"Steering Characteristics of Ships in Calm Water and Waves," Transactions, SNAME, Vol. 73, 1965.

5. Crane, C.L.,Jr.,"Maneuvering Safety of Large Tankers: Stopping, Turning, and Speed Selection," Transactons, SNAME, Vol. 81, 1973.

6. Eda, Haruzo, Falls, Robert, and Walden, David A.,"Ship Maneuvering Safety Studies," Transactions, SNAME, Vol. 87, 1979.

II. SHIP GEOMETRY

A. PRINCIPAL GEOMETRIC CHARACTERISTICS

Hull	Ship	Model	Rudder	Ship	Model
L, m	232.56	1.5504	$\bar{b}$, m		
B, m	38.10	0.2540	c_r, m		
T, m	12.16	0.0811	c_t, m		
Trim, m by stern			A_T, m^2	48.081	0.00214
Δ, tons, lbs	86980.	0.02507	A_F, m^2	6.731	0.00300
∇, meters^3	86207	0.02554	A_M, m^2	41.350	0.00184
S, m^2			$a = \bar{b}^2/A_T$	1.500	1.500
LCG, m fwd of AP			Balance, percent		
VCG, m above			A_T/LT	0.017	0.017
L/B	6.104		δ_r, deg max.	35.0	40.0
B/T	3.133		$\dot{\delta}_r$, deg/sec	2.33	-
C_B	0.80				
C_V(1000)	6.853		Propeller (Rotation -)		
LCG/L			No. of Blades		
Bilge Keels			D, m		
b, m			P(0.7 R), m		
c, m			P/D		
			D/T		

Note: Geometry for full-load.

B. LINES

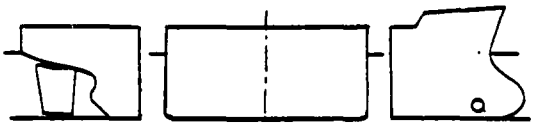

C. RUDDER DETAILS

III. MATHEMATICAL MODEL

SUMMARY OF EQUATIONS OF MOTION

DL Standard Equations - Restated in dimensional format using SNAME standard notation

A. BASIC EQUATIONS

Axial Force

$$
\begin{aligned}
m[\dot{u} - vr] = &+ \frac{\rho}{2} L^2[X_{uu}' u^2] + \frac{\rho}{2} L^3[X_{vr}' vr] \\
&+ \frac{\rho}{2} L^2[1/2 X_{vv}' v^2] + \frac{\rho}{2} L^2[1/2 X_{\delta r \delta r}' u^2 \delta r^2] \\
&+ \frac{\rho}{2} L^3[X_{u}' \dot{u}] + \frac{\rho}{2} L^2 [X_{(p)}' u^2] \\
&+ \frac{\rho}{2} L^2 u^2[X_{(a)}' + X_{(t)}' + X_{(m)}'] \\
&+ \frac{\rho}{2} L^2 u^2[X_{(A)}' + X_{(f)}']
\end{aligned}
$$

Lateral Force

$$
\begin{aligned}
m[\dot{v} + ur] = &+ \frac{\rho}{2} L^2[Y_{*}' u^2] + \frac{\rho}{2} L^2[Y_{v}' uv] \\
&+ \frac{\rho}{2} L^3[Y_{r}' ur] + \frac{\rho}{2} L^2[Y_{\delta r}' u^2 \delta r] \\
&+ \frac{\rho}{2} L[Y_{yo}' u^2 yo] + \frac{\rho}{2} L^3[Y_{vvr}' v^2 r \div u] \\
&+ \frac{\rho}{2} L^4[Y_{vrr}' vr^2 \div u] + \frac{\rho}{2} L^2[Y_{vvv}' v^3 \div u] \\
&+ \frac{\rho}{2} L^5[Y_{rrr}' r^3 \div u] + \frac{\rho}{2} L^2[Y_{\delta r \delta r \delta r}' u^2 \delta r^3] \\
&+ \frac{\rho}{2} \frac{1}{L}[Y_{yoyoyo}' u^2 yo^3] + \frac{\rho}{2} L^4[Y_{r}' \dot{r}] \\
&+ \frac{\rho}{2} L^3[Y_{v}' \dot{v}] + \frac{\rho}{2} L^2[Y_{(p)}'] \\
&+ \frac{\rho}{2} L^2 u^2[Y_{(a)}' + Y_{(b)}' + Y_{(t)}' + Y_{(m)}'] \\
&+ \frac{\rho}{2} L^2 u^2[Y_{(A)}' + Y_{(f)}']
\end{aligned}
$$

Yaw Moment

$$
\begin{aligned}
I_z \dot{r} = &+ \frac{\rho}{2} L^3[N_{*}' u^2] + \frac{\rho}{2} L^2[N_{v}' uv] + \frac{\rho}{2} L^4[N_{r}' ur] \\
&+ \frac{\rho}{2} L^3[N_{\delta r}' u^2 \delta r] + \frac{\rho}{2} L^2[N_{yo}' u^2 yo] \\
&+ \frac{\rho}{2} L^4[N_{vvr}' v^2 r \div u] + \frac{\rho}{2} L^5[N_{vrr}' vr^2 \div u] \\
&+ \frac{\rho}{2} L^3[N_{vvv}' v^3 \div u] + \frac{\rho}{2} L^6[N_{rrr}' r^3 \div u] \\
&+ \frac{\rho}{2} L^3[N_{\delta r \delta r \delta r}' u^2 \delta r^3] + \frac{\rho}{2}[N_{yoyoyo}' u^2 yo^3] \\
&+ \frac{\rho}{2} L^5[N_{r}' \dot{r}'] + \frac{\rho}{2} L^4[N_{v}' \dot{v}'] + \frac{\rho}{2} L^3[N_{(p)}' u^2] \\
&+ \frac{\rho}{2} L^3 u^2[Y_{(a)}' + N_{(b)}' + N_{(t)}' + N_{(m)}' + N_{(A)}' \\
&\quad + N_{(f)}' + N_{(c)}']
\end{aligned}
$$

B. SUPPLEMENTARY EQUATIONS

Autopilot:

$$\delta r_{(d)} = a(\psi - \psi_{(d)}) + b'\dot{\psi}' + c'p' + d'\dot{p}' + \delta r_{(e)}$$

where:

$\delta r_{(d)}$ is the desired rudder angle;
a, b', c', d' are the yaw, yaw-rate, path-deviation, path-deviation-rate gain constants, respectively;
p' is the perpendicular distance from the ship LCG to the channel centerline, positive or negative when the ship is proceeding either on the righthand or lefthand side of the channel, respectively;
$\dot{p}'$ is the path-deviation rate; and
$\delta r_{(e)}$ is the equilibrium rudder angle required to maintain steady straight course.

Auxiliary Relationships: Effect of propeller advance coefficient J or slip ratio s on longitudinal force and rudder coefficients;

$X_{(p)}' = T'(1-t)$ which is a nonlinear function of J or s and equal to $-X_{uu}'$ at ship propulsion point ($\eta = 1.0$)

$$Y_{\delta r(i)}' = \left[\frac{1 + ks_{(i)}^{1.5}}{1 + ks^{1.5}}\right] Y_{\delta r}'$$

$$N_{\delta r(i)}' = \left[\frac{1 + ks_{(i)}^{1.5}}{1 + ks^{1.5}}\right] N_{\delta r}'$$

$$Y_{\delta r \delta r \delta r(i)}' = \left[\frac{1 + ks_{(i)}^{1.5}}{1 + ks^{1.5}}\right] Y_{\delta r \delta r \delta r}'$$

$$N_{\delta r \delta r \delta r(i)}' = \left[\frac{1 + ks_{(i)}^{1.5}}{1 + ks^{1.5}}\right] N_{\delta r \delta r \delta r}'$$

where subscript i denotes instantaneous value

Notes: The above equations are referred to a right-handed orthogonal system of moving axis, fixed in the ship, with it's origin at the ship center of mass ($x_G = 0$). The equations include the restricted channel case and can be used to simulate maneuvers in water of constant depth (either deep or shallow) by substitution of the appropriate coefficient values.

III. MATHEMATICAL MODEL (CONTINUED)

SUMMARY OF EQUATIONS OF MOTION

DL Standard Equations - Original Nondimensional Presentation

A. BASIC EQUATIONS

Axial Force

$$m'(\dot{u}' - v'r') =$$

$$X' = c_o + c_1 v'r' + c_2 v'^2 + c_3 \delta^2 + c_4 \dot{u}' + X_p' + X_a' + X_t' + X_m' + X_n' + X_f'$$

Lateral Force

$$m'(\dot{v}' + u'r') =$$

$$Y' = b_o + b_1 v' + b_2 r' + b_3 \delta + b_4 y_o' + b_5 v'^2 r' + b_6 v' r'^2 + b_7 v'^3 + b_8 r'^3 + b_9 \delta^3 + b_{10} y_o'^3 + b_{11} \dot{r}' + b_{12} \dot{v}' + Y_p' + Y_a' + Y_b' + Y_t' + Y_m' + Y_n' + Y_f'$$

Yaw Moment

$$I_z'\dot{r}' =$$

$$N' = a_o + a_1 v' + a_2 r' + a_3 \delta + a_4 y_o' + a_5 v'^2 r' + a_6 v' r'^2 + a_7 v'^3 + a_8 r'^3 + a_9 \delta^3 + a_{10} y_o'^3 + a_{11} \dot{r}' + a_{12} \dot{v}' + N_p' + N_a' + N_b' + N_t' + N_m' + N_n' + N_f' + N_c'$$

B. SUPPLEMENTARY EQUATIONS

Autopilot:

$$\delta_d = a(\psi - \psi_d) + b'\dot{\psi}' + c'(\text{sign})p_\ell' + d'\dot{p}_\ell' + \delta_e$$

where:

δ_d is the desired rudder angle;
a,b',c',d' are the yaw, yaw-rate, path-deviation, and path-deviation-rate, gain constants, respectively;
ψ_d is the desired yaw angle:
p_ℓ' is the perpendicular distance from the ship LCG to the channel centerline;
(sign) is positive or negative when ship is proceeding either at the righthand or lefthand side of the channel, respectively; and
δ_e is the equilibrium rudder angle for steady straight course condition.

Auxiliary Relationships: Effect of propeller slip ratio $S = 1 - u/pn$ on rudder coefficients-

$$a_3 = \left[\frac{1 + ks^{1.5}}{1 + ks_e^{1.5}}\right] a_{3e}$$

$$a_9 = \left[\frac{1 + ks^{1.5}}{1 + ks_e^{1.5}}\right] a_{9e}$$

$$b_3 = \left[\frac{1 + ks^{1.5}}{1 + ks_e^{1.5}}\right] b_{3e}$$

$$b_9 = \left[\frac{1 + ks^{1.5}}{1 + ks_e^{1.5}}\right] b_{9e}$$

Where

k is a semi-empirical constant and subscript e denotes straight course equilibriumvalues.

Notes: The above equations are referred to a right-handed orthogonal system of moving axis, fixed in the ship, with it's origin at the ship center of mass ($x_G = 0$). The equations include the restricted channel case and can be used to simulate maneuvers in water of constant depth (either deep or shallow) by substitution of the appropriate coefficient values. Primed quantities and coefficients a,b,c in basic equations are nondimensionalized using powers L (standard SNAME system). For definition of symbols see Sheet 3-7 and standard notation.

III. MATHEMATICAL MODEL (CONCLUDED)

NONDIMENSIONAL HYDRODYNAMIC COEFFICIENTS

C. COEFFICIENT VALUES

X - Equation			Y - Equation			N - Equation		
Nondimensional Coefficient		Value	Nondimensional Coefficient		Value	Nondimensional Coefficient		Value
DL	SNAME		DL	SNAME		DL	SNAME	
c_0	X'_{uu}	-0.00064	b_o	Y'_*	0.00000	a_o	N'_*	0.00000
c_1	X'_{vr}	0.01086	b_1	Y'_v	-0.01650	a_1	N'_v	-0.00600
c_2	$\frac{1}{2}X'_{vv}$	-0.00384	b_2	Y'_r	-0.00395	a_2	N'_r	-0.00310
c_3	$\frac{1}{2}X'_{\delta r\delta r}$	-0.00152	b_3	$Y'_{\delta r}$	0.00305	a_3	$N'_{\delta r}$	-0.00140
c_4	$X.'_u$	-0.00030	b_4	Y'_{yo}	0.00000	a_4	N'_{yo}	0.00000
X'_p	$X'_{(p)}$		b_5	Y'_{vvr}	0.02000	a_5	N'_{vvr}	-0.03000
X'_a	$X'_{(a)}$		b_6	Y'_{vrr}	-0.02900	a_6	N'_{vrr}	0.01400
X'_t	$X'_{(t)}$		b_7	Y'_{vvv}	-0.03900	a_7	N'_{vvv}	0.00300
X'_m	$X'_{(m)}$		b_8	Y'_{rrr}	0.00000	a_8	N'_{rrr}	0.00000
X'_n	$X'_{(n)}$		b_9	$Y'_{\delta r\delta r\delta r}$	-0.00100	a_9	$N'_{\delta r\delta r\delta r}$	-0.00200
X'_f	$X'_{(f)}$		b_{10}	Y'_{yoyoyo}	0.00000	a_{10}	N'_{yoyoyo}	0.00000
			b_{11}	$Y.'_r$	0.00000	a_{11}	$N.'_r$	-0.000718
			b_{12}	$Y.'_v$	-0.01086	a_{12}	$N.'_v$	0.00000
			Y'_a	$Y'_{(a)}$		N'_p	$N'_{(p)}$	
			Y'_p	$Y'_{(p)}$		N'_a	$N'_{(a)}$	
			Y'_t	$Y'_{(t)}$		N'_b	$N'_{(b)}$	
			Y'_m	$Y'_{(m)}$		N'_t	$N'_{(t)}$	
			Y'_n	$Y'_{(n)}$		N'_c	$N'_{(c)}$	
			Y'_f	$Y'_{(f)}$		N'_m	$N'_{(m)}$	
			m'	m'	0.01370	N'_n	$N'_{(n)}$	
						N'_f	$N'_{(f)}$	
						I'_z	I'_z	0.000802

NOTES:

The above nondimensional coefficients are referred to a set of moving axis, fixed in the body, with its origin at the ship center of gravity ($x_G = 0$). Separate columns are used to equate the DL with SNAME-based notation. Prime denotes that coefficients are nondimensionalized using powers of L in accordance with SNAME standards. The a,b,c coefficients (DL Notation) are not primed but are nondimensionalized in the same manner. Parentheses are used with subscripts of some of the coefficients in the SNAME columns to distiguish them from derivatives.

IV. SHIP MANEUVERING CHARACTERISTICS

A. STABILITY AND CONTROL DERIVATIVES AND INDICES

Derivative or Index	Value	
	Fully Appended, n = 1	Bare Hull
Y_v'	-0.01650	
N_v'	-0.0060	
Y_r'	0.00395	
N_r'	-0.00310	
$Y_{\dot{v}}'$	-0.01086	
$N_{\dot{v}}'$	0.00000	
$Y_{\dot{r}}'$	0.00000	
$N_{\dot{r}}'$	-0.000718	
$Y_{\delta r}'$	0.00305	
$N_{\delta r}'$	-0.00140	
m'	0.01370	
I_z'	0.000802	
$-Y_{\dot{v}}'/m'$	0.79270	
σ_{1h}'	0.07077	
σ_{2h}'	-2.78207	
σ_{1h}''	0.01344	
ℓ_v'	0.36364	
ℓ_r'	0.31795	
ℓ_d'	-0.04569	
$N_{\delta r}'/Y_{\delta r}'$	-0.45902	
$N_{\delta r}'/(N_{\dot{r}}'-I_z')$	0.92105	

NOTE:

Nondimensional derivatives and indices are referred to an origin at the ship C.G. ($x_G = 0$). Values apply to full-load conditions in calm deep water.

IV. SHIP MANEUVERING CHARACTERISTICS (CONTINUED)

B. NUMERICAL MEASURES FROM DEFINITIVE MANEUVERS

SPIRALS	8 Knot Approach Speed		16 Knot Approach Speed	
	Simulated	Full Scale	Simulated	Full Scale
Loop height, deg/sec	0.352		0.704	
Loop width, deg	2.22		2.22	
Neutral rudder angle, deg	0.00		0.00	
Steady-turning rate, deg/sec				
δ_r = 20 deg R	0.227		0.454	
δ_r = 10 deg R	0.222		0.444	
δ_r = 0 deg	±0.176		±0.352	
δ_r = 10 deg L	-0.222		-0.444	
δ_r = 20 deg L	-0.227		-0.454	

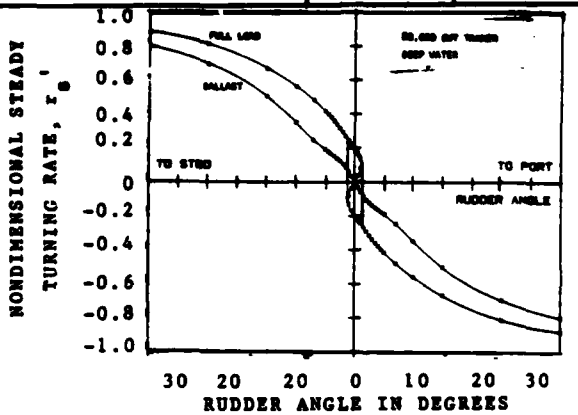

RESULTS OF SIMULATED SPIRAL MANEUVERS FOR 80,000 DWT TANKER

5-5 ZIGZAGS	Knot Approach Speed		Knot Approach Speed	
	Simulated	Full Scale	Simulated	Full Scale
First Overshoot				
Time to reach execute heading change, sec				
Overshoot heading angle, deg				
Total heading angle change, deg				
Path width at execute, m				
Overshoot path width, m				
Total path width, m				
Second overshoot heading angle, deg				
Third overshoot heading angle, deg				
Period, sec				

Note:

Simulator predictions are based on zero neutral rudder angle (Y ', N ' = 0). Therefore, numerical measures derived from predicted definitive maneuvers such as spirals and steady-state turns have equal values corresponding to equal right and left rudder angles.

IV. SHIP MANEUVERING CHARACTERISTICS (CONTINUED)

B. NUMERICAL MEASURES FROM DEFINITIVE MANEUVERS

10-10 ZIGZAGS	8 Knot Approach Speed		15 Knot Approach Speed	
	Simulated	Full Scale	Simulated	Full Scale
First Overshoot				
Time to reach execute heading change, sec				
Overshoot heading angle, deg				
Total heading angle change, deg				
Path width at execute, m				
Overshoot path width, m				
Total path width, m				
Second overshoot heading angle, deg				
Third overshoot heading angle, deg				
Period, sec				
20-20 ZIGZAGS				
First Overshoot				
Time to reach execute heading change, sec			61.8	
Overshoot heading angle, deg			11.4	
Total heading angle change, deg			31.4	
Path width at execute, m				
Overshoot path width, m				
Total path width, m				
Second overshoot heading angle, deg			10.9	
Third overshoot heading angle, deg			10.3	
Period, sec			348.9	

Note: For calm deep water at full-load.

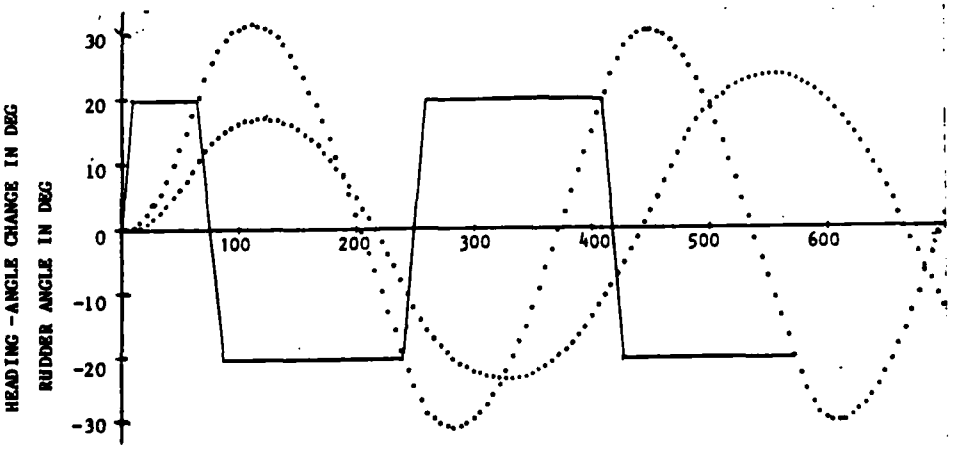

PREDICTED TRAJECTORIES OF A 20-20 ZIGZAG FOR 80,000 DWT TANKER
(Full-load condition in calm deep water)

IV. SHIP MANEUVERING CHARACTERISTICS (CONTINUED)

B. NUMERICAL MEASURES FROM DEFINITIVE MANEUVERS

STEADY TURNS (20-DEG R RUDDER)	8 Knot Approach Speed		16 Knot Approach Speed	
	Simulated	Full Scale	Simulated	Full Scale
Time to change heading 90 deg, sec				
Time to change heading 180 deg, sec				
Speed after 90 deg heading change, knots				
Speed after 180 deg heading change, knots				
Speed loss in steady turn, percent	70.7		70.7	
Advance, m				
Transfer, m				
Tactical diameter, m				
Steady-turning diameter, m	610.4		610.4	
Steady-turning rate, deg/sec	0.227		0.454	
STEADY TURNS (35-DEG R RUDDER)				
Time to change heading 90 deg, sec				
Time to change heading 180 deg, sec				
Speed after 90 deg heading change, knots				
Speed after 180 deg heading change, knots				
Speed loss in steady turn, percent	74.4		74.4	
Advance, m				
Transfer, m				
Tactical diameter, m				
Steady-turning diameter, m	523.8		523.8	
Steady-turning rate, deg/sec	0.230		0.460	

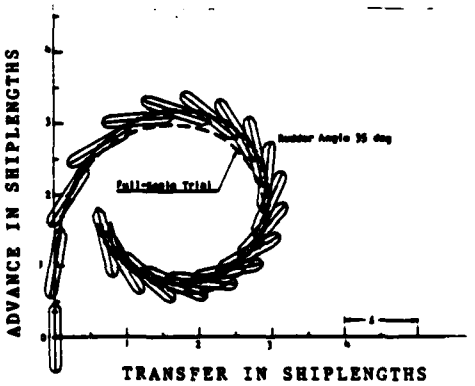

FROM REF. 6
14 APRIL 1968 TRIAL
HALF AHEAD SPEED
SHIP SHOWN AT ONE MINUTE INTERVALS
FULL LOAD, DEEP WATER

PREDICTED AND FULL-SCALE TRIALS TRAJECTORIES FOR 80,000 DWT TANKER

IV. SHIP MANEUVERING CHARACTERISTICS (CONCLUDED)

B. NUMERICAL MEASURES FROM DEFINITIVE MANEUVERS

STEADY TURNS (20-DEG L RUDDER)	8 Knot Approach Speed		16 Knot Approach Speed	
	Simulated	Full Scale	Simulated	Full Scale
Time to change heading 90 deg, sec				
Time to change heading 180 deg, sec				
Speed after 90 deg heading change, knots				
Speed after 180 deg heading change, knots				
Speed loss in steady turn, percent	70.7		70.7	
Advance, m				
Transfer, m				
Tactical diameter, m				
Steady-turning diameter, m	610.4		610.4	
Steady-turning rate, deg/sec	0.227		0.454	
STEADY TURNS (35-DEG L RUDDER)				
Time to change heading 90 deg, sec				
Time to change heading 180 deg, sec				
Speed after 90 deg heading change, knots				
Speed after 180 deg heading change, knots				
Speed loss in steady turn, percent	74.4		74.4	
Advance, m				
Transfer, m				
Tactical diameter, m				
Steady-turning diameter, m	523.8		523.8	
Steady-turning rate, deg/sec	0.230		0.460	
STEADY TURNS (45-DEG L RUDDER)				
Time to change heading 90 deg, sec				
Time to change heading 180 deg, sec				
Speed after 90 deg heading change, knots				
Speed after 180 deg heading change, knots				
Speed loss in steady turn, percent				
Advance, m				
Transfer, m				
Tactical diameter, m				
Steady-turning diameter, m				
Steady-turning rate, deg/sec				

AD-P003 823

Tracor Hydronautics

TECHNICAL PAPER

A Proposed Basis for Evaluating Ship Maneuvering Performance

Roderick A. Barr
Eugene R. Miller, Jr.

August 1983

Prepared for the
20th American Towing Tank Conference
Maneuvering Session

Tracor Hydronautics

INTRODUCTION

Tracor Hydronautics, Incorporated completed a study designed to provide a rational, quantitative basis for evaluating the maneuvering performance and capabilities of commercial vessels larger than 1,000 metric ton displacement. This work, which was carried out for the U. S. Coast Guard under Contract DTCG23-80-C-20037, is described in detail by Barr, et al (1).

The study was motivated by a long term awareness of the need for maneuvering performance standards and by the requirement that the Coast Guard provide rules and regulations governing ship safety and pollution control. In particular, the Coast Guard has been charged (2) to:

> "Begin publication as soon as practicable of proposed rules and regulations setting forth minimum standards of design, construction, alteration, and repair of vessels ... such rules and regulations shall, to the extent possible, include but not be limited to improved vessel maneuvering and stopping ability and otherwise reduce the possibility of collisions, grounding or other accident...." (emphasis added)

At the initiation of the study, few standards or requirements for ship maneuvering and stopping performance were known to exist. There were a number of reasons for this: Most ships traditionally have at least acceptable maneuvering performance; human operators are highly adaptable and can compensate, at least in part, for poor ship capability; and owners

do not have any clear economic incentive to improve maneuvering performance. Any meaningful and successful standards needed to reflect these considerations and to avoid rigid or inflexible (go/no go) requirements.

It seemed clear ~~at the beginning of the study~~ that standards should be based on some type of performance rating, should be generally acceptable in format to industry, and should reflect inherent ship controllability under conditions typical of those under which most ship maneuvering, and most CRG (collision, ramming, and grounding) casualties, occur.

The imposition, by regulatory agencies such as the Coast Guard, or the voluntary acceptance, by industry, of any maneuvering performance standards, will have important implications for ship design and model testing. It will become desirable, if not essential, to insure, during the design process, that a ship will have acceptable maneuvering performance. At present, this can only be done using captive or free running model tests, and towing tanks will need to develop suitable means for conducting such tests with models of adequate size.

This paper summarizes the work of the study and the resulting proposed maneuvering standards. Reference 1 presents a detailed description of the study, including a summary of all trials data used in the study.

APPROACH TO DEVELOPMENT OF STANDARDS

The approach selected for developing standards involved a three-level process in which available data were used to establish:

- "Criteria" which could be used as a basis for selecting specific measures of performance.
- "Measures" of performance which would provide a basis for selecting quantitative performance levels.
- "Levels" of performance which would represent specific quantitative definitions of performance, i.e., superior performance, average performance, etc.

In establishing the proposed maneuvering performance standards, several separate approaches were followed, including:

- An analysis of ship casualty data to see what correlation could be established between ship maneuvering performance and maneuvering related casualties.
- Collection and analysis of a large enough body of ship trials data to rate ship maneuvering performance primarily on the basis of ship's peformance in selected trials maneuvers.
- Simulations of the effect of ship aerodynamic characteristics on the ability of a ship to maintain course and/or execute a desired maneuver.

Nature of Standards

Performance standards were developed based on the following assumpions:

(1) All vessels must have the inherent maneuvering capability to permit navigation from Point A to Point B;

(2) The greatest demands on maneuvering performance occur in restricted waters, and all vessels must be able to initiate and check a turn, maintain course, stop, operate at

moderate speeds and not be overly sensitive to the environment;

(3) Standards should cover normal operating conditions and provide a ranking of performance relative to other vessels of a similar size and type. Measures of maneuvering performance should reflect the following criteria:

- The measures should be directly related to the type of performance being rated, i.e., head reach is a good measure of stopping ability,
- The measures should be ones which can be based on available data for existing ships since the rankings are relative,
- The performance in a given measure should be able to be determined from trials,
- There should be no significant increase in the complexity or length of trials, in order to obtain data needed to establish performance standards,
- The measures should reflect the effects of environment, and particularly wind, on maneuvering performance.

For each measure considered, quantitative levels of performance must be established. For the proposed standards, five levels of performance were used: superior, above average, average, below average, and marginal. These levels were established based on the following considerations:

- Performance levels which are known, on the basis of operating experience or simulation studies, to increase or reduce casualty risk.
- Performance levels that significantly differ from those of other vessels of similar size and type, i.e., performance which a pilot would not expect.

- Performance levels of vessels identified by pilots as "problem vessels" or "superior vessels."
- Performance levels of vessels with a large number of casualties.

Reference 1 describes in detail the establishment of rankings based on levels of performance defined by these considerations. It should be noted that the proposed rankings are based almost entirely on the first two of these factors. The latter two factors need further study so that performance rankings can adequately reflect all four factors.

One important factor which must be considered in establishing performance measures and levels is whether to use dimensional or nondimensional parameters. The particular measures selected in this study are those which are felt to provide the best means for assessing performance. Most of the measures selected involve some degree of nondimensionalization in order to suitably systematize the data.

In addition, there are other aspects of ship maneuvering which have been identified as important but which are not covered by these measures. They include the effects of wind and current and special maneuvering requirements imposed in restricted water situations. The effects of windage can be significant, but it is not practical to quantify it by the conduct of routine trials. Thus, it is proposed to require a special investigation of the effect of wind during the design stages for vessels which exceed a certain ratio of above water profile area to below water profile area, as described in Reference 1.

Discussions of pilots indicate that one of the most important aspects of maneuverability in restricted waters is the ability to maintain control while coasting and slowing down. This can be done by direct control with the rudder and/or alternately going astern and ahead and using the improved rudder effectiveness from the propeller slip stream. This aspect of a ship's maneuvering performance could be characterized by a coasting zig-zag maneuver. Such maneuvers are not routinely performed so there is no body of data against which to compare performance. Such a maneuver would also increase the time and complexity of the trials. An alternate to an additional trial maneuver is to require special investigation of the maneuvering performance of vessels which have characteristics which are known to cause poor low speed control. These include vessels with rudders located outside the propeller race and diesel powered vessels with such a small amount of starting air that the engines cannot be reversed as often as desired. At this time, it is recommended that the approach of special investigation for vessels with such characteristics be followed. This should be considered further.

The proposed standards are based entirely on deep water trials data, as shallow water trials data were available for only one vessel, the ESSO OSAKA (2). However, maneuvering is usually most important in relatively shallow water where bottom effects are important. It may soon be possible to propose maneuvering performance standards for shallow water, at least for tankers, based on the growing body of captive model test and simulation results. Shallow water trials are far more difficult and costly to conduct than are deep water trials.

Therefore, when and if shallow water performance standards are developed and adopted, model tests will probably become the accepted method for evaluating ship performance.

Trial Maneuvers

In the development of maneuvering standards, the types of maneuvering problems associated with CRG casualties should be considered. Much more work should have been done in this area than has been the case. However, a number of references do address this. Reference 1 presents a summary of results of analyses of CRG casualty reports.

Miller, et al (3) showed that in cases in which vessel controllability could have affected the result, typical casualty situations reoccurred. That paper also suggested a number of controllability evaluation maneuvers that could be related to the typical casualty situations. These maneuvers and their relationship to the typical casualty situations are listed in Table 1 of the paper. The important conclusion from this table is that controllability evaluation maneuvers can be related to CRG casualty situations and that these evaluation maneuvers are <u>not necessarily</u> the same as the maneuvers performed on normal trials and for which data are available.

At present, commercial ship maneuvering performance is generally characterized by performance of two standards trial maneuvers, maximum rudder angle turns and crash stop. It has now become standard practice to post results of these maneuvers on the ship's bridge, as discussed by Landsburg, et al (4). In many cases, trials also include additional standard maneuvers such as zig-zags, and spiral maneuvers or turns at

smaller rudder angles. The nature and conduct of various standard maneuvers are discussed in detail in a SNAME Research Bulletin (5) and in the Maneuvering Committee Report to the Fourteenth International Towing Tank Conference (6).

Table 1, from the 1975 ITTC report, compares recommended or proposed maneuvering trials from various sources. The most widely proposed tests are the full speed turning test and the zig-zag (all five sources) and the full speed crash stop (four sources). These are, in fact, the most widely conducted maneuvers. Each of the maneuvers of Table 1 is described in Reference 6, as are the usual performance measures derived from these maneuvers.

Based on these considerations and on the previously defined "criteria," appropriate "measures" of maneuvering performance were selected for use in the performance standards.

TABLE 1

Maneuvering Trials Recommended
by Various Organizations

	BSRA	SNAME	DnV	10th ITTC	14th ITTC
Crash-stop (AV) at full speed	x	x	x		x
Stopping trial at low speed					x
Coasting stop test			x		
Crash-stop (AR)		x			
Stopping by use of rudder			x		
Turning test at full speed	x	x	x	x	x
Turning test at medium speed					x
Turning test at slow speed	x		x		x
Turning test with propulsion stopped			x		
Turning test from zero speed	x				x
Pull-out	x				x
Weave manoeuvre	x				
Zigzag	x	x	x	x	x
Direct spiral	x			x	x
Reverse spiral	x		x		x
Statistical method	x				
Change of heading				x	x
Lateral thruster :					
- Turning test			x		x
- Zigzag test, ahead			x		x
- Zigzag test, astern			x		x
- Course-keep test, astern			x		

Development and Use of a Ship Maneuvering Data Base

An important part of the study was the development of a ship maneuvering trials data base program and the use of this program to analyze available trials data for standard maneuvers. Data for 603 ships were collected and used. These ships are listed by ship type in Table 2. The general structure of the data format used is described in Table 3. It includes data for the ship and for three types of maneuvers: stops, turns, and zig-zags. These three maneuvers were selected as the only ship trials maneuvers for which a statistically significant body of data were available.

TABLE 2

Distribution of Ship by Type in Maneuvering Data Base

Ship Type	No. of Ships
Tankers	364
Bulk Carriers	90
Cargo Ships	4
Container Ships	4
Others	4
Not Identified[1]	137
Total	603

[1] For these ships, which were primarily from data provided to IMCO, all necessary ship characteristics and maneuvering performance data were provided, but the ship type was not identified. These data have been determined to be suitable for inclusion in the data base, despite the fact that the ship types were not identified.

A primary purpose for creating the maneuvering performance data file was to provide a means for analyzing and assessing maneuvering performance. The data file was used to make three types of analyses:

- Variation of direct measures of maneuvering performance (tactical diameter, head reach, etc.) with basic ship design parameters (length, displacement, etc.)
- Variation of nondimensional maneuvering performance parameters with nondimensional ship design parameters.
- Statistical variations of maneuvering performance data about observed mean behavior.

An extensive analysis of the trials data for all 603 ships contained in the maneuvering data file was carried out. Various analyses were carried out for stopping, turning and zig-zag maneuvers. For each of these maneuvers a number of dimensional and nondimensional maneuvering performance and ship parameters were considered in various combinations to determine how well results could be correlated. The final proposed standards were developed from the analyses which showed the best correlation of ship design parameters and performance.

SUMMARY OF PROPOSED MANEUVERING PERFORMANCE STANDARDS AND TRIALS

A set of proposed standards and a proposed ship trials agenda have been developed using the factors discussed earlier in this report and on an analysis of available ship trials data and maneuvering performance studies, as described in Reference 1. These standards are outlined below.

Proposed Maneuvering Performance Standards

The proposed maneuvering performance ratings for a given ship are assigned on the basis of measured performance in selected trial maneuvers supplemented by special investigations for vessels which fail to meet certain criteria. The standards are expressed in terms of a relative performance ranking, i.e., superior, above average, average, below average and marginal. These standards are applied to a vessel's turning, course changing and course keeping ability, a vessel's stopping ability and a vessel's ability to operate at a moderate speed suitable to a restricted water situation. The maneuvering trials agenda proposed for use in determining performance ranking of a vessel must include as a minimum:

- Turning maneuver from full maneuvering speed with maximum rudder angle.
- 20-20 zig-zag maneuver from full maneuvering speed.
- Stopping maneuver from reduced maneuvering speed.
- Demonstrated ability to operate at a continuous speed between four and six knots.

Rankings or rating of turning, course changing and course keeping ability have been assigned on the basis of performance in turning and zig-zag maneuvers. The lowest of the resulting ratings will be the rating applied to the vessel in the turning/course keeping area. The numerical measures used to establish the ratings are:

1. The tactical diameter/length ratio from a full rudder angle turn at full maneuver speed (8 to 10 knots).

2. The overshoot angle from a 20-20 zig-zag maneuver performed at full maneuvering speed.

3. The K'-T' relationship from a 20-20 zig-zag maneuver performed at full maneuvering speed.

The relationships between the numerical measures and ratings for each of these maneuvers are defined in Figures 1 through 5 as a function of ship displacement and, to a limited extent, ship type. K' and T' are the Norrbin-Nomoto parameters.

Rankings or rating of stopping ability are to be made on the basis of performance in a crash stopping maneuver carried out from a sustained speed of about eight knots. The relationship between the numerical measure and the performance ranking is defined in Figures 6 and 7 for tankers and for all other ship types. The numerical measure used is head reach divided by the product of ship length and Froude number at the initiation of the maneuver.

The ability of a vessel to maintain a course at a speed suitable to a restricted water situation must be demonstrated

on trial at a continuous speed between four and six knots for a period of one-half hour.

Finally, for vessels falling into one or more of the following categories, acceptable maneuvering performance must be demonstrated to United States Coast Guard satisfaction during the "design phase" by means of special investigations. These criteria include:

- The ratio of above water profile area to below water profile area exceeds three in the minimum operating draft condition.[2]
- No rudders are located in the slipstream of a propeller.
- Propeller direction of rotation (or direction of propeller thrust) cannot be changed at least four times in one minute (interim values).

Proposed Trial Agenda

The proposed maneuvering performance standards are based on numerical measures derived from performance in the following trial maneuvers:

- Turning maneuver from full maneuvering speed with maximum rudder angle.
- 20-20 zig-zag maneuvers from full maneuvering speed.

[2] The ratio three is based on a wind speed of 45 knots, which is a value that can be expected to exist for a significant period of time during a sudden squall, and a typical ship speed of seven knots. Other limiting ratios of above water to below water profile area will be defined for other assumed values of ship and wind speed, as described in Reference 1.

- Crash stopping maneuvers from reduced maneuvering speed.
- Demonstration of ability to operate at a continuous speed between four and six knots.

With the exception of the demonstration of ability to operate continuously at low speed, these maneuvers are similar to those usually carried out during a new ship trial. The trial procedures to be used for the turn, 20-20 zig-zag maneuvers and crash stop maneuver are defined in a SNAME Research Bulletin (5). As a test of ship machinery, crash stopping maneuvers will usually be carried out from design speed; for the purpose of the maneuvering performance ranking, an additional stopping maneuver carried out with the vessel operating at a reduced initial speed ahead is required.

For ships which have diesel power plants and thus may have problems operating continuously at low power levels, and for which trials are conducted at or near full load condition (as is typical for bulk carriers), the designer or builder may need to demonstrate, using approved computational procedures, that the ship can maintain steady-state operation at a speed between four and six knots at the minimum operating load condition.

Additional Trials Agenda

The proposed standards reflect the nature of available trials data. It was not possible to include other potentially important maneuvers and performance measures due to the lack of performance data for such maneuvers.

Based on our understanding of ship maneuvering and controllability, two additional trials maneuvers are considered

highly useful and should be strongly recommended during ship trials and model maneuvering studies:

- Coasting zig-zag in which a command to stop the propeller is issued at the initiation of the maneuver.
- Standing turn in which simultaneously the propeller is started and the rudder is put over with the ship at zero speed.

The performance measures to be derived from these maneuvers are the same as those for the standard zig-zag and turn. It would be highly desirable to include performance measures from one or both of these measures in future standards, if some representative body of trials data could be obtained. It might be feasible to supplement limited trials data with model test and/or simulation results.

CONCLUSIONS AND RECOMMENDATIONS

The most important conclusions of this study are reflected in the proposed performance standards and trials agenda. Other important conclusions include:

1. Ship performance in normal turns, crash stops and zig-zag maneuvers are all important for rating performance. Relative importances cannot be assigned to these maneuvers, although the proposed standards do give somewhat greater weight to the zig-zag maneuver.

2. Differences in maneuvering performance between different ship and machinery types exist, particularly variations of turning ability with ship type. Where appropriate, different ratings have been provided for different ship types.

3. If an overall ship performance rating is needed, this rating should be based on the lowest of the individual ratings rather than an average rating.

4. Trials used to determine maneuvering performance ratings should be conducted at typical maneuvering speeds rather than at ship design speed.

5. The proposed rating system is considered a significant first step and the proposed standards are considered suitable for immediate use in rating ship maneuvering performance. However, additional data and refinements are needed to fill out and improve the rating system.

6. The implementation of any maneuvering performance standards will undoubtedly result in a significant increase in the number of maneuvering model tests conducted for new ship designs.

REFERENCES

1. Barr, R A., E. R. Miller, Jr., V. Ankudinov and F. C. Lee, "Technical Basis for Maneuvering Performance Standards," U. S. Coast Guard Report CG-M-8-81, December 1981.

2. Crane, C. L., "Maneuvering Trials of a 278,000 DWT Tanker in Shallow and Deep Waters," Transactions of the SNAME, Vol. 87, 1979.

3. Miller, E., V. Ankudinov and T. Ternes, "Evaluation of Concepts for Improved Controllability of Tank Vessels," Marine Technology, Volume 18, No. 4, October 1981.

4. Landsburg, A., et al, "Proposed Shipboard Maneuvering Data," Proceedings of the Fifth Ship Technology and Research (STAR) Symposium, 1980.

5. Panel M-19 (Ship Trials) of the SNAME Ship's Machinery Committee, "Code for Sea Trials - 1973," SNAME Technical and Research Code C-2, 1974.

6. International Towing Tank Conference, "Discussion of Recommendations for an ITTC Maneuvering Trial Code," Volume 2 of the Proceedings of the Fourteenth International Towing Tank Conference, 1975.

TABLE 3

ORGANIZATION OF SHIP MANEUVERING PERFORMANCE DATA FILE

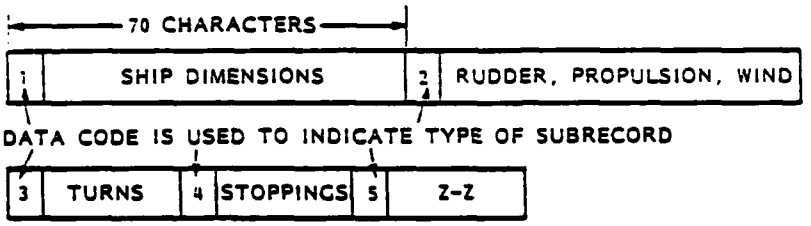

Each subrecord contains 70 characters

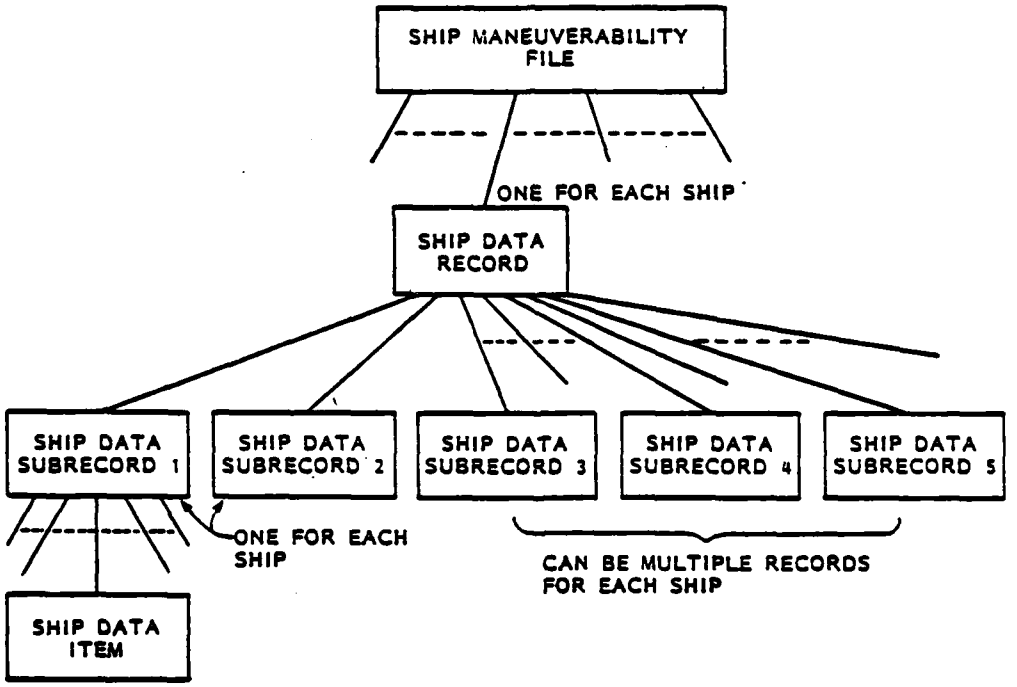

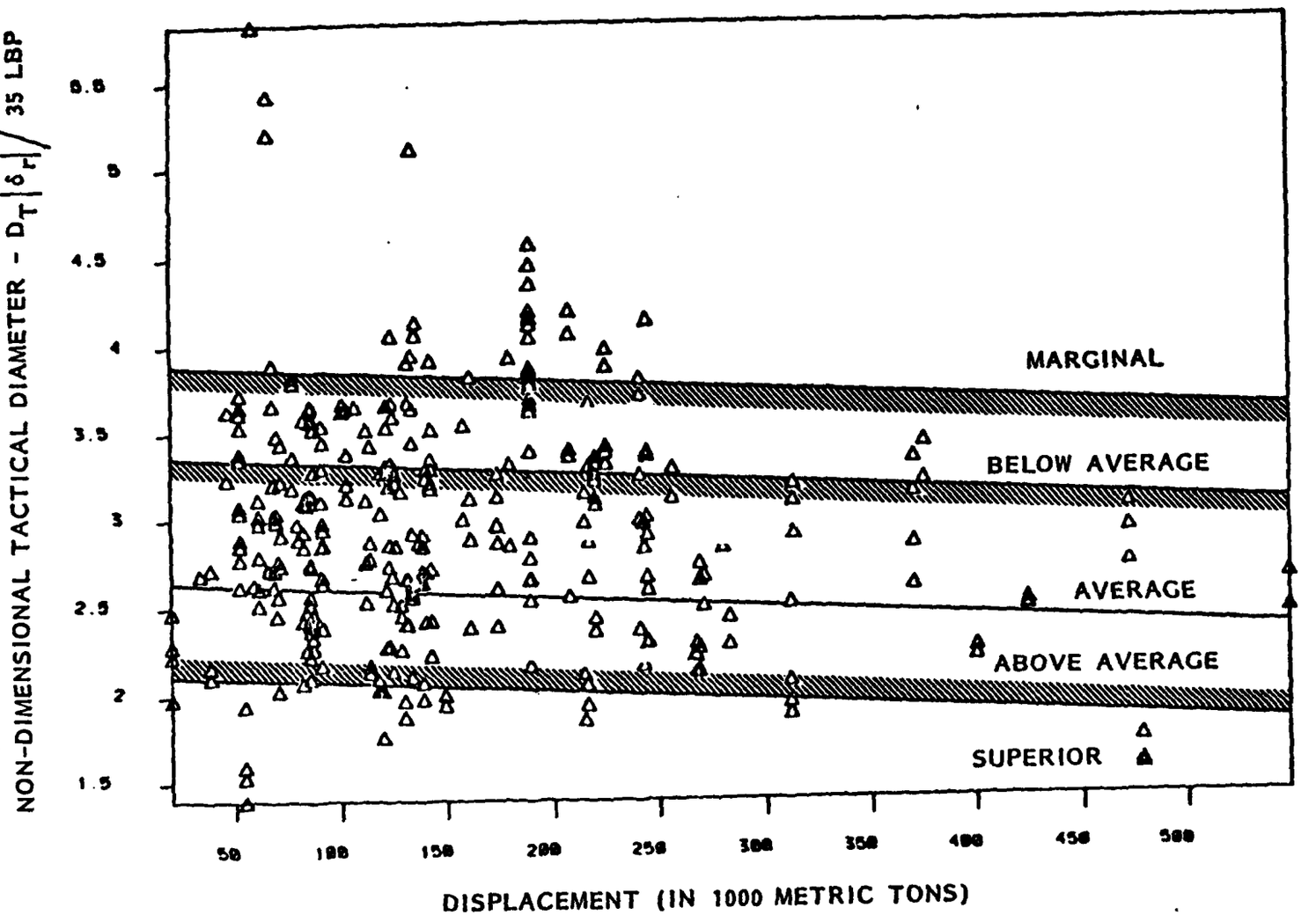

FIGURE 1 - PERFORMANCE RATINGS BASED ON TANKER TACTICAL DIAMETER

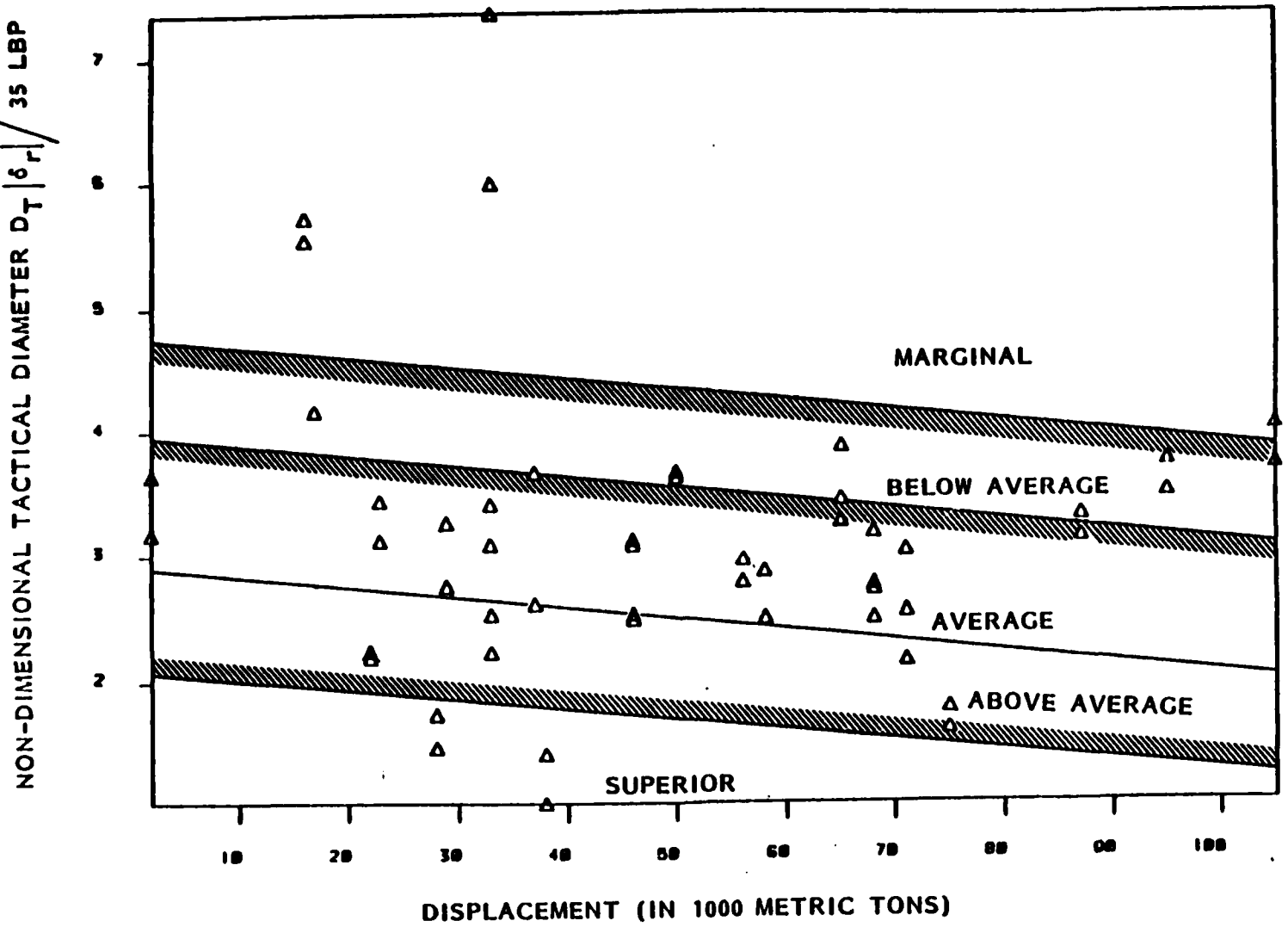

FIGURE 2 - PERFORMANCE RATINGS BASED ON BULK CARRIER TACTICAL DIAMETER

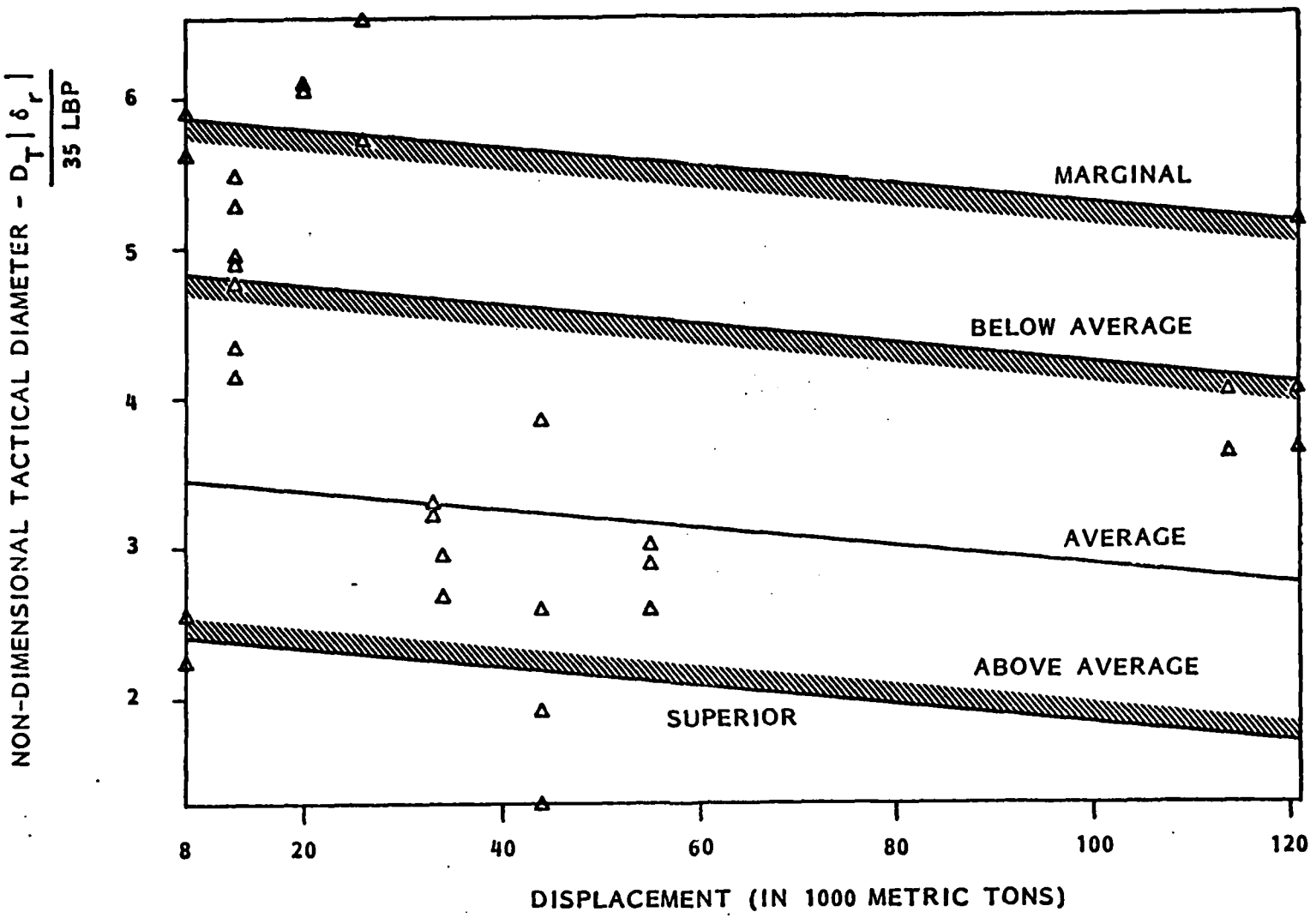

FIGURE 3 - PERFORMANCE RATINGS BASED ON CARGO AND CONTAINER SHIP TACTICAL DIAMETER

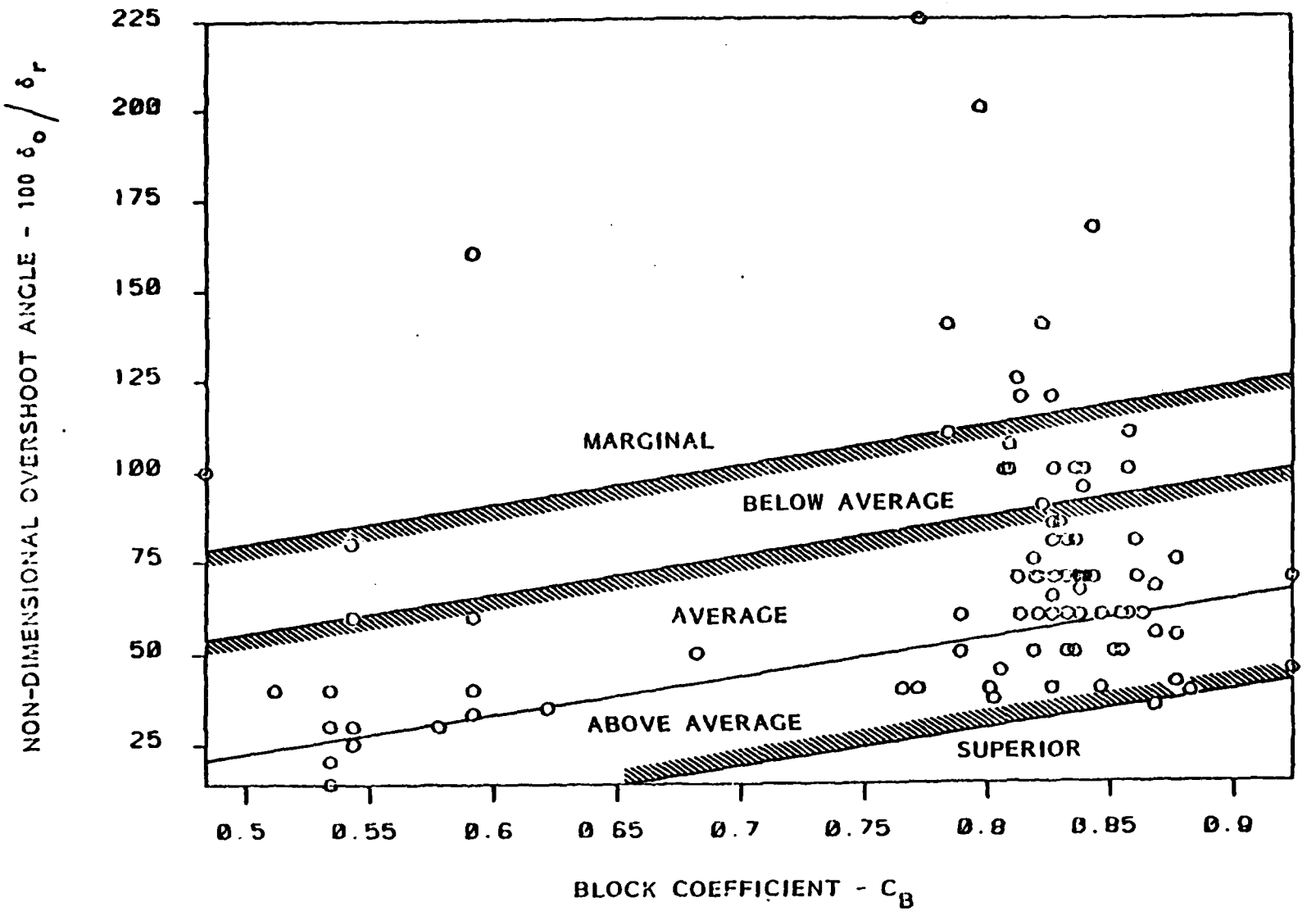

FIGURE 4 - PERFORMANCE RATINGS BASED ON OVERSHOOT ANGLE

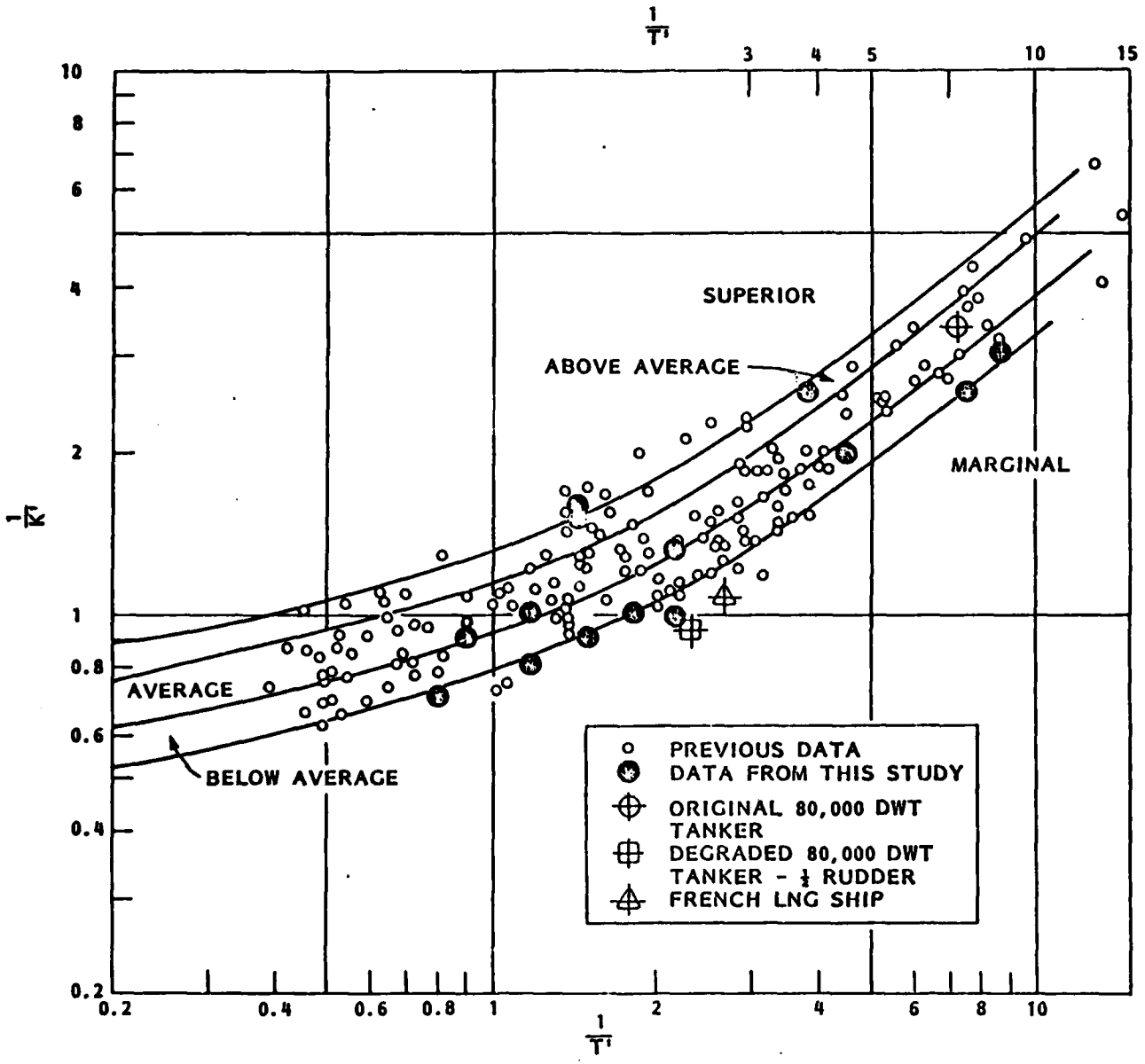

FIGURE 5 - PERFORMANCE RATINGS BASED ON ZIG-ZAG PARAMETERS K' AND T' APPLICABLE TO ALL SHIP TYPES

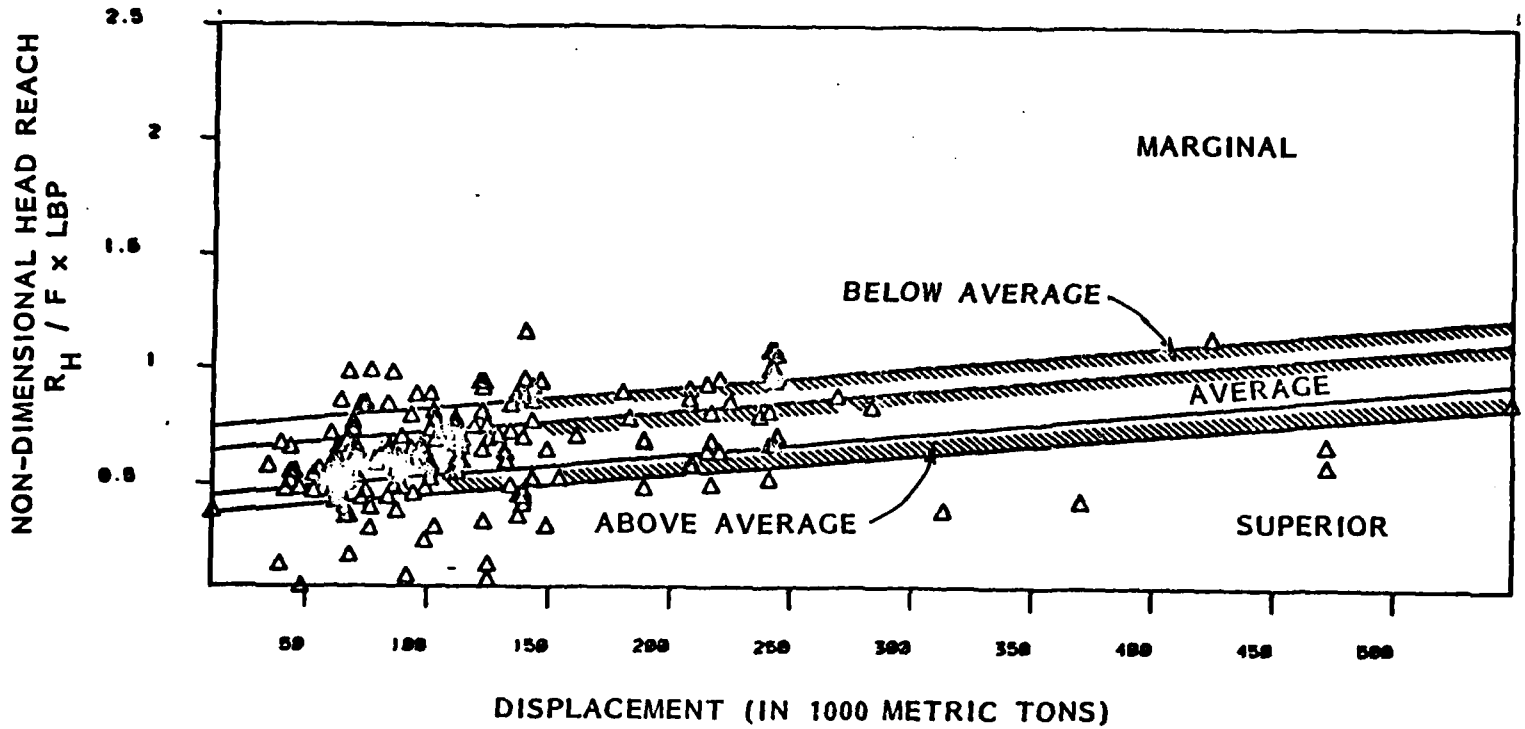

FIGURE 6 - PERFORMANCE RATINGS FOR TANKERS ONLY BASED ON STOPPING HEAD REACH

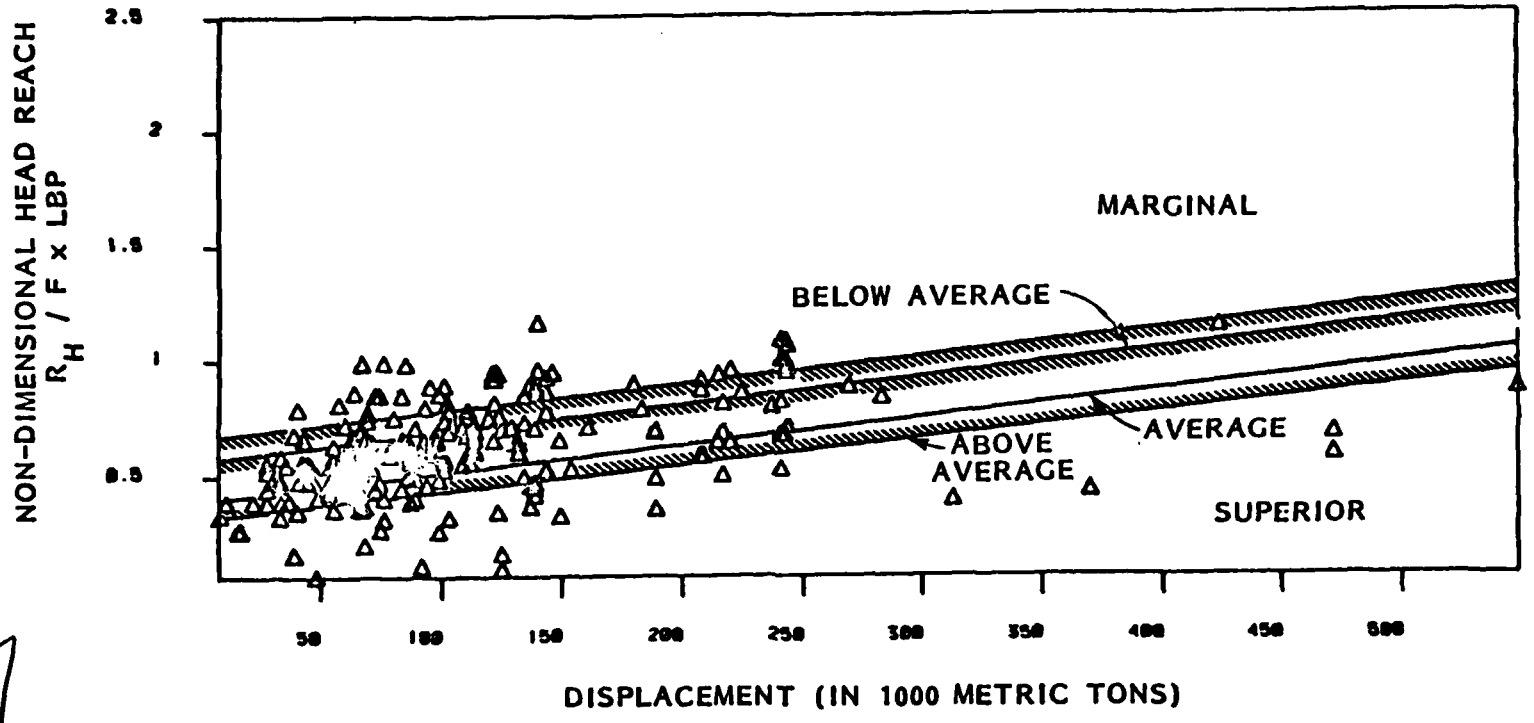

FIGURE 7 - PERFORMANCE RATINGS BASED ON STOPPING DATA FOR ALL SHIPS - APPLICABLE TO ALL SHIP TYPES BUT TANKERS

AD-P003 824

APPLICATION OF MICROCOMPUTER TECHNOLOGY TO PHYSICAL AND NUMERICAL ANALYSIS OF SHIP MANEUVERING

by F.W. DeBord Jr.
Offshore Technology Corporation

ABSTRACT

The recent availability of low cost, relatively powerful computers has had a major impact on experimental and analytic hydrodynamics. Application of these devices to control, data acquisition, and data analysis for ship maneuvering tests can result in improved cost efficiency, data quality, and interpretation of results. During the past year Offshore Technology Corporation has developed a low cost microcomputer-controlled planar motions mechanism, improved techniques for analysis of resulting data, and a simulation model capable of running on a small personal computer. Hardware design, software, operating features, and typical data resulting from these techniques are discussed. These are compared to typically used hardware and techniques and further design improvements are recommended. In addition, designs for a microprocessor-based model control system and a digital model tracking system, which are currently under development are discussed.

1. INTRODUCTION

During the past 20 to 30 years naval architects have developed a capability to reliably predict maneuvering behavior of ships in a wide variety of situations. To date, the most successful techniques used for this analysis have included model testing combined with computer modeling. Recent developments in digital electronics (past 10 years) have provided a new set of powerful, low cost tools which can be applied to both model testing and computer modeling to improve efficiency and make these techniques available to small experimental facilities and naval architects. The purpose of this paper is to explore specific applications of current microcomputer technology to analysis of ship maneuvering. Improvements to traditional techniques will be suggested and specific designs will be given. It will be shown that significant cost reductions can be realized and tools used in the analyses can be made more user friendly.

As of the last ATTC, three general techniques were available for ship maneuvering analyses: (1) full scale trials; (2) free-running model tests; and (3) captive model tests combined with numerical simulation models. Full scale testing has taken two basic forms. Traditionally specific maneuvers (turning circles, Z maneuvers, and spirals) have been executed to quantitatively compare different vessels and provide standards for performance. More recently, system identification

techniques have been applied to trials data to generate coefficients for numerical models similar to those resulting from captive model tests. Recent electronics advances greatly enhance data collection for either technique and system identification would not be possible without computer analysis.

Free-running model tests have typically been conducted similar to classical full scale trials i.e. turning circles, Z maneuvers, and spirals. In addition, these can be used to evaluate performance in specific situations such as harbor entrances with wind, current and waves and system identification techniques can be used to generate required data for numerical models. Again, data acquisition equipment has been substantially improved in recent years.

Captive model testing combined with numerical analysis is by far the most widely used method for prediction of maneuvering behavior. Model techniques include rotating arm tests, planar motions mechanism tests, oscillator tests, and impulse response tests. Results of these experiments are analysed to provide empirical coefficients for one of several published numerical simulation models which predict vessel response to rudder and propeller activity. Testing, data acquisition, data analysis, and operation of the simulation models are all dependent on the current state of the art in electronics.

Prior to discussing specific improvements to all of the above techniques, a brief review of recent advances in electronics technology is in order. In the late 1960's the first minicomputers were introduced, providing experimental facilities with greatly improved capabilities for data acquisition and analysis. More recently as a result of large scale integrated circuits, capabilities have increased dramatically and costs have gone down. Now the typical home computer is as capable as the first minis at one tenth the cost (as shown in Table 1). Currently very large scale integration is resulting in increasingly capable machines and in the very near future desktop computers will be available with the capabilities of a mainframe. Simultaneously, software has improved and more importantly design and application techniques have been made available. It is entirely possible for anyone with the most basic understanding of electronics to design and build microcomputer controllers, instrumentation, or interfacing devices.

2. CAPTIVE MODEL TESTS

Discussions here will concentrate on Planar Motions Mechanism tests as opposed to other captive model test techniques since the device is applicable to most towing basins (provided sufficient width is available) and the technique is currently used at most facilities which conduct captive tests. It should be noted however that hardware and some aspects of the the software which will be discussed are applicable to oscillator and impulse response techniques.

The classic PMM, as discussed by Strom-Tejsen et al (1966) and others, is essentially a pair of variable amplitude scotch yokes driven by variable speed electric motors. Construction of these electro-mechanical devices has

TABLE 1

TYPICAL SMALL COMPUTERS

MODEL	APPROX. COST*	MAXIMUM MEMORY	PROCESSOR	PERIOD
Digital PDP-8	$30,000	32K	12 bit mini	Early 1970's
HP 9845	30,000	489K	16 bit mini	Mid 1970's
Digital PDP 11/23	20,000	512K	16 bit LSI mini	Mid 1970's
APPLE II Plus	2,500	64K	8 bit micro	Late 1970's
HP 9816	8,000	7,000K	16 bit micro 32 bit arithmetic	Early 1980's

* Approximate typical cost with memory and peripherals

always been complicated by the need to vary amplitude, phase, and frequency of the two motions within constraints imposed by relatively infelxible control systems. In addition, complexity and costs are affected by the need to determine the in-phase and out-of-phase force components. Typically this has been accomplished either through manual analysis of analog time histories or analog signal processing with custom circuitry. As a result of the required mechanical and electrical complexity, PMM's have typically been extremely costly to build or purchase, with recently quoted prices as high as $500,000.00.

In 1981, several upcoming projects required that OTC develop (or purchase) a PMM suitable for vertical or horizontal motions. A design effort was initiated with critical requirements identified as low cost and flexibility. Based on a review of existing hardware, experience with forced oscillation tests with marine risers, and a review of current technology, a decision was made to pursue an electro-hydraulic design. This approach provided several principal advantages over an electro-mechanical device: (1) a number of components were available in-house and the hydraulic carriage drive system could be modified to provide power for the PMM; (2) flexibility in model size, mass, and required motion amplitude would be available through component changes and rearrangement; and (3) amplitude and frequency variations would be achievable without mechanical adjustments and could in fact be varied during a test if required.

Hardware used in the final design is illustrated in Figure 1. Basically, models are attached to a rotating ring on a transverse subcarriage with 2 heave staffs. Transverse and angular position of the ring are controlled by 2 hydraulic cylinders. These are driven by a constant pressure hydraulic pump and individual servo-valves. Depending on test requirements, maximum amplitude is variable from 0.5 ft to 3.0 ft and model attachment point spacing is variable from 0-10 ft. Vertical motions are achieved by orientating the cylinders vertically and providing surge and sway restraint with vertical rails and linear bearings.

Based on the need to provide two time-varying command signals (analog voltages) with independent phase angles and variable magnitude to the servo valves, control through computer generated signals was selected. This approach provided improved flexibility and ease of operation as compared to a system of analog generated signals. A block diagram of the control system is shown in Figure 2. A desktop computer (Tektronix 4052 later replaced by an APPLE II) generates a digital time varying signal for each of the two cylinders as required by the specific test conditions. These signals are simultaneously output to a D/A converter, filtered, and fed into the servo amplifiers as a D.C. voltage proportional to the desired cylinder position. Feedback from cylinder position potentiometers is provided within the servo amplifiers.

Initially, control was provided through BASIC programs on a Tektronix 4052 with a Tranzero D/A converter. These programs were modifications of existing wave generation routines. Later, due to the cost of this computer, motions generation software was developed for an APPLE II which could be dedicated to the PMM. Since motions must be generated over a wide range of frequencies, the primary problem to be solved was calculation and D/A conversion of two simultaneous signals at a rate which could be filtered to

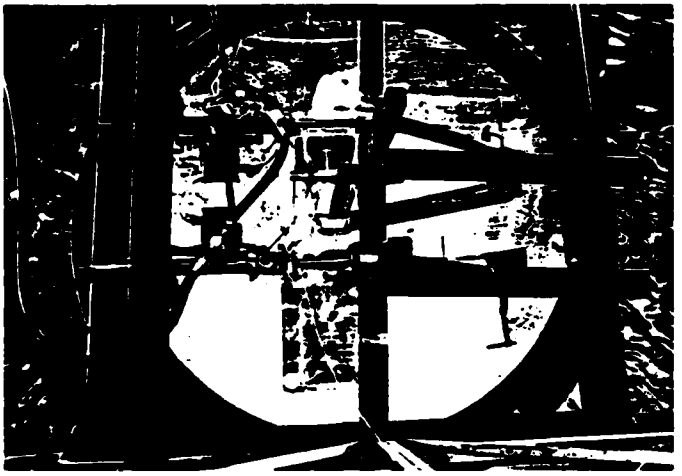

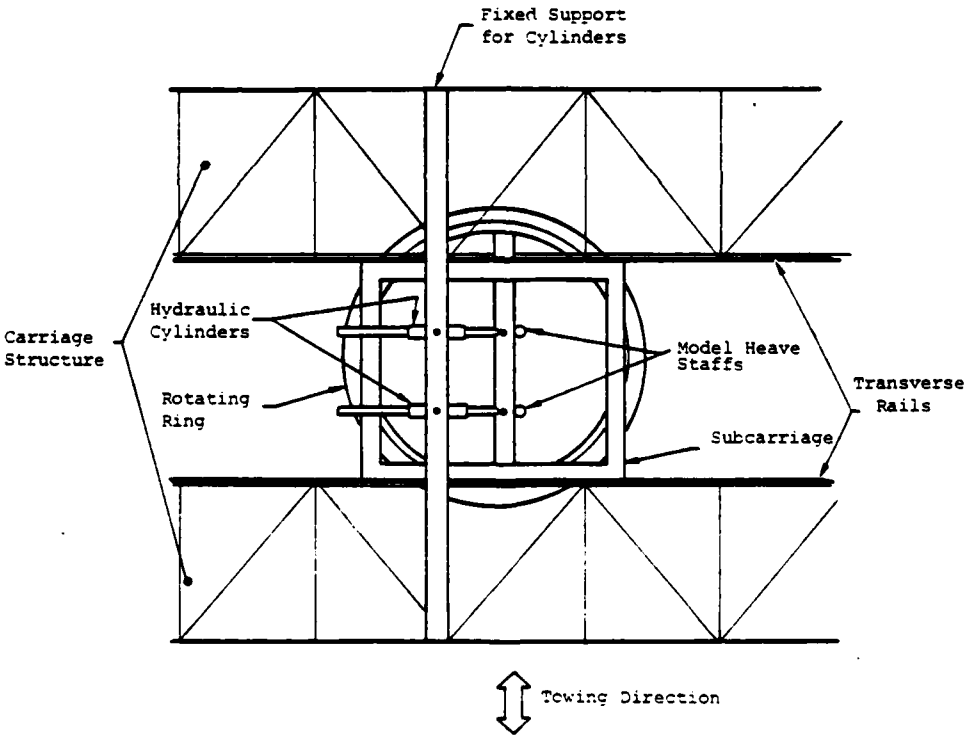

Figure 1 PMM Hardware Arrangement for Horizontal Motions

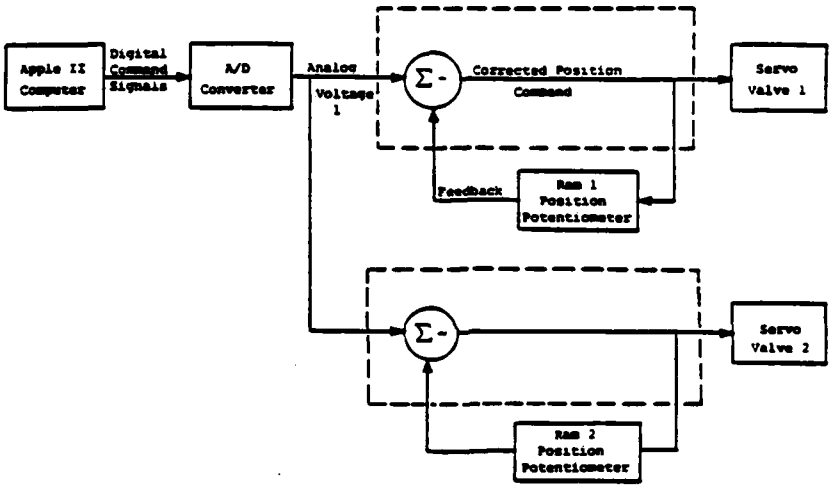

Figure 2 PMM Controller Block Diagram

provide smooth motions over the desired frequency range. The approach taken with both machines was to generate an array of digital data in BASIC as per the governing equations for the desired motion (Mandel 1967) prior to the test, and then output the array at the required rate under control of a real-time clock. Realization of adequate speed with the APPLE required use of a machine language output routine operating on interupts from the clock. Output to 2 channels at rates up to 1000 Hz are possible with this approach. A hardware diagram for this system is shown in Figure 3.

Software listings for the BASIC main program and the 6502 assembly language output routine are included in APPENDIX A. During a test program operation of the system is as follows. Prior to the test the test engineer selects the type of motion desired (Figure 4) and inputs parameters in engineering units. The computer then completes the required calculations to generate 2 arrays of voltage levels to be output. On command from the operator, the machine language routine outputs data to the D/A converter based on clock interupts until the stop command is given. Input of test parameters and generation of the output arrays requires approximately 45 seconds prior to the beginning of the test. The engineer communicates with the control system in units which are consistent with development of the test plan and parameters are infinitely variable within constraints imposed by fixed maximum amplitude. If parameters are requested which are outside the available range, the operator is so informed.

A cost breakdown for all required hardware and estimates of development labor costs are given in Table 2. These should be in the range available for development at most experimental facilities. Obviously, costs will vary slightly depending on carriage construction and availability of parts in-house.

To date, the new PMM has been used on two major projects, vertical added mass and damping tests with a drillship, and horizontal tests with an amphibious vehicle. Initial problems consisted primarily of mechanical noise in the model restraining system. An example of an early force time history is shown in Figure 5A. These high frequency accelerations were reduced by careful redesign of all attachments and bearings with the result that current force histories (filtered at the same rate) exhibit no noticeable high frequency components as shown in Figure 5B. Additional tests have been conducted with a single cylinder to evaluate the response of marine risers and an upcoming project will use the device to analyze added mass and damping of ice floes in 6 degrees of freedom.

Planned improvements in the system include minor software modifications to further improve user interface, addition of ramp up and down start and stop routines to eliminate manual start and stop control, and inclusion of a random motion generation capability. This later feature has the potential to reduce the number of tests required to determine zero-frequency maneuvering coefficients and will minimize the number of tests required to determine seakeeping added mass and damping. The intent is to excite the model with a white-noise motion spectrum and analyse resulting data with standard random data correlation techniques as discussed by Bendat et al (1981) and Hoste (1983). Output from these tests will be similar to that shown in Figure 6 for seakeeping test data. This will be discussed in detail in the following section.

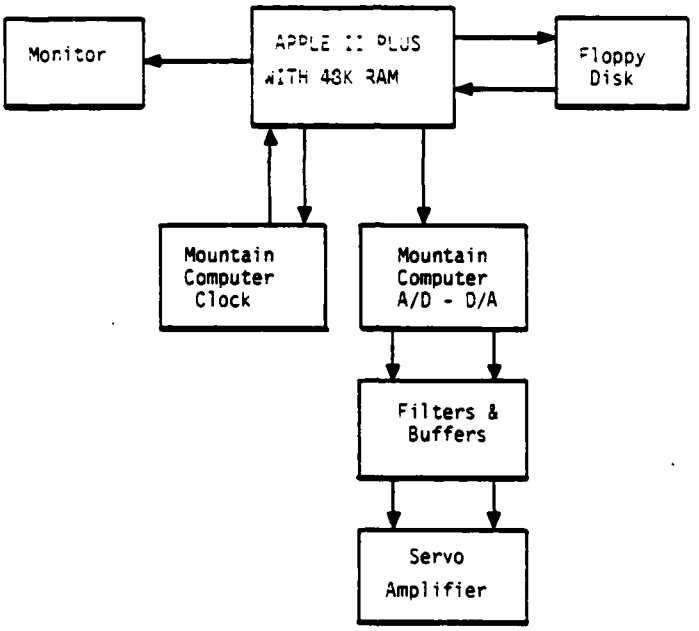

Figure 3 APPLE Controller Hardware

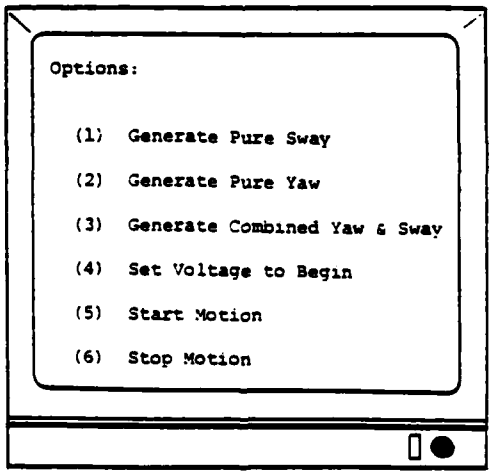

Figure 4 Software Main Menu

TABLE 2

PMM COST SUMMARY

PARTS	
Hydraulic Pump	$6,000.00
Servo Valves (2)	2,000.00
Hydraulic Rams (2)	2,000.00
Servo Amplifiers (2)	2,000.00
Hoses and Parts	1,000.00
APPLE II Plus w/Peripherals	3,000.00
Miscellaneous Electronics Parts	200.00
SUB-TOTAL	$16,200.00
LABOR	
Hardware Assembly	1,200.00
Software Development	1,500.00
Electronics Assembly	800.00
SUB-TOTAL	$ 3,500.00
TOTAL	$19,700.00

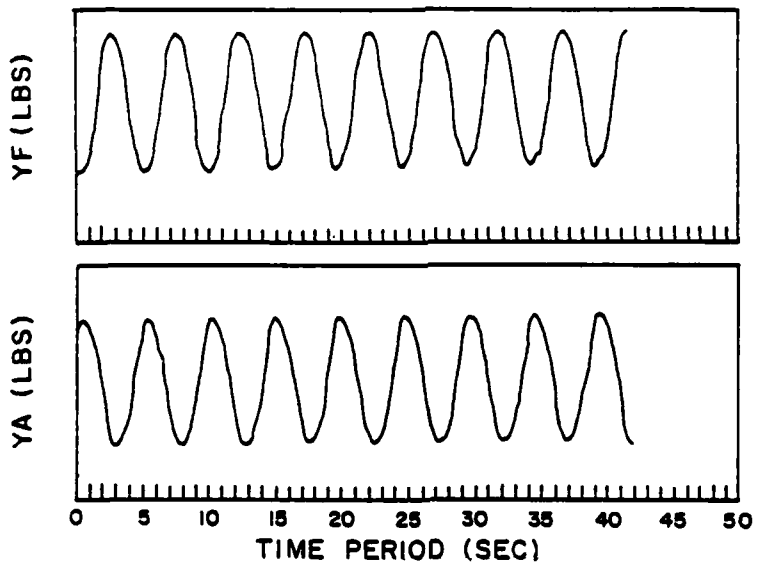

B. With Technical Improvement (Current)

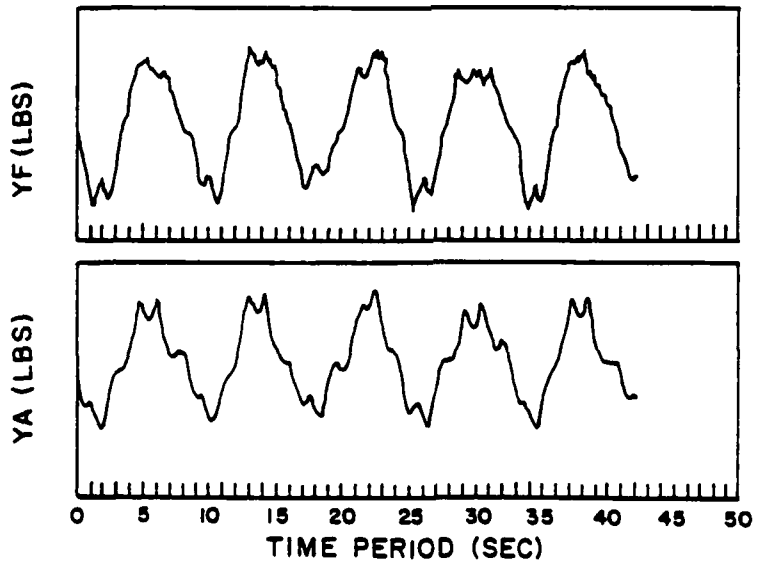

A. With Mecnanical Noise (Initial)

Figure 5 Typical PMM Force Time Histories

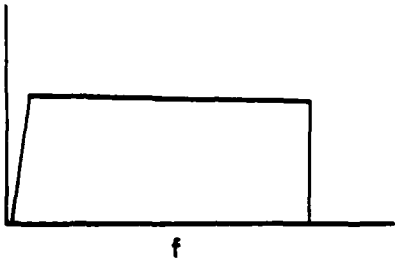

FORCED MOTION SPECTRUM

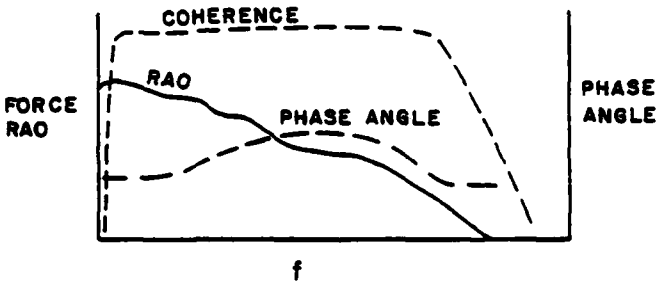

RAO & PHASE

Figure 6 Planned Presentation of Random PMM Test Results

3. PLANAR MOTIONS DATA ANALYSIS

As discussed by Mandel (1967) and others, development of hydrodynamic coefficients from Planar Motions Mechanism test results requires determination of the in-phase and out-of-phase forces and moment and subsequent solution of the following equations:

$$Y_v = = \frac{(Y_B)\ \text{out} + (Y_S)\ \text{out}}{-a_0\ \omega} \qquad Y_r - mu_1, = = \frac{(Y_B)\ \text{out} + (Y_S)\ \text{out}}{-\psi_0\ \omega}$$

$$N_v = = \frac{[(Y_B\ \text{out} - (Y_S)\ \text{out}]\ X_S}{-a_0\ \omega} \qquad N_r - mX_G u_1 = \frac{= [(Y_B)\ \text{out} + (Y_S)\ \text{out}]\ X_S}{-\psi_0\ \omega}$$

$$Y_{\dot{v}} - m = \frac{(Y_B)\ \text{in} + (Y_S)\ \text{in}}{-a_0\ \omega^2} \qquad Y_{\dot{r}} - mX_G = \frac{= [(Y_B)\ \text{in} + (Y_S)\ \text{in}\ ]}{-\psi_0\ \omega^2}$$

$$N_{\dot{v}} - m X_G = = \frac{[(Y_B)\ \text{in} - (Y_S)\ \text{in}]\ X_S}{-a_0\ \omega^2} \qquad N_{\dot{r}} - I_Z = = \frac{[(Y_B)\ \text{in} - (Y_S)\ \text{in}\ ]\ X_S}{-\psi_0\ \omega^2}$$

where: Y_v, N_v, $Y_{\dot{v}}$, $N_{\dot{v}}$, Y_r, N_r, $Y_{\dot{r}}$, $N_{\dot{r}}$ = velocity and acceleration derivatives

Y_B = measured bow side force

Y_S = measured stern side force

a_0 = sway amplitude

ψ_0 = yaw amplitude

ω = frequency of motion

m = model mass

X_G = location of C.G.

X_S = distance from ⊗ to heave staffs

I_Z = model moment of inertia

u_1 = carriage velocity

Historically, the in-phase and out-of-phase force components have been determined using two methods. Obviously, analog records of the force

transducer outputs can be manually analyzed to determine these components, however this approach is tedious at best. The solution typically taken is to determine these components directly with analog electronics installed as part of the PMM. As discussed by Strom-Tejsen et al (1966), the in-phase and out-of-phase components can be determined through signal integration with appropriately chosen periodic polarity reversals. In most cases this equipment contributes greatly to the high cost of the current generation of PMM's.

During development of the PMM described in the previous section it was realized that an alternate approach would be desirable. Therefore, a method was developed to use existing time series analysis routines to complete the required calculations from digital time histories of measured ram positions, side forces, and drag force. Currently, the procedure used is as follows:

1. Based on measured data, compute derived time series for velocities, accelerations, total side force, and yaw moment. The capability to derive new time series from measured data is a standard feature of existing PDP 11/23 data acquisition stations.

2. Using a standard Fourier Analysis routine, compute the 1st sinusoidal component magnitude and phase for each variable including the derived variables. A sample output from this program is included as Table 3.

3. Finally, coefficients are calculated based on the phase and magnitude information using the following equations which are derived from those given above:

$$Y_v = \pm \frac{\frac{Ym\ RAO}{Ydis\ RAO} * \sin\phi}{\omega}$$

$$N_v = \pm \frac{\frac{Nm\ RAO}{Ydis\ RAO} * \sin\phi}{\omega}$$

$$Y_{\dot{v}} - m = \pm \frac{\frac{Ym\ RAO}{Ydis\ RAO} * \cos\phi}{\omega^2}$$

$$N_{\dot{v}} - mX_G = \pm \frac{\frac{Nm\ RAO}{Ydis\ RAO} * \cos\phi}{\omega^2}$$

$$Y_r - mu_1 = \pm \frac{\frac{Ym\ RAO}{psi\ RAO} * \sin\phi}{\omega}$$

* * REGULAR WAVE * *
* * * PHASE ANGLES * * *

Base Channel: YB
Heading: 0.0 deg.
Period: 4.85 sec.
Model Scale: 6.000
Sample Rate: 20.00 hz.

No. of Cycles: 8
Start Time: 0.02 min.
Test Duration: 0.65 min.
Total Duration: 0.70 min.
Samples / Chan: 342

VARIABLE	UNITS	RAO	PHASE
YB	FEET	1.000	0.
YS	FEET	1.028	179.
WAVE	FEET	0.097	23.
VM	FT/S	0.021	-137.
XF	LBS.	6.118	49.
YF	LBS.	122.843	-22.
XA	LBS.	4.634	137.
YA	LBS.	215.880	146.
D.P.	FT2/S2	24.955	-155.
BACC	FT/S/S	0.346	18.
CGACC	FT/S/S	0.831	56.
HEAVE	FEET	0.015	-114.
PITCH	DEGREE	0.442	5.
BWAVE		0.017	-30.
RPM	RPM	0.065	2.
----------	derived channels	----------	----------
XM	LBS.	7.777	85.
YM	LBS.	99.539	130.
NM	FT-LBS	252.652	-30.
YDIS	FT.	0.018	141.
PSIM	RAD.	1.456	179.
YDOTM	FT/S	0.056	-134.
VDOTM	FT/S*S	0.174	-48.
RM	RAD/S	4.563	-95.
RDOTM	RA/S*S	14.378	-10.

TABLE 3

TYPICAL FOURIER ANALYSIS OUTPUT

$$N_r - mX_G u_1 = \pm \frac{\frac{Nm\ RAO}{psi\ RAO} * \sin \phi}{\omega}$$

$$Y_{\dot{r}} - mX_G = \pm \frac{\frac{Ym\ RAO}{psi\ RAO} * \cos \phi}{\omega^2}$$

$$N_{\dot{r}} - I_Z = \pm \frac{\frac{Nm\ RAO}{psi\ RAO} * \cos \phi}{\omega^2}$$

Where:

Ym RAO = total side force divided by ram displacement

Ydis RAO = sway amplitude divided by ram displacement

Nm RAO = yaw moment divided by ram displacement

psi RAO = yaw amplitude divided by ram displacement

ϕ = phase angle of response

Currently, this later analysis is completed on a desktop computer after testing is complete. In the future, these equations will be integrated into the menu-driven data acquisition software such that all analysis is completed automatically after each test. This approach will provide coefficients between tests and thus insure intelligent control of the test program. A hardware diagram and list of calculations are given in Figures 7 and 8.

As discussed briefly in the previous section, an additional feature to be tested is model excitation with white noise and analysis of the resulting data to produce coefficients as functions of frequency. Existing wave generation software will be used to excite the model with constant amplitude motion over the desired range of frequencies. Existing random time series data analysis routines will then be used to calculate transfer functions between motions and forces and the corresponding phase angles. Finally, the analysis described in 3 above will be completed in the frequency domain to output coefficients as functions of frequency. Output will include the coherence function such that the validity of coefficients at each frequency can be assessed.

Although the feasibility of using random excitation to determine maneuvering coefficients must still be determined in light of constraints imposed by test duration, the technique is currently successfully used for seakeeeping motions and will certainly be applicable to determination of seakeeping added mass and damping. If successful, the number of tests required to determine coefficients should be reduced significantly.

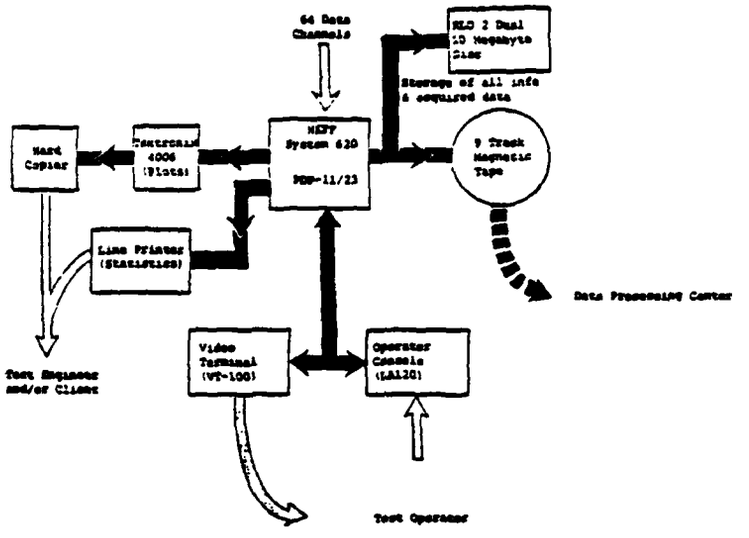

Figure 7 Hardware to Implement Between-Test Coefficient Calculations

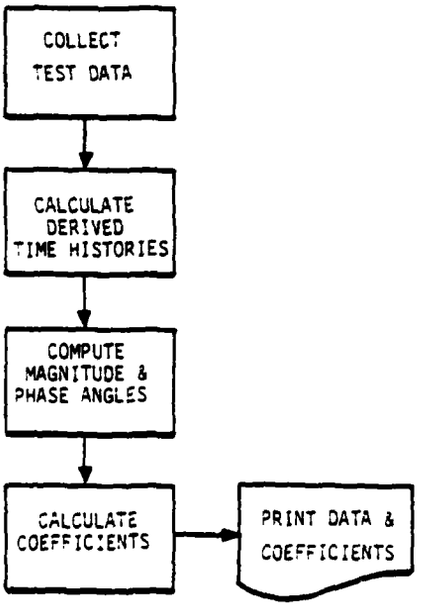

Figure 8 Calculation Procedure

4. FREE-RUNNING MODEL TESTS

As discussed previously, free-running model tests are typically conducted to assess behavior during standard maneuvers or in specific harbor situations. Two aspects of these tests where improvements are possible through application of the current microcomputer technology are model control and model tracking. Both of these problems can be addressed through creative application of available hardware components.

With respect to model control, we have in the past used manual radio control of models for turning circles and Z-maneuvers. This technique has been successful, however the precision of executed maneuvers (especially Z-maneuvers) has not been as repeatable as desired due to the human operator. Currently a microprocessor data acquisition, control, and telemetry system is under development. A processor aboard the model will collect data and control rudder actions based on the measured data. At the end of a test manual radio control will be envoked. In addition, the same processor will control data transmission to the fixed basin data acquisition system.

Hardware for this system is based on a modification to an existing microprocessor data acquisition system (ARCDATS) built by ARCTEC Incorporated. This system is illustrated in Figures 9 and 10. The model mounted hardware is approximately 10 inches by 8 inches by 8 inches and should easily fit into most models. Through variations in installed firmware specific maneuvers can be executed or a pilot can be represented for tests in realistic harbor situations.

The availability of low-cost microcomputers along with recent advances in video imaging for robotics has recently provided hardware capable of tracking free-running models. Several commercial systems are currently available which track models using variations in video sensing techniques. These range in cost from $80,000.00 to $150,000.00 and are typically configured to measure motions in six degrees of freedom with sufficient accuracy for seakeeping work. As an alternative, components can be purchased separately and integrated into a custom system. Such an approach is currently in the design phase at OTC to provide model tracking for both seakeeping and maneuvering tests. The system is illustrated in Figure 11 and hardware costs for one complete system are currently estimated at $10,000.00. This approach incorporates commercial line array video cameras with a single-board microcomputer. The microcomputer will control target and camera operation and transfer data to the basin data acquisition system.

5. SIMULATION MODELS

In recent years, a wide variety of simulators have been developed for both training and analysis. These range from elaborate bridge mockups with realistic visual displays such as CAORF and the MSI facility to the recently introduced TRACMAN system which runs on a BBC microcomputer. In between these extremes, are the smaller training simulators such as that developed by Hydronautics and the commonly used fast simulation models which are run on a number of different mainframe computers.

The point to be made is that with the current availability of a wide variety of computer hardware, analysis of maneuvering behavior can be com-

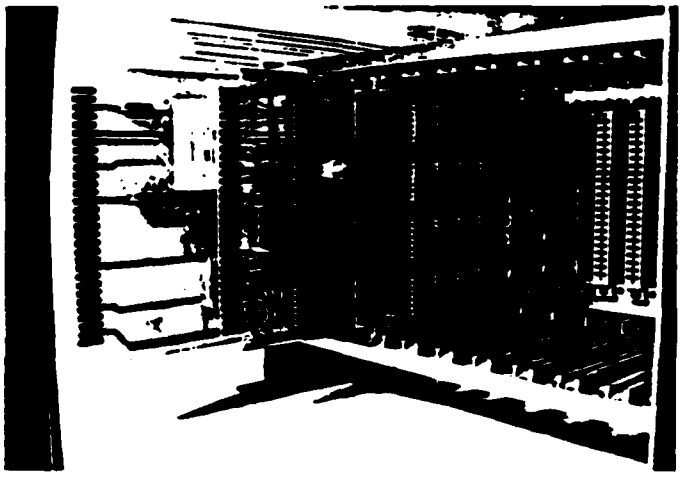

Figure 9 Model Microprocessor Data Acquisition and Control Package

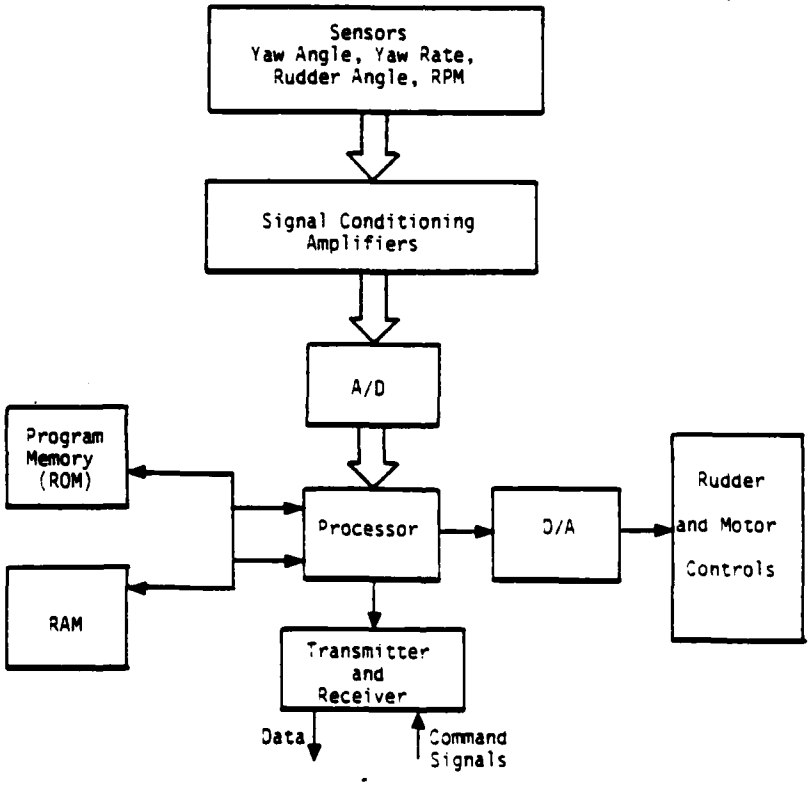

Figure 10 Schematic of Model Control System

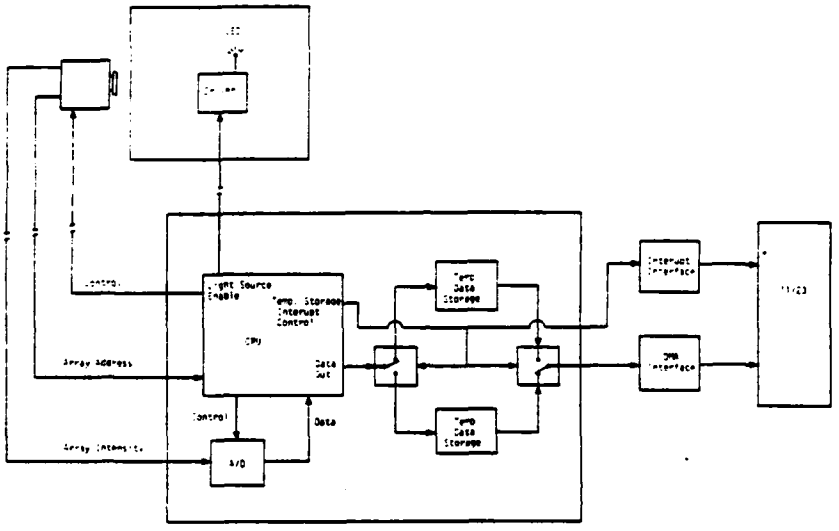

Figure 11 Model Tracking Hardware

pleted on hardware with capabilities (and costs) matched to the task. Majid et al (1983) completed a review of training simulators and found that minimum required hardware for this purpose is similar to a PDP 11/23. On the other hand, the author recently used a standard APPLE II to solve the complete equations of motion as given by Eda (1979). Although this later calculation was made at less than real time speeds, the desired analysis was completed on hardware costing less than $3,000.00 with accuracy comparable to much larger machines. The current generation of 16 bit micros provide order of magnitude increases in speed with only modest cost increases.

Based on available hardware, any small laboratory, design office, or owner should be capable of installing a machine which can complete analyses of maneuvering behavior with a realistic model and provide output in a useable form. Also, small, accurate training simulators are within the financial resources of most organizations. A schematic of such a system is given in Figure 12. This hardware should be available for under $15,000.00.

6. FULL-SCALE TRIALS

As illustrated by the technical impact of the ESSO OSAKA trials (Crane 1979), high quality full-scale experiments are extremely valuable for developing a better understanding of performance and validating model, analysis, and simulation techniques. Unfortunately, the cost to conduct similar experiments can be prohibitive, expecially when the cost of the ship is included. As suggested by Abkowitz (1980), the use of ships of opportunity might greatly reduce this problem and in fact, if high quality data can be collected during normal operations costs could be reduced to a level comparable with model tests.

The high quality of data resulting from the OSAKA trails is a credit to the entire project team. OTNSRDC used a small desktop computer to control the instrumentation and record data. A large number of measurements were taken from the ships instruments and periodic readouts were provided to insure data quality. If data collection on ships of opportunity is to be realized, quality similar to the OSAKA trials must be insured, however equipment should be portable and minimum interfacing with ship systems should be required.

With the current state-of-the-art, such a system could be easily assembled with properly selected transducers and existing microprocessor controlled data acquisition systems. One such data acquisition system is shown in Figure 13. This unit contains signal conditioning, amplifiers, a control and calculation processor, a digital tape recorder, and interfaces for communication with telemetry equipment and other computers. In fact, the package illustrated in the figure contains sufficient space for transducers, and if transducers are required at several locations on the ship, telemetry is available to eliminate the need for cables. The U.S. Maritime Administration is currently working on a different system, however details have not been published to date.

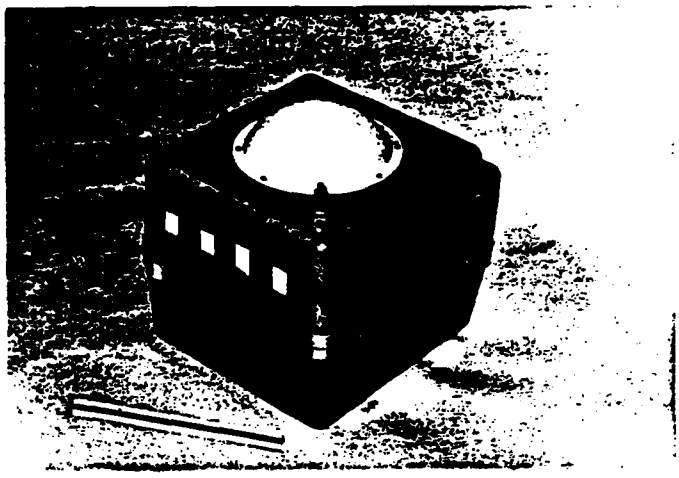

Figure 13 Portable Data Acquisition and Telemetry Package

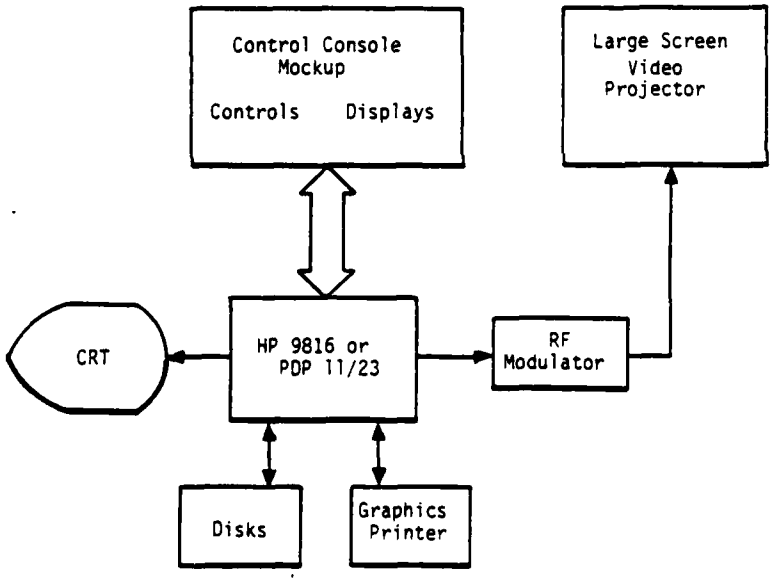

Figure 12 Training Simulator Hardware

7. SUMMARY

A number of ideas have been presented which have varying amounts of potential to improve our ability to analyse ship maneuvering. Hopefully, these ideas will inspire others to creatively apply current technology in an effort to improve our capabilities. In this effort several points should be kept in mind. First, although recent advances in electronics are exciting, we will benefit from these only if they are applied intelligently. Our objectives should be to improve the quality of our work while improving efficiency such that the U.S. industry is more competitive. In addition, if technology can be applied to reduce costs and make systems easier to use, experimental and analysis techniques can be made available to a larger number of organizations with the result that a larger number of advances should be realized. Also, as equipment costs are reduced and reliability is improved, techniques which are currently in the realm of R & D should become commonplace in operations.

The second key point to be made is that design and construction of microprocessor devices is not beyond the capabilities of any organization represented at this conference. The question which must be answered when considering new systems is; for similar end results, is construction of custom equipment or purchase of existing equipment more cost effective?

REFERENCES

Abkowitz, M.A., "Measurement of Hydrodynamic Characteristics from Ship Maneuvering Trials by System Identification" TRANSACTIONS, Vol. 88, S.N.A.M.E., 1980, New York, N.Y.

Bendat, J. S., A.G. Piersol Engineering Applications of Correlation and Spectral Analysis, John Wiley and Sons, 1980, New York, N.Y.

Crane, C. L. Jr. "Maneuvering Trials of a 278,000 DWT Tanker in Shallow and Deep Waters", TRANSACTIONS, Vol. 87, S.N.A.M.E. 1979, New York, N.Y.

Eda, H., R. Falls and D.A.Walden "Ship Maneuvering Safety Studies" TRANSACTIONS, Vol. 87, S.N.A.M.E., 1979, New York, N.Y.

Hoste, J., Dillingham, J.T. "Data Analysis Techniques in Model Testing" 20th American Towing Tank Conference, 1983, Hoboken, N.J.

Majid, I., B. Menon "Investigative Studies on Arctic Marine Simulators", Transport Development Center, Canadian Department of Transportation, Feb. 1983

Mandel, P. "Ship Maneuvering and Control", Principles of Naval Architecture, S.N.A.M.E., 1967, New York, N.Y.

Strom-Tejsen, J., M.S. Chislett "A Model Testing Technique and Method of Analysis for the Prediction of Steering and Maneuvering Qualities of Surface Vessels", Sixth Symposium on Naval Hydrodynamics, 1966, Washington, D.C.

APPENDIX

Listings of Planar Motions Mechanism Driven Programs

```
100  REM       PROGRAM PMMDRIVER
110  REM
120  REM       OUTPUTS SINE WAVES TO
130  REM      GENERATE PURE SWAY.PURE
140  REM     YAW.OR COMBINED YAW AND SWAY
150  REM
160  REM       REQUIRES CLOCK IN SLOT 4
170  REM     AND D/A IN SLOT 5.  CALLS
180  REM     MACHINE LANGUAGE ROUTINE TO
190  REM     GENERATE OUTPUT ON CLOCK
200  REM     INTERRUPTS.
210  REM
215  HIMEM: 28671
220  DIM IA(520),IB(520)
230 PI = 3.14159265:RAD = 180 / PI:XS = 0.75
240 D$ =  CHR$ (4)
250  PRINT D$;"BLOAD CLOCKWAVE.OBJ"
260  HOME : HTAB 10: INVERSE
270  PRINT " PLANAR MOTIONS PROGRAM "
280  NORMAL : PRINT : PRINT
290  PRINT "OPTIONS:": PRINT : PRINT
300  HTAB 5: PRINT "<1> GENERATE PURE SWAY": PRINT
320  HTAB 5: PRINT "<2> GENERATE PURE YAW": PRINT
330  HTAB 5: PRINT "<3> GENERATE YAW AND SWAY": PRINT
340  HTAB 5: PRINT "<4> SET VOLTAGES TO BEGIN": PRINT
350  HTAB 5: PRINT "<5> START MOTION": PRINT
360  HTAB 5: PRINT "<6> STOP MOTION": PRINT
370  GET A$:CODE =  VAL (A$): IF CODE >  = 1 AND CODE <  = 6 THEN 390
380  PRINT "ILLEGAL ENTRY": GOTO 370
390  ON CODE GOTO 1000,2000,3000,4000,5000,6000
1000  REM
1010  REM    GENERATE WAVE TABLES FOR
1020  REM          PURE SWAY
1030  REM
1040  HOME : INVERSE : PRINT "GENERATE PURE SWAY WAVE TABLES": NORMAL
1050  POKE 34,2
1060  PRINT : PRINT : INPUT "ENTER MODEL VELOCITY (FT/SEC)";VM
1070  PRINT : INPUT "ENTER MAX. DRIFT ANGLE (DEG)";BETA
1080  PRINT : INPUT "ENTER FREQUENCY (HZ)";FH
1090 BETA = BETA / RAD
1100 FR = FH * 2 * PI
1110 AMAX = VM *  SIN (BETA) / FR
1120  IF AMAX > .45 THEN  GOTO 1080
1130  INVERSE : PRINT "WORKING": NORMAL
1140  FOR I = 0 TO 511
1150 A = AMAX *  COS (FR * I * .01)
1160 IB(I) =  ABS ( INT (A * 256.0 - 128))
1170 IA(I) = IB(I)
1171  PRINT IB(I)
1180  NEXT
1190 CYCLE = 1 / (FH * .01)
1200  POKE 34,0
1210  GOTO 260
2000  REM
2010  REM     GENERATE WAVE TABLES FOR
2020  REM           PURE YAW
2030  REM
2040  HOME : INVERSE : PRINT "GENERATE PURE YAW WAVE TABLES": NORMAL
2050  POKE 34,2
```

```
2080  PRINT : INPUT "ENTER FREQUENCY
2090 R = R / RAD
2100 FR = FH * 2 * PI
2110 PHASE =  ATN (FR * XS
2120 PSIMAX = R / FR
2130 YMAX = XS *  SIN (PSIMAX *  COS  PHASE))
2140  IF YMAX > .45 THEN  GOTO 2080
2150  INVERSE : PRINT "WORKING": NORMAL
2160  FOR I = 0 TO 511
2170 YB = YMAX *  SIN (FR * I * .01 - PHASE)
2180 IB(I) =  ABS ( INT (YB * 256.0 - 128))
2190 YS = YMAX *  SIN (FR * I * .01 - PHASE)
2200 IA(I) =  ABS ( INT (YS * 256.0 - 128))
2205  PRINT IB(I); TAB( 5):IA(I)
2210  NEXT
2220 CYCLE = 1 / (FH * .01)
2230  POKE 34,0
2240  GOTO 260
3000  REM
3010  REM   GENERATE WAVE TABLE FOR
3020  REM   COMBINED SWAY AND YAW
3030  REM
3040  HOME : INVERSE : PRINT "GENERATE SWAY AND YAW WAVE TABLES": NORMAL

3050  POKE 34,2
3060  PRINT : INPUT "ENTER MODEL VELOCITY (FT/SEC)":VM
3070  PRINT : INPUT "ENTER DRIFT ANGLE (DEG)";BETA
3080  PRINT : INPUT "ENTER MAX. R (DEG/SEC)":R
3090  PRINT : INPUT "ENTER FREQUENCY (HZ)";FH
3100 BETA = BETA / RAD
3110 R = R / RAD
3120 FR = FH * 2 * PI
3130 PHASE =  ATN (FR * XS / VM)
3140 PSIMAX = R / FR
3150 YMAX = XS *  SIN (PSIMAX *  COS (PHASE))
3160  IF YMAX + XS *  SIN (BETA) > .45 THEN  GOTO 3090
3170  INVERSE : PRINT "WORKING": NORMAL
3180 YC = XS *  SIN (BETA)
3190  FOR I = 0 TO 511
3200 YB = YMAX *  SIN (FR * I * .01 + PHASE) + YC
3210 IB(I) =  ABS ( INT (YB * 256.0 - 128))
3220 YS = YMAX *  SIN (FR * I * .01 - PHASE) - YC
3230 IA(I) =  ABS ( INT (YS * 256.0 - 128))
3235  PRINT IB(I); TAB( 5):IA(I)
3240  NEXT
3250 CYCLE = 1 / (FH * .01)
3260  POKE 34,0
3270  GOTO 260
4000  REM
4010  REM   SET VOLTAGES TO BEGIN
4020  REM
4030  HOME : INVERSE : PRINT "   SET VOLTAGES TO BEGIN": NORMAL
4040  POKE 34,2
4050 ZB =  PEEK (49360):ZB =  PEEK (49360)
4060 ZA =  PEEK (49361):ZA =  PEEK (49361)
4070 E1 = IB(0) - ZB:E2 = IA(0) - ZA
4080  PRINT "PRESS ANY KEY TO START"
4090  GET A$
4100  INVERSE : PRINT "WORKING": NORMAL
4110  IF E1 < 0 GOTO 4200
4120  FOR I = 1 TO E1
4130  POKE 49360,ZB + I
4140  NEXT
4150  IF E2 < 0 GOTO 4250
```

```
4180  NEXT
4190  GOTO 4200
4200  FOR I =  - 1 TO 21 STEP  - 1
4210  POKE 49360,IB + I
4220  NEXT
4240  GOTO 4150
4250  FOR I =  - 1 TO 21 STEP  - 1
4260  POKE 49361,IA + I
4270  NEXT
4300  POKE 34,0
4310  GOTO 260
5000  REM
5010  REM   START MOTION
5020  REM
5030  HOME : INVERSE : PRINT "START MOTION": NORMAL
5040  POKE 34,2
5050 CH = 0
5060 CL = CYCLE
5070  IF CYCLE >  = 255 THEN CH = 1
5080  IF CYCLE >  = 255 THEN CL = CYCLE - 256
5090  POKE (32774),CL
5100  POKE (32775),CH
5110  FOR I = 0 TO CYCLE - 1
5120  POKE (33024 + I),IB(I)
5130  POKE (33536 + I),IA(I)
5140  NEXT
5150  PRINT : PRINT "PRESS ANY KEY TO START MOTION"
5160  GET A$
5170  CALL 34304
5180  POKE 34,0
5190  GOTO 260
6000  REM
6010  REM  STOP MOTION
6020  REM
6030  HOME : INVERSE : PRINT "STOP MOTION": NORMAL
6040  POKE 34,2
6050  PRINT : PRINT "PRESS ANY KEY TO STOP MOTION"
6060  GET A$
6070  CALL 34308
6080  POKE 34,0
6090  GOTO 260
6100  END

]PR#0
```

```
:ASM

                    1000          .OR $8000
                    1010          .TA $0800
                    1020 *--------------------------------
                    1030 *
                    1040 * PROGRAM CLOCKWAVE
                    1050 *
                    1060 * OUTPUTS SPECIFIED WAVE FORMS ON
                    1070 * D/A CHANNELS 0&1 ON INTERRUPTS
                    1080 * FROM CLOCK
                    1090 *
                    1100 * MOUNTAIN A/D IN SLOT 5 AND
                    1110 * CLOCK IN SLOT 4
                    1120 *
                    1130 *--------------------------------
                    1140 *
                    1150 * ENTRY POINTS
                    1160 *
8600- 78            1170 START  SEI             DISABLE INT &
8601- 4C 74 86      1180        JMP INIT        JUMP TO INIT
8604- 78            1190 STOP   SEI             DISABLE INT &
8605- 4C AF 86      1200        JMP FINISH      JUMP TO STOP
                    1210 *--------------------------------
                    1220 *
                    1230 * EQUATES
                    1240 *
                    1250 *--------------------------------
0000-               1260 CHNLF  .EQ $00         1ST CHAN NO.
0001-               1270 CHNLA  .EQ $01         2ND CHAN NO.
0081-               1290 STARTF .EQ $81         PAGE NOS. OF
0083-               1290 STARTA .EQ $83         WAVE TABLES
00FC-               1300 WAVF   .EQ $FC         ADDRESSES
00FE-               1310 WAVA   .EQ $FE
8004-               1320 PTRL   .EQ $8004       COUNTERS
8005-               1330 PTRH   .EQ $8005
8006-               1340 CYCL   .EQ $8006       TABLE LENGTH
8007-               1350 CYCH   .EQ $8007
C0C0-               1360 CLOCK  .EQ $C0C0       CLOCK
0009-               1370 SETINT .EQ 9           INT EN ADDR
0007-               1380 CLRIRQ .EQ 7           CLOCK IRQ
0008-               1390 CLRINT .EQ 8           CLOCK INT
03FE-               1400 IRQVEC .EQ $03FE       INT VECTOR
C0D0-               1410 DTOA   .EQ $C0D0       D/A ADDR
                    1420 *--------------------------------
                    1430 *
                    1440 * INTERRUPT HANDLER
                    1450 *
                    1460 *--------------------------------
8608- A5 45         1470 IHNDLR LDA $45         SAVE REGS.
860A- 48            1480        PHA
860B- 8A            1490        TXA
860C- 48            1500        PHA
860D- 98            1510        TYA
860E- 48            1520        PHA
860F- AC 04 80      1530        LDY PTRL        SET INDEX
8612- A2 00         1540        LDX #CHNLF      1ST CHAN NO
8614- B1 FC         1550        LDA (WAVF),Y    GET VALUE
8616- 9D D0 C0      1560        STA DTOA,X      OUTPUT TO D/A
8619- A2 01         1570        LDX #CHNLA      2ND CHAN NO
861B- B1 FE         1580        LDA (WAVA),Y    GET VALUE
```

```
8621-  18          1810          CLC
8622-  69 01       1820          ADC #$01       INCREMENT
8624-  A5 FD       1830          LDA WAVF+1     IF CARY SET,
8626-  69 00       1840          ADC #$00       INCREMENT
8628-  85 FD       1850          STA WAVF+1     PAGE NOS.
862A-  AD 04 80    1860          LDA PTRL
862D-  18          1870          CLC
862E-  69 01       1880          ADC #$01
8630-  A5 FF       1890          LDA WAVA+1
8632-  69 00       1900          ADC #$00
8634-  85 FF       1910          STA WAVA+1
8636-  AD 04 80    1920          LDA PTRL
8639-  18          1930          CLC
863A-  69 01       1940          ADC #$01
863C-  8D 04 80    1950          STA PTRL
863F-  AD 05 80    1960          LDA PTRH
8642-  69 00       1970          ADC #$00
8644-  8D 05 80    1980          STA PTRH
8647-  CD 07 80    1990          CMP CYCH       COMPARE TO
864A-  D0 18       2000          BNE RSTCLK     TABLE LENGTH
864C-  AD 04 80    2010          LDA PTRL
864F-  CD 06 80    2020          CMP CYCL
8652-  D0 10       2030          BNE RSTCLK
8654-  A9 81       2040          LDA #STARTF    SET UP FOR
8656-  85 FD       2050          STA WAVF+1     BEGINNING
8658-  A9 83       2060          LDA #STARTA
865A-  85 FF       2070          STA WAVA+1
865C-  A9 00       2080          LDA #$00
865E-  8D 04 80    2090          STA PTRL
8661-  8D 05 80    2100          STA PTRH
8664-  A2 07       2110 RSTCLK   LDX #CLRIRQ    RESET FOR
8666-  BD C0 C0    2120          LDA CLOCK,X    NEXT INT
8669-  A2 08       2130          LDX #CLRINT
866B-  BD C0 C0    2140          LDA CLOCK,X
866E-  68          2150          PLA            RESTORE REGS
866F-  A8          2160          TAY
8670-  68          2170          PLA
8671-  AA          2180          TAX
8672-  68          2190          PLA
8673-  40          2200          RTI            RETURN
                   2210 *-------------------------------
                   2220 *
                   2230 * INITIALIZATION ROUTINE
                   2240 *
                   2250 *-------------------------------
8674-  48          2260 INIT     PHA            SAVE REGS
8675-  8A          2270          TXA
8676-  48          2280          PHA
8677-  98          2290          TYA
8678-  48          2300          PHA
8679-  A9 00       2310          LDA #$00       INITIALIZE
867B-  8D 04 80    2320          STA PTRL       POINTERS
867E-  8D 05 80    2330          STA PTRH
8681-  85 FC       2340          STA WAVF
8683-  85 FE       2350          STA WAVA
8685-  A9 81       2360          LDA #STARTF
8687-  85 FD       2370          STA WAVF+1
8689-  A9 83       2380          LDA #STARTA
868B-  85 FF       2390          STA WAVA+1
868D-  A9 08       2400          LDA #IHNDLR    STORE HANDLER
868F-  8D FE 03    2410          STA IRQVEC     ADDRESS INTO
8692-  A9 86       2420          LDA /IHNDLR    INT VECTOR
8694-  8D FF 03    2430          STA IRQVEC+1
8697-  A2 07       2440          LDX #CLRIRQ    CLEAR CLOCK
```

```
86[illegible]-  [illegible]     2260        LDX #CLRIN
86[illegible]-  BD C0 C0  2270        LDA CLOCK,X
86A1- A9 01       2280        LDA #$01      TURN ON CLOCK
86A3- A2 09       2290        LDX #SETINT   INTERRUPTS
86A5- 9D C0 C0    2300        STA CLOCK,X
86A8- 68          2310        PLA           RESTORE REGS
86A9- A8          2320        TAY
86AA- 68          2330        PLA
86AB- AA          2340        TAX
86AC- 68          2350        PLA
86AD- 58          2360        CLI           ENABLE INT
86AE- 60          2370        RTS           RETURN
                  2380 *-------------------------------
                  2390 *
                  2400 * FINISH SUBROUTINE
                  2410 *
                  2420 *-------------------------------
86AF- 48          2430 FINISH PHA           SAVE REGS
86B0- 8A          2440        TXA
86B1- 48          2450        PHA
86B2- 98          2460        TYA
86B3- 48          2470        PHA
86B4- A9 00       2480        LDA #$00      TURN OFF INTS
86B6- A2 09       2490        LDX #SETINT
86B8- 9D C0 C0    2500        STA CLOCK,X
86BB- A2 07       2510        LDX #CLRIRQ
86BD- 9D C0 C0    2520        STA CLOCK,X
86C0- A2 08       2530        LDX #CLRINT
86C2- 9D C0 C0    2540        STA CLOCK,X
86C5- A9 65       2550        LDA #$65      RESTORE INT
86C7- 8D FE 03    2560        STA IRQVEC    VECTOR
86CA- A9 FF       2570        LDA #$FF
86CC- 8D FF 03    2580        STA IRQVEC+1
86CF- 68          2590        PLA           RESTORE REGS
86D0- A8          2600        TAY
86D1- 68          2610        PLA
86D2- AA          2620        TAX
86D3- 68          2630        PLA
86D4- 58          2640        CLI           ENABLE INTS
86D5- 60          2650        RTS           RETURN
```

SYMBOL TABLE

```
0001- CHNLA
0000- CHNLF
C0C0- CLOCK
0008- CLRINT
0007- CLRIRQ
0007- CYCH
0006- CYCL
C0D0- DTOA
86AF- FINISH
8608- IHNDLR
8674- INIT
03FE- IRQVEC
0005- PTRH
0004- PTRL
8664- RSTCLK
0009- SETINT
8600- START
0083- STARTA
0081- STARTF
8604- STOP
00FE- WAVA
```

AD-P003 825

AIR-PATH ACOUSTIC TRACKING SYSTEM

by

L. E. Motter & D. Huminik

David W. Taylor Naval Ship R&D Center

ABSTRACT

A two-dimensional acoustic tracking system has been developed and installed in the Maneuvering and Seakeeping(MASK) Facility at ~~David~~ DTNSRDC, Taylor Naval Ship Research and Development Center. The system consists of an acoustic pinger in the vehicle being tracked, eight microphones positioned around the basin and a shoreborne microprocessor. In operation, the acoustic pinger in the vehicle is monitored by the eight microphones and the arrival time of the pulses are fed into the microprocessor. The microprocessor computes the travel time of the pulses, uses the times combined with known frequency propagation characteristics, microphone positions and test facility geometry to determine the position of the vehicle. The X and Y coordinates of the vehicle location can be recorded along with other model data on a digital computer and/or plotted in real time on an X-Y plotter.

INTRODUCTION

Over the past two decades, major advancements have been made in the electronics industry. The development of miniaturized data multiplexing and telemetry equipment has made it possible to use radio controlled ship models to investigate maneuvering characteristics that were previously considered impractical. The David W. Taylor Naval Ship R&D Center(DTNSRDC) anticipated the advent of radio control model experiments when the Harold E. Saunders Maneuvering and Seakeeping (MASK) Facility was constructed at the Center in the early 60's. The facility included a 360 ft(110m) x 240 ft(73m) x 20 ft(6m) basin and was designed to accommodate experiments under the towing carriage or with radio-controlled (RC) models. The towing carriage is on railroad tracks so that it can be positioned near the side of the tank for minimum interference when RC models are used.

The tracking of RC models was originally accomplished by two cameras installed in the roof. This photographic tracking system worked well but is not in real time, and consequently was uneconomical and cumbersome to use. The photographic film had to be specially ordered in bulk quantity, months in advance of the experiment. In addition some regions of the tank are out of range of the cameras. Finally analysis of the film is a labor intensive and imprecise procedure. For these reasons, a search was made for a more modern tracking system.

The requirements for the new system were as follows:

(1) The system must have sufficient range to track the model anywhere in the tank;
(2) Data from the tracking system should be immediately

available during a run to determine the success of that run;
(3) The system should be simple to operate and add no more than one person to the model experiment crew;
(4) Last, but not least, it must be affordable.

A scaled down version of the "Mini-Ranger" microwave tracking system manufactured by Motorola was given careful consideration. In discussions with technical representatives, it was determined that the system accuracy would be limited to only $\pm$1.0 ft(0.3m) due to the wavelength limitations of the system. Because of this, the system was rejected.

An opto-electronic measurement system referred to as Selective Spot Recognition(SELSPOT) System is manufactured by Selcom A/B in Sweden. L. Abelseth and O. Rotvold reported, at the 16th International Towing Tank Conference, on their attempts to install a version of the SELSPOT system at the Norwegian Hydrodynamic Laboratories(NHL). They did not adopt the system because it had insufficient range to cover their 50 x 80 m tank and because it was sensitive to light reflections from the water surface.

Using the experience gained from experiments with SELSPOT, NHL developed their own opto-electronic system referred to as Optical Positioning (OPTOPOS) System. This system appears to have good accuracy on the order of 0.04 percent, but it is unclear whether this system would operate effectively in the MASK. Because of the apparent complexity of the system, the estimated cost and the difficulty of purchasing from a foreign manufacture, these systems were ruled out.

AD-A144 227 PROCEEDINGS OF THE GENERAL MEETING OF THE AMERICAN 4/6
TOWING TANK CONFERENCE..(U) STEVENS INST OF TECH
HOBOKEN NJ DAVIDSON LAB D SAVITSKY ET AL. AUG 83
UNCLASSIFIED SIT-DL-TR-13029-VOL-2 N00167-83-M-4062 F/G 20/4 NL

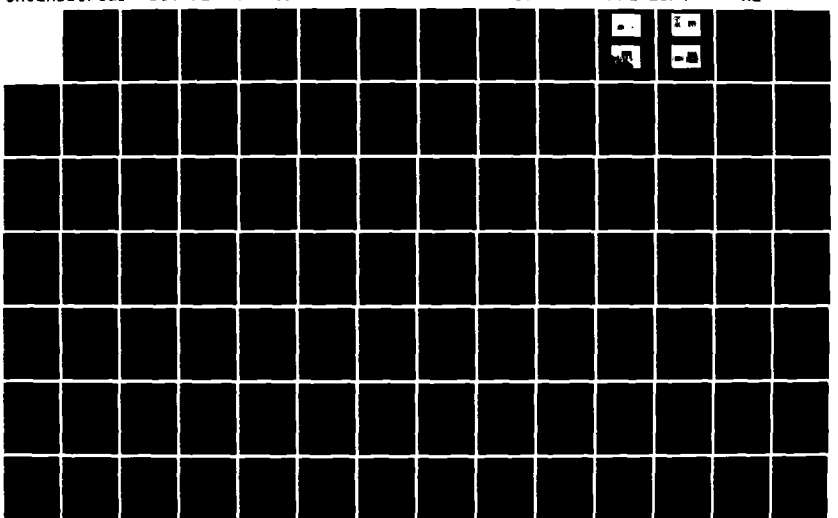

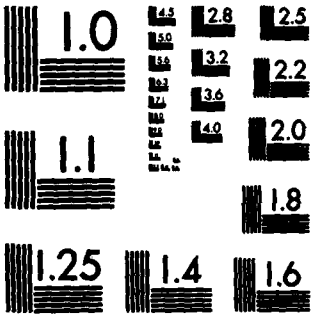

MICROCOPY RESOLUTION TEST CHART
NATIONAL BUREAU OF STANDARDS-1963-A

Ultrasonic technology has been used at the Center to measure relatively short distance with great success for many years. After careful consideration of the problem, it was concluded that an ultrasonic or acoustic tracking system could be developed to operate over the surface of the basin. The result is the Model ATS 821 Acoustic Air Path tracking system built for DTNSRDC by Novascan Corporation.

SYSTEM DESCRIPTION

The ATS 821 Tracking System is suitable for tracking the X-Y position and obtaining the velocity of a model over a horizontal area up to 240ft (73 m) x 360 ft(110 m). There is a trade off between the range and accuracy of the system, which is determined by the wave length and propagation characteristics of the carrier frequency. With a carrier frequency of 20.4 khz, the present system is believed to have sufficient range and accuracy to locate the position of the model to within $\pm$2.0 inches(5.1cm) anywhere in the tank.

System operation is controlled by a crystal oscillator in the main electronics unit, which sends pulses to four strobe units at the selected repetition rate. The strobe units flash simultaneously, and the flash is picked up by a ring of phototransistors in the pinger/strobe detector module. Each time a flash is received, the pinger sends an acoustic pulse, after a calibrated delay. The pulse is picked up by all detectors which are within range, and the pulse arrival times are transmitted back to the main electronics unit. A

microprocessor checks the arrival times against calculated range gates and uses the six shortest valid arrival times to calculate and verify the model position.

The system is quite sophisticated and has many features that will be obvious as the components of the system are considered.

Components of the Tracking System

Figure 1 shows a diagram of the basin with the location of the tracking system components indicated. Eight detectors, indicated as rectangles, and four strobes, indicated as circles are located around the periphery of the tank. The exact location of these components is specified by the user.

These are wired via RG-58 cables to the Main Electronics Unit shown on the shore. A pinger/strobe detector and a pinger electronics unit are mounted on the model.

Figure 2 shows a typical detector(left) and a strobe unit(right). The four strobes are wired in parallel and operate with +17 vdc power supplied by the main electronics unit. The xenon flash tube in the strobe is fired by a circuit which detects a momentary drop to zero of the power input.

The shore mounted detector units, as shown in Figure 2, must be rigidly mounted at the same distance above the water surface and have an unobstructed view of the water surface. Each acoustic detector consists of an electret condenser microphone and a series of signal amplification stages which are designed to keep the gain as high as

possible without causing the detector to trigger on noise. Figure 3 shows the pinger/strobe detector(left) and the associated electronics(right) to be mounted on the model. The acoustic pinger element is a tubular transducer made of lead zirconate-lead titanate ceramic. It is mounted on top of a section of acrylic tubing containing a ring of phototransistors to sense the strobe flash. The total weight of the pinger/strobe detector and electronics is only 2.4 lbs (1.1 kgs) The sensitivity of the phototransistors is adjustable to compensate for existing lighting in the tank. In addition a circuit is used to control signal amplification gains and compensate for the noise level at the amplifier output. The output from the phototransistor electronics signals the pinger electronics unit each time a flash is detected.

The strobe detector will not work outdoors because the phototransistors are saturated by sunlight. Indoor lighting is not normally a problem, as long as strong lights are not present at close range. The primary sensitivity of the phototransistors is infrared, but they also have some sensitivity in the visible spectrum.

The pinger/strobe detector is designed to mount, if necessary, on a gyro-stabilized platform, furnished with the system and shown on the left in Figure 4. The pinger's beam pattern is omnidirectional in a horizontal plane, but highly directional in a vertical plane, so the pinger needs to be mounted on a surface which will not deviate from horizontal by more than 10 to 15 degrees. This angle is highly dependent on detector locations and sensitivity settings. In operation

analog pitch and roll must be supplied to control servo motors which stabilize the mounting platform. The gyro-stabilized platform weighs 6.75 lbs (3.1 kgs) not including pitch and roll transducers.

Figure 5 shows the main electronics unit, the X-Y plotter and the terminal used to communicate with the tracking system. The electronics unit is housed in an aluminum cabinet 17 x 8.75 x 16 inches (43.2 x 22.2 x 40.6 cm). The front panel contains power switch/circuit breaker, system status indicator, reset switch, RS-232 port, and digital meters for display of X-Y coordinates. The back panel has jacks for detectors, strobes and X-Y analog outputs, and connector for the parallel data output. Inside is a power supply and a card cage containing a Texas Instruments 9900 Microprocessor Central Processor Unit(CPU) board, and a system interface board.

Central Processing Unit Functions

The Central Processing Unit(CPU) controls all tracking system operations. It controls when the strobes flash, determines which are the correct return signals received at the detectors and computes where the model is located and the X and Y speed components. In order to reduce the effects of external noise during normal tracking, the CPU computes the anticipated location of the model at the next time step repetition and allows the operator the option of adjusting the size of a window, referred to as range gates, to be opened only when the next pulse is expected at the detector.

When the power is first turned on, or either the reset circuit is

activated or the position of the model is lost for four consecutive pulses, the CPU reverts to an "Acquisition Mode" in which the range gates are ignored and arrival times are used directly. Once the system establishes the location of the model, it reverts to the normal tracking mode. The System Status Indicator light shows which tracking mode is in process.

The CPU supplies the instantaneous X and Y coordinates both to digital meters on the front panel and to a parallel data output port for transfer to an online data collection computer. The output port also supplies date, time, and X and Y velocity. In addition the CPU supplies analog X and Y coordinates which can be connected directly to an X-Y plotter for obtaining a plot of the model path during the run. A typical plot is shown in Figure 6.

The CPU also can be used to calibrate the system, including the local speed of the transmitted pulse and the location of the detectors around the tank. In operation, the CPU must be supplied with the X and Y Coordinates of the first two detectors and the Y Coordinate of detectors 1, 2, and 3 must be the same.

Communication with the CPU is carried out with a Texas Instruments Silent 700 computer terminal. The terminal is used to set up system constants such as detector locations, range gate windows, repetition rates etc, and to control the mode of operation, i.e., calibrate or run.

PERFORMANCE EVALUATION

At the time of writing, there has not been a opportunity to use the tracking system during an actual model experiment. However, the strobe detector/pinger and associated electronics were mounted in a work boat to aid in the evaluation of the system. Because of its sophistication, it was necessary to have a combination adjustment and training session.

It was discovered that the range gate adjustment is absolutely necessary to eliminate external background noise interference and pinger echoes. Without proper adjustment, the detectors frequently locked on to extraneous noise sources such as jingling keys and dropped tools.

The phototransistor sensitivity adjustment is critical to eliminate extraneous light interference such as from open doors. This feature could present a serious problem in a well lighted tank. The purpose of the xenon light and phototransistor is to trigger the pinger in the model. With a minimum of modification, the pinger could be triggered by a different technique such as through a telemetry data channel. This was avoided on the present system to save the telemetry channel for data and to avoid time delays in the multiplex and telemetry process.

The system has a choice of repetition(sample) rates of 1, 2, 3, 4

or 5 Hz. As was expected, dropout was severe at 5 Hz with the present distribution of detectors. In a smaller facility this sample rate may be possible. At 4 Hz, dropouts occurred occasionally but they were not a serious problem. The system was found to be virtually dropout free for repetition rates of 3 Hz or less.

The auto calibration feature to establish the relative location of shore detectors was not of great value. The shore detectors are rigidly mounted and are not subject to accidental location changes. The locations of the detectors can be measured with a tape measure to a greater degree of accuracy than with the auto calibration function.

The auto calibration feature for the speed of sound has been very useful. The speed of sound does depend on the changing atmospheric conditions in the tank, and must be checked daily.

Figures 6 through 9 show samples of 4 different tracked model paths as recorded directly on the X-Y plotter during the turns. All four paths were recorded with a pulse repetition rate of 3 Hz, and the same plotter scale ratio of 20 ft = 1 inch(2.4 m = 1.0 cm). The plotter scale ratio is adjustable so that the user can change the scale to include all of the tank or only a small portion of the tank on the plot.

The turns in Figure 6, 7, and 8 were made in calm water and the one in Figure 9 was made in regular waves. As seen in the figures, the path is not absolutely smooth and there is a signal loss glitch shown in Figure 6 and 9. However the results are more than satisfactory for assessing model maneuvering performance.

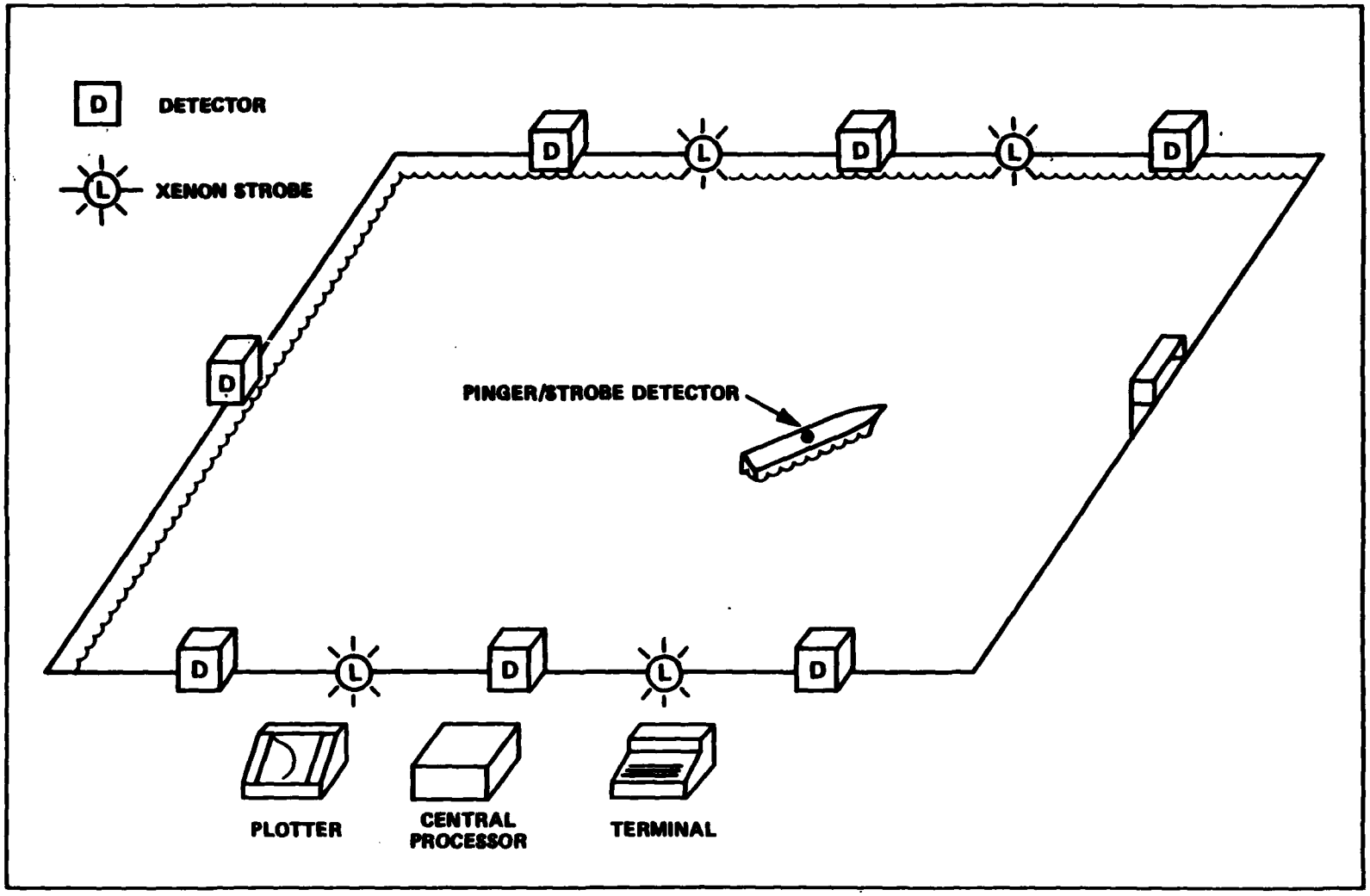

Figure 1 - Layout of Tracking System in MASK

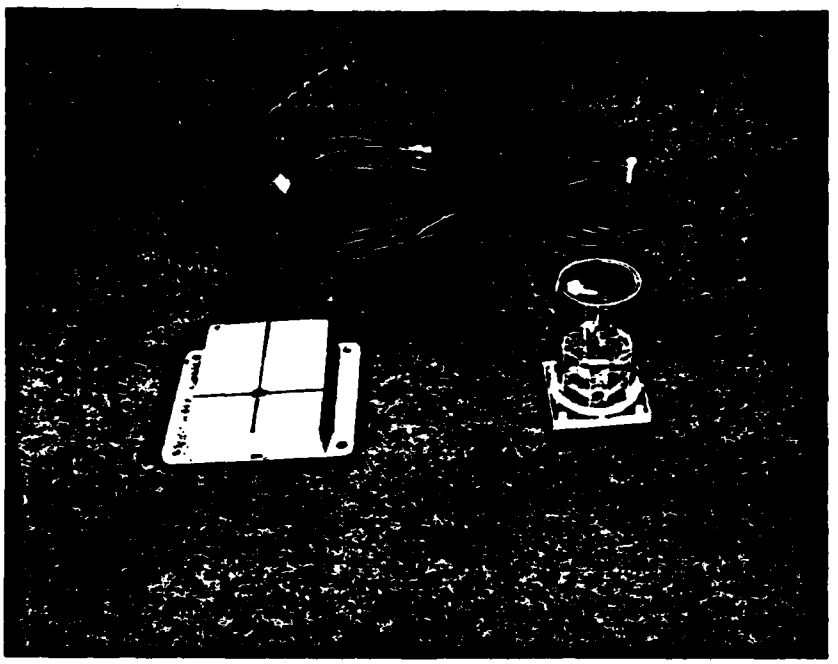

Figure 2 - Shore Mounted Strobe and Detector

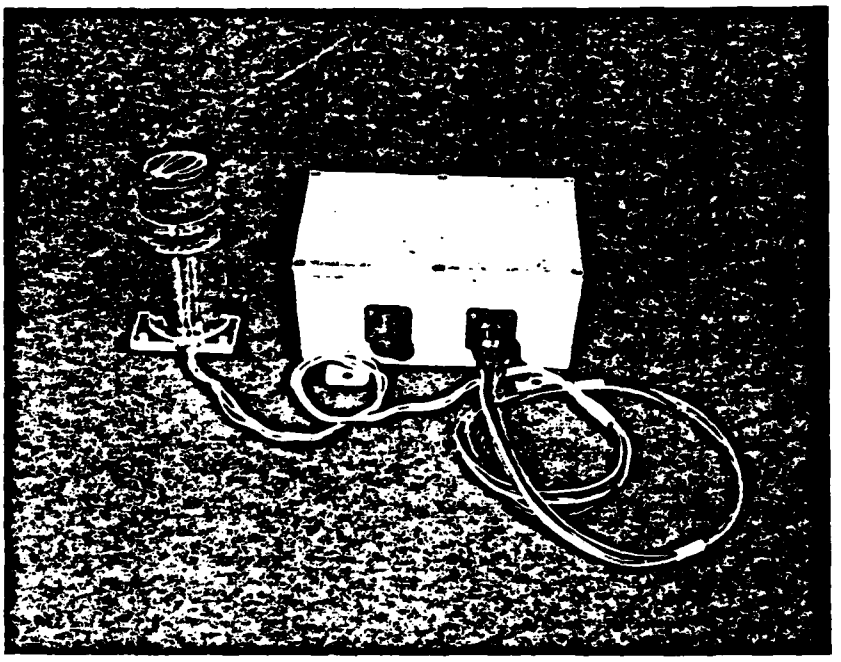

Figure 3 - Model Borne Pinger/Strobe Detector Module and Electronics Housing

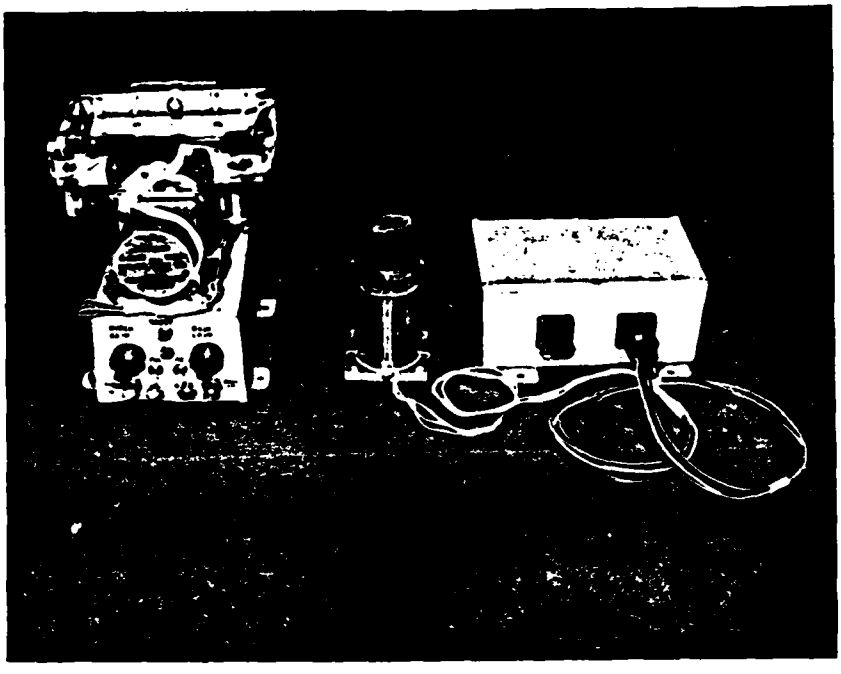

Figure 4 - Gyro-Stabilized Platform and Pinger/Strobe Detector Unit

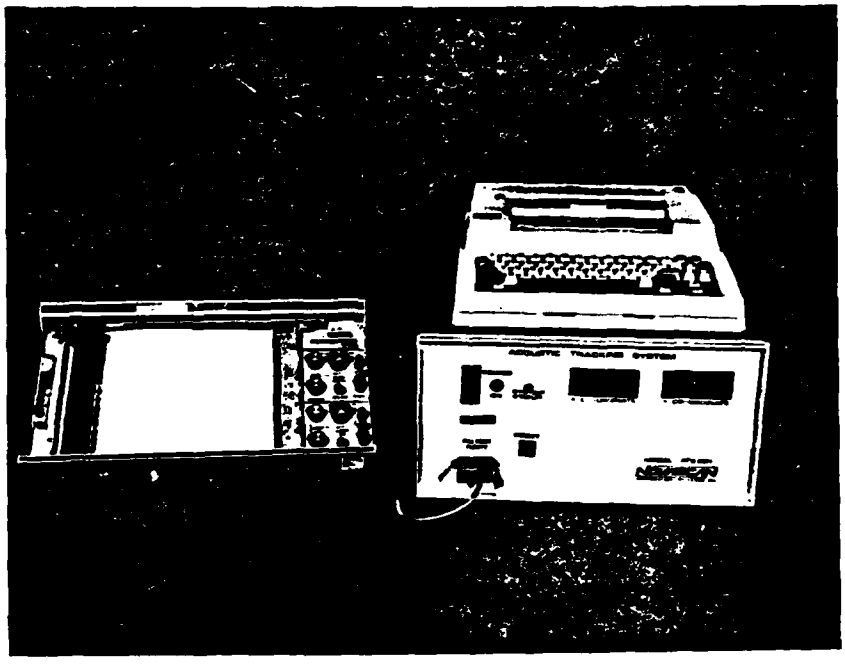

Figure 5 - Main Electronics Unit, the X-Y Plotter and Computer Terminal

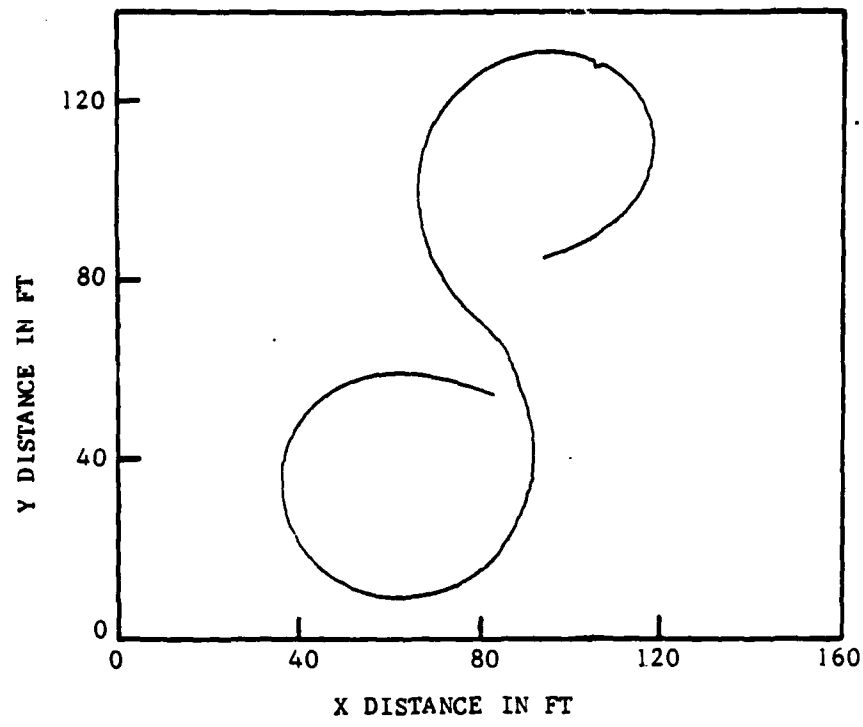

Figure 6 - Figure 8 Path in Calm Water

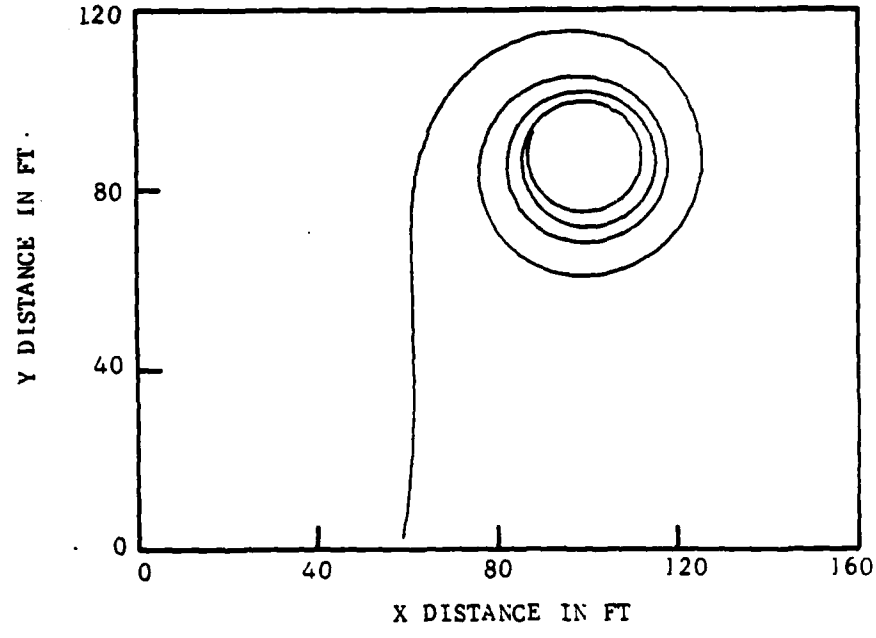

Figure 7 - Path with Constant Command Speed and Rudder in Calm Water

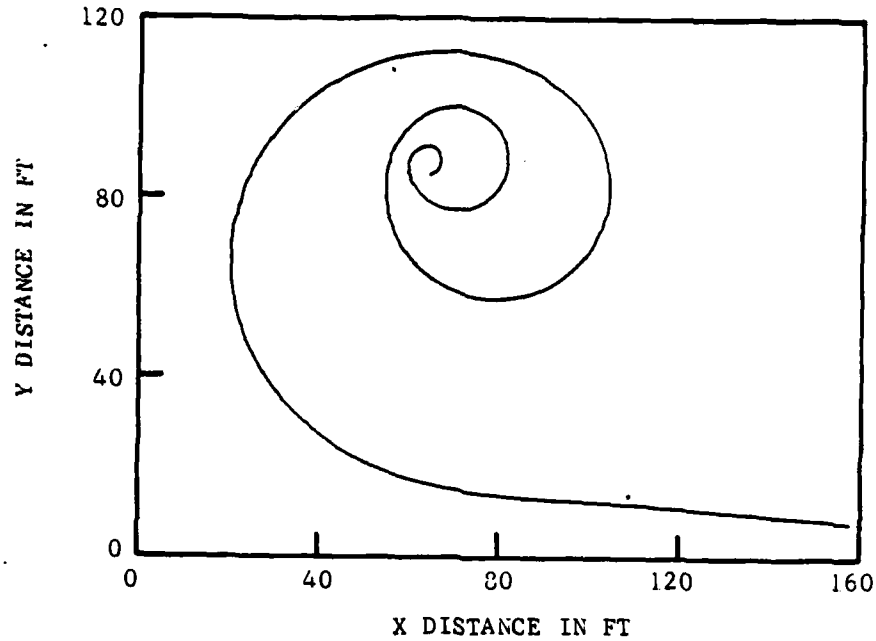

Figure 8 - Spiral Path in Calm Water

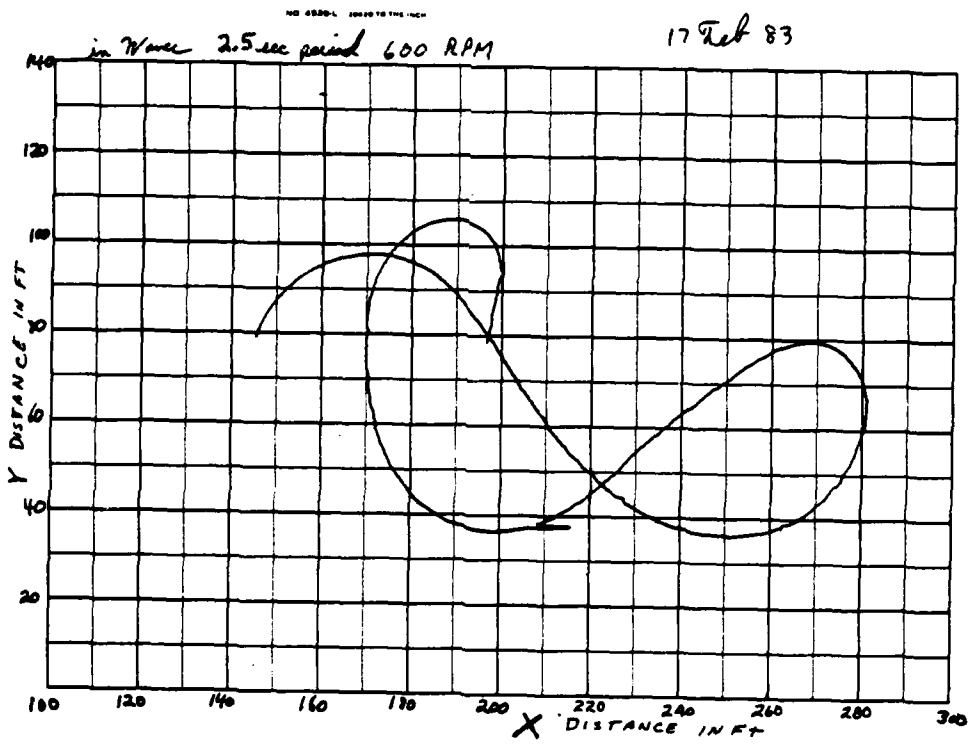

Figure 9 - Figure 8 Path in Waves

REPORTS OF THE

SEAKEEPING

COMMITTEE

Report of the Seakeeping Committee

INTRODUCTION

The Seakeeping Committee for the Twentieth American Towing Tank Conference is composed of the following members:

Professor Martin Abkowitz
Massachusetts Institute of Technology

Dr. Roderick A. Barr
TRACOR Hydronautics, Inc.

Professor Robert F. Beck (Chairman)
The University of Michigan

Professor Roger H. Compton
U.S. Naval Academy

Mr. Geoffrey G. Cox
David Taylor R&D Center

Mr. John Dalzell (Corresponding Member)
Stevens Institute of Technology

Dr. Jeff Dillingham
Offshore Technology Corp.

Dr. Adrian R.J. Lloyd
U.S. Naval Academy

Mr. David C. Murdey
National Research Council

Professor J. Randy Paulling
University of California

The work of the committee was accomplished by telephone and letter. It consisted of two major areas:

(1) The preparation of the Report of the Seakeeping Committee using individual reports prepared by committee members on their institutions' principal seakeeping activities since the ninetheeth ATTC.

(2) The review of abstracts of papers submitted for presentation and discussion during the seakeeping session.

The individual reports of committee members are presented as the main body of the Report of the Seakeeping Committee. They indicate the wide range of seakeeping activities that are being carried on by member institutions. From a general review of the individual reports, the following observations can be made:

* Much of the seakeeping work on normal ship types involves the development of analytic prediction methods and their verification using experimental data. Several institutions report on new and/or improved seakeeping computer programs.

* To improve full scale predictions, improved analytic methods must be accompanied by improved environmental data. DTNSRDC has continued to refine the quality, quantity and presentation of ocean environmental data. NRC has incorporated the North Atlantic wave condition model into their ship motion program. OTC has experimently investigated the impact of icebergs with fixed structures. A new technique for generating random seas in a towing tank has been developed at U of M.

* The area of offshore engineering continues to be of major interest to towing tanks. Investigations on tension leg platforms, OTEC, jack-up rigs, wave forces on cylinders, stability of bottom fixed structures, and wave energy devices have all been performed since the last ATTC.

* Several institutions report work on roll motion. The effects of forward speed on roll damping and cross-coupling with yaw has been investigated by MIT and DTNSRDC. Davidson Laboratory investigated the effects of lateral drifting speed on roll motion amplitude. A joint project of Hydronautics and USNA has studied the capsizing of sailing yachts.

* The effects of hull form on seakeeping performance has received considerable attention. In Canada, motion and propulsion data is being measured on a series of Fast Surface Ships. Also, systematic work on the seakeeping of fishing vessels is being carried out. At DTNSRDC work continues on validating the seakeeping characteristics of an "optimum seakeeping" hull and indentifying its calm water resistance. At Berkeley the effects of above water bow shape on ship performance in head seas for four variations of a Series 60, C_B = .60, hull has been measured.

* Relative motion and deck wetness experients have been conducted at DTNSRDC and the U of M. The work includes the measurement and theoretical prediction of the various components of relative motion on a mathematical model and the SL-7 container ship. The experiments at Berkeley on the effects of above water bow shape included relative motion measurements.

The following individual reports have been submitted by member institutions:

Summary of Activity in Seakeeping at Massachusetts Institute of Technology

by Martin A. Abkowitz

The following is a brief summary of the work done (or being done) over the last few years in the seakeeping area at our Department at MIT. The first two are studies in the experimental area and the remainder are in the theoretical and analytical areas.

1) Model tests are being carried out to determine the effect of forward speed on wave roll damping at roll resonance frequencies, to check the results of three dimensional theory.

2) Seakeeping tests were carried out on a series of fishing boat designs in order to determine added drag in a seaway for purposes of estimating towing power required by the rescue vessel.

3) Design studies of unusual ship forms, for minimum motion in a seaway at zero forward speed, to be utilized as storage platforms.

4) The MIT 5 degree of motion freedom seakeeping program has been extended to predict hull deflection in a seaway under quasi-static analysis.

5) Extension of strip theory to include surge motion effects on diffraction and vice versa.

6) Corrections for bow and stern (end effects) by solving the analytic problem of a cylinder in surge motion in association with towing cable problems.

7) A physical look at the non-linear free surface condition and its effects on body excitation.

8) A hybrid numerical scheme involving matching inner and outer solutions has been developed for the determination of added mass and damping coefficients of ship-like sections (2-D).

9) Formulation and solution of the diffraction problem of slender bodies in waves of all practical lengths and angles of incidence. Solution completed and tested for slender spheroids.

10) Theoretical study on the validity of forward speed reciprocity relations for calculating the exciting forces in pitch and heave, with comparison to direct pressure integration.

11) Studies of end effects on slender body analysis by the introduction of double body flow as a model of the steady state flow - a first step in the attack on 3-D end effects.

12) Ship motions calculations using unified theory are presently underway.

13) Wave damping in roll, sway and yaw with forward speed using slender body theory.

14) Ship to ship wave interactions at zero forward speed.

15) A study of the characteristics and impact forces of large breaking waves (from irregular seas) is being carried out in the Ship Model Towing Tank, using preprogrammed wave generator input.

STATE OF THE ART IN SEAKEEPING WORK AT TRACOR HYDRONAUTICS, INCORPORATED

By Dr. Roderick A. Barr

Since the last ATTC Conference in 1980, a variety of experimental and analytical seakeeping studies have been carried out for ships and offshore systems at TRACOR HYDRONAUTICS. Many of these studies have involved well-established test techniques and theoretical methods. Several studies which may be of particular interest are reviewed below.

An extensive study of seakeeping performance of two candidate OTEC platforms and their multi-point moorings was conducted for NOAA, Kloetzli and Zseleczky (1). Two platforms, a barge-like hull and a semi-submersible, were tested with an elastically scaled cold water pipe (CWP) and four rigid discharge pipes modeled. Tests were conducted with the CWPs and the transition platform at the top of the CWP attached to, and disconnected from, the platform. Measurements included surface platform motions and accelerations, mooring line forces, transition platform motions (relative to surface platform) and forces between the hull and CWP transition platform. Three of the most interesting aspects of this study were the modeling of the moorings, the modeling of the CWP and the split image movies of the tests.

A four-element mooring system was modeled in all tests. Two methods were used for simulating the desired mooring leg force displacement or stiffness characteristics. The first used two series linear springs, of much different stiffness, on each leg. The second used an electro-mechanical mooring line simulation developed at TRACOR HYDRONAUTICS. This simulation, which uses a constant-speed electric motor and limited

ship clutch, as described in Reference 4, can be programmed to provide a desired linear or non-linear stiffness characteristic. Both linear and non-linear stiffnesses were used in the tests described in Reference 1.

Elastic scaling of the CWP models was difficult due to the large scale ratios (λ = 50 to 85) and the fact that proper scaling requires a CWP cross section or bending stiffness, EI, which varies [see Barr and Johnson (2)] as:

$$EI \sim \lambda^{-5}.$$

The model CWP construction technique used was considerably simpler than previous techniques, such as those discussed in Reference 2 and 3. The CWP has a small diameter central spine of commercial aluminum tubing surrounded by a very flexible sleeve which is made of highly permeable foam and has the required CWP OD. Figure 1 shows a photograph of this model. Buoyant, free ascent tests with two CWP sections, one having no exterior covering and one having an impermeable cloth covering, indicated only small differences in mass and hydrodynamic properties of the two sections (1). An uncovered model was, therefore, used for all tests. This modeling technique is applicable to any model having requirements for submerged, elastic members.

A large number of split-image, 16 mm color movies were made during the tests. Two cameras, one above and one below the surface, were synchronously operated. A one-half frame image was recorded by each camera and the resulting films were used to produce a final film print which presents, side-by-side, the above-water motions of the surface platform and the below-water motions of CWP and transition platform.

Several years ago, a computer program for calculating the seakeeping behavior of multiple, three-dimensional bodies was developed at TRACOR HYDRONAUTICS. This zero-speed, linear, frequency-domain program was based on the method of Garrison (5). Initially, the program was used to study wave energy absorption multi-body arrays, Duncan and Brown (6). Recently, the program has been used to predict the motions of two connected ships in close proximity. The connection was modeled by linear springs. The program can treat arbitrary body shapes and water depths.

TRACOR HYDRONAUTICS has been involved for some time in studies of capsizing of sailing yachts. The most recent work has been carried out in a joint project with the U. S. Naval Academy. A recent paper by Kirkman, et al (7) describes results of recent tests in breaking waves of models of varying geometric and inertial properties. The test results indicate interesting and somewhat surprising influences of model properties on resistance to capsizing. The ultimate goal of this work is to establish adequate intact stability criteria for sailing yachts.

REFERENCES

1. Kloetzli, J. and J. Zseleczky, "Model Test Report for Two Configurations of a Moored Pipe/Mobile Platform OTEC Plant," Hydronautics, Incorporated Technical Report 8032-2, May 1982.

2. Barr, R. A. and V. E. Johnson, Jr., "Analytical and Experimental Methods for Determining OTEC Plant Dynamics and CWP Loads," Proceedings of the Sixth OTEC Conference, June 1979.

3. Hove, D., et al, "Ocean Systems Operations Project Final Report," SAI Report SAI-464-820-013-LA, May 1981.

4. Kloetzli, J. and J. Zseleczky, "Model Test Plan for Two Configurations of a Moored Pipe/Mobile Platform OTEC Plant," Hydronautics, Incorporated Technical Report 8032-1, January 1982.

5. Garrison, C. J., "Hydrodynamic Interaction of Waves with a Large Displacement Floating Body," Naval Postgraduate School Report NPS-69 GM 77091, September 1977.

6. Duncan, J. H. and C. E. Brown, "Development of a Numerical Method for the Calculation of Power Absorption by Arrays of Similar Arbitrarily Shaped Bodies in a Seaway," Journal of Research, Volume 26, No. 1, March 1982.

7. Kirkman, K. L., T. Nagle and J. Salsich, "Sailing Yacht Capsizing," Paper presented at the Sixth Chesapeake Sailing Yacht Symposium, January 1983.

Seakeeping Activities of the University of Michigan

by Armin W. Troesch

The towing tank at the University of Michigan was built in 1904. Due to its age, periodic upgradings are required and one such effort to modernize the facility is currently underway. In addition to the complete replacement of all mechanical parts on the towing carriage, new motors and a carriage speed control have been installed. The result is a stable platform from which ocean engineering and seakeeping experiments may be conducted.

A replacement wedge shaped wave maker has been installed and is in the process of being checked out. It is powered by a DC servo/ballscrew drive. The atypical design was selected to be compatible with the non-rectangular cross section of the tank.

A low cost but effective beach has been installed at the end opposite to the wavemaker. The beach extends to the tank bottom and has an average slope of 10°. Expanded Uniroyal Royalite© plastic sheets were placed over a galvanized Unistrut© framework. To provide the viscous damping mechanism required in wave dissipation, eighteen to twenty four inches of Ford Motor Company Truck grills cover the plastic sheets. The grills are held in place by expanded galvanized metal.

Various eductional, commercial, and sponsored research projects investigating seakeeping and ocean engineering related topics have been completed in the past three years. Some of these are described below.

Random Wave Generation

A simple procedure to generate digital random time histories is described by Cuong, Troesch, and Birdsall (1982). This

method produces a random number sequence that is shaped to give the desired spectral density curve. The finite set of numbers is then Inverse Fast Fourier Transformed (IFFT). The result is a pseudo random time history which has given spectral characteristics. Using linear transfer function theory, the application of the method in the generation of random waves is outlined. The paper demonstrates that an essential part in the generation of scale irregular waves is the accurate description of the transfer function of wavemaker.

One difficulty associated with the use of irregular waves in the towing tank is that they are not truly representative unless the records are excessively long. Finite tank dimensions and imperfect wave absorbers place a practical limit on the run time. If it is desired to create a sea that represents the most extreme condition a vessel or structure is to encounter during its lifetime, then care must be exercised in the generation of the wave form. This problem has been addressed by Toki (1982) who constructed a rational basis for the selection of one or a few "design irregular waves." The word "design wave" means a wave which represents the design condition of a structure such as the survival condition. Toki (1982) assumed that the significant wave height and mean wave period corresponding to the severest storm condition could be given by the examination of long term statistical data of sea waves, and that irregular wave elevations were stationary random process in the short term. On the basis of these assumptions a probabilistic model which can create a number of samples of irregular waves shapes with the same maximum wave elevation and the same wave spectrum was developed. There was a large variation in the individual wave shapes that had the 1/10000 highest wave elevation. Adopting four parameters based upon the steepness of the front and rear crest, and the level of vertical and horizontal wave asymmetry, a variety of extreme wave shapes was investigated. A "design irregular wave" was then identified as one that had a maximum

wave height and an exceedance probability of 1/10 of the value of the crest front steepness.

Relative Motion and Deck Wetness

The total relative motion in the bow region of a ship is made up of components which result from the incident waves, ship motion, radiated waves, diffracted waves, and waves due to steady forward speed. As reported by Beck (1982), each of these components have been experimentally measured and theoretically calculated on a wall-sided, mathematical form in head seas.

The idealized model was both fixed and forced to oscillate in heave and pitch in order to measure the diffracted and radiated wave components respectively. The total relative motion was obtained by towing the model in sinusoidal head waves with freedom to heave and pitch. The experiments show that the various components are linear functions of the input amplitude and can be added to give the total relative motion within experimental accuracy. The total relative motion tends to increase with forward speed and decrease as one moves aft from the bow towards midship. The radiated and diffracted wave components normally increase the relative motion 10 to 30% over a simple incident wave minus local vertical motion analysis.

The theoretical calculations were made using a strip-theory approach for the radiated wave components and a slender-body theory for the diffracted waves. The rigid-body motions were predicted using a standard strip-theory computer program. The agreement between theory and experiment is reasonable for the radiated wave component. The theoretical diffracted wave amplitudes are much less than the experimentally measured values. The agreement for the total relative motion is also reasonable; but only because the theoretical heave and pitch amplitudes are significantly larger than the experimental motions.

Wave Energy

A series of model experiments with a twin-flap wave-energy absorbing device is described by Scher, Troesch, and Zhou (1983), and the results compared with numerical predictions based on previous theoretical work. Measurements were made of absorption efficiency, flap motion responses, and total flap forces (mooring forces), all with the supporting structure held fixed, with normal wave encounter. Both 2-D and 3-D finite-flap-length experiments were conducted.

Generally, fair agreement was obtained between theory and experiments with regard to efficiency. A slight but consistent tendency for theory to underestimate measured efficiency was apparent from these experiments. Maximum efficiencies approaching 100% (as predicted analytically) were confirmed by experiments. Further, the predicted behavior of curves of efficiency versus wave number and applied external damping coefficient was generally matched by experimental results.

Results for flap motion responses and forces showed good agreement with theory.

Some basic conclusions are drawn with regard to practical design and economic considerations for a twin-flap power generating system.

Non-Linear Ship Springing

Springing is defined as the dynamic structural response of a vessel due to incident wave excitation. If the wave length is short relative to the ship length, then the process can be described as essentially linear. Results of a theoretical and experimental investigation of linear ship springing is described by Troesch (1980).

However, if an incident wave of a single frequency has a length that is long relative to the ship length, then it is

possible to have hull resonance excited by encounter frequencies that are one half or one third the natural frequency of the main hull girder, ω_o . This phenomenon is a non-linear process involving harmonic excitation due to a low frequency, long wave. The sea is not composed of a single wave component, but rather a complete spectrum. The steepness of the water surface and the interaction of different wave components introduce non-linearities. Wave components at one frequency will interact with components at other frequencies. The result will be pressures and particle velocities with frequencies $\omega_i - \omega_j$ and $\omega_i + \omega_j$, where ω_i and ω_j are the frequencies of the first order wave components. The implication of this for ship springing is that, in addition to the long wave harmonic excitation resulting from 2ω and 3ω , there will also be long wave excitation from $\omega_i + \omega_j$.

Slocum and Troesch (1983) describe how the non-linear behavior of Great Lakes ship springing was investigated through model tests. Both the harmonic ($\omega_o = 2\omega_1$) and the sum frequency ($\omega_o = \omega_1 + \omega_2$) conditions were investigated. A description of the experimental equipment and data collection procedures is included. An empirical form of the equation describing the non-linear springing response is given and verification offered. The use of the model test results in statistically evaluating the importance of the non-linear springing is shown through an example.

The report concludes that the non-linear excitation and response are basically quadratic in wave amplitude and are dependent upon ship speed, wave frequency of encounter, and wave height. The level of the response is also influenced by the relatively small heave and pitch motions of the Great Lakes "thousand footer" used in the experiments.

Wall Reflection Problems

A number of slow speed ocean engineering experiments have

been conducted in the Michigan towing tank. One problem encountered when testing a low speed model is that of tank wall reflection. In addition to the incident waves generated by the wavemaker, the model itself produces a wave pattern. This wave pattern travels away from the model toward the boundaries of the tank. If the tank walls are not equipped with some absorption mechanism, the waves will be reflected back towards the model where they will combine with the incident waves and cause potentially large experimental errors. Tank wall reflection occurs in all hydrodynamic testing facilities of finite dimensions. However, the problem has been observed to be most severe when the model dimensions are relatively large compared to tank dimensions.

By understanding the hydrodynamics of bodies in confined areas, a procedure may be developed in which experimental results from restricted towing tanks can be corrected for side wall reflective effects. A project sponsored by the Michigan Sea Grant Program has been initiated to study the problem. The method for correcting the data will use both experimental and theoretical techniques.

Educational Projects

The Ship Hydrodynamics Laboratory is used by the students at the University for either required class work or individual directed study. A growing number of the projects involve seakeeping or offshore engineering experiments. For example, two student sailing enthusiasts designed and constructed two different sailing catamaran hulls. These were tested in waves and the students determined that reducing pitch motions significantly reduced the added resistance.

A graduate level laboratory course that combines seakeeping theory with experiment is taught in the Spring half term. One experiment shows how motion RAO's are determined. In this part of the course, the transient wave technique is explained and

then demonstrated. The students are given the opportunity to run the entire experiment, from the set up of the equipment to the writing of the data analysis computer programs. This real life experience gives the students a chance to demonstrate their management and technical skills.

References

1. Beck, R.F., "Relative Motion Components for a Mathematical Form in Regular Waves," 14th Symposium on Naval Hydrodynamics, University of Michigan, Ann Arbor, Michigan, 1982.

2. Cuong, H.T., Troesch, A.W., and Birdsall, T.G., "The Generation of Digital Random Time Histories," *Ocean Engineering*, Vol. 9, No. 6, 1982.

3. Scher, R.M., Troesch, A.W., and Zhou, G., "Experimental and Theoretical Evaluation of a Twin-Flap Wave Energy Absorbing Device," *Ocean Engineering* (to appear), 1983.

4. Slocum, S., and Troesch, A.W., "Non-Linear Ship Springing Experiments," University of Michigan, Department of Naval Architecture and Marine Engineering, Report No. 266, 1983.

5. Toki, N., "Preliminary Study on the Concept of Design Irregular Wave With Emphasis on the Generation of It," University of Michigan, Department of Naval Archtiecture and Marine Engineering, Report No. 252, 1982.

6. Troesch, A.W., "Ship Springing - An Experimental and Theoretical Study," University of Michigan, Department of Naval Architecture and Marine Engineering, Report No. 219, 1980.

Review of Seakeeping Activities at the U.S. Naval Academy 1980 - 1983

by Roger H. Compton

Experimental research in seakeeping at the Hydromechanics Laboratory of the U.S. Naval Academy since 1980 has resulted in the publishing of 21 technical reports listed chronologically at the end of this brief summary. The research described in these reports can be categorized as either (1) Ship Motion Studies, or (2) Ocean Wave Studies.

Within the first category, experimental programs investigating head sea wave responses were performed in both the 120' and the 380' tanks in regular and irregular long-crested waves. Wave time histories were measured with either resistance wave wires (stationary measurements) or sonic transducers (moving measurements). Model motions (absolute) were measured by mechanical means using potentiometers for signal generation or sonic transducers while relative motions (point on hull relative to water surface) were normally measured visually. The effects of varying pitch gyradius from about 21% to 29% of model length showed measurable differences in vertical plane, head sea responses - a finding not agreed upon by many. The addition of a stern wedge also affected head sea responses with, in general, a decrease in absolute motions but an increase in relative bow motion at higher speeds.

In the tests involving zero speed beam sea rolling, the model was either completely free and employed sonic sensors (SWATH study) or attached to the carriage by a dynamometer which allowed freedom in roll, heave, pitch, and sway (limited travel). It was noted that wave disturbances from the responding model made wave sensor placement relative to the model an important consideration. It also appeared that even a small model, relative to the tank width of 26 feet, would block the tank at certain frequencies and cause wave reflection to occur.

The extreme wave responses studied by Moran and the capsizing studies employed color videotape recording of the model behavior. A repeatable breaking wave pattern has been developed which works in either tank for capsizing studies. The wave system will break at the same predetermined point in the tank on every run. The controlling program operates on a Tektronics 4051 and is written in BASIC. Preliminary results indicate the roll moment of inertia is a major factor in determining whether a yacht will capsize or not in an extreme beam sea.

The 1983 NAVSEA Research Professor, Dr. Adrian Lloyd, is currently studying the effects of varying amounts of bow flare on deck wetness of frigate forms in long crested head seas. The subject model is a 10 foot model of a recent frigate with seven systematically varied above water bow shapes. Relative bow motion and deck wetness, as measured by a pressure transducer array on the fo'c'sle will be the principal measured motion variables.

Dr. Johnson's state-of-the-art report on irregular wave generation techniques currently employed was produced in collaboration with the ATTC's Seakeeping Committee.

In the second category, Ocean Wave Studies, Dr. Michael McCormick continues to study various methods of extracting useful energy from ocean

waves. Primary among the schemes studied is a bidirectional, pneumatic turbine mounted atop a vertical, hollow, circular cylinder which is partially submerged in a wave system. Heaving cylinder and hinged barge techniques have also been studied experimentally at the Academy's Hydromechanics Laboratory. Basic wave mechanics topics including wave focusing, wave refraction, and wave reflection have been studied by Dr. McCormick and his student investigators. Surface wave forces on tubular offshore structures were studied experimentally by Trident Scholar Mark Rolfes under the supervision of Prof. Thomas Dawson in 1980.

LIST OF TECHNICAL REPORTS

Watkins, R. M., "Experimental Stability Investigation of the Fast Surface Delivery Sled (FSD)", U.S. Naval Academy Division of Engineering and Weapons Report EW-5-80, February 1980.

McCormick, M. E., Coffey, J. P., Richardson, J. B., "An Experimental Study of Wave Power Conversion By A Heaving, Vertical, Circular Cylinder in Restricted Waters", U.S. Naval Academy Division of Engineering and Weapons Report EW-10-80, May 1980. Also published in the Journal of Applied Ocean Research.

Rolfes, M. H., "Wave Force and Structure Response: A Comparison of Theoretical and Experimental Results Using Regular and Irregular Waves", Trident Scholar Report No. 108, U.S. Naval Academy, Annapolis, MD, June 1980.

McCormick, M. E., Kastner, R. J., Glover, L., "An Experimental Study of Water-Wave Focusing by Lens-Shaped Structures", U.S. Naval Academy Division of Engineering and Weapons Report EW-14-80, November 1980. Also published in Marine Technology Society Journal.

Ales, M. R., McGettigan, "An Experimental Analysis of the Effects of Pitch Gyradius on Ship Motions in Head Seas", U.S. Naval Academy Division of Engineering and Weapons Report EW-2-81, April 1981. (Student paper prepared under the direction of Dr. R. H. Compton.)

Compton, R. H., Hoyt, J. G. III, Hough, J. J., "USNA YP Replacement Model Test Program: Zero Speed Beam Sea Rolling Tests", U.S. Naval Academy Division of Engineering and Weapons Report EW-3-81, March 1981.

Enzinger, S. W., "Stability Investigation of U.S. Coast Guard Fast Surface Delivery (FSD) Sled", U.S. Naval Academy Division of Engineering and Weapons Report EW-11-81, September 1981.

Salsich, J. O., Chatterton, H. A., "Investigation of Capsizing in Breaking Waves of the U.S. Coast Guard 41 Foot Utility Boat", U.S. Naval Academy Division of Engineering and Weapons Report EW-5-82, March 1982.

Salsich, J. O., "Bilge Keel Trace Verification Study for FFG-7", U.S. Naval Academy Division of Engineering and Weapons Report EW-6-82, March 1982.

Johnson, B., "A State-of-the-Art Review of Irregular Wave Generation and Analysis", U.S. Naval Academy Division of Engineering and Weapons Report EW-9-82, April 1982.

Salvesen, N., "Nonlinear Large-Amplitude Low-Frequency Ship Motions", U.S. Naval Academy Division of Engineering and Weapons Report EW-10-82, April 1982.

Moran, D. D., "Seakeeping Response of the USCG Cutter HAMILTON In Head Seas", U.S. Naval Academy Division of Engineering and Weapons Report EW-12-82, July 1982.

McCormick, M. E., Brown, T., Dixon, D., Ward, R., "A Theoretical and Experimental Study of the McCabe Wave Energy Pump", U.S. Naval Academy Division of Engineering and Weapons Report EW-15-82, June 1982.

Kirkman, K. L., Salsich, J. O., "SNAME/USYRU Safety from Capsize Study - A Progress Report", Ancient Interface XII, San Francisco, CA, October 1982.

Righter, J. R., "The Effects of a Bow Bulb and a Stern Wedge on a Large Waterplane, Transom Sterned Hullform", U.S. Naval Academy Division of Engineering and Weapons Report EW-25-82 (Vols I, II, III), October 1982. (Student project report prepared under the guidance of Dr. R. H. Compton.)

McCormick, M. E., "An Analysis of Optimal Wave Energy Conversion by Two Single Degree-of-Freedom Devices", U.S. Naval Academy Division of Engineering and Weapons Report EW-27-82, November 1982.

Salsich, J. O., "Experimental Studies of Variable Geometry Bilge Keels", U.S Naval Academy Division of Engineering and Weapons Report EW-9-83, January 1983.

Kirkman, K. L., Nagle, T. J., Salsich, J. O., "Sailing Yacht Capsizing", SNAME Chesapeake Sailing Yacht Symposium, Annapolis, MD, January 1983.

McCormick, M. E., "The Determination of the Directional Spectrum from Cross-Correlation Wave Measurements", U.S. Naval Academy Division of Engineering and Weapons Report EW-14-83, April 1983.

Voight, B. D., McPherson, J. L., "An Experimental Comparison of Zero Speed Seakeeping Characteristics of Single and Double Strut SWATHS", U.S. Naval Academy Division of Engineering and Weapons Report EW-15-83, April 1983. (Student SNAME paper written under the guidance of Dr. R. H. Compton.)

Chatterton, H. A., "Investigation of Capsizing in Breaking Waves of the U.S. Coast Guard 44 Foot Motor Lifeboat", U.S. Naval Academy Division of Engineering and Weapons Report EW-18-83, May 1983.

Salsich, J. O., Zseleczky, J., "Experimental Studies of Capsizing in Breaking Waves", Ancient Interface XIII, San Diego, CA, October 1983.

Significant Areas of Progress for Seakeeping at DTNSRDC

by Geoffrey G. Cox

There continues to be considerable effort devoted to conventional ship seakeeping at DTNSRDC but changes of emphasis, initiated over recent years to provide designers and operators with timely and pertinent seakeeping design and performance assessment information, are becoming increasingly important. Present efforts are mostly devoted to:

a) better definition, verification and presentation of the ocean environment as it applies to ship operation;

b) improved accuracy and convenience of analytical tools and methods;

c) improved seakeeping hull forms, including motion stabilization methods;

d) ability of ship, its subsystems (including aircraft) and crew to perform effectively in a seaway.

Since 1980 there has been a major effort under the leadership of Bales[1,2] to improve the quality, quantity, scope and utility of ocean environment data, including verification and progress in the identification and measurement of short crested seas. Significant features of this work are wave and wind statistics for the North Atlantic[3] and North Pacific based on hindcast climatology, identification of multidirectional characteristics in the Northern North Atlantic[4] and the application development of a directional wave buoy which is convenient for ship use[5].

Basic research has continued over the last three years to improve accuracy in the prediction of relative motion, since this response is essential in carrying out most performance assessments. At the time of writing forced oscillation

experiments are being carried out to supplement free running experiments carried out with a model of the SL-7 container ship and reported by Lee and O'Dea[6] and O'Dea[7].

The new DTNSRDC Ship Motion Prediction Program (SMP) was discussed in the committee report of the last conference. Since that time a significant improvement has been made to the oblique wave roll response for a ship at high speed. This is due to more careful attention being paid to yaw coupling into roll due to dynamic lift effects.

The pioneering work of N.K. Bales[8] to identify the influence of hull form geometry on seakeeping characteristics, including the associated technology, has already had a major impact on U.S. Navy destroyer-type design. It permits the development of superior seakeeping hulls from the earliest stages of the ship design process. Further work validating the seakeeping characteristics of an "optimum seakeeping" hull and identifying its calm water resistance characteristics was published in 1982[9]. Further analytical and experimental work continues in this area, particularly regarding the minimization of possible resistance penalties associated with such hulls.

The seakeeping community suffered a sad loss with the death of Kinney Bales in late 1981. Kinney was an excellent experimenter in addition to his other professional attributes, and members will remember his fine contribution to the last conference on the measurement of flare slamming and deck wetness. Ken received the DTNSRDC David W. Taylor Award for 1980 in recognition of his outstanding achievements for seakeeping research.

References 10 and 11 are examples of how current seakeeping assessment tools can assist the Navy's decision making process and ship operators respectively. Their usefulness depends on

the accuracy, or otherwise, of all the issues identified above. They also serve to emphasize the critical importance of quantitative seakeeping criteria as a component of seakeeping performance assessment. Present state-of-art for seakeeping criteria almost solely consists of simple go/no go values of varying validity, see Appendix E of reference 8 and reference 10, with little information about how a ship subsystem or function gradually degrades with sea state severity, etc. Continued progress in this area depends on considerable efforts using a variety of methods ranging from questionnaires to operators, instrument assisted operator data collection, special trials and simulation studies of varying complexity. Reference 12 includes the results of a recent simulation study to determine the probability of stumbling for a ship's crew engaged in helicopter shipboard functions.

References

1. Bales, S.L., Cummins, W.E. and E.W. Foley, "New Environmental Data for Towing Tank Simulation," contributed paper to Seakeeping Committee Report, Proc. 19th ATTC, July 1980.

2. Bales, S.L., "Review of Ocean Environment Technology for Use in Ship Performance Evaluation," contributed paper to Seakeeping Committee Report, Proc. 16th ITTC, September 1981.

3. Bales, S.L., Lee, W.T. and J.M. Voelker, "Standardized Wave and Wind Environments for NATO Operational Areas," DTNSRDC Report No. SPD-0919-01, July 1981.

4. Cummins, W.E., Bales, S.L. and D.M. Gentile, "Hindcasting Waves for Engineering Applications," Proc. International Symposium on Hydrodynamics in Ocean Engineering, Norwegian Inst. of Tech., August 1981.

5. Foley, E.W., Backman, R.J. and S.L. Bales, "Open Ocean Wave Buoy Comparisons in the North Atlantic," Proc. MTS/NDBC 1983 Symposium on Buoy Technology, April 1983.

6. Lee, C.M., O'Dea, J.F. and W.G. Meyers, "Prediction of Relative Motion of Ships in Waves," Proc., 14th ONR Symposium on Naval Hydrodynamics, August 1983.

7. O'Dea, J.F., "Relative Motion and Deck Wetness Investigation of the SL-7 Container Ship," DTNSRDC Report No. SPD-

8. Bales, N.K., "Optimizing the Seakeeping Performance of Destroyer-Type Hulls," Proc. 13th ONR Symposium on Naval Hydrodynamics, October 1980.

9. Bales, N.K. and W.G. Day, "Experimental Evaluation of a Destroyer-Type Hull Optimized for Seakeeping," Proc. 7th Ship Technology and Research (STAR) Symposium, April 1983.

10. Comstock, E.N., Bales, S.L. and D.M. Gentile, "Seakeeping Performance Comparison of Air Capable Ships," Naval Engineers Journal, Vol. 94, No. 2, April 1983.

11. Bales, S.L. and E.W. Foley, "Development of a Heavy Weather Operator Guidance Catalog for FF-1052 Class Ships," DTNSRDC Report SPD-773-02, February 1979.

12. Baitis, A.E., Applebee, T.R. and T.M. McNamara, "Human Factors Considerations Applied to Operations of the FFG-8 and LAMPS MK.111," submitted for publication in the Naval Engineers Journal.

SUMMARY OF ACTIVITY IN SEAKEEPING AT DAVIDSON LABORATORY SINCE THE 19th ATTC

by John F. Dalzell

Since the last ATTC the Davidson Laboratory has been moderately busy in the experimental, and somewhat less busy in the analytical aspects of seakeeping. The largest part of the effort has been in two dozen experimental projects since then. All but two of these projects have been developmental and thus are proprietary or restricted in some other way. The list includes five drill rigs, two planing hulls, a bulk carrier, three special purpose displacement mono hulls, five SWATH vessels, and several amphibious craft. Most of the test work has been in head and following seas. No new experimental techniques have been involved. The Laboratory has also conducted one abbreviated full scale trial on a SWATH vessel.

Reference 1 is one of the two unrestricted seakeeping projects. Experiments were conducted with a 1/96 scale model of AMERICAN RACER in the wide tank to study the effect of lateral drifting speed on beam sea excited rolling. To the extent possible the experimental program duplicated that of an earlier program in MIT's narrow tank in which a lateral drifting velocity was found to significantly reduce roll motion. No confirmation of the previous results were obtained in the present experiments in which both the conditions of model restraint and the proximity of tank sides were different.

In the second unrestricted project, Reference 2, experiments were conducted with a model of a single-strut-per-hull SWATH ship and three variants (Higher GM, Wide Spacing, Deep Draft) at zero speed in beam regular and irregular waves. Each model configuration tended to roll at its natural frequency ω when excited by regular waves with a frequency 2ω, or by irregular waves with a modal frequency of 2ω. Rolling amplitude extremes for all configurations generally were characterized by the upwave hull just broaching the wave surface. This observation appears to explain both the larger rolling amplitudes of the Deep Draft variants and the smaller rolling amplitudes of the Wide Spacing (of demihulls) variant.

On the analytical side, development of strip methods for the second order drift forces has continued (Reference 3), as well as refinement of strip methods for relative motion, pressure distribution, and the estimation of the effect of shallow water, Reference 4. Finally, some exploratory work has been completed in the modeling of third order statistical systems and the development of a cross-tri-spectral estimation technique, Reference 5.

REFERENCES

1. Dalzell, J.F., "Model Tests of a Drifting Vessel," SIT-DL-81-9-2204, June 1981.

2. Numata, E., "Experimental Study of SWATH Model Rolling in Beam Waves," SIT-DL-81-9-2200, August 1981.

3. Kim, C.H. and Dalzell, J.F., "An Analysis of the Quadratic Frequency Response Function for Lateral Drifting Forces and Moment," JSR, Vol. 25, No. 2, June 1981.

4. Kim, C.H., Chou, F.S. and Tien, D., "Motions and Hydrodynamic Loads of a Ship Advancing in Oblique Waves," SNAME. Vol 88, 1980.

5. Dalzell, J.F., "An Investigation of the Applicability of the Third Degree Function Polynomial Model to Non-Linear Ship Motion Problems," SIT-DL-82-9-2275, December 1982.

Seakeeping Research at Offshore Technology Corporation

by Jeffrey T. Dillingham

The following areas represent a few of the most significant research activities at Offshore Technology Corporation in the area of seakeeping over the last two years.

1) Towing Resistance and Seakeeping Measurements

A great deal of effort has been expended on the improvement of methods and equipment for conducting seakeeping measurements of vessels underway. Among these are the installation of a towing carriage in the shallow water basin and the development of an improved multi-channel telemetry system for transmitting data from free running models to the data acquisition system.

The new towing carriage was developed primarily for a series of tests performed on an amphibious combat vehicle. Due to the multiple functions of the craft it has a hull form which is very unlike conventional ships. This posed many interesting problems in the design which have been studied extensively in a multi-phase program. The areas of investigation include: 1) Calm water resistance and self-propulsion, 2) Resistance and behavior in waves, 3) Free floating survival in waves, and 4) Large amplitude PMM tests to evaluate maneuverability.

A new telemetry system was designed to transmit data from a free running model of a submarine during shallow water maneuvering and seakeeping tests. These tests were designed to determine whether bottom impact would occur during transit through shallow water in waves.

2) Tension Leg Platform Modeling

In the last two years there have been five separate model tests of TLP's conducted at OTC. These have gradually increased

in complexity and sophistication as we have come to better understand the importance of various parameters and the difficulties of the physical modeling. In addition to the basic 6-degree-of-freedom platform motions we have successfully developed instrumentation and techniques to measure, for example: 1) tensions and lateral loads of the tendon/platform connection, 2) tendon bending stresses by means of strain gauges placed on the tendons, 3) Flex joint motions, 4) Hydrodynamic loading on individual hull members, 5) Second order responses, e.g. low frequency drift motions and high frequency ringing phenomenon. In addition, some fundamental experiments have been performed to determine the effects of combined current and waves on the mean offset and low frequency drift motions of a TLP.

3) On-Bottom Stability of Flat-Bottom Structures

This is a deceptively difficult measurement to make for the following reason. A flat bottomed structure sitting on the ocean floor experiences wave-induced pressures on the hull bottom which are a function of the nature of the sea floor material. For most types of bottom material the pressure fluctuation will not be felt significantly on the portions of the hull which is buried in the mud. In order to determine the overturning moments on this structure it is necessary to mount the model on the basin floor in such a fashion that the pressures on the underside of the hull are constant as the waves pass. At the same time all of the forces and moments at the support must be measured. To accomplish this, a system has been developed which allows the small space between the hull bottom and basin floor to be filled with air at a constant pressure. In order to prevent the air from escaping while avoiding any physical contact between the model and basin floor other than through the load cells the model is fitted with a small metal skirt at the turn of the bilge which is immersed in a narrow trough of mercury. As the pressure on the outside of the hull fluctuates in the

waves the mercury level varies slightly, thus preventing any significant portion of this pressure from being transmitted to the air underneath the hull. The model may be supported by load cells either from above or from the underside of the hull. Normally, three three-axis loads cells with simple supports are used since this allows determination of all the forces and moments.

This technique has been used successfully to measure overturning moments on the ARCO Seep Structure and on a submersible drilling rig model.

4) Ice Impact Experiments

Tests have been conducted to study the mechanisms of impact between an iceberg and a fixed structure. The impact force and motions of the iceberg were measured. In order to obtain motion measurements during the impact while not having any physical encumberences attached to the model iceberg a method was developed to compute all 6 degrees-of-freedom of motions using measurements made with accelerometers and gyroscopes mounted on the berg. The data was transmitted to the computer using a battery-powered telemetry system.

Measurement of all of the forces and motions allows computation of energy balances. This has provided some valuable insight into the mechanisms of the collision and given some clues about how to predict maximum impact loads.

5) Wave Energy System

A model of a novel wave energy extraction system was tested to determine efficiency and the effect of variations of numerous parameters. Tests were conducted in shallow water with uni-directional and multi-directional waves. The complicated hydraulic system which is designed to transmit the mechanical energy to an electric generator was modeled physically. It was

thus possible to actually measure the power output from the model and adjust the physical parameters toward an optimum configuration during the model tests.

SEAKEEPING RESEARCH IN CANADA SINCE THE 19TH ATTC.

by David C. Murdey

There has been considerable activity in seakeeping in Canada during the last three years. At the Arctic Vessel and Marine Research Institute of the National Research Council of Canada, the work has fallen into two main categories of which the first, the use of well established techniques for the testing and evaluation of designs for commercial clients, falls outside the scope of this report. The second category includes research projects in areas such as the use of standard techniques to build up an empirical data base, comparison of experiment and theoretical results, and the development of improved testing methods.

Work has continued on the NRC Hull Form Series for Fast Surface Ships. Seakeeping data from this series were presented to the 19th ATTC.(1) and an application to a practical design was described in (2). The motions and propulsion data have now been incorporated in the Defence Research Establishment Atlantic head seas ship theory program PHHS7(3), to produce a semi-empirical model of warship performance in head seas. Additional models have now been manufactured both to complete the series as originally conceived and to extend it. Figure 1 shows all the models now available and identifies those tested since the last Conference. Resistance experiments have been carried out with these new models and seakeeping experiments are well in hand. The extensions of the Series to cover a wide range of length/displacement ratios, and to large beam/draught ratios are considered to be of importance not only in providing trends of performance but also for evaluation of strip theory calculations over a wide range of ship proportions.

The Series data have so far concentrated on pitch and heave responses and power increase, and the slamming characteristics have only been taken into account by means of a simple theoretical model(2). Steps are now being taken to remedy this situation, both by developing test techniques to measure slamming pressure and making improvements in the analytical model. This interest is shared by DREA who contracted Arctec Canada to perform an investigation of bow slamming. The investigation comprised an extensive literature survey followed by an experiment program. Experiments were conducted in Arctec's facilities using 'V', 'Normal' and 'U' forms from the NRC Series instrumented with pressure transducers. Free and pivoted drops were performed in still water and the pivoted drops were repeated in waves. The results were used to prepare an empirical time domain model. As part of the same project seakeeping experiments in regular head waves were carried out with the 'V' form model in the NRC ship model experiment tank. This latter series of tests covered wide ranges of model speed, wavelength and waveheight and included a group of 11 repeat runs to give information on the statistical variability of the results obtained. The data from the pressure transducers were recorded on an FM tape recorder and digitized later for direct computer analysis, which was considered essential for handling the large quantities of data involved. A multi-channel digital transient recorder is now being developed at NRC to overcome the time consuming digitizing process in such tests and to improve frequency response. Consideration is also being given to the use of a segmented model for slamming studies.

In addition to the fast surface ship series, NRC is also carrying out systematic work on the seakeeping of fishing vessels. In this case, the emphasis is on exploring the bounds of validity of strip theory as beam/draught ratio becomes very large. This work is described in detail in (4).

A unique facility at NRC is the outdoor seakeeping basin which is 122m long and 61m wide, and is fitted with a bank of 8 pneumatic wavemakers on one short side and a beach on the other. Work has recently been carried out on the control of the wavemakers to improve the uniformity of the waves across the tank. Waves are usually measured during a model test at two fixed points across the tank and the mean used in the analysis of model responses. However, recent analyses of tests with a free running model in oblique waves suggest spatial anomalies in the waveheight, believed to be due to transverse standingwaves, and more wave probes are being installed to investigate this further.

While current facilities at NRC are restricted to regular waves, the wavemakers to be installed at the new AVMRI laboratories in St.John's, Newfoundland, will enable in addition, both long and short crested irregular waves to be produced. The NRC Hydraulics Laboratory has been very active in the study of sea state simulation. Subjects covered recently include wave synthesis and wave generation, with consideration being given to wave asymmetries and wave grouping (5) (6) (7).

DREA have been developing a capability for radio controlled ship model testing (8). This makes use of the natural environment in Bedford Basin at the head of Halifax Harbour. Results to date have been based on the use of a destroyer model. Work is continuing with particular interest in rudder roll stabilization and a SWATH ship design developed in cooperation with the Royal Netherlands Navy in tests conducted at NSMB.

Research is being carried out at DREA and NRC into the prediction of pressure distribution on a hull's wetted surface. This work is resulting in hull loading software to be

used by DREA's Structural Mechanics Group for the development of comprehensive finite element computer programs for ship strength and vibration analysis. NRC's contribution is the measurement of the amplitude of pressure variation in waves at 12 locations on the hull of a model of a fast warship design. Instrumentation for the study of long-term stresses on warships is being developed by Arctec Canada.

The DREA Ship Dynamics Group have maintained involvment in the development of theory and computer software, including production of a six degree of freedom motions program SHIPMO(9) which has recently been extended to incorporate a loads prediction capability(10). The motion prediction capability was used as a foundation of MSPA(11), a program for the seakeeping performance assessment of mono-hull ships. MSPA utilizes SHIPMO and the North Atlantic wave condition model proposed by Bales and Cummins and since adopted by NATO(12) to compute motions for the entire range of sea conditions in a user specified area of the North Atlantic. Seakeeping criteria are applied to compute seakeeping performance parameters for each heading and sea condition. Parameters are averaged over heading to provide values for each sea condition and over sea condition with consideration of probability of occurence to derive a single valued criteria allowing convenient comparison of ship designs. Similar programs, SWATMO(13) and SWSPA(14), have been prepared for SWATH ships.

REFERENCES

1. Murdey, D.C.: Seakeeping of the NRC Hull Form Series - A Comparison between Experiment and Theory. Proc. 19th ATTC, Ann Arbor, August 1980.

2. Schmitke, R.T. and Murdey, D.C.: Seakeeping in Resistance Trade-Offs in Frigate Hull Form Design. Proc. 13th Symposium on Naval Hydrodynamics, Tokyo, October 1980..

3. Schmitke, R.T. and Colwell, J.L.: Addition of an Experimental Data Base to the PHHS Computer Program. DREA Technical Memorandum 82/H, June 1982.

4. Karppinen, G.T.: Comparison of Theoretical Predictions with Model Test Results for a Wide Beam Fishing Vessel. Proc. 20th ATTC, Hoboken, August 1983.

5. Funke, E.R. and Mansard, E.P.D.: On the Synthesis of Realistic Sea States. NRC/DME report LTR-HY-66, Hydraulics Laboratory, National Research Council, Ottawa, 1979.

6. Mansard, E.P.D. and Funke, E.R.: A New Approach to Transient Wave Generation. Proc. 18th Int. Conf. on Coastal Eng., Cape Town, South Africa, 1982.

7. Funke, E.R. and Mansard, E.P.D.: The Control of Wave Asymmetries in Random Waves. Proc. 18th Int. Conf. on Coastal Eng., Cape Town, South Africa, 1982.

8. Ellis, W.E. and Schmitke, R.T.: Open-Water Testing for Seakeeping Research. Defence Research Group Symposium on Research Facilities, The Hague, April 1982.

9. Schmitke, R.T. and Whitten, B.W.: SHIPMO - A Fortran Program to Predict Ship Motions in Waves. DREA Technical Memorandum 81/C, October 1981.

10. Ando, S.: Wave Load Prediction for the SHIPMO Computer Program. DREA Technical Memorandum 82/L, October 1982.

11. Schmitke, R.T.: MSPA - A Computer Program Package for Seakeeping Performance Assessment of Monohull Ships. DREA Technical Memorandum 83/A, February 1983.

12. Bales, S.L., Lee, W.T. and Voelcher, J.M.: Standardized Wave and Wind Environments for NATO Operational Areas. DTNSRDC Report SPD-0919, July 1981.

13. Nethercote, W.C.E., Piggott, S.D. and Savory, M.W.: SWATMO MOD 2: A Computer Program for the Prediction of SWATH Ship Motions in Regular and Irregular Waves. DREA Technical Memorandum (in review).

14. Nethercote, W.C.E.: SWSPA - A Computer Program Package for Seakeeping Performance Assessment of SWATH ships. DREA Technical Memorandum (in preparation).

FIGURE 1 NRC HULL FORM SERIES FOR FAST SURFACE SHIPS

	C_B	0.48		0.52	
	C_W	0.74	0.80	0.74	0.80
$\frac{L^2}{BT}$	B/T				
60	3.280		29		
105	3.280		30		
150	5.200	1	7	13	19
	4.200	2*	8*	14	20
	3.280	3	9	15	21
194	3.280		26		25
238	5.200	4	10	16	22
	4.200	5*	11*	17	23
	3.280	6	12	18	24

(Basic Form)

350	3.280	27
480	3.280	28

Designs for which tests are described in Ref. (1) and (2)

* Models not yet made

Recent Seakeeping Research at the University of California, Berkeley

by J. Randy Paulling

Wave Forces on Cylindrical Members of Offshore Structures

The forces exerted by waves on the slender cylindrical members of offshore structures are usually estimated by a variation of the so-called Morison formula. This procedure essentially replaces the rather complex orbital motion of the water under the wave by a simple to-and-fro rectilinear motion, and uses fluid force concepts derived from two-dimensional steady flow observations in computing the force exerted on the member. For real structures in waves, several effects are present which represent departures from such an idealization, and these include the above noted orbital motion, combined motions comprising waves plus platform rigid-body motion plus currents, and the three-dimensional nature of the flow in the vicinity of the junction of several members of the structure.

Several experimental studies have been conducted at the University of California for the purpose of evaluating the effects of some of these departures from the Morison formula idealizations. Three specific areas, of which one is reported in detail in another paper at this conference, have formed the focus of these studies, and they are:

a) The effect of cylinder orientation and wave orbital motion;

b) The effect of waves and current acting simultaneously;

c) The three-dimensional effects introduced by intersecting members.

In the first group of experiments, an instrument has been developed by means of which the fluid force acting on a narrow

transverse slice of the test cylinder may be measured. Cylinders of two different diameters have been used for experiments and the parameters varied have included cylinder orientation in the vertical, transverse, longitudinal and oblique directions relative to wave motion. Distinct effects which are correlated with cylinder orientation have been observed in the measured forces, and flow observations through dye injection techniques have yielded visual records of these effects.

Studies of the three-dimensional effects of member intersections and of simultaneous wave-current effects have been carried out through experiments in waves and through the use of constrained motion (PMM) experiments. In the cylinder joint experiments, models representing T-joints between two cylinders were tested in waves and in simple oscillatory surge motion. The experiment was conducted in such a way that the augment in drag force due to the intersection could be separated out of the total force record.

The effect of wave (oscillatory motion) combined with current (steady flow) has been studied by towing a vertical cylinder in the tank. Experiments were conducted in waves and in still water, in the latter case with a forced periodic surge motion imposed on the cylinder.

In all cases, discernable effects which could be attributed to the departure from the idealizations of the Morison formula, were observed. Tank and instrument limitations, to some extent, limited the range of Reynolds' and Keulegan-Carpenter numbers which could be attained to the lower part of the range of values expected in practice.

Effect of Above Water Bow Shape on Ship Performance in Waves

The shape of the bow sections above the waterline have an important influence on several aspects of ship seakeeping, especially in severe sea states. Effects are felt in the basic

rigid-body motions, bow accelerations, added resistance caused by waves, and the relative motion between deck and water surface. The latter, in turn, affects the taking of water on deck and the occurrence of slamming. Linear ship motion theory does not take the effect of above water hull shape into account and, therefore, predictions based on such theory are not able to distinguish the effect of flare even though linear predictions have proven useful for many other aspects of ship seakeeping evaluation.

In order to gain some insight into the phenomena involved and to evaluate the magnitude of some of the basic effects of above water hull shape, a program of experiments have been conducted in the towing tank of the University of California, Berkeley based upon a standard merchant ship hull form having a systematic series of variations in the bow flare shape above the load waterline.

The specific objectives of the work consisted of the following four items:

a) Resistance in waves;

b) Vertical acceleration at the bow;

c) Rigid body motions of the ship;

d) Relative motion between the ship and water surface, and the occurrence of green water on deck at five stations distributed over the forward one-third of the length.

All of the experiments have been conducted using the Series 60, Block 0.60 underwater form. Four bow shapes have been investigated, which may be described as follows:

a) Nearly vertical sides;

b) Standard Series 60 sheer and flare;

c) Extreme continuous flare;

d) Compound flare with knuckle.

Experiments were conducted in regular waves of from 0.65 to 3.0 times model length at a speed corresponding to a Froude Number of 0.25. Wave heights were 1/60 to 1/30 the wave length, with most of the experiments being conducted in 1/40 waves.

The following observations were made concerning the results.

Within the accuracy of experimental measurement, there was no difference among the four flare shapes in the observed first-order rigid body motions of the model. Similarly, there was no discernable difference in the added resistance due to waves for the four shapes.

The second-order motion effects were observed: a mean offset in pitch (but not in heave) and a second harmonic oscillatory motion. The magnitude of the pitch mean offset was about equal to the amplitude of the second harmonic motion. In terms of the bow form variations listed above, the second harmonic amplitude ranking was found to be (a)-(smallest amplitude), (b), (d) and (c).

The measured relative motion between bow and water surface exhibited about a ten percent change between the best, form (c)-extreme continuous flare, and worst, (a)-vertical sides.

The vertical acceleration at the bow was found to vary over a range of about twenty per cent from greatest, form (c) to least, form (a).

AD-P003 826

ADVANCES in ENVIRONMENT SPECIFICATION for SEAKEEPING ANALYSES*

Susan L. Bales, William E. Cummins and Wah T. Lee
David W. Taylor Naval Ship Research and Development Center

ABSTRACT

Substantial progress has been made in the specification of environmental statistics since the 19th ATTC in 1980. For the first time, reliable wind and wave statistics for the Northern Hemisphere are available. While the characteristics of wave directionality are still ~~illusive~~ elusive, some progress has been made in the quantification of spectral spreading. New stratified sampling techniques provide a statistically unbiased sample of directional wave spectra representative of all sea severities and ocean areas. The modified JONSWAP and the Wallops idealized spectral formulations offer alternative methods to the commonly applied Bretschneider family for applying surface wave spectra in seakeeping analyses. Highlights of these advances are provided in this paper. (This paper provides)

INTRODUCTION

Until recently, the natural environment has played a very minor role in ship design. The consideration of ship performance in the prevailing environment has focused primarily on optimaization of calm water resistance and other factors related to the ship propulsion system. In 1975, the U. S. Navy initiated a project to develop statistics of wave occurrences throughout the Northern Hemisphere. This work encompassed the hindcasting of directional wave spectra for a continuous period of twenty years at six hour intervals at about fifteen hundred locations or grid points. While the hindcast climatology is primarily intended for analytic applications, it provides valuable new information on wave directionality and variability

* For presentation at the 20th American Towing Tank conference, Stevens Institute of Technology, Hoboken, New Jersey, 4 August 1983

of spectral shape to the naval architect.

HINDCAST CLIMATOLOGY

The primary stimulant for much of the interest in environmental modeling in the United States is the U. S. Navy's Spectral Ocean Wave Model (SOWM) [1], [2]* hindcast wind and wave climatology. The hindcast climatology is derived by simultaneously predicting wave systems at specified locations and then propagating the wave energy throughout the ocean basins. The typical output consists of two-dimensional wave spectra as well as parameters derived from them such as significant wave height, modal wave period, primary wave direction, secondary wave direction, etc. This work has permitted the development of open-ocean wind and wave statistics for the North Atlantic, North Pacific, and the Caribbean and North Seas [3], [4], [5], [6], [7]. Table 1 provides annual percentage probabilities of occurrence for each Sea State in the North Atlantic [4]. It also identifies associated modal wave period ranges. The table was developed using the hindcast climatology. Tables 2 and 3 provide similar data for the North Pacific and the Northern Hemisphere [4], respectively.

While the confusion associated with Sea State numeral definitions has sometimes indicated the need to avoid such classifications, some ship operators and designers use no other means of describing the wave and wind environment. Many nations throughout the world utilize and endorse the definition proposed by the World Meteorological Organization (WMO). As most shipboard observations which are currently published also use WMO codings, it was felt that the WMO definitions would provide a good standard for Tables 1 through 3.

* Numbers in brackets refer of references given at the end of text.

VALIDATION and APPLICATION of HINDCAST CLIMATOLOGY

The U. S. Army Corps of Engineers has published an atlas of wave hindcasts for 1956-1975 at 13 stations adjacent to the U. S. Atlantic Coast (deep water) [8] and for some near shore locations [9]. Comparison of the Navy (SOWM) hindcasts with the those of Corps of Engineers has indicated that for U. S. East Coast areas, the SOWM data may predict a greater occurrence of longer waves while the heights are not as extreme. This is probably due to a refinement in the wind fields input to the Corps of Engineers model.

The National Maritime Institute (NMI), United Kingdom, is preparing a new wave atlas based on visual observations. The visual wave data are processed through an evolving suite of computer programs named "NMIMET." These include procedures for deriving wave statistics from wind statistics based on parametric modeling of their joint probability and a method for synthesising directional wave climate from simple wave and wind statistics [10]. A comparison of NMIMET data with visual and SOWM hindcasts for station India is provided in Figure 1. The correlation between the NMIMET and hindcast derived data is excellent, while the visual data provide somewhat lower percent frequencies of exceedence.

As wind data are generally available for many open and coastal ocean areas and one of the objectives of an ongoing Ship Structures Committee project [11] is to provide a simultaneous description of the winds and waves, the following method is proposed. The model permits the prediction of significant wave height (or modal wave period), given a distribution of observed/

measured wind speeds. The model depends on the application of a modified Weibull distribution, a versatile tool in many engineering applications. The method, reported in greater detail elsewhere [11], can be summarized as follows:

1. Using the predetermined coefficients for the third order polynomial equations, determine B and θ values for various wind speed intervals. Where B is the Weibull slope and θ is called the scale parameter.

2. Substituting the appropriate sets of B and θ values from Step 1 into the Weibull distribution, derive the significant wave height or modal wave period frequency of occurrence distributions for different wind speeds.

3. Then, using the total wind speed percentages from any source and the results may be obtained by multiplying each value in Step 2 by its corresponding wind speed probability.

A comparison of the hindcast and thusly predicted significant wave heights is given in Figure 2. As can be seen in this figure, the resulting wave height exceedences agree rather well. In general the procedure provides reasonable predictions for open-ocean and coastal locations.

The Corps of Engineers wave parameter statistics are only applicable along coasts and in relatively shallow water. Other open ocean statistics generally based on visual observations of the seas and are subject to inherent observer biases. However, the SOWM hindcasts are based on the localized barometric pressures and resulting wind velocity fields [1], [2]. Therefore, the wave observational biases of other wave models are excluded. The SOWM is best used by statistically averaging wave conditions over several years time, for a specific location and season. Using the SOWM statistics to predict a single event is also a goal, and recent progress and validation indicate

that this may be achievable in some situations.

DEVELOPMENT OF A STRATIFIED SAMPLE

A family of "stratified" directional wave spectra has been developed for the North Atlantic and will be reported in detail elsewhere. The primary stratification is with regard to significant wave height variation and the secondary is with regard to geographic variation. Seasonal variations are also included in the resulting approximately 2000 spectra. The development of the stratified sample is summarized by the following steps:

SAMPLE I - The total ocean area was divided into segments, with a grid point roughly central to each segment. The set of hindcasts for each grid point was considered to be representative of the climatology for its segment. The sample for each grid point was chosen by a random procedure which gave each hindcast an equal chance of being chosen. Using this procedure, each hindcast in SAMPLE I is assumed to have equal weight. In addition to being sorted by stratum (significant wave height), SAMPLE I was also sorted by region and season.

SAMPLE II - A total sample size for the second sample was chosen by a single compromise between accuracy and computer cost This was distributed among the various strata in such a way as to roughly minimize the variance of an estimate of the mean of a statistic which correlates strongly with significant wave height. The entire set in stratum 6 (significant wave heights over 8 m) in SAMPLE I was included in SAMPLE II. SAMPLE II is also sorted by region and season.

Figure 3 shows the geographic stratification of the samples [11]. Table 4 provides a breakdown by region and stratum of SAMPLE II of the approximately 2000 spectra. While general conclusions for the applications of the stratified sample are not yet drawn, data appear to provide a statistically unbiased sample of directional wave spectra representative of all sea severities and

ocean areas for seakeeping performance assessment.

SPECTRAL FAMILIES

Among the various statistical tools available to describe wave data, spectral analysis is a most effective and powerful means for summarizing the properties associated with the sea. The lack of availability of suitable measured spectra for ship motion calculations (the stratified sample is an alternative for the near future) has led to the use of empirical and mathematically derived spectra as a standard tool. Since the magnitude of ship motions is significantly influenced by the shape of the wave spectrum for a given sea severity (e.g., due to the randomness of the ocean waves), it is highly desirable to examine the characteristics and limitations of various idealized spectral formulations for ship motion calculations. [12].

Most of the idealized wave spectral models are adopted from the spectral function proposed by Phillips [13]. Phillips used dimensional analysis to derive the upper limit of the spectral saturation range. The resulting function is applicable to fully-developed seas only.

The International Towing Tank Conference (ITTC) recommends application of a two-parameter wave spectral formulation. This is similar to that developed by Bretschneider and recommended by the International Ship Structures Congress (ISSC) for open ocean conditions. The Bretschneider spectrum is applicable to fully-developed as well as the usual unsaturated seas tnat persist most of the time throughout the world oceans. The Bretschneider spectra contain total energy approximately equal to four times

the square root of the zeroth moment of the spectrum and also permit variations of frequency distribution for given significant wave heights.

When the seas are relatively shallow and at least partially surrounded by land, the Bretschneider spectral formulation may not be applicable. The effort to develop a generalized spectral function for fetch-limited seas was greatly advanced during the Joint North Sea Wave Project (JONSWAP), where the fetch dependence of the measured one-dimensional frequency spectra was investigated by parameterizing the spectra with an analytic function derived by least squares fit techniques [14]. The resulting function is known as the JONSWAP spectral density formulation. As it is usually written, the JONSWAP spectrum is dependent on the two parameters wind speed and fetch. However, for simplicity, as well as consistency with the current state-of-the-art in seakeeping performance assessment, a JONSWAP expression which is dependent only on the two parameters, significant wave height and modal wave period, is required. A new parameter, β, has been developed to replace the usual α parameter, correcting for the parameter's nonuniversality [15]. The modified JONSWAP spectrum satisfies the total energy content of the spectrum automatically. That is, the total energy of the modified spectrum is approximately equivalent to four times the square root of the zeroth moment of the spectrum.

In 1981, Huang and his associates proposed a unified two-parameter wave spectral model known as the Wallops spectrum [16]. The model is based on theoretical analysis and laboratory data. The spectrum maintains a variable bandwidth as a function of the significant slope, a measure of the nonlinearity of the waves in the seaway. One novel feature of the Wallops spectrum

is the possibility of using remotely sensed data as an input directly (e.g., radar sensed wave slopes).

Figure 4 shows the shape of the three idealized wave formulations mentioned above. The modified JONSWAP and the Wallops spectra are sharply peaked where the broader Bretschneider spectrum contains more energy at the high and low frequency ends. Clearly each spectrum may provoke varying ship motion magnitudes in seakeeping performance assessments.

WAVE DIRECTIONALITY

Over the years, due to the lack of suitable measured directional wave spectra, a continuing deficiency in seakeeping technology has been the inability to adequately model the directional characteristics of the seaway. Now with the availability of the directional wave spectra from hindcasts, it is possible to add another parameter to the usual significant wave height and modal wave period pairs. This, of course, is wave directionality, including some description of wave energy spreading. A notable value of the hindcasts here is that they can be used to determine the statistical occurrence of directional conditions which could then be incorporated into an analytical multi-parameter model.

In [17], a set of parameters for treating the directional spread of wave energy was introduced. These parameters are reviewed and extended in [18]. A brief description of these parameters is now given.

a. m_2 is a measure of the angular spread or width of the directionality and in a sense, corresponds to a variance; for a unidirectional swell, it has a value of 0; Figure 5

shows m^2 as a function of half spreading angle Φ for the cosine squared distribution ($m^2 = 0.25$ corresponds to $\pm$ 90 degree spreading)

b. p^2 is a measure of the "centralness" of the spreading and it corresponds to a moment of inertia of wave spreading; large values of p^2 (e.g., $p^2 > 0.1$) suggests a non-central distribution of wave directionality such as is present when two or more systems propagate into an area

c. q is a measure of skewness; small values reflect slightly skewed central distributions while large values of p^2, suggest wave systems from multiple sources

Distributions of these three parameters have been developed for three grid points in [18] for about a 10 year hindcast data set. The results suggested that about half of the hindcast directional spectra for these three locations can be approximated with a cosine squared distribution with half spreading angles near 90 degrees. Based on the results available to date, it is too soon to suggest any improvement to the cosine squared spreading function.

SUMMARY

The Spectral Ocean Wave Model (SOWM) has permitted the development of open ocean wind and wave statistics throughout the Northern Hemisphere. The hindcasts can also be used to develop a stratified sample of wave spectra. This sample provides a statistically unbiased sample of directional wave spectra representative of all sea severities and various ocean areas.

The two-parameter Bretschneider spectral formulation, recommended by both the ITTC and the ISSC, remains the most widely accepted representative of open ocean conditions. When the seas are relatively shallow and at least partially surrounded by land, the modified JONSWAP spectrum, is recommended. The Wallops formulation may be of additional future interest.

One novel feature of the Wallops spectrum is the possibility for using remotely sensed data as a direct input.

Future or continuing efforts in the U. S. Navy include the development of additional hindcasts for other ocean areas, determination of the utility of the stratified spectral family in seakeeping performance analyses, and development of further directional data. Validation of the hindcast wind and wave climatology will continue to be of paramount interest. Collaboration with NMI is expected to provide interesting comparisons with measured and observed wave data and a directional wave buoy [19] developed by ENDECO is providing full-scale data for comparison with SOWM forecasts.

REFERENCES

1. Lazanoff, S.M. and Stevenson, N.M., "An Evaluation of a Hemispheric Operational Wave Spectral Model," FNWC Technical Note 75-3,June 1975.

2. Pierson, W.J., "The Spectral Ocean Wave Model (SOWM), A Northern Hemisphere Model for Specifying and Forecasting Ocean Wave Spectra," DTNSRDC Report 82/011, July 1982.

3. Bales, S.L., W.T. Lee, and J.M. Voelker, "Standardized Wave and Wind Environments for NATO Operational Areas," Report DTNSRDC/SPD-0919-01, July 1981.

4. Bales, S.L., "Designing Ships to the Natural Environment," Naval Engineers Journal, Vol. 95, No. 2, March 1983.

5. DTNSRDC report identifying worst season environmental data for 16 global locations, to be published approximately late 1983.

6. Report similar to reference 3 except for the North Pacific, to be published approximately in late 1983.

7. "U.S. Navy Hindcast Spectral Ocean Wave Model Climatology Atlas: North Atlantic," Publication NAVAIR 50-1C-538, Naval Oceanography Command Detachment, Asheville, N.C., to be published in late 1983.

8. Corson, W.D., D.T. Resio, R.M. Brooks, B.A. Ebersole, R.E. Jensen, D.S. Ragsdale, and B.A. Terry, "Atlantic Coast Hindcast, Deepwater, Significant Wave Information," Waterways Experiment Station, WIS Report 2, January 1981.

9. Corson, W.D., D.T. Resio, R.M. Brooks, B.A. Ebersole, R.E. Jensen, D.S. Ragsdale, and B.A. Terry, "Atlantic Coast Hindcast, Phase II, Wave Information," Waterways Experiment Station, WIS Report 6, March 1982.

10. Andrews, K.S., N.M.C. Dacunha, and N. Hogben, "Wave Climate Synthesis," Report NMI R-149, January 1983.

11. Report to be published by Ship Structures Committee, Project No. SR-1287, approximately at end of 1983.

12. Ochi, M.K. and S.L. Bales, "Effect of Various Spectral Formulations in Predicting Responses of Marine Vehicles and Ocean Structures," Offshore Technology Conference Paper OTC 2743, May 1977.

13. Phillips, O.M., "The Equilibrium Range in the Spectrum of Wind Generated Waves," J. Fluid Mech., Vol. 4, 1958.

14. Hasselmann, K. et al., "Measurements of Wind-Wave Growth and Swell Decay During the Joint North Sea Wave Project (JONSWAP)," Deutschen Hydrographischen Zeitschrift, A8, No. 12 (1973).

15. Lee, W.T. and S.L. Bales, "A Modified JONSWAP Spectrum Dependent only on Wave Height and Period," DTNSRDC Report SPD-0918-01, May 1980.

16. Huang, N.E., S.R. Long, C-C. Tung, Y. Yuen, and L.E. Bliven, "A Unified Two-parameter Wave Spectral Model for a General Sea State," Journal of Fluid Mechanics, Vol. 112, pp. 203-224, 1981.

17. Cummins, W.E. and S.L. Bales, "Extreme Value and Rare Occurrence Statistics for Northern Hemispheric Shipping Lanes," Proceedings, Fifth SNAME Ship Technology and Research (STAR) Symposium, Coronado, California, June 1980.

18. Cummins, W.E., S.L.Bales, and D.M. Gentile, "Hindcasting Waves for Engineering Applications," presented at International Symposium on Hydrodynamics in Ocean Engineering, Trondheim, August 1981.

19. Foley, E.W., R.J. Bachman, and S.L. Bales, "Open Ocean Wave Buoy Comparisons in the North Atlantic," Precedings of the MT/NDBC 1983 Symposium on Buoy Technology, New Orleans, Louisiana, 27 - 29 April 1983.

Sea State Number	Significant Wave Height (m)		Sustained Wind Speed (Knots)*		Percentage Probability of Sea State	Modal Wave Period (Sec)	
	Range	Mean	Range	Mean		Range**	Most Probable***
0 - 1	0 - 0.1	0.05	0 - 6	3	0	–	–
2	0.1 - 0.5	0.3	7 - 10	8.5	7.2	3.3 - 12.8	7.5
3	0.5 - 1.25	0.88	11 - 16	13.5	22.4	5.0 - 14.8	7.5
4	1.25 - 2.5	1.88	17 - 21	19	28.7	6.1 - 15.2	8.8
5	2.5 - 4	3.25	22 - 27	24.5	15.5	8.3 - 15.5	9.7
6	4 - 6	5	28 - 47	37.5	18.7	9.8 - 16.2	12.4
7	6 - 9	7.5	48 - 55	51.5	6.1	11.8 - 18.5	15.0
8	9 - 14	11.5	56 - 63	59.5	1.2	14.2 - 18.6	16.4
>8	>14	>14	>63	>63	<0.05	18.0 - 23.7	20.0

*Ambient wind sustained at 19.5 m above surface to generate fully-developed seas. To convert to another altitude, H_2, apply $V_2 = V_1(H_2/19.5)^{1/7}$

**Minimum is 5 percentile and maximum is 95 percentile for periods given wave height range.

***Based on periods associated with central frequencies included in Hindcast Climatology.

TABLE 1
ANNUAL SEA STATE OCCURRENCES IN THE OPEN OCEAN
NORTH ATLANTIC

Sea State Number	Significant Wave Height (m)		Sustained Wind Speed (Knots)*		Percentage Probability of Sea State	Modal Wave Period (Sec)	
	Range	Mean	Range	Mean		Range**	Most Probable***
0 - 1	0 - 0.1	0.05	0 - 6	3	0	–	–
2	0.1 - 0.5	0.3	7 - 10	8.5	4.1	3.0 - 15.0	7.5
3	0.5 - 1.25	0.88	11 - 16	13.5	16.9	5.2 - 15.5	7.5
4	1.25 - 2.5	1.88	17 - 21	19	27.8	5.9 - 15.5	8.8
5	2.5 - 4	3.25	22 - 27	24.5	23.5	7.2 - 16.5	9.7
6	4 - 6	8	28 - 47	37.5	16.3	9.3 - 16.5	13.8
7	6 - 9	7.5	48 - 55	51.5	9.1	10.0 - 17.2	13.8
8	9 - 14	11.5	56 - 63	59.5	2.2	13.0 - 18.4	18.0
>8	>14	>14	>63	>63	0.1	20.0	20.0

*Ambient wind sustained at 19.5 m above surface to generate fully-developed seas. To convert to another altitude, H_2, apply $V_2 = V_1(H_2/19.5)^{1/7}$

**Minimum is 5 percentile and maximum is 95 percentile for periods given wave height range.

***Based on periods associated with central frequencies included in Hindcast Climatology.

TABLE 2
ANNUAL SEA STATE OCCURRENCES IN THE OPEN OCEAN
NORTH PACIFIC

Sea State Number	Significant Wave Height (m)		Sustained Wind Speed (Knots)*		Percentage Probability of Sea State	Modal Wave Period (Sec)	
	Range	Mean	Range	Mean		Range**	Most Probable
0 - 1	0 - 0.1	0.05	0 - 6	3	0	–	–
2	0.1 - 0.5	0.3	7 - 10	8.5	5.7	3 - 15	7
3	0.5 - 1.25	0.88	11 - 16	13.5	19.7	5 - 15.5	8
4	1.25 - 2.5	1.88	17 - 21	19	28.3	6 - 16	9
5	2.5 - 4	3.25	22 - 27	24.5	19.5	7 - 16.5	10
6	4 - 6	5	28 - 47	37.5	17.5	9 - 17	12
7	6 - 9	7.5	48 - 55	51.5	7.6	10 - 18	14
8	9 - 14	11.5	56 - 63	59.5	1.7	13 - 19	17
>8	>14	>14	>63	>63	0.1	18 - 24	20

*Ambient wind sustained at 19.5 m above surface to generate fully-developed seas. To convert to another altitude, H_2, apply $V_2 = V_1(H_2/19.5)^{1/7}$

**Minimum is 5 percentile and maximum is 95 percentile for periods given wave height range.

TABLE 3
ANNUAL SEA STATE OCCURRENCES IN THE OPEN OCEAN
NORTHERN HEMISPHERE

TABLE 4 — SAMPLE II SPECTRA

STRATUM SIG. WAVE HT.(M)		NUMBER OF SAMPLES 1 (0-1)	2 (1-2)	3 (2-3)	4 (3-5)	5 (5-8)	6 (>8)	TOTAL
Region	A	20	43	66	93	107	44	373
	B	42	65	94	106	138	58	503
	C	88	56	37	23	9	2	215
	D	155	131	110	100	87	22	605
	E	70	80	68	53	22	8	312
TOTAL		375	375	375	375	374	134	2008
NORTH SEA		20	30	30	30	11	4	125
GULF		20	30	24	6	0	0	80

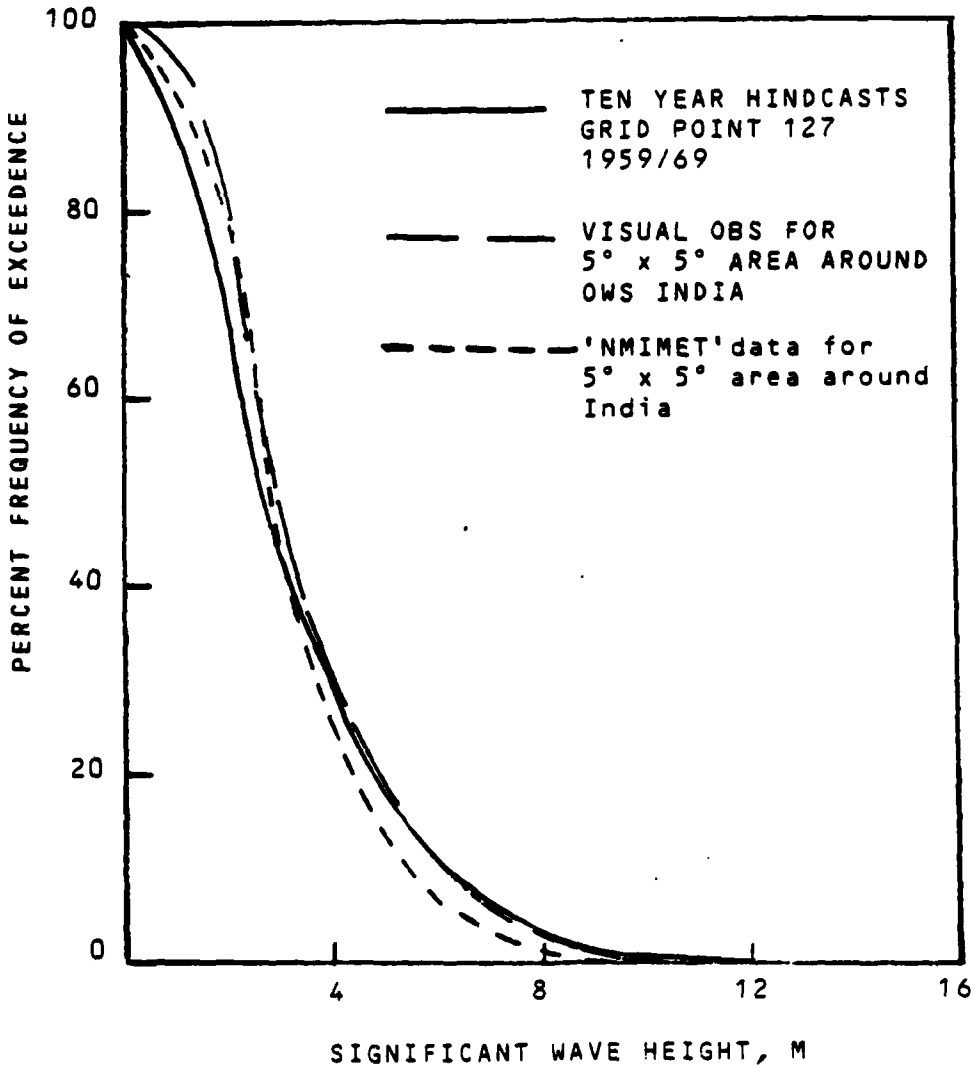

Figure 1 - Comparison of SOWN Hindcasts with Visual Data

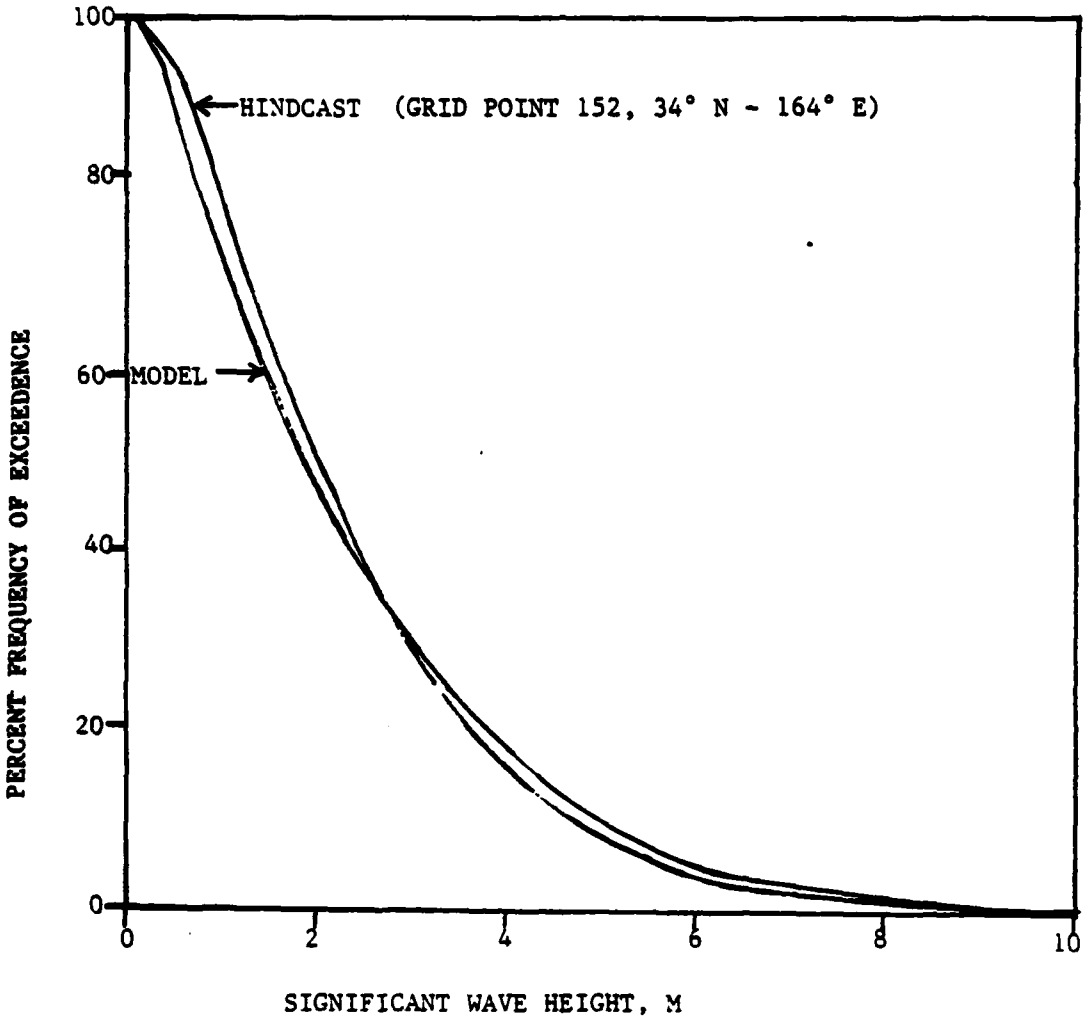

Figure 2 - Comparison of Wave Height Exceedances

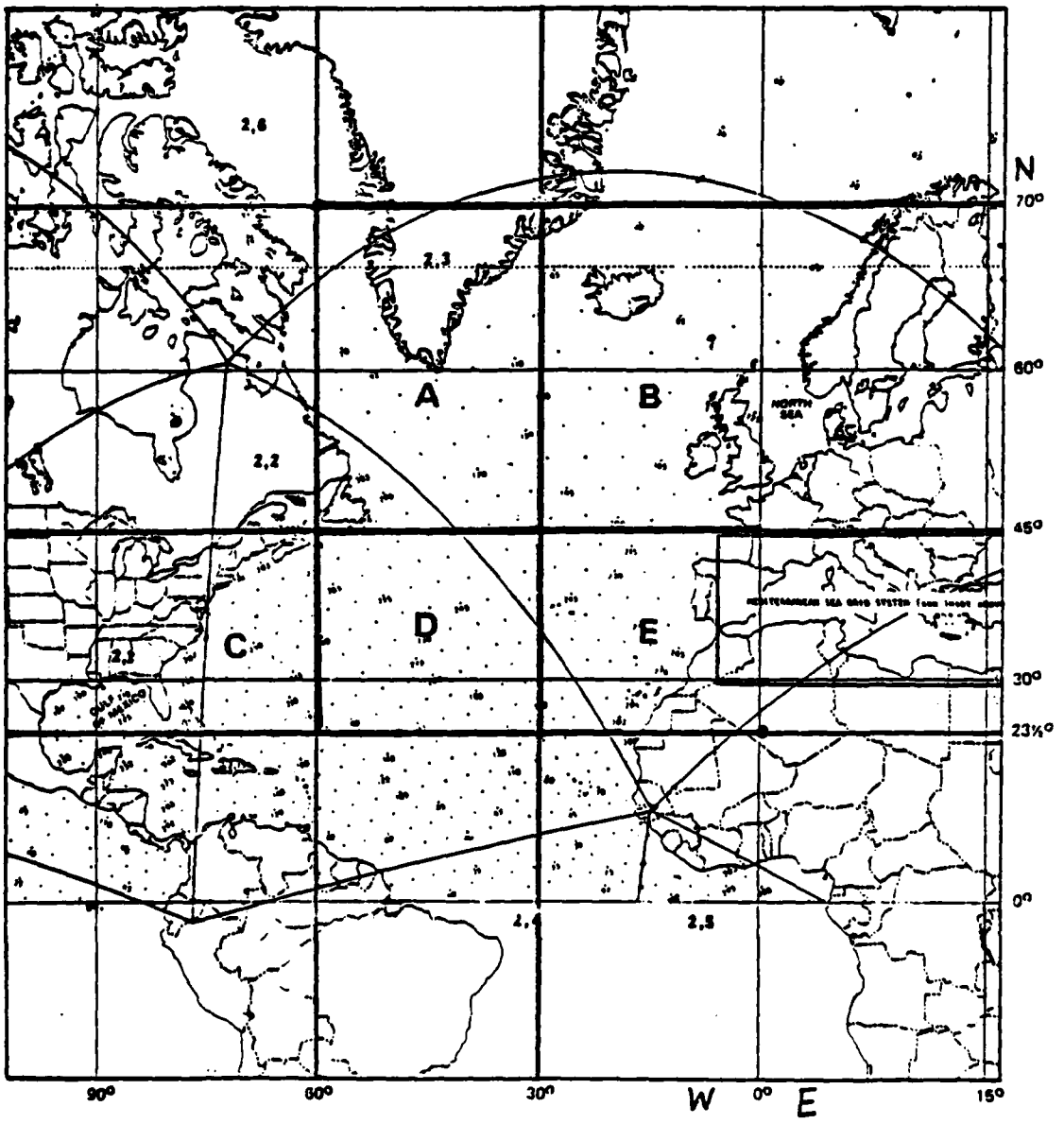

Figure 3 - Geographic Stratification of Sample

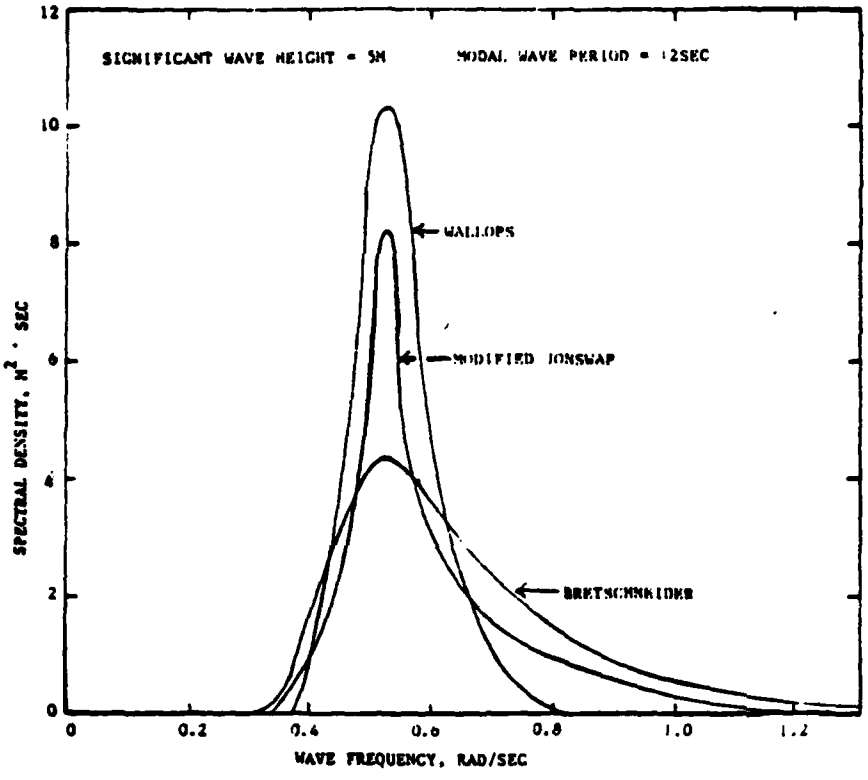

Figure 4 - Comparisons of the Bretschneider Spectrum with the Modified JONSWP Spectrum and the Wallops Spectrum

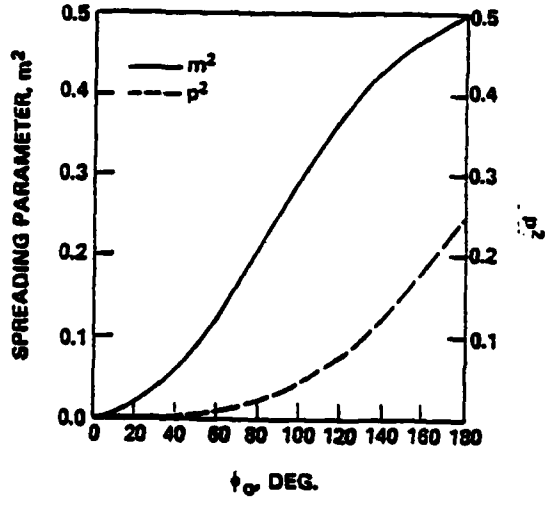

Figure 5 - Spreading Parameter m^2, and Parameter p^2 Versus Cosine Squared Spreading Angle, $\pm \phi_o$

AD-P003 827

A Transient Wave Generation Technique And Some Engineering Applications

by

Joseph O. Salsich, Bruce Johnson and Carvel Holton*
U. S. Naval Academy

ABSTRACT

Another method has been developed for generating transient waves ~~uti~~ using ~~lizing~~ the dispersion relationship of water waves. This technique consists of generating a drive signal which combines decreasing frequency with an exponentially increasing amplitude of specified form. The resulting wave energy which is focused at some point downstream of the wavemaker can result in some nonlinear, asymmetric, and/or breaking waves occurring repeatably at the same location in the tank. ~~The~~ location of the breaking wave relative to the predicted convergence point is discussed, and the derivation and computation of the drive signal as generated on a Tektronix 4051 microcomputer is described ~~herein~~.

Some specific examples of the model testing and research applications of this wave generation technique are also described. These include controlled extreme environment testing, capsizing of small vessels in breaking waves, ship responses to episodic waves, and a continuation of deck wetness experiments.

* now at United Technologies Research Center, East Hartford, Conn.

INTRODUCTION

The use of transient waves for towing tank tests was first implemented at DTNSRDC by Davis and Zarnick (1) in 1964, and further developed by Gersten and Johnson (2) in 1969. Takezawa and Hirayama (3) added computer generated drive signals to the wavemaker which improved the repeatability of the technique during the early 1970's. In 1974, Longuet-Higgins (4) proposed that the same decreasing frequency technique used to generate small amplitude transient waves be used to generate breaking waves in deep water. This concept was used by Kjeldsen (5) in 1978 and by Funke and Mansard (6) in 1979 to produce large plunging breakers in deep water wave flumes. Plunging breakers are generally not observed in randomly generated waves unless shoaling or opposing currents are present, or the channel is narrowed to concentrate the wave energy necessary to cause a plunging breaker (7).

Since 1978, the use of the computer to generate the wavemaker drive signals has resulted in many developments in deterministic transient wave techniques for extreme wave tests (8,9,10,11). Capsize tests on yacht models were performed by Kirkman and Salsich (12, 13) and Salsich and Zseleczky (14). Similar tests were performed on a Coast Guard utility boat by Salsich and Chatterton (15) and on a Coast Guard self-righting boat by Chatterton (16) at the U. S. Naval Academy. Tests were also conducted on life boat capsizing by Motora, Shimamota and Fujino (17) in Japan.

The characterization of extreme waves remains an unresolved issue (18). Kjeldsen and Myrhaug (19) have proposed four wave shape parameters which require a spatial domain description of the extreme or freak wave. At the present time, the Naval Academy is working on a time domain description of extreme wave steepness parameters so that this information can be extracted from wave staff recordings.

TRANSIENT WAVE CONVERGENCE

Following the development in Longuet - Higgins (4), convergence of a decreasing frequency wave train can be described for linear wave theory in deep water as follows:

The phase velocity of a simple harmonic small amplitude wave is expressed by

$$C = \frac{g}{\omega} \tanh \frac{2\pi h}{L} \qquad \text{where} \quad h = \text{water depth}$$

or $$C = \frac{g}{2\pi f} \quad \text{for deep water where } \tanh \frac{2\pi h}{L} \to 1$$

The group velocity in deep water is equal to one half the phase velocity and is assumed to be the speed at which the wave energy travels down the tank.

$$C_g = \frac{C}{2} = \frac{g}{4\pi f}$$

Thus the energy fronts of two waves of different frequency will converge if the higher frequency wave is started first, as illustrated in Figure 1.

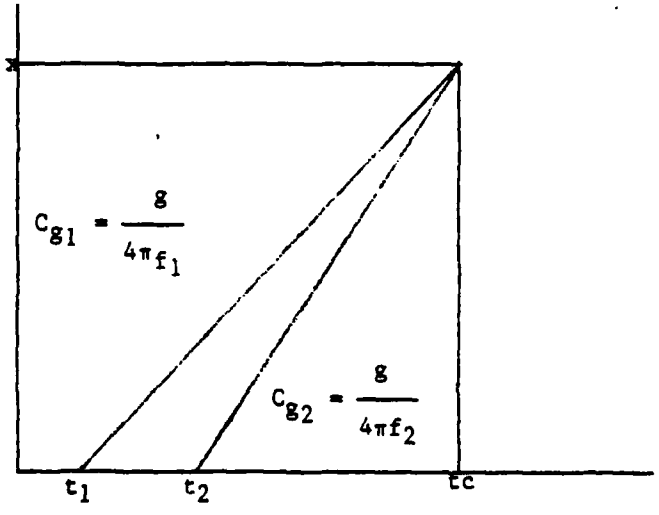

Figure 1. Convergence of two wave fronts

The time to convergence, t_c, can be expressed as

$$t_c - t_1 = \frac{x}{C_{g_1}} = \frac{4\pi f_1}{g} x \quad \text{for high frequency wave}$$

$$t_c - t_2 = \frac{x}{C_{g_2}} = \frac{4\pi f_2}{g} x \quad \text{for low frequency wave}$$

Eliminating t_c

$$t_2 - t_1 = \frac{4\pi x}{g} (f_1 - f_2)$$

or

$$\frac{f_2 - f_1}{t_2 - t_1} = \frac{-g}{4\pi x}$$

If the frequency is continuously varied

$$\frac{df}{dt} = \lim_{\Delta t \to 0} \frac{f_2 - f_1}{t_2 - t_1} = -\frac{g}{4\pi x} \qquad (1)$$

so that the convergence point x is defined by the sweep rate.

COMPUTATION OF WAVEMAKER DRIVE SIGNAL

The wavemaker drive signal was generated using a Basic computer program written for a Tektronix 4051 desktop computer with 32K memory. The 4051 is coupled to a Trans Era Model 620-DAC to convert the digital time series to an analog signal compatible with the wavemaker controller. The drive signal was not compensated for the wavemaker transfer function directly. Instead, the amplitude of the drive signal could be adjusted by exponential and polynomial multipliers to obtain the desired wave train by trial and error methods.

The linear frequency scan rate is set by incrementing equation (1) to give a desired minimum number of points per cycle within the total available points in the drive sequence (which is 1400 in this memory configuration). The drive signal amplitude which corresponds to each time increment is divided into three segments (delay; scan; hold and delay). During the initial delay time, the wavemaker runs at constant frequency, F1, to let the servo system gain reach the set value. The command delay time is modified by the program to allow the frequency scan to begin on the crest of a wave. During the scan time portion of the drive signal, the amplitude of the waveform is calculated from

$$A(I) = V \times \left[\frac{F2}{F(I)}\right]^{P} \times e^{E(F2 - F(I))/F2} \times \sin(2\pi F(I) T5) \qquad (2)$$

where V is the maximum output voltage of the D/A converter (9.995 volts)

F(I) is the current value of the frequency

F2 is the final value of the frequency scan

P is the polynomial multiplier

E is the exponential multiplier

T5 is the "phase time" parameter

The latter parameter, T5, represents a pseudo time increment which is initialized to zero during the delay time sequence and during the hold time sequence. During the scan time sequence when time and frequency are simultaneously increased linearly, a point is reached where a phase discontinuity is generated because

$$(2\pi F(I)\ T5(I)) - (2\pi F(I-1)\ T5(I-1)) \geq 180°$$

To remove this problem one must insure that phase continuity is maintained by

$$2\pi F(I)\ (T5(I) - \Delta T) = 2\pi F(I-1)\ T5(I-1)$$

or

$$T5(I) = \frac{F(I-1)}{F(I)} \times T5(I-1) + \Delta T \qquad (3)$$

where ΔT is the time increment

During the hold and decay time, the amplitude of the drive signal is held constant at the value calculated for F2 for a percentage of the time. Equation (2) is multiplied by an exponentially decaying function during the decay time portion of the sequence to return the waveboard smoothly to its rest position.

The entire sequence is displayed during computation on the Tektronix 4051 as illustrated in Figure2. The height of the actual wave record is set by varying the span settings on the wavemaker controller. The effect of varying the span setting is discussed in the next section.

The program just discussed is available on Tektronix tape format from the Hydromechanics Lab at the Naval Academy to anyone who has a compatible waveboard drive system.

LOCATION OF BREAKING WAVE

In his most recent paper, Kjeldsen (11) mentions that increasing the gain on the wavemaker command signal shifted the position of the plunging breaker downstream by about 10 percent, indicating non-linear behavior in the dispersion velocities. Most of the references concerning transient wave techniques do not discuss the location of breaking waves at positions other than the convergence point. It has been observed using the program just described, however, that the most severe breaking waves occur when the wavemaker gain is increased sufficiently to cause the wave to break between 40 and 80 percent of the distance to the convergence point. This is because plunging breakers are produced anytime the rate of change of the wave front steepness exceeds a critical value. Figure 3 represents an attempt to illustrate the observed strength of breaking waves as a function of relative wavemaker drive signal gain and the position of the breaking wave a percent of the distance to the convergence point defined by equation 1.

The tests summarized in Figure 3 were performed in the 120 foot (36.6 meter) tank at the Naval Academy. The convergence point for the drive signal in the top figure was set at 60 feet (18.3 meters) and the best breaking wave occured at 71 percent of that distance. The severity of the breaking wave is approximated by a 1 to 4 scale of intensity. At low wavemaker gain, a weak (spilling) breaker is produced near the convergence point. As the gain is increased, the location of the initial breaker moves upstream and increases in intensity. The break point location jumps in finite increments and does not vary continuosly. As can be seen from the figure, the location of a specific breaker may move downstream while additional breakers commence upstream of the orignal break point. A similar set of drive signal parameters but with the

convergence point set at 72 feet (22 meters) produced the breakers shown in the middle figure.

Note that the most severe plunging breakers were again located at about 71 percent of the convergence point. On the other hand, varying the drive signal so that the convergence point was located well beyond the end of the tank produced severe plunging breakers at only 41 percent of the convergence distance, although much higher wavemaker gain was used since the sweep rate was lower for the longer convergence distance.

Although the location of the best breaker is not presently predictable before a given signal is attempted, the location of the breaker can be adjusted to a particular location in the tank (centered in a window, for example) by trial and error methods. This location can be repeated time after time without variation by setting up the wavemaker gains and using the drive signal over and over again. This method is very appropriate for capsizing tests since one of the significant parameters is the location of the vessel relative to the position of the breaking wave.

APPLICATIONS

A wave generation technique such as this has many useful applications. Numerous experiments to date have been conducted in the previously mentioned basic research of capsizing of small vessels in breaking waves (12, 13, 14, 15). Other experiments with as yet unpublished results have been conducted in the areas of wave loadings on cylinders and ship responses in head seas. Future studies are planned to examine deck wetness in extreme conditions, to measure particle velocities in assymetric waves, to investigate mooring loads on a semi-submersible in survival conditions, and to attempt to define some time domain wave steepness parameters.

CAPSIZING STUDIES

The original impetus for sailing yacht capsizing research was the 1979 Fastnet disaster. A joint SNAME/USYRU committee was formed to focus on safety from capsizing and some of this committee's activities were reported in Reference 12.

The experimental research program that has been conducted at the Naval Academy was designed to aid in:

- understanding the basic physics of the capsizing process in breaking waves by observation under repeatable laboratory conditions
- creating a data bank of capsize trajectory and wave profile and flow field time histories for eventual comparison with computational schemes, and
- understanding the direct and independent effects of parametric variations.

The basic technique for these experiments was to attempt to simulate a worst case condition, lying still in the water beam to a breaking wave. The models used for these experiments were of constant cross section

(two-dimensional) for simplicity. These models were fitted with a horizontal and vertical movable weight mechanism to allow for variations of the VCG and the inertial properties in roll.

The preliminary conclusions drawn from these tests were that:

(1) The position of the model relative to the breaking wave is crucial. There is a definite critical region of capsize within a breaking wave.

(2) There were two distinct types of capsizes observed within this critical region of capsize. In the upstream portion of this region the model would ride up the face of the curling wave and absorb the impact of the crest while simultaneously losing waterplane stability. The second type of capsize occurred in the downstream portion of the critical region. At this point the wave had curled and fallen onto the face as a classic plunging breaker. The result of this mass of falling water was the production a second, explosive type wave which catapulted the model into a violent capsize.

The parametric study consisted of variations of the following characteristics:

(1) roll radius of gyration (k_{xx}) and moment of inertia (I_{xx})

(2) vertical center of gravity

(3) keel area and aspect ratio

(4) beam

Inertial variations seemed to exert the largest influence on capsize resistance. To establish a baseline roll gyradius for a representative sailing yacht, a series of 8 ocean racers were oscillated in still water and the resulting roll periods were measured. From these measurements it was deduced that the roll gyradii of these yachts in water varied from 0.62B to 0.78B. The baseline condition for the models were then chosen as a roll gyradius in air of 0.63B. This was measured by suspending the models horizontally from its ends and treating it as compound pendulum.

Figure 4 is a sample plot of some of the results obtained from the gyradius variation experiments. Each small pie chart on the plot represents the percentage of capsizes for twenty events. Since it had been seen earlier that location was a critical factor, the model was placed in ten different initial locations, twice at each spot. For a given gyradius condition, three transient waves of increasing height were generated and the model's responses noted. Then the gyradius was changed and the same waves repeated. Thus, this plot is a summary of 180 separate events. The percentage figures relate to the percentage of capsize during this testing sequence and have no bearing on probability of capsize in a seaway.

Figure 5 is a summary of the variation in the location of the vertical center of gravity experiments. The baseline location of the VCG was established at the waterline and then varied above and below the waterline. The percentage figures imply the same thing as previously explained for the inertial variations. The interesting thing to note is that as the VCG is raised, capsize resistance to a single breaking wave then increases. If one assumes that the axis of roll is somewhere below the waterline, then as the VCG is raised, the axis of roll in air (through the VCG) is moving further from the axis of roll in water. This could be a possible explanation of the trends seen in Figure 5.

Finally, Figure 6 illustrates the results of the experiments of changes in roll damping due to keel area. Clearly, the effects are not large. The changes in keel aspect ratio showed negligible difference. At this time there are no results available from the beam variation experiments.

It is hoped that these experiments will continue in the form of a complete two dimensional model series. Plans for a series of three dimensional models are being formulated as well.

OTHER STUDIES

Some experiments measuring a ship model's responses to extremely steep seas (head seas) have been conducted. A transient wave of a more persistent nature (narrower frequency content) was generated and the model's responses measured. The analysis of the data is not complete and the results should be published in the near future. As a continuation of the deck wetness experiments described by Lloyd (20), the same model with the variable bow forms will be studied in transient waves of varying steepness. Particle velocity measurements in these waves are also planned as well as a study of a semi-submersible's responses in a survival condition.

ACKNOWLEDGEMENTS

The authors would like to express their gratitude to the entire staff of the Hydromechanics Laboratory. A special note of thanks is due to Mr. Kevin Miller-Ihli for his assistance in completing the experiments described in this paper. Without his contributions this report could not have been completed.

REFERENCES

1. DAVIS, M, C., AND ZARNICK, E.C., "Testing Ship Models in Transient Waves", Proc. of the 5th Symposium on Naval Hydrodynamics, Bergen, Norway, September, 1964.

2. GERSTEN, A., AND JOHNSON,R.J., "Notes on Ship Model Testing in Transient Waves", DTNSRDC Report No. 2960, April 1969.

3. TAKEZAWA, S., AND HIRAYAMA, T., "Advanced Experimental Techniques for Testing Ship Models in Transient Water Waves: Part II, The Controlled Transient Water Waves for Using in Ship Motion Tests", Proc. of the 11th Symp. on Naval Hydrodynamics, London, 1976.

4. LONGUET-HIGGINS, M, S., "Breaking Waves in Deep or Shallow Water", Proc. of the 10th Symp. on Naval Hydrodynamics, MIT, Boston, Mass., June 1974.

5. KJELDSEN, S. P., AND MYRHAUG, D., "Breaking Waves in Deep Water and Resulting Wave Forces", Paper No. 3646, Proc. of the 11th OTC, Houston, Texas, 1979.

6. FUNKE, E. R., AND MANSARD, E. P. D., "SPLSH, A Program for the Synthesis of Episodic Waves", Hydraulics Laboratory Report LTR-HY-65, National Research Council of Canada, April 1979.

7. DAHLE, E. A., AND KJAERLAND, O., "The Capsizing of M/S Helland-Hansen", The Naval Architect, RINA, March 1980, No. 2.

8. TAKEZAWA, S., "New Wave Generation Techinques for Seakeeping Tests", Proc. of the 16th ITTC, Leningrad, 1981.

9. HIRAYAMA, T., AND TAKEZAWA, S., "Transient and Irregular Experiments for Predicting the Large Rolling in Beam Irregular Waves", Proc. of the Second International Conference on Stability of Ships and Ocean Vehicles, Tokyo, Japan, October 1982.

10. MANSARD, E. P. D., FUNKE, E.R., AND BARTHEL, "A New Approach to Transient Wave Generation", Proc. of the 18th International Conf. on Coastal Engineering, Cape Town, South Africa, November, 1982.

11. KJELDSEN, S. P., "2 - and 3 dimensional Deterministic Freak Waves", Proc. of the 18th International Conf. on Coastal Engineering, Cape Town, South Africa, November 1982.

12. KIRKMAN, K. L., NAGLE, T. J., AND SALSICH, J. O., "Sailing Yacht Capsizing", Proc. of the Chesapeake Sailing Yacht Symposium, Annapolis, Maryland, January 1983.

13. KIRKMAN, K. L., and SALSICH, J. O., "SNAME/USYRU Safety from Capsize Study - A Progress Report," Proc. of the Ancient Interface XII, San Francisco, CA, October, 1982.

14. SALSICH, J. O., and ZSELECZKY, J. J., "Experimental Studies of Capsizing in Breaking WAves," Proc. of the Ancient Interface XIII, San Diego, CA, October 1983.

15. SALSICH, J., AND CHATTERTON, H.A., "Investigation of Capsizing in Breaking Waves of the U. S. Coast Guard 41 Foot Utility Boat" Report EW-5-82, U. S. Naval Academy, March 1982

16. CHATTERTON, H. A. "Investigation of Capsizing in Breaking Waves of the U. S. Coast Guard 44 foot Motor Life Boat", Report EW-18-83, U. S. Naval Academy, May 1983.

17. MOTORA, S., SHIMAMOTO, S., AND FUJINO, M., "Capsizing Experiment on a Totally Enclosed Life Boat:, Proc. of the Second International Conf. on Stability of Ships and Ocean Vehicles, Tokyo, Japan, October, 1982.

18. JOHNSON, B., "A State of the Art Review of Irregular Wave Generation and Analysis". Proceedings of the 16th ITTC, Leningrad, USSR, September, 1981.

19. KJELDSEN, S. P., AND MYRHAUG, D., "Wave-Wave Interactions and Resulting Extreme Waves and Breaking Waves", Proc. 17th Conf. on Coastal Engineering, Sydney, Australia, 1980.

20. LLOYD, A., "Deck Wetness Experiments," Proceedings of the 20th ATTC, Hoboken, N.J., August 1983.

FIGURE 2. EXAMPLE WAVEMAKER DRIVE SIGNAL

```
LOG FILE012  120 WAVEMAKER PARAMETER SET 017      12/14/81
INITIAL FREQ., HZ = 1.1    FINAL FREQ., HZ = 0.7
BREAK POINT, FEET = 104  SPAN SETTINGS = 42/63
DELAY TIME, SEC. = 2.84545454545  HOLD TIME, SEC. = 6
SCAN TIME, SEC = 16.2479336594 HOLD TIME DECAY, % = 70
POLYNOMIAL EXPONENT=5 EXPONENTIAL MULTIPLIER=3
DECAY EXPONENT = 2  POINTS PER CYCLE = 50
PEAK VOLTAGE OF FINAL FREQ SINEWAVE, VOLTS = 9.995
PLOT? Y OR N - Y
+9.995 VOLTS
```

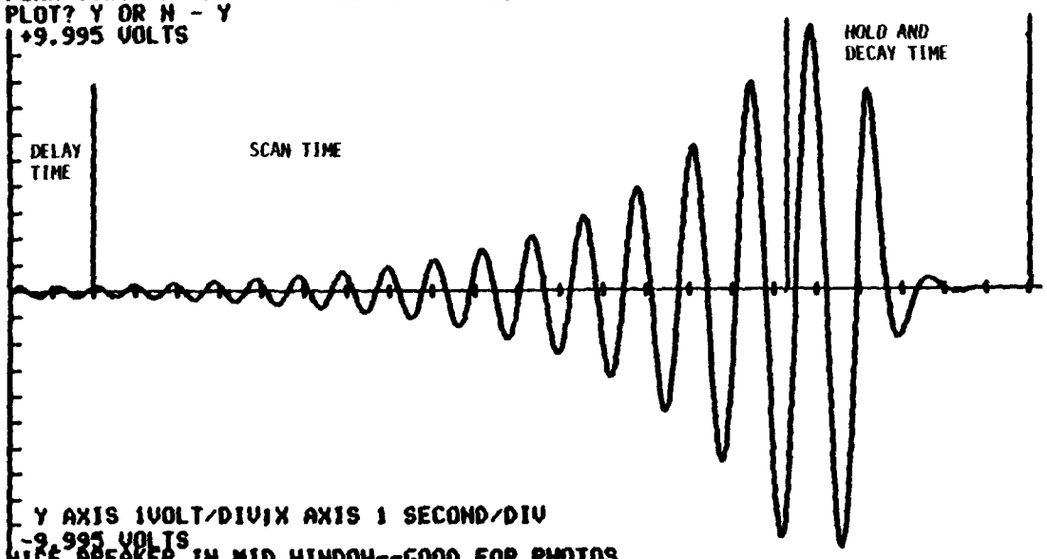


```
 Y AXIS 1VOLT/DIV;X AXIS 1 SECOND/DIV
-9.995 VOLTS
NICE BREAKER IN MID WINDOW--GOOD FOR PHOTOS
                        $$$$$ READY $$$$$
COMMAND?- BYE, LOG, POWER, RES, RUN, SCAN, SET, STOP, VOLTS:
```

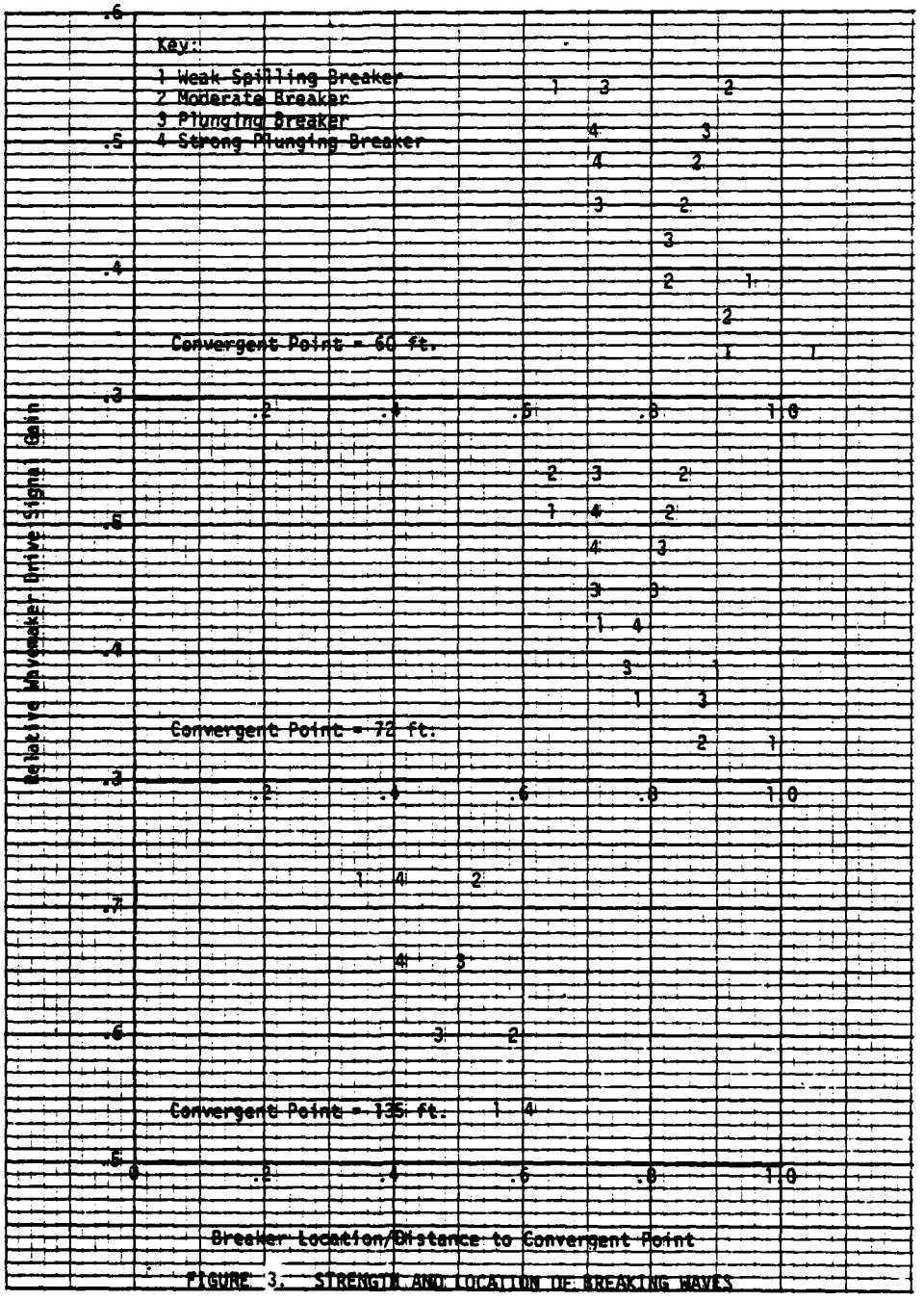

FIGURE 3. STRENGTH AND LOCATION OF BREAKING WAVES

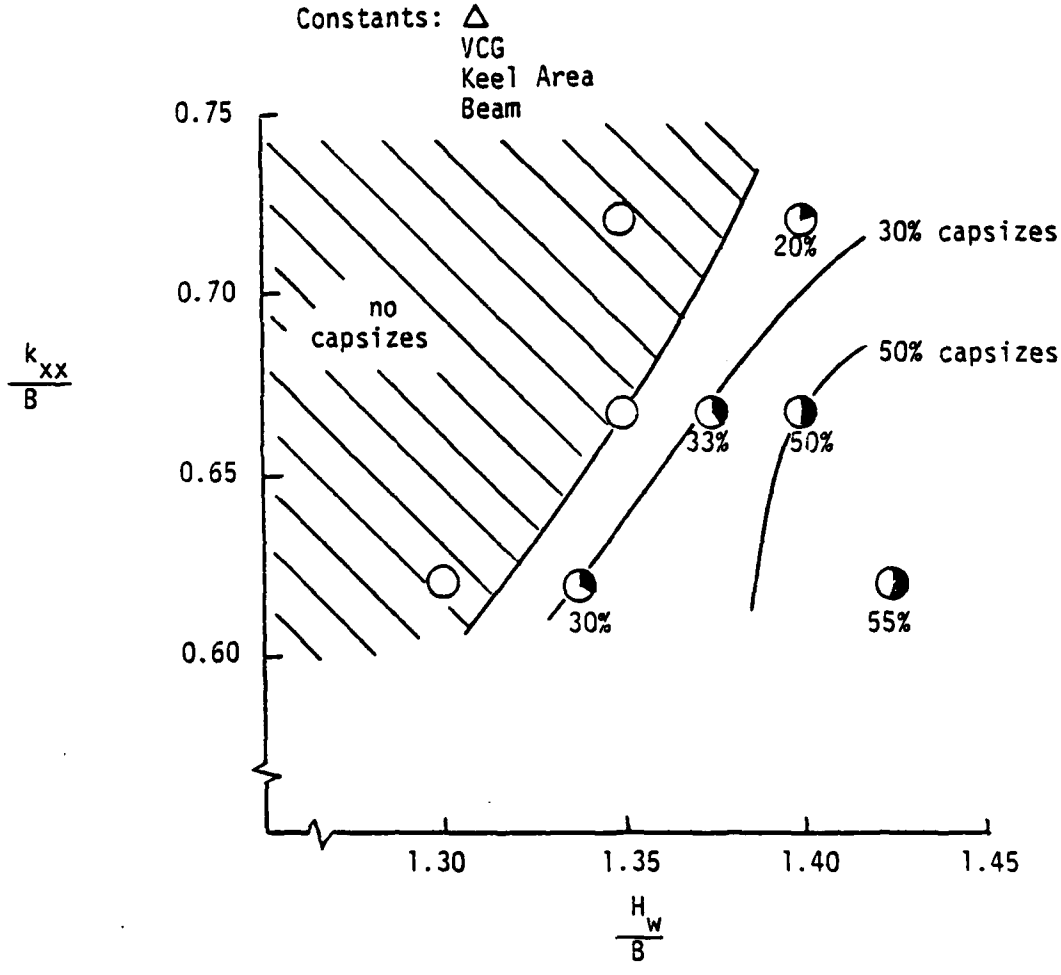

Fig 4. The Effect of Roll Gyradius Variation on Capsize Resistance

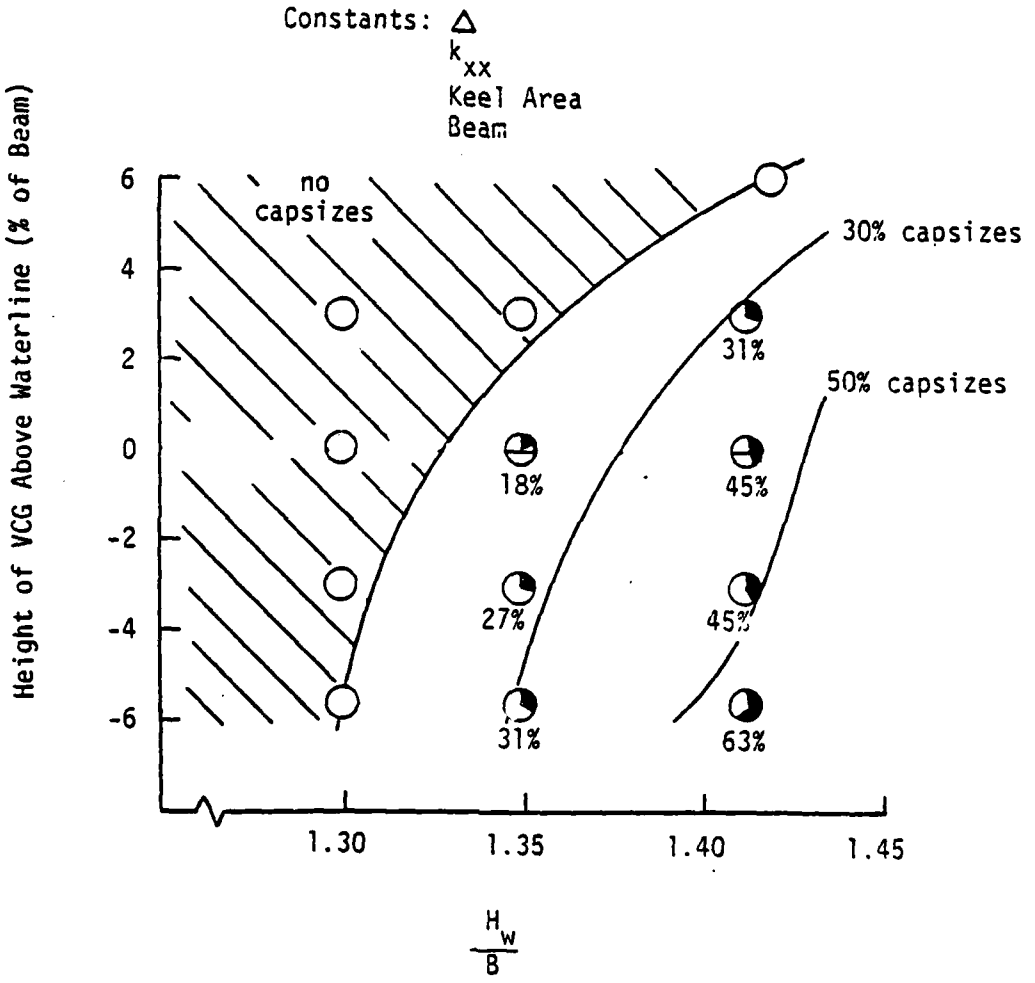

Fig 5. The Effect of VCG Variation on Capsize Resistance

AD-A144 227 PROCEEDINGS OF THE GENERAL MEETING OF THE AMERICAN TOWING TANK CONFERENCE..(U) STEVENS INST OF TECH HOBOKEN NJ DAVIDSON LAB D SAVITSKY ET AL. AUG 83 5/8

UNCLASSIFIED SIT-DL-TR-13029-VOL-2 N00167-83-M-4062 F/G 20/4 NL

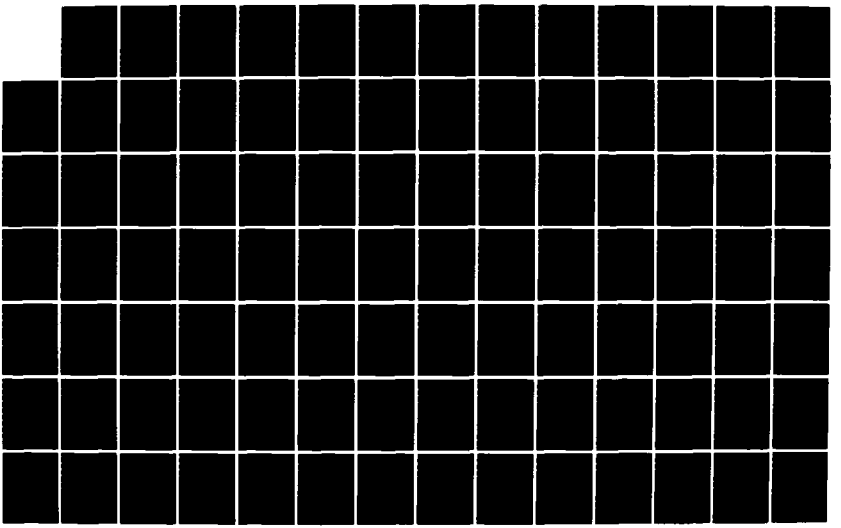

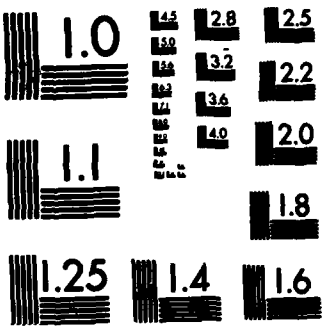

MICROCOPY RESOLUTION TEST CHART
NATIONAL BUREAU OF STANDARDS-1963-A

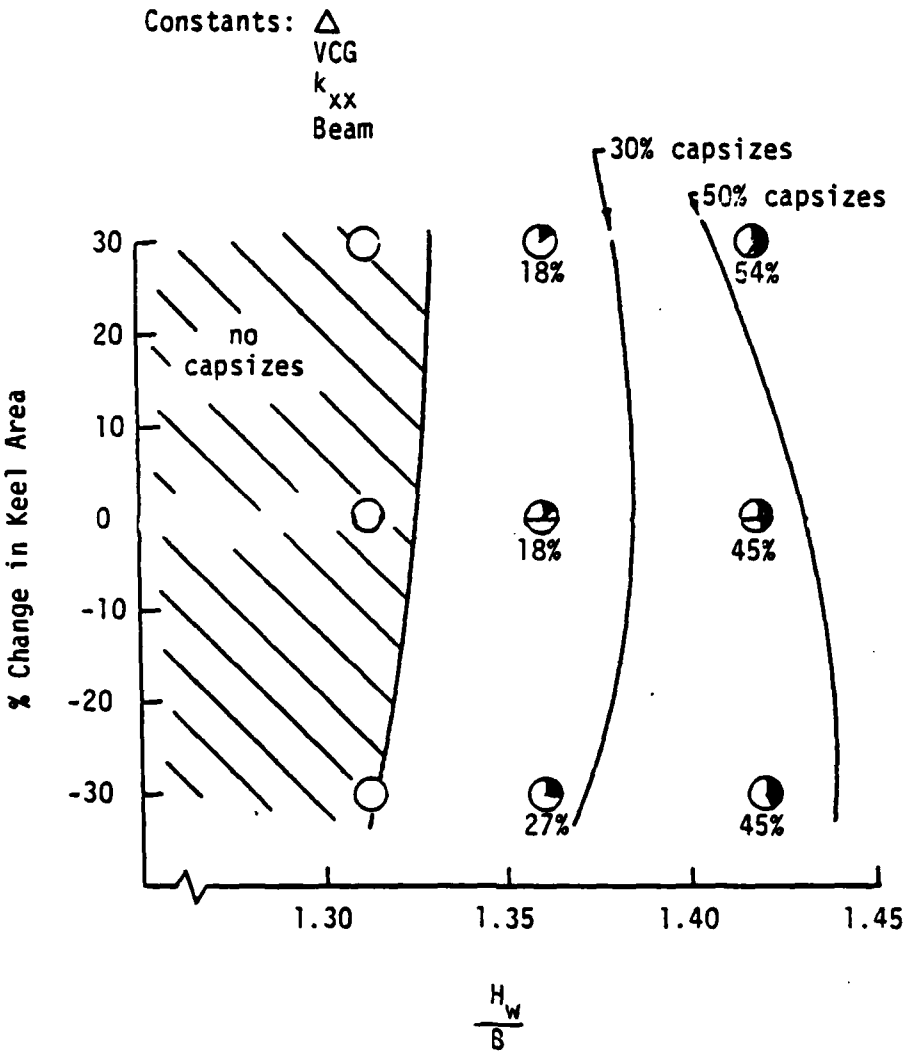

Fig 6. The Effect of Keel Area Variation on Capsize Resistance

AD-P003 828

DECK WETNESS EXPERIMENTS

by

ARJM Lloyd Ph.D. BSC FRINA
Admiralty Marine Technology Establishment
Haslar Gosport Hants UK

Currently NAVSEA Visiting Professor
US Naval Academy, Annapolis

(Seakeeping)

20th AMERICAN TOWING TANK CONFERENCE
Stevens Institute of Technology
Hoboken, New Jersey
August 1983

Summary

The history of model experiments to quantity the effect of above water bow form on the deck wetness characteristics of frigates in head seas is reviewed and the results obtained are reported. Suitable experiment techniques are discussed and recommended and plans for further experiments are described.

1. Introduction

Deck wetness has long been recognized as one of the factors which determine the seakindliness of a ship. In extreme conditions the frequent shipping of water may lead to the eventual capsize of the vessel: in more moderate conditions the loss of the vessel is unlikely but frequent deck wetness may still cause damage to exposed fittings and deck cargo and make the upper deck untenable for the crew. In a warship this may seriously reduce the ship's operational effectiveness by limiting the crew's ability to man and reload weapons and to complete tasks such as replenishment at sea.

The frequency and severity of deck wetness can, of course, be reduced by avoiding high speeds and head seas: but the resulting limitations on mobility can also be regarded as a reduction in operational effectiveness. In short the wet ship is likely to be a much less successful weapons platform than the dry ship.

The problem was graphically described by Kehoe in Reference 1 in which attention was drawn to the importance of adequate freeboard and appropriate above water bow design.

The interest in operational effectiveness and warship mobility has led to studies aimed at developing criteria for acceptable deck wetness frequency and severity. The author proposed a tentative criterion for wetness frequency in Reference 2. This was based on the reported limiting performance of a merchant ship (Reference 3) and a destroyer (Reference 4) in head seas. The criterion

was derived by using strip theory to calculate the average frequency and rms value of the relative bow motion of each ship in the reported sea conditions. The Rayleigh distribution formula was then used to calculate the average interval between deck wettings, defined as the relative motion exceeding the freeboard at the forward perpendicular. No allowance was made for the ship's bow wave or for "swell up", the local amplification of the incident wave at the bow caused by the presence of the ships' hull.

Based on these calculations a deck wetness interval criterion of 100 seconds was proposed. Thus the "average" captain would be prepared to tolerate one deck wetting every 100 seconds or 36 wettings per hour. No proposal for a wetness severity criterion was made.

This could only be regarded as a tentative result since it was recognized that the tolerable frequency of deck wetness would depend on the severity, the delicacy of the exposed fittings or deck cargo and on the immediate mission of the ship.

More detailed information was published in Reference 5 which described full scale trials in which two frigates were run side by side at high speed in rough weather. One of the ships was fitted with a video camera to monitor deck wetness: the highest deck wetness frequency exerienced in near limiting conditions was about 180 wettings per hour. The results were compared with predictions based on strip theory estimates of the relative bow motion at the forward perpendicular: it was immediately obvious that the theory overestimated the interval between wettings by a factor of about 2.0. Schmitke, in a contribution to Reference 5, reported results of calculations which included allowances for swell up and bow wave and these were in much closer agreement with the trial results.

The only above water characteristic of the bow which is taken into account in these calculations is the freeboard: the effects of flare, knuckle and other features of the bow above the waterline cannot, at present, be quantified.

Faced with this theoretical wilderness the designer must resort to experiment to obtain information on the effects of bow shape on deck wetness. To the author's knowledge the only well documented published work in this area is by Newton (Reference 6). He reported experiments with a model destroyer in regular head waves. The model was tested with five different above water bow designs involving:

a) a parent

b) two freeboard increments obtained by adding bulwarks

c) two forms of knuckle added to the basic parent bow.

All five bows had the same deck plan.

Wetness was visually ascribed to one of three categories: - "dry"; "wet"; or "very wet". It was found, as expected, that the additional freeboard and the two knuckles reduced the severity of the wetness and a tentative formula relating the geometric parameters defining the knuckle to an equivalent additional freeboard was derived.

In 1977 further experiments were conducted at AMTE Haslar. Since that time several more experiment series have been completed and appropriate techniques of measurement and experiment method have been developed. The author is currently engaged in similar experimental work at the U. S. Naval Academy.

This paper will describe these experiments and present some of the results obtained.

2. AMTE Experiments: First Series

The AMTE experiments were all run with a 1/45 scale model of a frigate in irregular head waves. Model length was 2.44 meters. The model was made in glass reinforced plastic and supplied with a total of nine alternative bow

forms. The underwater form and the above water form abaft station 2 (0.1 L from the forward perpendicular) was the same for all the experiments (see Figure 1).

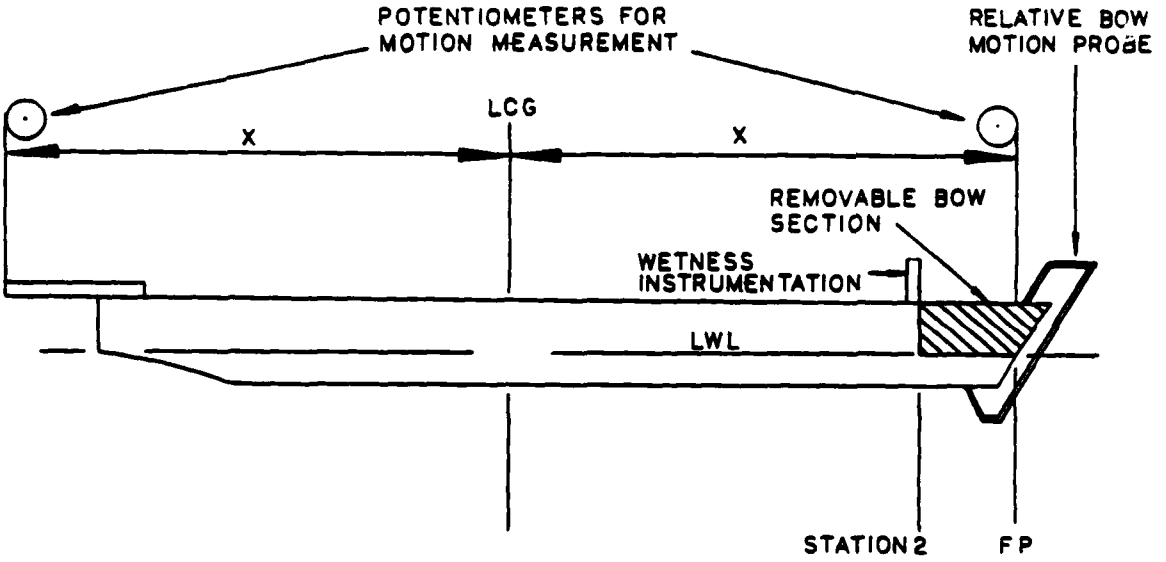

Figure 1. AMTE Deck Wetness Experiments

Each bow was thus designed to fare smoothly into the rest of the hull at station 2 and at the nominal load waterline. This was achieved by designing the bows using polynomial curves with suitable boundary conditions to describe the stem profile, the section shape at the forward perpendicular and the deck plan.

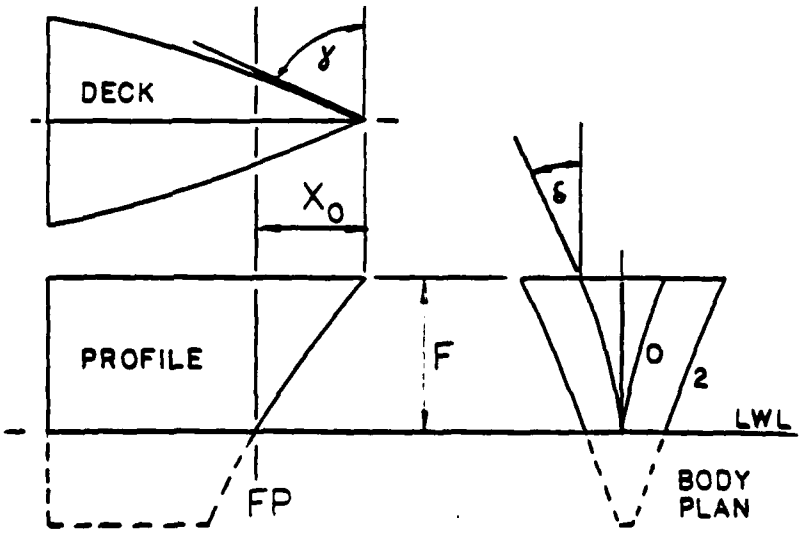

Figure 2. Bow Form Parameters

Four bow form parameters were varied:

a) freeboard F

b) overhang (or rake) X_0

c) stem sharpress (at deck) γ

d) Flare Angle at FP (at deck) δ

TABLE 1

Bow Form Parameters

	1st Series		2nd Series		3rd Series	
Model No.	$\frac{F}{L}$	$\frac{X_0}{L}$	$\frac{F}{L}$	$\frac{X_0}{L}$	γ degrees	δ degrees
1 (parent)	.07	.05	.06	.046	30	30
2	.06		.05			
3	.08		.07			
4		.03		.026		
5		.07		.066		
6					0	
7					60	
8						45
9						15

(Blanks indicate same values as parent).

These parameters are defined in Figure 2 and provided further boundary conditions to completely define the polynomial curves. Table 1 shows the form para-

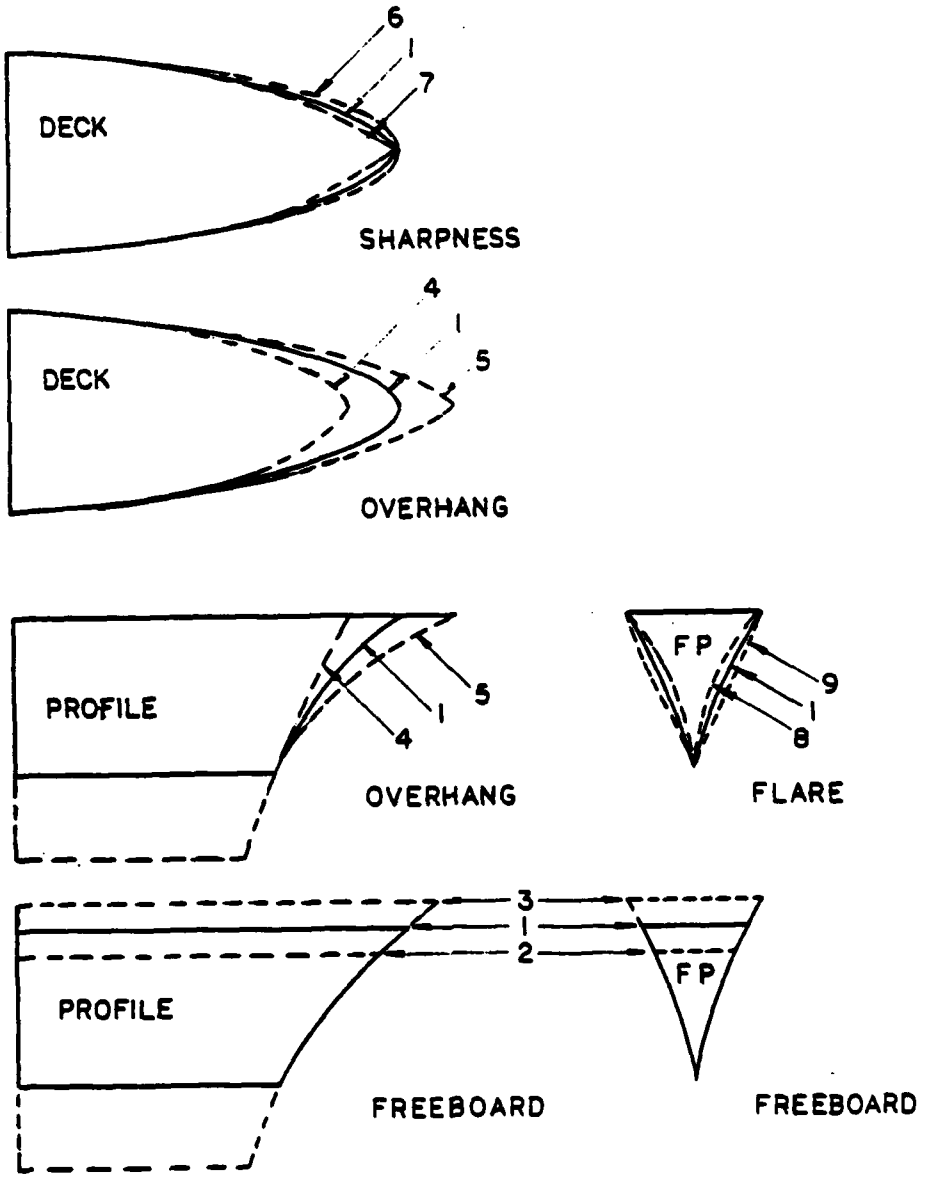

Figure 3. AMTE Bow Form Series

meters chosen and Figure 3 shows selected views of the resulting bow forms. It should be noted that the sharpness and overhang variations produced small changes in the deck width at the forward perpedicular: nevertheless the flare angle, as defined in Figure 2, was maintained at 30° for these bows. The freeboard variations were achieved by simply producing or truncating the calcu-

lated section shapes and stem profile for the parent form. Thus the freeboard variations inevitably involved small variation in flare and sharpness angles, measured at the deck and somewhat larger variations in overhang.

The bows were all made in wood and were ballasted to identical weights.

Wetness was monitored and quantified by recording the impacts experienced by an aluminum plate mounted on a vertical strain gauged post at Station 2 (see Figure 4). This arrangement enabled wettings to be objectively counted and some estimate of impact pressures to be made.

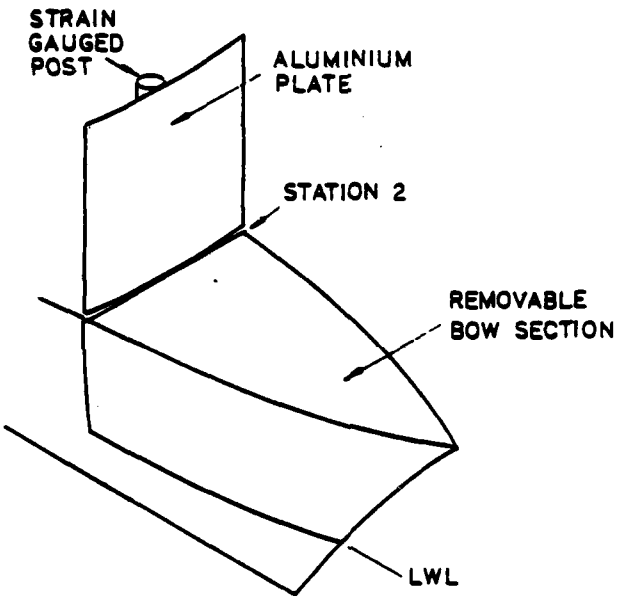

Figure 4. AMTE Experiments: 1st Series. Deck Wetness Instrumentation

Model motions were not recorded in these experiments.

The model was run at speeds equivalent to 15, 20, and 25 knots in a Pierson-Moskowitz head sea with significant wave height equivalent to 6.0 metres.

Each bow/speed combination was run three times using different wave time histories (but having the same spectral characteristics). The total run times for the three speeds were 20, 15 and 12 minutes respectively (in ship scale).

Figure 5 shows the results obtained for the freeboard variations (Bows 1, 2, and 3). As expected the wetness frequency decreases as freeboard increases and as speed is reduced. However the wetness frequency was generally much higher than was found to be tolerable in the subsequent full scale trials and it is now clear that these model tests were done in wave conditions which were unrealistically severe for the speeds chosen. With hindsight it is therefore

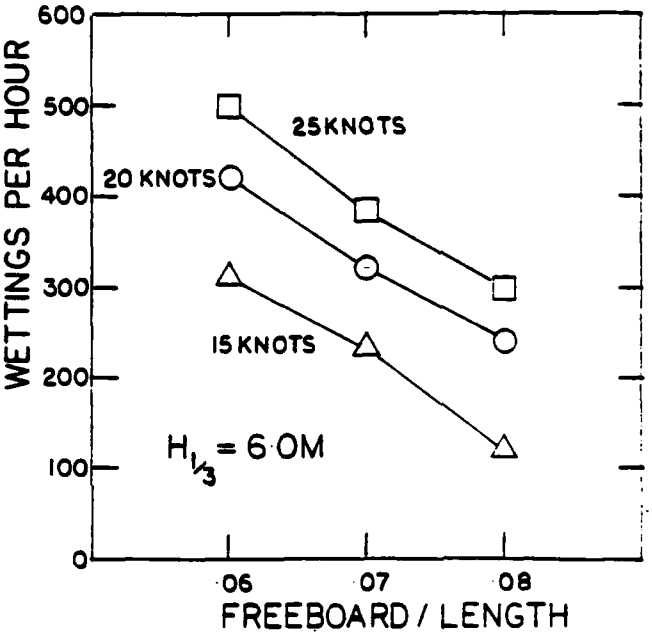

Figure 5. AMTE Experiments: 1st Series. Effect of Freeboard and Speed on Wetness Frequency

perhaps not surprising that the experiments failed to reveal any consistent trends of wetness frequency or severity with bow form (with the exception of the freeboard variations already discussed). Presumably the conditions were so severe that the comparatively minor variations in bow form could not affect wetness to any marked degree.

3. AMTE Experiments: Second Series

A second series of experiments was conducted at AMTE in 1980. The same model was used again with the same bow form variations but this time the bows

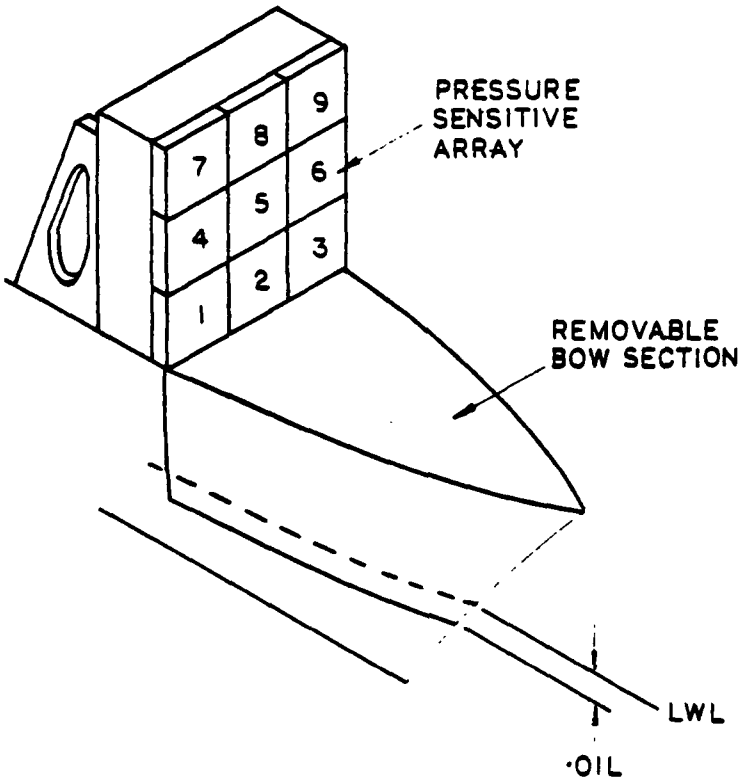

Figure 6. AMTE Experiments: 2nd Series
Deck Wetness Instrumentation

were manufactured in glass reinforced plastic. Figure 6 shows the improved deck wetness monitoring instrumentation used: an array of 9 square plates each mounted on a Sensotec load cell (+0.5 lbs, "D" series) enabled some indication of the distribution of impact pressures to obtained.

The model was also fitted with ship motion instrumentation as shown in Figure 1. The absolute motion of the forward perpendicular and a point equidistant abaft the LCG were recorded, together with the relative motion just forward of the forward perpendicular. In addition the incident wave was recorded alongside the forward perpendicular, about 1 metre away from the model.

The additional weight forward made it impossible to attain a realistic longitudinal radius of gyration at the original model displacement. The displacement was therefore increased to allow more freedom for adjusting the model's internal ballast to obtain a realistic pitch inertia: this resulted in a general reduction in freeboard and a marginal reduction in overhang (see Figure 6 and Table 1).

The model was again run in Pierson-Moskowitz head seas but the signifcant wave height was reduced to 4.24 metres (for ship) to reduce the wetness frequency. In order to keep the actual number of wettings at a reasonable level

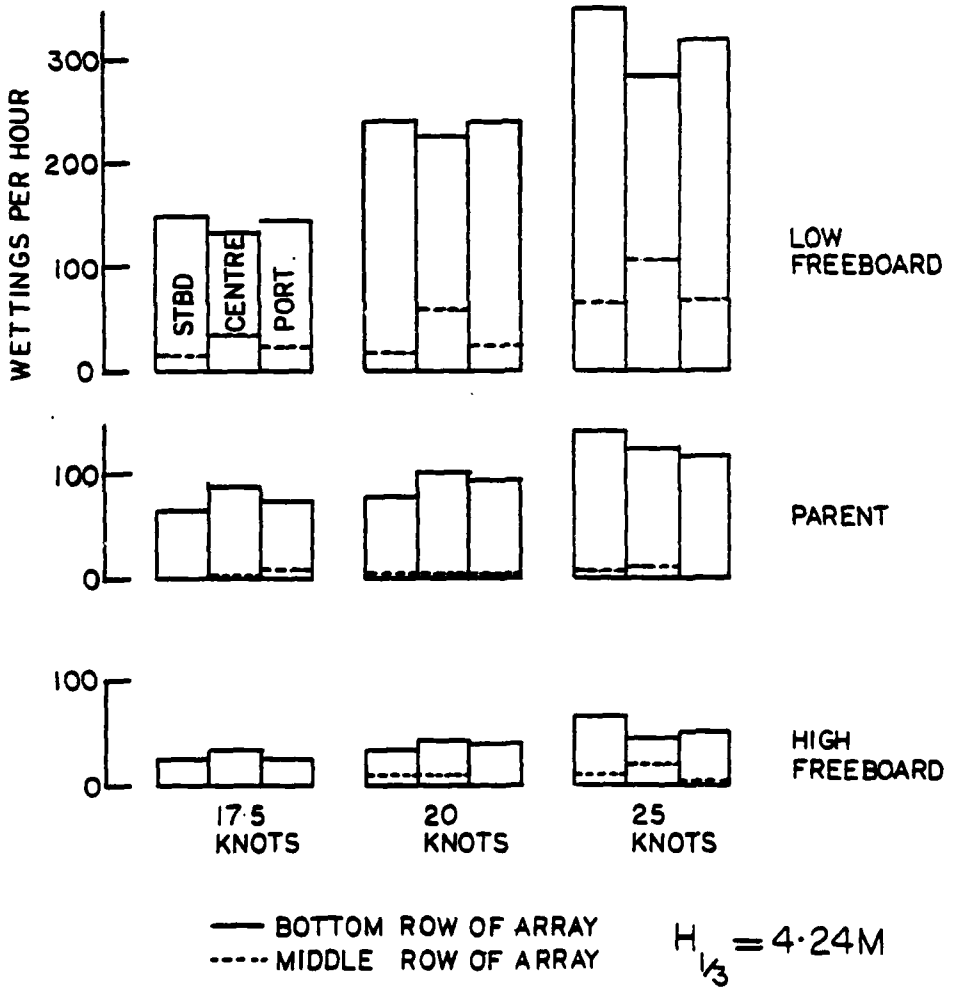

Figure 7. AMTE Experiments: 2nd Series
Distribution of Wetness Frequency:
Effect of Freeboard and Speed

the number of runs for each bow/speed combination was increased to five: each bow was tested at 17.5 and 20 knots giving a total run time of about 30 minutes (for ship). The freeboard variations were also tested at 25 knots.

Figure 7 shows a typical set of wetness frequency results: the diagram shows the distribution of wetness frequency as a function of freeboard and speed. As expected the wetness frequency again increases with speed and as the freeboard is reduced. Most impacts occurred close to the deck on the bottom row of the array, but a significant number were also recorded on the middle row of plates with the low freeboard low.

In very severe conditions (low freeboard, high speed) the greatest number of impacts were usually recorded on the outboard plates in the bottom row. Fewer impacts were recorded on the central plate. Perhaps this was a result of the centre plate being shielded by the relative motion probe. However, in these conditions the central plate experienced most impacts in the middle row of plates.

In less severe conditions (high freeboard, low speed) the central plate of the bottom row recorded most impacts: in these conditions the middle row of plates experienced very few impacts.

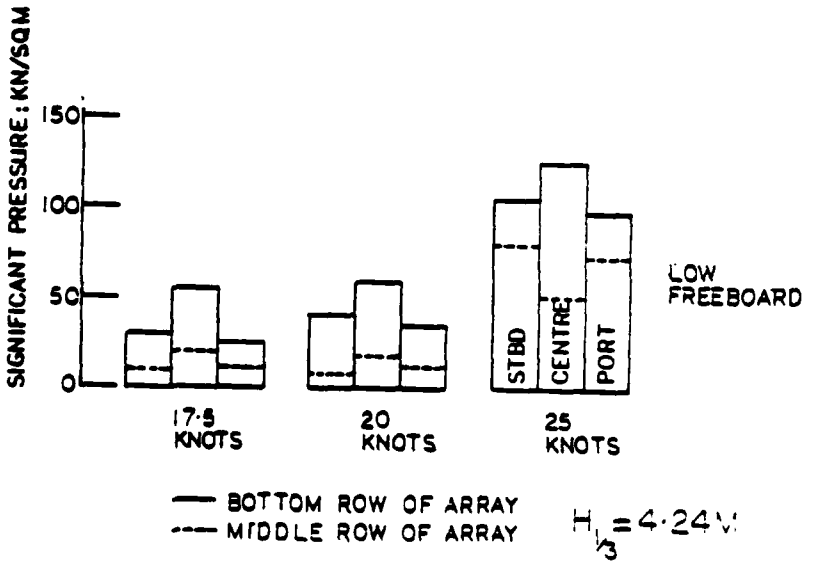

Figure 8. AMTE Experiments: 2nd Series
Impact Pressure Distribution with the Low Freeboard Bow

The low freeboard was the only one which produced a sufficient number of impacts to justify the calculation of pressure statistics for both active rows of the array. Figure 8 shows the distribution of significant impact pressure (defined as the mean value of the highest third of all recorded pressure peaks) for this bow. In most cases the highest pressures were recorded on the centreline of the model. However at 25 knots the outboard pressures on the middle row were higher than on the centreline even though fewer impacts were recorded (see Figure 7). This suggests that the frequent wetness experienced at 25 knots on the centreline of the middle row was largely relatively light spray rather than green water.

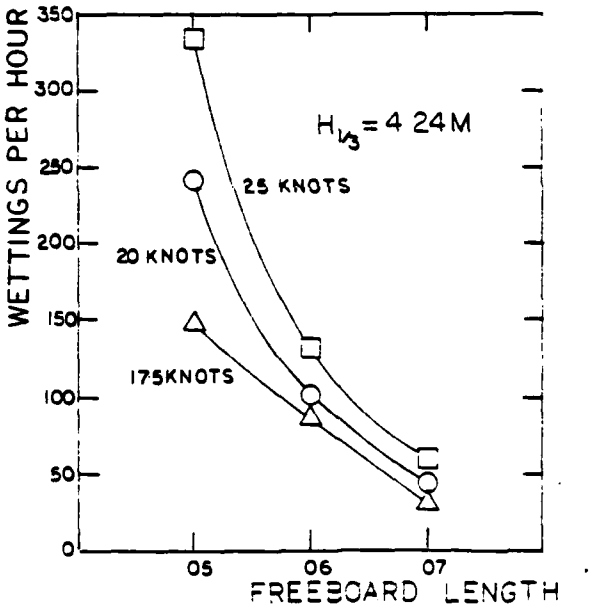

Figure 9. AMTE Experiments: 2nd Series
Effect of Freeboard and Speed on Deck Wetness Frequency

The highest wetness frequency recorded on any of the plates of the array was taken as the appropriate measure of deck wetness frequency for that particular bow and speed. Results for freeboard variations are plotted in Figure 9. Corresponding results for significant pressures are shown in Figure 10.

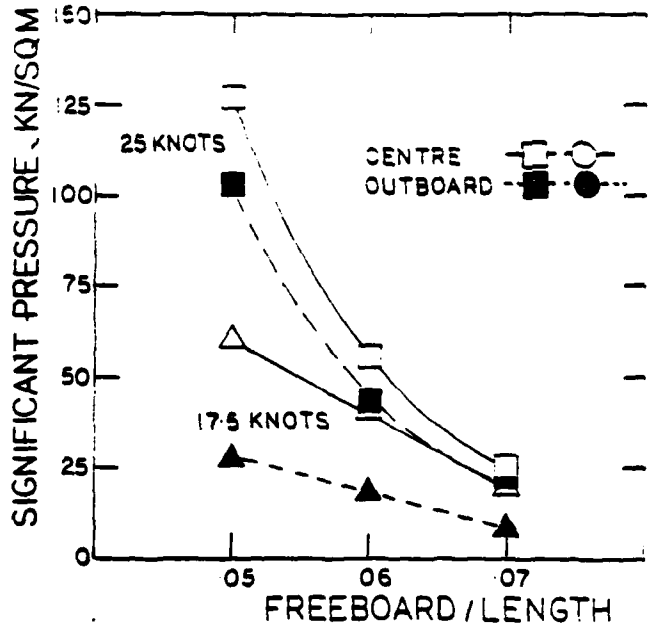

Figure 10. AMTE Experiments: 2nd Series
Effect of Freeboard and Speed on Impact Pressure Distribution

As expected the experiments show the dramatic effect of freeboard in reducing wetness frequency and severity, particularly at high speed.

Figure 11 shows the effect of overhang on deck wetness frequency: clearly a large overhang is beneficial in reducing wetness frequency. Overhang was found to have no consistent effects on significant impact pressure.

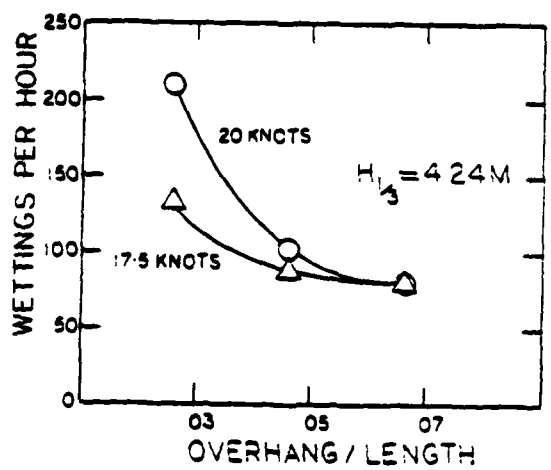

Figure 11. AMTE Experiments: 2nd Series.
Effect of Overhang and Speed on Deck Wetness Frequency

Figures 12 and 13 show the effect of flare angle on wetness frequency and impact pressures: these show unexpected results. Large flare angles seem to give increased wetness frequency and higher impact pressures.

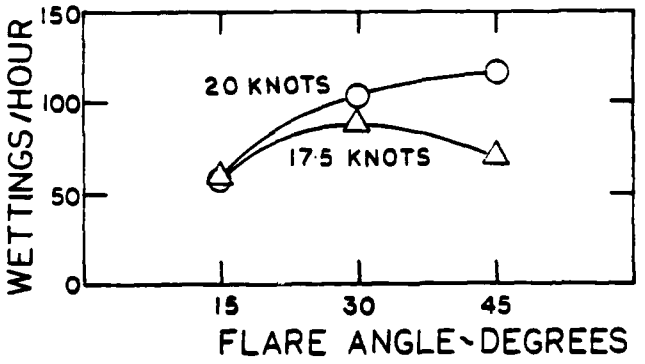

Figure 12. AMTE Experiments: 2nd Series.
Effect of Flare Angle and Speed on Deck Wetness Frequency

The ship motion measurements (see Figure 1) were manipulated to synthesise time histories for the following quantities:

a) pitch
b) heave
c) incident wave
d) actual relative bow motion
e) notional relative bow motion

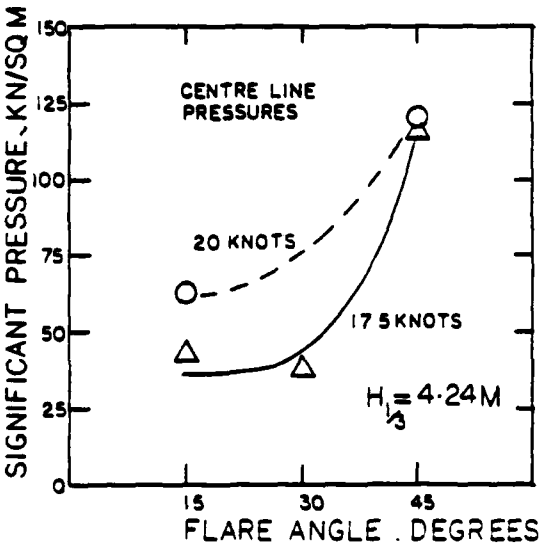

Figure 13. AMTE Experiments: 2nd Series
Effect of Flare Angle and Speed on Impact Pressures

Notional relative bow motion was obtained by subtracting the recorded incident wave time history from the absolute bow motion time history: The resulting quantity is a relative motion free from local swell up effects caused by the presence of the hull (since the wave was measured at a distance of about one metre from the model).

TABLE 2
RMS Motions
Mean Values for all Bows

Speed	Source of Data	Wave	Actual Relative Motion	Notional Relative Motion	Pitch	Heave
knots		metres	metres	metres	deg.	metres
17.5	Experiment	1.06	2.97	3.04	2.09	0.898
	Theory		2.84	2.84	2.02	0.924
20.0	Experiment	1.05	2.94	3.04	2.06	0.962
	Theory		2.94	2.94	2.02	1.00
25.0	Experiment	1.05	2.81	3.01	1.90	1.038
	Theory		3.04	3.04	1.94	1.15

It was found that the RMS values of pitch, heave and notional relative motion were not affected by above water bow form. Table 2 shows the mean values obtained for these quantities (averaged over all bow forms).

All of the individual RMS values were within ±5% of the mean for all bows and over 75% were within ±2%.

In constrast larger variations were found in the results for actual relative bow motion, and Table 3 shows the results obtained for each bow. Even here nearly 70% of the results are within ±5% of the mean for all bows.

Table 3
Effect of Bow Form on RMS Actual
Relative Bow Motion at FP

Bow No.	Difference from mean: per cent		
	17.5 knots	20 knots	25 knots
1	-3.0	-2.0	+5.3
2	0.0	+1.4	-5.3
3	-0.3	-0.3	+0.4
4	+3.0	-7.1	
5	-6.1	-6.1	
6	-1.0	+2.7	
7	-1.7	0.0	
8	+9.8	+10.9	
9	-1.7	-0.7	

Notable exceptions are Bow N°5 (high overhang) which has less than average relative motion and Bow N°8 (high flare) which has much greater than average relative motion. These trends are consistent with the results already described for wetness frequency and severity. Since all the bows experienced essentially identical notional relative motions it would appear that the differences in performance can be ascribed to differences in swell up resulting from the variation in detail design above the waterline: large overhang appears to reduce the swell up; large flare appears to increase swell up.

Table 2 also shows theoretical estimates of the rms motions using the AMTE PAT82 suite of computer programs (Reference 7) with the wave spectrum measured in the tank and the same results are plotted in Figure 14. Clearly the theory

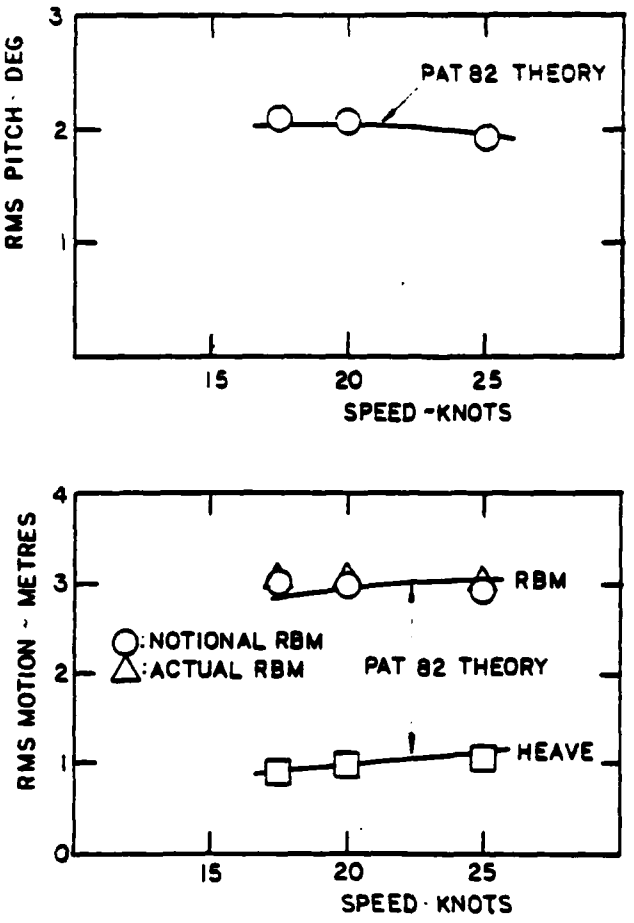

Figure 14. AMTE Experiments: 2nd Series
Ship Motions

gives generally good estimates of the motions although there is a tendency to overestimate motions at high speed (particularly heave) and to underestimate them at low speed (particularly relative motion). It should be noted that although the PAT-82 programs now include corrections for swell up as advocated by Schmitke in the discussion to Reference 5, these are supposedly zero at the forward perpendicular: consequently the theoretical estimates for actual and notional relative motion at this station are the same.

The PAT-82 programs have also been used to predict deck wetness frequency (on the basis of theoretically calculated relative motions) and the results are compared with the experiments in Figure 15. As expected the theory with no allowances for bow wave and swell up predicts deck wetness frequencies which are much too low: this confirms the trend found with the full scale results in Reference 5. Including corrections for bow wave and swell up improves the predictions but they are still too low, particularly when the wetness frequency is very high.

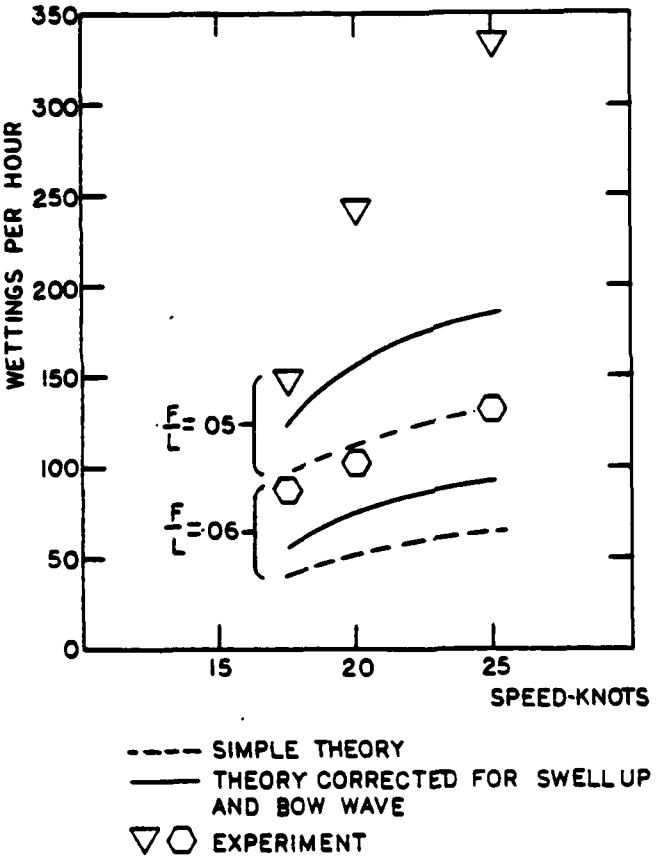

Figure 15. Predicted and Observed Deck Wetness Frequency. Effect of Freeboard and Speed

With swell up and bow wave effects included in the calculation the station at which the relative motion most often exceeds the freeboard is invariably some short distance abaft the FP (at least for conventional shear lines). The discrepancies in the results can only be caused by

a. underestimates of the notional relative motion at the appropriate station

b. underestimates of the swell up at the appropriate station

c. underestimates of the height of the bow wave at the appropriate station

d. the possibility that the relative motion peaks might exceed the freeboard more often than the Rayleigh formula would predict

e. the possiblity that additional wettings might occasionally result from other stations even when the most frequent wetness station remains dry.

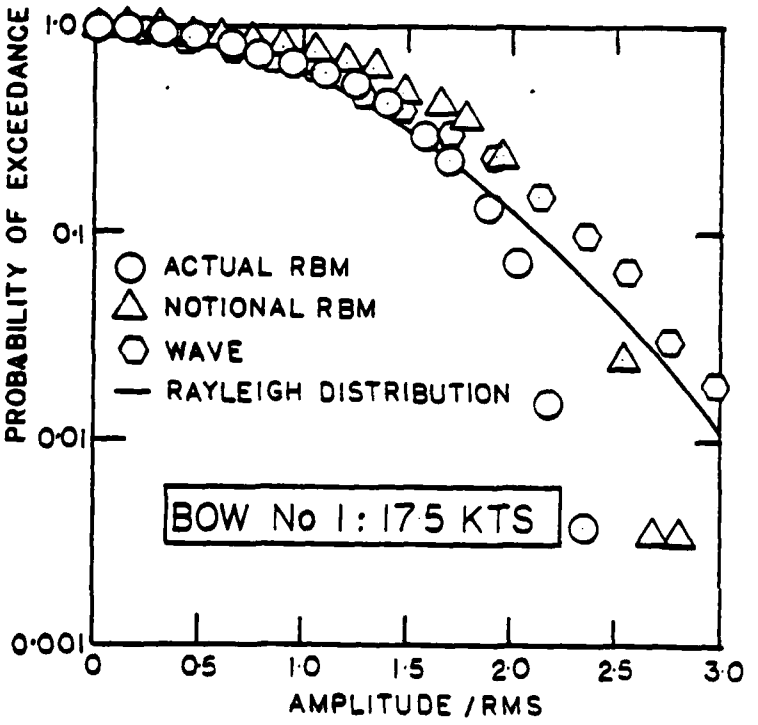

Figure 16. Distribution of Peaks of Relative Motions and Incident Waves

Unfortunately the only measurements of relative motion made in these experiments were at the Forward Perpendicular so none of these possibilities can be investigated without further experiments. However a limited analysis of the waves and the relative motion at the forward perpendicular was performed for comparison with the Rayleigh distribution: the results are shown in Figure 16, taken from Reference 8. Contrary to expectations the probability of both the actual and notional relative motions exceeding more than about twice the rms value is less than the Rayleigh distribution would predict. This occurs in spite of the fact that the results for the incident wave follow the Rayleigh distribution fairly well and are, if anything, underestimated.

Clearly these results need further investigation: in particular the same analysis should be applied to relative motions at stations other than the Forward Perpendicular.

4. AMTE Experiments: Catch Tank Series

Further experiments were conducted by MSC students from University College London at AMTE in 1980 and 1981 (References 9 and 10). These experiments used the same model and bows in identical wave conditions but employed a catch tank

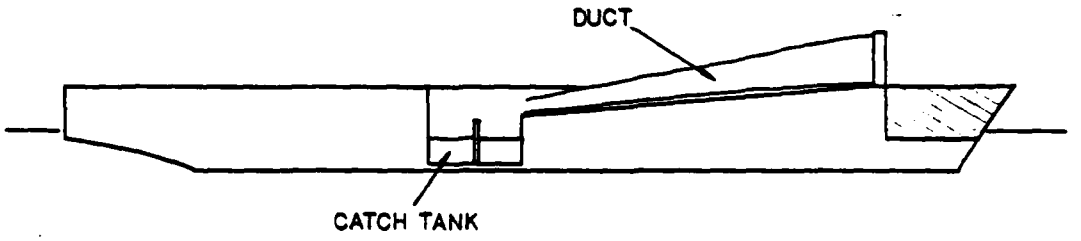

Figure 17. AMTE Catch Tank Experiments

technique to quantify deck wetness by measuring the quantity of water shipped in each run. The pressure sensitive array of the second series of experiments (Figure 5) was replaced by an open forward facing duct of identical dimensions (Figure 17). The duct led aft to a catch tank amidships: as wetness was experienced the water which would have struck the pressure array was collected in the catch tank. The collected water was continually pumped out to a sump on the carriage. After each bow's five runs had been completed the quantity of water collected was weighed. Wetness frequency was determined by visually counting the occasions when water was seen to enter the duct: these results were subsequently confirmed by observing video recordings of each run.

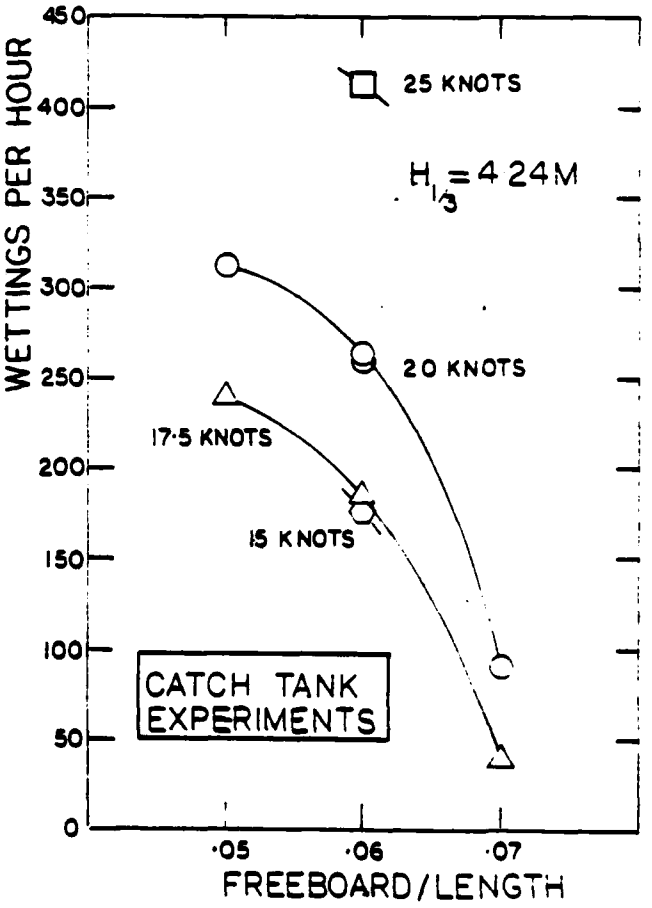

Figure 18. AMTE Catch Tank Experiments
Effect of Freeboard and Speed on Deck Wetness Frequency

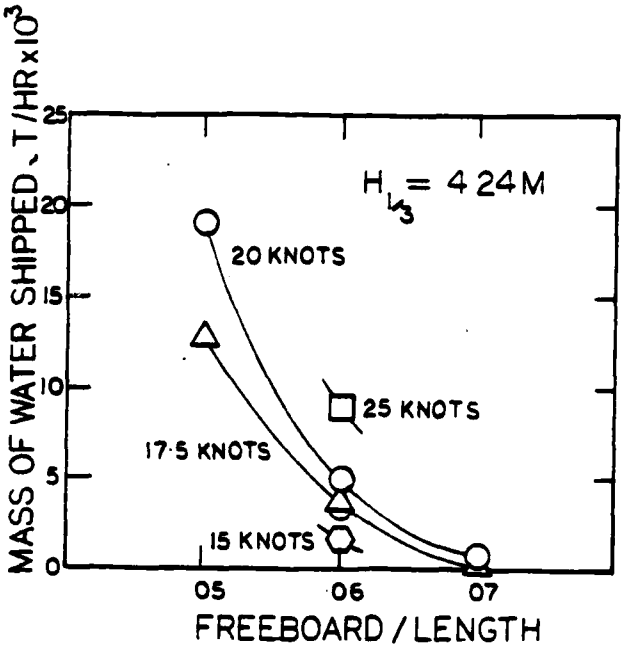

Figure 19. ATME Catch Tank Experiments
Effect of Freeboard and Speed on Mass of Water Shipped Per Hour

Figures 18 and 19 show some of the results obtained. It is immediately obvious that the wetness frequency observed in these experiments was much higher than in the second series (Figure 18) and the character of the curves is different in spite of the fact that the model was identical and tested in the same conditions in the same towing tank. For example the catch tank experimetns gave about 260 wettings per hour for the parent bow at 20 knots. The corresponding figure in the second series was about 100 per hour.

It is believed that this discrepancy is due to the effects of retaining the water shipped by the model: the weight of water flowing through the duct would tend to sink and trim the model bow down and reduce the freeboard so that the wetness frequency would tend to be increased. Another possibility is that the motion of the residual water in the catch tank may have adversely influenced the pitch motions of the model. Whatever the reasons it is clear that results of the catch tank technique need to be treated with caution.

5. AMTE Experiments: Conclusions

The experiments have shown that above water bow form does influence the frequency and severity of deck wetness in moderate head seas. In more severe conditions the influence of bow form is reduced. As expected freeboard has a dramatic influence on deck wetness but other more subtle characteristics have also been shown to be important. Since the experiments were confined to a single hull form in only one wave spectrum these results should be regarded as tentative: nevertheless there is clear evidence, at least for this case, that high overhang reduces the frequency of deck wetness and that large flare angles appear to increase wetness severity. This latter result is unexpected and needs further examination.

Above water bow form has been shown to have a neglible influence on ship motions like pitch, heave and notional relative bow motion, and these motions were well predicted using conventional strip theory. However there is some evidence to suggest that the above water bow form may influence local swell up effects and these trends appear to correlate well with observed wetness characteristics.

Current techniques for predicting deck wetness frequency on the basis of strip theory calculations of motions with allowances for bow wave and swell up appear to be inadequate especially when the wetness frequency is high. Further experiments to examine the wetness "process" in detail will be required to resolve these problems.

Experiments using a catch tank technique for quantifying wetness severity gave much more frequent wettings in spite of the fact that the model was tested in nominally identical conditions. It is concluded that this technique cannot be recommended.

Experiments to measure deck wetness in irregular seas require new techniques to be developed. On the basis of well established statistical rules of thumb it would appear that a minimum of about 100 wettings will be required for any one bow/speed/wave spectrum condition to ensure that reasonably reliable statistics for wetness and severity are obtained. This requirements tends to drive the experimenter towards very severe wave conditions. However it was shown in the first series of experiments that this leads to unrealistically frequent wetness so that the relatively minor bow form variations which are of practical interest can have no appreciable effect. The unpalatable alternative is to test the model over longer periods of time in less severe conditions. The second series of experiments were a step in the right direction with total run times equivalent to about 30 minutes at full scale. However these still only gave around 50 wettings for the parent form (100 wettings per hour): it is recommende that future experiments achieve a total of at least 100 actual wettings and this will call for total run times of the order of one hour at full scale, depending on the speed and bow form.

6. Proposed U. S. Naval Academy Experiments

The experience gained from the AMTE experiments has been used to design an improved series of similar experiments at the U. S. Naval Academy. These experiments will use a 3.45 metre model of another frigate to 1/36 scale and a total of 7 different above water bow forms. Like the AMTE bows the Academy bows will be designed using polynomial curves to ensure a consistent family of shapes and they will fare smoothly into the parent hull form at the waterline and at Station 5. Station 5 has been chosen rather than Station 2 to allow more scope for bow form variation.

The AMTE series varied each bow form parameter in isolation from its fellows in an attempt to determine its individual effects. While this approach

has classic scientific merit it would probably not appeal to the practising naval architect: normal practice would be to vary all the parameters simultaneously to produce an aestheticly attractive shape and to allow more scope for variation. Thus, for example, a large flare angle would almost invariably be associated with a wide fo'c's'le and a pronounced overhang.

Table 4
U. S. Naval Academy Bow Series

Flare Angle Degrees	Overhang / Length	Deck Width at Station 2 / Length
30	.06	.044
35	.07	.048
40	.08	.052
45	.09	.057
50	.10	.063
55	.11	.070

For this reason the Academy bows have been designed allowing all the parameters to vary simultaneously but in a unique, controlled manner. It has been found convenient to define a linear relationship between overhang and flare angle:

$$\frac{X_0}{L} = .002\delta \text{ (in degrees)}$$

and to specify the bow shapes in terms of the flare angle δ at Station 2. The above water section shape at station 2 and the stem profiles are defined by parabolas with suitable boundary conditions: the waterlines above the load waterline (including the deck plan) are defined by cubic polynomials.

The result is the family of bows listed in Table 4 and illustrated in Figure 20.

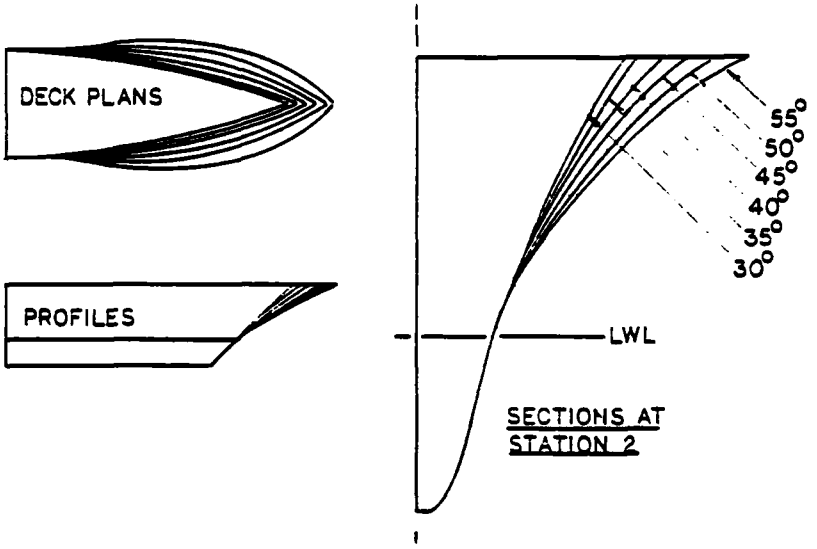

Figure 20. USNA Bow Form Series

In addition tests with a single bow incorporating a knuckle will be performed. This bow will have a 45° knuckle at .0375L above the LWL. The deck plan will be the same as the 35° bow as shown in Figure 21.

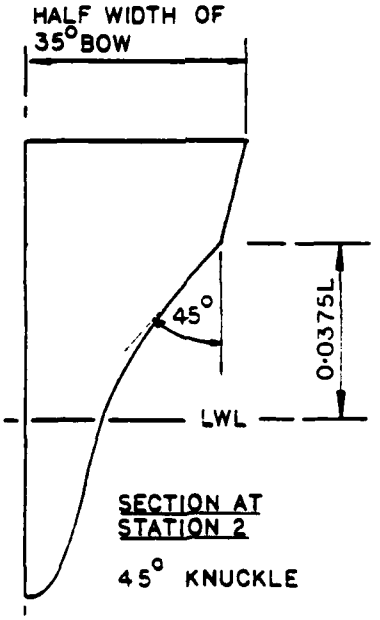

Figure 21. USNA Bow Form Series
Knuckle Bow

A limited number of these bows will be tested with a closely spaced array of flush mounted relative motion probes covering the region of interest immediately abaft the stem head, as shown in Figure 22. In addition the absolute motion and the incident wave will be measured at one of the stations selected for relative motion measurement. This will enable more data on swell up effects to be obtained.

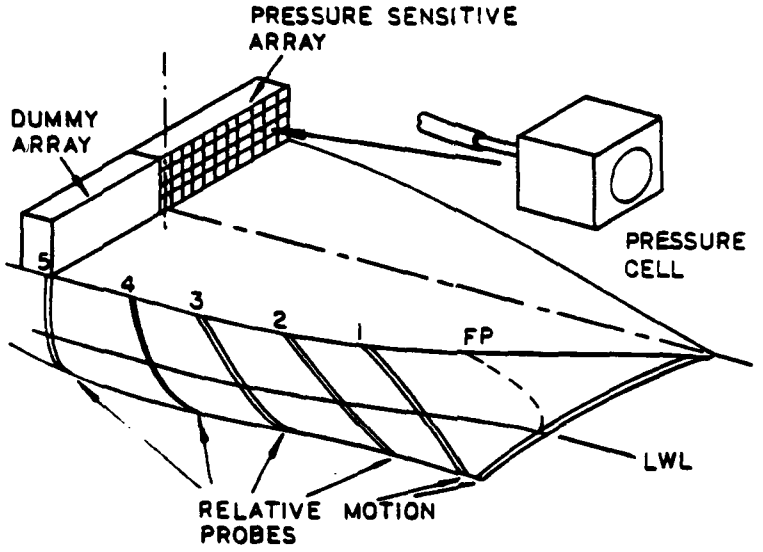

Figure 22. USNA Deck Wetness Experiments.
Proposed Instrumentation

Wetness will be quantified using a more sophisticated version of the AMTE pressure array illustrated in Figure 6: a number of pressure sensitive cells will be constructed and assembled into an array as shown in Figure 22. Each cell will be faced with a thin plastic membrane and filled with water from which all the air has been purged. Pressure pulses from the wettings will be hydraulically transmitted to remote pressure transducers to provide a record of wetness events and severity.

Each bow will be tested in at least one wave spectrum in the U. S. Naval Academy 380' towing tank for a time totalling at least one hour for ship. This will require a dozen or more runs in the tank for each speed and wave condition tested. If time permits the bows will be tested at additional speeds and in additional wave spectra.

7. Conclusions

This paper has described progress in the development of suitable techniques for model experiments to quantify deck wetness. The experiments were intended to investigate the effect of above water bow form on deck wetness frequency and severity: it was found that a high freeboard materially reduced deck wetness in all conditions but more subtle variations in bow form were only effective in moderate conditions. A large overhang and moderate flare angles were found to be beneficial.

Ship motions were found to be essentially independent of above water bow form; but there is some evidence to show that swell up may be affected by bow form and the trends found at least partially explain the observations of the effect of bow form on deck wetness.

Calculations of deck wetness frequency using strip theory with allowances for bow wave swell up effects generally gave estimates which were too low, especially in severe conditions.

The experienced gained from these experiments has been used to design a further series to be run at the U. S. Naval Academy.

The model will be run for times equivalent to about one hour at full scale to ensure an adequate number of deck wettings for reliable statistics to be obtained. Improved and more comprehensive instrumentation will enable the deck wetness process to be studied more thoroughly and provide a sound basis for further theoretical development.

8. Acknowledgements

The author would like to acknowlege the contributions of his colleagues at AMTE Haslar and at the U. S. Naval Academy to the work described in this paper. The author's stay at the U. S. Naval Academy were financially supported by the Naval Sea Systems Command and this support is gratefully acknowledged.

References

1. Kehoe, J. W., Destroyer Seakeeping: Ours and Theirs, U. S. Naval Institute Proceedings, November 1973.

2. Lloyd, ARJM and Andrew, R. N., Criteria for Ship Speed in Rough Weather, 18th ATTC, August 1977.

3. Aertssen, G., Service, Performance and Seakeeping Trials in MV JORDAENS, TRINA, Vol. 108, 1966.

4. Bledsoe, M. D., Bussemaker, O., and Cummins, W. E., Seakeeping Trials on Three Dutch Destroyers, Trans SNAME, Vol. 68, 1960.

5. Andrew, R. N. and Lloyd, ARJM, Full Scale Comparative Measurements of the Behaviour of Two Frigates in Severe Head Seas. TRINA, Vol. 123, 1981.

6. Newton, R. N., Wetness Related to Freeboard and Flare, TRINA, Vol. 102, 1960.

7. Loader, P. R., The User Guide for the PAT82 Ship Motion Program Suite. AMTE(H) TM 81022, December 1981.

8. Andrew, R. N., and Taylor, T., An Investigation of the Statistical Distribution of relative bow motion in irregular waves, AMTE(H) TM 82025 October 1982.

9. Sivaprakasam, S., Deck Wetness Experiments, MSC Project Report, Department of Mechanical Engineering, University College, London, 1980.

10. Tucker, A. M., Deck Wetness Experiments, MSC Project Report, Department of Mechanical Engineering, University College, London, 1981.

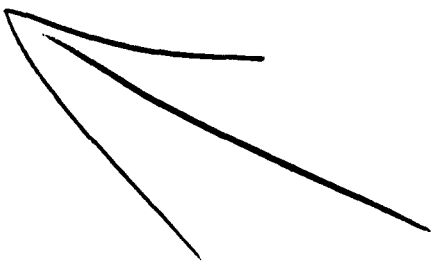

ABSOLUTE AND RELATIVE MOTION MEASUREMENTS ON A MODEL OF A HIGH-SPEED CONTAINERSHIP

Dupe

by

John F. O'Dea and Harry D. Jones
David W. Taylor Naval Ship Research and Development Center

ABSTRACT

A series of experiments was performed to measure the added mass and damping coefficients, and the radiated wave component of relative motion at the bow, for a model of the SL-7 containership. The coefficents of the uncoupled motions agree well with strip theory predictions, but the cross-coupling coefficients between heave and pitch are not well predicted. When the measured values of the coefficients are used in the equations of motion, the calculated motions agree well with the measured motions of a freely floating hull. The measured radiated wave component of relative motion is consistently larger than predicted by strip theory, and has a different phase angle.

INTRODUCTION

One of the important measures of a ship's seakeeping performance is the relative vertical motion between the ship and water surface, particularly near the bow. This relative motion has a strong influence on slamming and deck wetness in a seaway. In the past, the relative motion has been calculated using a kinematic approach, taking the difference between the absolute vertical motion at a given location on the hull and the undisturbed incident wave elevation at that location. This approach was not entirely satisfactory, since interference between the ship and waves (sometimes referred to as "dynamic swell-up") was not taken into account. Recently, several attempts have been made to improve calculations

of relative motion by calculating the hull diffraction effect on the incident waves and the waves generated by the oscillation of the hull (Beck[1], Lee et. al.[2]).

While there is no question that these effects must be included if improvements are to be made in the prediction of relative motion, it must also be recognized that accurate prediction of the rigid body motions is a prerequisite to calculation of relative motion. Both amplitude and phase of the heave and pitch transfer functions affect the calculation of absolute vertical motion in head seas, and if the absolute vertical motion near the bow is not accurately calculated the relative motion calculation will be in error.

It is commonly assumed that the strip theory presented by Salvesen,Tuck and Faltinsen[3] (STF) can be used with confidence to predict longitudinal motions of conventional, monohull displacement ships at moderate Froude number. However, this may not always be true. It has been found in previous experimental work with the SL-7 hull that, at moderately high speed (Froude number = 0.30) in head seas, the magnitude of heave was poorly predicted. There are also motion prediction methods, such as the rational strip theory of Ogilvie and Tuck[4], and the unified slender body theory of Newman and Sclavounos[5], which in some cases predict added mass and damping coefficients which are noticeably different from those calculated using the ordinary strip theory of Salvesen.

The discrepancy between prediction and measurement of the rigid body motions motivated a series of forced oscillation experiments on the SL-7

hull, designed to measure the various components of the rigid body equations of motion and determine the source of the discrepancy. At the same time, the relative motion in the region of the bow was measured so that the hull generated component of relative motion could be compared to strip theory predictions. The results of these oscillation experiments are presented in this paper.

EQUATIONS OF MOTION

The coupled equations of motion of a heaving and pitching ship may be written as:

$$\begin{aligned}(M + A_{ZZ})\ddot{Z} + B_{ZZ}\dot{Z} + C_{ZZ}Z + A_{Z\theta}\ddot{\theta} + B_{Z\theta}\dot{\theta} + C_{Z\theta}\theta &= F_Z \\ A_{\theta Z}\ddot{Z} + B_{\theta Z}\dot{Z} + C_{\theta Z}Z + (Mk_y^2 + A_{\theta\theta})\ddot{\theta} + B_{\theta\theta}\dot{\theta} + C_{\theta\theta}\theta &= M_\theta\end{aligned} \qquad (1)$$

where k_y is the radius of gyration in pitch, A, B, and C refer to the added mass, damping and hydrostatic coefficients, Z and θ are the heave and pitch motions, and F_Z and M_θ denote the heave exciting force and pitch exciting moment respectively. For steady sinusoidal motion the motion and excitation terms can be expressed as complex amplitudes containing both magnitude and phase information:

$$Z = \mathrm{Re}[Z_o e^{i\omega t}], \quad \dot{Z} = \mathrm{Re}[i\omega Z_o e^{i\omega t}], \text{ etc.}$$

It is also convenient to represent all the terms in the equations of motion in nondimensional from, as shown in Table 1. The equations of motion may then be written as a set of algebraic equations with complex coefficients:

$$\begin{aligned}[C'_{ZZ} - \sigma^2(1+A'_{ZZ}) + i\sigma B'_{ZZ}]Z'_o + [C'_{Z\theta} - \sigma^2 A'_{Z\theta} + i\sigma B'_{Z\theta}]\theta'_o &= F'_Z \\ [C'_{\theta Z} - \sigma^2 A'_{\theta Z} + i\sigma B'_{\theta Z}]Z'_o + [C'_{\theta\theta} - \sigma^2(k'^2_y + A'_{\theta\theta}) + i\sigma B'_{\theta\theta}]\theta'_o &= M'_\theta\end{aligned} \qquad (2)$$

For the purpose of determining the added mass and damping coefficients, the hull can be oscillated with a single degree of freedom at a time. The resultant force and moment on the hull may then be used to determine the coefficients. The hydrostatic coefficients may be calculated from the waterplane characteristics or measured by static displacement of the hull.

For example, for forced heave oscillation, let the heave motion Z be defined as a real quantity, so that it is the zero phase reference, and let the force and moment in this case be made nondimensional by heave amplitude rather than incident wave amplitude. The equations of motion then become:

$$\begin{aligned} C'_{ZZ} - \sigma^2(1 + A'_{ZZ}) + i\sigma B'_{ZZ} &= F'_Z \\ C'_{\theta Z} - \sigma^2 A'_{\theta Z} + i\sigma B'_{\theta Z} &= M'_\theta \end{aligned} \qquad (3)$$

and the added mass and damping terms associated with heave motion are found as:

$$\begin{aligned} A'_{ZZ} &= \frac{C'_{ZZ} - \mathrm{Re}[F'_Z]}{\sigma^2} - 1 \\ B'_{ZZ} &= \frac{\mathrm{Im}[F'_Z]}{\sigma} \\ A'_{\theta Z} &= \frac{C'_{\theta Z} - \mathrm{Re}[M'_\theta]}{\sigma^2} \\ B'_{\theta Z} &= \frac{\mathrm{Im}[M'_\theta]}{\sigma} \end{aligned} \qquad (4)$$

In a similar way, if a pure pitch motion (about the center of gravity) is applied to the hull, and the resulting force and moment F_Z, M_θ are made nondimensional as:

$$F_Z^* = \frac{F_Z}{\rho g \nabla \theta} \quad , \quad M_\theta^* = \frac{M_\theta}{\rho g \nabla L \theta}$$

then the added mass and damping terms are found to be:

$$\begin{aligned} A'_{Z\theta} &= \frac{C'_{Z\theta} - \mathrm{Re}[F_Z^*]}{\sigma^2} \\ B'_{Z\theta} &= \frac{\mathrm{Im}[F_Z^*]}{\sigma} \\ A'_{\theta\theta} &= \frac{C'_{\theta\theta} - \mathrm{Re}[M_\theta^*]}{\sigma^2} - k'^2_y \\ B'_{\theta\theta} &= \frac{\mathrm{Im}[M_\theta^*]}{\sigma} \end{aligned} \qquad (5)$$

EXPERIMENTAL SET UP and INSTRUMENTATION

The forced oscillation experiments were performed using a 1:60 scale model of the SL-7 containership ballasted to a 0.173m waterline with a pitch radius of gyration equal to 0.254 times the length between perpendiculars. The coordinate origin of the axis system used in the experiments was taken at the center of gravity of the hull, with heave motion and force defined as vertically upward and pitch motion and moment defined as bow down. The oscillator used was a single degree-of-freedom Scotch yoke type with maximum stroke of ± 1 inch(25.4mm) and a variable frequency controlled by a servo system on the DC driving motor. In the heave experiment the model

was connected to the oscillator through four load cells and a rigid frame (the load cells were mounted port and starboard, at approximately $\pm$ L/4 with pivot joints to avoid out-of-axis loads). For the pitch oscillation experiment the aft pair of load cells was moved to the hull center of gravity and attached to the carriage through pivots, while the oscillator was used to vertically oscillate the forward attachment point.

Using the full range of the oscillator, it was possible to achieve a heave magnitude equal to approximately 15% of the draft of the hull. It was also decided that a maximum nondimensional frequency ($\omega\sqrt{L/g}$) equal to 10 was desirable. This frequency corresponded to a wavelength ratio, $\lambda/L < 0.5$ at a Froude number of 0.3. Using these values, and estimates of added mass from strip theory, the maximum heave oscillation force was estimated to be approximately 1000 N, and the load cells were calibrated accordingly. Using the same load cell range in the pitch oscillation experiment the maximum pitch amplitude was limited to approximately $\pm$ 0.6 degrees. Since the intention was to check the linear coefficients of the equations of motion, these oscillation amplitudes were considered adequate.

Relative motion was measured at stations 0,1,2 and 3 using resistance-type probes mounted flush to the side of the hull. Time histories of force, oscillation amplitude, carriage speed and relative motion were digitized by an on-board DEC 11/23 computer and recorded on magnetic disk. The records were harmonically analyzed and resolved into inertia and damping coefficients according to equations 4 and 5.

RESULTS

The results of the oscillation experiments are shown in Figures 1 to 8. In each case, the experiments, were done at three speeds corresponding to Froude number = 0.1,0.2 and 0.3, and nondimensional frequency varied from approximately 2.0 to 8.5. The heave experiments were done over the full range of frequencies at an amplitude $Z_o/T = 0.037$, and repeated with amplitudes up to $Z_o/T = 0.147$ at selected frequencies. The pitch experiments were done over the full frequency range at an amplitude of 0.37 degrees, and repeated for selected frequencies at 0.19 and 0.56 degrees.

The uncoupled coefficients A_{ZZ}, B_{ZZ}, $A_{\theta\theta}$ and $B_{\theta\theta}$, shown in Figures 1 to 4 are generally in very good agreement with predictions made by strip theory. This is particularly true in the range $3<\sigma<5$, corresponding to a range of wavelengths near the ship length where motion predictions are most crucial. The only area where significant scatter is shown in the data is in the low speed results near $\sigma \leq 2.5$, corresponding to $\omega\frac{U}{g} = 1/4$ where free surface waves can be radiated ahead of the hull. The introduces the possibility of reflected waves reaching the hull, resulting in the poor data shown. The corresponding condition at the higher Froude numbers would occur outside the frequency range tested; therefore no such scatter appears in the data at these speeds.

Results for the cross coupling coefficients $A_{\theta Z}$, $B_{\theta Z}$, $A_{Z\theta}$ and $B_{Z\theta}$ are shown in Figures 5 to 8. There are significant discrepancies between predicted and measured values for all these coefficients. The predicted and measured coefficients converge at the highest frequencies but diverge

over much of the frequency range, particularly the range where cross coupling has a strong effect on the motions as discussed below. These discrepancies are qualitatively similar to those reported by Faltinsen [6], who found a significant improvement when the extra components of the Ogilvie-Tuck theory were added to the ordinary (STF) strip theory.

Experimental values of heave and pitch excitation were available from an earlier, unpublished experiment on this hull. These data were obtained with the model rigidly attached to the towing carriage, with incident waves of steepness $2\zeta_A/\lambda=1/50$. The results of these experiments are shown in Figures 9 to 12. In general, the heave excitation magnitude agrees well with strip theory predictions, as does the heave excitation phase angle except at high frequencies, corresponding to wave lengths shorter than the ship length where phase angles shift rapidly with changing frequency. Similar agreement is found for pitch excitation although there is an overall trend for the measured pitch excitation to be slightly less than the predicted values.

The experimentally measured added mass, damping and excitation coefficients have been used in the equations of motion to calculate the heave and pitch motions. The results are shown in Figures 13 and 14, together with strip theory predictions and experimental values on a freely floating model. The heave motion measured on the freely floating hull is considerably closer to the calculations made with the measured coefficients, than to the strip theory predictions. This is particularly true at Froude number = 0.3. The effect of using the measured coefficient in calculating pitch is less obvious, and at Froude number = 0.3 in the low frequency range, the use of

the measured coefficients actually gives slightly poorer predictions than strip theory.

The measured values of relative motion in the oscillation experiments are shown in Figures 15 to 18 for stations 0, 1, 2 and 3 respectively. These figures show the magnitude of relative motion measured by the resistance wire probes made nondimensional by the corresponding absolute vertical motion at the particular station (either heave amplitude or pitch amplitude times the lever arm to that station). Thus, even when no local wave is generated by the hull, the nondimensional relative motion has a value of 1.0. The degree to which the data in the figures deviates from a value of 1.0, therefore, is an indication of the importance of the hull-generated wave component in relative motion.

Relative motion data are shown in each figure for the four amplitudes of heave motion used in the oscillator experiments and for one pitch amplitude. There is a trend for the results at the smallest heave amplitude to be slightly larger than at the larger amplitudes. This was possibly caused by surface tension effects at the smallest amplitude or by a small bias in setting the oscillation amplitude. All the other results show no particular trend with oscillation amplitude. The results for the pitch oscillation are generally close to the results for heave oscillation, when both are nondimensionalized by the local absolate vertical motion.

The results for stations 0 and 1 show little effect from hull generated waves. This is not surprising, since the hull cross-section at these stations is very small. At station 2, the magnitude of the relative motion reaches

approximately 1.25, and at station 3 at high frequencies it reaches a value of 1.5, indicating a significant hull generated wave component. Athough not shown, the phase of the relative motion, referenced to the phase of the local absolute motion, was very close to 180 degrees at stations 0 and 1, since in the absence of a local wave effect the relative motion reaches a maximum positive value at the point where the hull reaches its deepest immersion (maximum negative absolute vertical motion). The phase of the relative motion at station 2 indicated a further phase lead of 5 to 10 degrees and at station 3 a lead of 15 to 20 degrees, compared to the phase at stations 0 and 1. This indicates that the hull generated wave at stations 2 and 3 was not exactly in phase with the motion.

The hull generated wave component of relative motion, as predicted by strip theory, is shown in figure 19 for station 2 at Froude number = 0.3. As shown, the phase angle of this component lags the absolute motion by approximately 90 degrees. Since the relative motion is the vector difference between the absolute motion and hull generated wave, and the latter is typically a fraction of the former, the relative motion predicted by strip theory would show very little influence from the hull generated wave if it is phase shifted 90 degrees from the absolute motion. In contrast, when the measured value of relative motion reaches a magnitude of approximately 1.25 at this station, it is an indication that the hull generated wave has a magnitude of at least 0.25, and the phase of this wave component is closer to 180 degrees than to 90 degrees.

EXPERIMENTAL ACCURACY

The accuracy of oscillation experiments can be affected by many factors. The first is the accuracy of the oscillation motion itself. If the oscillator motion is not purely sinusoidal, or if there is vibration of the carriage, the measured forces and moments will be distorted. While harmonic analysis of the time histories will filter most of the unwanted portion, the effective signal-to noise ratio will be reduced. It was found in the experiments reported here that there was a background noise level in all of the force gages of approximately one Newton RMS. This was presumably caused by carriage vibration, and did not vary with carriage speed. The oscillator motion itself was very nearly a pure sinusoid, with the first harmonic typically accounting for about 99% of the total mean square energy of the motion signal. The magnitude of the force signals was typically much large than the background noise level, except for the smallest oscillator amplitudes and lowest oscillation frequencies. However, even in these cases the first harmonic of the force signals typically were greater than 50% of the total energy.

Another factor in the accuracy of the experiments is the degree to which the hydrostatic coefficients, measured from static displacement of the hull, agree with calculations using the waterplane characteristics of the hull. It was found that the heave static coefficients, as measured by the slope of static force and moment against static heave displacement, agreed very well with calculated values. Of course, there was an offset of the

intercept of such calibration curves which increased with Froude number, This is recognized as the steady forward speed loads causing sinkage and trim on a freely floating hull and in fact the measured offset values correlated well with measured sinkage and trim values previousy measured on this hull. In the pitch oscillation experiments, there was a noticeable discrepancy between the measured and calculated pitch hydrostatic coefficient, $C_{\theta\theta}$. This was apparently caused by some residual stiffness in the hardware which was accentuated by the very small oscillation amplitudes used. There was also a small apparent tendency for this static coefficient to vary with forward speed. The experimentally measured values of all the static coefficients were used in analyzing the results according to equations 4 and 5, but the uncertainly concerning $C_{\theta\theta}$ makes the values of $A_{\theta\theta}$ perhaps the least reliable of all the dynamic coefficients.

The accuracy of the relative motion probes on the bow is a function of their linearity, sensivity, and possibly surface tension effects. These probes were originally designed to measure relative motion over a large range, from bottom emersion to deck immersion. However, their electronic sensitivity was adjusted for these experiments in recognition of the fact that oscillation amplitudes would only be a fraction of the draft, and in fact the small amplitudes served to reduce possible nonlinearities, since the hull was effectively wall-sided in the oscillation range. However, the small oscillation amplitudes may have introduced surface tension effects, since the probes were in physical contact with the water surface, and the size of the meniscus was not necessarily negligible in comparion to measured

magnitudes.

In considering the accuracy of the various coefficients, one must consider the magnitude of the force or moment component associated with a particular coefficient, in relation to the vector sum of all the forces or moments in the equations of motion. The relative balance between the components is a function of frequency. That is, at low frequencies the equations are dominated by hydrostatic effects, while at very high frequencies inertial effects predominate. This means that the accuracy of measuring added mass will be good at high frequencies, but at low frequencies one may expect rather more scatter in the added mass data since the inertial part is only a small fraction of the real part (or in-phase component) of the force or moment. If there is an error in the corresponding hydrostatic coefficient, a bias will be introduced into the low-frequency added mass estimates, in addition to increased scatter.

In an intermediate frequency range, the static and inertial terms tend to cancel each other, with the phase of the net force or moment approaching a 90 degree shift from the motion itself. This corresponds to the resonance condition for a mechanical oscillator. In this situation the total force or moment is dominated by the damping term, so that the most accurate measurements of damping are expected in the intermediate frequency range. Implicit in the discussion above is the need to measure phase angles accurately, since the forces and moments for arbitrary frequencies contain information about both damping and inertial coefficients, and the real and maginary parts must be carefully separated.

A final measure of the accuracy of the experiments is the repeating of conditions which was done at different oscillation ampltitudes. This is a check both on repeatability (the degree of scatter) and linearity (trends with amplitude). In these experiments, very little nonlinearity was observed. There is some tendency for the measurements at the very smallest oscillation amplitude to differ from other amplitudes, but this may be simply an indication of the limit of the accuracy with which the actual oscillation amplitude could be set. The smallest amplitudes corresponded to only a few millimeters at the oscillator attachment point so that even a tenth of a millimeter might bias the results. Other than this, there was no discernable nonlinear trend in any of the results, and the variation between results at different amplitudes would have been considered quite acceptable scatter even if only one amplitude had been repeated.

CONCLUSIONS

The measured coefficients of heave and pitch motion of the SL-7 show good agreement with strip theory for the uncoupled coefficients. However, the cross coupling coefficients show a considerable discrepancy at all but the highest frequencies of oscillation. The measured wave excitation loads are in reasonable agreement, with measured pitch exciting moment being somewhat less than predicted by strip theory. When the measured values of added mass, damping and excitation are used in the equations of motion, the resulting calculated values of heave and pitch response show improved correlation to the measured motions on a freely floating hull, particularly at high speed.

The measured relative motion near the bow due to forced heave or pitch motion is consistently higher than predicted by strip theory. The phase angle of the measured relative motion is close to 180 degrees from the motion phase, indcating that the hull generated wave is also near this phase angle. This tends to maximize the relative motion, while the 90 degree phase shift predicted by strip theory tends to minimize the effect of the generated wave on relative motion.

ACKNOWLEDGEMENT

This work was sponsored by the Naval Sea Systems Command under the General Hydromechanics Research Program administered by the David W. Taylor Naval Ship Research and Development Center.

REFERENCES

1. Beck, Robert F., "Relative Motion Components for a Mathematical Form in Regular Waves," 14th Symposium on Naval Hydrodynamics, Ann Arbor, Michigan, August 1982.

2. Lee, Choung M., John F. O'Dea and William G. Meyers, "Prediction of Relative Motion of Ships in Waves," 14th Symposium on Naval Hydrodynamics, Ann Arbor, Michigan, August 1982.

3. Salvesen, Nils, E. O. Tuck and Odd Faltinsen, "Ship Motions and Sea Loads," Transactions SNAME, 1970.

4. Ogilvie, T.F. and E.O. Tuck, "A Rational Strip Theory of Ship Motions, Part 1," University of Michigan, Department of Naval Architecture and Marine Engineering, Report 013, 1969.

5. Newman, J. Nicholas and Paul Sclavounos, "The Unified Theory of Ship Motions," 13th Symposium on Naval Hydrodynamics, Tokyo, 1980.

6. Faltinsen, Odd M., "A Numerical Investigation of the Ogilvie-Tuck Formulas for Added-Mass and Damping Coefficients," Journal of Ship Research, June 1974.

TABLE 1

Non-dimensional Coefficients

$$A'_{zz} = \frac{A_{zz}}{\rho\nabla} \qquad B'_{zz} = \frac{B_{zz}}{\rho\nabla}\sqrt{L/g} \qquad C'_{zz} = \frac{C_{zz}}{\rho g\nabla}$$

$$A'_{z\theta} = \frac{A_{z\theta}}{\rho\nabla L} \qquad B'_{z\theta} = \frac{B_{z\theta}}{\rho\nabla L}\sqrt{L/g} \qquad C'_{z\theta} = \frac{C_{z\theta}}{\rho g\nabla}$$

$$A'_{\theta z} = \frac{A_{\theta z}}{\rho\nabla L} \qquad B'_{\theta z} = \frac{B_{\theta z}}{\rho\nabla L}\sqrt{L/g} \qquad C'_{\theta z} = \frac{C_{\theta z}}{\rho g\nabla}$$

$$A'_{\theta\theta} = \frac{A_{\theta\theta}}{\rho\nabla L^2} \qquad B'_{\theta\theta} = \frac{B_{\theta\theta}}{\rho\nabla L^2}\sqrt{L/g} \qquad C'_{\theta\theta} = \frac{C_{\theta\theta}}{\rho g\nabla L}$$

$$F'_Z = \frac{F_Z}{\rho g(\nabla/L)\zeta_A} \qquad M'_\theta = \frac{M_\theta}{\rho g\nabla\zeta_A}$$

$$Z'_o = \frac{Z_o}{\zeta_A} \qquad \Theta'_o = \frac{L\Theta_o}{\zeta_A}$$

$$k'_y = \frac{k_y}{L} \qquad \sigma = \omega\sqrt{L/g}$$

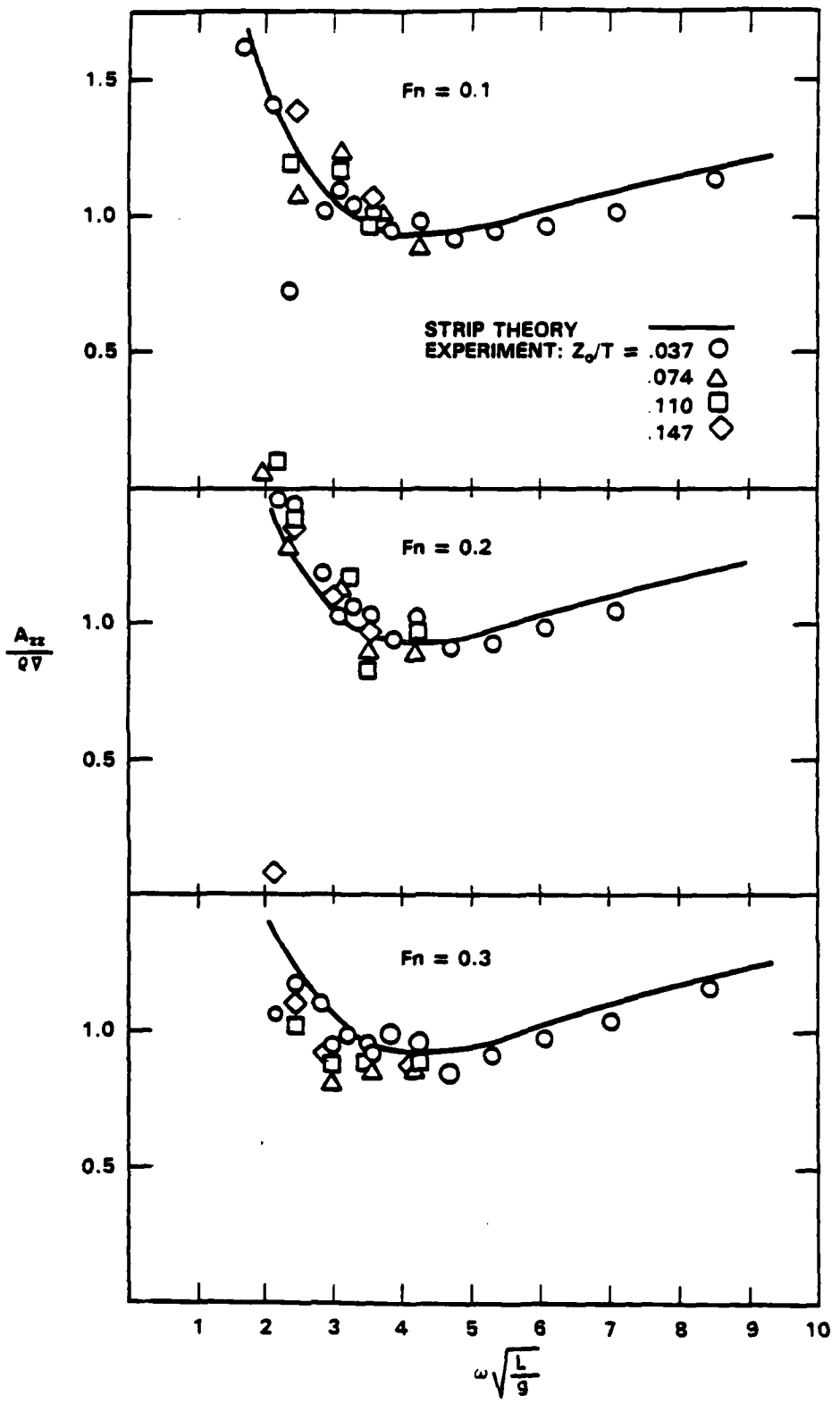

Figure 1 - Heave Added Mass Coefficient A_{zz}

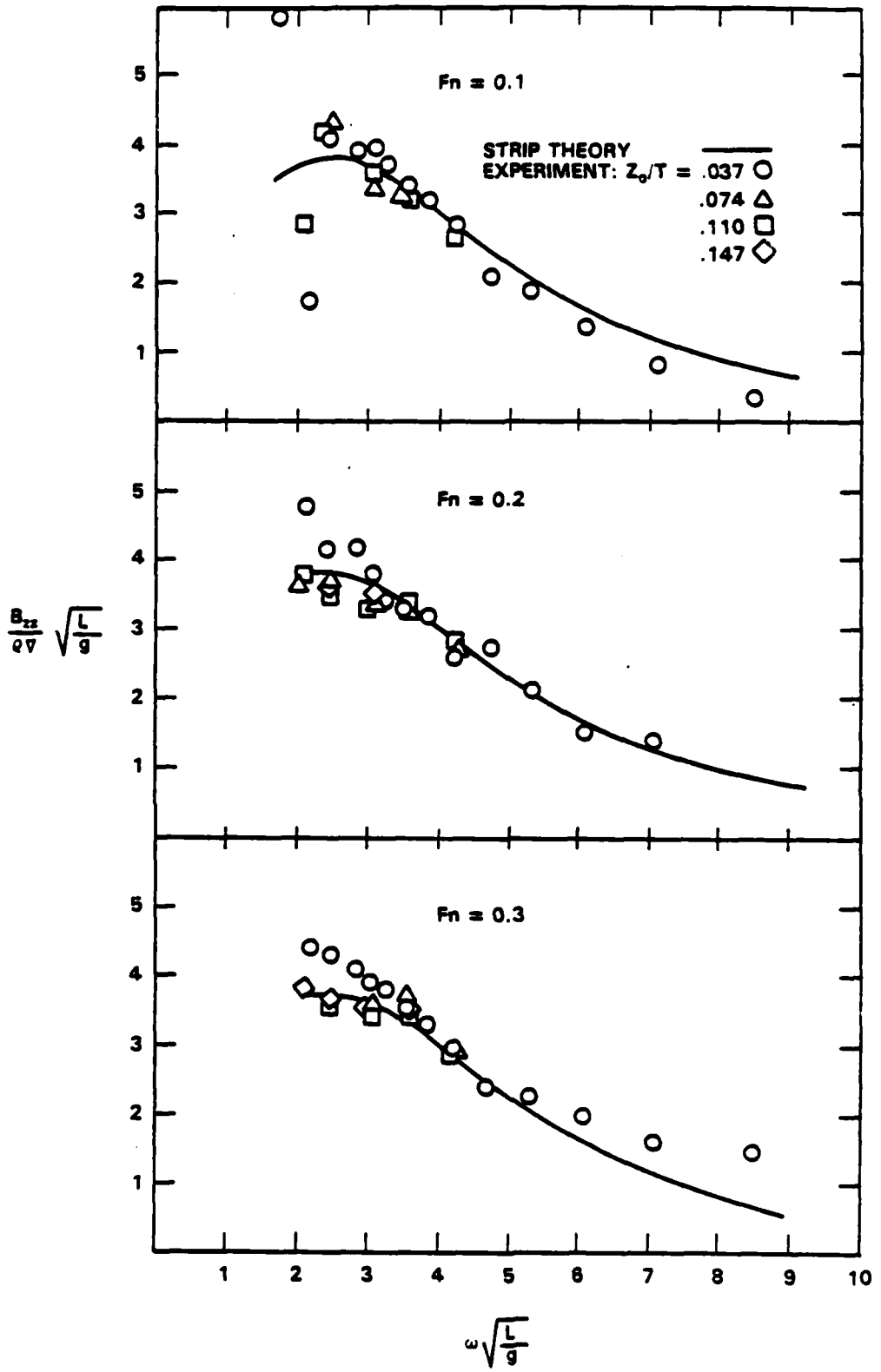

Figure 2 - Heave Damping Coefficient B_{zz}

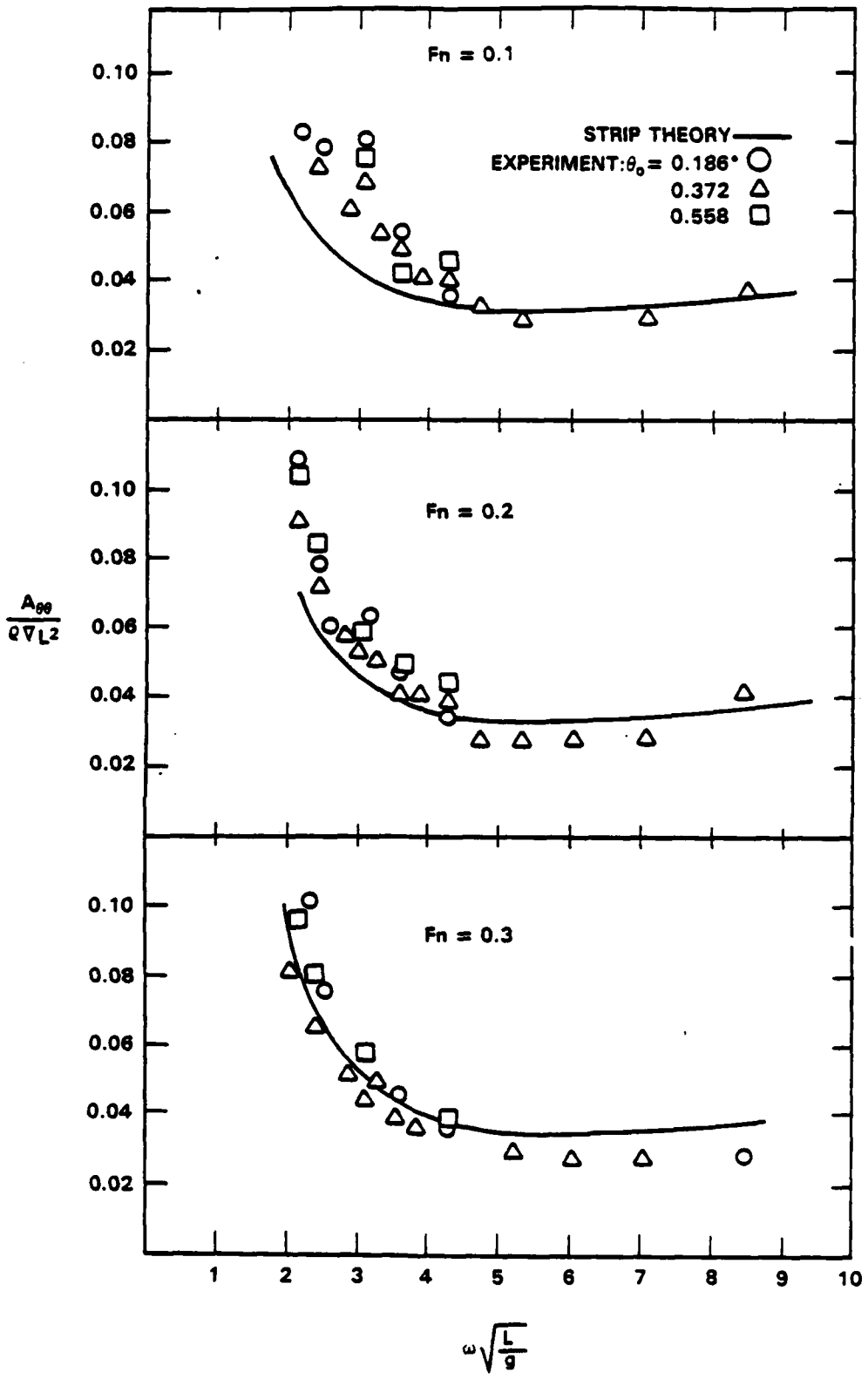

Figure 3 - Pitch Added Mass Coefficient $A_{\theta\theta}$

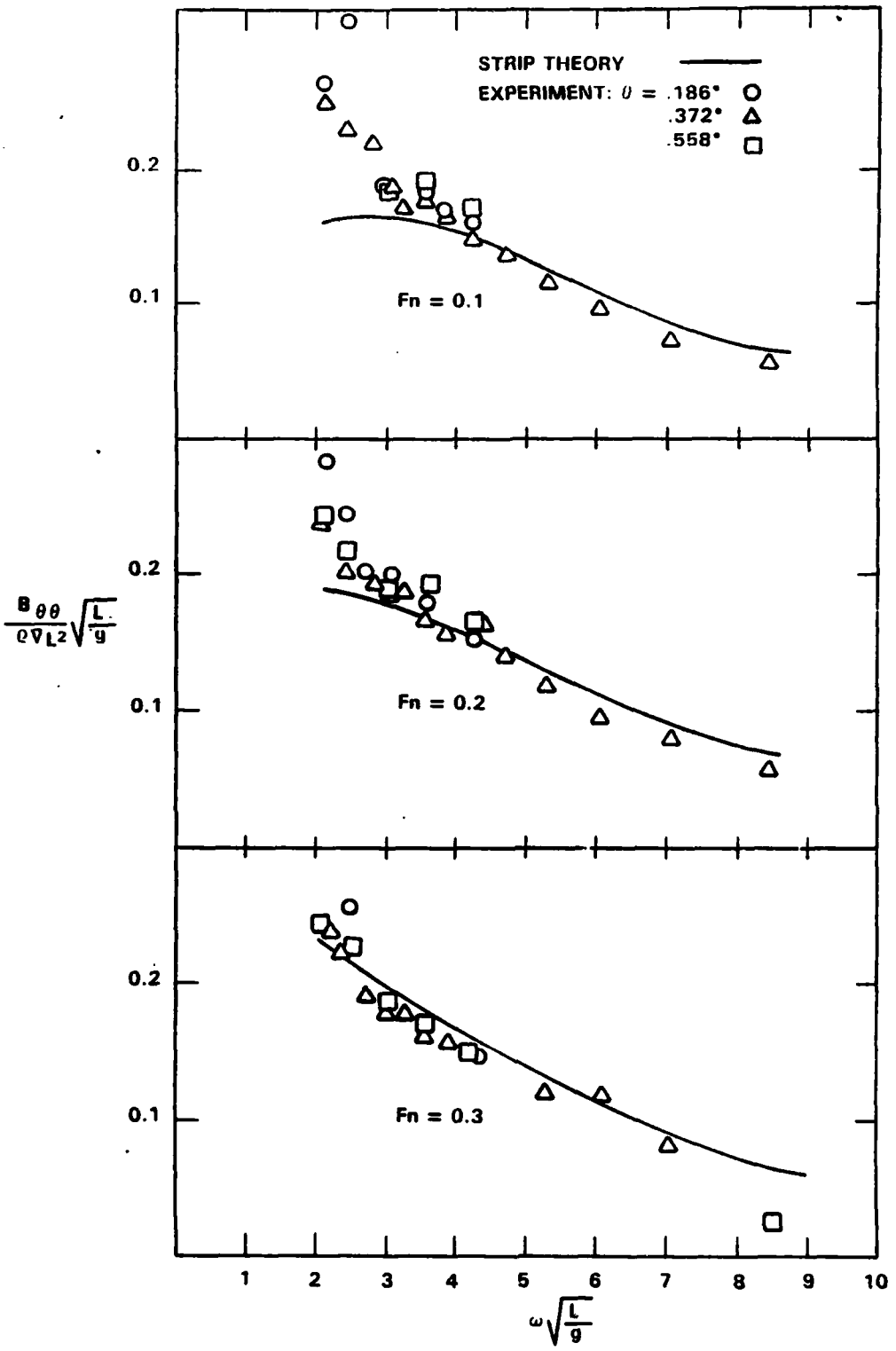

Figure 4 - Pitch Damping Coefficient $B_{\theta\theta}$

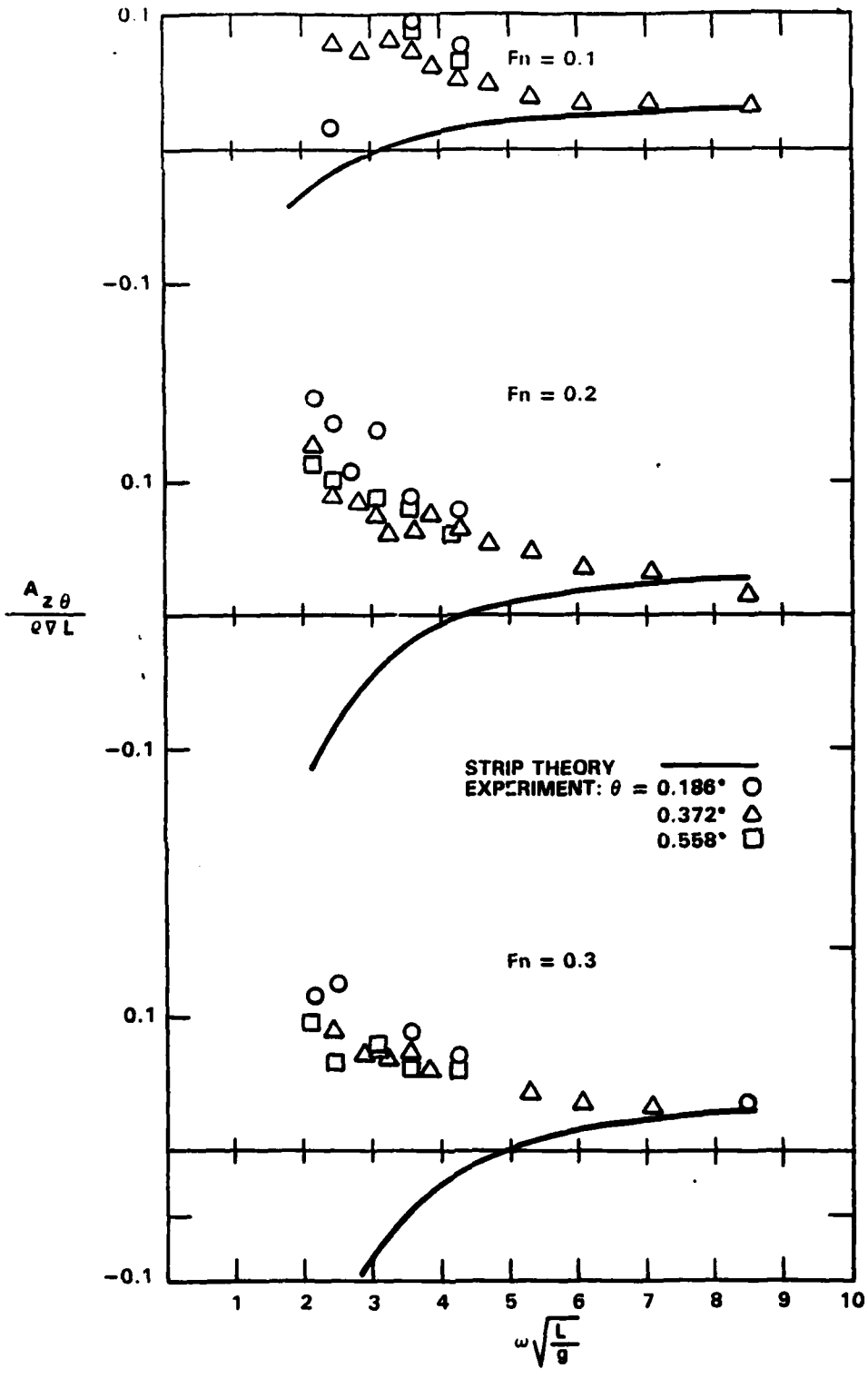

Figure 5 - Heave-Pitch Coupling Coefficient $A_{z\theta}$

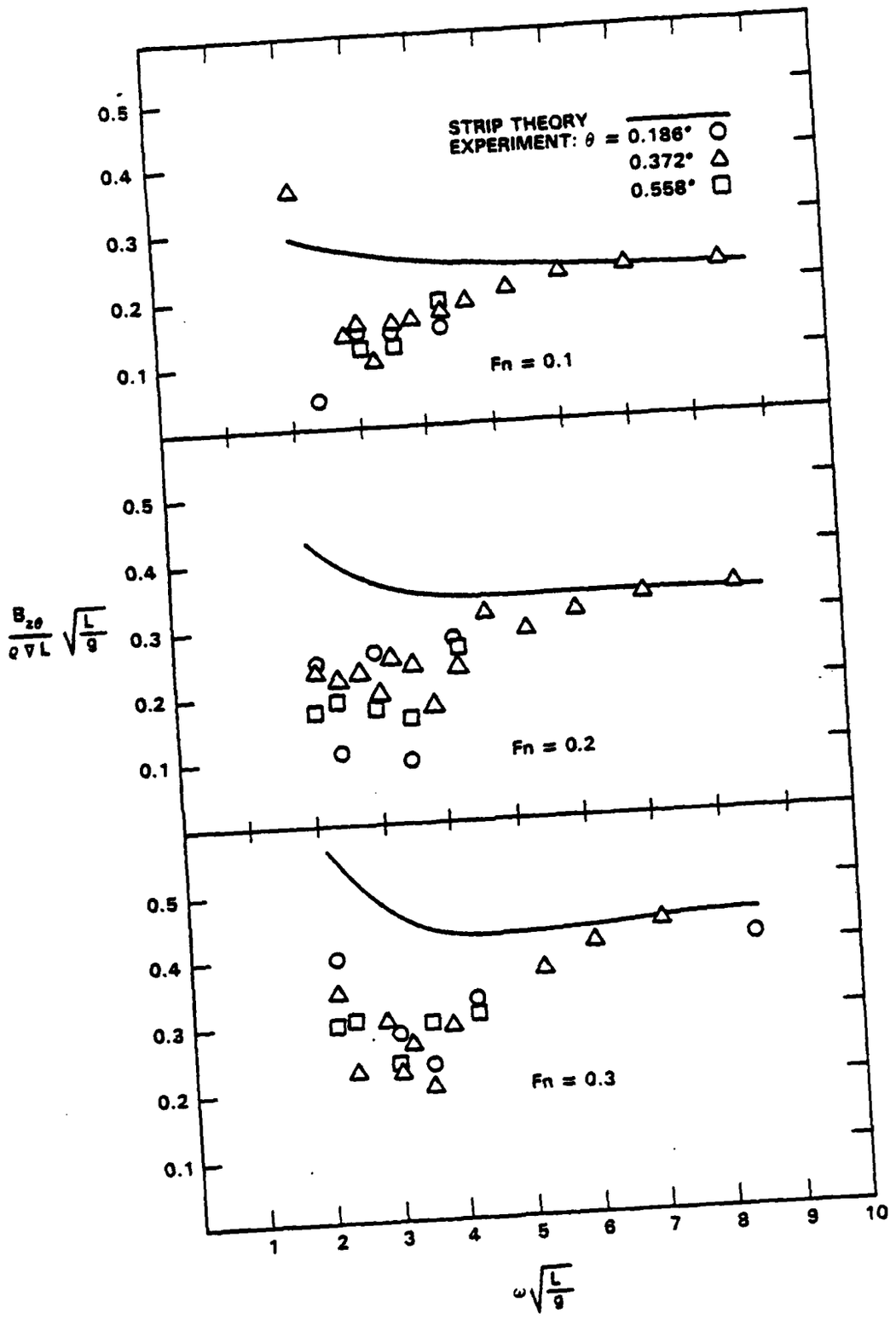

Figure 6 - Heave-Pitch Coupling Coefficient $B_{z\theta}$

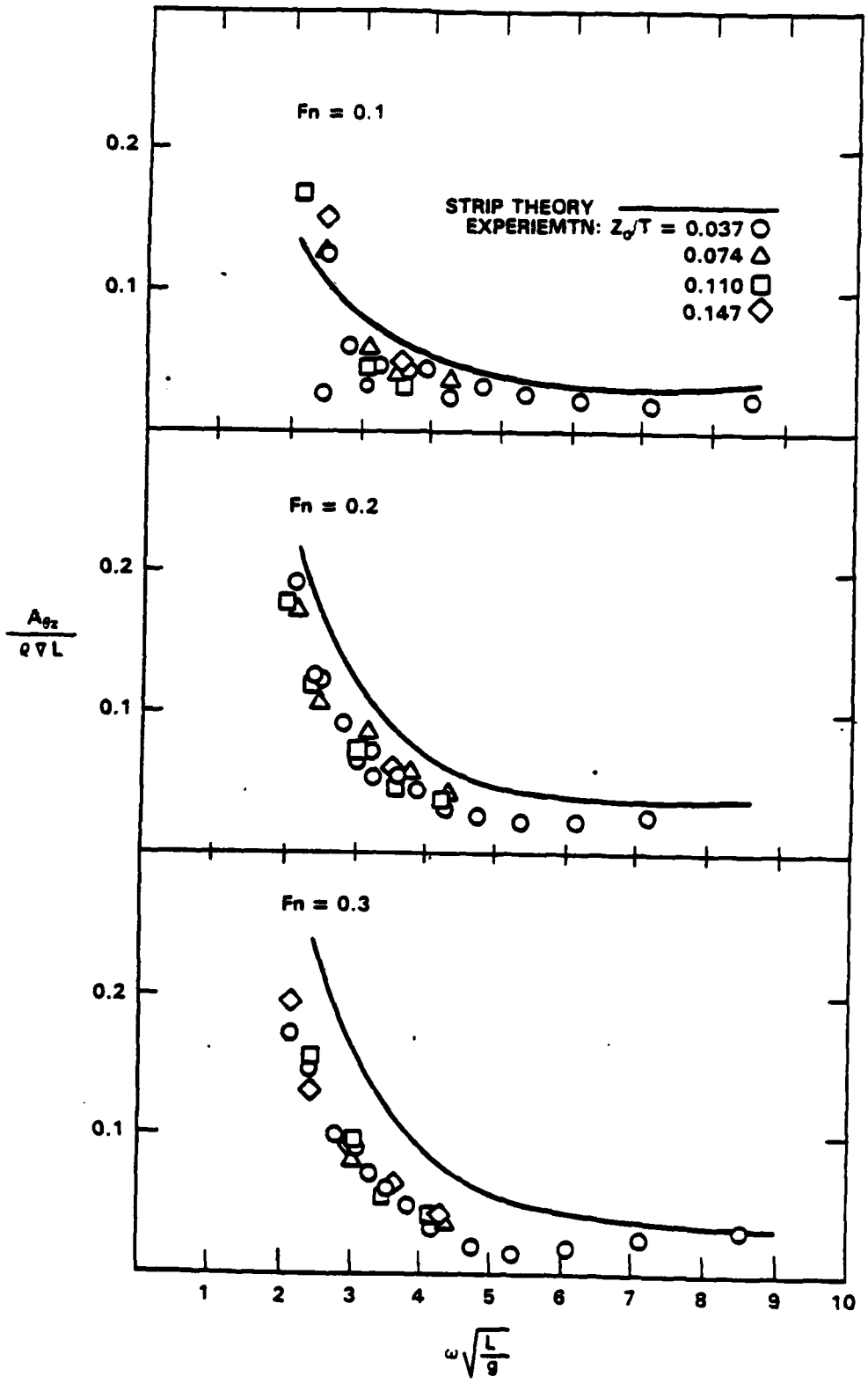

Figure 7 - Pitch-Heave Coupling Coefficient $A_{\theta z}$

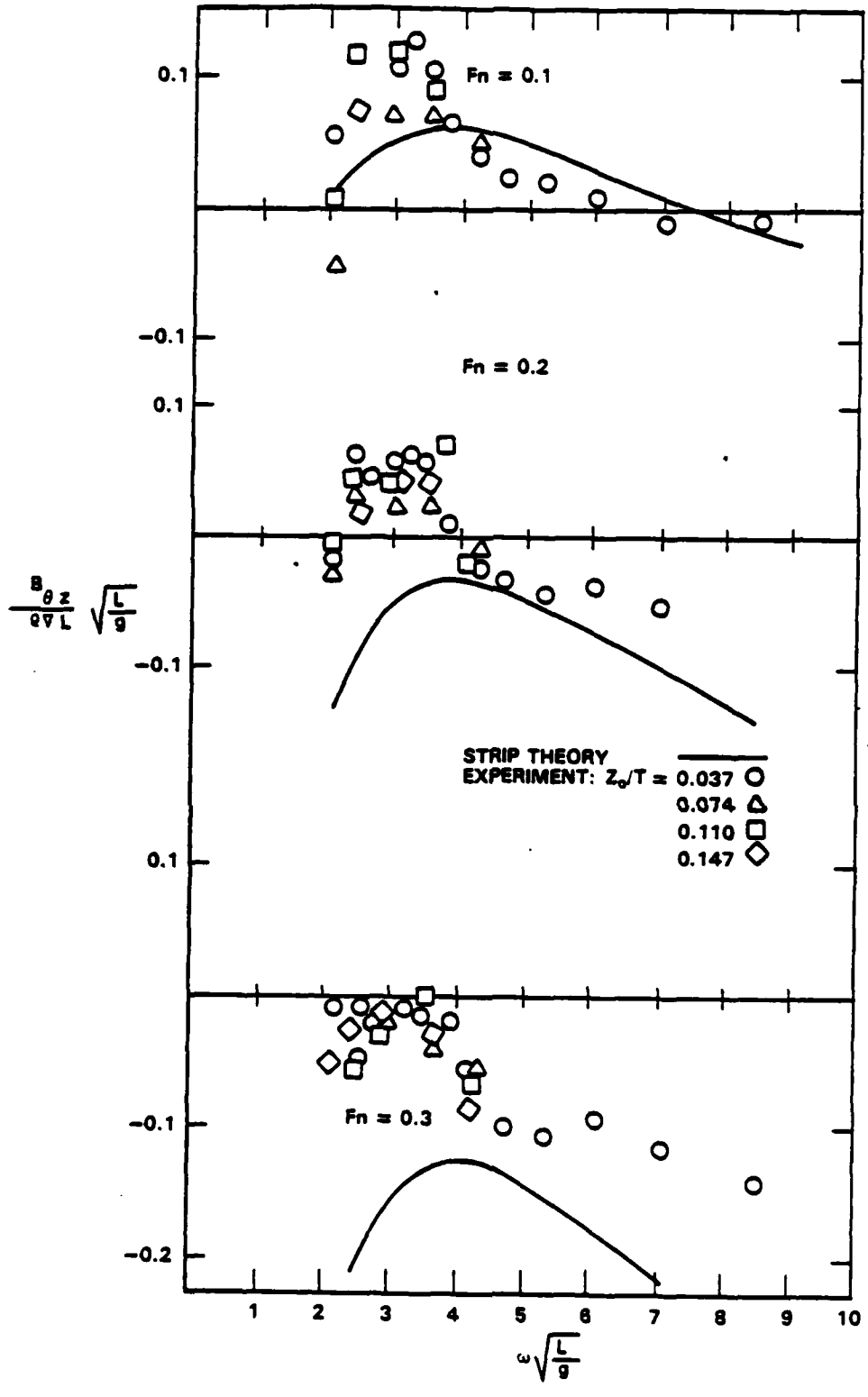

Figure 8 - Pitch-Heave Coupling Coefficient $B_{\theta z}$

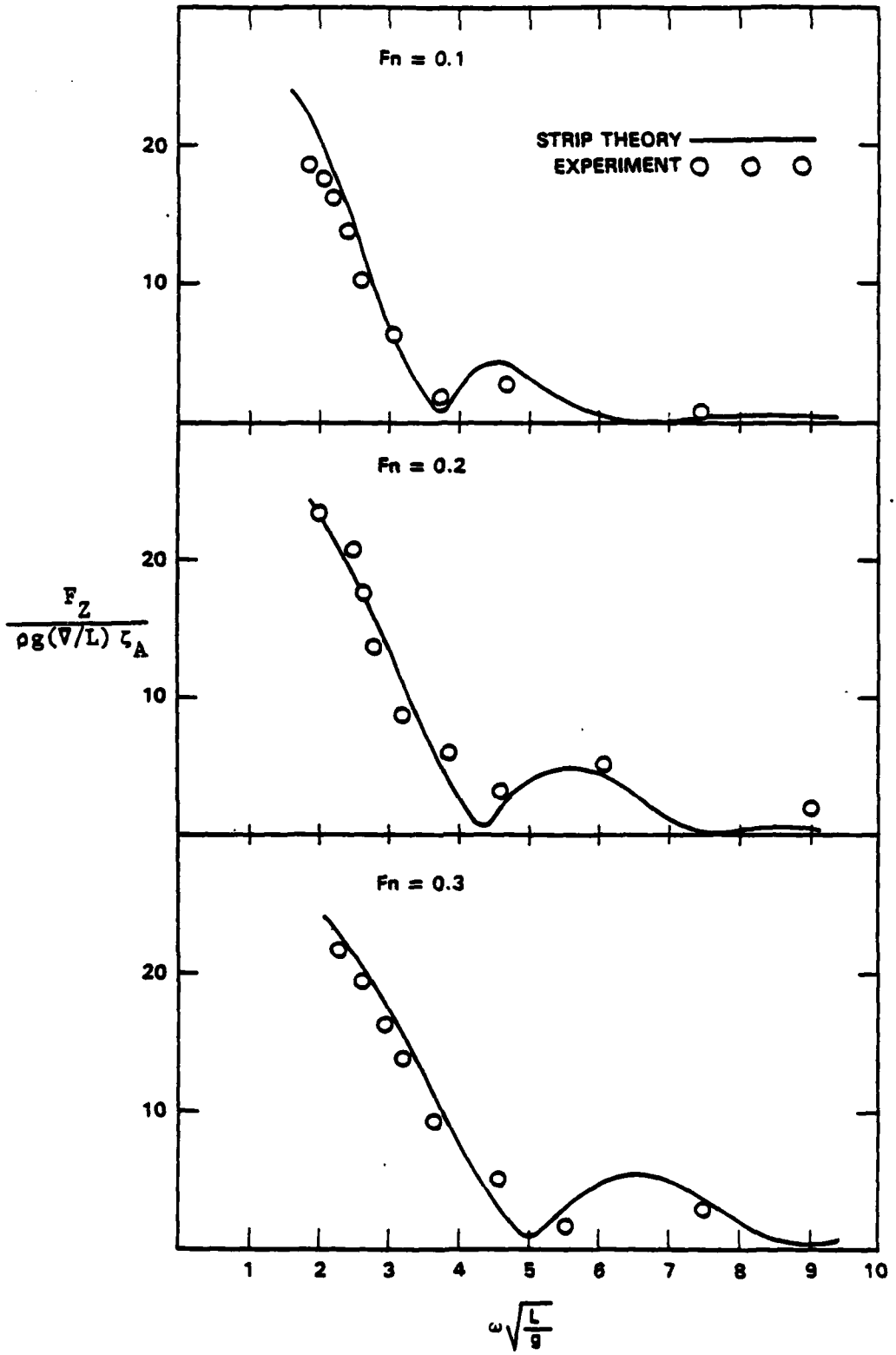

Figure 9 - Amplitude of Heave Exciting Force

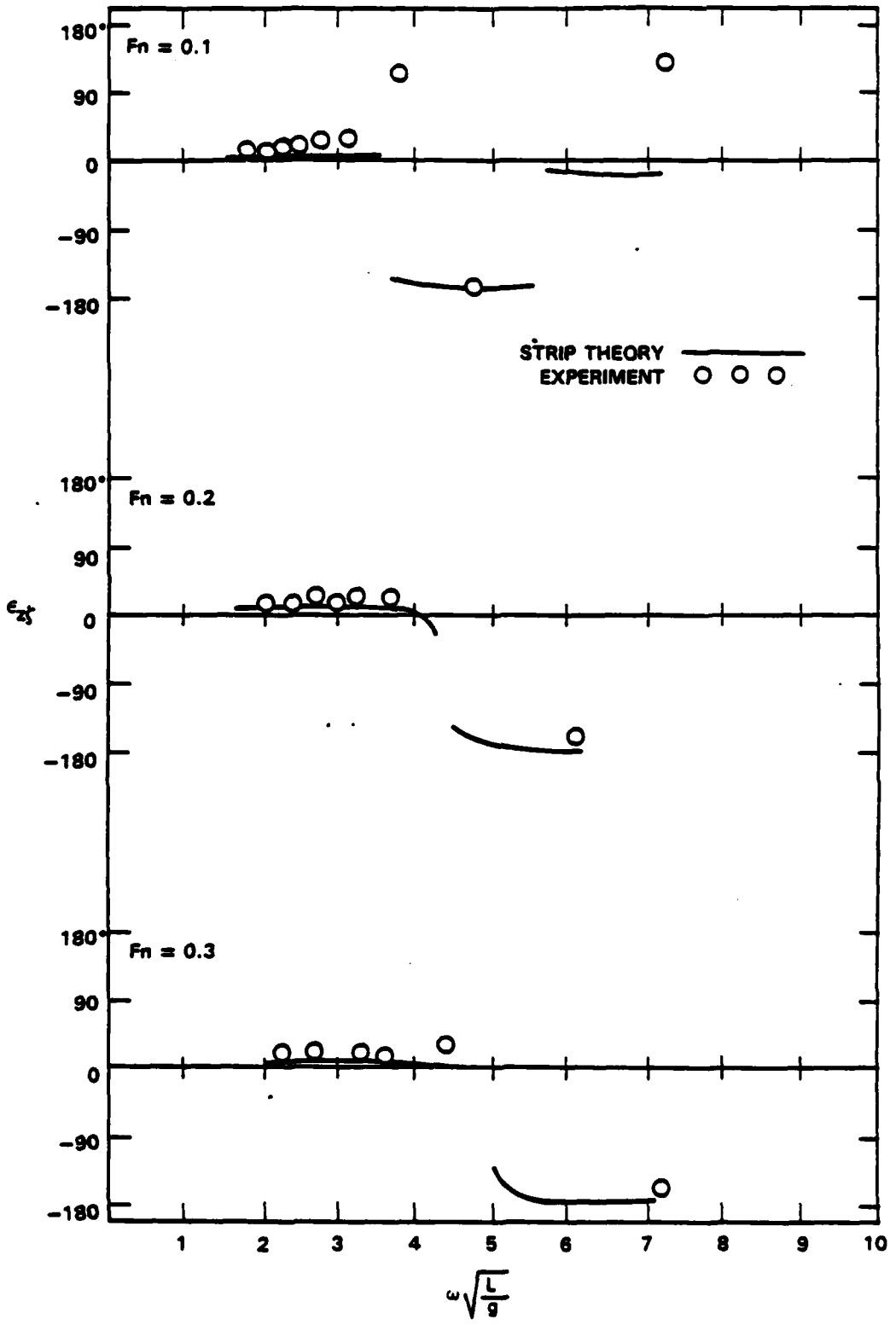

Figure 10 - Phase of Heave Exciting Force

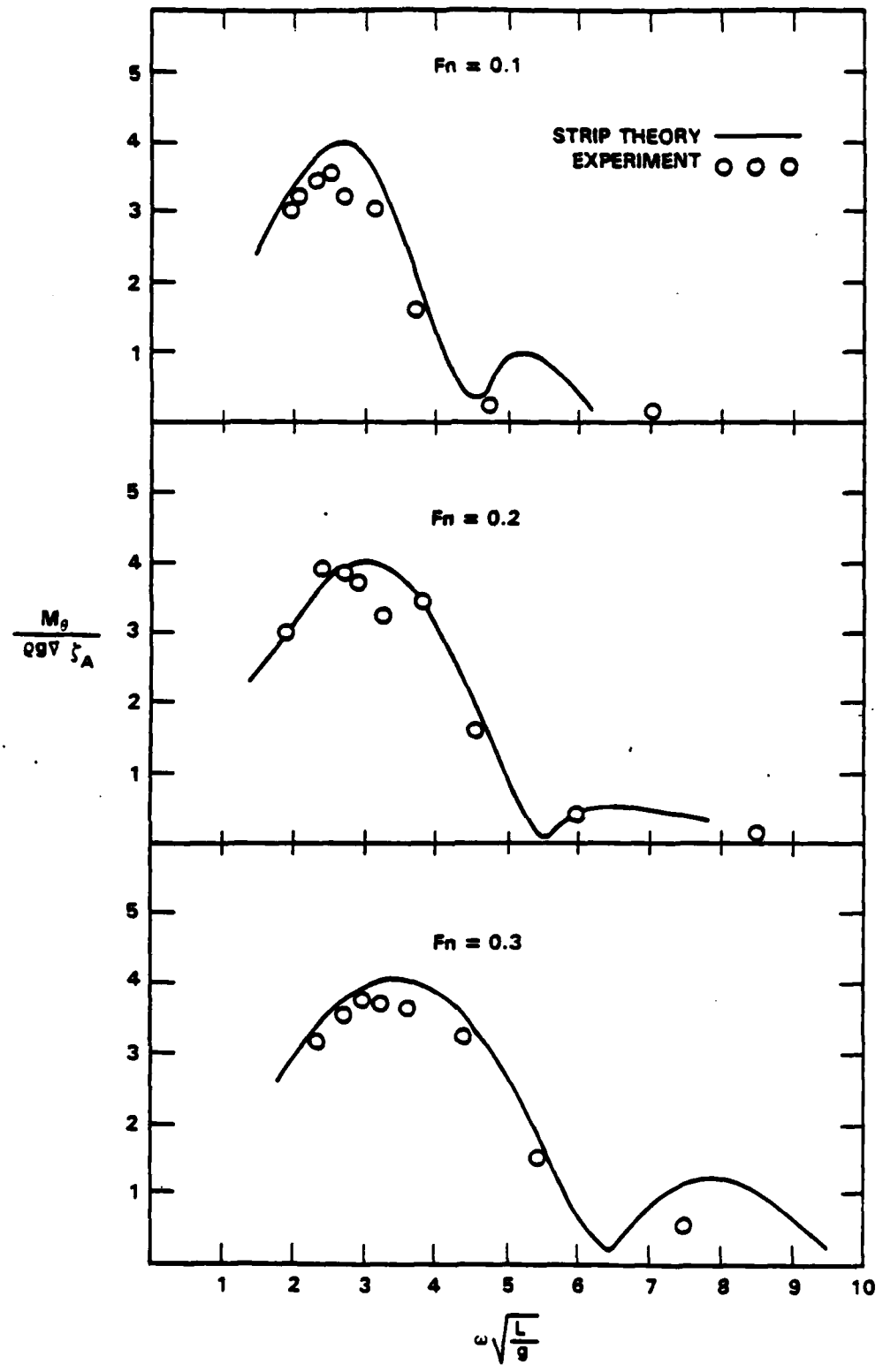

Figure 11 - Amplitude of Pitch Exciting Moment

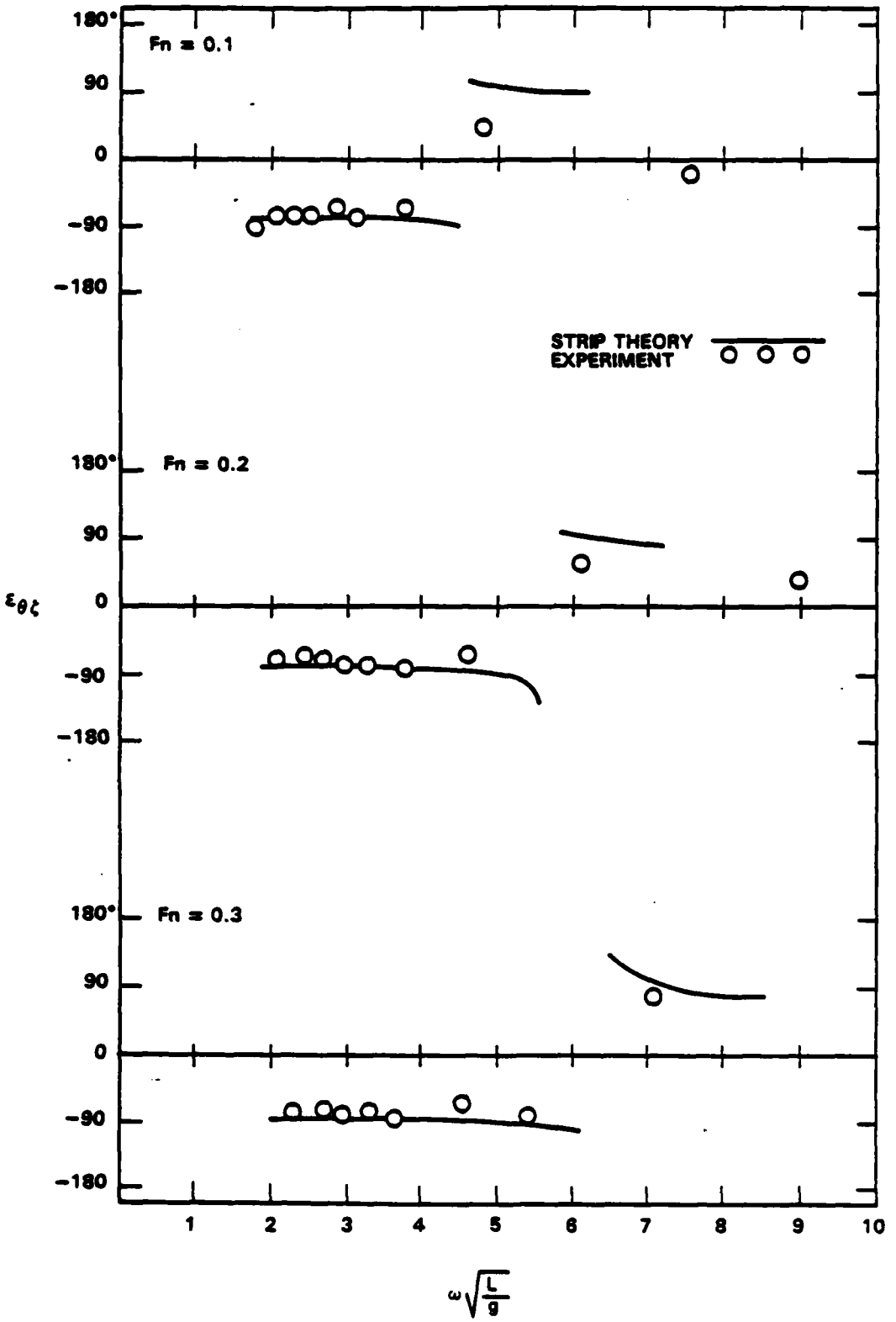

Figure 12 - Phase of Pitch Exciting Moment

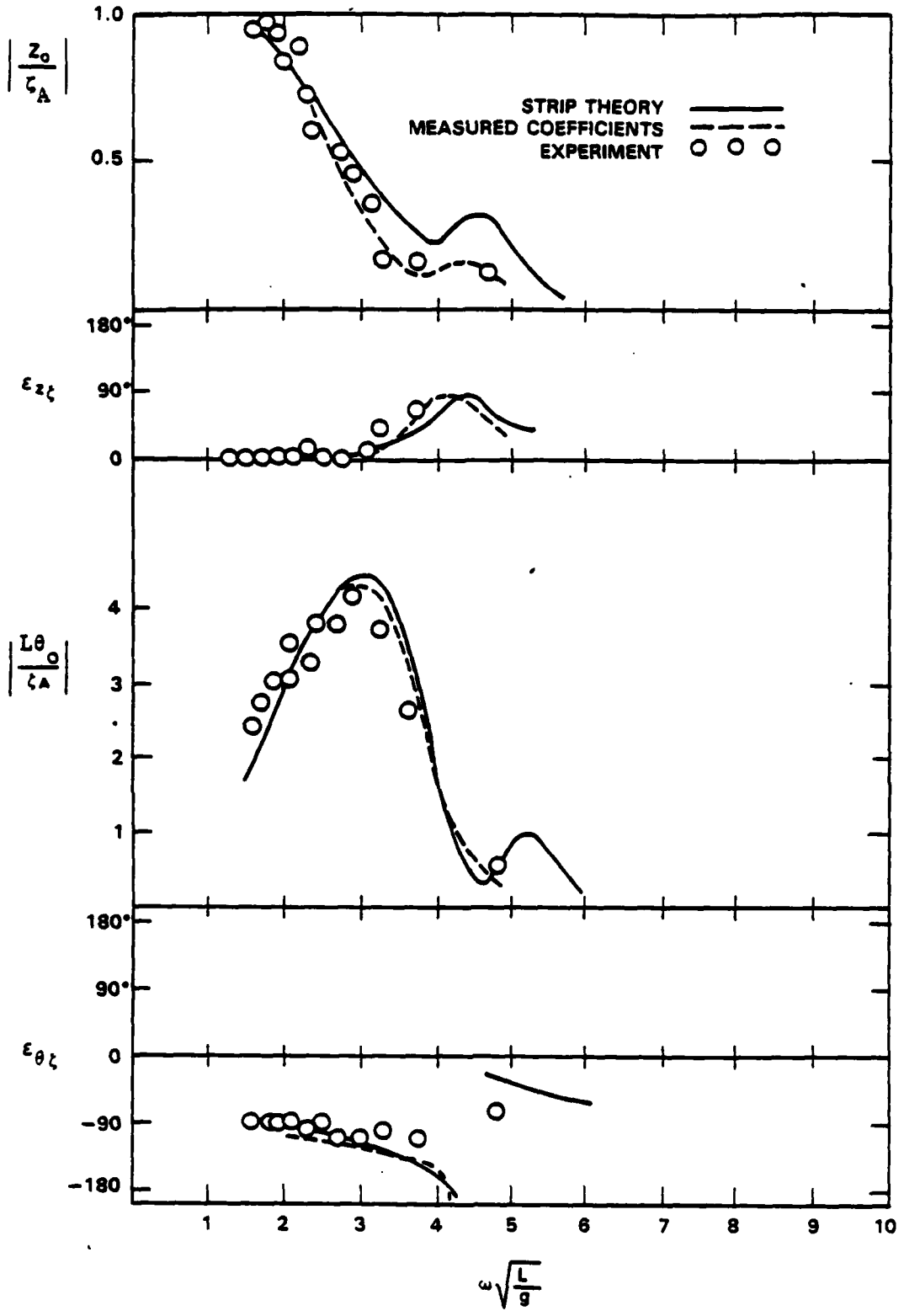

Figure 13 - Heave and Pitch Transfer Functions, Froude Number = 0.1

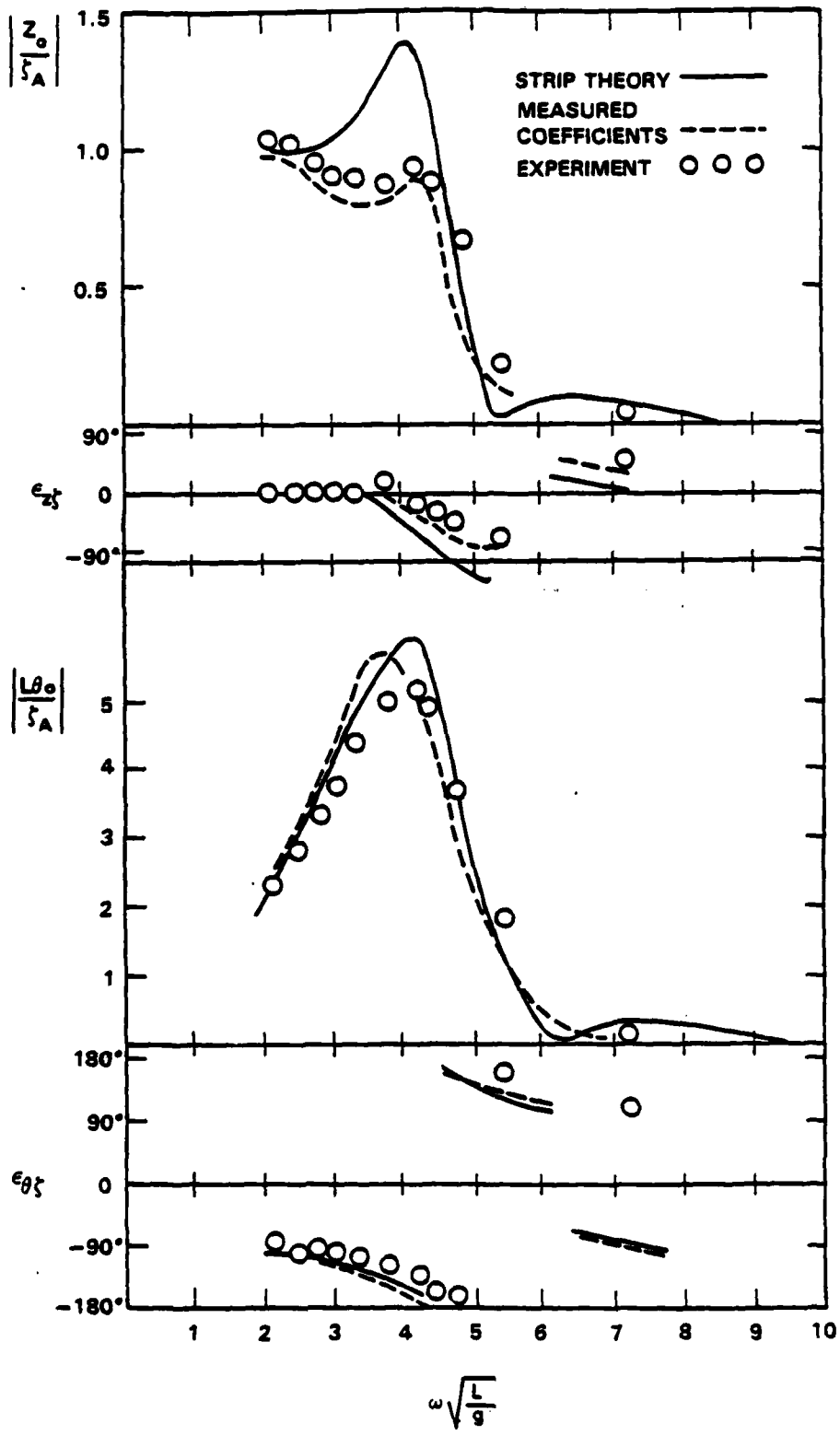

Figure 14 - Heave and Pitch Transfer Functions, Froude Number = 0.3

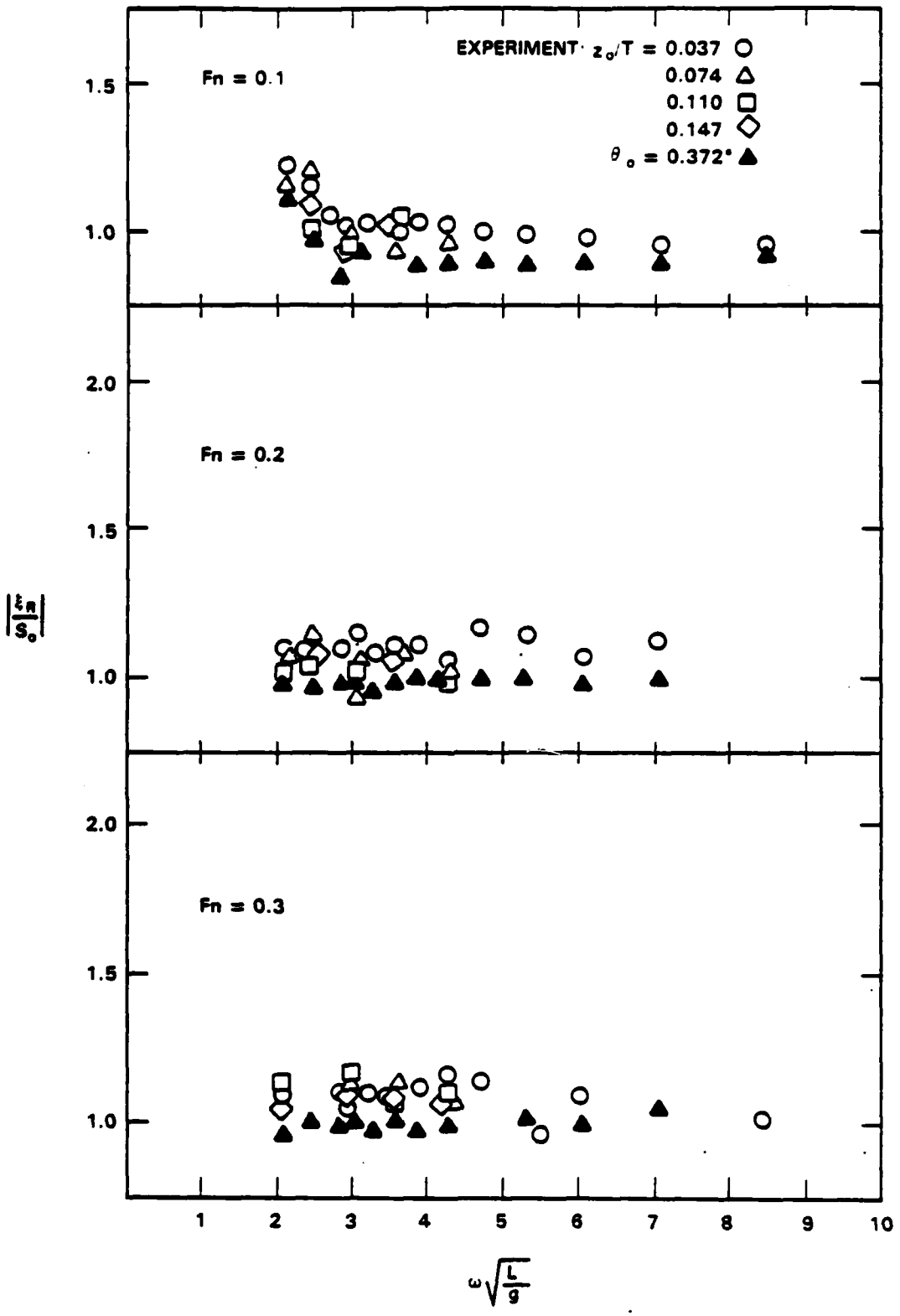

Figure 15 - Relative Motion at Station 0

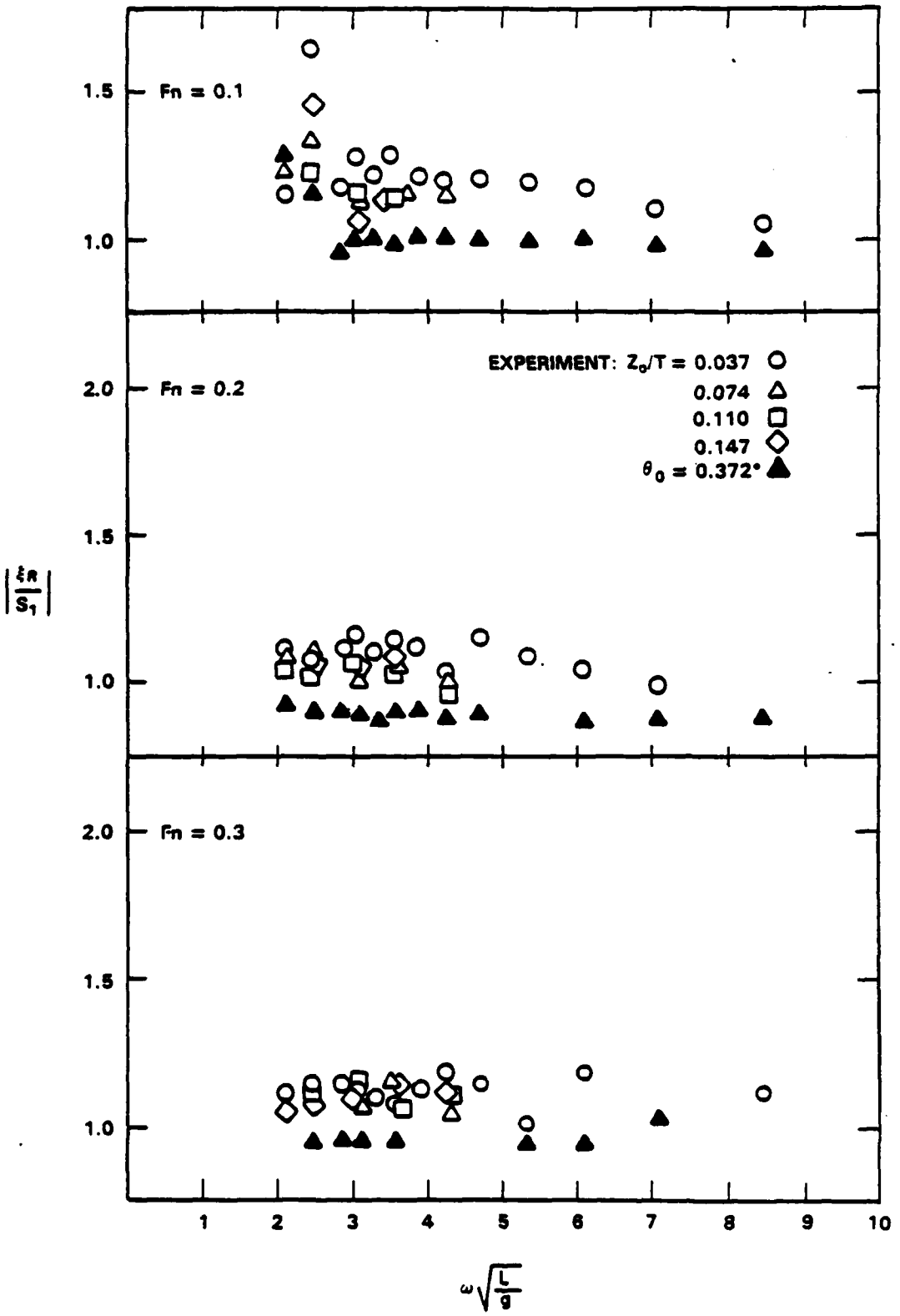

Figure 16 - Relative Motion at Station 1

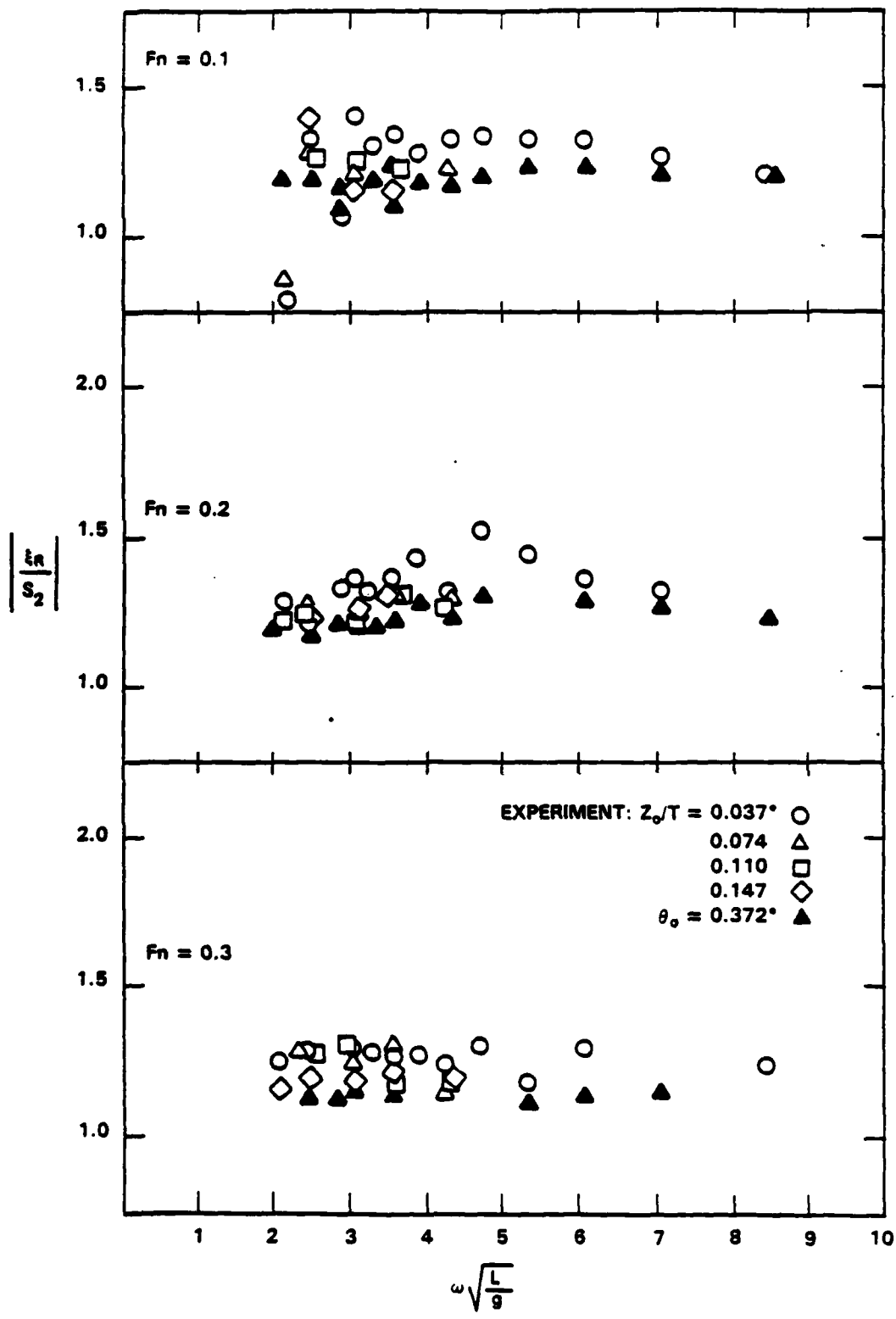

Figure 17 - Relative Motion at Station 2

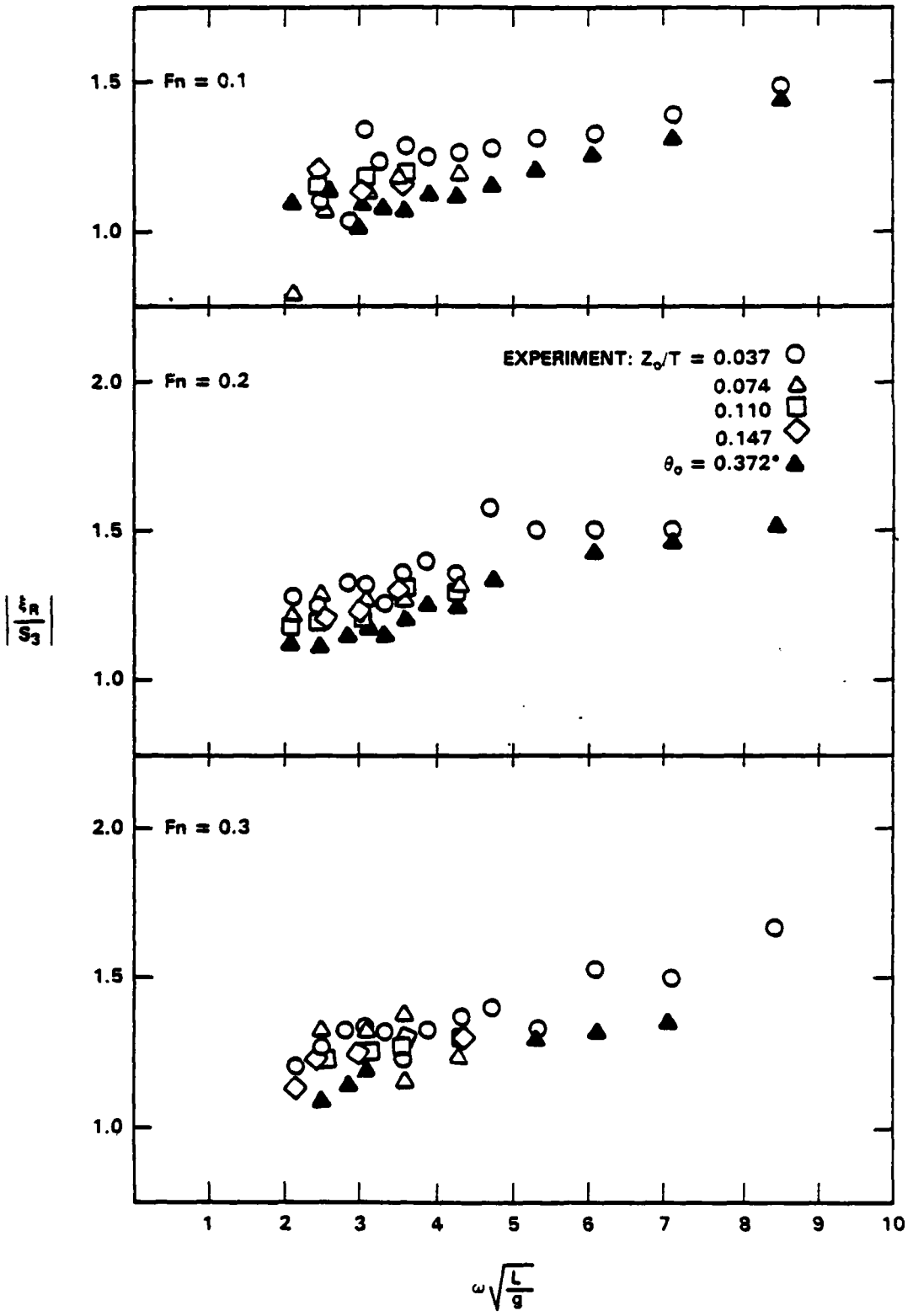

Figure 18 - Relative Motion at Station 3

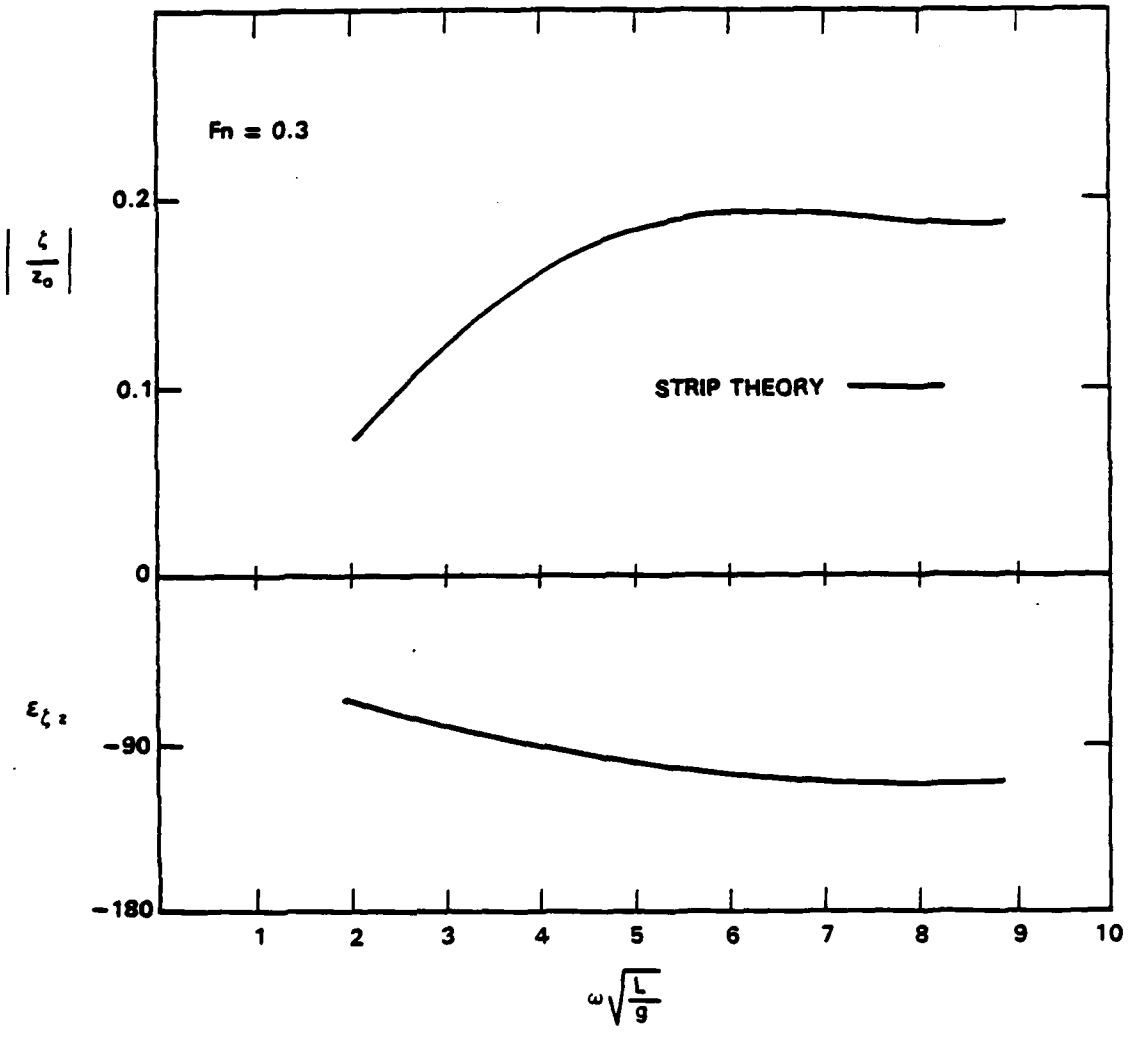

Figure 19 - Wave Component Caused by Heave Oscillation at Station 2

EXTENSION OF THE BALES SEAKEEPING RANK FACTOR CONCEPT

by

David A. Walden
David W. Taylor Naval Ship Research and Development Center

ABSTRACT

An additional term for the equation used to predict the Bales seakeeping rank factor R is described. This new term incorporates the effect of displacement, thus extending the usefulness of the predictor equation. Discussion and example applications of the new equation are given.

INTRODUCTION

The original work of Bales[1] on the seakeeping rank factor, R, was a milestone paper of particular interest to the naval architect, since it represented a breakthrough in an area for which no essential progress had been reported over the last 20 years. A means was now available for evaluating, and in fact ranking, ships in a quantitative sense, more specifically ship underwater hulls, on the basis of their seakeeping characteristics. (It should be noted that the seakeeping characteristics included in the R factor are vertical relative and absolute motions and accelerations of various stations and a slamming index, all calculated in head seas for a range of speeds and sea states.) Adding further to the value of the R factor, an equation was developed to predict R factor values based on six ship underwater hull characteristics. The previous work dealt with a group of 20 destroyer type ships all normalized to 4300t displacement. Based on the R factor predictor equation and the limits of the six ship characteristic values for

the group of 20 ships, values for the six characteristics were chosen that defined an 'optimum' ship.

Subsequent work by Bales and Cieslowski[2] describes the generation of an 'anti-optimum' hull. In that work, extensive calculations were carried out using the Navy Standard Ship Motion Program, for a range of speeds, headings, and sea states, of nine responses. These calculations were done for a series of geosims of the 'optimum' and 'anti-optimum' hull. These results were then used to establish ranges of operability index values as a function of displacement.

The operability index values are a function of the particular responses chosen and especially of the limiting values chosen for each response which are based on specified operations. However, for many applications the R factor may prove to be of value particularly when the details of ship missions and systems, which are required for the calculation of operability indices, are not available.

The present work will discuss a means of calculating R factors based on a more complete hull form description, rather than predicting R using only six ship hull characteristics. This method will then be used in an investigation of the effect of displacement on R factor values. Thus a means will be developed of comparing the seakeeping characteristics of different size destroyer type ships. This will make possible quantitative studies of the effect of increased displacement on improving seakeeping characteristics. Further, the present work will extend the R factor predictor equation to include the effect of displacement.

R FACTOR CALCULATION

For both the present effort and planned future work, a means of more quickly and efficiently calculating R factor values based on a hull form description was required. Since, as described in Bales,[1] the R factor essentially includes only pitch, heave, and related motions in head seas; a simple seakeeping program is entirely adequate. That chosen is described in Loukakis.[3] Lewis forms, and the MIT bulb are used to describe the hull form. Comparison with results for ships using Lewis forms in Bales[1] shows excellent agreement, e.g., an R factor of 6.53 for Bales Hull 14 which corresponds to R factor of 6.56 for the same ship using the present calculation.

The present program requires ship length as well as beam, draft and sectional area for 20 stations. Also included as a variable is a scale factor which allows R factors for geosims of a parent hull to be calculated. The results of interest are R factors and calculated displacements. It should be noted that the R factors are calculated as described in Bales.[1] Except for $(C_S)_3$, the average responses are inverted after being divided by their respective minima. This was also done in producing the results shown in Bales,[1] although not fully clarified in that text.

VARIATION OF R WITH DISPLACEMENT

Using the program described in the previous section, the variation of R with displacement for a number of ships was studied. Seakeeping computations were carried out and R's based on these results were then calculated. The R predictor equation was not used. Figure 1 shows the results. Each line represents R factor values for a series of geosims of a parent hull. 21N is

an 'optimum' hull form, Hull 14 is a representative modern destroyer hull form, and 22N is an 'anti-optimum' hull. The normalization factors used here are the same as those used in the original work, thus R factors greater than 10 and less than 1 are to be expected.

The figure indicates a 8000t version of each of the hulls would have the following R's:

Hull	R
21N (Optimum)	23.7
14 (Destroyer)	18
22N (Anti-optimum)	8.5

Hull 14 is seen to be closer to the optimum then the anti-optimum, but improvement is still possible in seakeeping performance.

Of perhaps even greater interest is the interpretation of the figure which shows the displacement required to achieve a desired R value, for example, if an R value of 9 is desired the hulls would require the following displacement:

Hull	Displacement
21N	3620t
14	5030t
22N	8210t

This shows quite dramatically the difference between the seakeeping performance of a very good hull form compared to that of a very bad hull form. A 3620t version of the good hull form would achieve the same seakeeping

performance as an 8210t version of the bad hull form; the bad ship requiring more than twice the displacement for the same performance.

Since calculated R's rather than predicted R's are being used, it is possible to compare R's for different displacement, that is non-normalized ships. For example,

Ship	Hull Geosim	Displacement	R
A	21N	4000	10.4
B	14	6000	11.8
C	22N	7000	6.3

Here Ship B would have the best seakeeping performance as measured by the R factor. Ship A is second, even though it has the best hull form, because the additional displacement of Ship B more than makes up the difference. Ship C is worst, its greater displacement not being able to overcome the disadvantage of its hull form.

EXTENDED R FACTOR

Using the results shown in Figure 1, an additional term can be added to the R factor predictor equation to incorporate the effect of displacement. In order to maintain consistency with the other terms, a linear term in a nondimensional ship characteristic is required. Using normalized displacement variation and the average of the slopes of the 21N and 22N curves, this additional term is given by:

$$\frac{12.9\ (\Delta - 4300)}{4300}$$

where displacement Δ is in tonnes. The R factor predictor equation thus becomes:

$$\hat{R} = 8.422 + 45.104\ C_{WF} + 10.078\ C_{WA} - 378.465\ T/L + 1.273\ c/L$$
$$- 23.501\ C_{VPF} - 15.875\ C_{VPA} + 12.9\ \frac{(\Delta - 4300)}{4300}$$

where all notation is as in Bales.[1] The range of displacement is limited to 3000t to 9000t.

CONCLUSIONS

The usefulness of the R factor has been increased by extending the predictor equation to include displacement. It should however, be remembered that it is always dangerous to attempt to summarize such a complicated phenomenon as seakeeping in a single number. All the caveats concerning the R factor cited in Bales[1] still apply and should be carefully reviewed before any application is attempted. Using R factors based on seakeeping computations avoids the problem of the limited range of the input parameters associated with the predictor equation, but caution is still required.

ACKNOWLEDGEMENTS

Funds were provided by the Surface Ship Hydromechanics Program under Project Number 62543N, Block Number SF-43-421-301. The work was performed at the David W. Taylor Naval Ship Research and Development Center (DTNSRDC) where Work Unit Number 1506-103 was used to identify the work.

REFERENCES

1. Bales, N.K., "Optimizing the Seakeeping Performance of Destroyer-Type Hulls," 13th Symposium on Naval Hydrodynamics, Tokyo, Japan (1980).

2. Bales, N.K. and D.S. Cieslowski, "A Guide to Generic Seakeeping Assessment," Naval Engineers Journal (1981).

3. Loukakis, T.A., "Computer Aided Prediction of Seakeeping Performance in Ship Design," MIT Report No. 70-3 (1970).

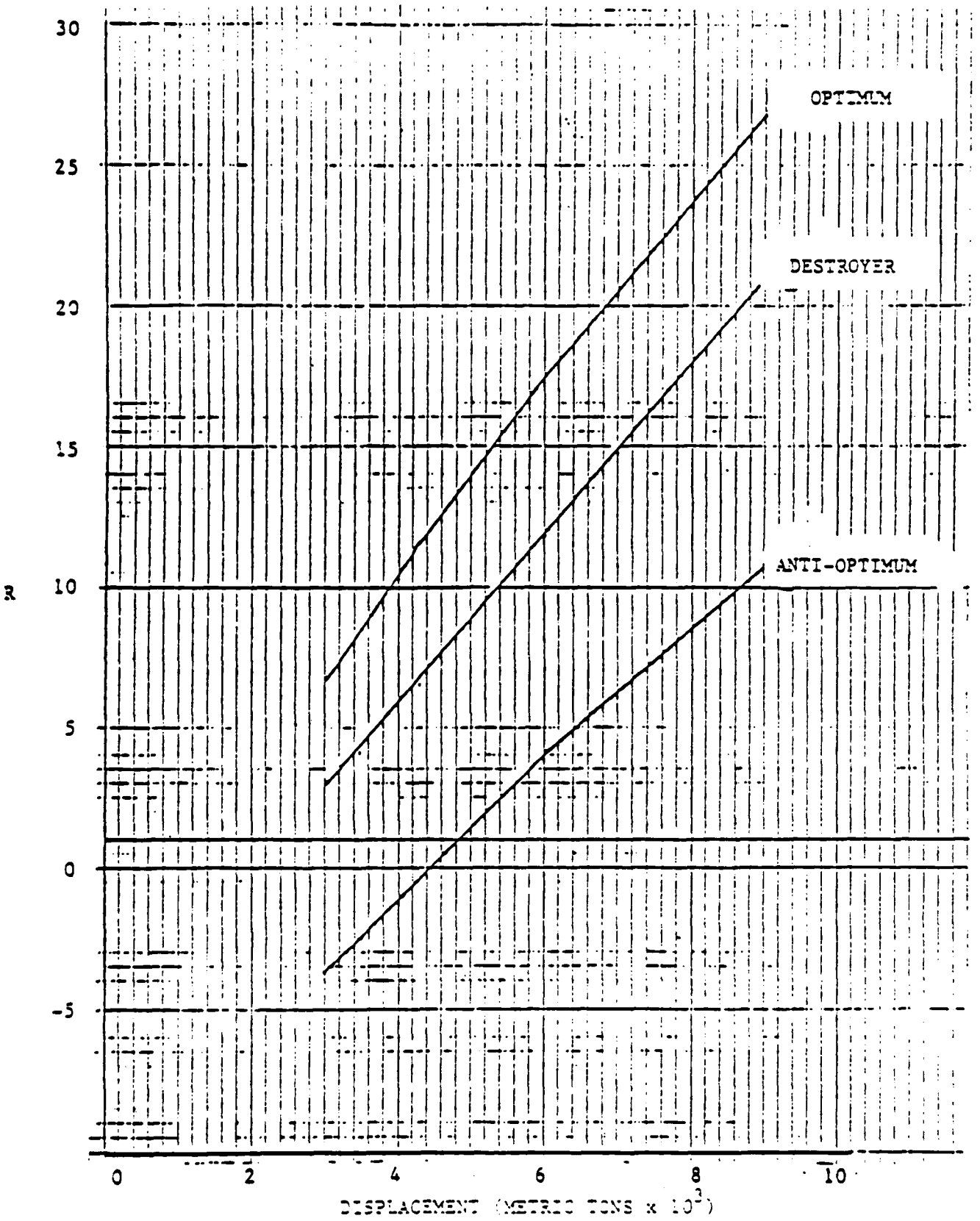

Figure 1 - Variation of R with Displacement

DISCUSSIONS

Bruce Johnson
U.S. Naval Academy

My congratulations on a very useful extension of the Bales Seakeeping rank factor. I was always bothered by the conclusion in Reference 2 in your paper that the DD-963 hull form ranked very low when discussions with ship captains indicated otherwise. The displacement corrections puts a better perspective on the concept of rank factor. I also appreciate your careful attention to caveats. Since deck wetness is not considered in the rank factor, a good underwater design might have a poor above waterline form and vice versa. I have reservations about putting Bales "drooping bow" which lacks adequate freeboard at the stem from a deck wetness point of view with an otherwise good underwater hull form and calling the results optimum.

A.R.J.M. Lloyd
U.S. Naval Academy

The regression equation suggests that a shallow draught is beneficial for seakeeping. Common sense would suggest that this would encourage frequent slamming. Would the author care to comment?

The British LEANDER frigate has a ranking of about 3.6 under the original equation. Inclusion of the new term in displacement (approximately 3000 tons) will reduce this to about zero, in spite of the ships widely accepted reputation for good seakeeping. This result calls into question the validity of the rank concept when compared with practical experience at sea.

AD-P003 829

COMPARISON OF THEORETICAL SEAKEEPING PREDICTIONS WITH MODEL TEST RESULTS FOR A WIDE BEAM FISHING VESSEL

T.O. Karppinen
Arctic Vessel and Marine Research Institute
National Research Council
Ottawa, Canada

ABSTRACT

Motion transfer functions and phase lags computed by linear strip theory for a very wide and short fishing vessel are compared with model test data and theoretical results determined by the three-dimensional, linear sink-source method. Results are presented for beam waves at zero speed and for head seas at the trawling speed and at the top speed. Heave in head seas is predicted by the strip theory equally well for this wide beam vessel as for more slender, ordinary hulls. Problems arise in pitch prediction, particularly at the higher speed. Roll computed by a new strip theory computer program is in close agreement with experimental roll data. The strip theory gives either a much better or at least equally good fit to the model test data than the three-dimensional method.

INTRODUCTION

There seems to be a growing interest in the seakeeping of smaller craft, such as yachts, supply vessels and fishing vessels, which often are short and broad. It is well known that the linear strip theory, due to its basic assumptions, is not particularly well suited to predicting wave induced motions of vessels with low length to beam ratio. In a comparison made by Bales et al. (1975) the strip theory overpredicted heave and pitch of a fishing vessel in head seas roughly by a factor of two. Use of the dynamic waterline in the computations did not improve the prediction accuracy (Watkins & Bales, 1976). The poor correlation may have been due in part to the high Froude number used in the tests. It has been generally observed that the strip theory usually fails to predict heave and pitch accurately at Froude numbers higher than approximately 0.3 even for quite slender ships. This has been for instance pointed out by Dalzell (1977) in his review of published strip theory correlations with experimental data and by Murdey (1980) in a paper dealing with accuracy of the strip theory heave and pitch predictions for a systematic series of destroyer type hulls.

The three-dimensional nature of the flow around a wide hull is taken into account in the three-dimensional, linear sink-source method, but the computations are very time consuming compared with the computations by the strip theory and computer programs based on the sink-source method are not nearly so generally available as strip theory programs. Furthermore, at low speeds heave and pitch depend mainly on the hydrostatic terms, which the strip theory predicts correctly. Thus, there seems to be an understandable temptation to apply strip theory also to wide beam vessels violating quite badly the basic assumptions of the method.

The present paper tries to sound the boundaries of the strip theory by comparing strip method predictions for an extremely wide fishing vessel with model test data and with results computed by the three-dimensional sink-source method. At the A.V.M.R.I., as part of a study concerning seakeeping of fishing vessels, motion transfer functions and phase lags of a model with length to beam ratio of 2.4 have been measured in regular beam and head waves. In the head wave runs the Froude numbers of 0.19 and 0.38 were somewhat smaller than in the investigation of Bales et al. (1975). The lower Froude number corresponds approximately to the trawling speed.

MODEL TESTS

Seakeeping tests were carried out in the towing tank of the A.V.M.R.I. with a wooden model representing a prototype wide beam fishing vessel at a scale ratio of 1:8. The model was built up to the top of bulwark both on the forecastle deck and on the main deck. Main particulars of the full sized vessel are given in Table 1 and the body plan of the vessel is shown in Figure 1. Characteristics of the vessel are a hull formed of developable surfaces with two hard chines and a wide transom stern, which was just out of water at the shallower draft tested and

approximately one-third submerged at the deeper draft. The vessel also has a large skeg. The model was equipped with a working propeller in a nozzle, which in the prototype is turning and is intended to be used also for manoeuvring. Thus, the model did not have a separate, conventional rudder.

In head seas the model was tested at two draughts, shallow and deep, which correspond to the departure and arrival displacements, respectively. At both loading conditions tests were conducted at Froude numbers of 0.19 and 0.38 corresponding to 5 and 10 knots in full scale. In beam seas the test program comprised three loading conditions; the shallow and deep draughts as tested in head waves and the model ballasted to an additional lower metacentric height (GM) at the deep draught. Beam wave tests were made only at zero speed.

Motion transfer functions and phase lags were determined by measurements in regular waves with various lengths. Due to difficulties in controlling the waveheight the wave slope was not constant throughout the tests. In the range of frequencies covering the roll natural periods of the model in the tested loading conditions the wave steepness varied from 1/50 to 1/30, the wave height remaining approximately constant. In short waves the wave steepness varied from 1/30 to 1/20.

In the head sea runs the standard measurement procedure of the A.V.M.R.I. was used. In order to maintain the model speed of advance the same as the speed of the carriage the model was self-propelled with manual rpm control. Two vertical guide poles kept the model on straight course under the carriage. The model was free to move in surge, heave and pitch. The longitudinal movement of the model with respect to the carriage was measured by a sonic probe. A similar transducer was used for recording the waves encountered. Heave and pitch were determined from vertical accelerations measured at bow, longitudinal center of bouyancy and stern. Spectral analysis was used to determine the motion amplitudes and phase lags.

In beam waves the model was virtually free to move in all six degrees of freedom. In order to measure the transverse drift force (not discussed in this paper) the model was connected to the carriage through thin fishing lines and prestressed, long rubber bands. The two fishing lines pointing diagonally upwards from the model bow and stern were fixed on the centerline of the model approximately at the height of the waterplane. Before the measurements were started the model was allowed to drift to a stable position. However, at some higher wave frequencies the model tended to change heading, since the mooring system was very soft. Thus, the heading during the test runs was not always exactly beam on. This excited pitch motion which also influenced heave due to the quite strong heave-pitch coupling resulting from the wide transom stern. In short waves the change of heading has probably had some effect on the scatter of data.

Again accelerometers fixed in the model provided the basic data for determining sway, heave and roll displacements. In addition a roll gyro was installed to give a direct reading of roll angle. The roll angles obtained from the accelerometers and from the gyro were found to be identical.

A typical feature of using a sonic wave probe in short, steep waves is to get some sharp spikes in the recording. The spikes can have a significant effect on the spectrum. Therefore prior to spectral analysis the spikes were removed numerically. In some cases it was impossible to remove all the spikes without on the same time distorting the wave signal. In these cases several short, clean parts of the recording were analysed separately. The unclean wave recordings have probably had some effect on the scatter of data at high frequencies.

THEORETICAL COMPUTATIONS

Transfer functions have been computed by the strip theory for all the tested loading conditions and speeds using two computer programs: SMP81, described in Meyers et al. (1981), and HANSEL, described in Meyers et al. (1975). The programs were developed at the David W. Taylor N.S.R.D.C. SMP81 is a new, revised version of HANSEL. Motion transfer functions computed by SMP81 are compared with model test data in the report Baitis et al. (July 1981) and the improved roll damping prediction method of the new program has been validated in the report Baitis et al. (June 1981). Overall good agreement was found between theory and experiment for naval type vessels. Both SMP81 and HANSEL are based on the strip theory of Salvesen et al. (1970) and use Frank's (1967) close-fit source distribution technique for solving the two-dimensional potential flow problem in the cross-section planes.

The main differences between the programs are that SMP81 takes into account the speed-dependent dynamic lift damping due to the hull and appendages, which is neglected in HANSEL, and SMP81 provides seakeeping predictions also for irregular seas while HANSEL computes just the regular wave responses. However, these differences are not relevant from the point of view of the present study, since model test data for roll are only available at zero speed and all comparisons are made between theoretical and experimental transfer functions and phase angles. In addition the viscous roll damping in HANSEL has been modified in the SMP81 program on basis of recent Japanese work. Finally there are differences between the two programs as far as hull definition is concerned. In HANSEL a hull cross section is approximated by a polygon defined by maximum of eight offset points, while SMP81 allows ten offsets and fits a curve through the points using a parametric spline routine. By this latter method conventional rounded hull forms can be described well. Considering the

fishing vessel hull with two hard chines and a large skeg ten offset points were too few to concentrate a couple of points at the chines in order to get really sharp corners. However, it is considered that the slightly crude representation of the station shape has had probably only a minor effect on the computed results. Zero speed added mass and damping coefficients for the total hull predicted by SMP81 and HANSEL were found to be in fairly good agreement.

The same set of input offsets for fourteen stations were used both in SMP81 and HANSEL. In SMP81 the skeg was defined with four points per station and in HANSEL with just two. In HANSEL the cross-sectional area of the extreme forward and aft stations is set to zero. At the deeper draft this caused a loss of displaced volume of about five percent.

The strip theory of Salvesen et al. (1970) incorporates in the coefficients of the equations of motion and in the exciting forces several forward speed dependent end terms associated with the added mass, damping and diffraction of the aftermost section. The HANSEL program has the provision of adding the end terms to the coefficients while SMP81 disregards the end-effects. In some cases better correlation with experimental data for ships with wide transom sterns has been obtained with the end terms included (Salvesen et al. 1970).

The computer program used for determining the transfer functions by the three-dimensional method is based on the approach described by Garrison (1974). The original program written by Dr. Garrison was modified at the Ship Laboratory of the State Research Centre of Finland to incorporate a triangular element and the provision of including the effect of low forward speed.

In this three-dimensional approach the wetted surface of the body is subdivided into small, plane quadrilateral or triangular elements. Stationary pulsating sources are distributed over the wetted surface, at the centroid of each element. The source strengths, assumed constant over the area elements, are solved numerically from an integral equation obtained by applying the body boundary condition. The velocity potentials are finally determined as summations of contributions from each source potential.

The effect of speed of advance is taken into account within this framework in an approximative way as described by Inglis & Price (1979 and 1980). The strip theory assumptions of low forward speed and high frequency of oscillation are retained in order to neglect the forward speed dependence of the free surface condition. Thus, the velocity potentials satisfy the classical, linearized zero speed boundary condition on the free fluid surface. In fact, the approach is similar to the strip theory of Salvesen et al. (1970) up to their equations (98) - (100). While Salvesen et al. determine the speed independent unit potentials appearing in the

equations (98) - (100) by applying the strip method and circumvent the diffraction problem by using Haskind relations with the strip method, in this three-dimensional approach the speed independent potentials are solved by the three-dimensional source distribution technique outlined in the preceeding paragraph.

For the fishing vessel 126 elements were used to represent the underwater part of the hull at the deep draft and 122 elements at the shallow draft. Most of the elements were quadrilaterals but a few triangular elements were used at the forebody. The coordinates of the corners of the elements were mainly taken from the input offsets to the strip theory computer programs SMP81 and HANSEL. Due to limitations of computer capacity a more sparse station subdivision had to be used in the three-dimensional computations than in the computations by the strip method.

Transfer functions were computed by the three-dimensional method for the deep draft, large GM loading condition in beam waves at zero speed and for the speed of 10 knots in head seas. At the shallow draft results were computed only for the beam seas.

COMPARISON OF THEORETICAL RESULTS WITH EXPERIMENTAL DATA

Examples of typical correlation between theoretical non-dimensional transfer functions and model test data are presented in Figures 2-7. The translational displacements, sway and heave, are made non-dimensional dividing the response amplitude by wave amplitude and the angular displacements dividing by the maximum wave slope. Responses are expressed as functions of non-dimensional incident wave frequency. Length between perpendiculars and acceleration of gravity have been used in non-dimensionalizing the wave frequency. Phase lag of sway in beam seas is expressed relative to heave. In the figures model test data are represented by open squares and triangles, results computed by the three-dimensional sink-source method by stars, SMP81 results by a continuous line, results computed by HANSEL the end terms neglected by a dashed line and HANSEL results the end terms included by a dashed line with dots.

In order to provide a quantitative measure of the agreement between experiment and theory the motion indices of correlation, defined by Dalzell (1977), have been used. These indices are defined as the largest deviation between theory and experiment divided by the largest experimental value, in percent. The values of the indices are given in Table 2 for heave and pitch in head seas and in Table 3 for sway, heave and roll in beam seas. In Table 2 the frequency range where the largest deviation between theory and experiment occurs has been indicated by the three words short, peak and long, short referring to short waves, peak to the frequency range around the peak response and long to long waves, where the model has been conturing the waves.

A negative index of correlation indicates that the theory underpredicts the response at the largest deviation. Due to the larger scatter of experimental data in beam sea tests the values of the indices of correlation in Table 3 are more approximative than in Table 2 and the frequency range and sign of the maximum deviation have not been given.

Head Seas

Comparing the indices of correlation in Table 2 with the values presented in Dalzell's (1977) general review on the accuracy of the strip theory it may be seen that the strip theory predicts heave equally well for this wide beam vessel as for more slender-hulled ordinary ships. Contrary to the general trend in Dalzell's Table 1 the accuracy of the pitch prediction is in this case much worse than the accuracy of the heave prediction.

The strip theory gives a significantly better correlation with experimental data than the three-dimensional method. The differences between the strip theory predictions and the predictions by the three-dimensional sink-source method are surprisingly large considering the quite close agreement obtained by Inglis & Price (1980) for a fine form ship at a Froude number of 0.15. It seems that the combination of wide hull and quite high Froude number is too much for the approximative way in which the effect of forward speed has been taken into account in the three-dimensional method.

Inclusion of the end terms shifts the transfer functions predicted by the strip theory towards the results of the three-dimensional method, but still the results of the two methods are far apart. The end terms have only a minor effect on heave at the lower speed. At the higher Froude number and particularly for pitch the peak of the transfer function is considerably underpredicted when the end terms are added to the coefficients. In short waves, where the largest deviations between the strip theory heave prediction and experimental data are, the end terms lift the transfer function slightly closer to the model test data. The three-dimensional method overpredicts in short waves particularly for pitch.

A surprising result is that the largest difference between pitch predicted by SMP81 and the experimental data is at low frequencies, where the model has been in practice conturing the waves. Since the strip theory has the correct hydrostatic terms it should give the right limiting values of heave and pitch in long waves. Without the end terms the older strip theory computer program HANSEL seems to predict the long wave limit of pitch quite well, but when the end terms are included at the higher speed a pitch transfer function increasing with decreasing frequency is obtained at low frequencies.

The phase lags are, in general, quite well predicted by the strip theory. The largest deviation between theory and experiment occurs at the higher Froude number in short waves, where the strip theory gives heave and pitch phase angles sharply decreasing with increasing frequency while the experimental data shows a slightly increasing trend.

Beam Seas

Roll is amazingly well predicted by SMP81 while HANSEL underestimates the magnitude of the roll peak roughly by a factor of half. The three-dimensional method does not take into account viscous damping so that comparison with experimental roll is not meaningful at the roll natural frequency. Outside of the resonance peak the roll predicted by the three-dimensional method agrees well with the model test data. At the deep draft, the largest deviation between the experimental roll and the prediction by the three-dimensional method, given in Table 3, is measured quite close to the roll resonance frequency. The somewhat larger roll index of correlation for SMP81 at the deep draft small GM loading condition is due to a small shift of the theoretical transfer function towards low frequencies compared with experimental data. This discrepancy could result for instance from a small inaccuracy in the estimate of the roll gyradius of the model.

The model test sway data seems to indicate a peak in the sway transfer function at a slightly higher frequency than the roll natural frequency and a minimum point just before the roll peak. The theoretical sway transfer functions have a peak approximately at the roll natural frequency. It is interesting to note that in this same frequency region the experimental sway phase lag relative to heave has a distinct minimum while the strip theory predicts a maximum. The sway phase lag computed by the three-dimensional method falls in this region closer to the experimental data than the prediction by the strip theory. In general the three-dimensional method gives perhaps a slightly better fit to the model test sway data than the strip method.

In the range of frequencies of large rolling the model test heave data is quite scattered and the scatter seems to follow an oscillating pattern. There seems to be no obvious explanation for an oscillatory behaviour of the heave transfer function. The linear strip theory and the three-dimensional method predict that the heave of the vessel should follow closely the wave displacement in this frequency region. In short waves both the strip theory and the three-dimensional method overpredict heave, the results of the two theoretical methods being in fairly close agreement.

CONCLUSIONS

The strip theory predicts heave in head seas for this extremely wide and short fishing vessel equally well as for more slender ordinary ships. Contrary to the general trend with ordinary ships pitch is not so well predicted. Problems in pitch prediction arise at the higher Froude number at the peak response and, surprisingly, in long waves, where the model has been conturing the waves. Although the vessel has a wide transom stern the inclusion of the end terms impairs the correlation with experimental data. With the end terms added the pitch response peak is considerably under-predicted. The three-dimensional sink-source method with the effect of forward speed taken into account in an approximative way gives in head waves a much worse fit to the experimental data than the strip theory. In beam waves at zero speed heave and sway computed by the two- and three-dimensional theories are in fairly close agreement. Roll in beam waves at zero speed is very well predicted by the new strip theory computer program with improved roll damping prediction. The maximum roll response is in good agreement with experimental data indicating that the semi-empirical method used in estimating the viscous damping applies fairly well also for this quite extreme hull form. Considering this vessel there seems to be no benefit in using for motion transfer function prediction the much slower sink-source method.

ACKNOWLEDGEMENT

The study reported here has been conducted while the author has been working as a visiting scientist at the Arctic Vessel and Marine Research Institute. The author is very grateful to the National Research Council for the possibility to work in Canada. The computations by the three-dimensional sink-source method have been carried out at the Ship Laboratory of the Technical Research Centre of Finland by Mr. S. Kalske. The permission to use the program and the contribution of Mr. Kalske are gratefully acknowledged. Finally the author wishes to express his gratitude to Mr. D.C. Murdey who critically reviewed the manuscript and suggested important improvements.

REFERENCES

Baitis, A.E. et al.. Validation of the Standard Ship Motion Program, SMP: Improved Roll Damping Prediction. DTNSRDC Report SPD-0936-02, June 1981.

Baitis, A.E. et al. Validation of the Standard Ship Motion Program, SMP: Ship Motion Transfer Function Prediction. DTNSRDC Report SPD-0936-03, July 1981.

Bales, N.K. et al. Validity of a Strip Theory-Linear Superposition Approach to Predicting the Probabilities of Deck Wetness for a Fishing Vessel. DTNSRDC Report SPD-643-01, November 1975.

Dalzell, J.F. Experiment-Theory Correlation: Linear Ship Motion and Loading Theory. Proc. of the 18th ATTC, Vol. 2, Seakeeping Session, Annapolis, Maryland, August 1977.

Frank, W. Oscillation of Cylinders In or Below the Free Surface of Deep Fluids. NSRDC Report 2375, 1967.

Garrison, C.J. Hydrodynamics of Large Objects in the Sea, Part I - Hydrodynamic Analysis. Journal of Hydronautics, Vol. 8, No. 1, January 1974.

Inglis, R.B. & Price, W.G. Motions of Ships in Shallow Water. Transactions of the RINA, Paper W10, 1979.

Inglis, R.B. & Price, W.G. Comparison of Calculated Responses for Arbitrary Shaped Bodies Using Two and Three-Dimensional Theories. International Shipbuilding Progress, Vol. 27, No. 308, April 1980.

Meyers, W.G. et al. Manual-NSRDC Ship-Motion and Sea-Load Computer Program. NSRDC Report 3376, February 1975.

Meyers, W.G. et al. User's Manual for the Standardd Ship Motion Program, SMP. DTNSRDC Report SPD-0936-01, September 1981.

Murdey, D.C. Seakeeping of the NRC Hull Form Series: A Comparison Between Experiment and Theory. Proc. of the 19th ATTC, Vol. 1, Seakeeping, Ann Arbor, Michigan, July 1980.

Watkins, R.M. & Bales, N.K. Dynamic Waterline Seakeeping Predictions for a Fishing Vessel. DTNSRDC Report SPD-643-02, May 1976.

TABLE 1A

MAIN PARTICULARS FOR A FULL SIZED VESSEL REPRESENTED BY THE MODEL 350 AT A SCALE RATIO OF 1:8.

	SHALLOW DRAFT	DEEP DRAFT
Length between perpendiculars [m], L	18.29	18.29
Length on waterline [m]	17.70	18.36
Maximum beam [m], B	7.59	7.59
Waterline beam at midships [m]	6.77	7.43
Draught above keel line at aft perp. [m]	2.76	3.68
Draught above keel line at forward perp. [m]	1.31	2.23
Displacement, metric tons of fresh water	92.0	187.4
Longitudinal center of bouyancy, aft of midships [m]	0.38	0.72
Wetted surface [m^2]	127.2	173.6
Skeg length along keel [m]	6.4	6.4
Block coefficient for naked hull	0.40	0.49
Prismatic coefficient for naked hull	0.61	0.68
Waterplane coefficient	0.77	0.83

TABLE 1B

LOADING CONDITIONS DURING THE SEAKEEPING TESTS
GIVEN IN FULL SCALE VALUES.

	BEAM SEA TESTS			HEAD SEA TESTS	
	SHALLOW DRAFT	DEEP DRAFT		SHALLOW DRAFT	DEEP DRAFT
		LARGE GM	SMALL GM		
Metacentric height GM					
Transverse [m]	0.96	1.32	1.04	1.40	1.32
Longitudinal [m]	16.92	12.24	12.00	17.36	12.24
Vertical center of gravity above keel [m]	3.56	3.04	3.32	3.12	3.04
Roll gyradius/B	0.30	0.30	0.33	0.30	0.30
Pitch gyradius/L	0.27	0.25	0.25	0.27	0.25
Yaw gyradius/L	0.27	0.25	0.25	0.27	0.25

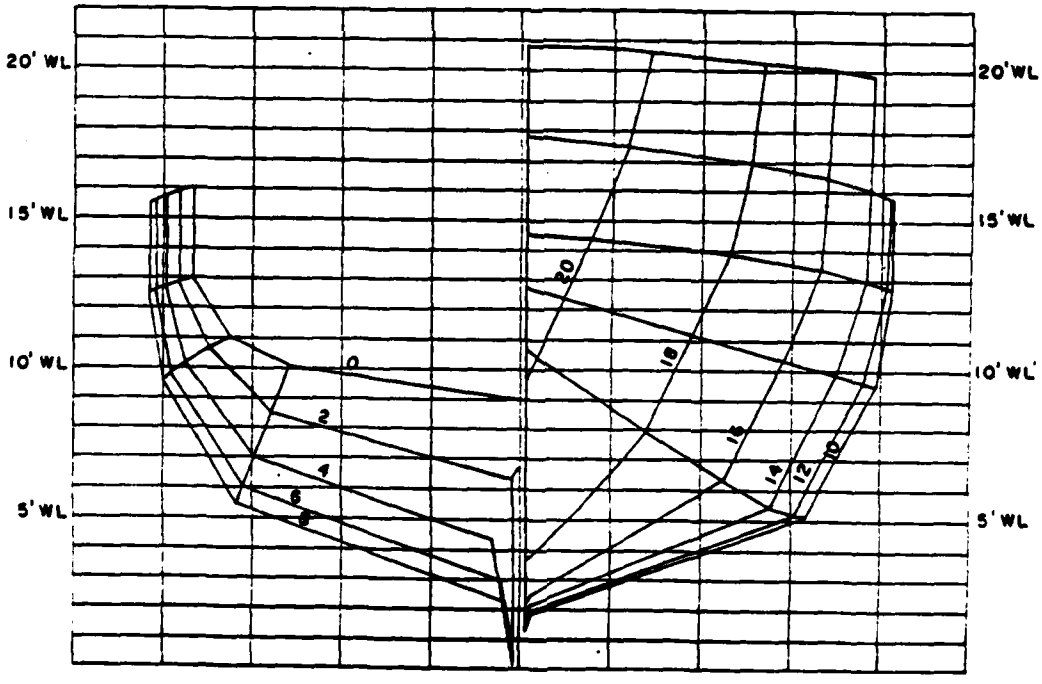

FIGURE 1. BODY PLAN, M-350.

TABLE 2

MOTION INDEX OF CORRELATION IN PERCENT
WIDE BEAM FISHING VESSEL, MODEL 350
HEAD WAVES

	HEAVE		PITCH	
	Fn = 0.19	Fn = 0.38	Fn=0.19	Fn=0.38
Deep Draft				
SMP81	-12.5% short	-13% short	+21.5% long	+30% long
HANSEL, no end terms	-12% short	+14.5% peak	- 8.5% short	+26% peak
HANSEL, end terms incl.	-10% short	-24.5% peak	-32.5% peak	-38% peak
3-Dim. Method		-67% peak		-59.5% peak
Shallow Draft				
SMP81	-14% short	-10.5% short	+23% long	+41% long
HANSEL, no end terms	-10% short	+14% peak	-22% peak	+43% peak
HANSEL, end terms incl.	- 9% short	-13% peak	-36% peak	-26.5% peak

$$\text{Index of Correlation} = \frac{\text{Largest deviation of theory from experiment} \times 100}{\text{Largest experimental value}}$$

Plus (+) sign indicates that the theory overpredicts the response at the largest deviation and respectively minus (-) sign indicates that the theory underpredicts the experimental data at the largest deviation.

The three words short, peak and long refer to the frequency range where the largest deviation between theory and experiment is observed. Short refers to short waves, peak to frequencies around the peak response and long to long waves.

Fn = Froude number.

TABLE 3

APPROXIMATE MOTION INDEX OF CORRELATION IN PERCENT
WIDE BEAM FISHING VESSEL, MODEL 350
BEAM WAVES

	SWAY	HEAVE	ROLL
Deep Draft, Large GM			
SMP81	50%	26%	9%
HANSEL	50%	24%	50%
3-Dim. Method	60%	30%	40%
Deep Draft, Small GM			
SMP81	50%		20%
HANSEL	50%		50%
Shallow Draft			
SMP81	30%	25%	7%
HANSEL	15%	21%	60%
3-Dim. Method	12%	20%	9%

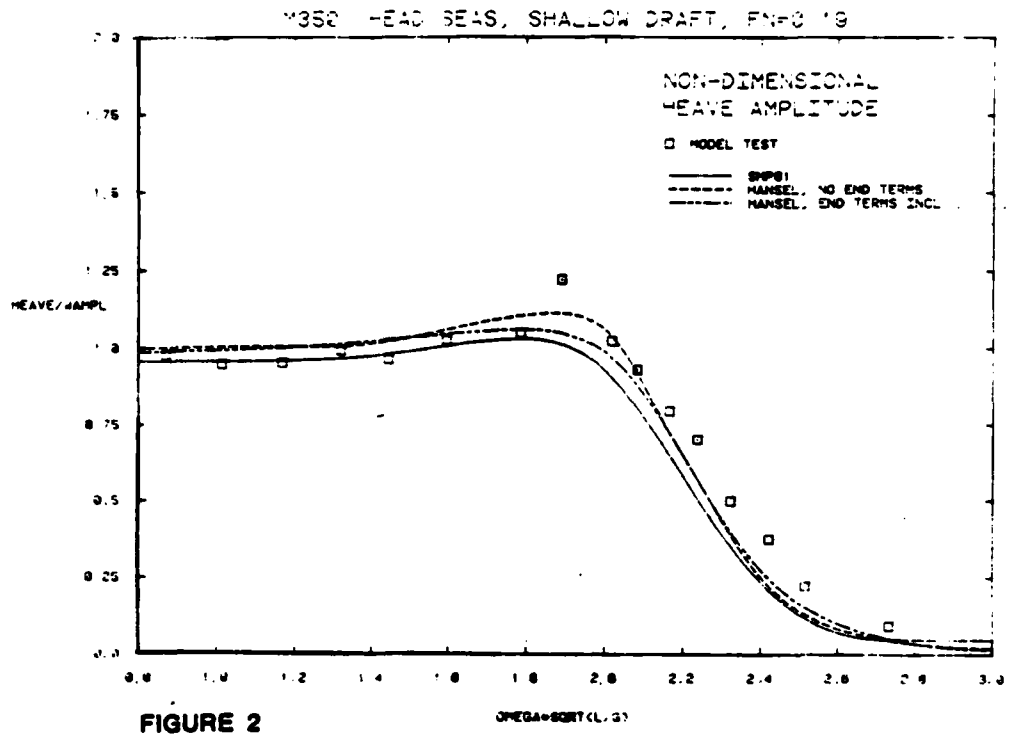

FIGURE 2

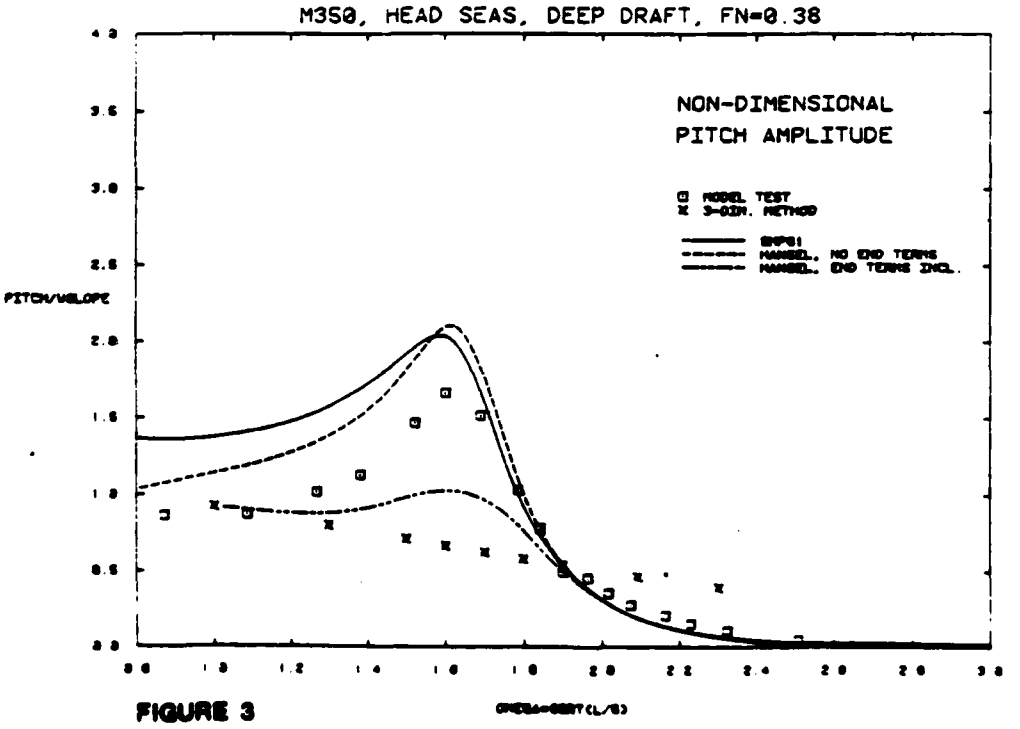

FIGURE 3

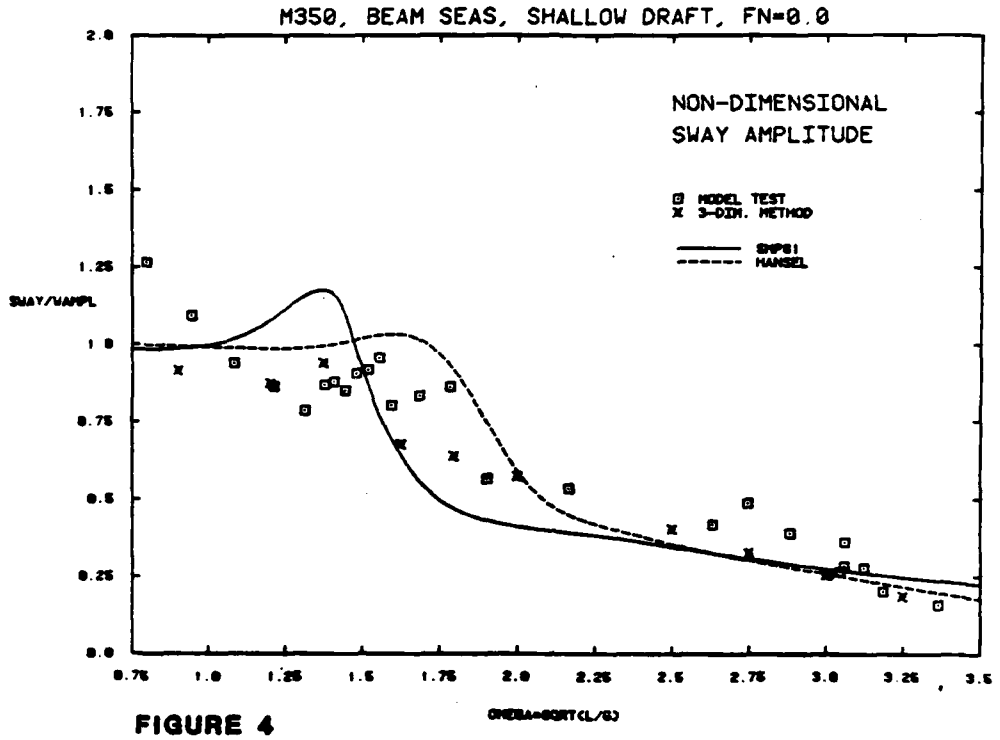

FIGURE 4

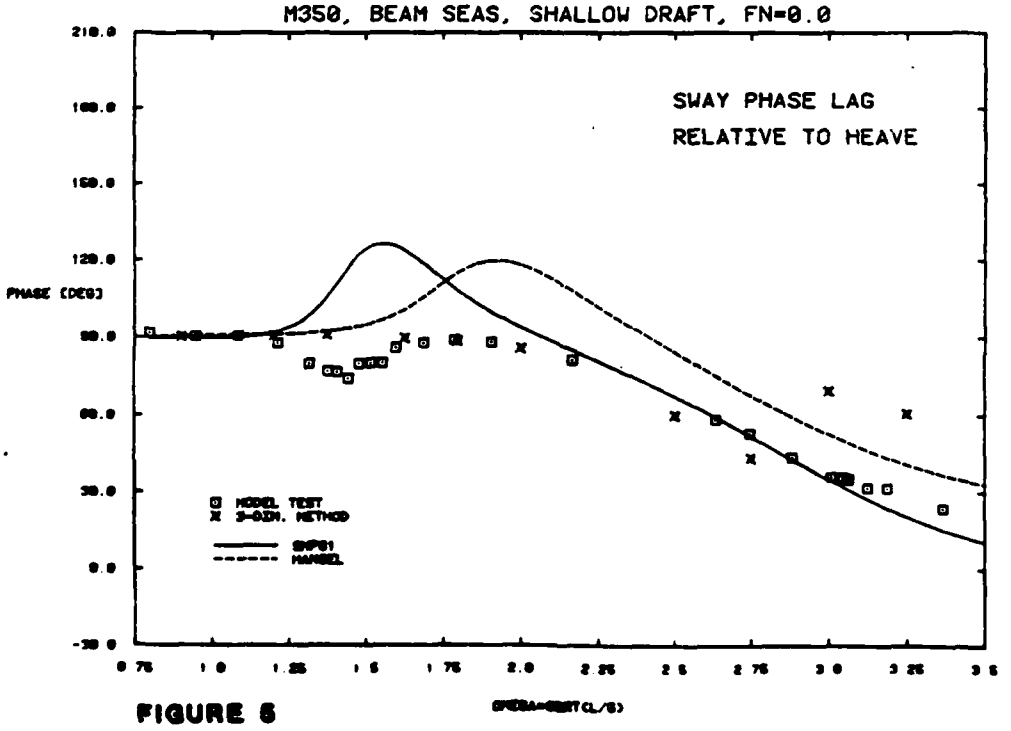

FIGURE 5

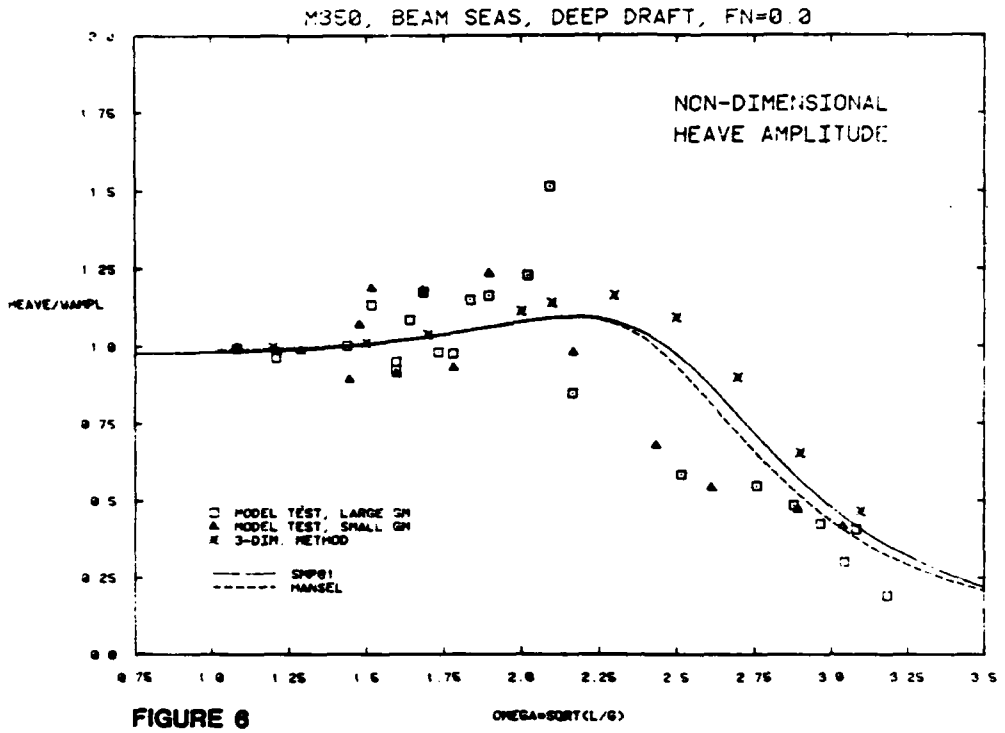

FIGURE 6

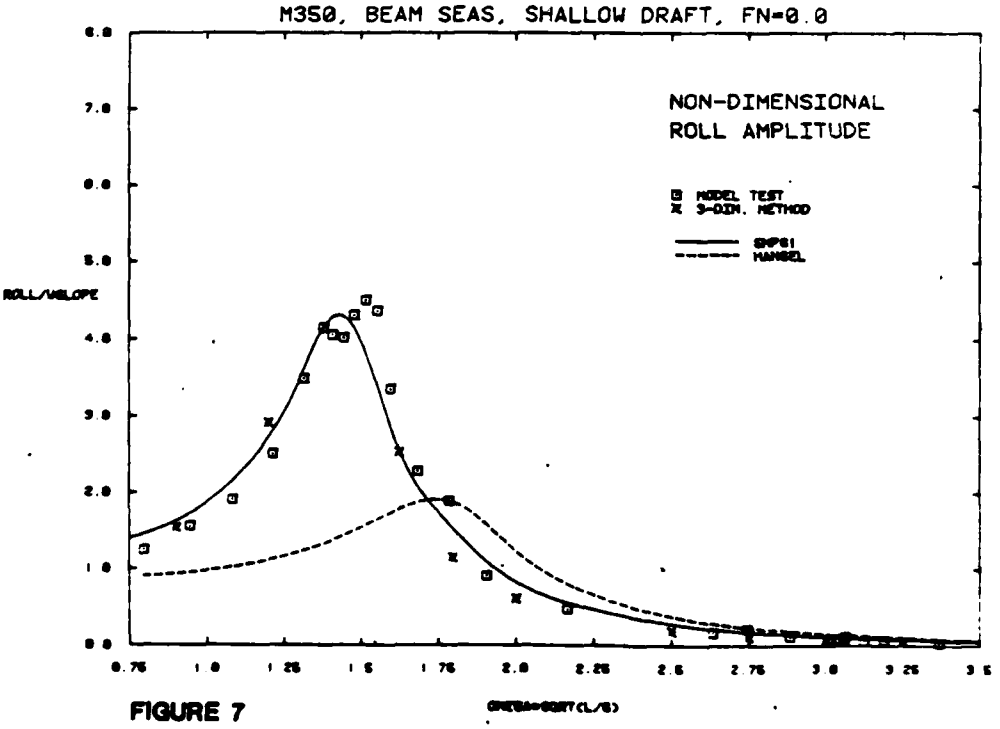

FIGURE 7

AD-A144 227 PROCEEDINGS OF THE GENERAL MEETING OF THE AMERICAN TOWING TANK CONFERENCE.. (U) STEVENS INST OF TECH HOBOKEN NJ DAVIDSON LAB D SAVITSKY ET AL. AUG 83 6/8

UNCLASSIFIED SIT-DL-TR-13029-VOL-2 N00167-83-M-4062 F/G 20/4 NL

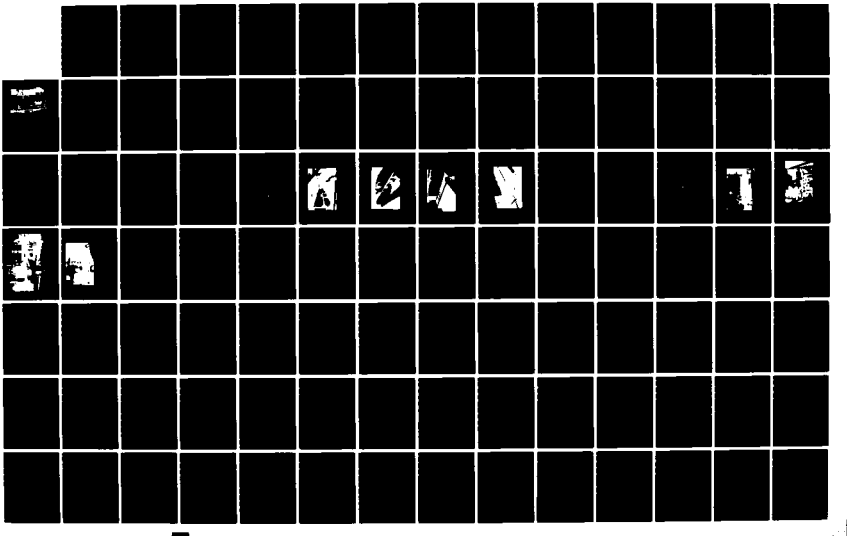

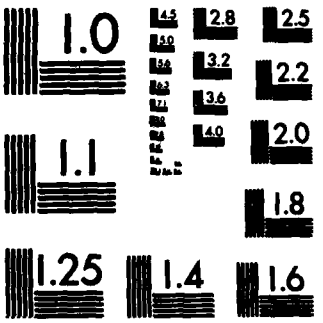

MICROCOPY RESOLUTION TEST CHART
NATIONAL BUREAU OF STANDARDS-1963-A

DISCUSSION

John O'Dea
David W. Taylor Naval Ship Research
and Development Center

The coupling between surge and pitch is usually ignored in ship motion predictions. This is justified because the moment arm by which surge forces cause pitch moments is typically of the order of the ship draft, and the coupling moments are thus negligible compared to pitch exciting, damping or inertial moments for a slender ship. In the case of the fishing vessels tested, with L/B as low as 2.5, this assumption may not be correct. Do you think this coupling could be the cause of the discrepancy between your pitch measurements and predictions?

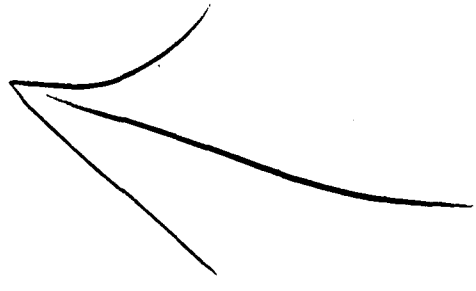

AD-P003 830

ROLL DAMPING AT FORWARD SPEED

by

Martin A. Abkowitz

Massachusetts Institute of Technology

(Steering and Maneuvering)

20th American Towing Tank Conference

Davidson Laboratory
Stevens Institute of Technology
Hoboken, New Jersey

August 1983

ROLL DAMPING AT FORWARD SPEED

Martin A. Abkowitz

ABSTRACT

Three dimensional body theories indicate a significant effect of forward speed on the linear roll damping coefficient, whereas two dimensional and strip-slender body theories indicate that the effect is small. Model tests, carried out many years ago, demonstrated a strong effect of forward speed on the roll damping of a battleship. The three dimensional body theories indicate a significant reduction in damping at pitch resonant frequencies and a significant increase in damping at roll resonant frequencies. Forced rolling tests on a model of the MARINER at various forward speeds have been carried out in the MIT Ship Model Towing Tank to measure the effect of forward speed on roll damping. The results confirm the three dimensional theory trend. Ability to closely estimate the roll damping at ship speeds will improve seakeeping motion prediction and improve operational procedures with respect to efficiency and safety.

1. INTRODUCTION

Significant roll responce to wave excitation can seriously degrade the safety and operational efficiency of the ship. If the seaway contains wave lengths which can excite resonant or near resonant frequencies, at the desired heading and speeds, the motion response will be approximately inversely proportional to the damping coefficient. Because of the elongated shape of the normal displacement type vessel, the beam-draft ratios are such that roll damping (due to wave generation) is small, resulting in significant roll response at resonant frequencies.

In order to predict ship roll response, one needs to estimate the magnitude of the roll damping coefficients (linear and nonlinear contributions i.e. wave and viscous effects) with reasonable accuracy. Many theories for calculating roll damping for displacement hull shapes have been presented with the associated equations, calculations, and computer programs.

The most popular theory is the strip-slender body theory, which is essentially a two dimensional theory with a correction for forward speed effects involving the body shape, but without a free surface condition. Therefore Froude effects involving the interaction between the frequency generated waves and the waves generated by the forward speed are not properly taken into consideration.

The truly three dimensional (3D) theories and resulting calculations developed to date demonstrate a very strong effect of forward speed on the damping coefficients (in several degrees of motion freedom), much more than the strip-slender body theory indicates. Figure 1 (taken from Reference 1) shows the results of a calculation by a 3D theory of the heave damping coefficient as a function of frequency number and Froude number. This 3D theory involves the distribution of pulsating sources on the centerline plane, the strengths of which are determined by ship geometry, and the free surface condition is satisfied. The above conditions limit the results to that of "thin ship" theory but do not in any way limit the three dimensionability of the theory. From the figure it can be observed that, in the middle range of frequencies which are the usual heave resonant frequencies, the effect of forward speed (Froude number) is to decrease the damping coefficient by the order of 15 to 20 percent at ship normal operating speeds. Strip-slender body theory shows no such reduction in damping coefficient. The difference in results between the two theories is significant, but only affects the predicted heave response by the order of 15 to 20 %. Figure 2 (taken from Reference 2), shows the roll damping coefficient, as a function of frequency number and Froude number, for a near water surface submerged ellipsoid, satisfying the free surface

condition and the hull surface boundary condition. The theory does not have the "thin ship" assumption but the ellipsoid is not representative of a body which is ship shape and penetrates the water surface. Nevertheless, it still is a valid three dimensional theory and results of the calculations would still be qualitatively true.

It can be observed from Figure 2, that at middle frequencies, the effect of forward speed is to reduce the roll damping coefficient, however at low frequencies, which are the roll resonant frequencies (where the response is very dependent on the damping coefficient), the effect of forward speed is to increase the damping coefficient by a factor of four or more. Therefore, the roll response at resonance predicted by strip-slender body would be several times greater than is to be expected for the real 3D ship situation. With respect to ship operations in a seaway, slowing down increases the heave damping (wave) thereby reducing heave, whereas slowing down in beam seas will significantly reduce the roll damping (wave) at resonant frequencies thereby significantly increasing the roll response.

From both an academic and practical point of view, it is interesting and useful to find out if this strong affect of forward speed on roll damping, as predicted by 3D theory, holds for the actual ship. A model test program was carried out at the MIT Ship Model Towing Tank to determine the effect of forward speed on the roll damping coefficient for the MARINER ship type.

2. TEST PROGRAM

A convenient way to measure the damping coefficient (equivalent linear) is to measure the roll response, at roll natural frequency, resulting from a known roll excitation. The response is inversely proportional to the roll damping coefficient at resonant frequency. Many years ago, in 1938, a free running self-propelled model of a battleship was tested in this manner at various forward speeds to investigate the roll damping effect of continuous and discontinuous bilge keels of varying sizes and shapes. Two sets of counter rotating eccentric weights, with a set located equally above and below the roll axis, provided roll moment excitation without pitch, yaw, sway or heave excitation. One of the test conditions was hull without any bilge keels. Figure 3 (taken from reference 3) shows the results of this test, and one can observe the strong effect of forward speed on the roll damping coefficient at roll natural frequencies. The results show a strong increase in linear roll damping at the larger forward speeds indicating a significant increase in roll wave damping with forward speed. Since the tests described above were self-propelled and since rotating propellers will tend to increase the linear roll damping coefficient with forward speed, these test results do not conclusively attribute the increase in roll damping to damping resulting from wave generation. Also the tests were run near only one natural frequency. The model of the MARINER tested in the MIT Ship Model Towing Tank was towed with freedom to roll but with the sway, yaw, heave and pitch restrained. Therefore, roll excitation could be accomplished with only one set of counter rotating eccentric weights mounted above the roll axis. Figure 4 shows the excitation instrumentation mounted in the model. Natural frequencies in roll were varied by testing the model ballasted at various metacentric heights at the same displacement. The

model was tested at several forward speeds at each of several resonant frequencies. The measured roll responses were analyzed and converted into corresponding roll damping coefficients.

3. TEST RESULTS AND CONCLUSION

Figures 5 and 6 (taken from Reference 4) show the results of the model tests. Figure 5 shows the roll damping coefficient for the model when ballasted to the design metacentric height of the MARINER. It is clear that an increase in forward speed causes a significant increase in roll damping at this frequency. This confirms the trend of the results of the battleship model tests. Since the model tests results indicate wave plus vicous roll damping, the value of the damping coefficient at zero Froude number at this frequency may be indicative of the magnitude of viscous damping. Figure 6 shows the results of the model tests at several resonant frequencies with all values of $\frac{\omega^2 L}{2g}$, except at the value of 3.98, at the same model displacement (MARINER load displacement). In order to obtain a resonant roll frequency which was high enough to move toward the range where increasing forward speed reduces the damping, it was necessary to increase the displacement of the model in order to obtain a low enough center of gravity. Therefore, the values of the non-dimensionalized roll damping coefficient at $\frac{\omega^2 L}{2g} = 3.98$ are not quantitatively related to those at other values of $\frac{\omega^2 L}{2g}$ but are qualitatively related. In a sense they indicate that at the higher frequencies, the effect of Froude number on roll damping is reduced.

A comparison between Figure 6 and Figure 2, taking into account that the values shown in Figure 6 include viscous as well as wave damping, shows that the strong effect of forward speed on the wave roll damping coefficient, as predicted by three dimensional theories, holds for the real situation.

REFERENCES

1. J. Gerritsma, J.E. Kerwin, and J.N. Newman "Polynomial Representation and Damping of Series 60 Hull Forms", International Shipbuilding Progress, Vol. 9, 1962

2. J.N. Newman, "The Damping of an Oscillating Ellipsoid Near a Free Surface" Journal of Ship Research, Vol. 5, no. 3, December 1961

3. J.G. Thews, "Discontinuous Anti-Rolling Keels", United States Experimental Model Basin, Report no. 450, May 1938

4. B. Colbourne, "The Effect of Forward Speed on Ship Roll Damping", S.M. Thesis, Department of Ocean Engineering, MIT, August 1983

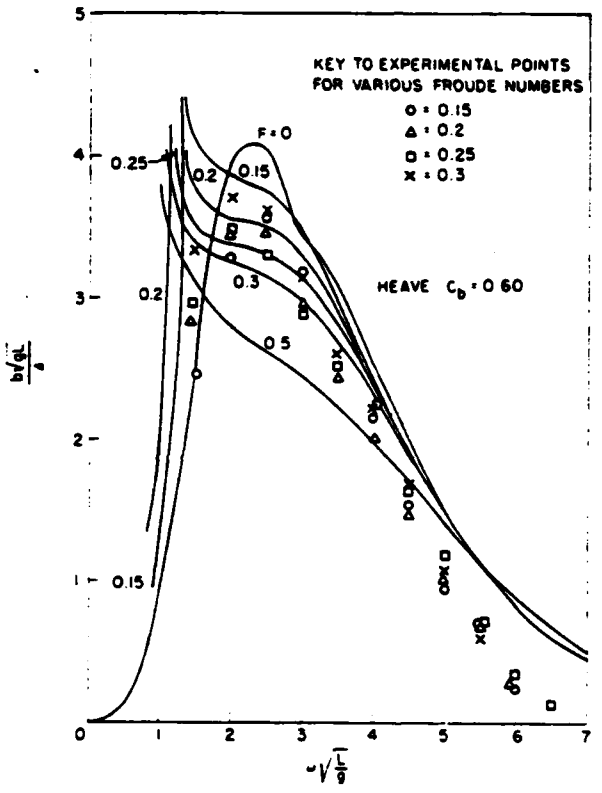

Heave Damping Coefficient for Series
60 Block 0.60 Hull

FIGURE 1

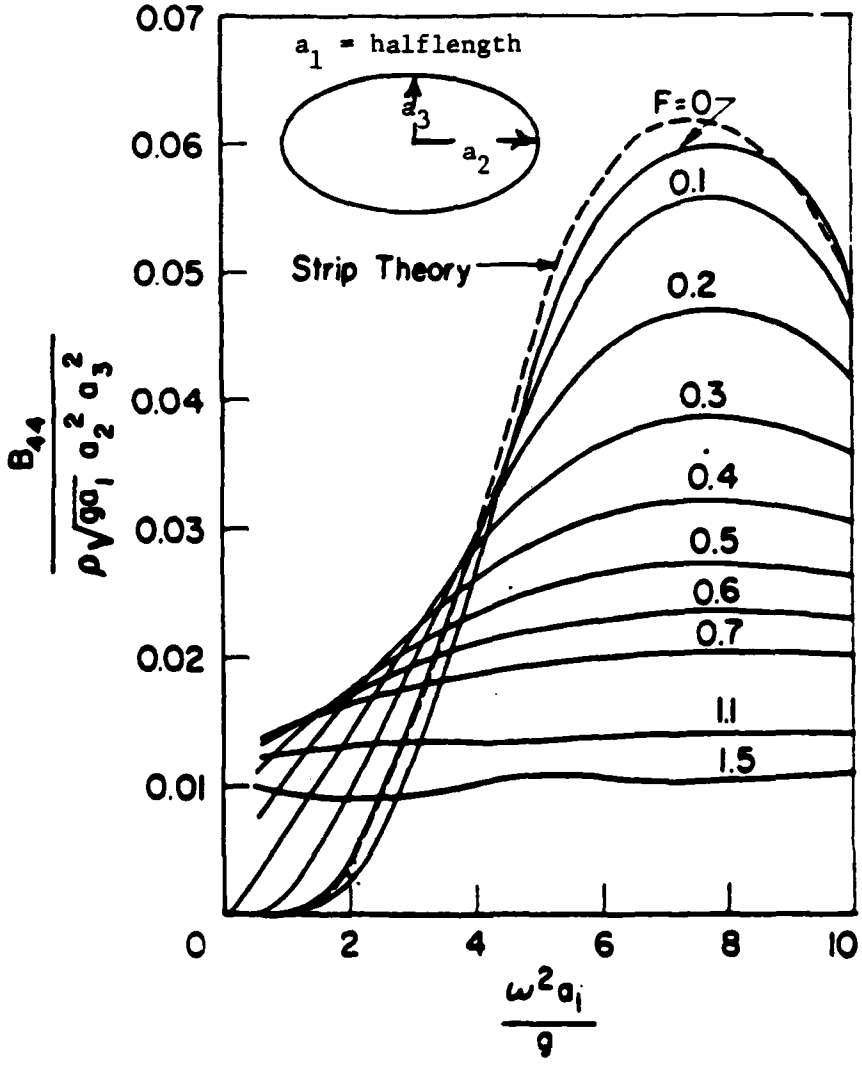

Roll Damping Coefficient of An Ellipsoid

FIGURE 2

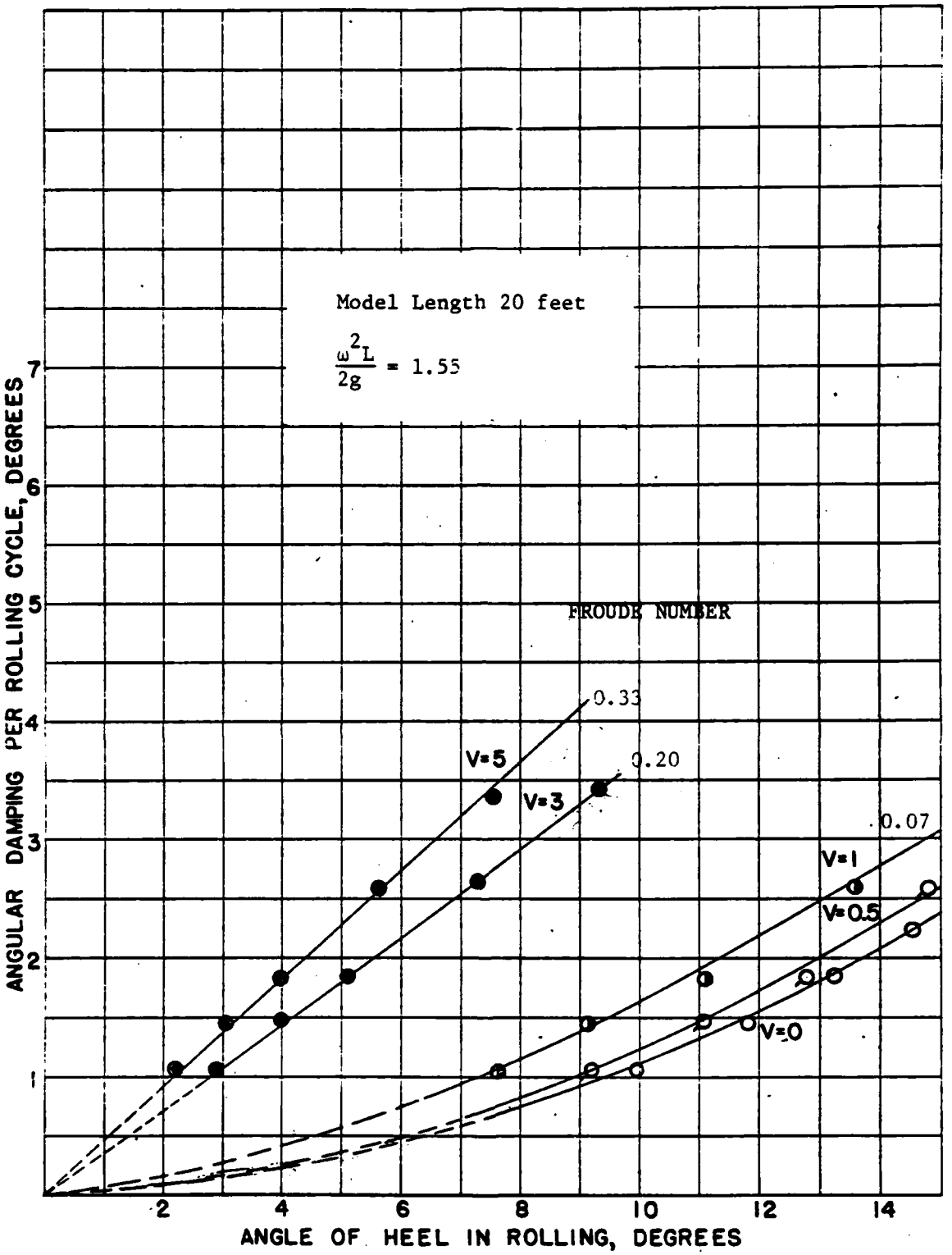

MODEL NO. 3400. TOTAL ANGULAR DAMPING WITH NO BILGE KEELS AT SPEEDS OF 0, 0.5, 1, 3, & 5 KNOTS.

FIGURE 3

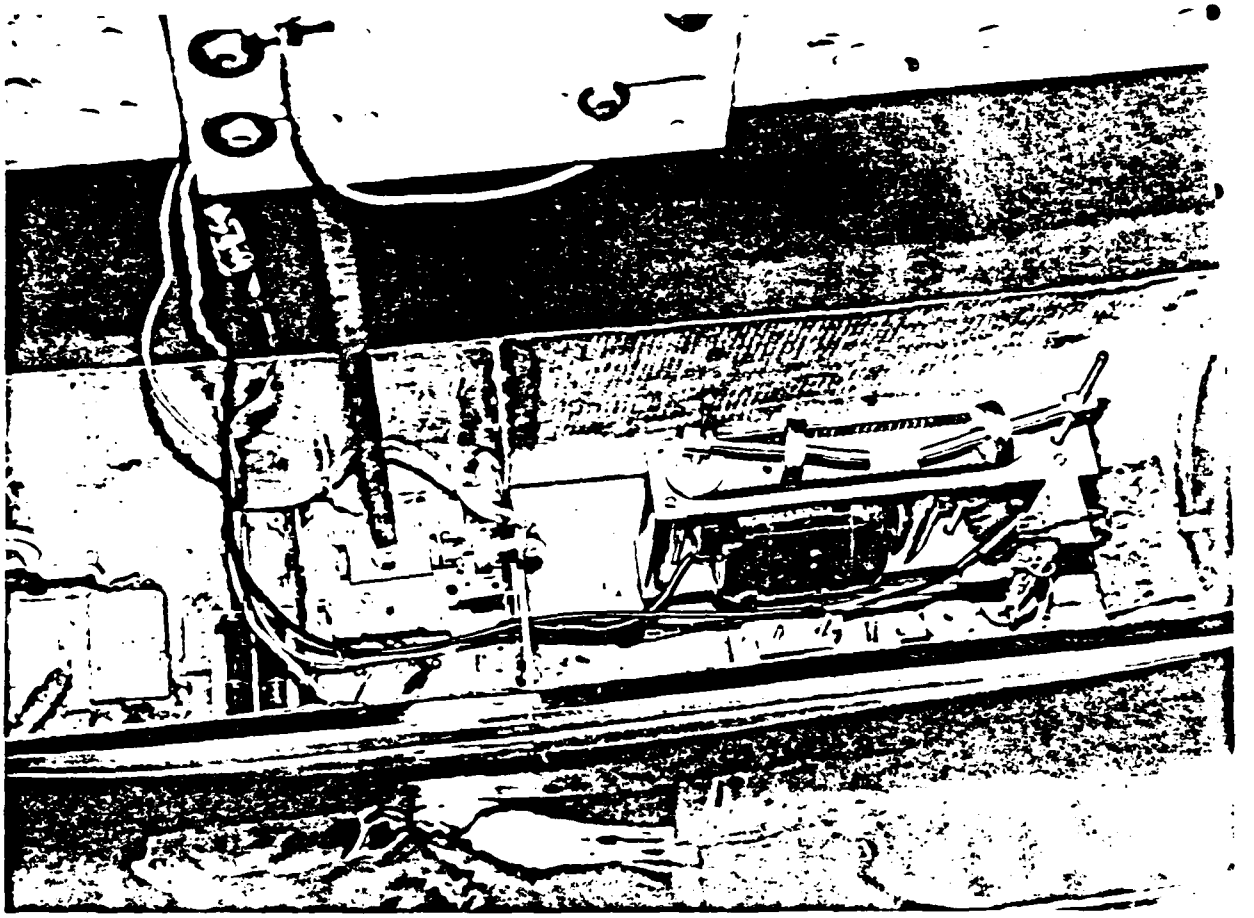

Counter-Rotating Eccentric Weights
in MARINER Model

FIGURE 4

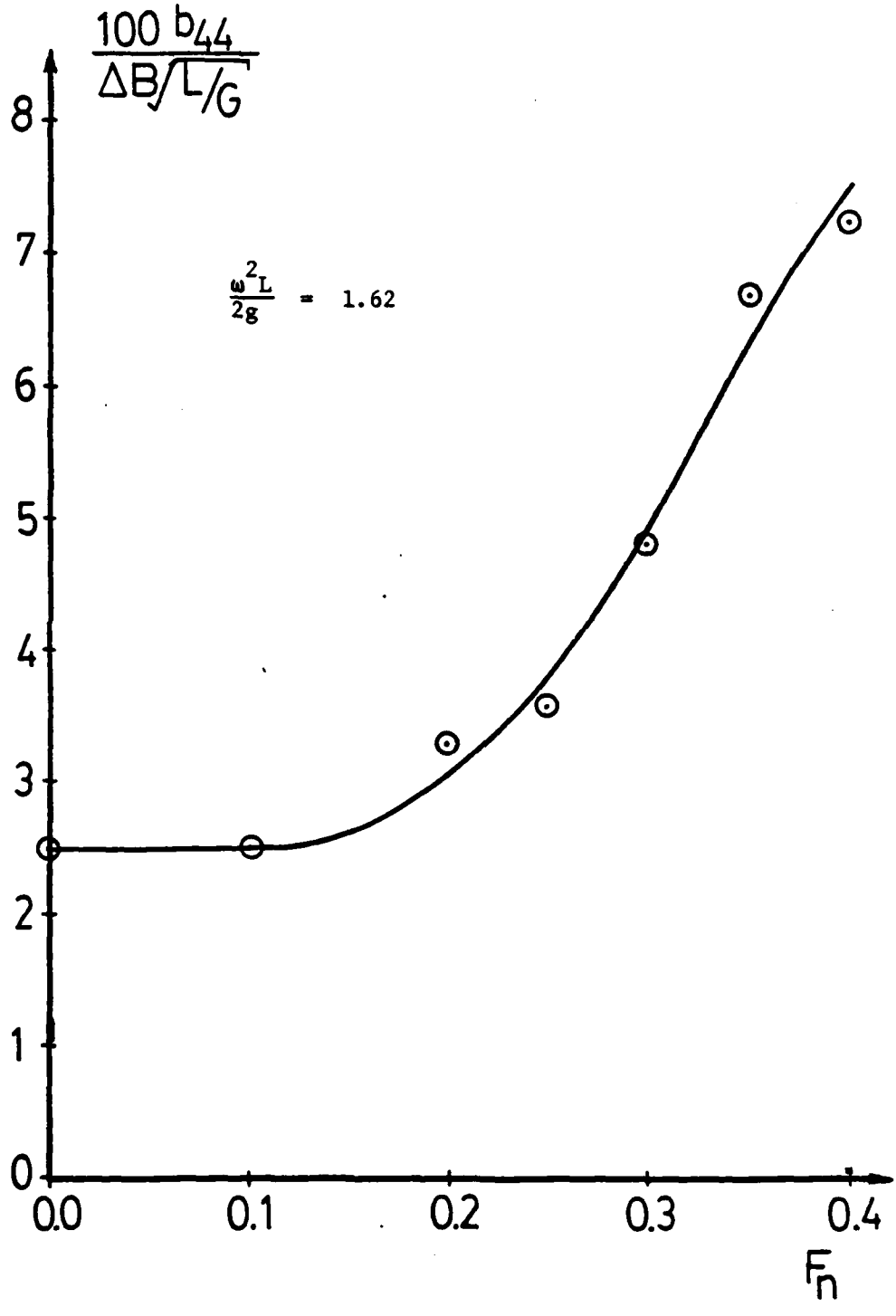

Roll Damping Coefficient of MARINER Model

FIGURE 5

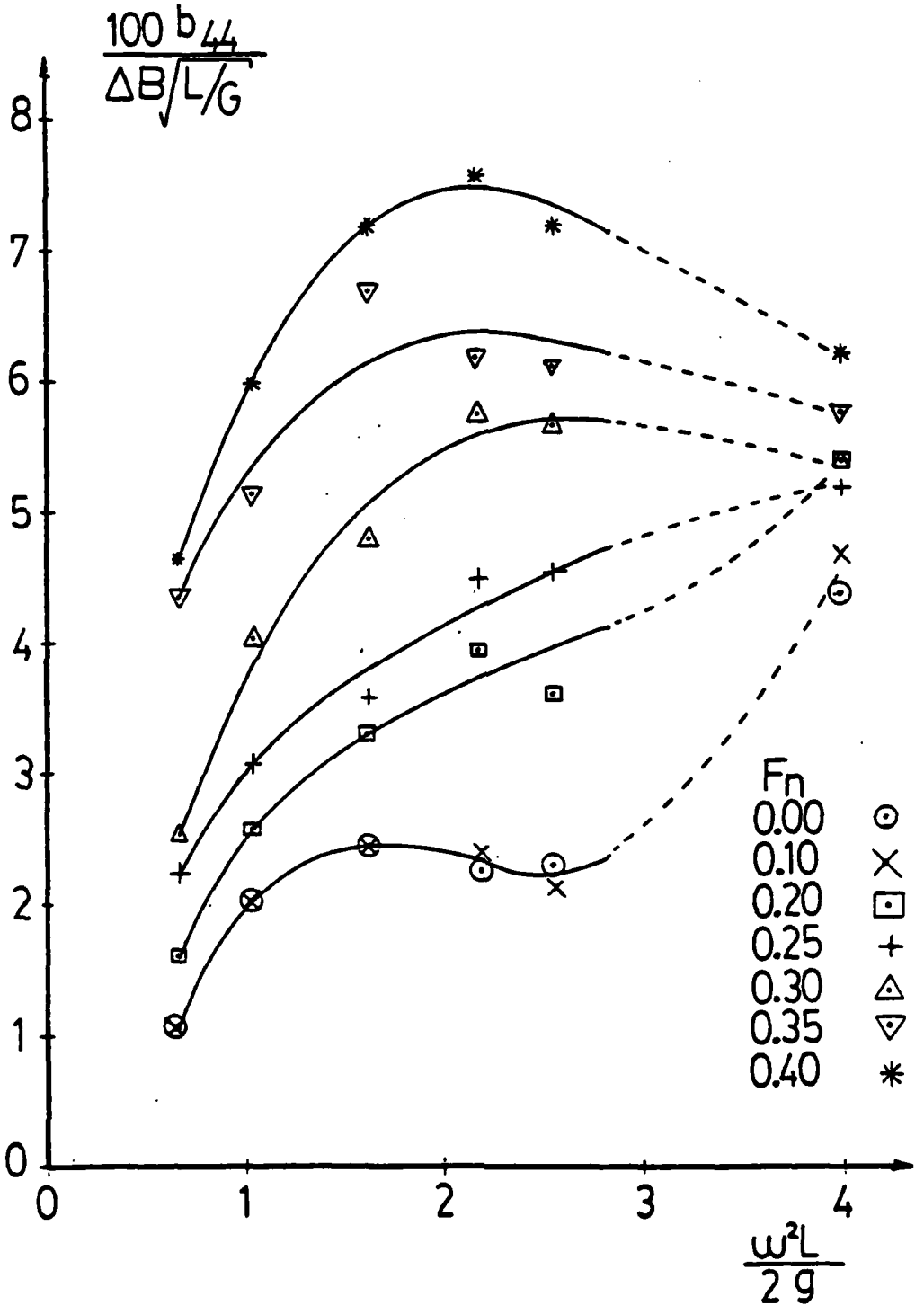

Roll Damping Coefficient of MARINER Model

FIGURE 6

REPORTS OF THE

SYSTEMS AND TECHNIQUES

COMMITTEE

REPORT OF THE COMMITTEE ON SYSTEMS AND TECHNIQUES

The Systems and Techniques Committee for the 20th ATTC consisted of:

Prof. Bruce Johnson, U. S. Naval Academy, Chairman

Dr. R. S. Rothblum, David W. Taylor Naval Ship Research and Development Center

Mr. Michael D. Miles, National Research Council

Mr. Alex Goodman, Hydronautics, Inc.

Mr. Stuart B. Cohen, The University of Michigan

Dr. Jeffrey T. Dillingham, Offshore Technology Corporation

Mr. D. R. Mullinix, David W. Taylor Naval Ship Research and Development Center

Dr. D. Gospondnetic, National Research Council

Mr. Peter W. Brown, Davidson Laboratory

Prof. Armin W. Troesch, The University of Michigan

The work of the committee was accomplished by telephone, letter and personal contacts. Contributions to the session on systems and techniques were solicited from committee members and from representatives of the various organizations attending the ATTC. The papers were grouped in three areas: new facilities, techniques, and instrumentation.

New Facilities

Several new facilities have been planned since the 19th ATTC.

1. A towing carriage has been designed and is being installed on an existing 61m x 4.6m x 2.4m wave-tank at Memorial University of Newfoundland, St. John's Newfoundland, Canada. Dr. Chi-Chao Hsiung presented a description of the facility as prepared by himself and several co-authors.

2. Adjacent to the campus at Memorial University, St. John's, the National Research Council of Canada has planned several new model testing facilities

for the Artic Vessel and Marine Research Institute (AVMRI). Dr. Drasco Gospodnetic and Mr. Michael D. Miles presented a paper describing the new 80m x 12m x 3m ice model basin, a 200m by 12m by 7m clearwater towing tank, and a 75m by 32m x 3.5m seakeeping and manoeuvring basin. These tanks and associated equipment are slated for operation in 1986.

3. A large cavitation channel with a test section 3m x 3m x 12m in length is in the design stages at DTNSRDC. Dr. Richard S. Rothblum presented a summary of the current status of this very large project.

In addition, Mr. Duncan Brown of the Naval Underwater Systems Center made a brief report on the re-commissioning of the 2800 ft long salt water basin at Langley Field in Virginia.

Techniques

John Hoste and Dr. Jeffrey T. Dillingham of Offshore Technology Corporation prepared a comprehensive paper on data analysis techniques in model testing. The increased use of sophisticated time series analysis techniques in model testing has led to setting criteria for sampling rates and record lengths based on desired estimated errors in the analysis. Examples of well annotated plots of spectral density and transfer functions for various model tests are included.

Instrumentation

Professor Armin Troesch and Frederic Phelps described the new speed control system for the University of Michigan towing tank. The system, installed in 1982, exhibits speed variations of less than ± .003 ft/sec and repeatability over a measured distance of ± .001 ft/sec from 0 to 20 ft/sec. Plots of the carriage speed control calibrations are included.

Also in the area of control systems, Harry D. Harper presented a comprehensive report on the modernized control system for the DTNSRDC 36 inch variable pressure water tunnel. The new control system is expected to improve the daily operating functions of the facility and to obtain experimental data at a higher level of productivity. It makes use of a distributed processing network consisting of a host processor, five node processors, and microprocessor-based digital controllers. It also represents a pilot program for the control system for the large cavitation channel mentioned earlier.

A paper of great interest to the sailors and yacht-racing community was presented by Charles Gommers and Dr. Peter van Oossanen of the Netherlands Ship Model Basin. In it they describe the evolution of yacht dynamometer systems leading up to the new wind-force dynamometer which was developed to test yacht models at NSMB. The use of this dynamometer was instrumental in the development of the unusual keel configuration of the America's cup yacht Australia II. The dynamometer can be described as an active system because close-loop servo-systems are incorporated in its operation.

A less complex but much less expensive two-component force balance for towing tanks and flumes was described by Professor Ted Kowalski of the University of Rhode Island and Mr. Duncan Brown of the Naval Underwater Systems Center. The force balance was designed to measure drag and side forces and allow for pitch and heave motions. The initial testing of the dynamometer was carried out using a 1/6 scale model of a sailing yacht.

Finally, David Coder, Benjamin Wisler and Michael Jeffers of DTNSRDC described a high precision differential force balance and experimental method to measure small fluid-dynamic forces due to small geometry changes. This system was developed for wind tunnel tests of appendage drag on models of

ships. It was used to evaluate various types of fillets by rotating the fillets into the flow and using a nulling force mechanism to measure the very small differences in drag produced by the effect of the fillet geometry on the appendage drag.

AD-P003 831

NEW TOWING FACILITIES AT MEMORIAL UNIVERSITY OF NEWFOUNDLAND

by

C.C. Hsiung*, D. Friis*, W. Milne*,
G.R. Peters*, and H.W. Weber**

for

20th American Towing Tank Conference at
Davidson Laboratory, Stevens Institute of Technology,
Hoboken, New Jersey, August 1983

* Faculty of Engineering and Applied Science, Memorial University of Newfoundland, St. John's, Newfoundland, Canada

**Kempf & Remmers GmbH, Hamburg, W. Germany

ABSTRACT

A towing carriage is being installed on an existing 61m x 4.6m x 2.4m wave-tank at Memorial University of Newfoundland, St. John's, Newfoundland, Canada. This is the first towing carriage of this kind and size at a Canadian university. It will support the new educational program in shipbuilding engineering and research work in the area of ship and marine hydrodynamics. The facilities can be used by undergraduate students for experimental work, by graduate students for thesis projects and by the faculty for contracted and academic research. With the maximum acceleration and maximum velocity of the carriage being 2.0 m/sec^2 and 5.0 m/sec, respectively, together with the wave-making capability of the tank, a wide range of hydrodynamic research can be performed. The wave-tank lay-out and the towing facilities are described.

INTRODUCTION

A full undergraduate degree program in Shipbuilding Engineering (Naval Architecture) has been offered at Memorial University since 1979. Even before starting the program, there was a plan to convert the existing 61m (200 ft) wave tank into a model towing tank for supporting the ongoing ocean engineering research as well as the new educational program in shipbuilding engineering. It is through the joint financial support of the National Research Council of Canada and the Government of the Province of Newfoundland that the installation of the new towing facility is possible.

The towing facility design is a common effort of Memorial faculty members and Kempf & Remmers' design staff. Since the facilities are restricted to fit the existing wave tank, special design considerations have been given for various conditions. Kempf & Remmers will deliver the finished towing carriage to Memorial by the end of July 1983. At the time of writing this report, the towing carriage is en route to St. John's.

Wave Tank

The existing wave tank, shown in Figs. 1 and 2, is a reinforced concrete structure situated in the basement of the S.J. Carew Building where the Faculty of Engineering is located. The tank dimensions are 61m (200 ft) long, 4.6m (15 ft) wide and 2.4m (8 ft) deep. However, the wave-maker takes a length of 5m (16 ft) and the beach (above water portion) occupies 4.6 m (15 ft), the effective length of the tank is approximately 49m (160 ft). The operating depth of the tank is 1.83m (6 ft).

At one end of the wave tank, there is a hydraulically operated piston-type wave-maker manufactured by MTS (Figs. 3 and 4). An aluminum wave-board is driven by a hydraulic actuator with a 48.8 kN force capability over a 0.25m stroke. The hydraulic power supply delivers 6.62 L/s at 20.7 MPa. A pneumatic sealing gasket is attached to the three sides of the wave-board to ensure watertightness. With a closed-loop control system, regular and irregular waves can be generated according to testing specification. For regular waves, maximum wave height is 0.4m (1.3 ft) at 6.1m (20 ft) wave length and 0.91m (3.0 ft) water depth. For irregular waves, the Pierson-Moskowitz spectrum can be simulated [Ref. 1].

At present, the beach at the opposite end of the tank is constructed of five modules each consisting of orthogonal wood grids mounted on top of plywood (Fig. 5). It has reflection coefficients of less than 12% depending on wave conditions. The total length of the beach including the above water and below water portions plus the clearance between beach and the tank end, occupies a tank length about 10m to 12m. In order to increase the run distance of the future towing carriage, a shorter beach is expected to replace the present one. A curved and slatted beach model (Fig. 6) patterned after the beach used in the seakeeping basin at NSMB, Wageningen, the Netherlands [Ref. 2] has been built and tested in a small wave flume. The test results are shown in Fig. 7. It has been found that the slope of the beach should be set to less than 10°, and that this type of beach model has low reflection coefficients for high wave frequencies. Based on Froude's Law of similitude, the square of the frequency ratio of full-scale to

model is inversely proportional to the length ratio of full-scale to model. Therefore the curved, slatted beach is expected to have low reflection coefficients in the operating frequency range of the wave tank. A full-scale new beach based on the tested model will be built and tested for the tank in the near future.

Towing Facilities

The towing facilities are shown in Fig. 8. The particulars of the towing carriage are as follows:

1)	Weight	4000 kg
2)	Maximum speed	5 m/s
3)	Accuracy of the speed control in speed range 0.05 to 5 m/s	1%
4)	Minimum possible speed	0.05 m/s
5)	Maximum acceleration	2 m/s^2
6)	Maximum deceleration	2 m/s^2
7)	Length of working platform	2 m
8)	Total length	3.5 m

9) Driving system:

2 sets of thyristors and rectifiers for electronic control;

2 sets of shunt wound DC driving motors

10) Braking system:

Electro-magnetic deceleration and brake;

Pneumatic emergency brake

Other technical details are as follows:

1)	Gauge of rail	4.87 m

2) Length of rails 55 m

3) Length of current conductors 55 m

The main feature of the model-towing carriage is that the driving system is supported by the guide rail on one side of the tank which is an integral part of the building wall. This is because the opposite side of tank has several large view-windows which would not provide sufficient structural support for the carriage. While the guide rail on which the drive wheels engage is of relatively heavy design, the rail on the opposite side is lighter since the latter will carry considerably less weight. The carriage runs on four wheels, and is guided and driven by two sets of horizontal wheels at the forward end and at the rear end of the carriage. These wheels are on the guide rail side (Fig. 9).

Another special feature of the towing carriage is that the maximum carriage speed is 5 m/s. Since the available running length of the tank is only about 50m, a high acceleration is required so that a sufficient length of steady run can be obtained to acquire meaningful test data for such a speed. The maximum acceleration of 2 m/s^2 (or 0.2 g) will result in a speed of 5 m/s in 2.5 sec over a distance of 6m. This is achieved by a driving system with two sets of vertical driving motors acting on horizontal wheels which are pressed by spring action to the sides of the head of the guide rail (Fig. 10). The driving wheels which serve also for guiding the towing carriage.

One more special feature of the towing carriage is that the frame for support of measuring equipment is attached to the main carriage frame in such a way that its vertical position is adjustable (Fig. 11).

With such an arrangement, model tests for different water depths can be conducted. Particularly, for the shallow water experiments, one may let the water out until the required depth is reached, then lower the measuring frame accordingly for test runs.

The two sets of drive motors of the carriage are shunt wound D.C. motors which are provided with current from the three phase A.C. line via a high precision two quadrant thyristor type control which is arranged on the carriage. Acceleration and deceleration of the carriage can be adjusted with small potentiometers at the switch desk. The desired speed of the carriage is chosen according to a calibration table in the form of a preset stabilized voltage. One of the drive motors is connected to a tachometer generator and the speed control works so that the tachometer generator voltage and the preset voltage are kept equal with good precision, thus stabilizing the speed of the run at the desired value.

The speed of the carriage is measured with the help of a measuring wheel which is provided with a photo-electric pick-up giving 10,000 impulses per meter run. The measuring wheel will be connected to an electronic counter and a printer for read out and recording.

With normal operation of the carriage the operator brakes the carriage via the drive motors so that the drive motors act as braking generators and feed current back into the three phase A.C. line. In case the operator forgets to brake before reaching the minimum braking distance at the ends of the tank, automatic braking is enacted with the help of an end-limit-switch. The carriage is then braked using brakes with lifting magnets which are arranged on the motor shafts. Braking

is made with a deceleration of approximately 2 m/s^2 while the electric drive of the motors is automatically switched off. The carriage is also provided with a pneumatic braking system for normal operation as well as for emergency. This system is operated from the control panel in the carriage, or automatically activated by an end-limit-switch.

Electrical current supply for the towing carriage is from the three phase A.C. line via three current conductor rails (Fig. 12). The further current conductor rails are provided for transmitting single phase A.C. to the towing carriage, and a further current conductor rail is connected to give a good grounding for electronic measuring equipment on the carriage. The carriage has two current collectors for each current conductor rail in order to ensure a good connection.

Concluding Remarks

The existing wave tank has been used extensively for various ocean engineering research projects, such as measuring wave loads on offshore structures, studying wave attenuation in ice, etc. The installation of the towing facilities will further enhance its versatility. At present, the basic measuring instruments for ship resistance, seakeeping and maneuvering tests need to be purchased or developed in-house. A real-time micro-computer system on the carriage will be equipped for data processing. The control system of the carriage has been designed with possible access to computers. Therefore, it can be computerized for on-line control. It also will take time to conduct the tank blockage effect studies. Then meaningful experiments can finally be carried out.

However, this is the first towing facility of this kind and size at a Canadian university. It will offer a wide range of possibilities for testing ships, ship hull and propeller interactions, and other moving or fixed marine structures/bodies. It will support the new educational program in shipbuilding engineering (naval architecture) and research work in ship and marine hydrodynamics. The facilities can be used by undergraduate students for experimental work, by graduate students for thesis projects, and by faculty members for academic and contracted research.

Acknowledgements

The work of beach model tests carried out by Mr. Gam Yao and Mr. Roy Dawe is acknowledged.

References

1. Muggeridge, D.B. and Murray, J.J., "Calibration of a 58m Wave Flume", Can. J. of Civ. Eng., Vol. 8, 1981.

2. van Lammeren, W.P.A. and Lap, A.J.W., "The Combined Wave and Current Laboratory of the Netherlands Ship Model Basin", Int. Shipbuilding Progress, Vol. 11, No. 118, June 1964.

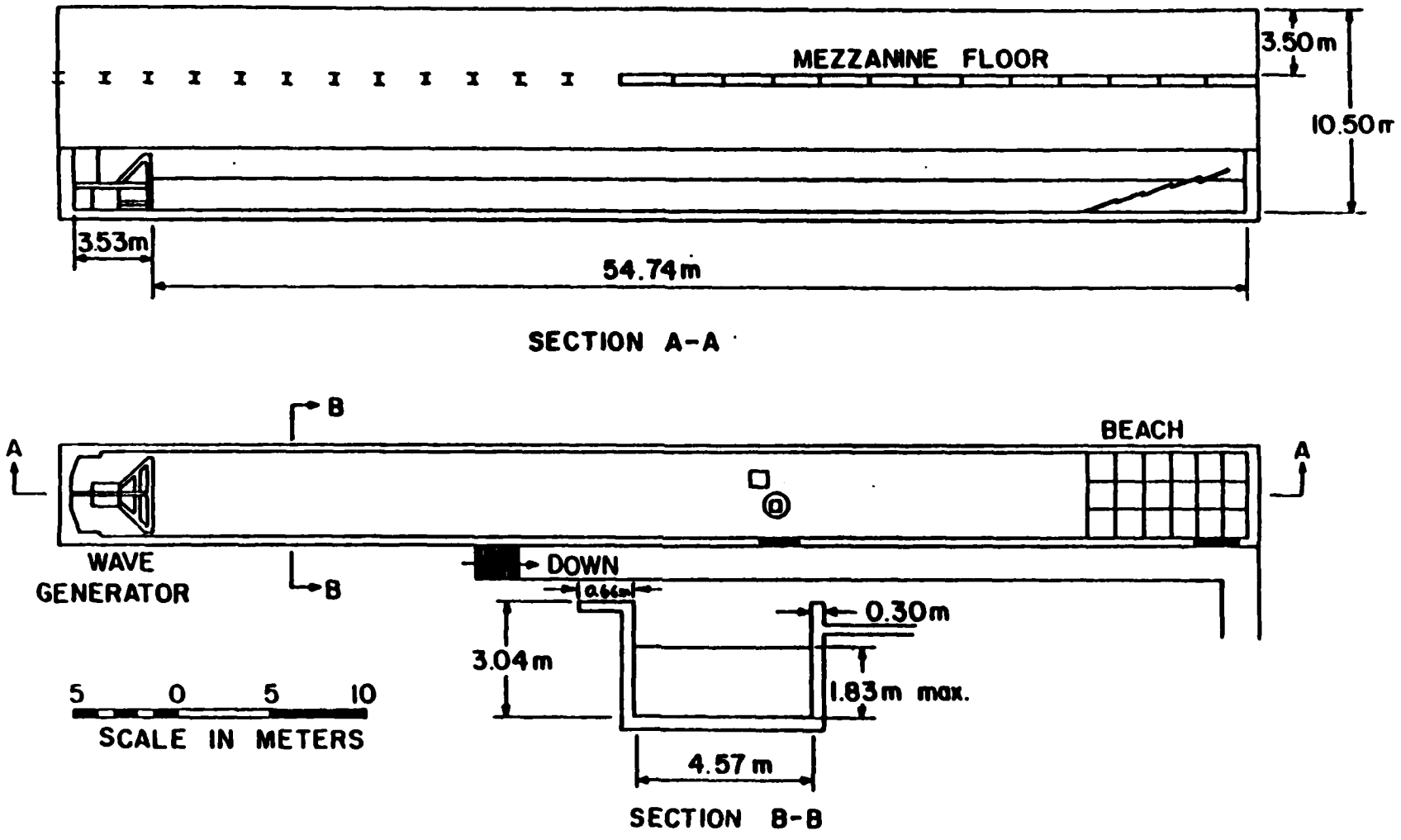

1094

Fig. 1 Elevation and Plan Views of Wave Tank

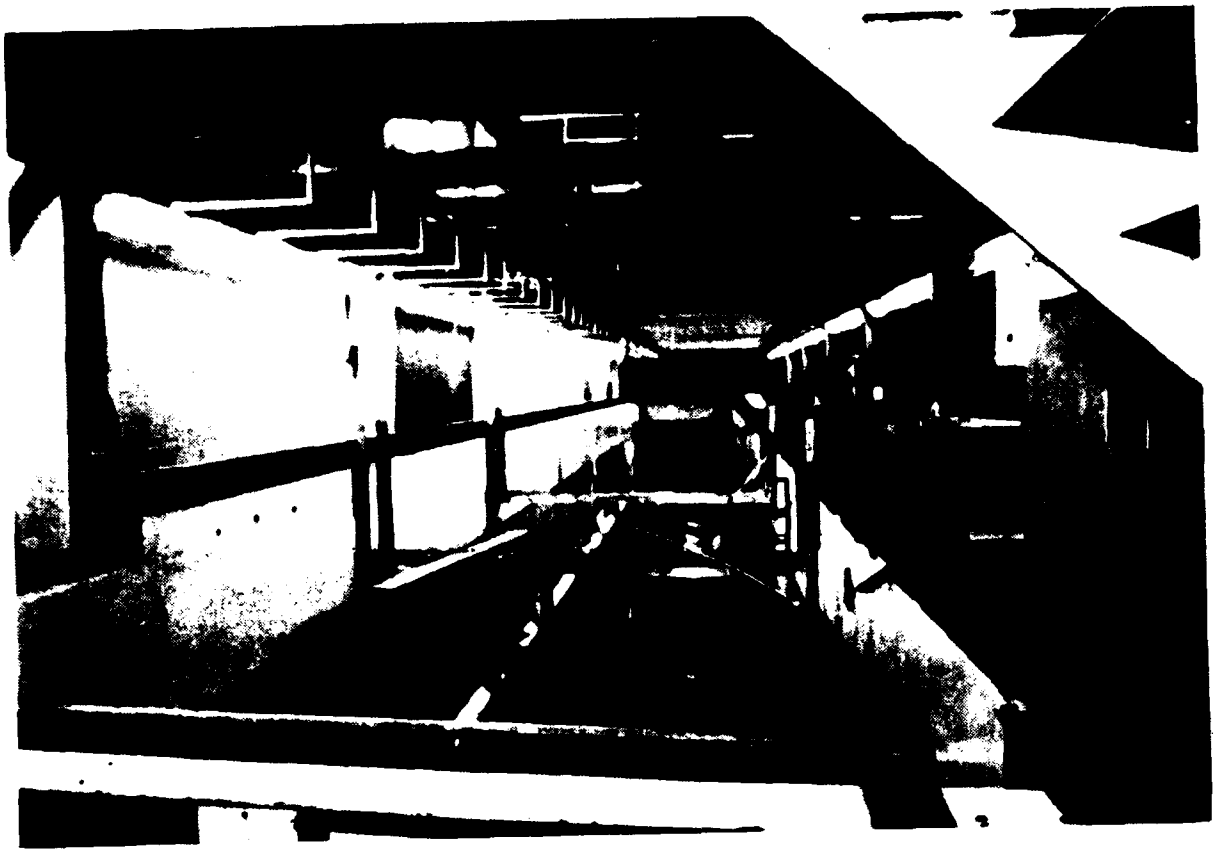

Fig. 2 Wave Tank with Rail Systems Installed

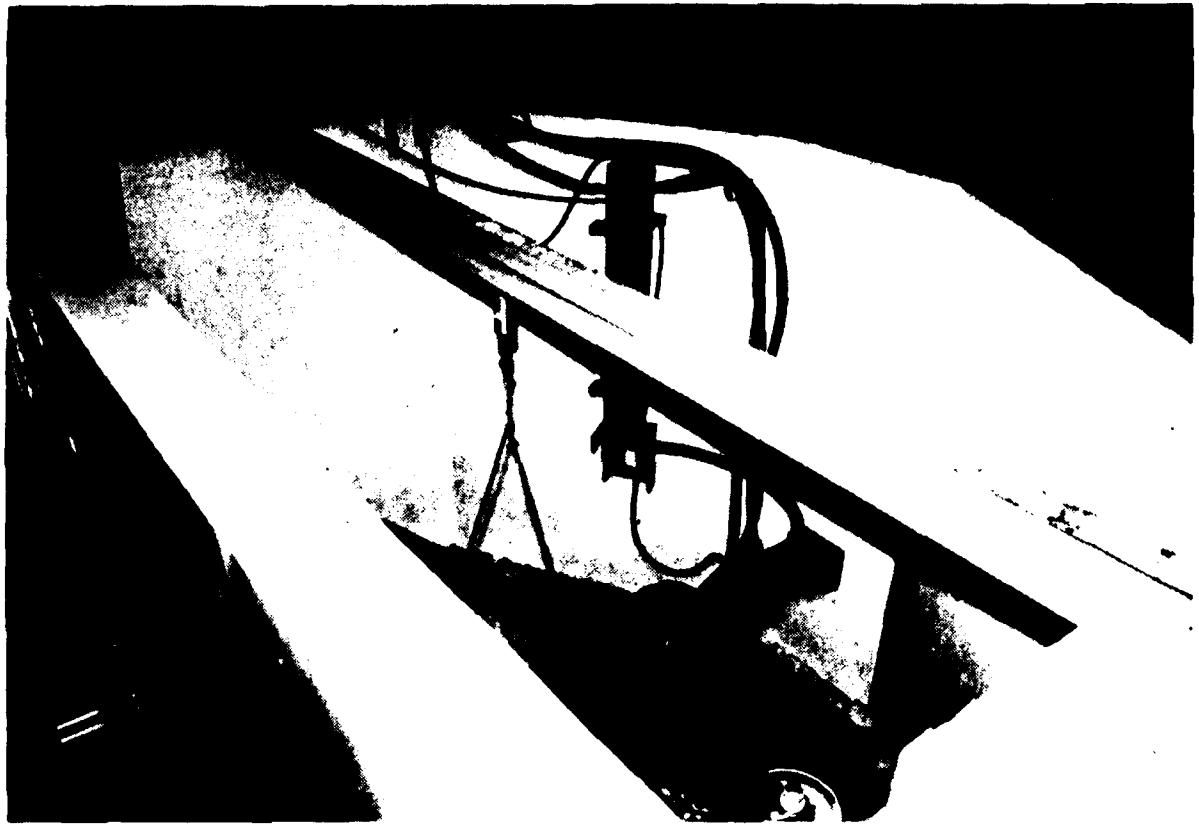

Fig. 3 Wave-Maker

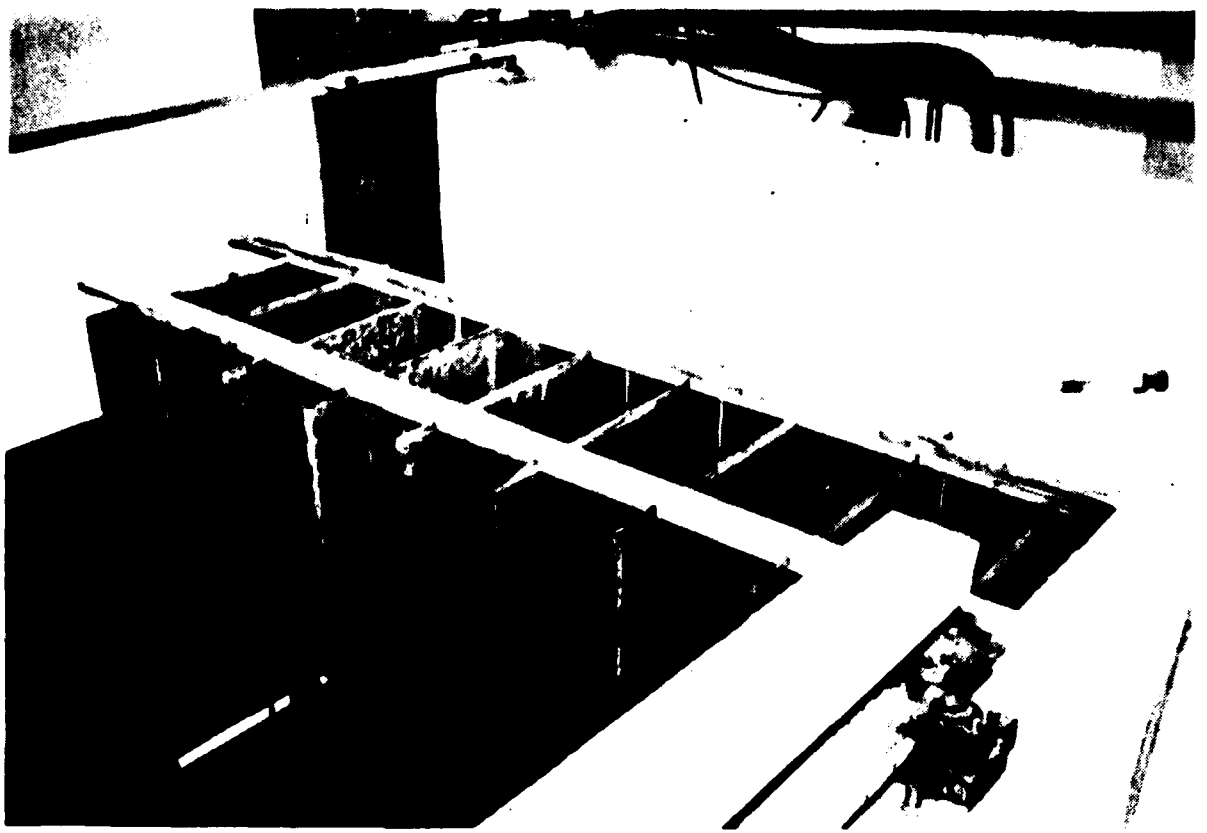

Fig. 4 Wave-Maker with Wave Rectifier

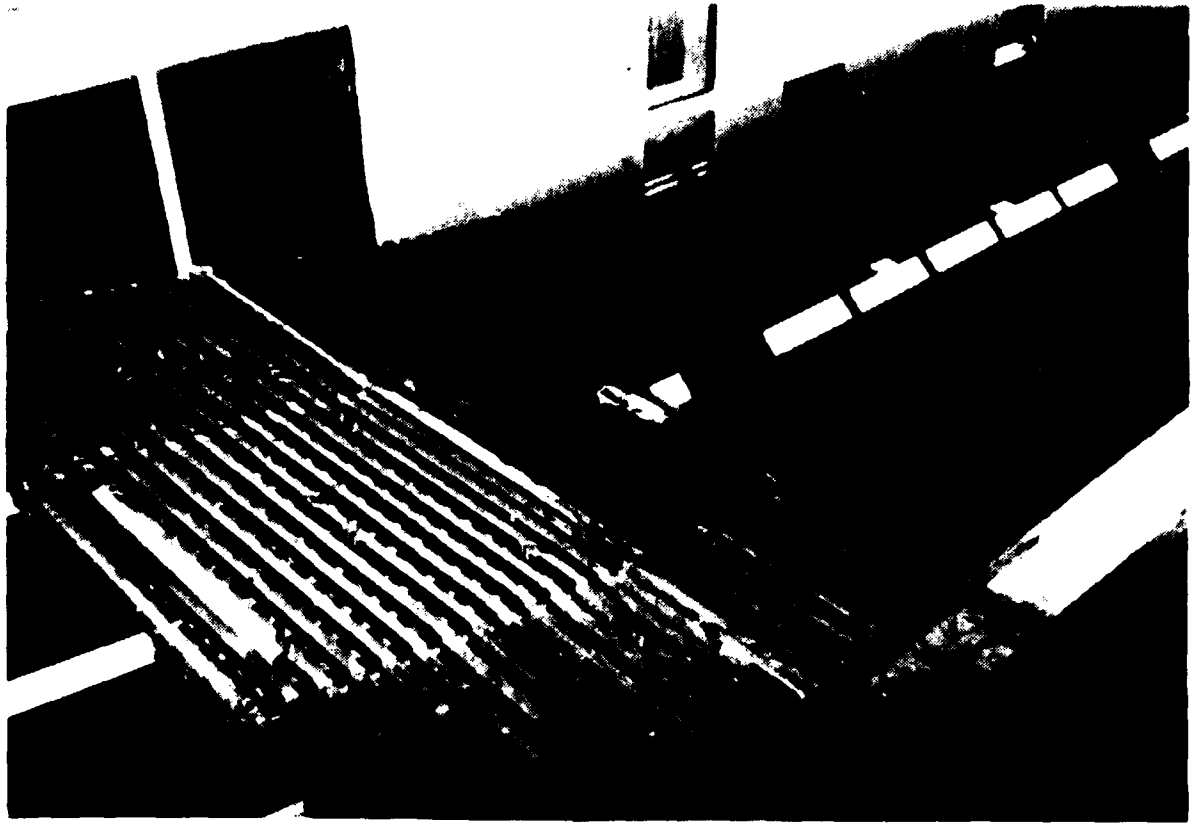

Fig. 5 Beach

1099

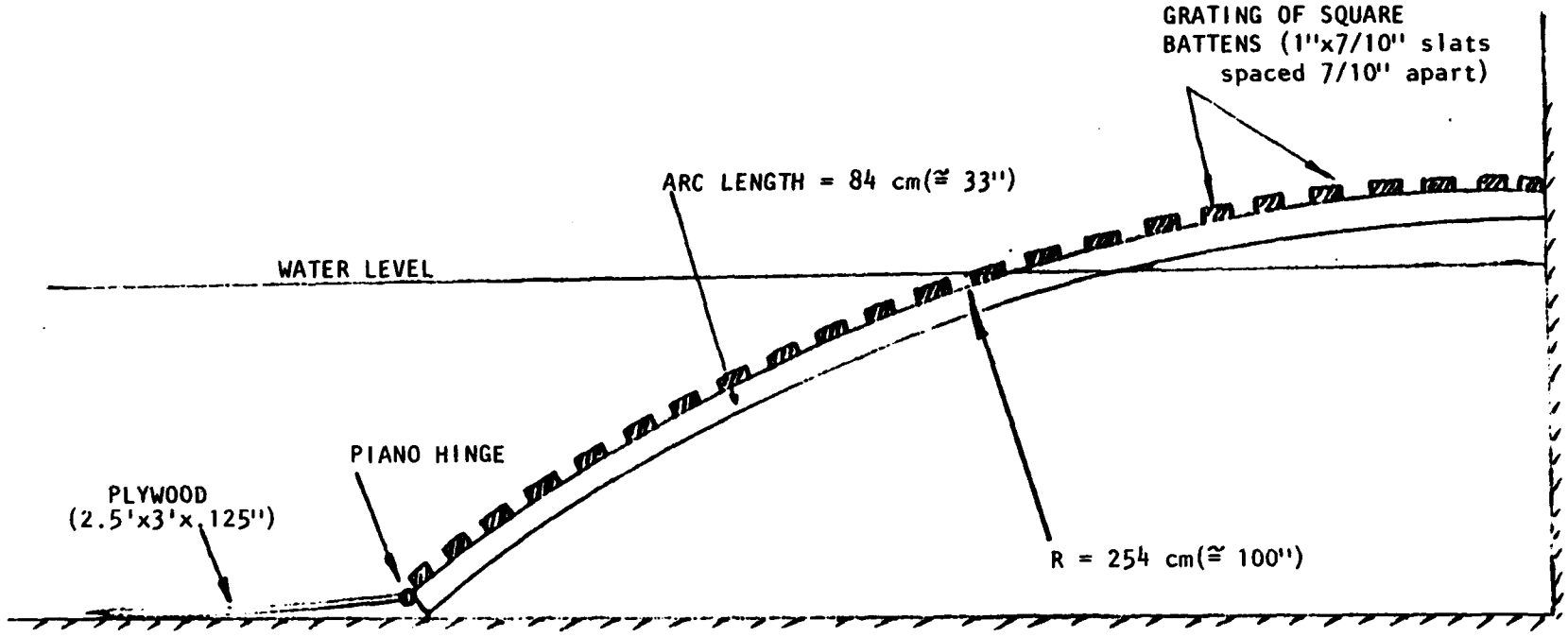

Fig. 6 Beach Model

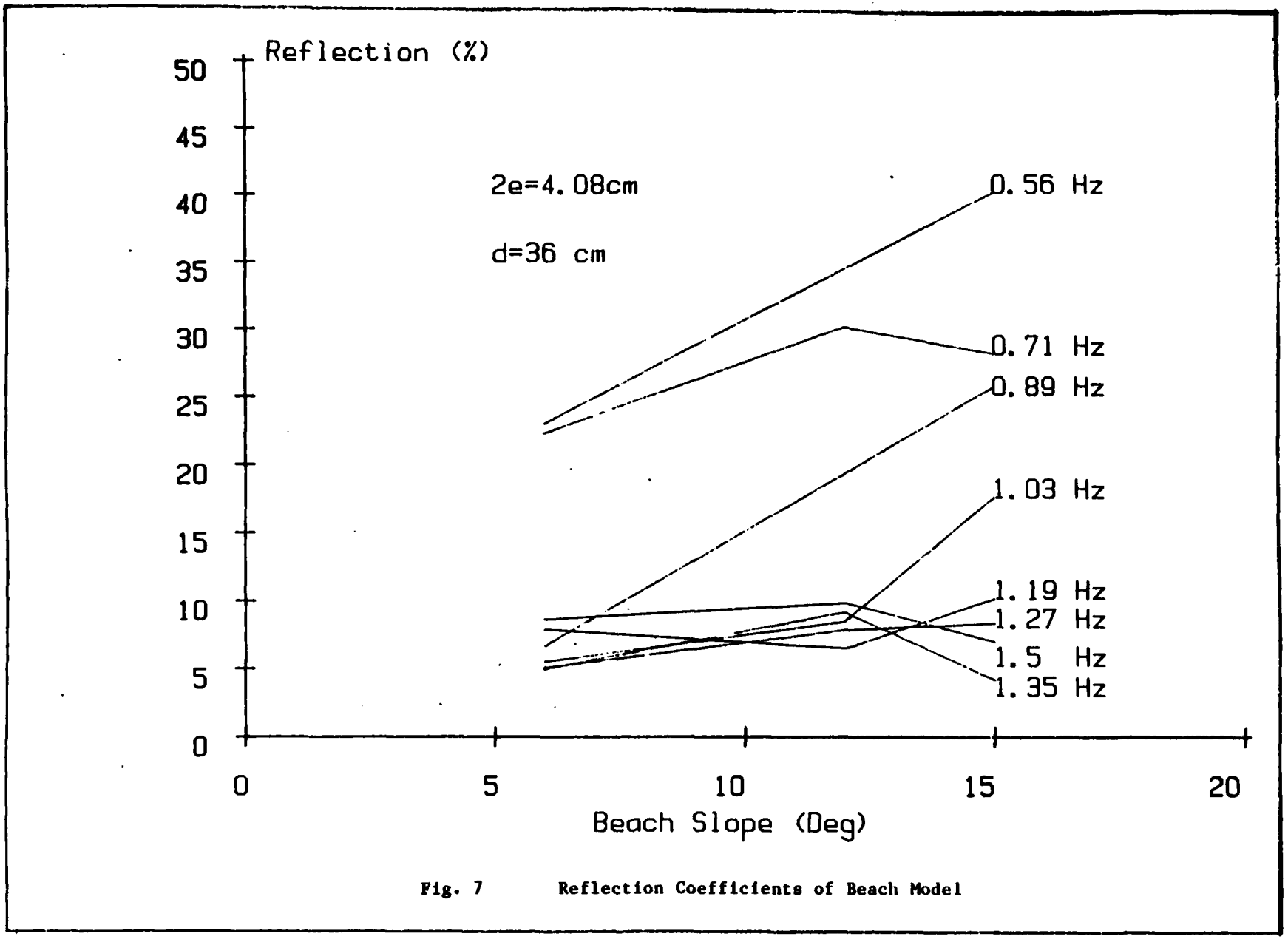

Fig. 7 Reflection Coefficients of Beach Model

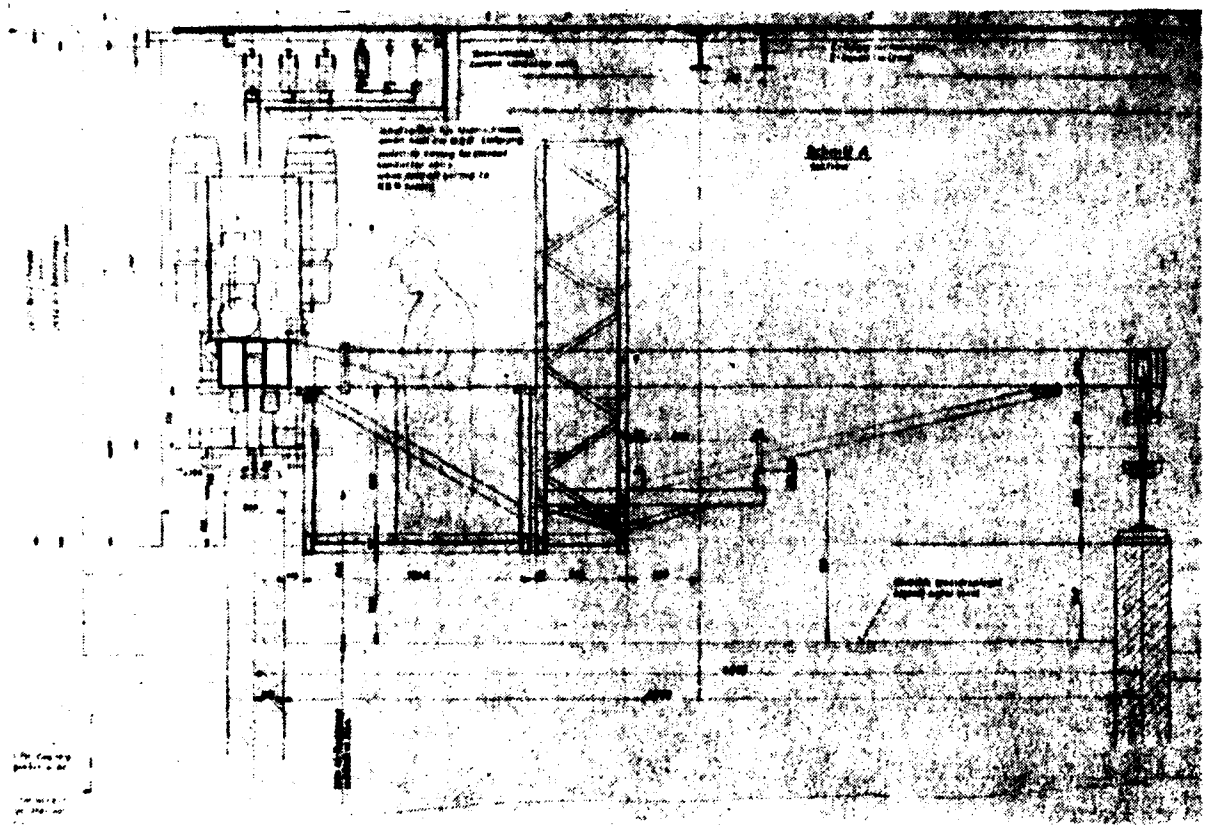

Fig. 8 Towing Carriage

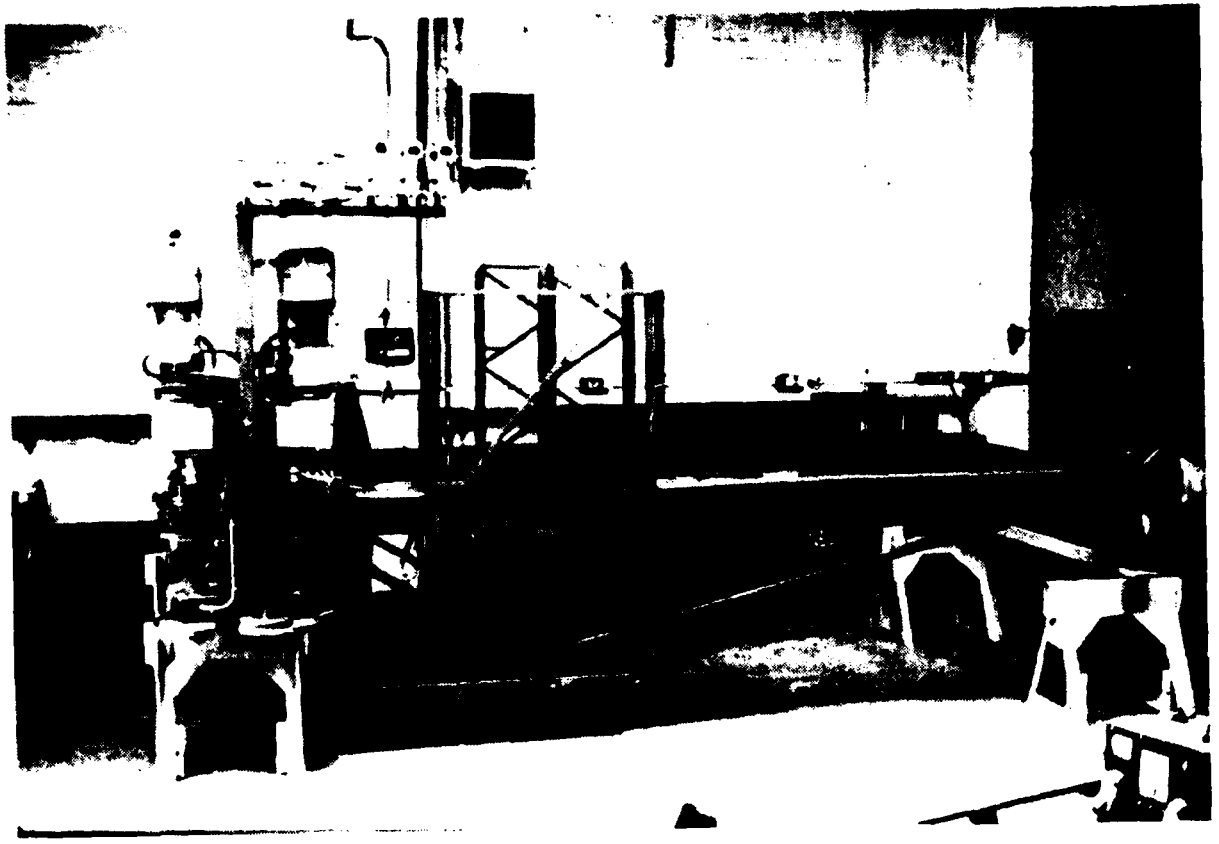

Fig. 9 Towing Carriage Assembly in Shop

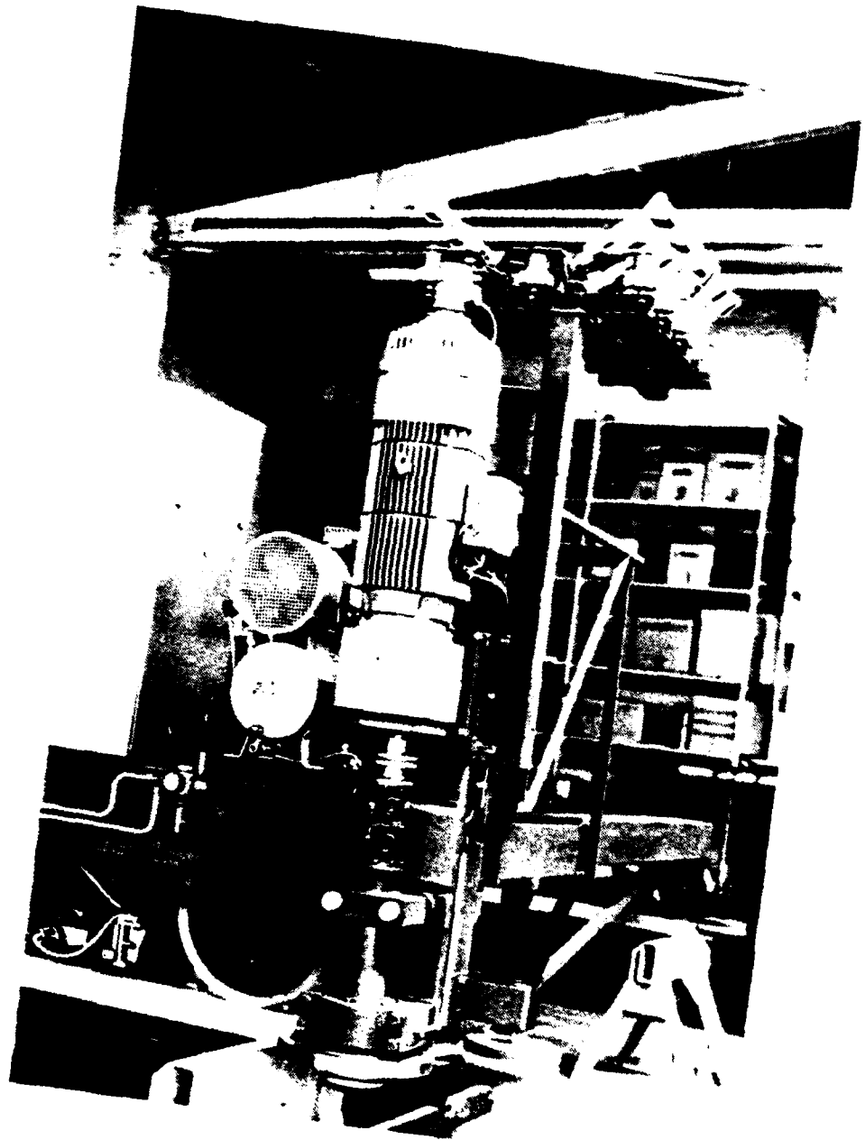

Fig. 10 Driving System and Current Conductor Post

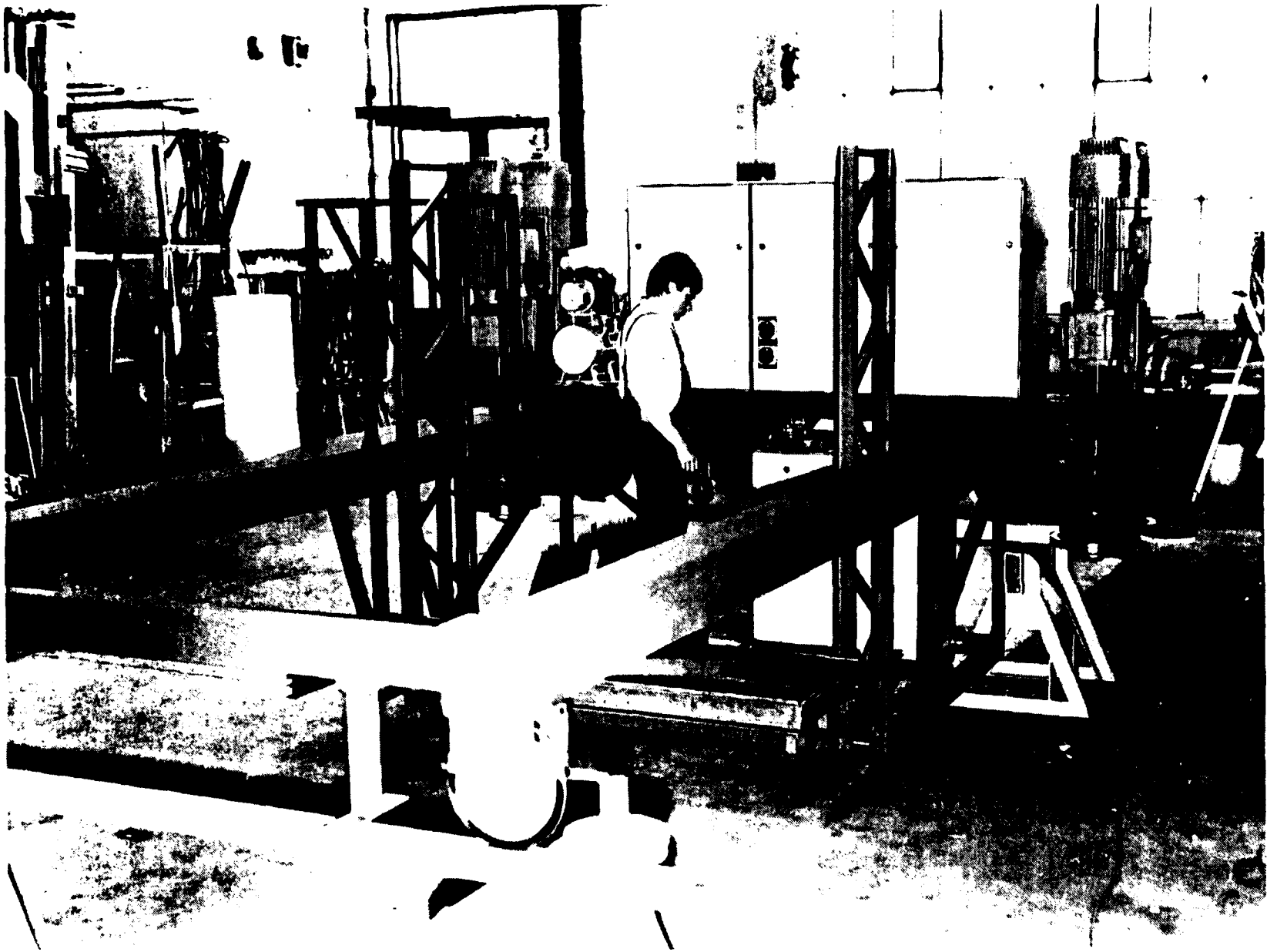

Fig. 11 Measuring Frame and Work Platform

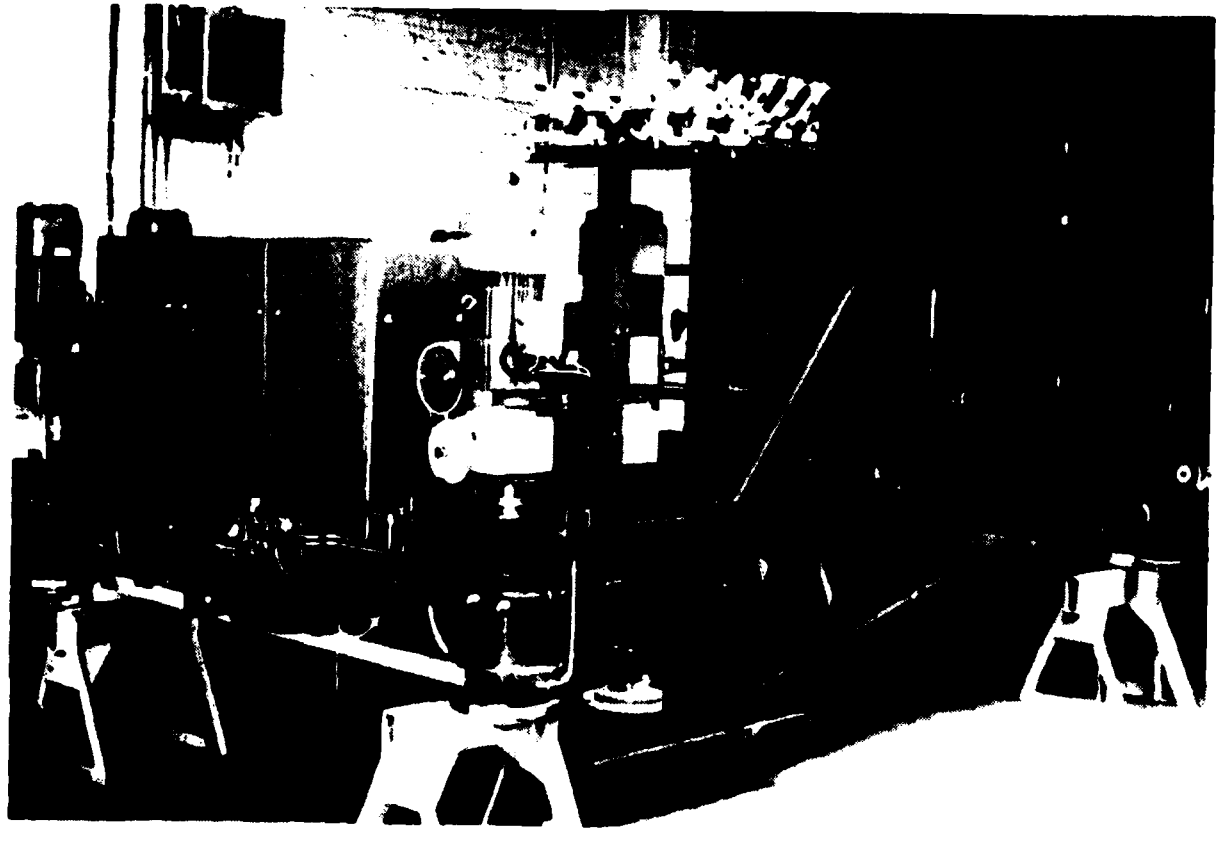

Fig. 12 Towing Carriage Assembly in Shop

AD-P003 832

NEW MODEL TESTING FACILITIES OF THE NRC ARCTIC VESSEL AND MARINE RESEARCH INSTITUTE

by

D. Gospodnetic and M.D. Miles
National Research Council of Canada

1. INTRODUCTION

In preparation for Canada's future development of natural resources, particularly in the Arctic and off the east coast, and also in support of its continuing role in hydrodynamic research and testing, the National Research Council has established a new Arctic Vessel and Marine Research Institute (AVMRI) which is currently under construction on the campus of Memorial University in St. John's, Newfoundland. AVMRI will evolve from the present NRC Marine Dynamics and Ship Laboratory located in Ottawa and the new laboratories should become operational late in 1985.

The institute is intended to provide NRC with an integrated centre for research in the fields of ship hydrodynamics, ice interaction and ocean engineering. Since the primary emphasis will be on physical model testing, the institute will contain a refrigerated ice model basin, a clearwater towing tank, a seakeeping/manoeuvring basin and various supporting facilities. ~~as shown in Figure 1.~~ Each of the main facilities is described in detail in the following sections.

2. ICE MODEL BASIN

The ice model basin has been designed primarily for resistance and propulsion tests of ships including flow visualization and detailed studies of ice interaction with hulls and propellers. The basin will also be used to study ice interaction with bottom-founded structures. The refrigerated towing tank will be the largest of its type in the world with a width of 12m, a depth of 3m and a usable length of 80m. A 15m long trim tank is located at one end of the towing tank and is separated from it by a thermal barrier gate. The opposite end of the tank has a sloped ramp leading into a melt pit which has an insulated cover to enable the next ice sheet to be grown while the remains of the previous one are melting.

The 12m width will allow larger scale models to be tested for propulsion and will also permit limited manoeuvring studies on smaller models. Since many tests will not require the full width, however, a removable centre barrier will allow the tank to be partitioned into two 6m lanes in order to obtain better ice sheet utilization. Typical model lengths will be 6 to 8m but models up to 12m in length can be accomodated.

The tank is constructed of steel reinforced concrete with a glass fibre reinforced epoxy liner and external polyurethane foam insulation. The walls and ceiling above the tank are constructed with prefabricated, steel-clad, urethane foam panels. The tank is supported on four rows of concrete columns with teflon pads to allow for thermal expansion. The basin has sufficient corrosion resistance to handle saline ice but carbamide (urea) doped ice will probably be used instead since studies at NRC have shown that it provides more accurately scaled model ice properties.

The refrigeration system will use two-stage mechanical compression and water cooled condensers. The rejected heat will be reclaimed for ice melting, domestic water preheat and tank wall perimeter heating via embedded pipes fed with glycol for ice sheet release. The ammonia refrigerant will be delivered to 28 ceiling hung evaporators in the main tank plus two similar units in the trim tank. Compressor capacity, evaporating pressure and fan speed will be computer controlled in order to obtain a uniform temperature distribution near the water surface. The aim is to provide a cold air supply over the upper part of the basin with heat transfer near the ice sheet/air interface by natural convection. The air temperature can be controlled from -30°C to +15°C and ice growth rates between 2.5 to 3mm/hour are anticipated with a maximum thickness of 15cm. A separate chiller system will control the water temperature between +1°C and -2°C.

The towing carriage will be about 14m long and weigh approximately 65 tonnes with a natural frequency of 12Hz. There will be two speed ranges; 1 to 200 mm/s and 0.02 to 4 m/s. The speed accuracy is specified at 1 mm/s at speeds below 1 m/s and 0.1% of setting at higher speeds. The maximum thrust available on the low speed range for testing fixed structures will be 6 tonnes on the centreline and 3 tonnes on the quarter points. A separate service carriage will be used for tasks such as skin clearing, seeding and testing samples of the ice sheet.

The main carriage will be equipped with a model test frame which can be moved 3 m transversely to accomodate either the full width or the partitioned tank. A U-shaped steel dock will be mounted on submerged rails in the trim tank so that the model and dock can be moved together when changing from one side of the partitioned tank to the other. It will also be possible to adjust the width of the dock to suit the beam of the model being tested.

A small, cable-towed, submerged carriage will carry a CCTV system and lights for observation of ice movement beneath the model being tested. The motion of the camera carriage will be automatically slaved to that of the main carriage with differential adjustment to allow for model surge.

3. CLEARWATER TOWING TANK

The tank is 200 m long, 12 m wide and 7 m deep. It is spanned by a towing carriage running on rails, electrically driven, capable of speeds up to 10 m/s. Specifications call for manual and for automatic drive mode in which speed and acceleration are selected leaving to the control to maintain the desired speed profile. Two speed ranges will be provided: 5 to 1000 mm/s, accurate to 1 mm/s and 0.5 to 10 m/s, accurate to 0.1% of the set speed. The carriage will be about 12 m long, weigh 65 tonnes and have a natural frequency of 12 Hz. It features computer controlled data acquisition, a movable model test frame and model access platform. At one end of the tank is a computer controlled double flap wavemaker, optimized for the range of wavelengths between 2 and 25 m. Maximum regular wave height is 1 m for wavelengths between 10 and 25 m. Maximum significant wave height is 0.5 m in irregular waves. The lower flap is 2.8 m high with the hinge at 4.0 m depth. The upper flap is 2.2 m high with the hinge at 1.2 m depth. Displacement of each flap is ± 16°. The back of the waveboard is dry. Separate hydraulic actuators balance the hydrostatic pressure and move the flaps. The wavemaker is driven by a microprocessor which accepts control signals generated by the data acquisition computer on the carriage. A parabolic beach with square transverse slats (70 mm square at 120 mm centres) is provided opposite the wavemaker. Overall length of the beach is 20 m; it's slope at the water surface is 10.5°.

4. SEAKEEPING AND MANOEUVRING BASIN

The seakeeping basin is located in the north building adjacent to the clearwater towing tank. It has been designed for three main types of tests:

(1) Seakeeping tests of moving vessels in oblique waves.

(2) Seakeeping tests of moored and bottom-founded offshore structures including hydroelastic effects.

(3) Manoeuvring tests of ships in deep water.

The basin is 75 m long, 32 m wide and has water depth variable from 0.4 to 3.5 m. A 4 m square pit in the centre of the tank will provide a maximum depth of 7.5 m for testing certain types of bottom-founded structures. A 3 by 8 m trim tank is located on the east side of the basin.

No carriage will be fitted to this tank, due primarily to cost considerations, so free-running, radio controlled ship models will be used with a typical length of 4 m. An X-Y crane with 4 tonne capacity will allow access platforms to be positioned anywhere in the basin for testing of moored structures, however.

The basin will be equipped with a computer-controlled, mixed frequency, serpentine wavemaker capable of generating both long and short-crested regular and irregular waves with angles of propagation up to 60 degrees from the normal. Wavelengths of 0.5 m and longer will be generated with a maximum wave height of 0.5 m for wavelengths from 5 to 9 m. The maximum significant wave height for irregular waves will be 0.3 m.

The wavemaker will consist of 190 individually-controlled segments with each segment being 0.5 m wide and 2 m high (1.5 m maximum immersion). The design of the wavemaker will not be finalized until January, 1984 but a 3-segment prototype is currently being tested in the NRC Hydraulics Laboratory. This unit uses hydraulic actuators and can operate in hinged flapper, piston and combined flapper/piston modes with maximum displacement of $\pm 20°$ in the flapper mode and ± 0.4 m in the piston mode. It should thus have sufficient displacement to control the second order boundary conditions required for proper generation of group-bound long waves and suppression of spurious free-running long waves. This is particularly important for testing moored structures such as semi-submersible rigs because of the very low resonant frequencies involved. The wavemaker will also be able to function as both a wave generator and an active wave absorber simultaneously by using feedback sensors to measure horizontal velocity and wave elevation on the board.

The wavemakers will be wall-mounted and adjustable in height to accomodate the range of water depths in the basin. Both the wavemakers and the passive beaches will be modular and portable so that their configuration can be altered to suit the particular type of test. Thus, an L-shaped configuration, similar to the NSMB seakeeping tank, will be used for tests of moving vessels but a U-shaped configuration may be used to obtain improved boundary conditions for testing moored structures, especially for short-crested seas and low frequency components.

Wind forces will be simulated by using either computer-controlled winches or fans. Although it would also be very useful to be able to generate currents in this facility, it has been necessary to defer this capability due to funding restrictions.

A six degree of freedom optical tracking system such as OPTOPOS or SELSPOT will be used to measure model motions during seakeeping and manoeuvring tests. A 32-channel digital radio telemetry system will be used to obtain data from various

types of model-mounted sensors such as force and pressure transducers. The radio control and telemetry equipment will be based on systems designed by NRC and currently in use at the AVMRI facilities in Ottawa.

5. MODEL MANUFACTURING FACILITIES

Ship model design and manufacture will follow the well established practices developed at the Ottawa Laboratory. The drawing office, using graphic terminals and plotters, interactively creates a lines plan and a digital definition of the hull, based on which the central computer prepares a cutting file. The raw wooden model (up to 12.0 m * 2.4 m * 1.2 m) is then cut according to that file by a gantry type CNC milling machine. A full implement of supporting equipment (large tables, glue press, lathes, etc.) is also available.

Ship model propellers are developed using similar computer-aided design techniques. The propellers are then cut on a standard 5 axes, vertical CNC milling machine capable of handling blades of up to 300 mm diameter.

6. COMPUTER SYSTEMS

The institute's computer system will basically consist of a large central 32-bit computer linked to four smaller 16-bit computers in a high-speed local area network. Three of the small systems will be dedicated to data acquisition, control and preliminary on-line analysis on the two towing carriages and in the seakeeping basin. The fourth system will be used for full scale trials.

The central system will perform a variety of tasks including final analysis of all test data, numerical modelling, CAD/CAM operations for model manufacturing, report generation and project management. Extensive use will be made of both high and medium resolution interactive graphics terminals. The central system will also compute the control signals for the segmented wavemaker in the seakeeping basin which will be driven in real time by a distributed system of microprocessors. It will also provide direct control of the two NC milling machines for production of model hulls and propellers.

The data acquisition systems will be able to function independently of the central system and will only transfer data to it at the end of a model test. This has been done for increased reliability and to prevent excessive loading of the central computer. Each system will be equipped with a graphics terminal, plotter and a 64-channel analog signal processor with 14-bit resolution and sampling rates up to 1000 samples per second on each channel. Transient recorders will provide higher burst rates up to 100,000 samples per second for slamming and impact tests.

7. BUILDING SCHEDULE

The project is divided in five phases:

Phase I Offices

Phase II Ice tank

Phase III Seakeeping, clearwater tanks

Phase IV Roads, landscaping

Phase V Installation of equipment

Phases I through IV are already underway and about 30% completed, to be finished by January 1985.

Installation of equipment (rails, carriages, wavemakers, milling machines, workshops etc.) will commence in the fall of 1984 and acceptance testing should be complete by the end of 1985.

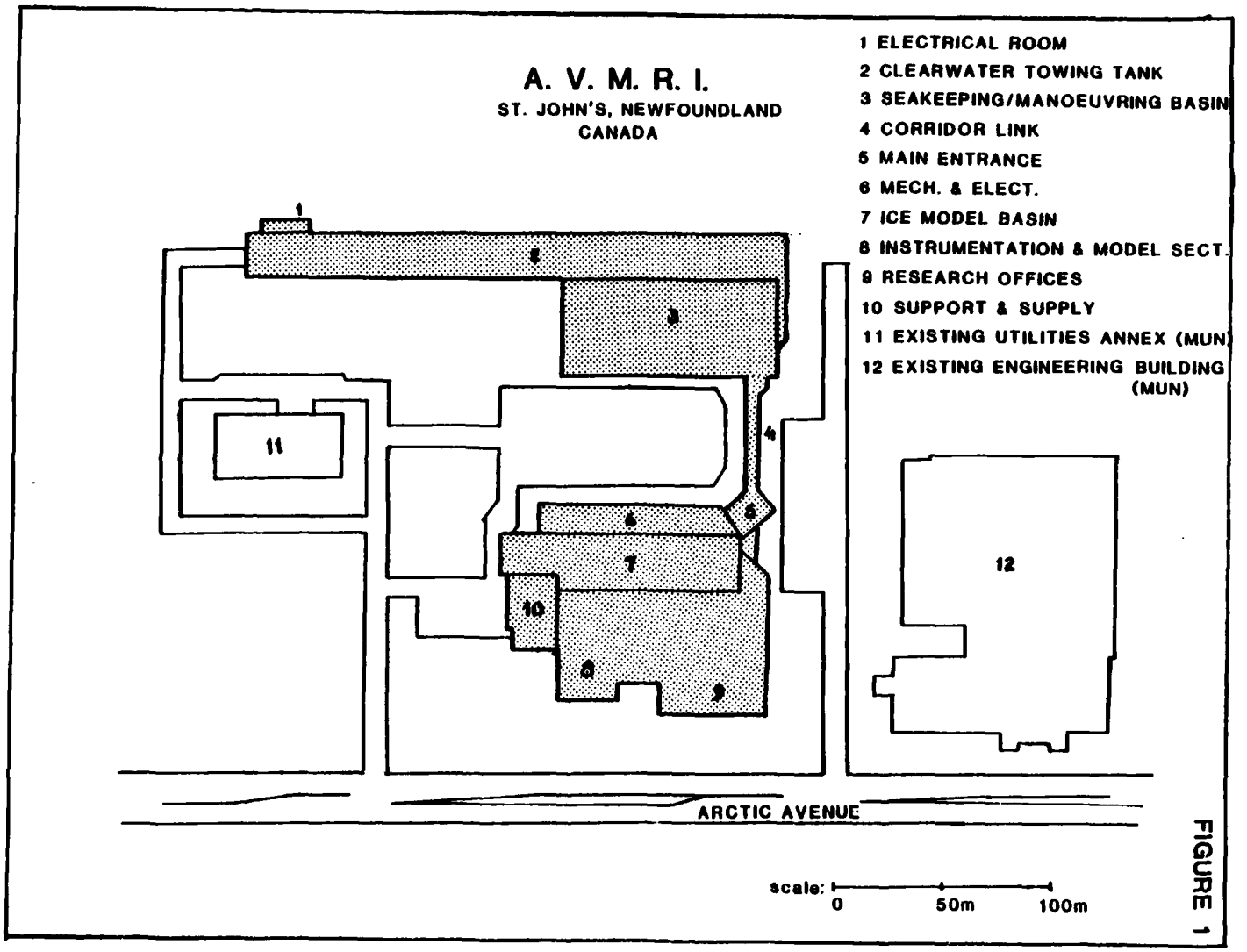
A. V. M. R. I.
ST. JOHN'S, NEWFOUNDLAND
CANADA
1 ELECTRICAL ROOM
2 CLEARWATER TOWING TANK
3 SEAKEEPING/MANOEUVRING BASIN
4 CORRIDOR LINK
5 MAIN ENTRANCE
6 MECH. & ELECT.
7 ICE MODEL BASIN
8 INSTRUMENTATION & MODEL SECT.
9 RESEARCH OFFICES
10 SUPPORT & SUPPLY
11 EXISTING UTILITIES ANNEX (MUN)
12 EXISTING ENGINEERING BUILDING (MUN)
ARCTIC AVENUE
scale: 0 50m 100m

FIGURE 1

A. V. M. R. I.

SEAKEEPING/MANOEUVRING BASIN
CLEARWATER TOWING TANK

ST. JOHN'S, NEWFOUNDLAND

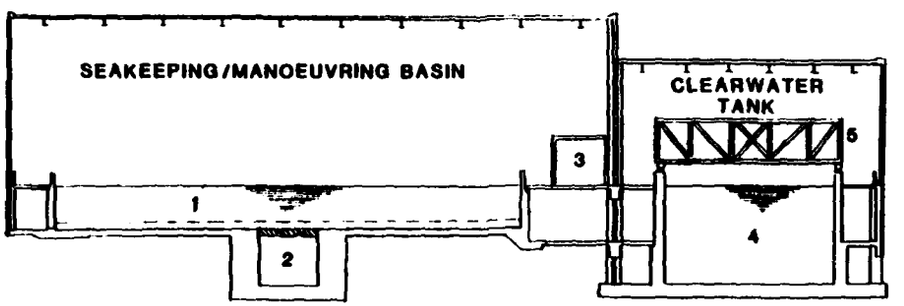

BUILDING SECTION

1 WATER DEPTH 3m
2 PIT 4 METRES SQUARE WITH REMOVABLE COVER
3 SEAKEEPING TANK CONTROL ROOM
4 WATER DEPTH 7m
5 TOWING CARRIAGE

scale: 0m 10m 20m

FIGURE 2

1114

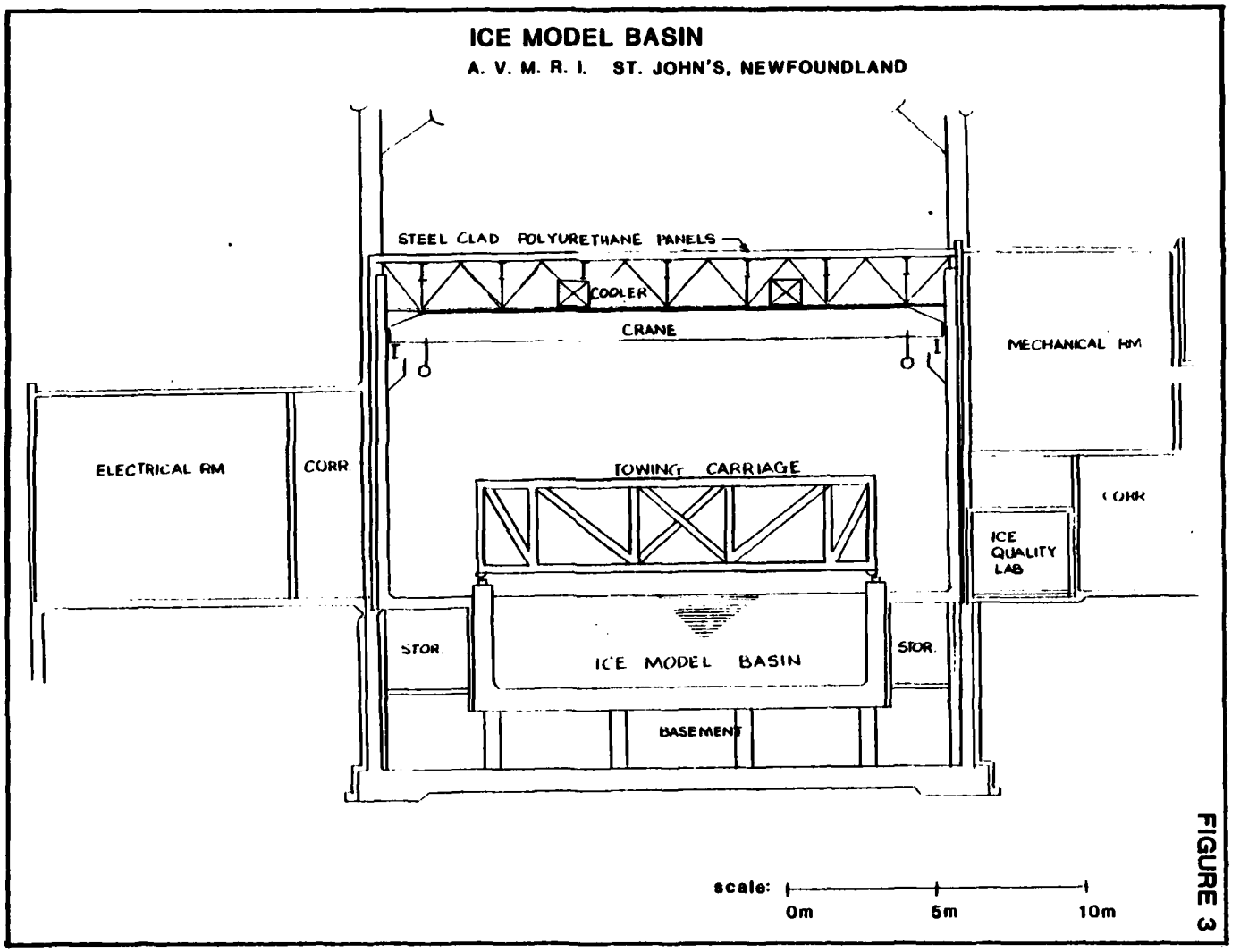
ICE MODEL BASIN
A. V. M. R. I. ST. JOHN'S, NEWFOUNDLAND
STEEL CLAD POLYURETHANE PANELS
COOLER
CRANE
MECHANICAL RM
ELECTRICAL RM
CORR.
TOWING CARRIAGE
CORR.
ICE QUALITY LAB
STOR.
ICE MODEL BASIN
STOR.
BASEMENT
scale:
0m
5m
10m

FIGURE 3

AD-P003 833

A MODERNIZED CONTROL SYSTEM FOR THE DAVID TAYLOR NAVAL SHIP R & D CENTER'S 36 INCH VARIABLE PRESSURE WATER TUNNEL

by

Harry D. Harper

David W. Taylor Naval Ship Research and Development Center
Bethesda, Maryland 20084

Paper presented at the
Systems and Techniques Symposium, 20th American Towing Tank Conference,
Davidson Laboratory, Stevens Institute of Technology,
Hoboken, New Jersey, 2-4 August 1983

ABSTRACT

The 36-Inch Variable Pressure Water Tunnel (VPWT) facility at David W. Taylor Naval Ship Research and Development Center (DTNSRDC) was placed in operation in 1963. Since then the tunnel has essentially been used full time, often on a two-shift-per- day basis, with only minor modifications to either the tunnel hardware or machinery. The original control system consisted of a vacuum tube type electronic control system that was upgraded to a discrete solid state electronic system in the mid 1960's.

In July 1980, DTNSRDC implemented a program to refurbish and upgrade the tunnel machinery and to replace the facility control system with state-of-the-art equipment. This should result in a more efficient facility capable of meeting the needs of our engineering staff and research scientists for the next two decades. The new control system is expected to improve the daily operating functions of the facility and to obtain experimental data at a higher level of productivity. The refurbishments consist of rebuilding and replacing certain pieces of machinery, modifying and upgrading the auxiliary water piping and replacing the control system.

This paper presents an overview of the functional operation of the 36-Inch VPWT and a description of the new system. The new approach taken by DTNSRDC with this facility is defined from an operational point of view. How and why the new computer based control system was selected is explained.

INTRODUCTION

The original facilities at The David Taylor Model Basin located at Carderock, Maryland became fully operational about 1940. The present 24-inch water tunnel was installed and placed in operation in late 1940 or early 1941. Although the addition of the 24-inch tunnel provided a moderate improvement in the Navy's ability to solve propulsion problems, it also pointed out the need for a larger, more flexible tunnel. With the United States entry into World War II, many new research problems surfaced. One of these was a need for a water tunnel test facility for propeller cavitation research with enough flexibility to perform various propeller and propulsion tests, as well as a facility for testing submerged bodies, hydrofoils, ship appendages, sonar domes, pump jets, etc.

At the end of World War II, work was started planning the present 36-Inch Variable-Pressure Water Tunnel (VPWT). Engineering plans and specifications were prepared by Seelye, Stevenson, Value, and Knecht, Consulting Engineers and The David Taylor Model Basin staff. They were completed in April 1951. Construction was started shortly after and the new tunnel was ready for acceptance testing and final calibration in early 1963.

DESCRIPTION

GENERAL DESIGN

The 36-Inch VPWT has been in operation for approximately twenty years in very much its original configuration of operational hardware. The tunnel is a closed loop circuit as shown in Figure 1; its vertical height between centerlines of the upper and lower horizontal legs is 28 feet 6 inches. The overall height of the entire tunnel with the resorber, which extends 78 feet into the ground below floor level, is 118 feet 6 inches. The overall length is 76 feet. In general, the tunnel

cross sections are circular. The tunnel may be operated with the resorber by-passed by interchanging the elbow and the upcomer; however, in the twenty years that the tunnel has been in operation there have been only two experiments requiring this configuration.

The tunnel is a variable-speed, variable pressure facility with two interchangeable test sections -- the open jet test section (Figure 2) and the closed jet test section (Figure 3). Model propellers up to 27 inches can be tested in the open jet test section (OJTS), propellers up to 18 inches in the closed jet test section (CJTS). The OJTS is used primarily for testing propellers and the CJTS, for testing appendages and bodies up to four feet in length. Both test sections have windows which permit visual and photographic observation. Both test sections also have access ports for model changes. The upper leg of the tunnel has two contrarotating dynamometer shafts each with a capacity of 1,000 SHP.

The primary drive system for the circulation of water in the tunnel consists of an S. Morgan Smith 78-inch diameter adjustable four blade propeller pump. The rated pump discharge is 597 cu.ft/sec for a head of 34 feet and 272 RPM. The rated input horsepower to the pump is 2,887. The pump is driven by a variable speed drive eddy current coupling built by Dynamatic Corp. The coupling is driven by a Westinghouse 3,500-hp, 2,300-volt, 3-phase, 60-cycle synchronous motor. The motor operates at a constant 300 RPM. The eddy current coupling is controlled by an electronic speed control system. This system controls the output shaft of the eddy current coupling from 0 to 272 RPM.

There are two propeller dynamometer drive systems, each driven by a 1750-hp induction motor. The speed of each dynamometer drive motor is controlled by a variable frequency alternating current generator. The output

of the generator is a function of the generator RPM which is controlled by an eddy current coupling. There is an individual coupling for each dynamometer drive motor. Two eddy current couplings are driven by a common 2,500-hp, 2,300-volt, 3-phase, 60-cycle induction motor which can operate at either 1,188 RPM or 596 RPM. Figure 4 is a simplified block diagram of the entire dynamometer drive system.

The test section pressure is regulated by the system shown in the block diagram Figure 5. The primary components of the system are a constant flow, positive displacement, 200 gal/min circulating pump whose input comes from the discharge manifold of the tunnel and the pressure regulating tank. The output of the pump feeds the intake manifold of the tunnel and the pressure regulating tank. The quantity of water passing through these two suction and discharge lines is controlled by a hydraulic servo valve system whose feedback comes from the test section pressure. When the set point pressure and the test section pressure are equal, each of the four valves passes 100 gal/min so that the amount of water leaving the tunnel at the discharge manifold is equal to the amount of water entering the tunnel at the intake manifold. At the same time the quantity of water entering and leaving the pressure regulating tank is equal. There is a secondary positive feedback control loop which senses the pressure head at the test section and adjust the head at the pressure regulating tank to equal that in the test section.

There are a number of systems which support the basic operating functions of the facility. They consist of tunnel filling and draining, tunnel filtering and circulating, vacuum-type deaerator, tunnel purge, impeller machinery lubrication, dynamometer drive system lubrication, machinery cooling water, and tunnel data. The original tunnel system

also included a refrigeration system for chilling the tunnel water. This system has been removed because it was found that it isn't necessary for experimental testing.

A much more detailed description of the original tunnel, its hardware and machinery are discussed in the W.F. Brownell Reports 1052 (June 1956) and 1690 (December 1962).

OPERATIONAL MODIFICATIONS

The original control system for the facility was mid-1950 technology which contained vacuum tube amplifier circuits and poorly regulated power supplies. After the tunnel was placed in operation in the early 1960's, it became apparent that the electronic control systems for the three drive systems were not providing the necessary regulation and tight control that was required for the experimental research being conducted in the facility. Rather than removing the entire electronic control system and starting over, it was determined that the original system could be modified and upgraded with solid state amplifiers and power supplies. This work was performed in the mid-1960's and did provide the necessary tight control parameter needed for experimental testing within the accuracy of available instrumentation at that time.

The control system for regulating tunnel pressure was also found to be inadequate in its original configuration. This system was also analyzed and modified to provide better pressure regulation. Similar to the three machinery drive systems, this system was upgraded with new solid state electronic control devices.

There have been many small changes made to the entire operating systems in the tunnel over the twenty years that it has been in service. Most of these were to correct known deficiencies that impeded operation or to improve

the operational efficiency of the facility. Also, a number of pressure gages, flow meters and other transducers have been added which provide the operating personnel with some information on how the tunnel is performing on a daily basis.

With the exception of these changes, the facility operates today very much as it did when it was placed in operation twenty years ago.

OPERATION

When the facility was placed in operation, an operating and maintenance manual was published which was used as a guide for tunnel operation. As is normal with all of the Ship Performance Department (SPD) facilities, the tunnel is operated and maintained by the Center's Industrial Department. The normal operation of the tunnel is performed by a test operations' electrician and machinist. These two people work as a team preparing the tunnel for operation on a daily basis. The electrician is responsible for the actual operation and is assisted by the machinist. Training basically consists of on-the-job training (OJT) on a one-to-one basis. Over the years a method of operation has been developed and passed on from operator-to-operator. The researcher or experimenter requests the tunnel operator to activate or deactivate various systems or subsystems depending on the requirements of an individual experiment. For a given experiment, the operator may be performing two or more sets of operating procedures simultaneously. Each operator follows his own sequence of events based on his knowledge and experience to accomplish the requested test conditions. The operating and maintenance manual does not provide detailed instructions on a sequence of events for the various experimental conditions which may be requested by the researcher or experimenter. It simply provides a generalized set of instructions on how the facility's various systems

operate. This has resulted in a wide range of procedures in performing the daily routine of preparing the tunnel for operation. The amount of time required to perform these functions also varies and is dependent on the individual experience and skill of the operating personnel. How these people work as a team also affects the time required to prepare the tunnel for operation or to change to new operating conditions. Industrial Department personnel are rotated in and out of the facility depending on the scheduled workload of that facility as well as the requirements for other Center facilities. Consequently, this results in no set routine procedure or predictable amount of time for daily preparation or operation of the facility.

The experience of the research scientist or experimenter also affects the operational efficiency of the facility. If the researcher is a senior engineer with many years of experience in conducting experimental test programs in the tunnel, the overall planning and implementation of the experiment flows much smoother. The experienced researcher has an understanding and knowledge of the impact of changing test conditions. He knows the when, why and how to plan the experiment so that time is efficiently allocated. He will plan his experiment so that changing operating conditions have a minimum impact on his test program. On the other hand, new or inexperienced test engineers are still involved in the process of learning the operational characteristics of the facility and often must rely on the tunnel operating personnel to advise them of the best sequence of operating conditions. This generally leads to some confusion and planning errors in conducting an experiment. The inexperienced project engineer also tends to be more concerned with many of the scientific details of a program and thus overlooks the operational

details which have a direct impact on the efficiency of daily operation of the facility.

The existing operating system in the tunnel has a large number of permissive electrical inlocks to prevent equipment damage in case of a system component failure. When this occurs, there are no troubleshooting guidelines for assisting the operating personnel in locating and correcting the malfunction. With each problem, the electrician or machinist starts from scratch and works toward finding and correcting the problem. With the experienced person, this can result in an efficient solution with only a small impact on tunnel productivity. Often even with a qualified test technician they must call for assistance from the Center's engineering staff.

Occasionally, problems arise because a researcher or experimental engineer feels that the data being collected is incorrect or is not what was expected. Sometimes a simple check calibration of tunnel parameters will resolve the problem. At other times, there is a need to carefully examine and analyze the mechanical or electrical systems involved before a solution can be validated. Although these types of malfunctions are rare, they have been found to be very time consuming and difficult to resolve. For example, as recently as two years ago a senior engineer detected deviation in a test propeller torque measurement. Three weeks working a minimum of sixteen hours per day were spent resolving the problem. The entire north dynamometer shaft and shaft housing was removed so that each of thirteen bearings in this drive system could be inspected. The results were, that an entire new set of bearings were installed and indeed the experimental torque data did improve. The unresolved question was which bearing or combination of bearings caused the

problem or was there, in fact, a shaft alignment problem that was corrected with the re-installation of the system. Downtime of this magnitude doesn't occur often but it is devastating to both the test program being run and future projects that have scheduled facility test time and are delayed.

There is a much more detailed discussion of the problems related to the operation of the facility in the Seidle (July 1982) Technical Report Number 2120 which was prepared by ORI, Inc. for the David W. Taylor Naval Ship Research and Development Center (DTNSRDC) under Contract N00167-81-D-F269. This report was part of a study to determine what should be done to increase the productivity and operational efficiency of the 36-Inch VPWT.

IMPROVEMENT PROGRAM

PLANS AND GOALS

In the early part of 1980, DTNSRDC was informed that the Navy would have funds available for capital improvements which would enhance the productivity of operations. DTNSRDC was instructed to identify programs to meet these goals. The 36-Inch VPWT was selected as a potential candidate for the program and necessary documentation was submitted to the Navy Material Command (NAVMAT) for funding approval. The upgrading of the 36-Inch VPWT was selected and approved for funding under the FY82 Cost of Ownership Reduction Investment (COORI) Program.

The goals for the program included the following:

(1) More efficient daily operation. Establish a more systematic operating procedure and minimize the requirements for human intervention into the process.

(2) Improve the methods of locating system problems, defining the problem and providing guidelines for the systematic correction of the problem.

(3) Predicting machinery or equipment faults/problems before they become critical rendering the facility inoperative and, based on the prediction of a probable fault, taking the necessary corrective action to eliminate or minimize the impact on daily operations.

(4) Obtain experimental data in a more productive manner and to develop basic data reduction programs to meet the needs of a broad base of experimental researchers.

(5) Improve the working environment for both the operating personnel and facility users. (It is felt that providing the operating personnel with a good work environment and adequate test and operating equipment will improve their overall ability to do work in a more productive manner.)

With the above goals as a guide, it was determined that the following objectives would lead to the desired results.

(1) Overhaul the entire impeller drive machinery system. This system has had twenty years of operating service without a major overhaul. The primary purpose of the overhaul was to insure that another twenty to thirty years of dependable service could be expected from the facility's number one priority system. (Experimental research can't be performed without the ability to move water.)

(2) Replace the existing control system with a system using the latest advances in control technology. The replacement control system would be computer based and have the ability to control, monitor, and do at least preliminary diagnostics of facility problems.

(3) Remodel the facility control room. Included in this objective was the replacement of the existing floor with a raised

floor similar to those in computer equipment centers. This provides flexibility for the installation of new equipment, modification of existing equipment, and the ability to maintain a clean functional work space. Also included is the replacement of the control room lighting system, electrical system, and the heating/air-conditioning systems.

(4) Replace the facility experimental instrumentation system. The existing instrumentation is mid-1960 technology and has become costly and time consuming to maintain in a good operational state.

IMPLEMENTATION

The first step in implementing the productivity enhancement program was the preparation of specifications and requirements for the overhaul of the impeller drive system machinery. This work was initiated in June 1981 and the contract was awarded in August 1982. Concurrent with this task a team of DTNSRDC engineers was formed to study the existing tunnel operations and control system. In order to get a better overall understanding of the operation and control of the facility, the Navy also awarded a contract to ORI, Inc. to assist with these tasks. It was felt that a new or different point of view would uncover areas in the existing operation and control that needed changes and that the Government team might overlook critical changes because of their familiarity with the existing procedures and equipment. It was also felt that the in-house staff, though capable of doing all of the necessary study requirements, had limited experience in modern control theory and applications. Using a contractor allowed the Government flexibility in studying and planning the best possible solution for improving the overall operational efficiency and productivity of the facility.

The combination team of Government-contractor engineers first did an in depth study of existing operating procedures, experimental procedures, and methods of troubleshooting/repair of malfunctions. This resulted in the operational flow charts which are Appendix A of this report.

Traditionally, the facility had been viewed as one large operational system. In the course of reviewing the entire tunnel operating system, the study team broke the tunnel functions down into clearly defined subsystem and prepared functional diagrams of each individual subsystem. They studied each subsystem and its functional relationship to all other subsystems, as well as its relationship to operation of the facility to carry out the requirements of the researcher or experimenter.

The tunnel was redefined into the following subsystems:

(1) Impeller Drive Subsystem

(2) North Dynamometer Drive Subsystem

(3) South Dynamometer Drive Subsystem

(4) North Dynamometer Drive Lubrication Subsystem

(5) South Dynamometer Drive Lubrication Subsystem

(6) Machinery Lubrication Cooling Water Subsystem

  (a) North and South Dynamometer

  (b) Impeller

(7) Impeller Drive Lubrication Subsystem

(8) Auxiliary Water Subsystem

  (a) Tunnel Pressure Regulation

  (b) Tunnel Deaerator

  (c) Tunnel Purge

  (d) Tunnel Water Filling, Draining, and Filtering

(9) Tunnel Control Center Subsystem

(10) Tunnel Experimental Data Collection Subsystem

DESCRIPTION OF SUBSYSTEMS

A brief description of each subsystem is given in the subsequent paragraphs.

Impeller Drive Subsystem

The basic equipment which is a part of the impeller drive system was described earlier in this report. Figure 6 is a diagram showing the primary components and their relationship to each other. The primary function of this subsystem is to pump water through the the tunnel loop at a predetermined velocity and to maintain that velocity within the prescribed limits. The drive system is capable of water velocities up to and including 50 knots. The impeller has a variable pitch blade angle mechanism which allows the experimenter to vary tunnel vibration and noise characteristics for a given test velocity. The impeller lubrication and cooling water subsystems are used in conjunction with this drive system.

North and South Dynamometer Drive Subsystems

The primary purpose of these two drive systems is to rotate test propellers at the desired test RPM. The experimenter may use either drive subsystem individually as required by his research test program or he may operate both subsystems simultaneously as a contrarotating drive system for testing twin propellers. The subsystems have some common components as was described earlier in this report and are shown in Figure 4. Each system has its own 1,750 hp induction drive motor, thrust bearing, slip ring assembly for experimental data retrieval, and tunnel seal. Each system has two primary speed ranges. The low speed range is from 0 to 2,300 RPM and the high speed range is from 0 to 4,600 RPM. A 2.15:1 ration gear box

may be added in the drive shaft to increase the maximum operating speed to 10,000 RPM. Each dynamometer drive system depends on both a lubrication and cooling water system for operation.

The instrumentation dynamometers for measuring torque, thrust, and bending moment are located at the end of each shaft just in front of the test propellers. The electrical excitation and the resultant electrical data signals are transmitted to and from the dynamometer via the slip ring assembly.

North and South Dynamometer Drive Lubrication Subsystems

These subsystems are used to provide the necessary oil lubrication for the bearings and other rotating machinery. Included in this is the main drive motor, the eddy current coupling, and alternator, the dynamometer shaft induction motor, the thrust bearing, the gear box, and the slip ring bearings. These systems consist of oil pumps, oil reservoirs, heaters, heat exchangers, and operational piping with valves.

Machinery Lubrication Cooling Water Subsystems

It is necessary to maintain the correct oil temperatures for the various lubrication systems and equipment. There are a number of heat exchangers for these oil lubrication systems through which cooling water is pumped from a storage tank through the equipment, then to a cooling tower adjacent to the building and back to the storage tank. Each of the three eddy current couplings (impeller, north dynamometer, and south dynamometer) is built with a cooling water jacket intergal to the equipment. Similar to the oil system, cooling water is pumped from a storage tank through the couplings, into a cooling tower, and back to the storage

tank. On all of these systems there are temperature sensors measuring oil and water temperatures and controlling valves which adjust the water flow to provide the correct amount of cooling for maintaining the proper operating temperatures of the machinery.

Impeller Drive Lubrication Subsystem

Similar to the dynamometer drive subsystem, the impeller drive oil lubrication subsystem provides the necessary oil lube for the rotating machinery which makes up the drive system. It consists of oil pumps and reservoirs and the necessary operational piping, valves and flow transducers to control oil flow to the drive motor, eddy current coupling, blade angle servo motor, and thrust bearing.

Auxiliary Water Subsystems

As stated previously, the auxiliary water subsystem performs a variety of functions. The most important of these is regulation of the tunnel pressure. A functional diagram of this system is shown in Figure 5 and a description of its operation has already been presented. The system control is furnished by the four proportional control hydraulic servo valves and a control valve for head pressure adjustment between the test section and the pressure regulating tank.

The tunnel deaerator subsystem transfers water from the tunnel to the deaerator tank. The tunnel water enters the tank at the top and falls through a system of baffles and trays which breaks it up into small droplets with the air being removed by a vacuum pump which maintains 28 inches of vacuum above the deaerator tank water level. The water at the bottom of the tank is returned to the tunnel. The air content can be reduced from saturation at 60 degrees F to 2 cc/liter in approximately eight hours.

Figure 7 is a functional diagram of this subsystem.

The tunnel purge subsystem used to remove from the tunnel any air which has separated from the water and collects at the high points in the tunnel, including the resorber. The system consists of a 150-gpm pump and two water powered vacuum jets (eductors) which form a system to remove air from the top of the tunnel. Figure 8 is a functional diagram of this subsystem.

Other functions which must be controlled include filling, draining and filtering the tunnel water. These functions are performed by pumps, valves, and operational piping which can be implemented as needed to meet test requirements.

Tunnel Control Subsystem

In the existing facility, the tunnel control subsystem is in reality the control console. This is the operational center for controlling the necessary functions of each subsystem. The tunnel operator is the key element in this operational arrangement. It is his responsibility to start and operate each subsystem. He must be cognizant of each subsystem and its relationship to all other subsystems. Depending on test or operational requirements, he will direct the work of other tunnel operating personnel, instructing them to open or close valves, start or stop pumps, etc. The control console does have a number of hardwired electrical permissives which assist the operator in placing the given subsystem in the proper operating mode. The control console also has a large number of status indicators which the operator must be aware of and understand their relationship to tunnel operation. The present control system is a labor-intentive system which requires a highly skilled operator who knows thoroughly the various nuances of the facility.

Tunnel Experimental Data Collection Subsystem

The experimental data collection subsystem is the basic tool of the researcher or experimenter using the facility. It measures, records, and operates or calculates the experimental data for each experimental test condition. The system measures the basic tunnel parameters of tunnel velocity, tunnel pressure, and tunnel temperature. It also measures the test propeller speed, torque, thrust, and bending moment. The system can be expanded to measure other test parameters as required for each individual experiment. For instance, if a shape or body is being tested that requires pressure distribution data, then the measurement system can be configured to measure any number of pressures on the surface of the body being tested. It is not the intention of this report to describe in detail the experimental capabilities of the facility so no further description of this subsystem will be addressed.

All of the facility's operating subsystems are described and shown in much greater detail in the specifications and functional diagrams which were developed for the purchase of the upgraded computerized control system for the facility.

DESCRIPTION OF NEW CONTROL SYSTEM

MODELING AND SIMULATION

The initial phase of implementing the new computer-based control system will consist of computer math modeling of the primary subsystems of the facility. There are four primary subsystems to be modeled to establish the control algorithms. These are the pressure regulation subsystem, the water velocity (impeller) subsystem, and two test body rotation (dynamometer) subsystems. Of these, pressure regulation is the more complex.

The complexity of pressure regulation in the 36-Inch VPWT system and inadequate performance of analog servo controllers requires that a model of the system be used to develop control algorithms which will provide acceptable operation over the wide operating range. This approach to development of the control system--firmly grounded on a math model of the facility, its subsystems, and existing sensors--provides assurance that the capacity and performance of all selected hardware and system components are adequately specified prior to implementation.

Since pressure regulation is achieved primarily through control of mass flux into or out of the tunnel, all subsystems which influence the amount of water in the system or the effective volume occupied by the water must be considered. These include the deaerator, purge, filter and circulate, storage, and pressure regulation subsystems. Additionally, unintentional mass flux due to leakage at the dynamometer and impeller seals must be modeled.

The air content of the water and air and water removed by the purge system at various locations in the tunnel and reinjection upstream of the impeller must be included. Although water compressibility is defined in terms of bulk modulus, the compressibility effects vary significantly as a result of air and water vapor bubbles. These effects are considered as well as tunnel expansion. While tunnel expansion is difficult to quantify, it is important that these effects be included in the model if the control system is to be designed with adequate stability margins over the entire operating range.

The approach is to describe the system using several control volumes and a lumped parameter technique. Within a control volume,

system parameters are treated as being time-dependent only. The effects of spatial dependency, such as friction losses through piping, or momentum changes through corners, are lumped instead at a point between control volumes. For each lumped control volume, the fundamental relationships of momentum, mass conservation, and energy conservation are applied. The preliminary analysis indicates that energy conservation considerations are not significant since the system is nearly isothermal. For completeness, however, these effects will be incorporated where applicable. Momentum considerations and conservation of mass relationships are much more significant. For example, application of conservation of mass to a control volume for the VPWT results in the following equation:

$$\Sigma \dot{m}_{in} - \Sigma \dot{m}_{out} = [\beta_w \rho_w V_T + (\beta_A \rho_A + \beta_w \rho_w) V_A + \rho_w \frac{\partial V_T}{\partial P}] \frac{dP}{dt}$$

where

$\Sigma \dot{m}$ is the sum of mass flux into or out of the tunnel, including both air and water

$\beta_w p_w V_t$ is a function defining the compressibility of water

$(\beta_A p_A + \beta_w p_w) V_A$ is a function defining the compressibility of air and water vapor bubbles within the control volume

$\rho_w \frac{\partial V_T}{\partial P}$ is a function defining the expansion of the control volume (i.e., tunnel) with respect to Pressure

$\frac{dP}{dt}$ is the rate of change of pressure in the control volume

From this relationship alone, it can be seen that the following effects must included:

(1) Compressibility of water - this is typically expressed in terms of a bulk modulus.

(2) Compressibility of air and water vapor bubbles - although

the compressibility of air is straightforward, the problem is complicated because first, the exact amount of air in the tunnel is indeterminant and second, water vapor bubbles can form and then collapse again as pressure varies throughout the tunnel and with time. The net result is that the combined compressibility effect of water, air bubbles, and water vapor bubbles can vary significantly from element to element within the tunnel. These effects must be so modeled that a control law can be devised which is tolerant of a wide range of these effects.

(3) Tunnel expansion - since the tunnel walls are not rigid, they expand with increasing pressure. While a nominal value for tunnel expansion can be calculated, expansion effects will vary throughout the tunnel as a function of tunnel geometry and local pressure. As with air and water compressibility effects, tunnel expansion must be so modeled that a sufficiently robust control law is developed.

(4) Mass Flux - All sources of mass entering or leaving the tunnel must be modeled. If empirical data are not available on leakage rates, leakage will be treated as a variable to be evaluated parametrically over a reasonable range in the same manner as compressibility effects and tunnel expansion are treated.

HARDWARE

There are a number of factors which affected the decision as to whether the configuration for the control system should utilize centralized or distributed processing. Of these, the major technical considera-

tion was throughput. For the VPWT, throughput relates to either how fast an out-of-limit parameter can be detected and corrective action taken or to how fast a digital control algorithm can be updated so as to maintain specified controller characteristics. Both of these can only be quantified by careful analysis of the associated process time constants. Specifying throughput in turn specifies data acquisition rates, transmission rates, and processing rates.

Since the data acquisition rate is a function of sampling speed and the number of inputs, higher effective rates can be achieved by using multiple collector units. For the VPWT, this is especially important because of the high common mode voltages which necessitate relay multiplexing. The transmission rate between the data system and the processor depends upon distance and the type of interface. Whereas close coupled systems can incorporate high-speed techniques, the distances involved for the VPWT will require slower interfaces. Finally, the processing rate is dependent upon processor characteristics and the application software.

The VPWT control system (Figure 9) is a distributed processing network consisting of a host processor, five node processors, and microprocessor-based digital controllers. This arrangement was chosen for three reasons:

(1) Distributed processing provides for higher effective throughput rates. With this arrangement, inputs can be checked for limits at the node processors. This enables detection to be made locally by the node processor rather than remotely by the host thus reducing communications.

(2) Distributed processing provides for expansion without significant degradation of system performance. Considering the requirements for hardware expansion, this is a significant factor affecting future performance.

(3) This network provides both flexibility and maintainability by utilizing remote processors which incorporate self-diagnostics.

The host processor will be a high-performance mini-computer equipped with 1-MByte main memory, a 65-MByte Winchester disc, a floating-point processor, and supporting peripherals. The key features are: a base performance of 2 million instructions per second, capability of 234k single precision floating point instructions per second, memory capacity of 4,096-MBytes, memory cycle time of 500 nanoseconds, and built in diagnostics. The node processors are 16-bit task processors which interface the remote multiplexers to the host using a coaxial communications link. The key features of the distributed processors are: common mode voltage of 350v peak, common mode rejection of 104 db, crosstalk of 120 db, accuracy $\pm$ 0.05 percent full scale, sampling rate of 500 samples per second, with 14-bit resolution, and built in diagnostics. The node processors are expandable to 2,000 points.

As a consequence of both the large number of I/O points (approximately 800) and the distances associated with the VPWT, it is economically attractive to use multiple remote data collectors rather than route all I/O wiring to a central location. Tentatively, five remote collectors are planned. However, the optimum number of collectors and their location will be established based on I/O geographical distribution density, cabling and installation cost, and equipment costs. By incorporating a

processor with each remote unit, the collectors will function as pre-processors thus improving overall response.

As shown, the system uses microprocessor-based digital controllers for the continuous control loops. Digital controllers with a self-tuning PID algorithm were chosen for all loops both to provide an interface for the operator at the console and to incorporate a keep-alive signal. For loops where it is determined from the process simulation that the control algorithm requires a more sophisticated technique than a self-tuning PID, the controllers will be set to use strictly the proportional feature with unity gain. For these loops, the control algorithm will be executed in the host processor. In the event the computer loses power, the controllers will detect the loss of the keep-alive signal and will maintain the last setpoint. The digital controllers interface to existing analog controllers using a switch located at the controller combined with a customized controller interface circuit.

APPLICATION SOFTWARE

As a consequence of the VPWT's numerous subsystems and extensive interactions, extensive application software is required to implement coordinated control. The system must be capable of ascertaining at all times the status of all subsystems. This, combined with pre-defined startup, control and shutdown strategies, is used to ensure that all subsystems are properly integrated and operated as a total system. The various operations that the control system provides include the following:

1. Impeller ON/OFF and speed control plus associated lubrication, cooling, and hydraulic systems;

2. North dynamometer ON/OFF and speed control plus associated lubrication and cooling systems;

3. South dynamometer ON/OFF and speed control plus associated lubrication and cooling systems;

4. Tunnel filling;

5. Tunnel draining;

6. Filtering;

7. Pressure regulator ON/OFF and pressure control plus associated hydraulic and water level control systems;

8. Purge system ON/OFF;

9. Deaerator system ON/OFF and water level control system; and

10. Certain building ventilation systems. (Future Growth)

During tunnel operation, the system will continuously monitor in real-time critical parameters associated with both the tunnel and its subsystems. In the event that an abnormal condition is detected the control system will automatically implement a pre-defined shut-down strategy designed to ensure that the tunnel equipment is shutdown safely and with minimal damage to the test body. Minimizing damage to the test body requires that the dynamometer and impeller speeds be continuously controlled so as to maintain thrust and torque with acceptable boundaries while at the same time assuring that no damage will occur to the machinery.

In addition to the primary control functions, the system will be capable to predicting failures of various equipment prior to the actual failure. This will be accomplished by first-of-all establishing base-line or standard values for various parameters such as pressure, temperature, noise, vibration levels, flow, and power at specific conditions. Once this data base has been established, then data will be periodically obtained and used to statistically determine if the variations are significant.

CONCLUSIONS

The addition of the computer-based control system will provide a marked improvement on the 36"-VPWT operational productivity. The system will also provide the necessary data for prediction of faults or problems before they reach a critical stage. It will be possible to schedule both routine and non-routine maintenance and repair for better utilization of time thus creating an overall scheduling program that is more productive and more cost effective. It is anticipated that there will also be an improvement in the morale of operating personnel. Both the tools (computer supported control system) and the working environment will be well grounded in current technology and personnel development programs.

The testing capability of the facility will be substantially improved. The computer control of basic tunnel test parameters (i.e., test section velocity, test section pressure, test propeller RPM) will be more accurate. The ability to maintain test parameters will be enhanced which will result in improved experimental data. The efficiency of planning test programs will be improved because of the systematic flexibility that results from subsystem interaction being controlled at all times by the computer based control system. Finally, the system has enough expansion capability to meet the needs of new test programs that will be necessary to support experimental testing well into the next century.

As with all major changes, there can also be disadvantages. In this particular endeavor the existing facility and the equipment associated with its daily operation are familiar to the operating personnel. Most of the equipment has been in operation for twenty years and has been tested by time, experience and simplification of operation. For example,

a manually operated valve only requires that the handle be turned to open or close it.

With the upgraded facility there will be a substantial increase in the required technical expertise to understand and maintain the facility. It will be necessary for DTNSRDC to program adequate training for operating personnel and to monitor the daily operation of the facility so that the maximum benefits of the modifications are realized.

ACKNOWLEDGEMENTS

The computer-based control system for the 36" VPWT described in this paper are due to the efforts of many people. I would like to especially thank the DTNSRDC personnel from the Central Instrumentation Department, Code 29 and the Industrial Department, Code 42, for their expert advice and assistance from the conception of the program. Acknowledgement is given to Mr. Normal Seidel and his staff from ORI, Inc. for assistance in the preliminary study and preparation of the specifications for the control system contract. In addition, acknowledgement is given to Mr. Jim Taylor and his staff of Sverdrup Technology, Inc. who are tasked to design, install and fully implement the new control system. Their contribution has been exceptional.

REFERENCES

1. Brownell, W. F., "A 36-Inch Variable Pressure Water Tunnel," David Taylor Model Basin Report 1052 (Jun 1956).

2. Brownell, W. F., "Two New Hydromechanics Research Facilities at the David Taylor Model Basin," David Taylor Model Basin Report 1690 (December 1962).

3. Seidle, Norman, "Control System for 36-Inch Variable Pressure Water Tunnel," ORI, Inc. Technical Report 2120 (July 1982).

4. Seidle, Norman and Ware, John, "Pressure Regulating System for 36-Inch Variable Presure Water Tunnel," ORI, Inc. Technical Report 2114 (August 1982).

5. Brenckman, R. D. and Goodson, R. C., "36-Inch Variable Pressure Water Tunnel Operating and Maintenance Instruction Manual," David W. Taylor Naval Ship Research and Development Center (March 1977).

6. Contract N00167-83-C-0067, "Procurement Specifications for Upgraded Control System for 36-Inch Variable Pressure Water Tunnel," David Taylor Naval Ship Research and Development Center (November 1982)

7. Technical/Management Proposal, "Design, Furnish and Install a Computer-Based Control System for the DTNSRDC 36-Inch Variable Pressure Water Tunnel, "Sverdrup Technology, Inc. (February 1983).

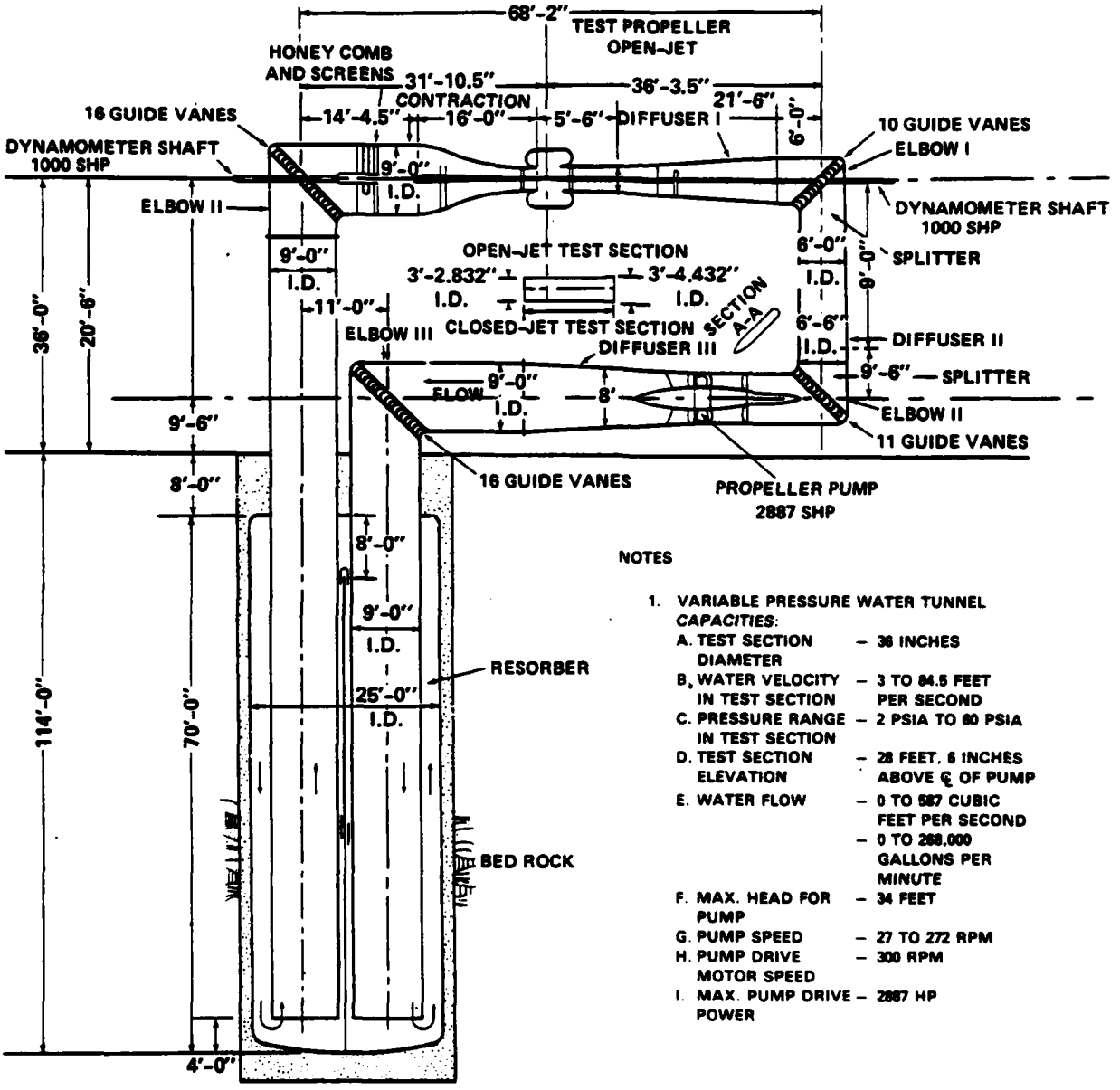

NOTES

1. VARIABLE PRESSURE WATER TUNNEL *CAPACITIES*:

A. TEST SECTION DIAMETER	– 36 INCHES
B. WATER VELOCITY IN TEST SECTION	– 3 TO 84.5 FEET PER SECOND
C. PRESSURE RANGE IN TEST SECTION	– 2 PSIA TO 60 PSIA
D. TEST SECTION ELEVATION	– 28 FEET, 6 INCHES ABOVE ℄ OF PUMP
E. WATER FLOW	– 0 TO 587 CUBIC FEET PER SECOND – 0 TO 268,000 GALLONS PER MINUTE
F. MAX. HEAD FOR PUMP	– 34 FEET
G. PUMP SPEED	– 27 TO 272 RPM
H. PUMP DRIVE MOTOR SPEED	– 300 RPM
I. MAX. PUMP DRIVE POWER	– 2887 HP

Figure 1. 36 Inch Variable Pressure Water Tunnel-Vertical Elevation

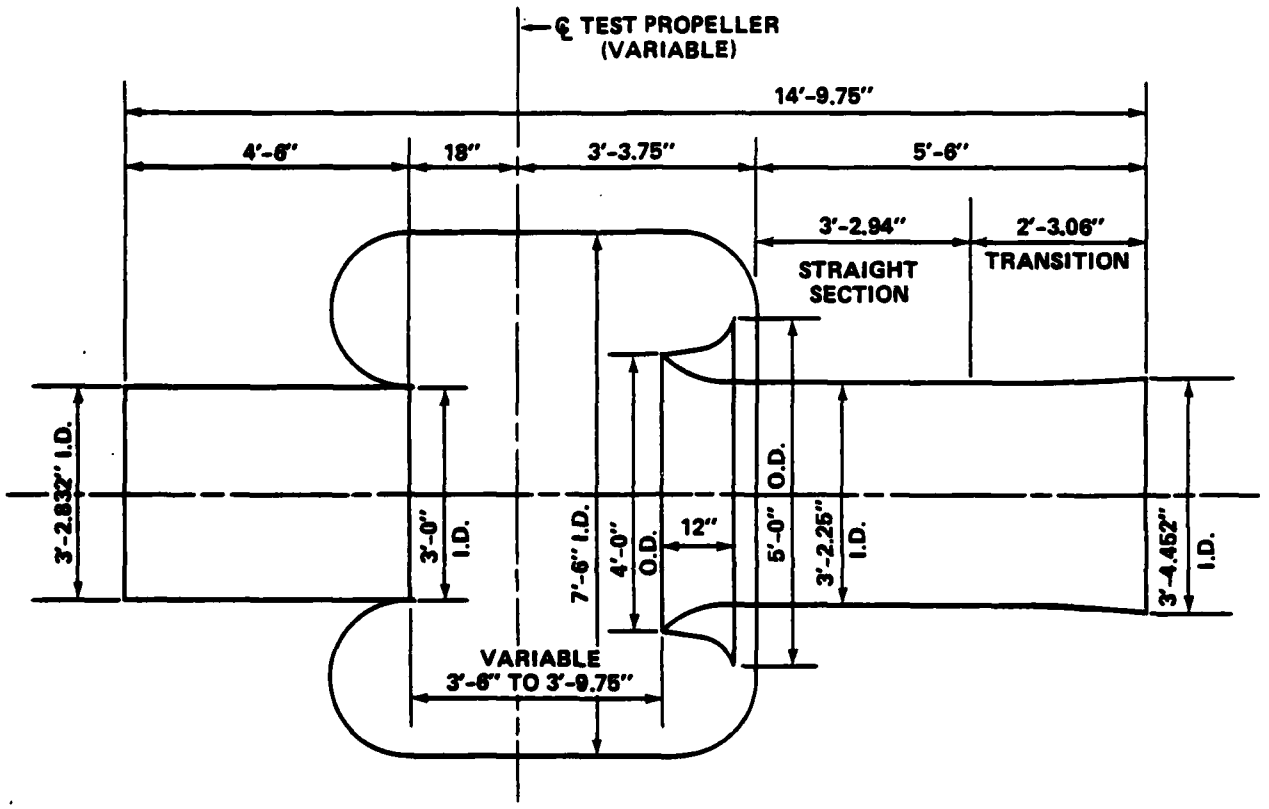

Figure 2. Open Jet Test Section - 36" VPWT

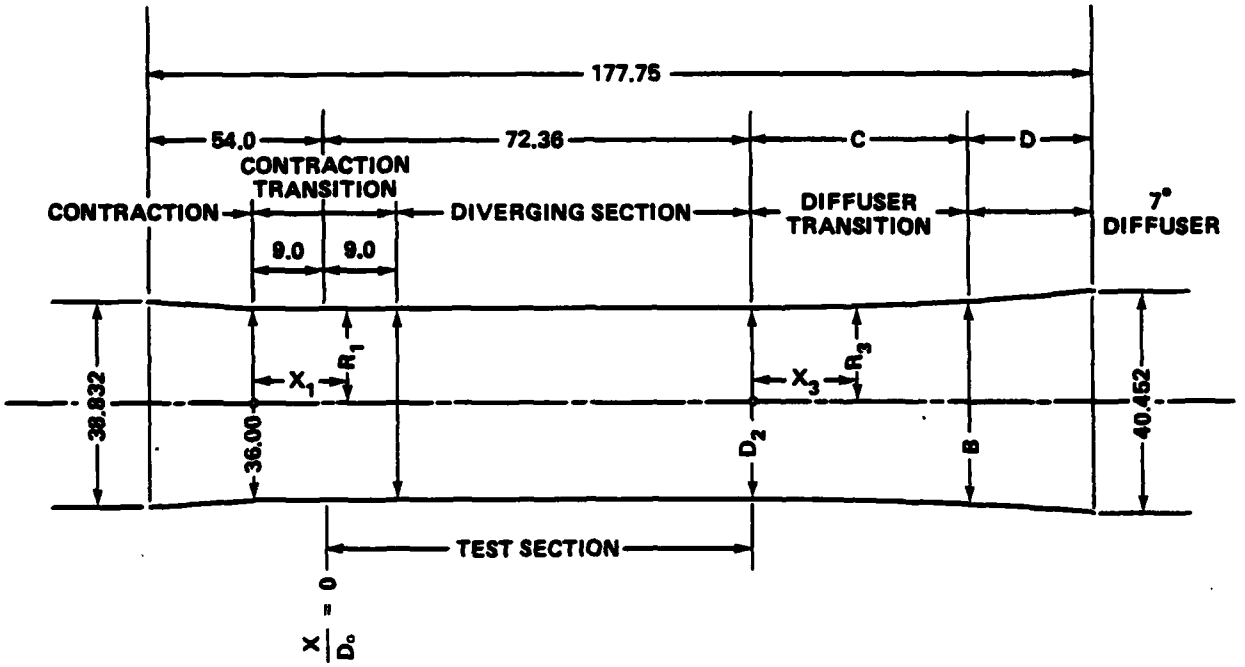

DIMENSIONS IN INCHES

Figure 3. Closed Jet Test Section - 36" VPWT

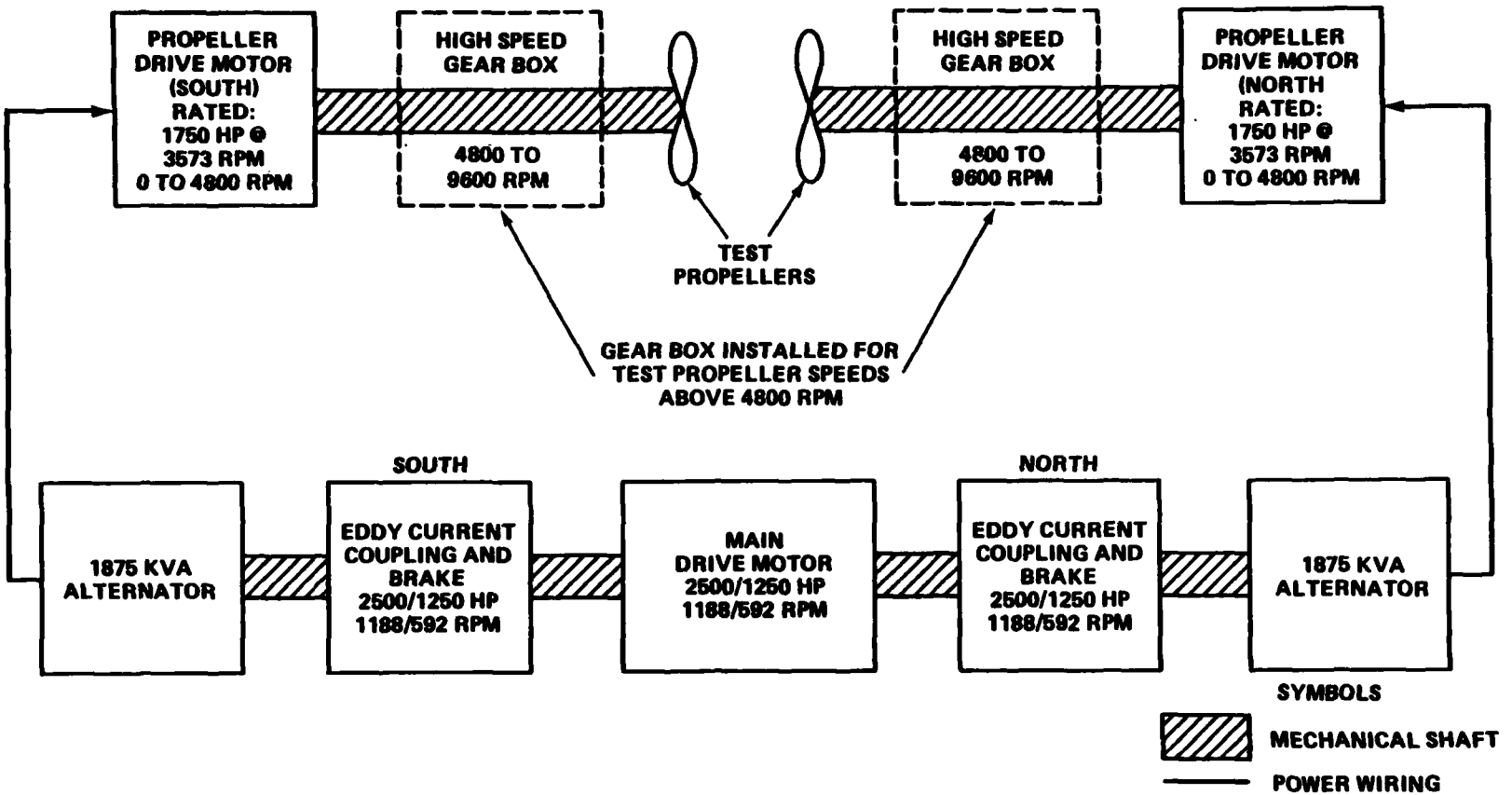

Figure 4. Block Diagram of the North and South Dynamometer Drive System for Propeller Testing

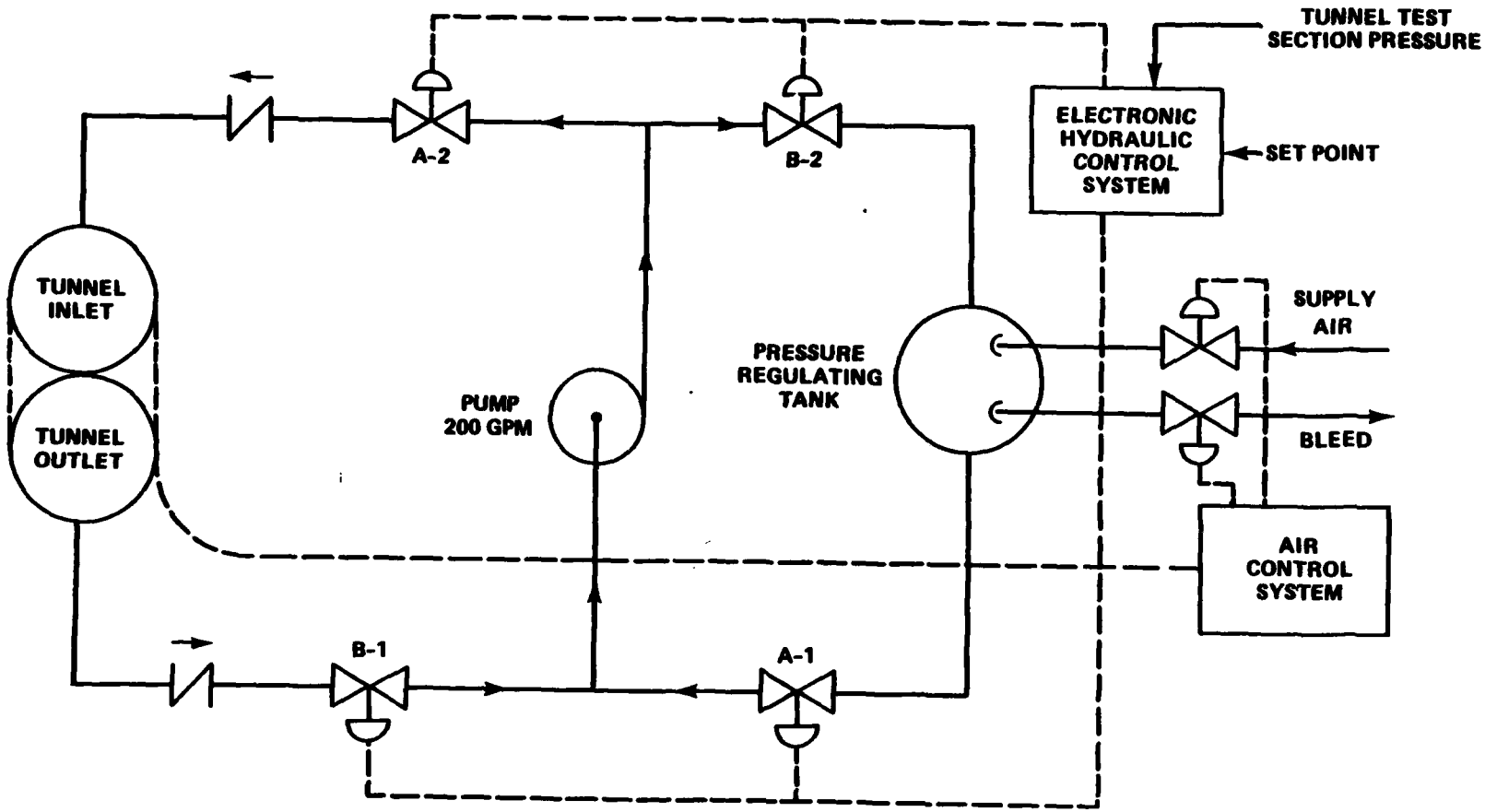

Figure 5. Simplified Diagram of the Pressure Regulating System for the 36" VPWT

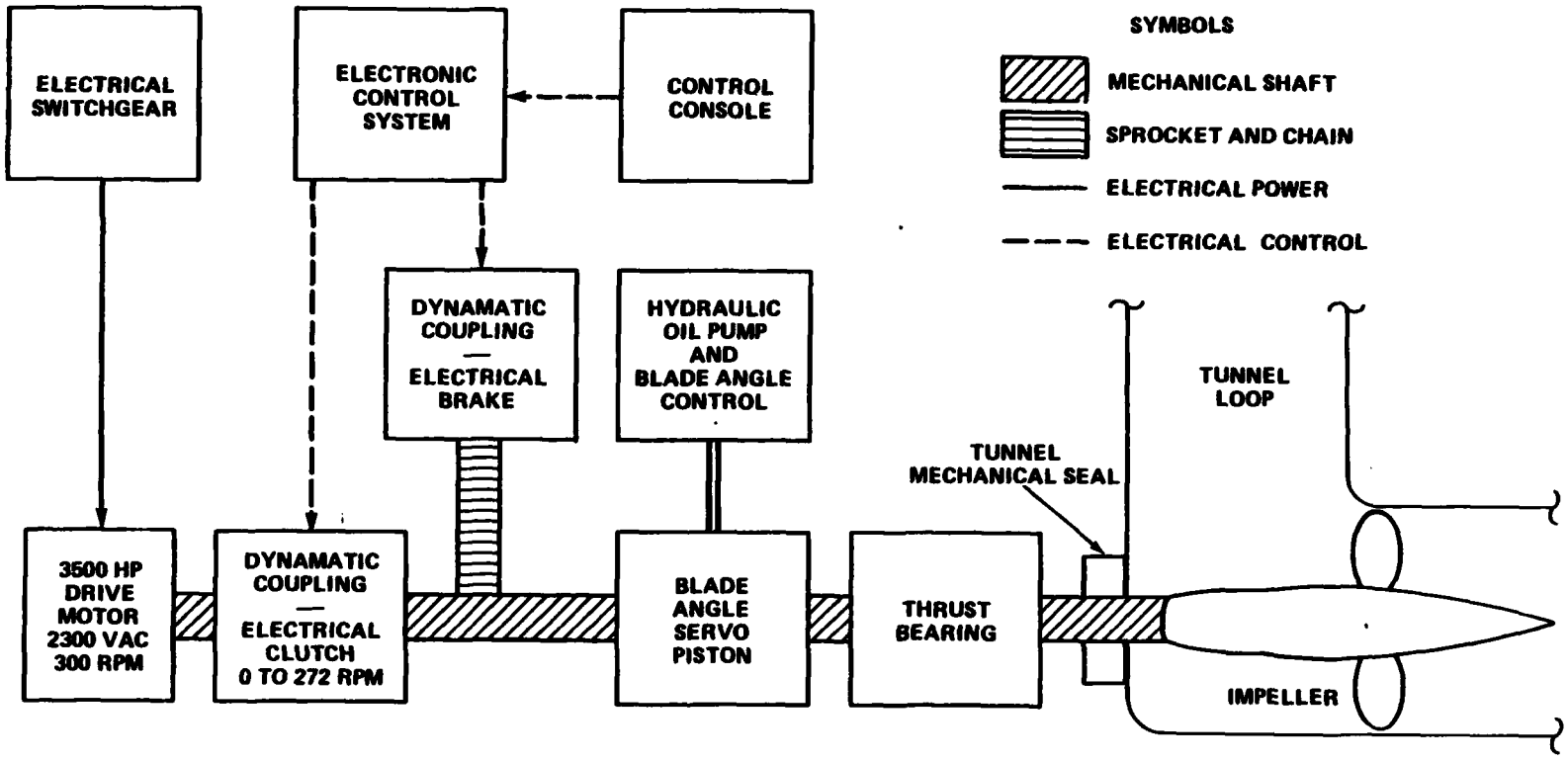

Figure 6. Impeller Drive Subsystem for the 36" VPWT

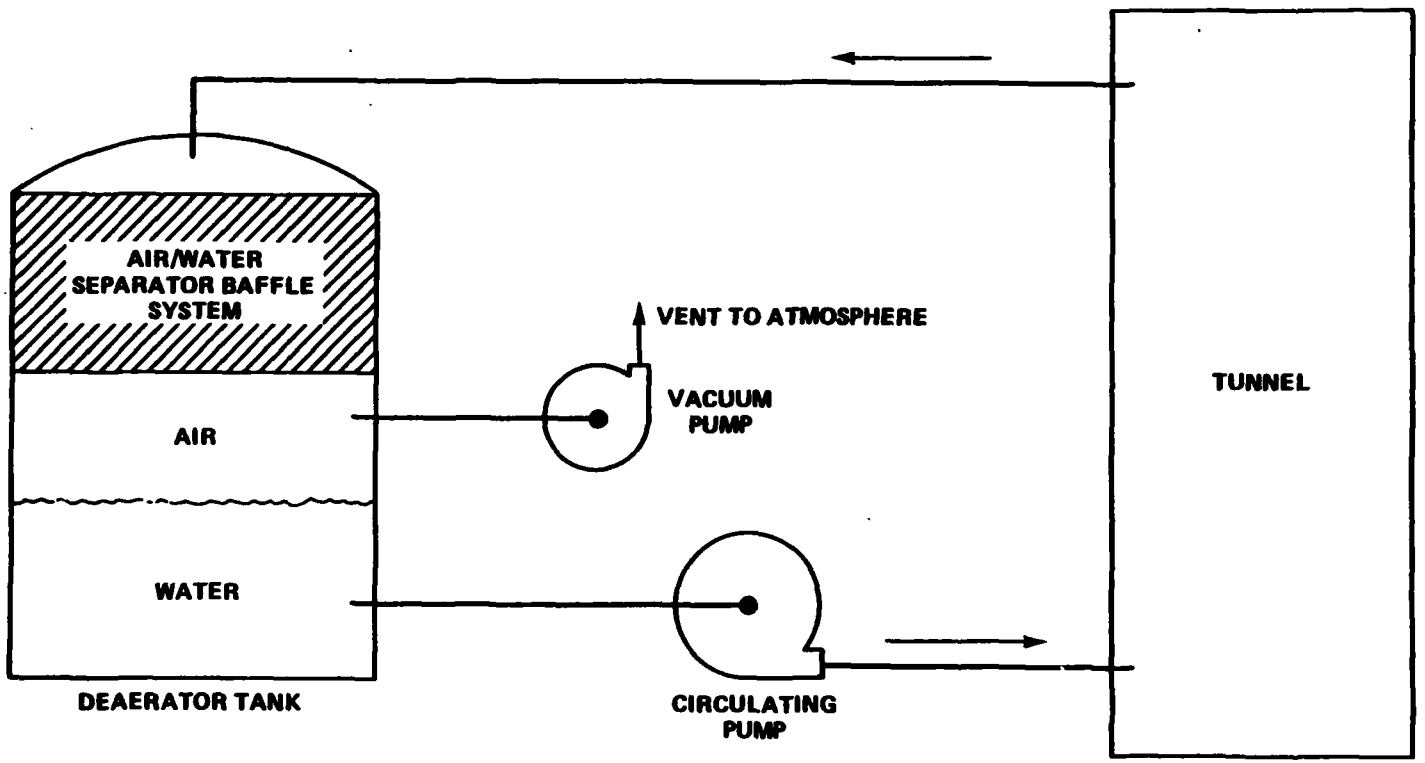

Figure 7. Functional Diagram of Deaerator System - 36" VPWT

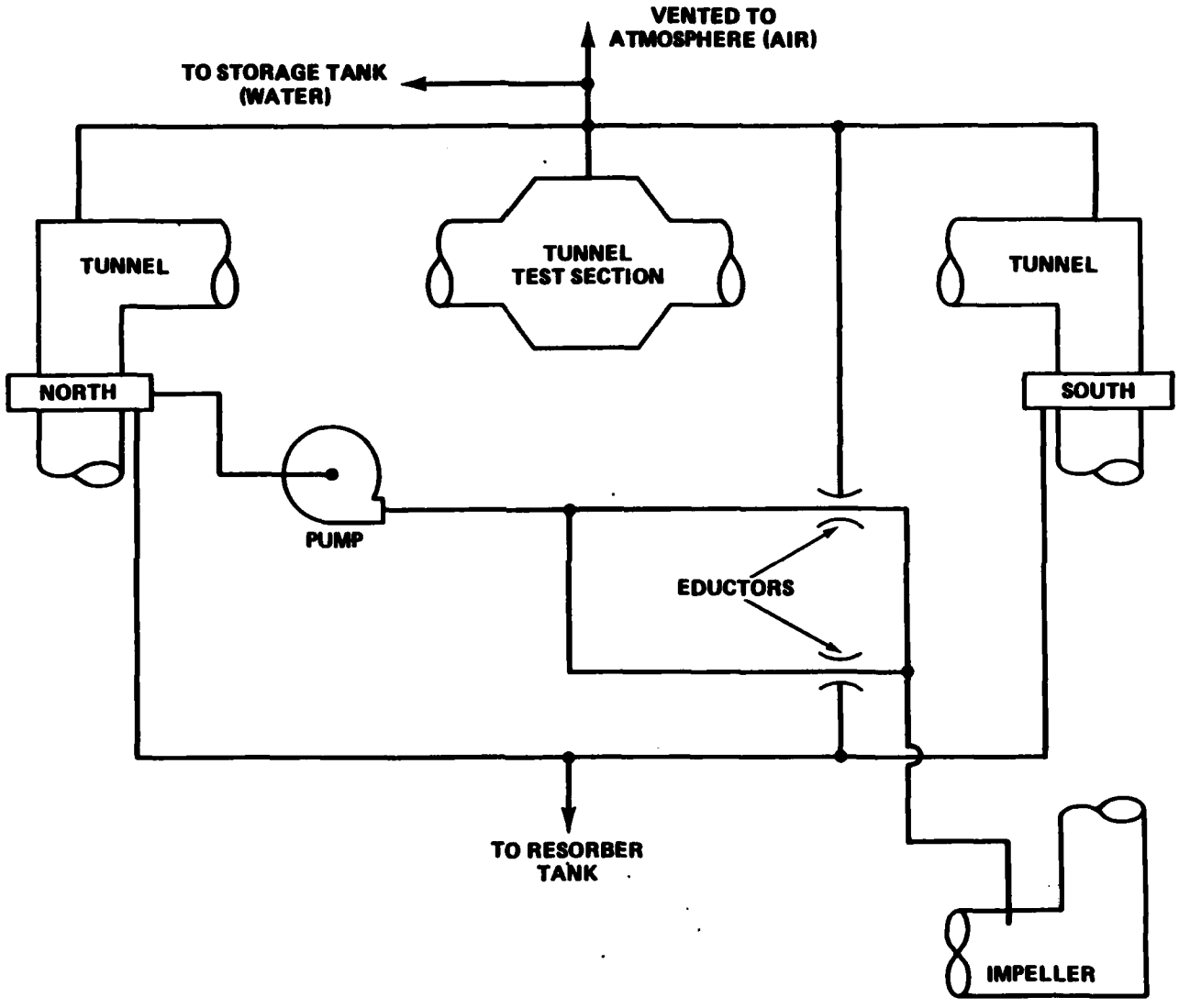

Figure 8. Functional Diagram of Purge System for the 36" VPWT

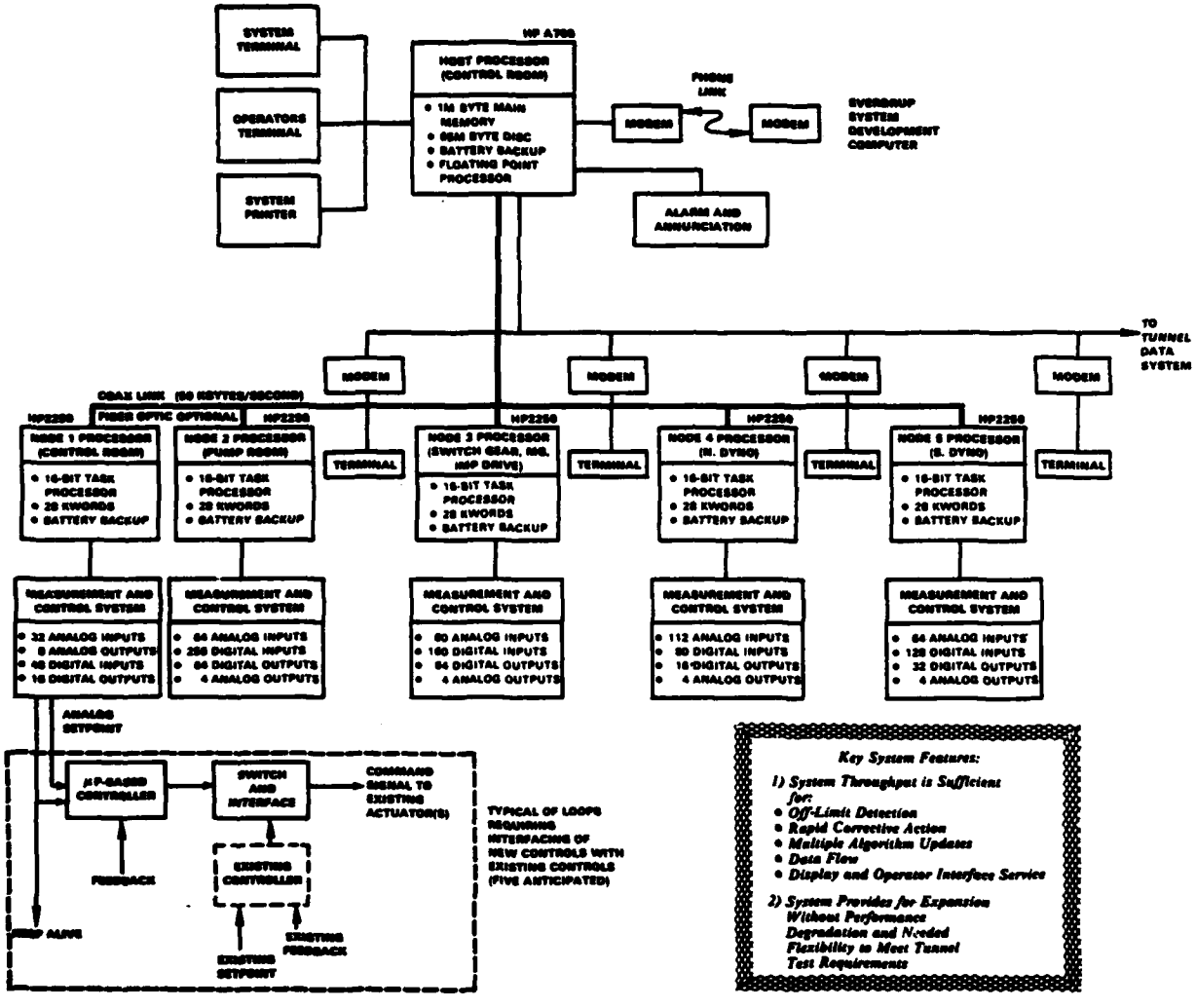

FIGURE 9. BASELINE CONFIGURATION FOR THE 36-INCH VPWT COMPUTER-BASED CONTROL SYSTEM

APPENDIX A

36-INCH VARIABLE PRESSURE WATER TUNNEL OPERATIONAL PROCEDURE

15 APRIL 1982

36" VPWT
OPERATIONAL PROCEDURE

FILL TUNNEL (FOR TOP SECTION)

DEAERATOR START-UP

DEAERATOR SHUT-DOWN

FILTERING FOR TUNNEL WATER - START-UP

FILTERING FOR TUNNEL WATER - SHUT-DOWN

PRESSURE REGULATOR START-UP

PRESSURE REGULATOR SHUT-DOWN

IMPELLER DRIVE START-UP

IMPELLER DRIVE SHUT-DOWN

DYNAMOMETER START-UP

DYNAMOMETER SHUT-DOWN

DRAIN TUNNEL (FOR TOP SECTION ONLY)

SLOW DRAIN (OPEN JET TEST SECTION ONLY)

15 APRIL 82

FILL TUNNEL (FOR TOP SECTION)

LOCATION	OPERATION	CHECK

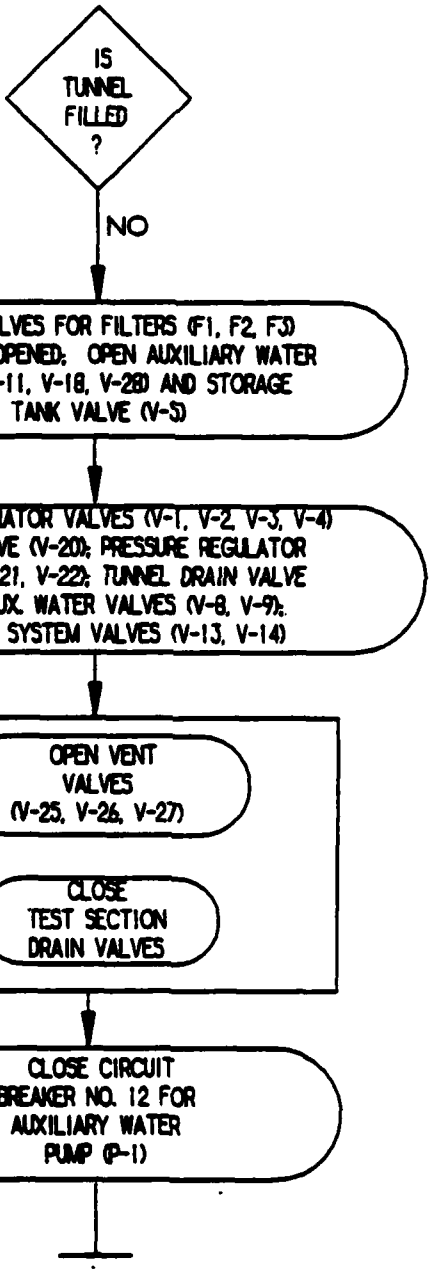

FILL TUNNEL (FOR TOP SECTION)
CONT

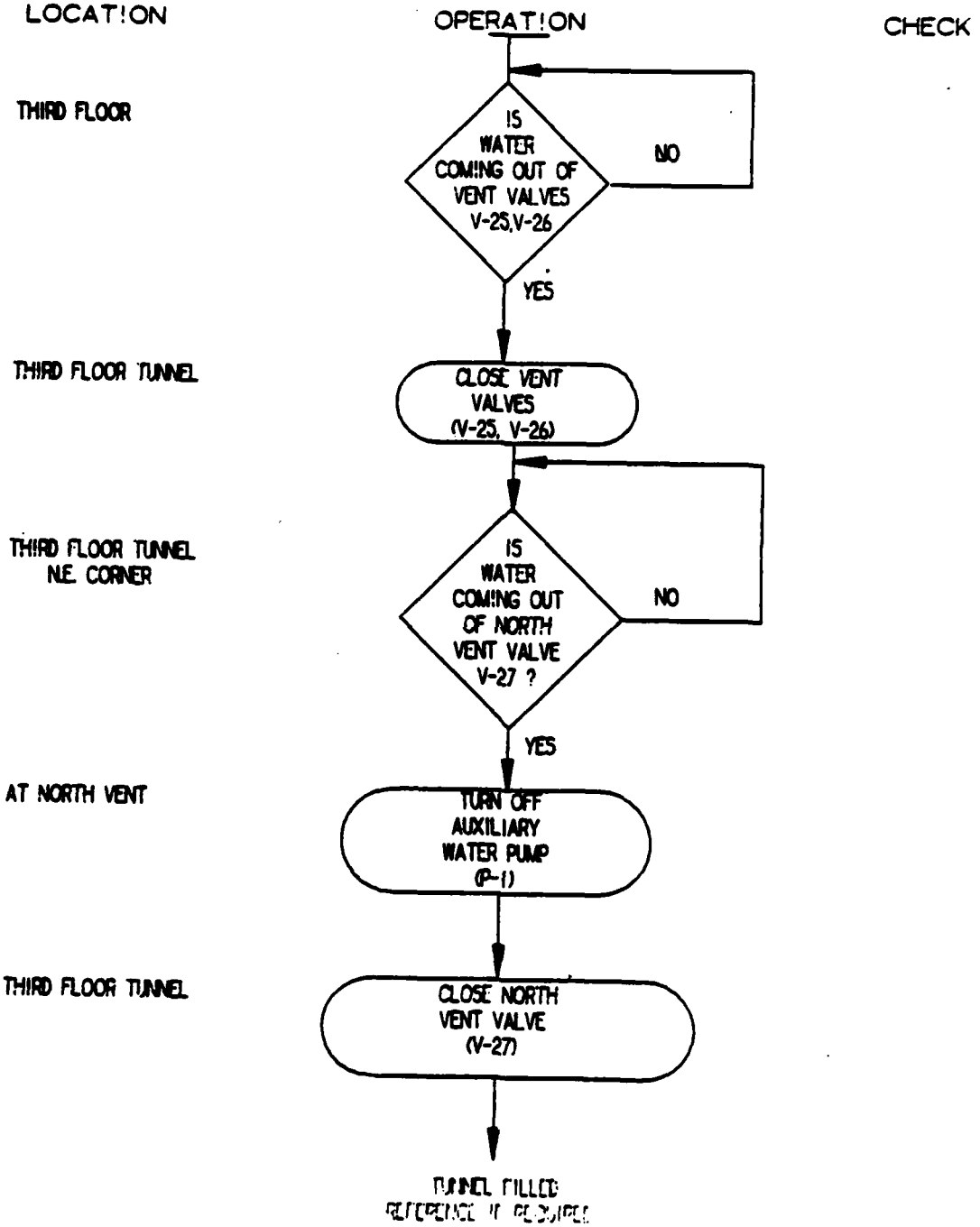

DEAERATOR START-UP

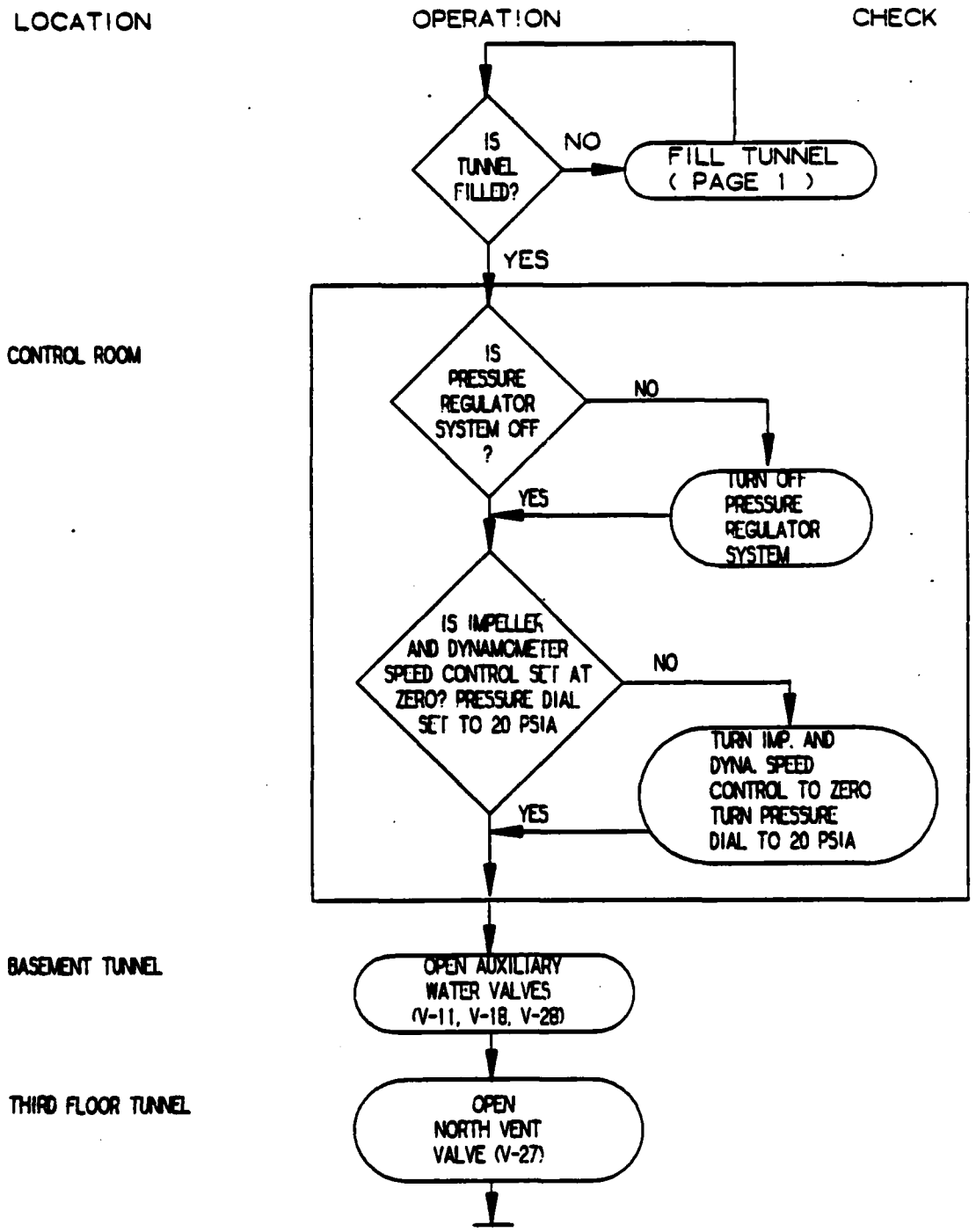

AD-A144 227 PROCEEDINGS OF THE GENERAL MEETING OF THE AMERICAN TOWING TANK CONFERENCE.. (U) STEVENS INST OF TECH HOBOKEN NJ DAVIDSON LAB D SAVITSKY ET AL. AUG 83 7/8

UNCLASSIFIED SIT-DL-TR-13029-VOL-2 N00167-83-M-4062 F/G 20/4 NL

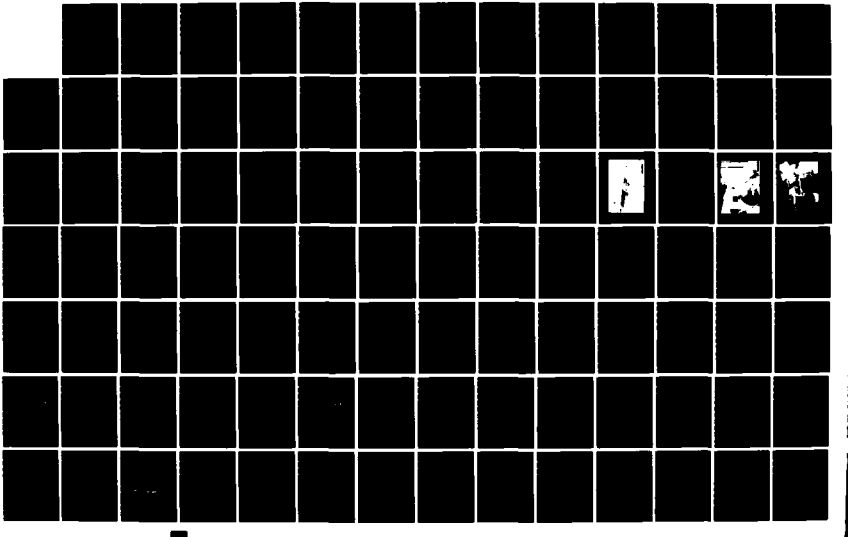

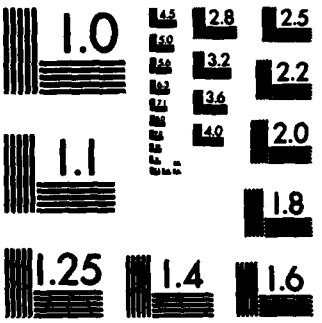

MICROCOPY RESOLUTION TEST CHART
NATIONAL BUREAU OF STANDARDS-1963-A

DEARATOR START UP
CONT

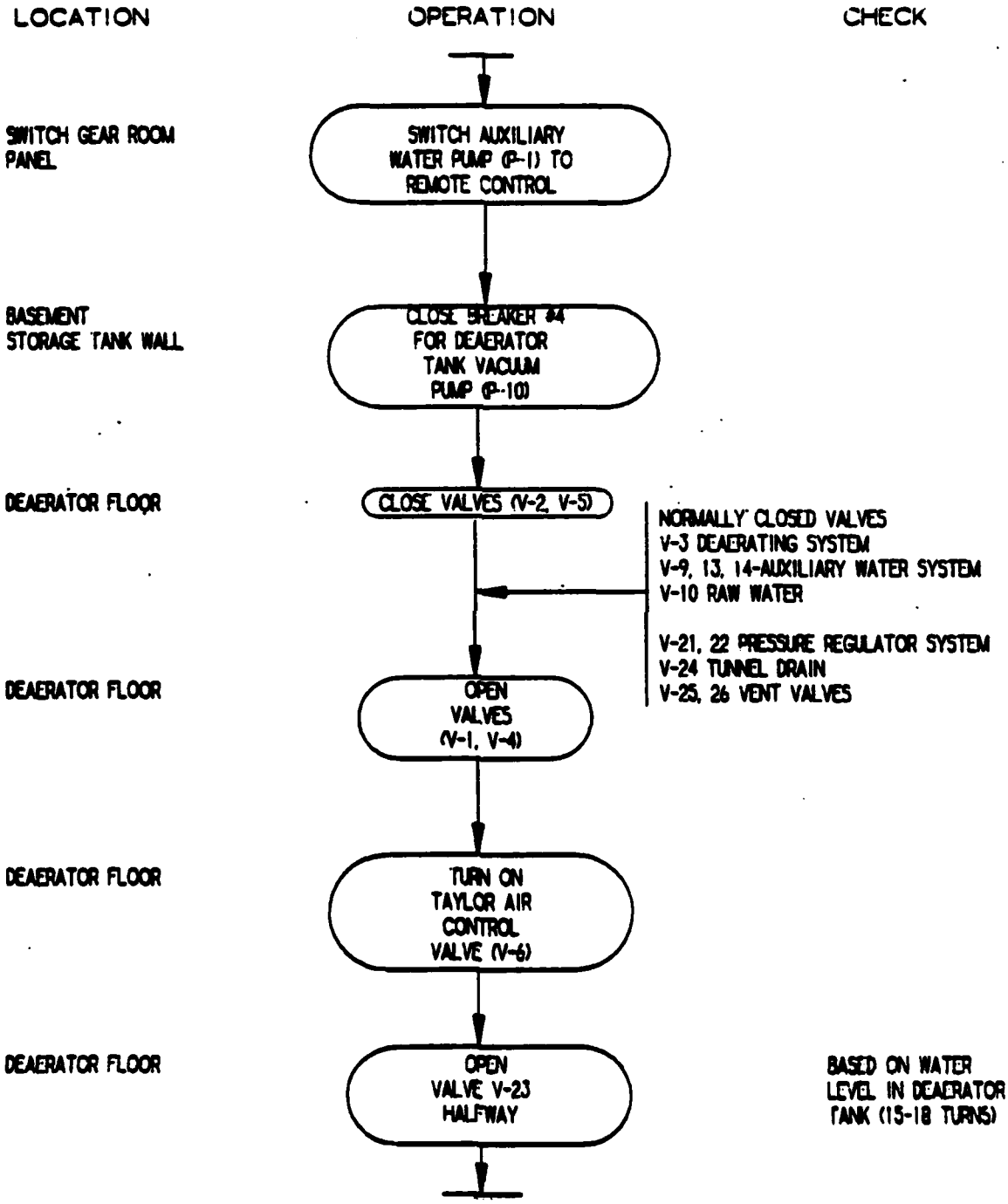

DEARATOR START UP
CON'T

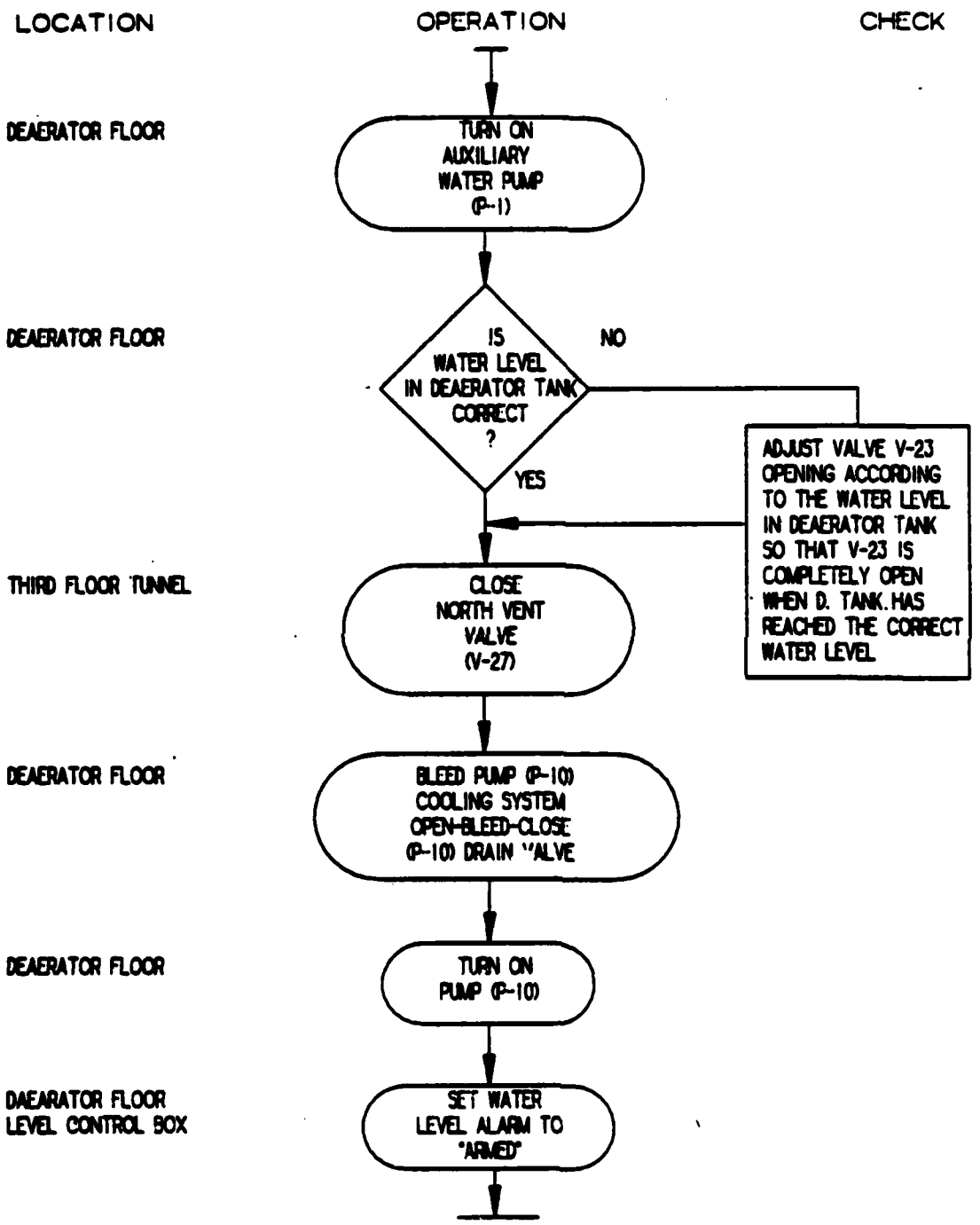

DEARATOR START UP
CONT

LOCATION	OPERATION	CHECK
	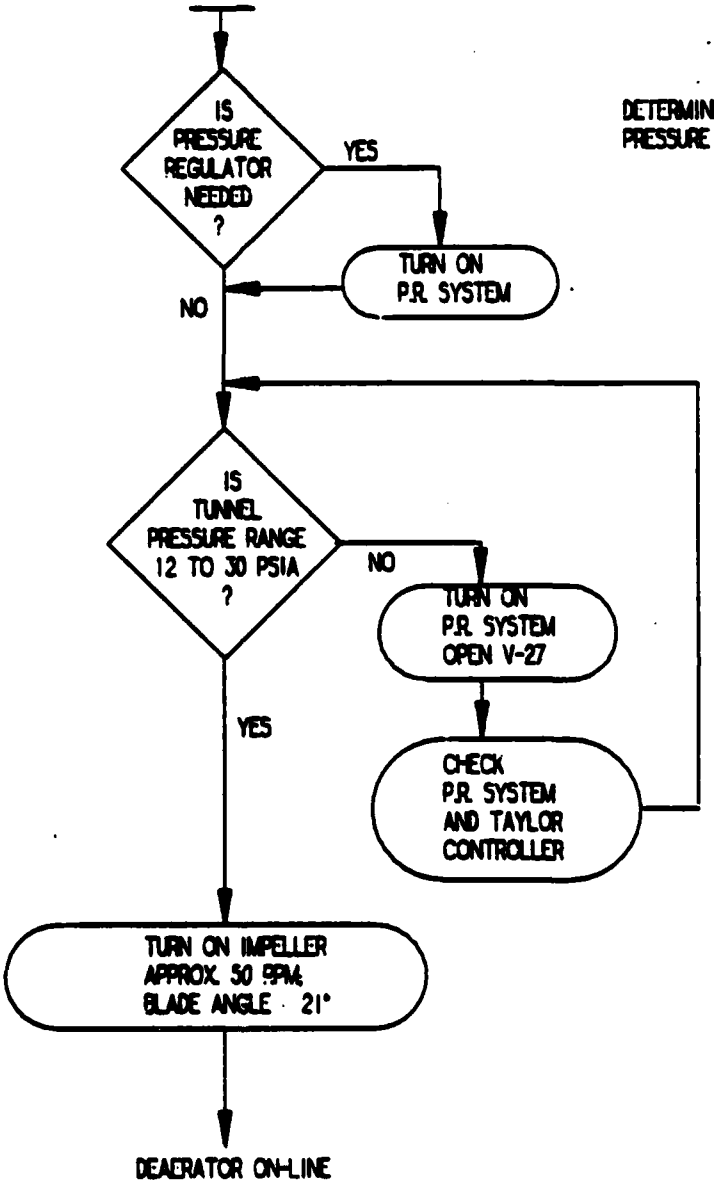	DETERMINED BY PRESSURE
CONTROL ROOM		

DEAERATOR SHUT-DOWN

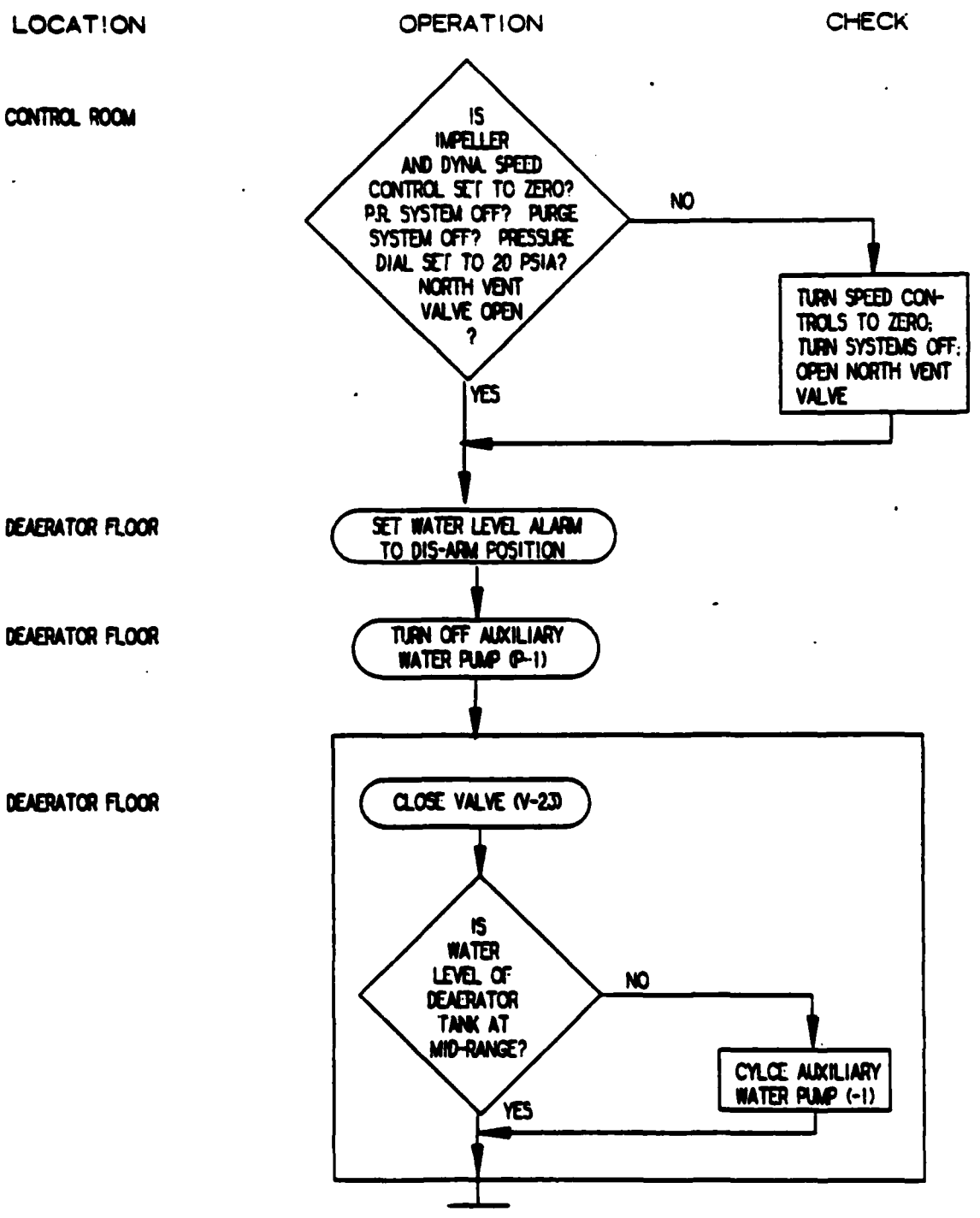

DEARATOR SHUT-DOWN
CONT

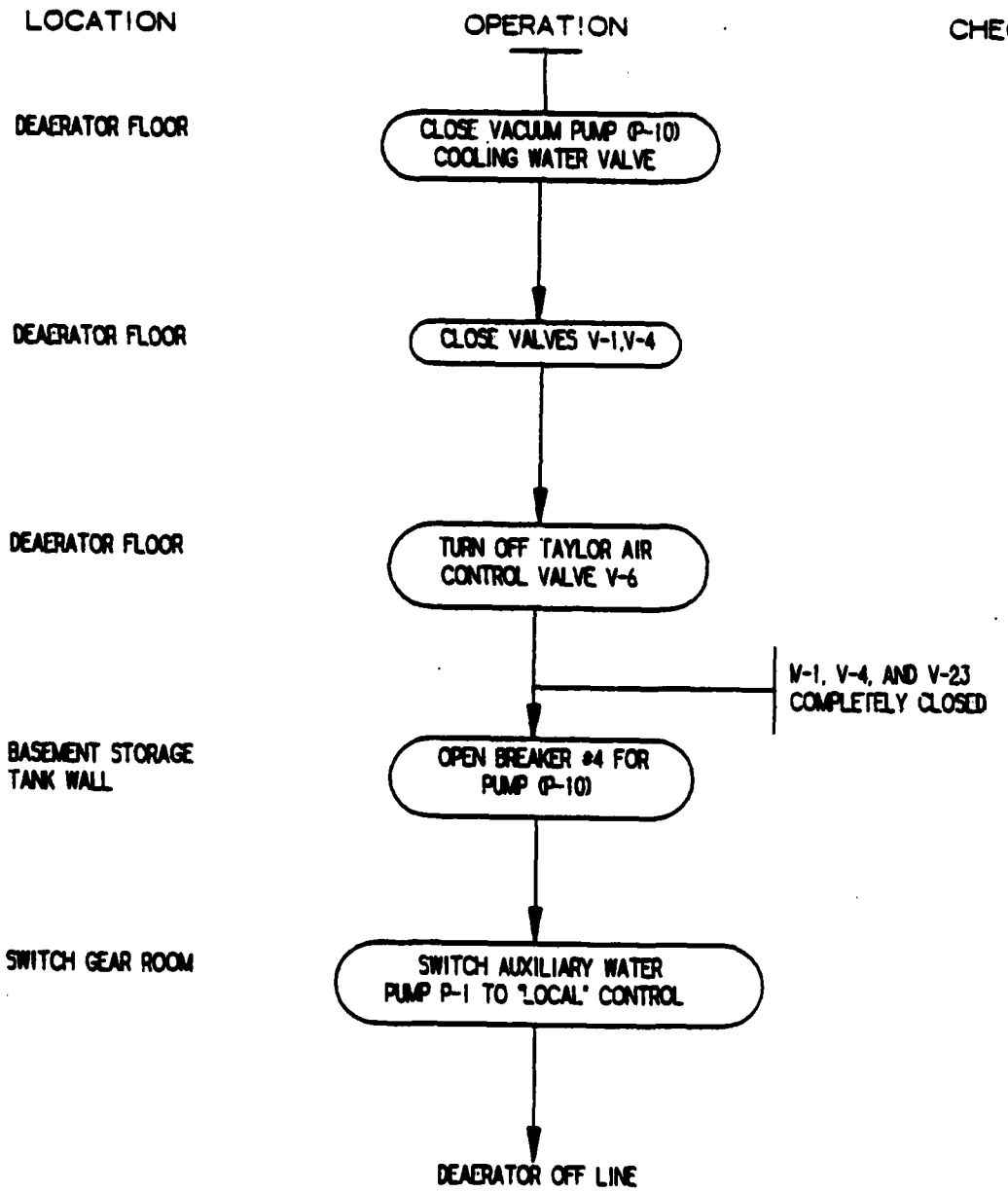

FILTERING FOR TUNNEL WATER START-UP

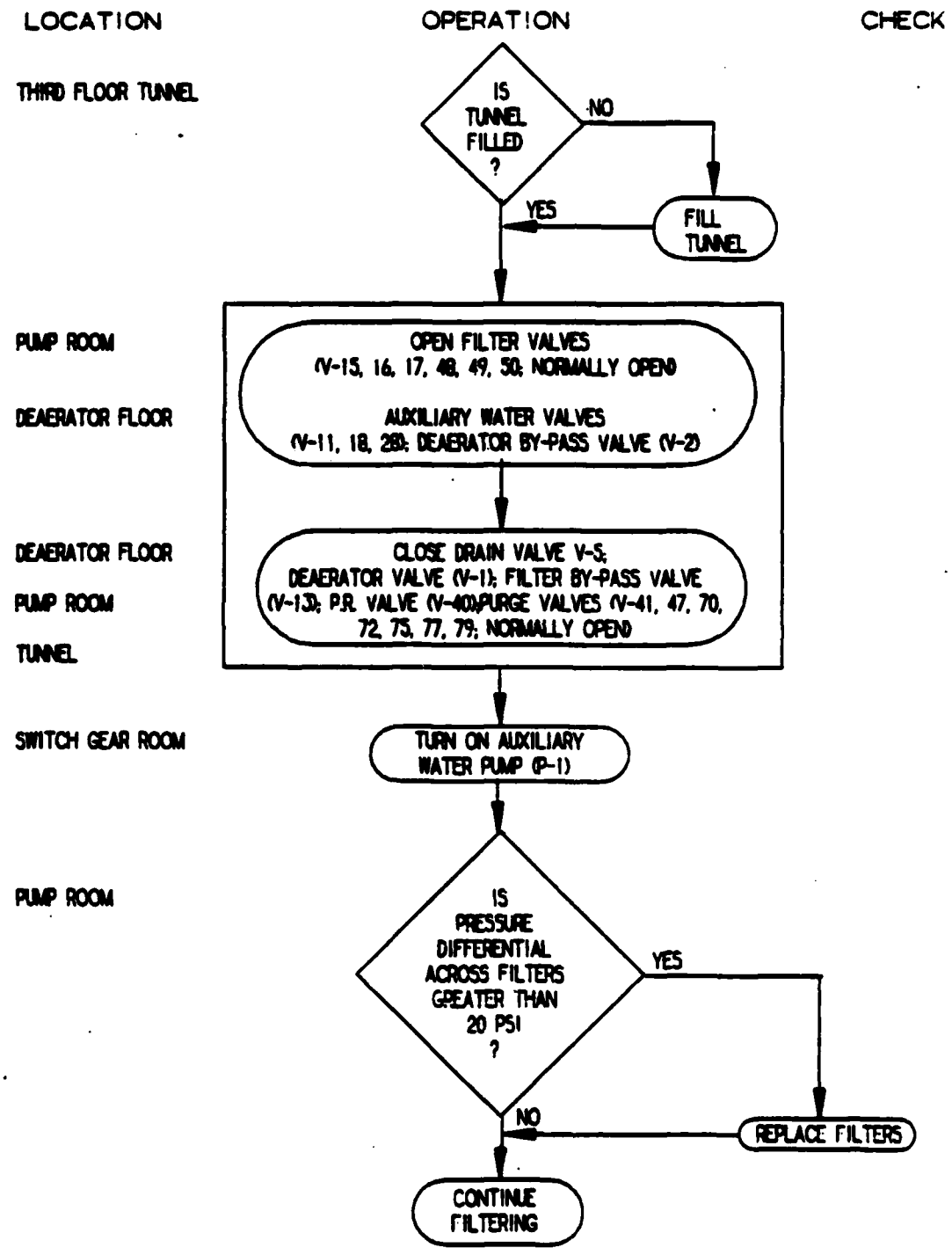

FILTERING FOR TUNNEL WATER SHUT DOWN

LOCATION	OPERATION	CHECK
	IS DEAERATOR ACTIVATED? — YES → USE DEAERATOR SHUT DOWN SEQUENCE	
	NO	
SWITCH GEAR ROOM OR THIRD FLOOR CONTROL ROOM	TURN P-1 OFF	P-1 OFF (VISUAL)
DEAERATOR FLOOR PUMP ROOM TUNNEL	CLOSE V-11, V-15, V-2	
	FILTERING OFF LINE	

PRESSURE REGULATOR START-UP

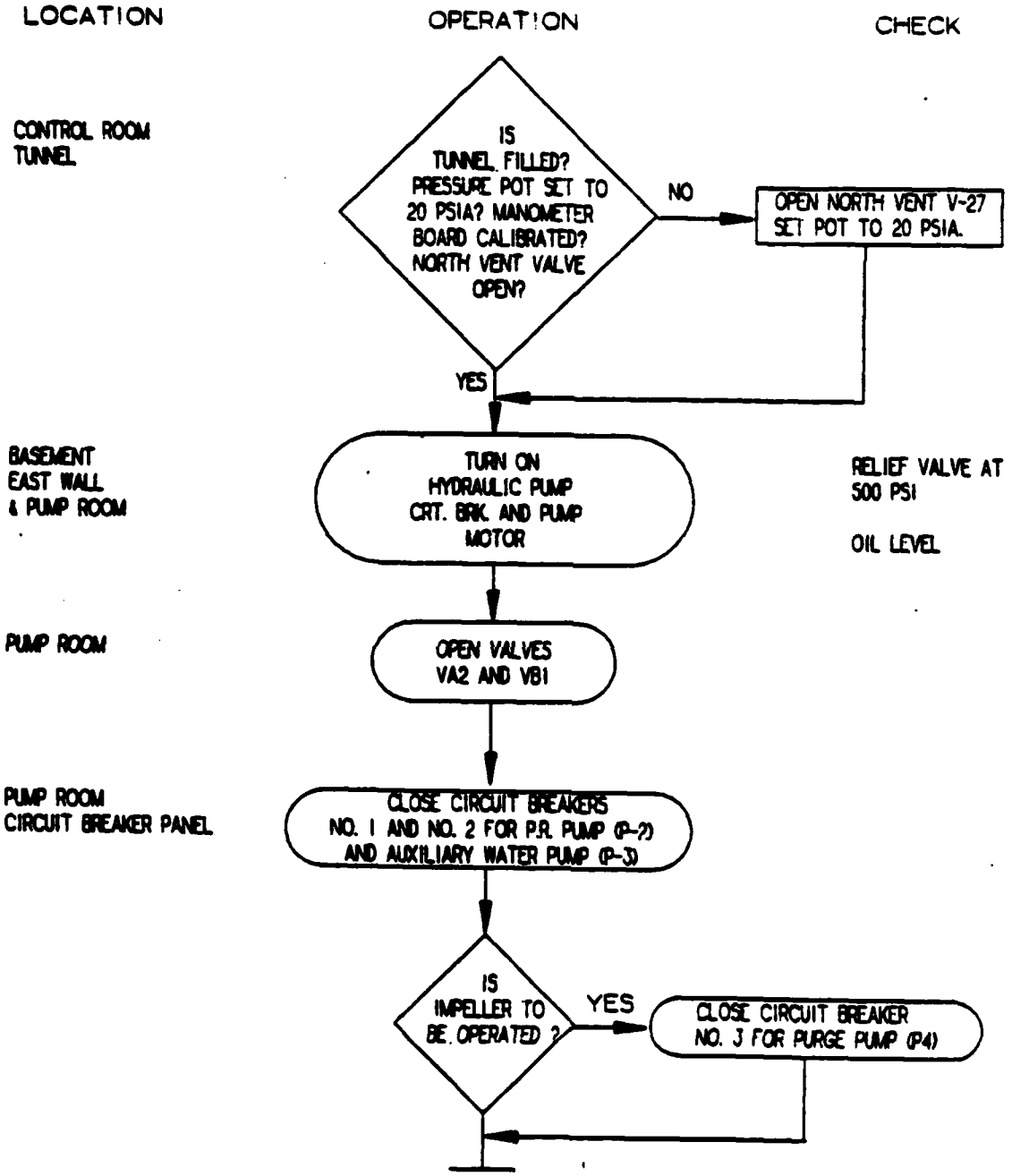

PRESSURE REGULATOR START-UP
CON'T

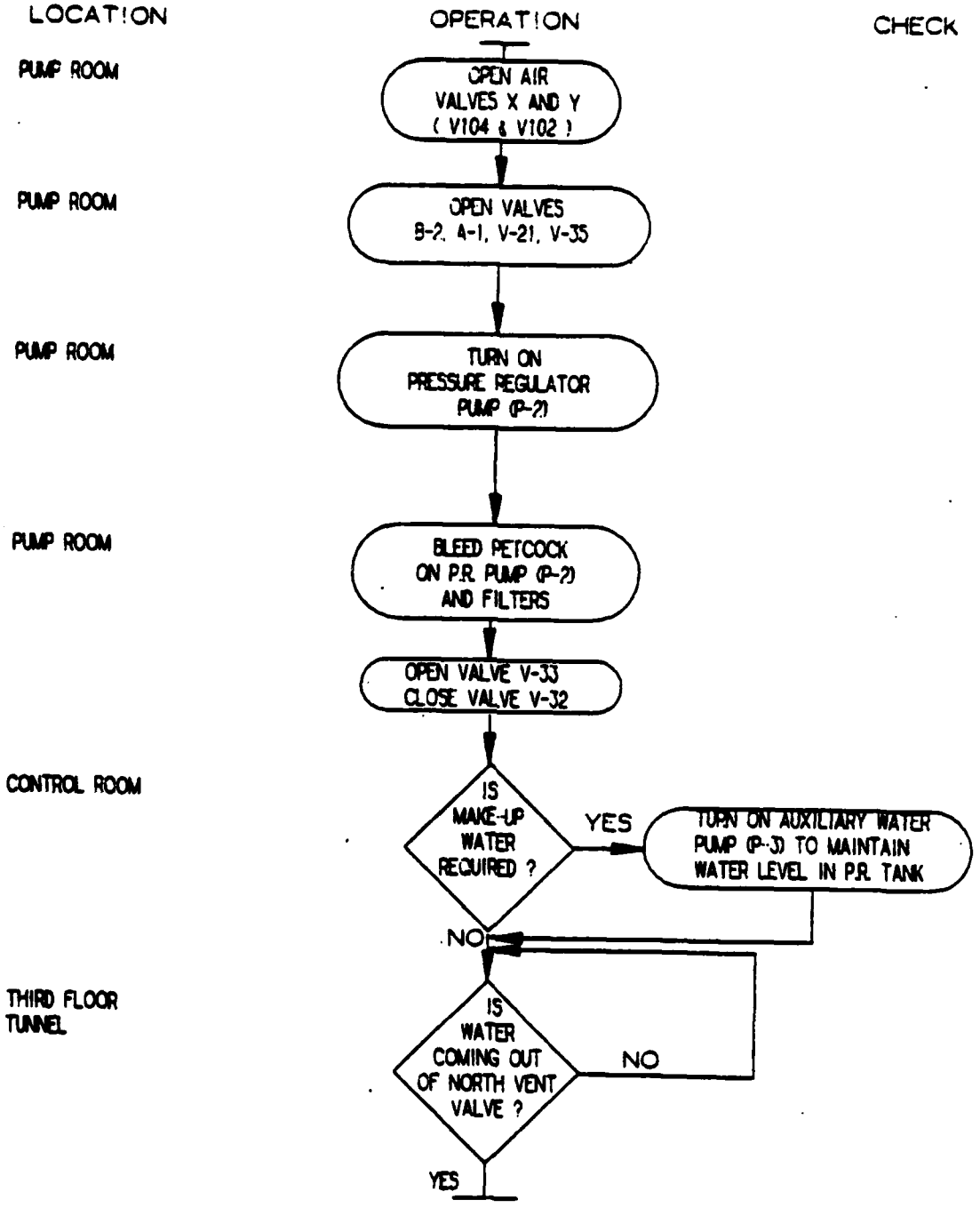

PRESSURE REGULATOR START-UP
CON'T

LOCATION	OPERATION	CHECK
THIRD FLOOR TUNNEL	CLOSE NORTH VENT VALVE V-27	

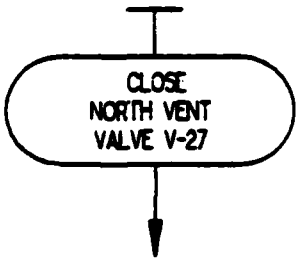

PRESSURE REGULATOR SYSTEM ON LINE

PRESSURE REGULATOR SHUT-DOWN

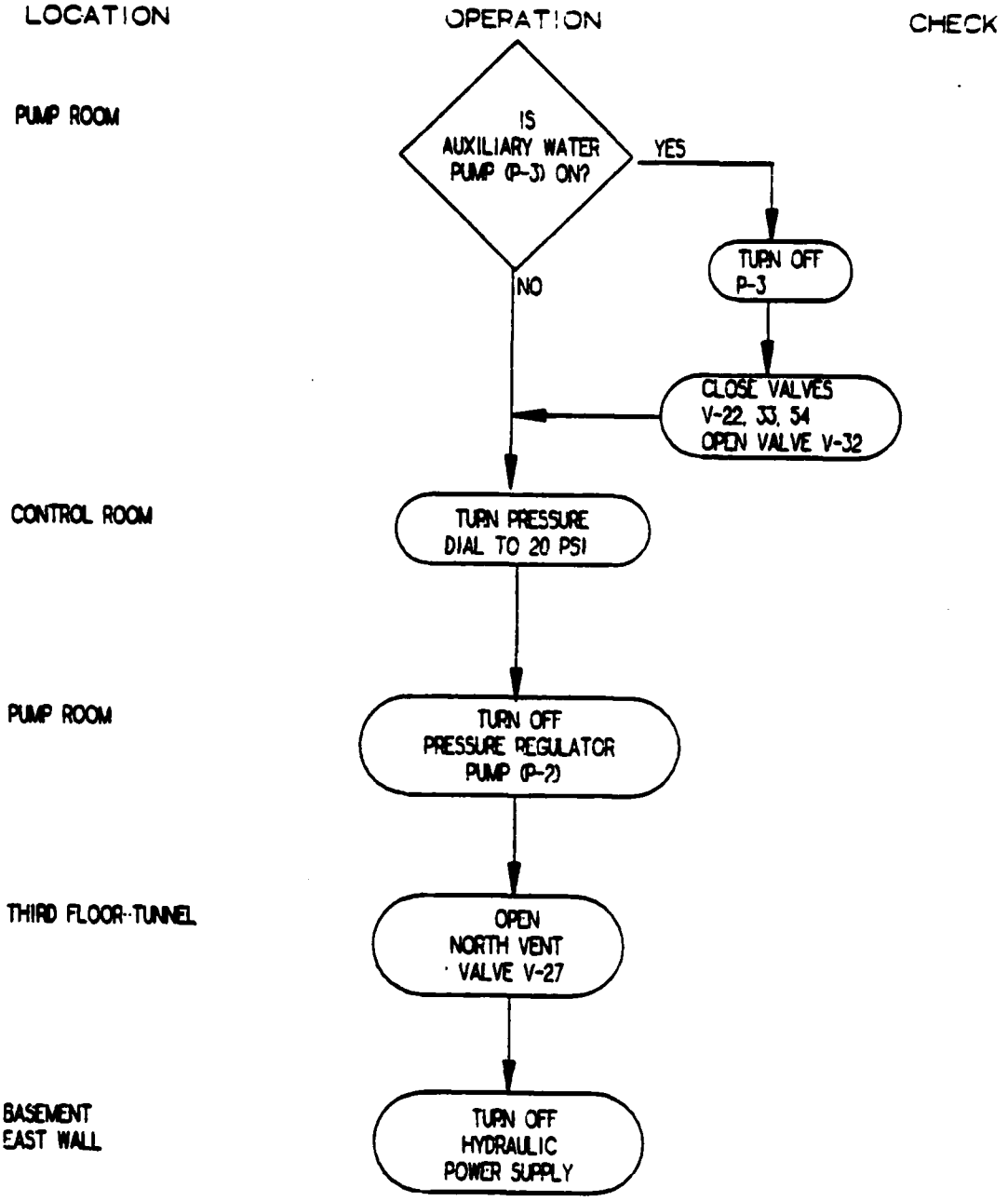

PRESSURE REGULATOR SHUT-DOWN
CONT

LOCATION	OPERATION	CHECK
SOUTH AND NORTH LEG OF TUNNEL; PUMP ROOM	CLOSE VALVES VA2, A-1, V51, B-2, V-21, V-35, X, Y (V104 & V102)	
PUMP ROOM CIRCUIT BREAKER PANEL	OPEN CIRCUIT BREAKERS NO. 1 , 2 AND 3 FOR PRESSURE REGULATOR PUMP (P-2) AND AUXILIARY WATER PUMP (P-3)	

PRESSURE REGULATOR SYSTEM OFF LINE

IMPELLER DRIVE START-UP

LOCATION	OPERATION	CHECK
SWITCH GEAR ROOM	2400V AND 125V SWITCH GEAR ON ?	'ON' LIGHT RED
	NO → TURN ON 2400V AND 125V SWITCHES	
	YES	
LOWER SOUTH ELBOW OF TUNNEL	RELEASE CARBON SEAL JACK	CHECK SEAL OIL PRESSURE
SWITCH GEAR ROOM IMPELLER CUBICLE	TURN ON	PRESSURE LIGHT VACUUM LIGHT 30 MINUTE OFF TIMER
	DYNAMATIC COUPLING LUBE OIL PRESSURE (CPLG #1)	
	DYNAMATIC COUPLING (#1) ELECTRONICS	READY LIGHT
	ANNUNICATOR AND RECORDER	LIGHT

IMPELLER DRIVE START-UP
CONT

LOCATION	OPERATION	CHECK
M/G ROOM	TURN ON: EXCITER FOR IMPELLER MOTOR	AUDIBLE
BASEMENT WALL (WEST) (TUNNEL ROOM)	THRUST BEARING LUBE OIL PUMP	AUDIBLE MONITOR GAGE INSTALLED IN 1981. PRESS. CHECK
	BLADE ANGLE CHANGE? YES / NO	SWITCH POSITION FOR THRUST BEARING OIL FLOW DIRECTION
	BLADE ANGLE ROUTINE	
PUMP ROOM CIRCUIT BREAKER PANEL 480 V CB	CLOSE CIRCUIT BREAKERS FOR: WATER TOWER PUMPS P-6, 7 AND 8 HYDRAULIC PUMP (14)	
OUTSIDE	IS TEMP. OUTSIDE BELOW FREEZING YES / NO	
	CHECK TOWER A FOR FROZEN WATER YES / NO	

IMPELLER DRIVE START-UP
CONT

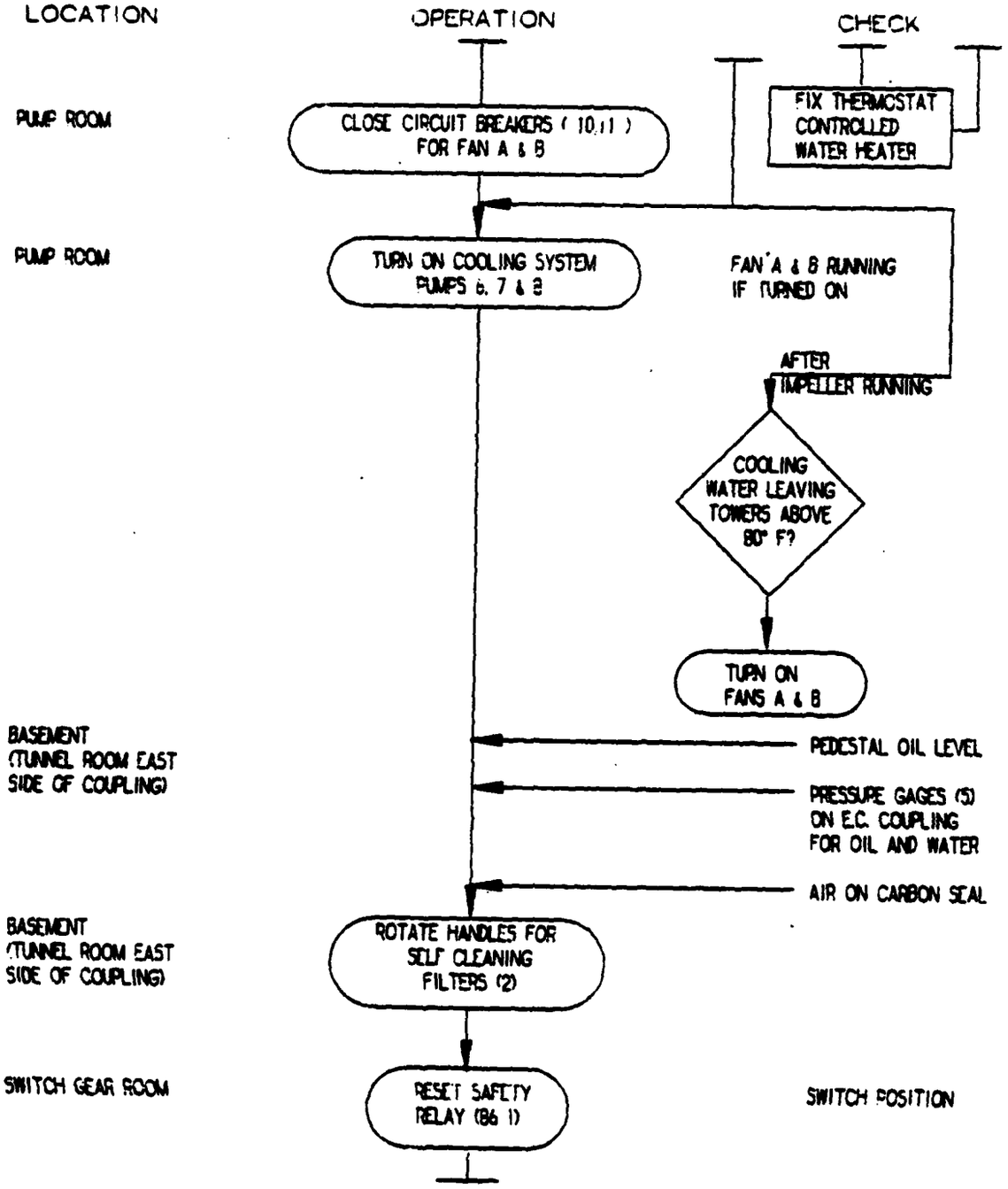

IMPELLER DRIVE START-UP
CONT

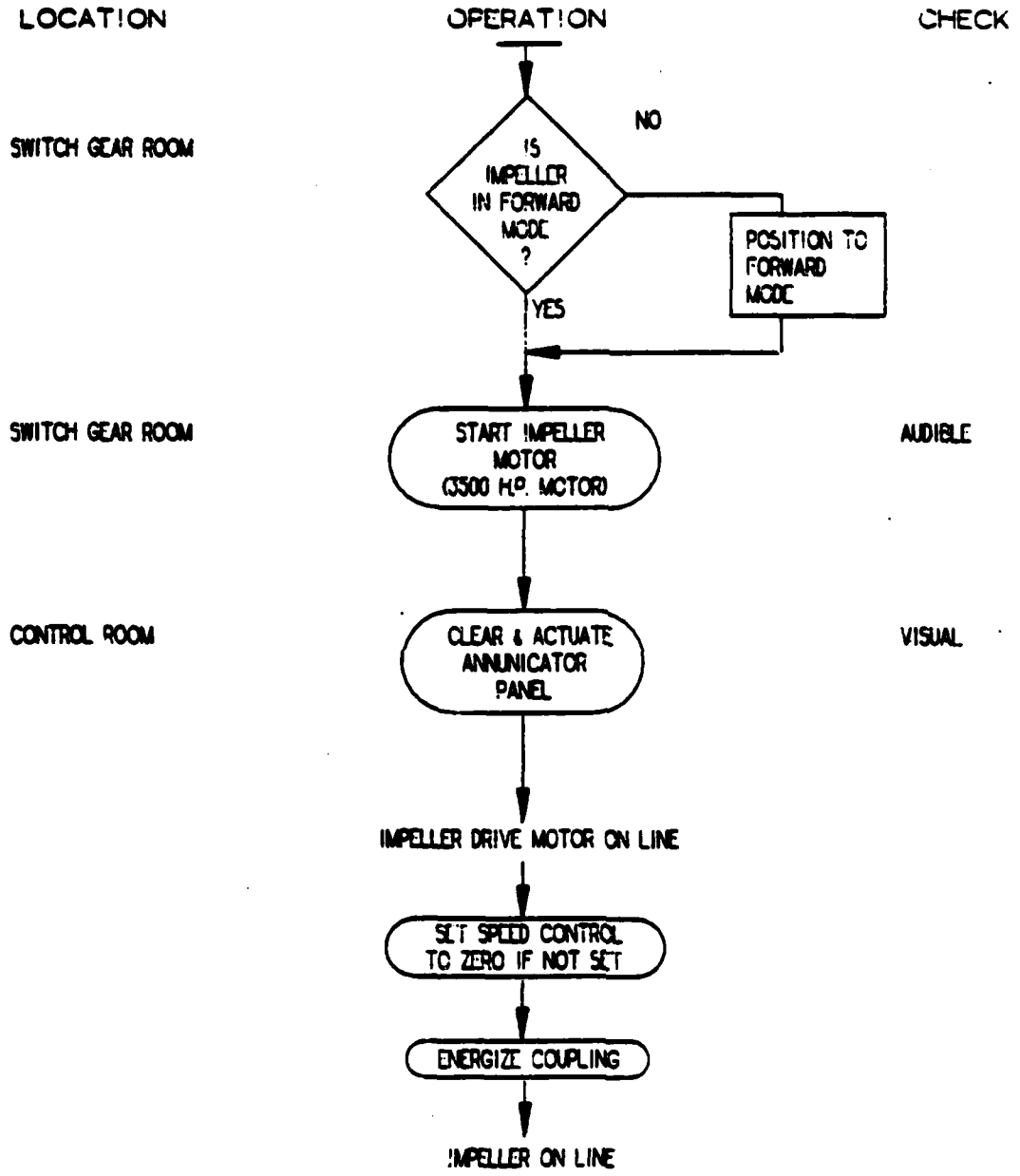

IMPELLER DRIVE SHUT-DOWN

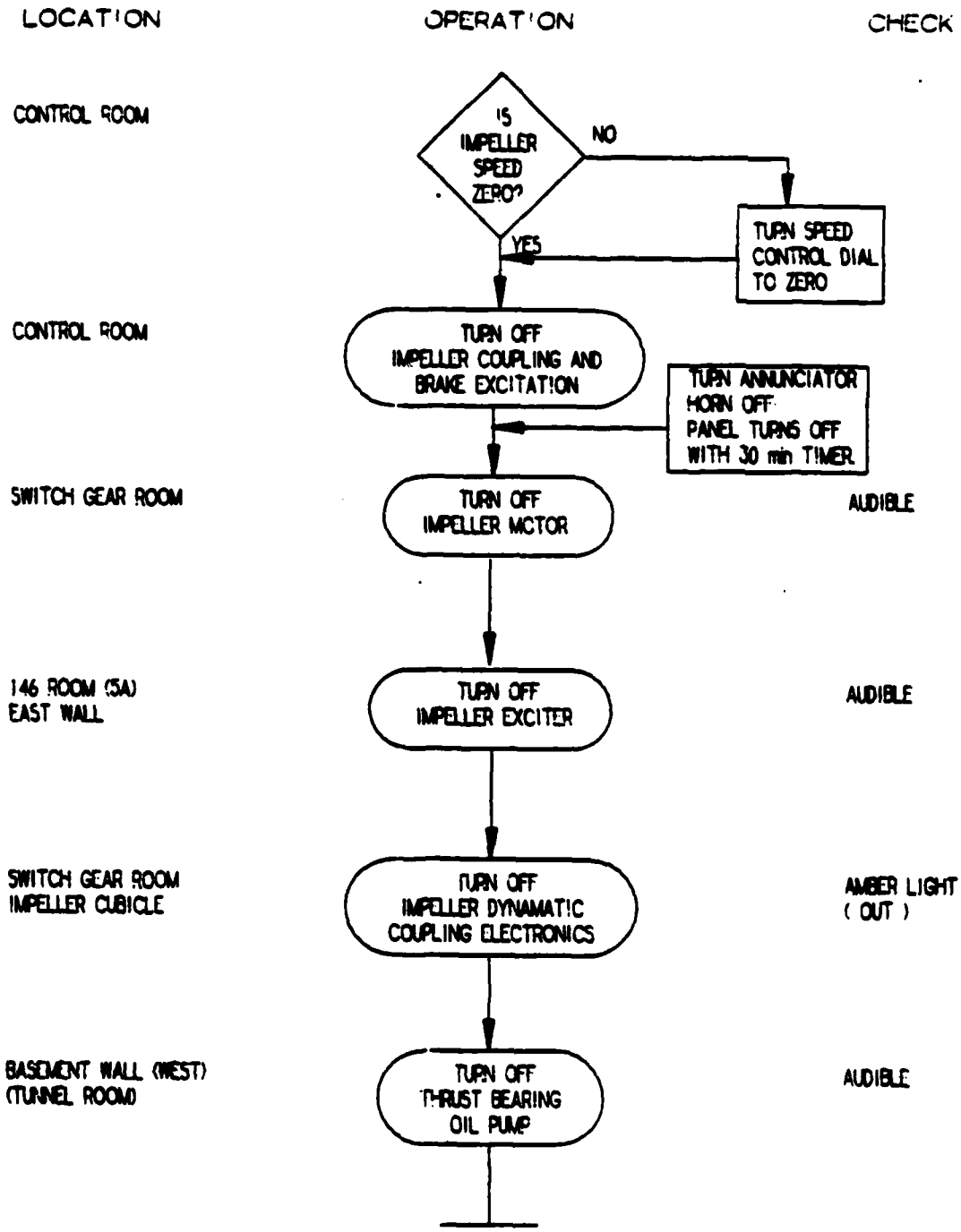

IMPELLER DRIVE SHUT-DOWN
CON'T

LOCATION	OPERATION	CHECK
PUMP ROOM	SHOULD PUMP ROOM BE SECURED ? — NO / YES	
	PUMP ROOM SECURED? — NO: FOLLOW PROCEDURES FOR SECURING PUMP ROOM / YES	
LOWER SOUTH ELBOW OF TUNNEL	IMPELLER OFF LINE	
	JACK-IN CARBON SEAL.	

DYNAMOMETER START-UP

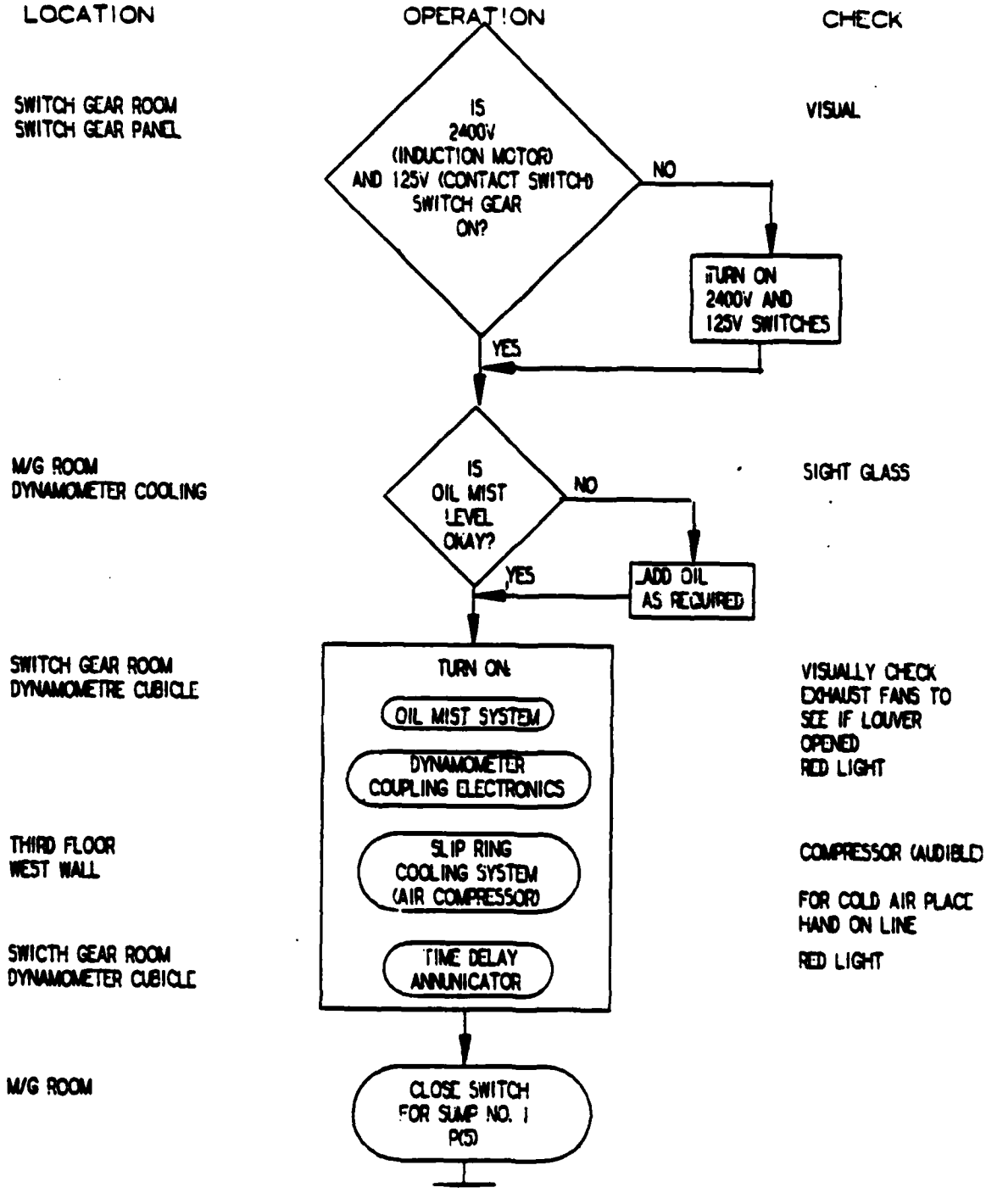

DYNAMOMETER START-UP CONT

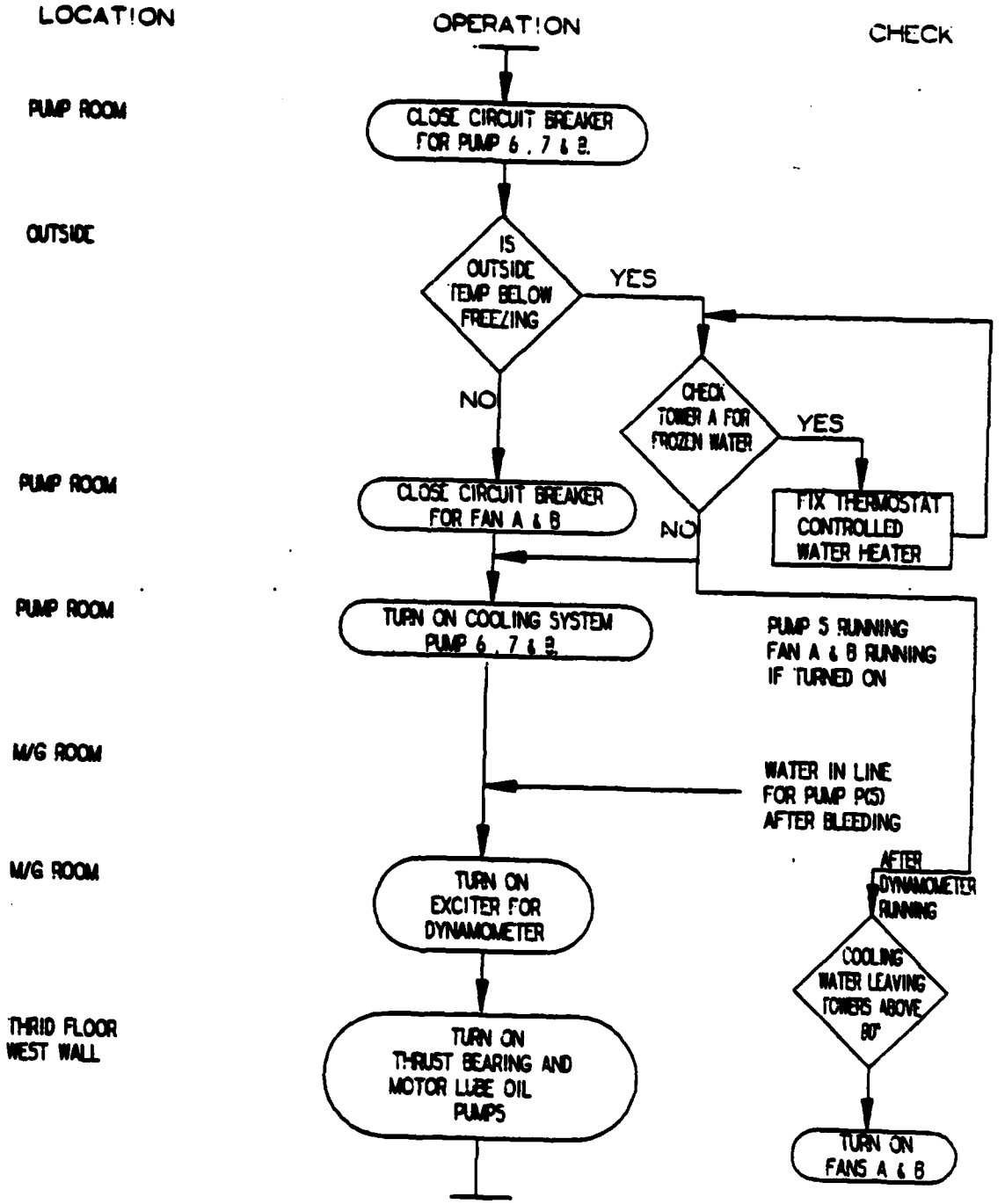

DYNAMOMETER START-UP
CONT

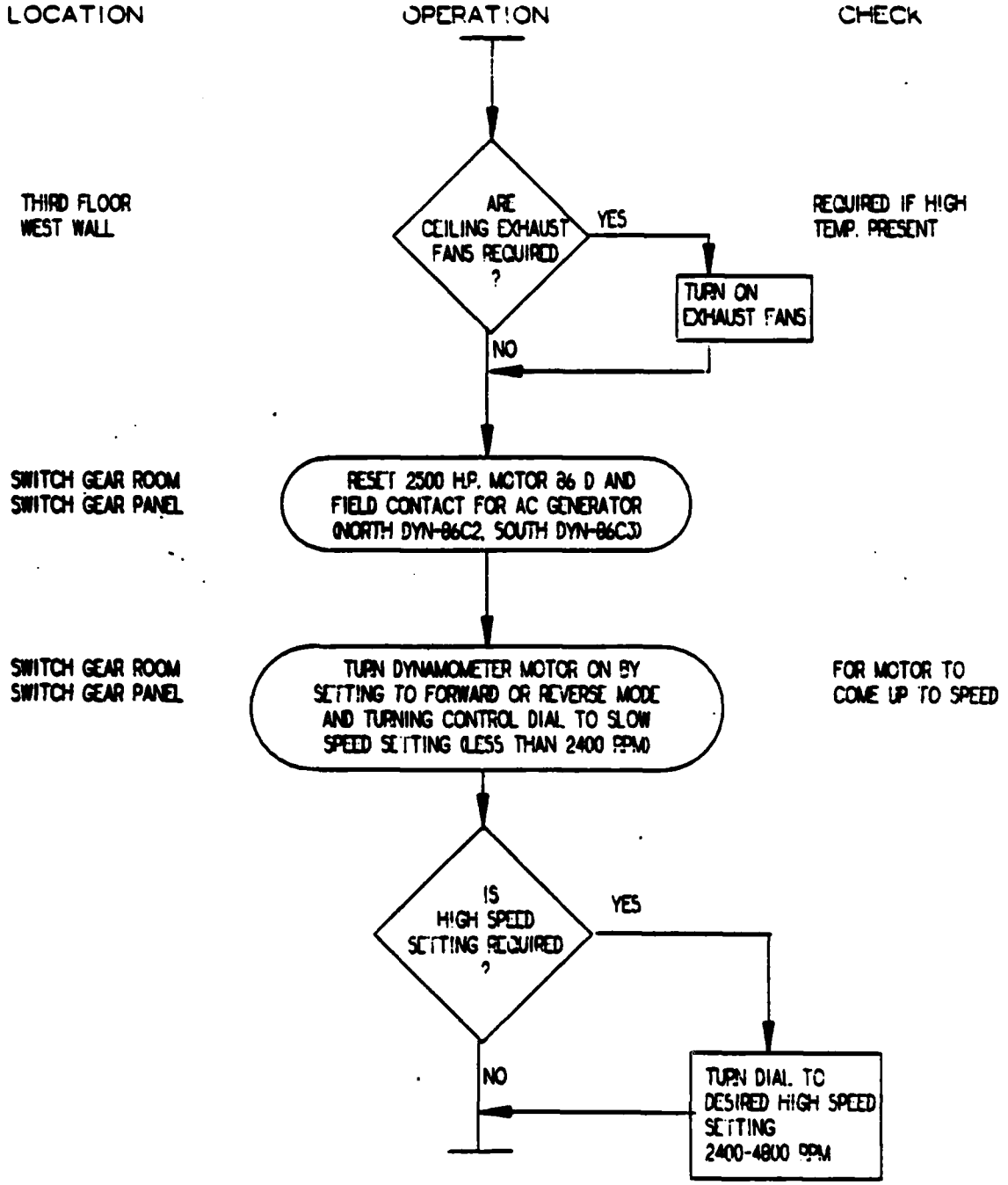

DYNAMOMETER START-UP
CONT

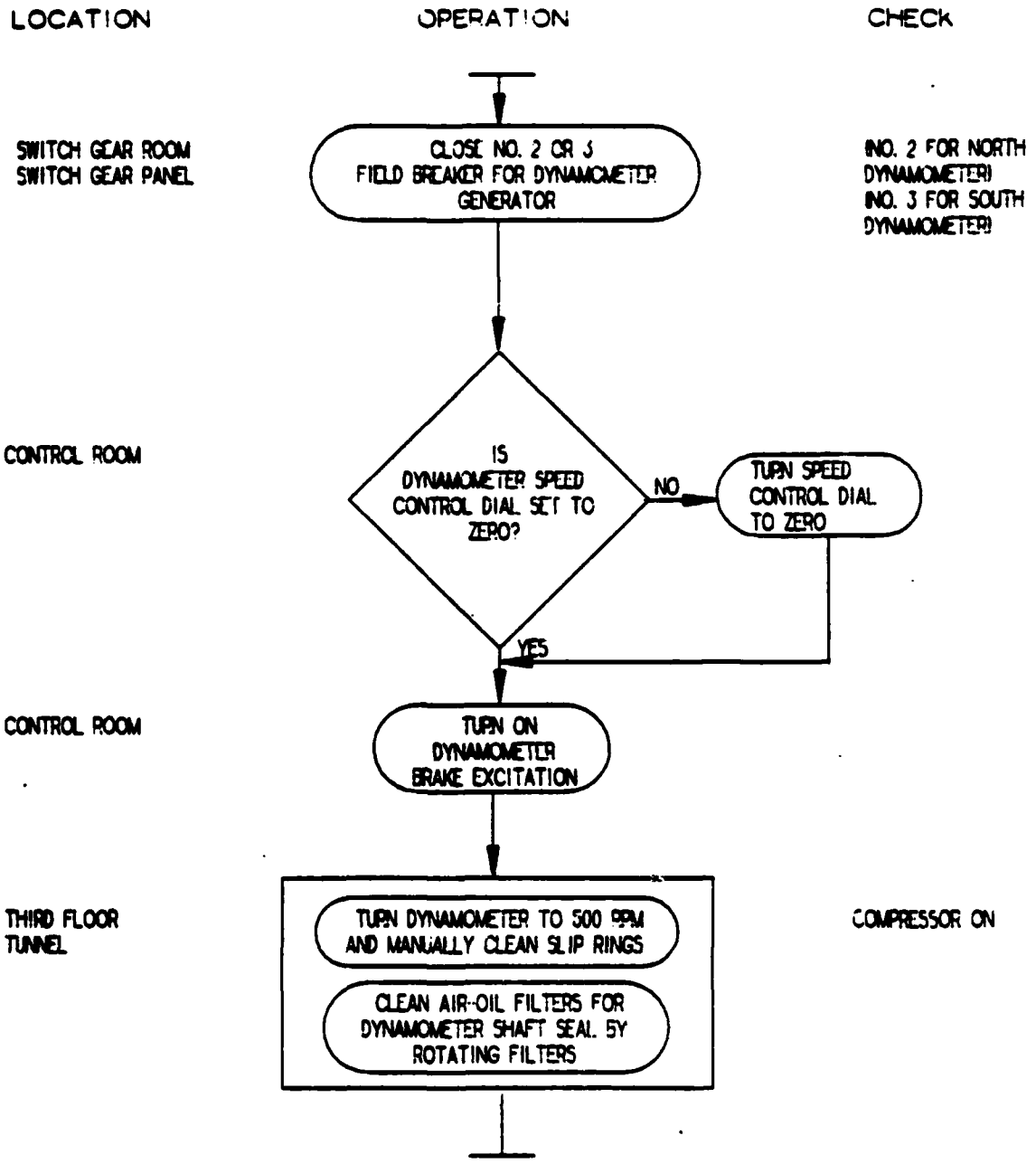

DYNAMOMETER START-UP
CONT

LOCATION	OPERATION	CHECK

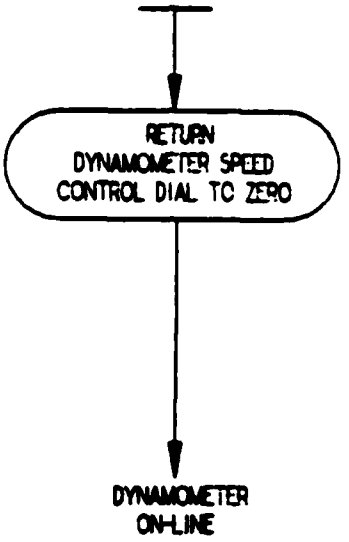

DYNAMOMETER SHUT-DOWN

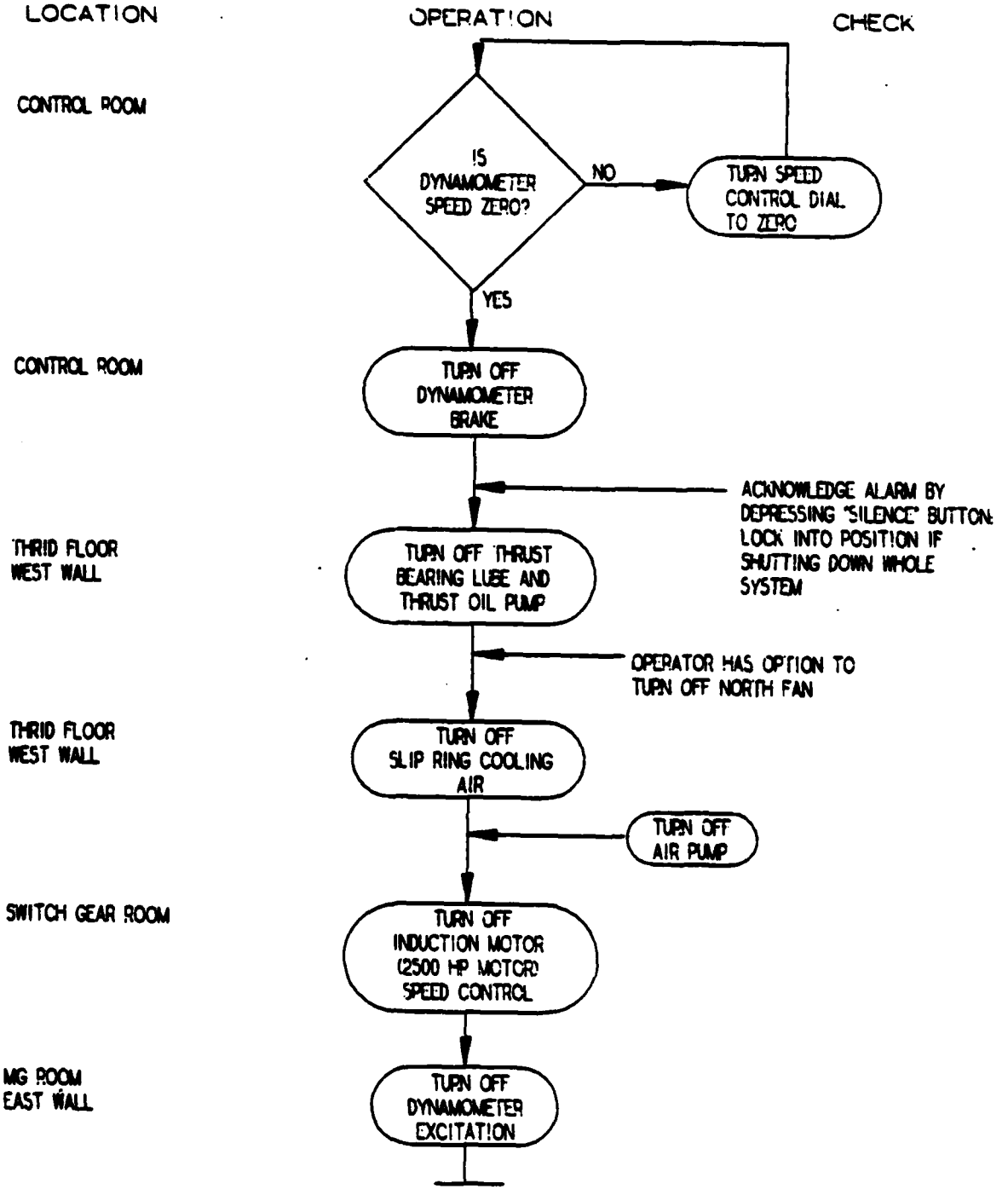

DYNAMOMETER SHUT-DOWN
CONT

LOCATION	OPERATION	CHECK
MG ROOM BELOW ECC	TURN OFF SUMP NO. 1 PUMP (P-5)	
SWITCH GEAR ROOM DYNAMOMETER CUBICLE	TURN OFF DYNAMOMETER ELECTRONIC EXCITATION	
	SHOULD PUMP ROOM BE SECURED ? — NO	
	YES	
	PUMP ROOM SECURED ? — NO	
PUMP ROOM	YES — FOLLOW PROCEDURES FOR SECURING PUMP ROOM	
	DYNAMOMETER OFF LINE	

DRAIN TUNNEL (FOR TOP SECTION ONLY)

LOCATION	OPERATION	CHECK
	FAST DRAIN (OPEN OR CLOSED JET TEST SECTIONS)	
CONTROL ROOM	ARE ALL SYSTEMS OFF ?	IMPELLER DYNAMOMETER COOLING WATER AUXILIARY WATER DEAERATOR PURGE PRESSURE REGULATOR
	TURN OFF ALL SYSTEMS	
	OPEN VENT VALVES (V-25, V-26, V-27)	
BASEMENT	OPEN AUXILIARY WATER SYSTEM VALVE (V-2)	
BASEMENT	OPEN VALVE V-5 (REGULATE FLOW IN SYSTEM)	
THIRD FLOOR TUNNEL	IS WATER LEVEL TO BOTTOM OF UPPER LEG ?	
	NO	
	YES	

DRAIN TUNNEL (FOR TOP SECTION ONLY)
CONT

LOCATION	OPERATION	CHECK
BASEMENT	YES CLOSE VALVES V-2, V-5 TUNNEL TOP SECTION DRAINED	

SLOW DRAIN (OPEN JET TEST SECTION ONLY)

LOCATION	OPERATION	CHECK
CONTROL ROOM	ARE ALL SYSTEMS OFF ? — NO → TURN OFF ALL SYSTEMS; YES →	IMPELLER DYNAMOMETER COOLING WATER AUXILIARY WATER DEAERATOR PURGE PRESSURE REGULATOR
THIRD FLOOR TUNNEL	OPEN VENT VALVES V-25, V-26, V-27	
THIRD FLOOR TUNNEL	OPEN TEST SECTION DRAIN VALVE: 68, 69	
	OPEN JET TEST SECTION DRAINED	

AD-P003 834

A HIGH PRECISION DIFFERENTIAL FORCE BALANCE AND EXPERIMENTAL METHOD TO MEASURE SMALL FLUID-DYNAMIC FORCES DUE TO SMALL GEOMETRY CHANGES

by

David W. Coder

Benjamin B. Wisler, Jr.

and

Michael F. Jeffers, Jr.

David W. Taylor Naval Ship Research and Development Center

Bethesda, Md. 20084

(Tele. 202/2271547)

To be presented at the

Systems and Techniques Symposium, 20th American Towing Tank Conference,

Davidson Laboratory, Stevens Institute of Technology,

Hoboken, New Jersey, 2-4 August 1983

A HIGH PRECISION DIFFERENTIAL FORCE BALANCE AND EXPERIMENTAL METHOD TO MEASURE SMALL FLUID-DYNAMIC FORCES DUE TO SMALL GEOMETRY CHANGES

by

David W. Coder

Benjamin B. Wisler, Jr.

Michael F. Jeffers, Jr.

INTRODUCTION

As the technical community attempts to capture the last few percentage points of vehicle fluid-dynamic resistance reduction, it becomes more and more important to be able to measure small improvements (reductions in resistance) due to small geometry modifications to the exterior of the vehicle. Examples of some of these modifications to reduce resistance are: smoothing of the surface, changing the size, shape, and location of control surfaces, filling in cavities and gaps , and filleting of appendage-main body intersections. While none of the above modifications may improve the resistance appreciably by themselves (and may not even be measurable separately by conventional means), several of these modifications taken together may produce a sizeable improvement (reduction in resistance) that could result in a significant savings in energy consumption over the lifetime of a ship. Thus it is desirable to measure these small resistance effects independently in order to obtain information to be used as input to various cost versus payoff studies.

The conventional model experiment to determine the effect of some small geometry change would involve the separate measurement of the total resistance of the baseline model and the model with the modification. The results would then be compared to see any difference. As long as the measured difference in resistance is sufficiently larger than the uncertainty in the measurements, this method may yield statistically meaningful results. Methods outlined by Schenck (1961), Lipson and Sheth (1973), and others may be useful in the design of such experiments. After analyzing the results of some high quality conventional resistance experiments, Sandell (1977) found that these experiments could be expected to produce statistically significant differences between hull form modifications down only to about 1 percent of the total resistance at a 95 percent confidence level. However, when it is desired to measure more accurately than this, the conventional method requires many repetitions, which are costly, to reduce the precision error and/or may fail because of high bias errors. In the present paper, a new improved method with its supporting hardware is described that has considerably improved the accuracy and has made possible the measurement of differences of resistance down to about 0.1 percent of the total resistance at a 95 percent confidence level.

METHOD

The resistance of a model may be represented in the form

$$Cd = Cd\ (Geometry, Fn, Rn)$$

where Cd is drag coefficient (=D/(qA)), Fn is Froude number ($=V/\sqrt{gL}$), Rn is Reynolds number ($=VL/\nu$), D is drag, q is dynamic pressure ($=0.5\rho V^2$), A is a characteristic area such as wetted area or cross-sectional area, V is free stream velocity, ν is kinematic viscosity of fluid, ρ is density of fluid, and "Geometry" is the outside geometry of the model. Uncertainties in the experimental data enter into the measurements and are propagated through all parameters and may be calculated and presented according to the methods presented in Kline and McClintock (1953), the ASME standard for many years, and now in Abernethy (1982), the new ASME standard. Uncertainty is an estimate of the error (difference between the measurement and the true value) which consists of a fixed error (referred to as "bias error" by Abernethy (1982) but previously referred to as "accuracy error" in texts such as Schenck (1961)) and a random error (refered to as "precision error" almost universally). Following Abernethy (1982), the recent ASME standard for reporting mean data with an uncertainty band (in this case a confidence interval) is

$$\bar{X} \pm U, \text{ where,}$$

$$U = \begin{cases} B + t95*S/\sqrt{N} \\ \quad \text{or} \\ (B^2 + (t95*S/\sqrt{N})^2)^{1/2} \end{cases} \qquad (1)$$

where $\bar{X}$ is mean value, U is uncertainty, B is bias error, t95 is the 95th percentile point for the two-tailed Students t-distribution (about equal to 2.0 for large number of samples), S is an estimate of the standard deviation of the population, N is the number of samples, and t95*S is the precision error expressed as the half-width of the confidence interval about the true mean.

While it appears possible to reduce the precision error of an experiment by obtaining better and better equipment (reducing S) and making more and more measurements (reducing t95 towards 2.0 and increasing N in the denominator), the bias error may be impossible to reduce down to the 0.1 percent level. It is often found that bias errors for the same experimental hardware and repeat conditions are much greater than this. It may even be impossible to reduce this error by the desired amount during the same run. Thus, it appears that the only way to reduce the bias error sufficiently in many cases is to conduct a "relative" experiment -- one in which the two separate configurations are tested at or near the same time under the same test conditions. In this case, the bias error does not change significantly between the two measurements and drops out of the measurement when the difference is taken. The only thing left in the equation is the precision error which should be reducible to an acceptable level. With this testing method in mind, the development of supporting hardware to allow the measurement of the effect of a small modification to the geometry of the exterior of the model will now be discussed in the next section.

INSTRUMENTATION DESIGN

For the work presented in the present paper, it was desired to measure the effect on total-model fluid-dynamic resistance, of placing a small fillet at the juncture of the main body (hull or fuselage) and the leading edge of an appendage. However, the same principles used here also apply to many other situations. What is needed for the testing methodology to work is for a mechanism to be developed to change configurations while testing and a force balance to be developed that has sufficient precision.

The overall mechanical system devised to solve the present measurement problem is shown schematically in Figure 1. A double model is shown mounted in a wind tunnel on two large bipod struts (the same system would work in a water tunnel with sufficient water-proofing of the instrumentation). Between the model and the supporting structure is a high precision differential force balance which will be described later. A rotating fillet mechanism on the model allows the changing of fillet configurations during testing. During a run, and actuated from outside the tunnel, a section of the hull and appendage without a fillet rotates out of place as shown schematically in Figure 2a and is replaced with a hull and appendage section with a fillet. The hull and fillet sections were carefully machined and fitted to the model so that any dissimilarities between the two sections except for the fillet geometry were minimized. From the local geometry as shown in Figure 2b, it is seen that the maximum possible height of the section that can be cut out of the appendage depends on the local hull geometry where the hidden section is stored. For the case where the local hull radius is R, the maximum height is $(\sqrt{2} - 1)R$. This height allows testing of rather high fillets if desired. The length of the rotating section along the hull forward of the appendage is made just long enough to accomodate the longest fillet to be tested.

The precision differential drag balance was designed as follows: As shown in Figure 1, the model "hangs" via four flexures from the support structure and is free to float as free of friction as possible on the flexures and deflect rearward under the action of drag (D). Three sets of flexures were designed to give a displacement of about $\pm$0.25 mm ($\pm$0.010 in.) for loads of $\pm$18, $\pm$36, and $\pm$71N ($\pm$4, $\pm$8, and $\pm$16 lbf), respectively. A nulling force mechanism (shown on the bench in Figure 3) is located inside the beam and is supported at the top of the beam with a flexural pivot. From outside the tunnel, the mechanism may be actuated to apply a nulling force (F) to the model directly below the pivot through a knife-edge/V-block arrangement in opposition to the drag. The magnitude of this nulling force, generated by moving weights on lead screws, is adjustable from 0 to about 700 N (0 to 175 lbf) and was designed to be repeatable and precise over the range of deflection, $\pm$0.25 mm ($\pm$0.010 in.). The maximum presision error in nulling force over this range considering the factors that might affect it (jack screw backlash, flexural pivot torque, flexural pivot hysterisis, jack screw deflection, etc.) is estimated to be less than 0.054 N (0.014 lbf). The deflection of the model on its flexures is measured using two calibrated linear voltage differential transducers (LVDT's), one of $\pm$0.025 mm ($\pm$0.010 in.) range and one of $\pm$0.125 mm ($\pm$0.050 in.) range, mounted with the cores attached to the model and the casings attached to the support beam. The flexures were also strain-gaged so that they could be used as an alternate drag-measuring device.

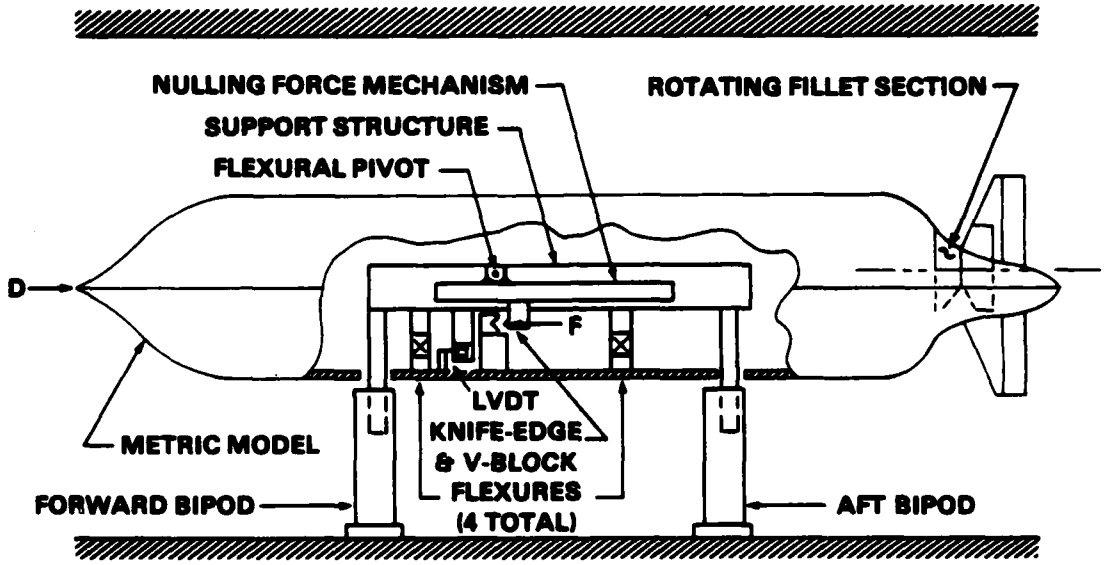

Figure 1 - Schematic of Model Mechanical System

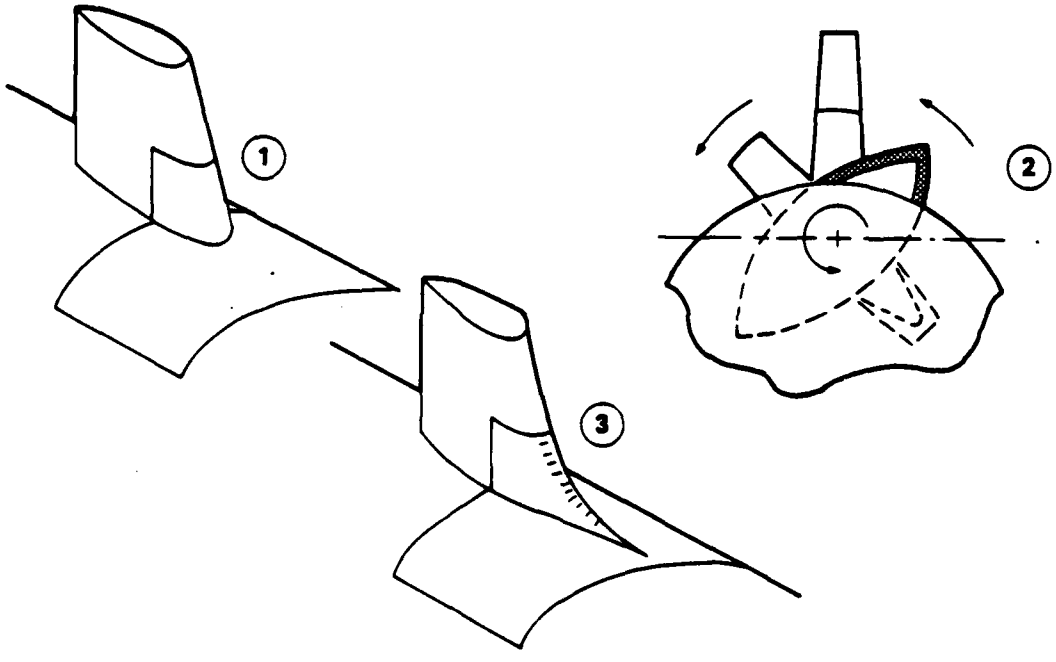

Figure 2 - Rotating Fillet Mechanism

Figure 2a - Schematic of Concept

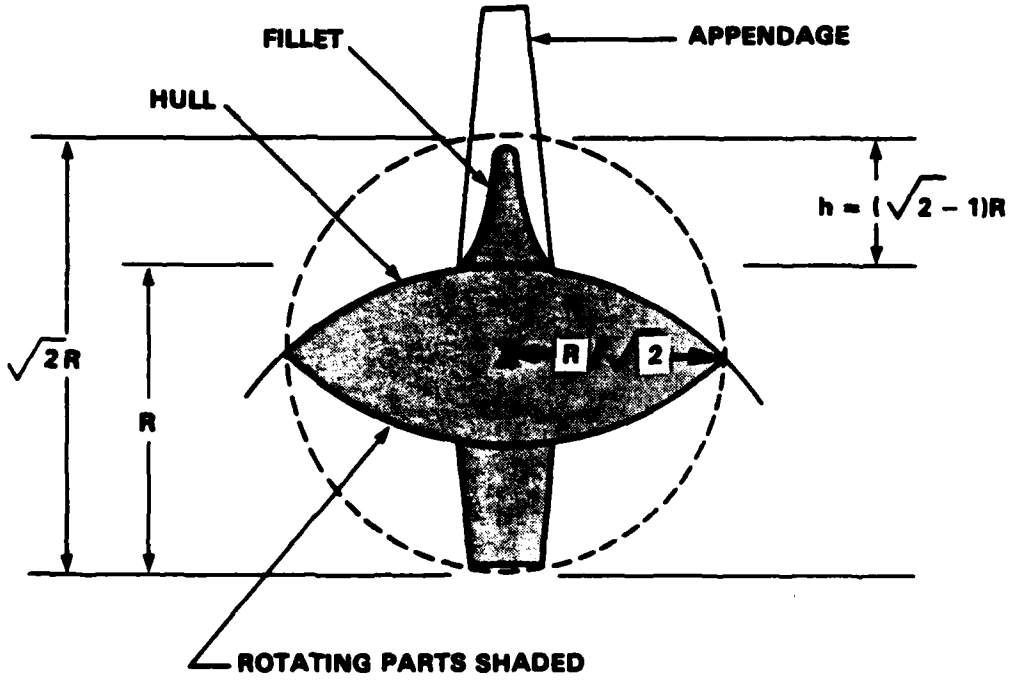

Figure 2b - Geometric Constraints of Mechanism

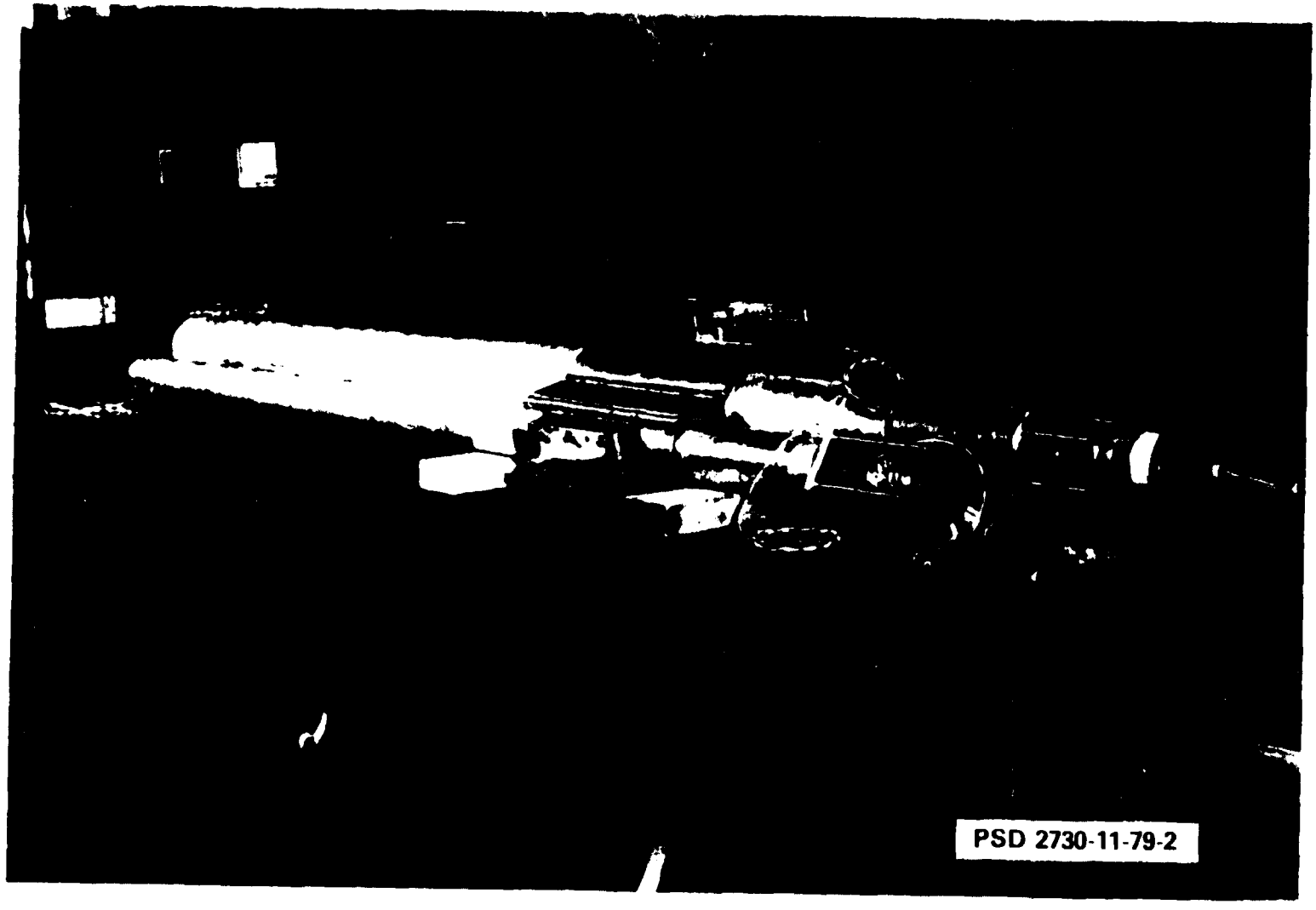

Figure 3 - Hulling Force Mechanism Shown on Bench

With this balance, differential resistance measurements may be measured as follows: Before a run the model deflections and the flexure strains are zeroed out. The flow velocity is brought up to speed and the drag deflects the model backward. The nulling force mechanism is used to place a force in opposition to the drag and the deflection or the strain may be nulled out (D - F = 0). While running at a given tunnel condition, small differentials between the two forces (D - F = small) are measured by the calibrated LVDT's and calibrated strain gages. Thus, if configuration changes are made while running at a constant tunnel condition, the measurement of small differences in drag are possible. The effect on resistance due to leading edge filleting was determined in this way. The drag reduction (if any) between the two conditions can be calculated as

$$\Delta D = Dw - Dwo = (Dw - F) - (Dwo - F) = \Delta Dw - \Delta Dwo \qquad (2)$$

where ΔD is drag reduction, Dw is drag with fillet, Dwo is drag without fillet, F is nulling force, ΔDw is differential drag with fillet, and ΔDwo is differential drag without fillet. This drag reduction for the given fillet may be converted to coefficient form using the tunnel conditions and a characteristic area,

$$\Delta Cd = \Delta D/(qA) \qquad (3)$$

where ΔCd is drag reduction coefficient, q is tunnel dynamic pressure, and A is sail profile area, body surface area, or body cross section area. The above process may be performed in reverse order (with fillet to without fillet) and as many times as necessary (from outside the tunnel) to obtain the desired precision. These calculations can be made as the test procedes to assure that enough data points are taken.

The balance described above was calibrated in the laboratory with precision weights as shown in Figure 4. Friction was reduced in the 90 deg force turning mechanism utilizing a knife-edge/V-block arrangement as shown in Figure 4b instead of a conventional pulley. In order to demonstrate how the differential drag balance performs, a laboratory simulation of a drag run is shown in Figure 5. Here a 222 N (50 lbf) simulated drag force was placed on the model as shown in Figure 4 and was zeroed out with the nulling force mechanism controlled by a computer. A small simulated drag force of 0.44 N (0.10 lbf) was alternately added to and removed from the 222 N (50 lbf) large weight. As the test proceeded the computer analyzed the data statistically and produced mean values and confidence intervals on the measured difference in simulated drag. As shown on the figure, there is enough data to produce statistical results by the fourth sample (two with and two without the small weight), the results improve (the confidence interval decreases) with some additional samples, but after about 10 samples, cease to improve significantly. Thus, by making calculations as the test proceeds, the test can be terminated whenever enough data is obtained thereby holding the testing time to a minimum. For the simulated drag run shown in Figure 5, a measurement of a simulated differential drag of about 0.2 percent of the total simulated drag was measured with a 95 percent confidence interval of $\pm$ 0.015 percent of the total imposed simulated drag. Thus the precision error due to the balance should be negligible compared with error from other real world sources when attempting to make measurements of differential drag down to a 95 percent confidence intervalon the mean of $\pm$ 0.1 percent of full scale.

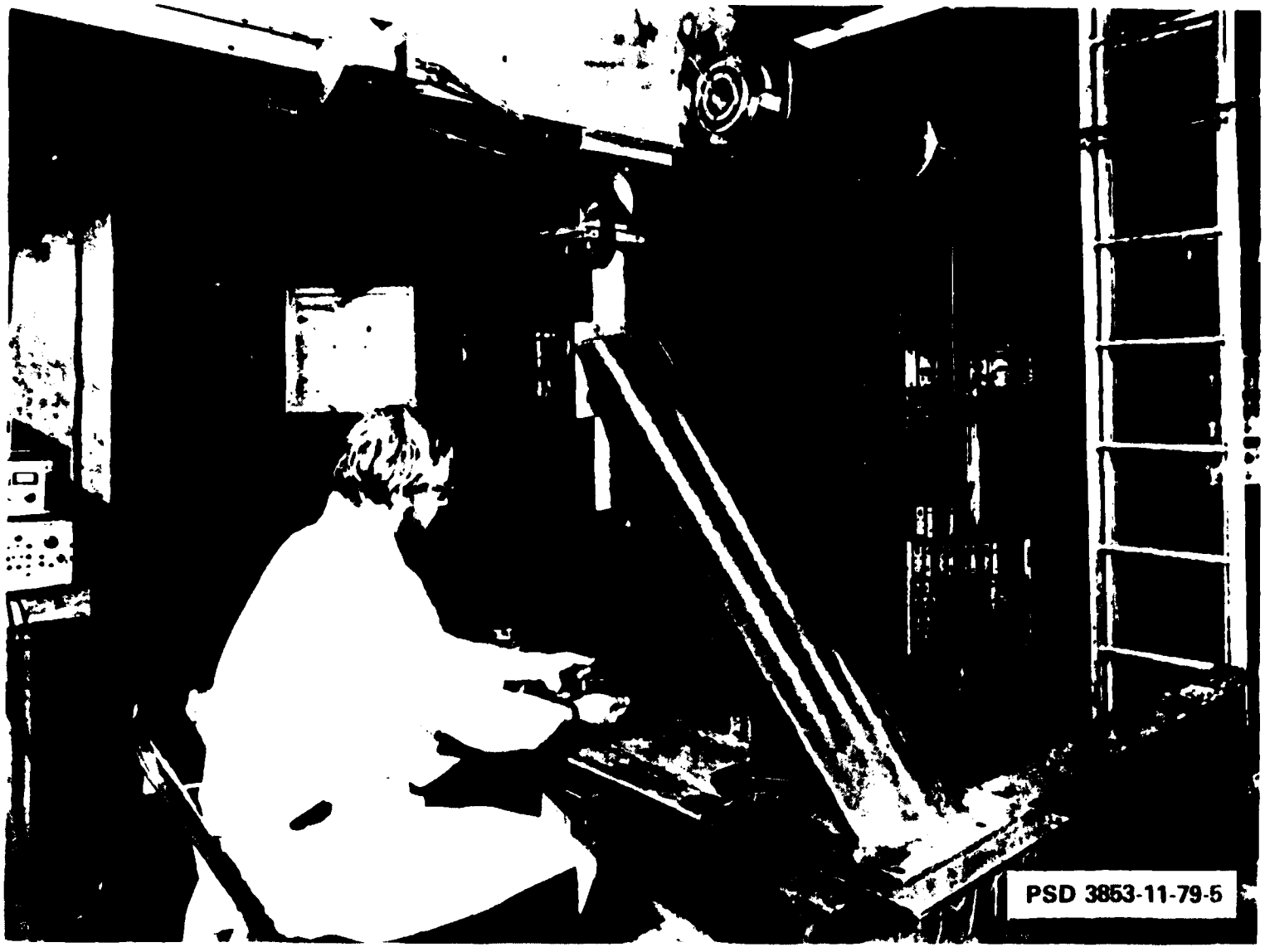

Figure 4 - Balance Calibration Set-Up

Figure 4a - Simulated Drag Loading Technique

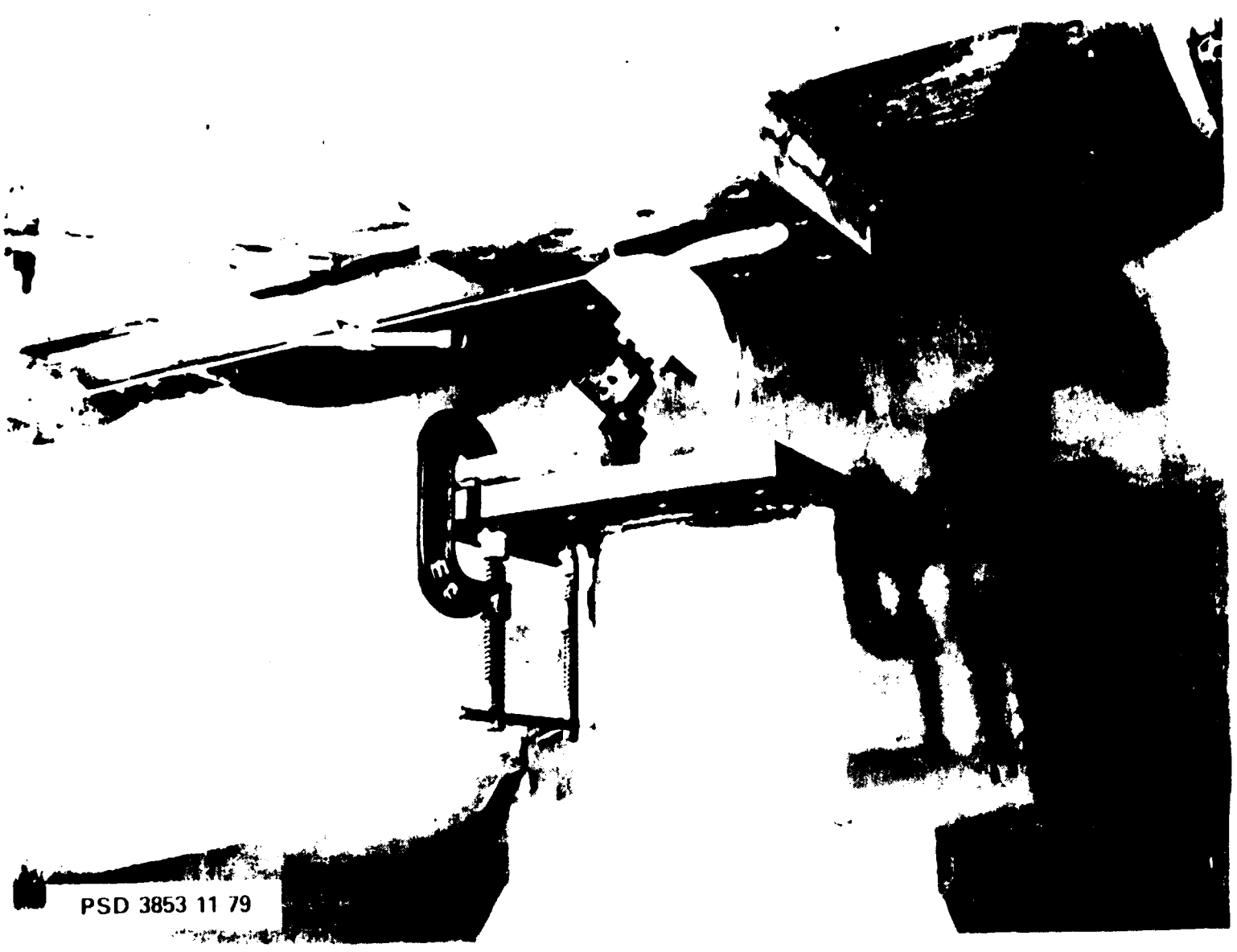

Figure 4b - Closeup of the Knife Edge/V-Block Pulley

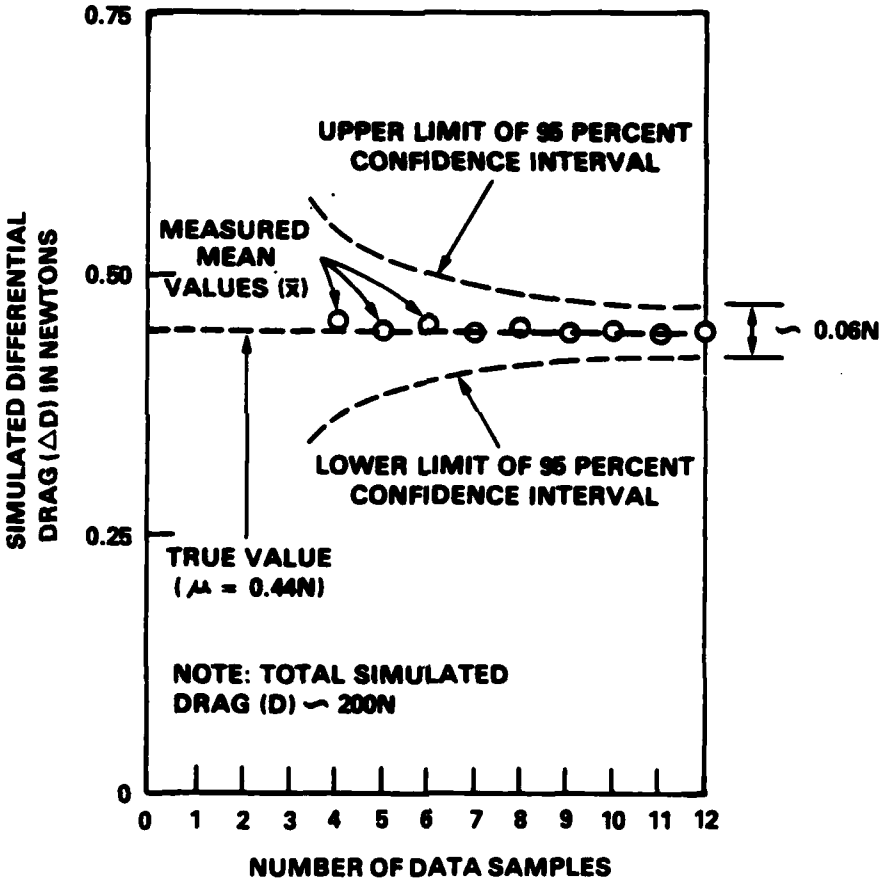

Figure 5 - Simulated Differential Drag Results

EXPERIMENTAL RESULTS AND ANALYSIS

A sketch of a qualitative analog signal from a LVDT or strain gage during testing is shown in Figure 6. The differential drag for one condition, say without a fillet, is adjusted onto the range of the balance using the nulling force mechanism. Several hundred samples were taken at a scan rate of 300 Hz and these data were averaged to obtain a mean. After data were taken without a fillet, the filleted section is rotated into place causing a drag increase during rotation, and then a drop in drag below the initial value whenever the fillet is in place. Data were again taken for this different configuration. This process was reversed, going from filleted to unfilleted, and repeated to obtain about 10 to 20 measurement samples. The data were then analyzed as follows:

(a) The raw data from the various transducers (LVDT's and strain gages) and the tunnel conditions were transformed into coefficient form (Cd and Rn).

(b) It was noted that these data from the three transducers tracked fairly well with each other. For a few cases, these three sets of data were analyzed separately and then compared — it made virtually no difference in the final results for the mean values. Even though there may be some benefit derived from analyzing these data separately and combining them at some later step, for simplicity it was decided to average the measurements at this point in the analysis.

(c) The resultant Cd and Rn data showed that, during a run, the Cd and Rn data drifted up and down with samples (taken at approximately equal time steps) but with an inverse correlation (i.e., the Cd tended to decrease when the Rn increased and vica versa). The change in Cd versus the change in Rn for each pair of samples at the same condition (every other point) was plotted and fit with a least-squares straight line. The slope was used to normalize all of the data to the average Reynolds number of the run. The resulting data were plotted as a function of sample number (sampling occurred at approximately equal time intervals of about 2 min.). A typical run as shown in Figure 7.

(d) Figure 7 shows an evident "drift" or time trend in the drag coefficient. A number of phenomena might plausibly account for the presence of this trend including electronic drift in the instrumentation, slowly changing temperature in the tunnel, thermal effects on the model, etc. In any case, it is apparent that the experimental environment in the real world varies significantly from the ideal of "constant tunnel conditions". Nevertheless, even with these contaminating effects, it seems obvious to the eye that the data for Configuration B (fillet) are consistantly lower than the data for Configuration A (no fillet) by an amount of roughly 0.02E-03. One set of differential resistance observations was generated by taking differences between all pairs of successive measurements in Figure 7. In all cases the resistance of Configuration B was subtracted from the adjacent value for Configuration A. This results in a set of 17 observations of the resistance difference attributable to the fillet. A second set of 8 observations was generated by comparing the measurement for Configuration B with the average of those for Configuration A just preceding and just following. A third set of 8 observations was gererated similarly to the second set but switching the configurations.

(e) A straightforward statistical analysis is used to determine if the apparent reduction in resistance attributable to the presence of the fillet is statistically significant and to provide an estimate of its magnitude and uncertainty in the form of a confidence level (using equation (1)). For the three sets of observations

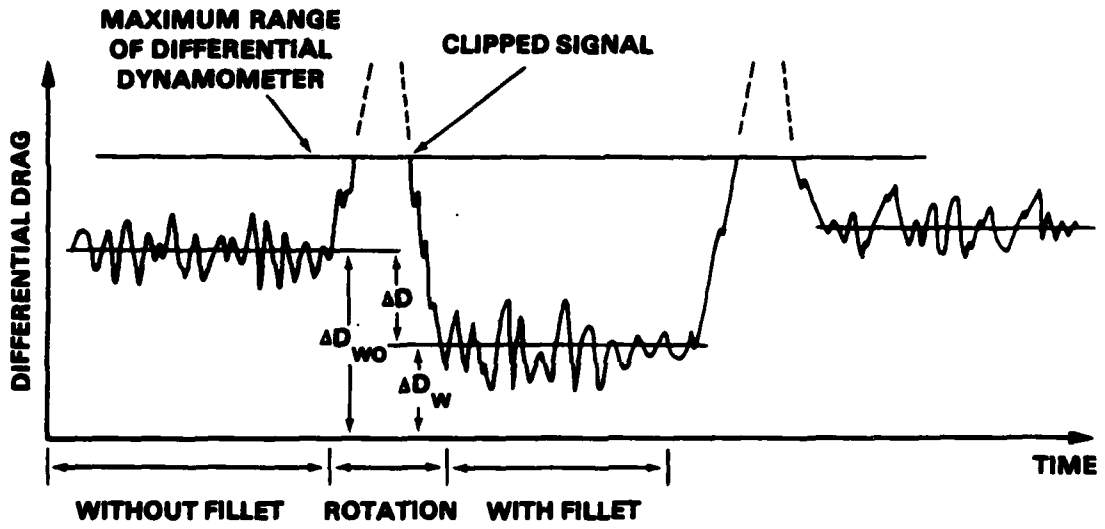

Figure 6 - Schematic of Balance Analog Signal During Testing

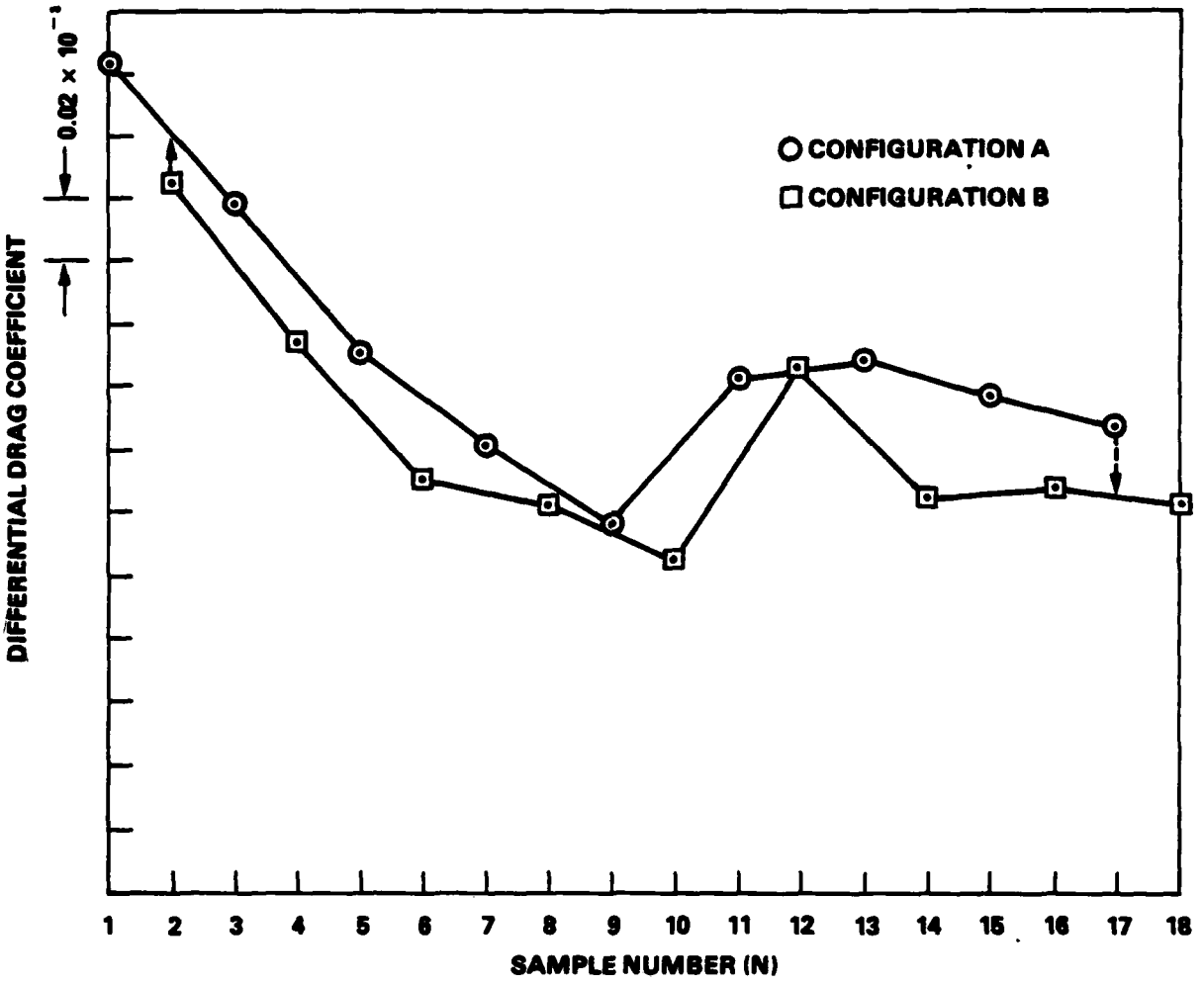

Figure 7 — Differential Drag Versus Sample Number (Time) for a Typical Run

Figure 7a - Mathematically Interpolated Data

determined above, the means, standard deviations, and 95 percent confidence intervals were calculated and are shown in Table 1. It is seen that the means and confidence intervals are approximately the same for the three sets of observations -- the 95 percent confidence interval for the resistance attributable to the fillet is $\Delta Cd = 0.021 \pm 0.010$. Thus, for this run it is shown that the force difference is measured within about 0.2 percent of the full scale value of about 5.0E-03, even in the presence of substantial variations in test conditions. For this run, the confidence interval no doubt could have been reduced down to about 0.1 percent of full scale by taking about four times as many points. Also, improving the fillet changing mechanism so that the measurements could be made quicker would admit less of the "drift" to the calculated precision error. However, even without these improvements, some of the data obtained during the same experiment (but not shown here) indicate 95 percent confidence intervals of about 0.1 percent.

SUMMARY AND CONCLUSIONS

In the present paper, the experimental hardware and method developed to make the measurement of the effect on fluid-dynamic resistance of placing a small fillet at the juncture of the main body (hull or fuslage) and the leading edge of an appendage was discussed. Since the conventional measurement method, in which the total resistance of each configuration is measured separately and then compared, was considered inadequate to accurately measure this effect, a new improved method was developed, one in which the separate configurations were tested at or near the same time under the same test conditions. This was accomplished by using a rotating fillet mechanism that was remotely actuated to change fillet configurations during testing. Thus the bias error that would occur during separate testing was reduced to a minimum.

By making multiple measurements of the differential resistance with the high precision differential balance, developed specifically for the experiment, the precision error was reduced to an acceptable level. Calibrations of the measurement system under laboratory conditions showed that the balance was able to measure a simulated differential resistance (a small weight on the order of 0.4 N) with a 95% percent confidence interval of ± 0.015 percent of the total simulated resistance. (large weight on the order of 200 N).

Typical experimental results obtained with a model in a wind tunnel with the above hardware and measurement method show that differential resistance measurements of the filleting effect were made with a 95 percent confidence interval down to about ± 0.1 percent of the total model resistance.

REFERENCES

1. Abernethy, R., editor, "Measurement Uncertainty for Fluid Flow in Closed Conduits," ASME (1982)
2. Kline, S.J. and McClintock, F.A., "Describing Uncertainties in Single-Sample Experiments," Mechanical Engineering, ASME (January 1953)
3. Lipson, C. and Sheth, N.J., Statistical Design and Analysis of Engineering Experiments, McGraw-Hill Book Company, New York, N.Y. (1973)
4. Sandell, D.A., "Statistical Design of Experiments for Submarine Speed Improvement Program," Report No. CGARD-04-77 (August 1977)
5. Schenck, H., Jr., Theories of Engineering Experimentation, McGraw-Hill Book Company, New York, N.Y. (1961)

TABLE 1 - STATISICAL ANALYSIS

OBSERVATIONS OBTAINED BY SUCCESSIVE DIFFERENCES		OBSERVATIONS CENTERED ON CONFIGURATION B (FILLET)		OBSERVATIONS CENTERED ON CONFIGURATION A (UNFILLETED)	
N	X	N	X	N	X
1	0.039	1	0.017	1	0.019
2	-0.006	2	0.021	2	0.019
3	0.045	3	0.027	3	0.016
4	-0.003	4	0.007	4	0.002
5	0.041	5	0.034	5	0.026
6	0.012	6	-0.001	6	0.023
7	0.020	7	0.039	7	0.031
8	-0.006	8	0.030	8	0.027
9	0.011				
10	0.057				
11	-0.004				
12	0.002				
13	0.044				
14	0.033				
15	0.030				
16	0.020				
17	0.026				
$\bar{X}$ = 0.0212		$\bar{X}$ = 0.0218		$\bar{X}$ = 0.0204	
S = 0.0203		S = 0.0136		S = 0.0089	
N = 17		N = 8		N = 8	
t95 = 2.110		t95 = 2.306		t95 = 2.306	
$t95*S/\sqrt{N}$ = 0.0104		$t95*S/\sqrt{N}$ = 0.0111		$t95*S/\sqrt{N}$ = 0.0073	
= 0.21%FS		= 0.22%FS		= 0.15%FS	

AD-P003 835

"AN INEXPENSIVE TWO-COMPONENT FORCE BALANCE FOR TOWING TANKS AND FLUMES"

T. Kowalski, Professor
Dept. of Ocean Engineering
University of Rhode Island

D. Brown, Research Engineer
Naval Underwater Systems Center
Newport, Rhode Island

Abstract

This paper describes the design, calibration and testing of an inexpensive, yet accurate two component dynamometer. The force balance was designed to measure drag and side forces, and to allow for pitch and heave motions. Testing of the dynamometer was carried out using a 1/6-scale model of the 5.5 meter sailing yacht Antiope.

Introduction

There are two types of force measuring dynamometers one can build. One is a direct force measuring device using strain gages or similar electronic pick ups. The other utilizes displacement transducers.

A direct force type balance is set up such that a material whose stress-strain properties are known is subjected to a force. The force is then measured by strain gages. This type of force dynamometer is typically quite accurate but also quite expensive.

In the displacement type dynamometer the deflection of a flat spring under the action of a force is measured by a transducer. The system is designed so that the deflection is linear within the range of the forces. This type of system can be quite inexpensive and if properly designed, can be quite accurate.

Description

There are two major requirements for the dynamometer. First the measurement of forces and second the freedom of movement of the model.

Force Measurement:

The measurement of drag and side force simultaneously simply involves the proper arrangement of the springs to be deflected.

In order to measure two forces simultaneously we look at the effect a force F_b, (i.e. a side force), has on spring 1 shown in Figure 1. Very little deflection is produced. This is due to the proper orientation of the spring. If we take two springs or sets of springs and mount them orthogonally to each other as shown in Figure 1 we can see that spring 1 and 2 deflect quite easily to F_a and F_b respectively. Spring 1, however, does not deflect easily to F_b nor does spring 2 deflect easily to F_a. All that is left in terms of building the force balance is to mount the springs properly and measure their deflections accurately.

Direct Current Displacement Transducers (DCDTs) are used to measure displacements. The DCDTs chosen were made by Hewlet Packard, Model # 24DCDT-100. They had a range of $\pm$ 0.1 inches with an error of less then 0.5%.

The flat springs used were made from Starret shim stock. Thickness ranged from 0.005 to 0.020 inches. The widths and lengths were kept constant at 0.5 and 3.0 inches respectively. The actual length of a spring experiencing displacement was 1 inch. One inch was used at either end for clamping purposes. Figures 2 and 3 are sketches of the dynamometer's spring arrangement.

The dynamometer was built in three tiers. The top and middle are connected by the drag springs. The thinnest sections of these springs are mounted at right angles to the direction of the model's advance. The top tier is connected to the towing carriage while the middle and bottom tiers,

are connected to each other by the side force springs. These are mounted, with their thin section parallel to the direction of motion. The bottom tier is much larger and stronger than the other two tiers as it serves to connect the dynamometer to models.

The most impressive feature of this dynamometer, in addition to its reasonable price, is its combination of range and accuracy when measuring forces. Springs in either drag or side force can easily be removed and replaced. For example, if the test range involves low values of force, then thin shim stock is used. For higher values of drag or side force, thicker shim stock is used. Of equal importance is the flexibility of using thin shim stock for drag measurements while thick shim stock is used for side force measurements, or vica versa. This extreme capability of both range and accuracy is comparable to a volt-ohm meter where one simply changes scales setting the range to the highest value intended measured.

Model Attachment:

The ability of the dynamometer to allow a model to trim is accomplished as follows. The heel of the model is preset by counter-weighting. Heel brackets attached to the model allow for rotation about the drag axis and the locking in of a given heel angle. Yaw is also preset. This is accomplished by fixing the heel brackets to specific locations on the model. Squat and sinkage are allowed by using a combination of rods, linear bearings and roller bearings. The rods are allowed to move freely in the vertical direction guided by the linear bearings. In addition the roller bearings allow the heel brackets to rotate about the side force axis. Surge and sway are prevented. Figures 2 and 3 show the details.

The nature of the heel brackets is such that stainless steel rods can, quite easily be inserted, into them. The rods are then kept in place by set screws. This allows for attachment and disconnect of the model prior to and after a test series. The heel brackets could of course be used on other models. All that is necessary is to mount them to plates which span a model's gunwales.

The heel brackets as well as the stainless steel rods were of a fairly heavy nature so it was necessary to counterweight them. This was accomplished by the use of Neg'ator springs. A Neg'ator spring is very simply a coil of thin material on a roller which when unrolled develops its resisting force incrementally rather than cumulatively as does a convential spring. These springs were quite inexpensive and were quite constant in their force unloading characteristics.

Electrical Set Up

A diagram of the electrical set up is shown in Figure 4. The DCDT's power was supplied by a 24 volt variable D.C. power supply. The transducers were wired in parallel to the supply. The maximum deflection of the chosen transducers was $\pm$ 0.1 inch. This corresponded to 10 volts or a 100 to 1 voltage to displacement ratio. The accuracy of the transducers were better than 99.5%.

The outputs from the transducers were filtered by an RC circuit. A resistor of 10K ohms was placed in series, and a 50 μfarahd capacitor in parallel with the output. The output was then fed to strip chart recorder. Each DCDT output was placed on a recorder alongside a speed trace which was obtained from a tachometer mounted on the towing carriage.

Calibration

Calibration was performed in the usual way using weights to apply force to the dynamometer and recording the voltage output of the transducer. Weight versus voltage was plotted and a linear regression analysis performed. A correlation coefficient of 0.9997 was typical. A typical calibration curve is shown in Figure 5.

Cross Coupling and Height Of Loading

Simultaneous drag and side force loads were applied to the dynamometer during the calibration to insure that cross coupling was not a problem. The highest interference occurs for high ratios of side force to drag or

drag to side force. The change in a value of either side force or drag was typically less then 2% for ratios less then two.

Loads were also applied to the dynamometer at various heights. That is the calibration line was attached at different points above or below which the model might move. No perceptable change was encountered.

Testing

The scale model of the Antiope was tested in several conditions. They were 0, 2, 4, and 6 degrees of yaw each with 0, 10, 20 and 30 degrees of heel. An angle of yaw was set on the model. The model would then be tested at various angles of heel. Again, yaw was preset by the relative positions of the heel brackets on the model and heel by counterweighting and the subsequent locking of the heel brackets. An inclinometer was placed on the stern of the model for ease in determining the angle of heel. At a given yaw and heel the model was run through a range of speeds. Typically a high speed run followed by a slow speed run working toward the middle of the range was followed. The time allowed between runs was based on the time needed to calm the water in the tank. This varried according to the speed of a previous run.

Results

A very simple but admittedly incomplete documentation of the capability of the dynamometer is drag versus speed for the upright condition (i.e., 0 degrees of yaw and heel). This is presented in Figure 6 as total model drag coefficient versus Froude number. This figure shows that URI's measurements are consistant with those of other facilities.

A total measure of the capability of the dynamometer would be to look at how well the performance of the Antiope, as measured in our tank, compares

against performance measurements from other facilities. The performance of a sailing yacht is found by plotting the drag coefficient versus the square of the side force coefficient. This comparison is not presented as all of the data have not been compiled. However, a preliminary look at the data reveals nothing inconsistent.

Conclusions

The two component dynamometer designed and built at the University of Rhode Island (URI) performed as designed. In calibration tests a regression analysis correlation coefficient of 0.9997 was typical. Cross coupling was minimal, less than 2% for the range of values tested with the Antiope, and calibration effects due to vertical placement of the model were negligible.

A preliminary workup of model performance data indicate that the URI tests and hence the dynamometer are working satisfactorily. It must be remembered that the dynamometer was quite inexpensive. Also, attachment and trim of a model were made quite easy by the use of the heel brackets.

Acknowledgement

The authors would like to express their appreciation to Edward Numata for lending the Antiope model, Paul Spens for making available data for use in Figure 6, both of the Davidson Laboratory and Michael Russo of the Marine Advisory Service, URI who helped with the improvements to the towing facility.

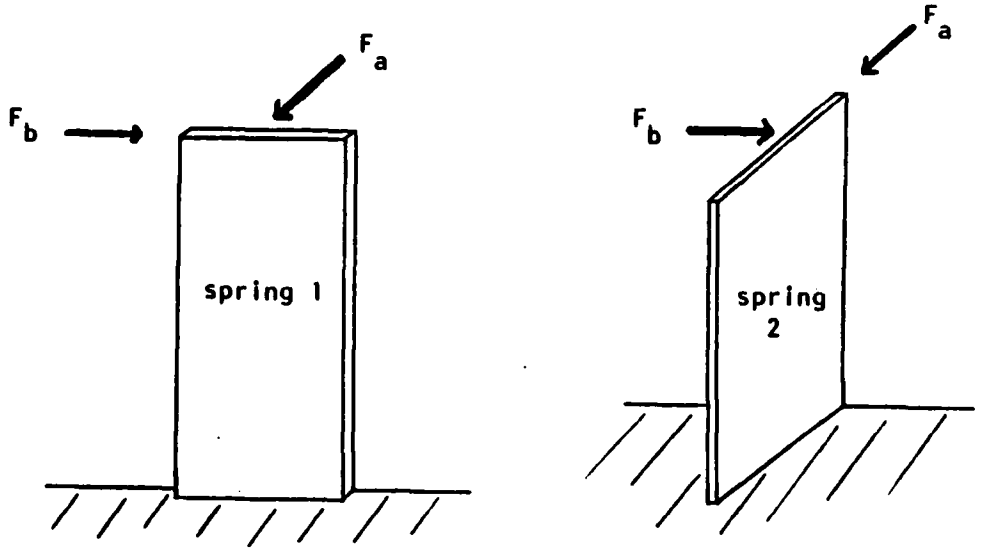

Figure 1: Spring and Force Arangment

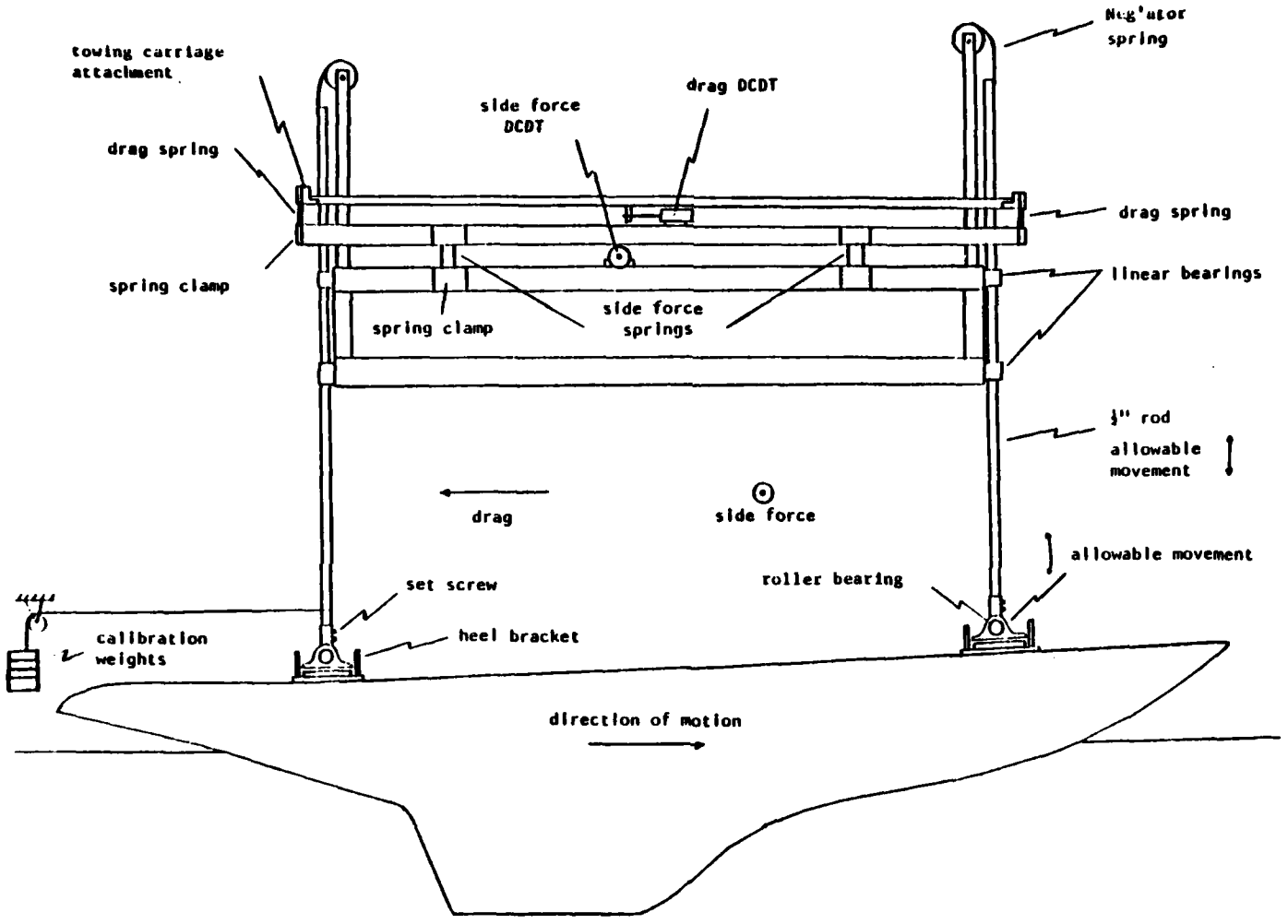

Figure 2: Two Force Dynamometer (side view)

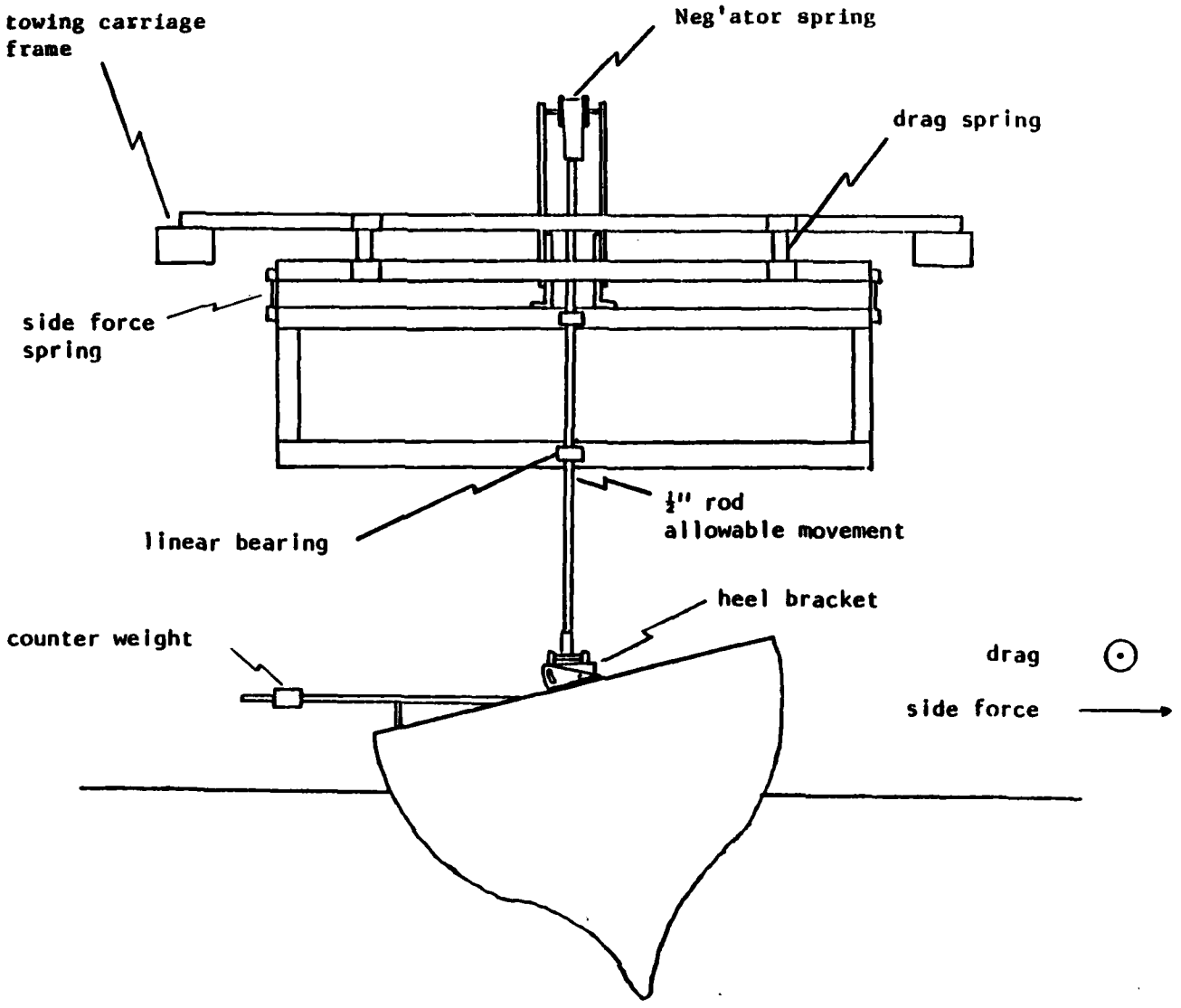

Figure 3: Two Force Dynamometer (front view)

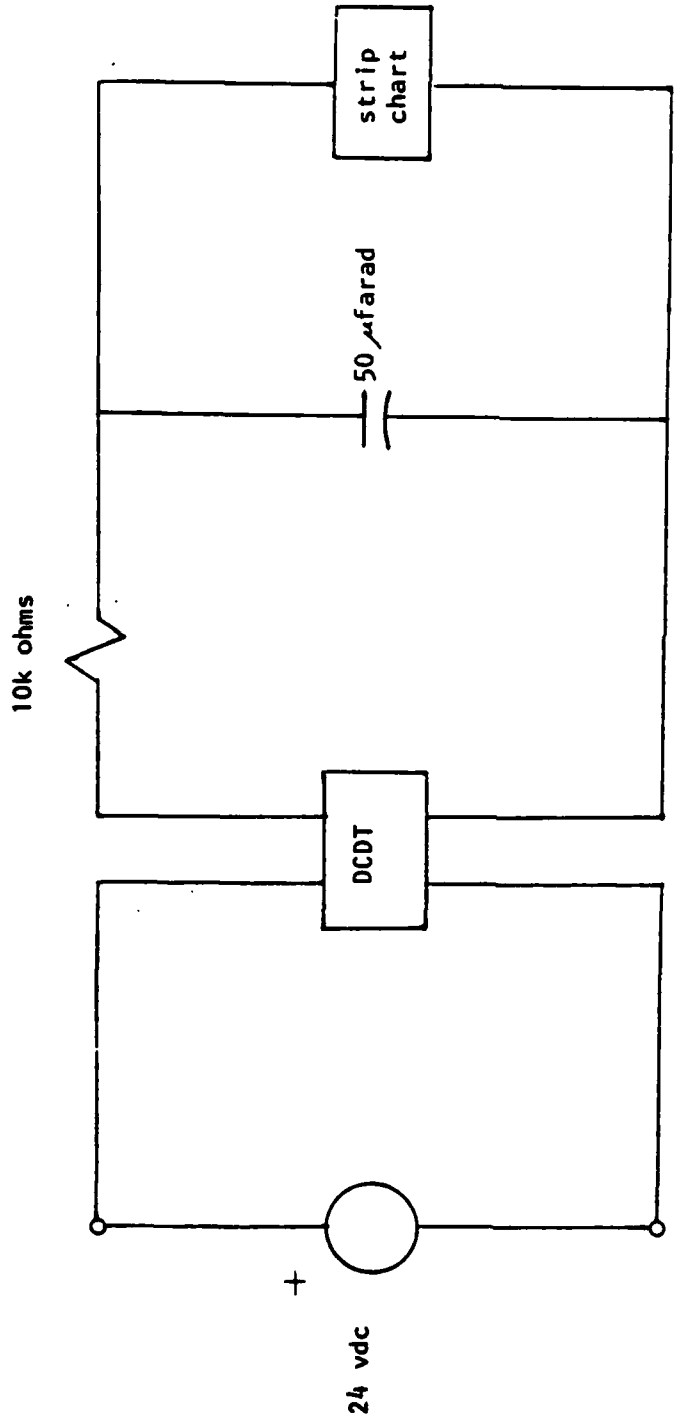

Figure 4: Electrical Set Up

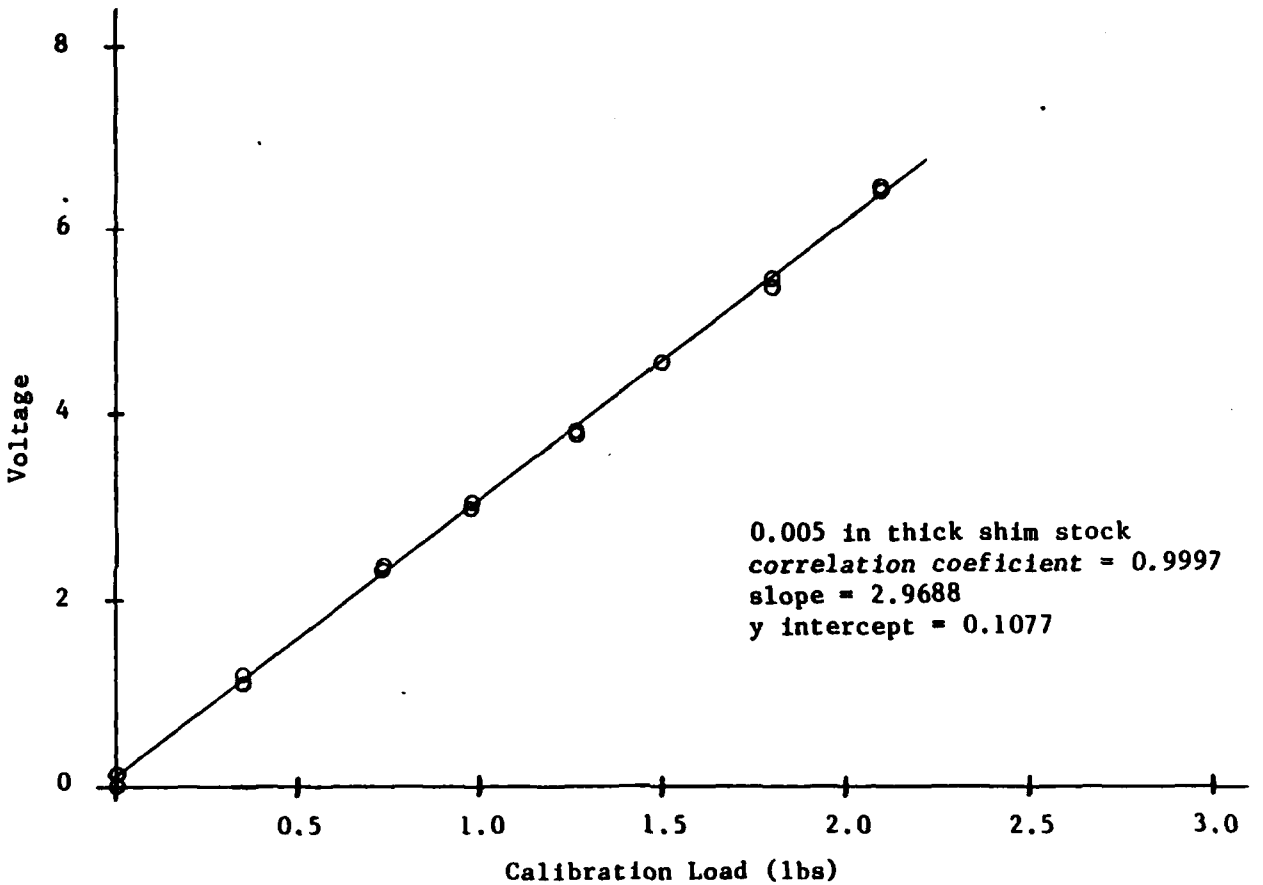

Figure 5: Sample Calibration Curve Drag versus Voltage

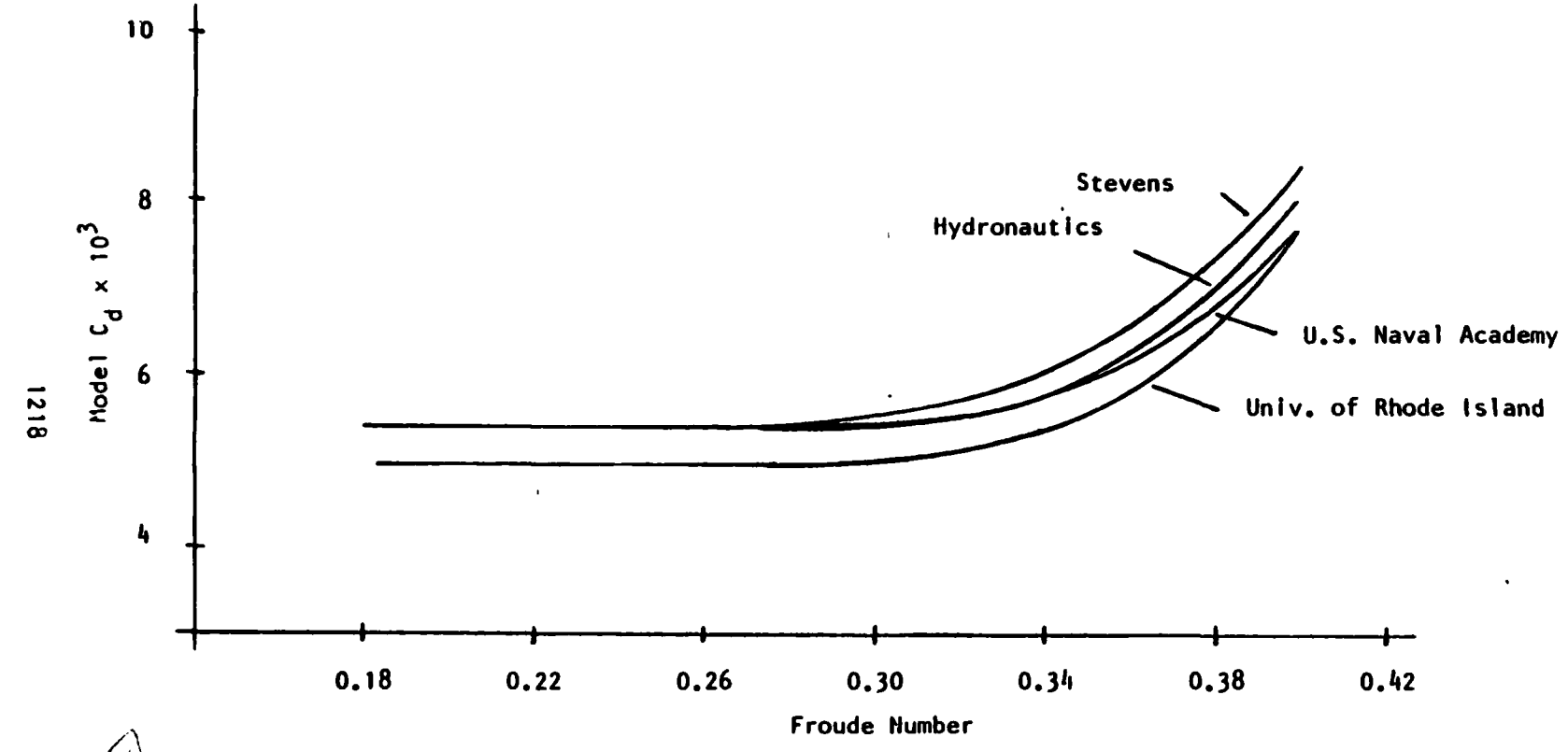

1218

Figure 6: Drag Coeficient vs Froude Number

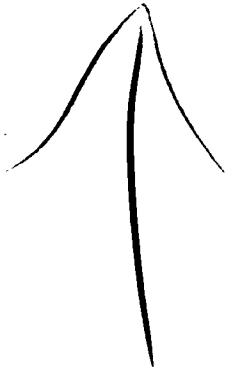

AD-P003 836

DATA ANALYSIS TECHNIQUES IN MODEL TESTING

PRESENTED TO

20th AMERICAN TOWING TANK CONFERENCE

2 - 4 AUGUST 1983

BY

J.T. DILLINGHAM
J.H. HOSTE

OFFSHORE TECHNOLOGY CORPORATION
578 ENTERPRISE STREET
ESCONDIDO, CALIFORNIA 92025

ABSTRACT

The extensive use of high speed digital data acquisition systems and computer systems has revolutionized model testing procedures. In particular most forms of data analysis can be performed within seconds or minutes after a test. Criteria for selection of sampling and filtering rates and record lengths may now be established on the basis of known error estimation formulas and desired accuracy rather than on instrument limitations. Notational conventions are recommended and formulas for estimating errors and validity of test results are presented. Applications of modern data analysis methods to model testing are discussed. Particular emphasis is placed on fast correlation and spectral analysis of time series and how these methods may be used to extract more useful information from model test data. Specific examples taken from recent model tests are presented.

NOTE OF ACKNOWLEDGEMENT

Almost all of the spectral analysis descriptions and suggestions reported here are taken from the work of Messers. J.S. Bendat and A. G. Piersol. Several of their publications are listed as references. In addition, over the last year Mr. Bendat has personally reviewed and revised our analysis methods here at Offshore Technology Corporation, and has suggested many improvements and extensions.

TABLE OF CONTENTS

ABSTRACT

NOTE OF ACKNOWLEDGEMENT

1. INTRODUCTION

2. TESTING CRITERIA

3. DATA ANALYSIS METHODS/APPLICATIONS

4. ERROR ESTIMATION

5. EXTENDED AREAS OF ANALYSIS

APPENDICES

A. Recommendation on Notation Conventions and Spectral Definitions

B. Review of a State-of-the-art Data Acquisition System

REFERENCES

BIOGRAPHIES

1.0 INTRODUCTION

In the field of model testing a variety of data analysis techniques have become important tools in the understanding of test results. The increased speed and larger memory capacity of even small laboratory computers compared to computers of only a few years ago make it practical to perform sophisticated data analysis routinely on a large scale. We find ourselves relying more heavily on techniques of spectral analysis which require performing Fourier transforms on long time series. The high data acquisition speeds which are available and the capabilty to process the data means that specifications for sampling rates and record lengths of time series may be based on the desired error bounds and frequency resolution of the final results, rather than on the limitations of the hardware.

Spectral analysis methods are not new, however in recent years they have come to be relied upon more extensively due partly to the proliferation of more powerful and less expensive computer hardware. The improvements in the hardware have had two major effects on the way in which data is acquired and analysed and the manner in which tests are conducted:

1) The increase in data gathering speeds and the capacity of fast storage devices have surpassed the requirements of all but a few types of tests which are normally conducted in a model basin. A notable exception is the performance of slamming experiments where the event of interest may last only about 1 or 2 milliseconds (here non-standard digital acquisition equipment would be used).

2) The increased speed of processors which are available for small laboratory computers has made it possible to perform a substantial amount of data analysis on line during the course of a test program. This has made it possible to conduct laboratory tests on a commercial scale with the capability of obtaining the final results during the program and changing the course of the experiments based on these results. This has greatly enhanced the quality control capabilities of the test engineer and made it cost effective to conduct research oriented test programs which would previously have been conducted only in a university environment due to the large amount of basin time required for data collection and processing.

The following list of data analysis techniques are some of the means available to the test engineer and client:

Statistics - Irregular, Periodic
Time Series Plots
Natural Period/Damping
Power Spectral Density Plots
Response Amplitude Operator and Phase Angle
Filtering
SIWEH (Wave Groupiness)
Probability Distributions - Histogram, Rayleigh, Weibull, Gumbel Plots
Zero Crossing Analysis
Forced Oscillation Analysis

Real advantages can be gained at test time by having these tools readily available. Problems with instrumentation, wave generation or the model itself can be more quickly identified and corrected. Unanticipated effects can be found in time to modify the instrumentation, sampling rates or test plan as testing progresses. The availability of this range of methods greatly increases the flexibility of the testing.

Today's powerful and inexpensive computer hardware allow high sampling rates, up to 40,000+ samples/sec; mixed sampling rates, some channels at 20 Hz some at 60 Hz and some at 960 Hz; and large test size, 1 to 4 million samples is not uncommmon. The above test parameters have become everyday practice at Offshore Technology Corporation. Under certain conditions, up to 40 data channels can each be sampled at 1000 Hz, or one channel at up to 40,000 samples/sec, or the test length could reach to over 40 million samples.

This paper will present a wide variety of data analysis techniques put into commercial use at the model testing basins of Offshore Technology Corporation. The primary motivation in developing these capabilities was to provide state-of-the-art data analysis, added testing capability, and real-time flexibility in the conducting of the test program, and better verification of data acquired.

2.0 TEST CRITERIA

Prior to acquiring any test data, decisions must be made regarding instrumentation, filters, sampling rates and length of test. These decisions are effected not only by the instrumentation and hardware available, but also by the desired results and analysis methods available.

Instrumentation should be chosen so as to provide multiple paths to the desired result. That is, if the desired analysis requires use of the model's angular velocity it is wise to include in the instrumentation either angular acceleration or a measurement of angular displacement. This "redundant" measurement could always be processed and used to replace the required angular velocity measurement if it were to fail.

2.1 Instrumentation

Decisions concerning the selection of instrumentation are included here because the proper instrumentation can make the later analysis more accurate, run quicker and guarantee the desired results. The instrumentation used is, of course, primarily dependent on the type of test and the results required. However, careful consideration of the analyses to be performed may show certain instruments not to have fine enough resolution or perhaps an instrument can be eliminated by calculating the desired data from other instrument readings. Another choice would be to leave the instrument in place thereby providing the data directly and at the same time having a redundant path to the desired result in case of instrument failure. Other considerations in choosing instrumentation should include:

Sensitivity, Range, Redundancy of Data
Size, Weight, Environmental Suitability

2.2 Data Acquisition

Decisions concerning the actual digitizing of the data include: quantization, calibration, highest expected frequency, filtering, band width versus variance, sampling rates, mixed rates, test length and test size.

The first two, quantization and calibration, have to do with the fact that we have a limited range of integer values to convert the analog data to. For instance, if we have a 12 bit analog-to-digital converter we have 4096 digital values that the analog data can be converted to. The error in converting to one of two discrete digital values is ± 1/2 the least significant bit, or .012%. Then we calibrate the data channel so that the digital range of 0 to 4095 covers the expected range of the acquired data. If measuring roll of the model, the expected range may be ± 30 degrees and we have:

$$\frac{60 \text{ degrees}}{4096}$$

giving a resolution of 0.0146 degrees per digital increment, and a quantizaton error of 0.000178 degrees. This quantization error is generally much smaller

than the instrument error itself. Two other digitization errors to consider are:

Aperture error - due to the fact that the analog-to-digital conversion is taken over some finite (very small) period of time rather than instantaneously.

Jitter - arising from the fact a finite time interval exists between the conversion of successive samples. Much of this can be avoided by the use of sample-and-hold circuits.

The selecton of data sampling rates results mainly from the compromise in spectral analysis techniques between band width resolution and random error. Other consideratons include the highest expected data frequency, available filters, and of course hardware limitations on maximum sampling rate and storage limitations. If the highest expected frequency content in your data is f_d, then in order to properly digitize the data, one should sample that data at something greater than twice f_d; i.e. the sampling rate $f_s=2.0* f_d$. If this is not possible then a cutoff filter should be included in the instrumentation so as to limit the input signal frequencies to $1/2f_s$. The smoothed spectral band width resolution, B_e, and random error are related as follows:

$$B_e = \frac{d}{T_r}$$

$$\epsilon_r = \frac{1}{(B_e T_r)^{1/2}} = \frac{1}{\sqrt{d}}$$

Where T_r is the record (test) length in seconds and d is the number of averages used.

2.3 Problems

One of the most frequently encountered problems is that the wave elevation was not measured at a point transversely in line with the model. This means that when analyzing model data versus the wave exciting force the two records cannot be directly compared. RAOs must be caluculated by ratioing the individual auto-spectra, which leaves noise and non-linearities in the final result. Likewise, phase relationships are in error.

A second common problem is that of test records that are either too short or too long to be properly handled by the analysis methods. Short records cause statistical problems (high random error, large band width resolution....), while very long records generally cause difficulties with the analysis method itself (size or too time consuming). For spectral analysis it is necessary to have 2^n, n = 1, 2, 3, 4....number of samples per channel in the test. In practice this usually means acquiring just over 2^n points per channel (e.g., 1024 ⟶ 1048, 2048 ⟶ 2060, 4096 ⟶ 4120, 8192 ⟶ 8220, and 16384⟶ 16410 samples). In this way, large tests can be cut in half and analyzed, or short tests can be ensemble averaged. Of course, as the

normalized standard error is reduced by averaging, the band width resolution is decreased.

The final problem to be mentioned here is that of signal noise. Of course, everything must be done that is possible to reduce noise sources. These include:

Faulty instruments, electrical connections....
Wave reflections
Structural vibrations

to name just a few. Analytically, noise at an input that passes on through the system is not nearly as bad as noise seen only in an output signal. Spectral analysis techniques can effectively eliminate noise (and non-linearities) if the noise is seen throughout the system. Noise seen only in an output signal (e.g., a "noisy" gyro) will probably have to be digitally filtered before it can be used. Many such filtering techniques are available today.

3.0 DATA ANALYSIS METHODS/APPLICATIONS

The following analysis methods form an integral part of most tests now performed at Offshore Technology Corporation. These capabilities were developed and brought on-line during the last two years. The thrust behind this effort was to provide comprehensive analytical capabilities to the test engineer at the test control station. Most of the analysis have been made fast enough to allow them to be run and the results evaluated between tests. In this way errors or problems can be found quickly; and the test program can be modified in response to any unexpected results. These capabilities have greatly changed the way test programs are conducted; they are now much more flexible and usually provide the client with more of the kind of information he is really interested in.

3.1 General Baseline Analyses

These simple analysis routines form the minimum set of analyses required for any test. They give the test engineer his first look at the data from which to decide if the test was a "good" one or not, and to determine what further analyses should be done before the next test is run. Good clear report outputs and generous use of graphics makes them easily and quickly read. These basic routines include:

Instrument calibration plot
Fast CRT display
Wave statistics immediately after test
Statistics - max, min, average, standard deviation/RAO, phase angle
Time series plot
Natural period/damping plot

and are described below along with examples.

The calibration plot is of course used prior to testing while calibrating. Its visual display of the calibration points along with the calibration line and 95% confidence bounds gives the test engineer immediate feedback as to the quality of the calibration. In addition, the calibration is quantified by the printed statistics. See Figure 3.1A.

Immediately on completion of a test, statistics on one channel is printed out. This channel, usually the wave elevation data, is processed in real-time so as to give an immediate result as to the "goodness" of the test. If acceptable, all data channels can then be flashed on a CRT display to quickly check that all instruments functioned properly (no spikes, dropouts or lost signals). The is purely a "hardware" display and yields no hardcopies.

Statistics are then run on all channels of the test. For an irregular wave test these consist of the maximum data value, minimum, average and the standard deviation. For a periodic (regular) wave test the maximum, minimum, average, RAO by wave height and by wave slope, and the phase angle. See Figures 3.1B and 3.1C.

The ability to plot a data channel versus time during testing is an important one. It is especially valuable to be able to plot two or three channels, one below the other on one plot. This can be very helpful in

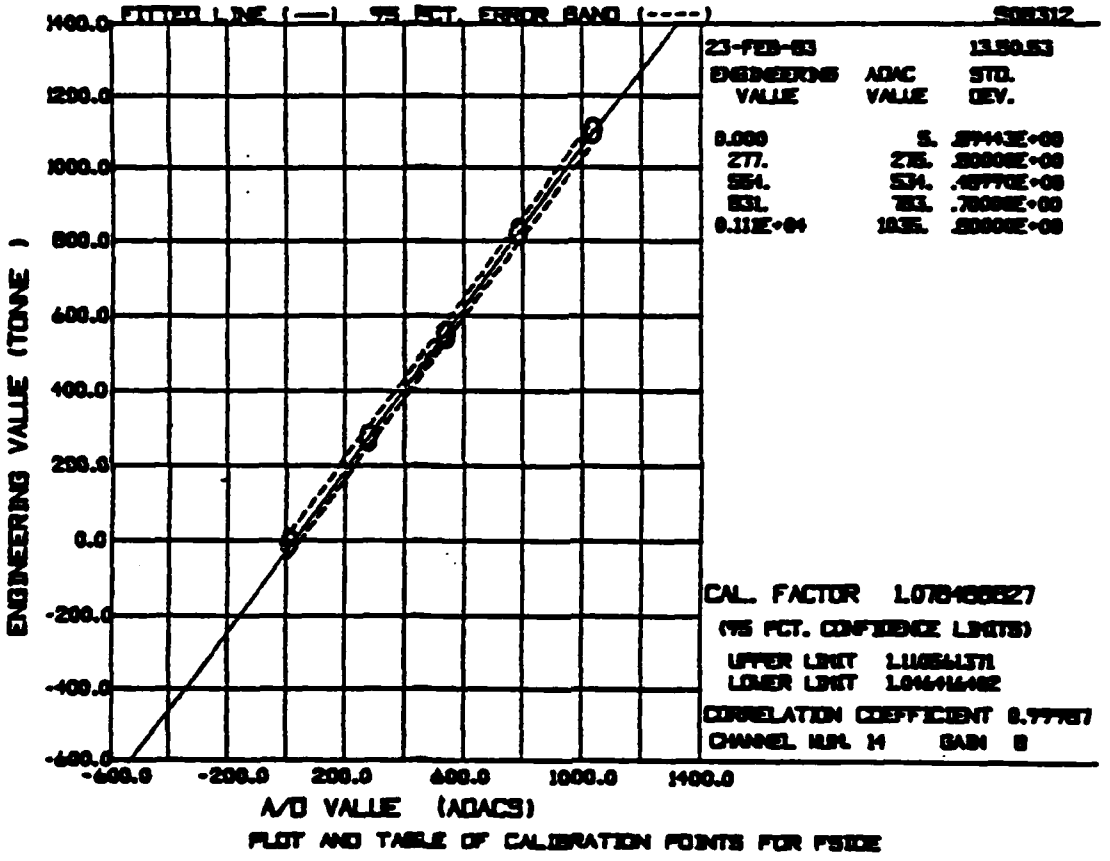

PLOT AND TABLE OF CALIBRATION POINTS FOR PSIDE

Figure 3.1A

Project: S08312 * * REGULAR WAVE * * Test Date: 21-FEB-83
Page 1 of 1 * * * PHASE ANGLES * * * Test Time: 17:45:15

TEST: 222

Base Channel: WAVE
Heading: 0.0 deg.
Period: 26.89 sec.
Model Scale: 49.200
Sample Rate: 14.00 hz.

No. of Cycles: 3
Start Time: 0.20 min.
Test Duration: 1.34 min.
Total Duration: 1.75 min.
Samples / Chan: 210

VARIABLE	UNITS	RAO	PHASE
WAVE	METERS	1.000	0.
SURANG	DEGREE	0.020	106.
SWANG	SWANG	0.427	97.
DRANG	METERS	1.174	179.
PITANG	DEGREE	0.003	-109.
ROLANG	DEGREE	0.244	-78.
YANG	DEGREE	0.029	-180.
GAPFWD	METERS	0.218	162.
GAPORT	METERS	0.310	146.
---------- derived channels ----------			
PITCH	DEGREE	0.018	-70.
ROLL	DEGREE	0.184	91.
YAW	DEGREE	0.029	0.
SURGCG	METERS	0.049	82.
SWAYCG	METERS	1.003	96.
HEAVCG	METERS	1.177	-2.

Project: S08312 * * REGULAR WAVE * * Test Date: 21-FEB-83
* * * STATISTICS * * * Test Time: 17:50:54

TEST: 223

No. of Waves: 2
Test Duration: 0.99 min.
Total Duration: 1.76 min.
Channels acquired: 9
Sampling Rate: 14.00 hz.

Heading: 0.0 degs.
Period: 29.56 sec.
Model Scale: 49.200
Samples / Chan.: 211.

CH	VARIABLE	UNITS	MAX	MIN	AVE	AVG P-P	RAO P-P/WH	RAO AMP/WS
1	WAVE	METERS	10.51	-7.65	0.51	17.44	1.00	0.11
5	SURANG	DEGREE	-0.88	-1.44	-1.16	0.55	0.03	0.00
6	SWANG	SWANG	4.90	-4.27	0.09	8.75	0.50	0.05
7	DRANG	METERS	9.24	-10.62	0.03	19.28	1.11	0.12
9	PITANG	DEGREE	-0.03	-0.36	-0.16	0.33	0.00	0.00
10	ROLANG	DEGREE	3.32	-3.37	0.13	6.11	0.35	0.04
11	YANG	DEGREE	0.87	-0.26	0.51	0.60	0.03	0.00
13	GAPFWD	METERS	1.55	-2.64	-0.04	4.42	0.25	0.03
14	GAPORT	METERS	2.14	-3.00	-0.25	4.77	0.27	0.03

Figure 3.18

Project: ERE136 * * RANDOM WAVE * * Test Date: 15-APR-83
Page 1 of 1 * * * STATISTICS * * * Test Time: 10:33:19

==========
TEST: 606
==========

Wave Height (sig): 4.0
Headings: 0.0 deg.
Model Scale: 48.000
Max. Sample Rate: 20 hz.

Start Time: 0.00 min.
Test Duration: 14.09 min.
Total Duration: 14.09 min.
Max. Samples / Chan: 2440.

VARIABLE	UNITS	MAX	MIN	AVE	STDV	5.1 x STDV	4.0 x STDV
WAVE	FEET	-1.641	-1.740	-1.701	0.024	0.123	0.096
CURRY	KNOT	2.308	1.525	1.891	0.146	0.744	0.584
WIND	KNOT	22.380	14.760	18.364	1.623	8.277	6.492
LINE 1	STON	17.251	13.912	15.328	0.991	5.055	3.965
LINE 2	STON	7.708	6.056	7.157	0.227	1.158	0.908
LINE 3	STON	8.343	7.230	7.741	0.323	1.647	1.291
LINE 4	STON	28.656	18.737	23.997	2.210	11.270	8.839
HAWSER	STON	22.398	18.847	20.810	1.064	5.425	4.255

Figure 3.1C

clearly seeing the relationship between data channels. See Figure 3.1D. A natural extension of the time-series plots is a natural period plot. Knowing the natural period and damping of the model being tested (or some part thereof) is a requirement of almost every test program. This natural period analysis quickly calculates the average period and damping using a zero-crossing method. See Figure 3.1E.

3.2 Autospectral (Power Spectral) Density

The Power Spectral Density (PSD) plot graphically displays a signal's energy content across frequency. It is calculated using the Fast Fourier Transform (FFT) method, requiring the record length to be an integral power of 2. FFT's on up to 16k points have become common. The mathematical definition is,

$$Gxx(f) = \frac{1}{B_e T_{total}} \int_0^{T_{total}} X^2(t,f,B_e)dt$$

where $X(t,f,B_e)$ is the result of passing $X(t)$ through a narrow band-pass filter of bandwidth B_e centered at f after which the output is squared to yield $X^2(t,f,B_e)$. In other words, $Gxx(f)$ is an estimate of the rate of change of the mean-square value with frequency.

The PSD is the standard method of defining theoretical seas such as Pierson-Moskowitz, Bretschneider, ISSC, Scott-Weigal and others. In plotting PSDs we have chosen to plot the Amplitude Half Spectrum as the ordinate. Other formulations are sometimes used as well (see Reference 10). Using this formulation the area under the PSD curve ($\sqrt{M_0}$) is equivalent to the standard deviation in the data, σ. For narrow-band data where the wave peaks follow a Rayleigh probability density function, the significant wave height is given by:

$$H_{1/3} = 4.0\,\sigma = 4.0\sqrt{M_0}$$

A number of interesting quantities can be derived from the various moments, M_n, of the PSD curve, where:

$$M_n = \int_0^\infty f^n G_{xx}(f)df \quad , \; n = 0,1,2...$$

Several of these quantities are given in the following table. Figure 3.2A shows a typical wave PSD plot. Note that the moments are printed on the plot along with several spectral quantities. Also included on the plot is information about the number of sample points used in the FFT, the effective sampling rate and the number of points used to smooth over. For a wave PSD like this one, it is bery useful to include the desired theoretical spectrum as a dashed line as well.

Standard Deviation, $\sigma = \sqrt{M_0}$ = area under curve

Spectral Width, $\varepsilon = \left[1 - (M_2^2/M_0M_4)^{1/2} \right]$

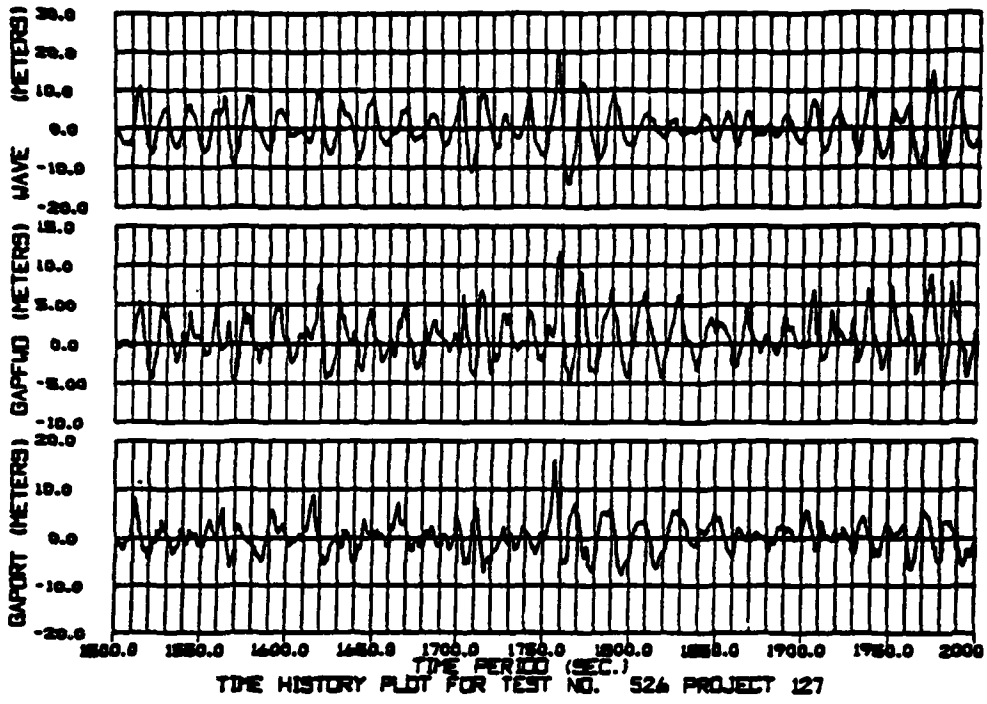

Figure 3.1D

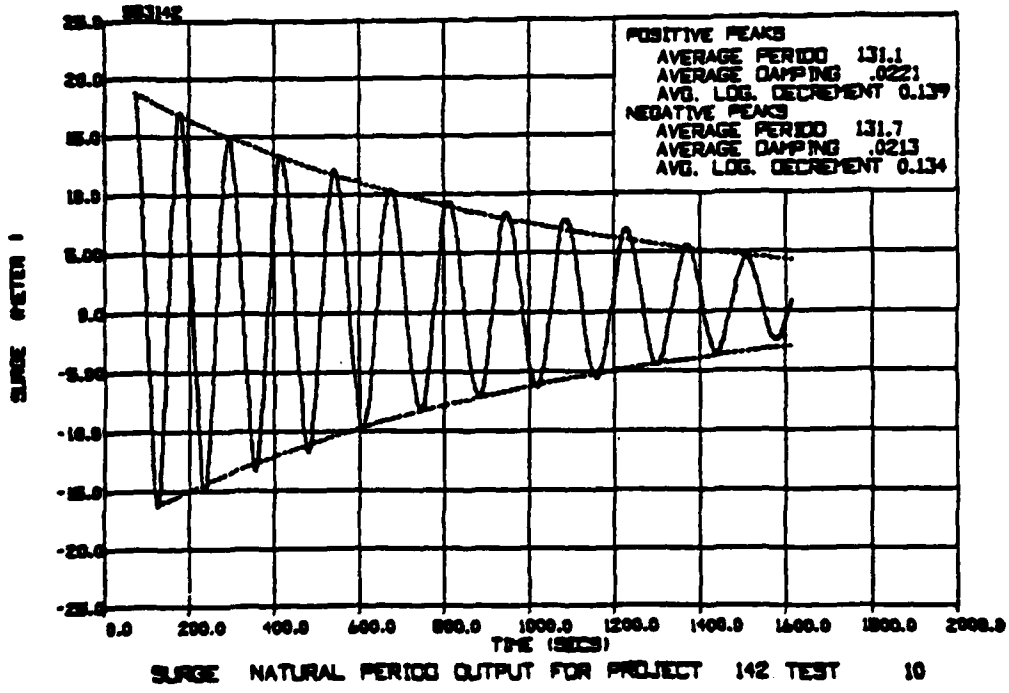

Figure 3.1E

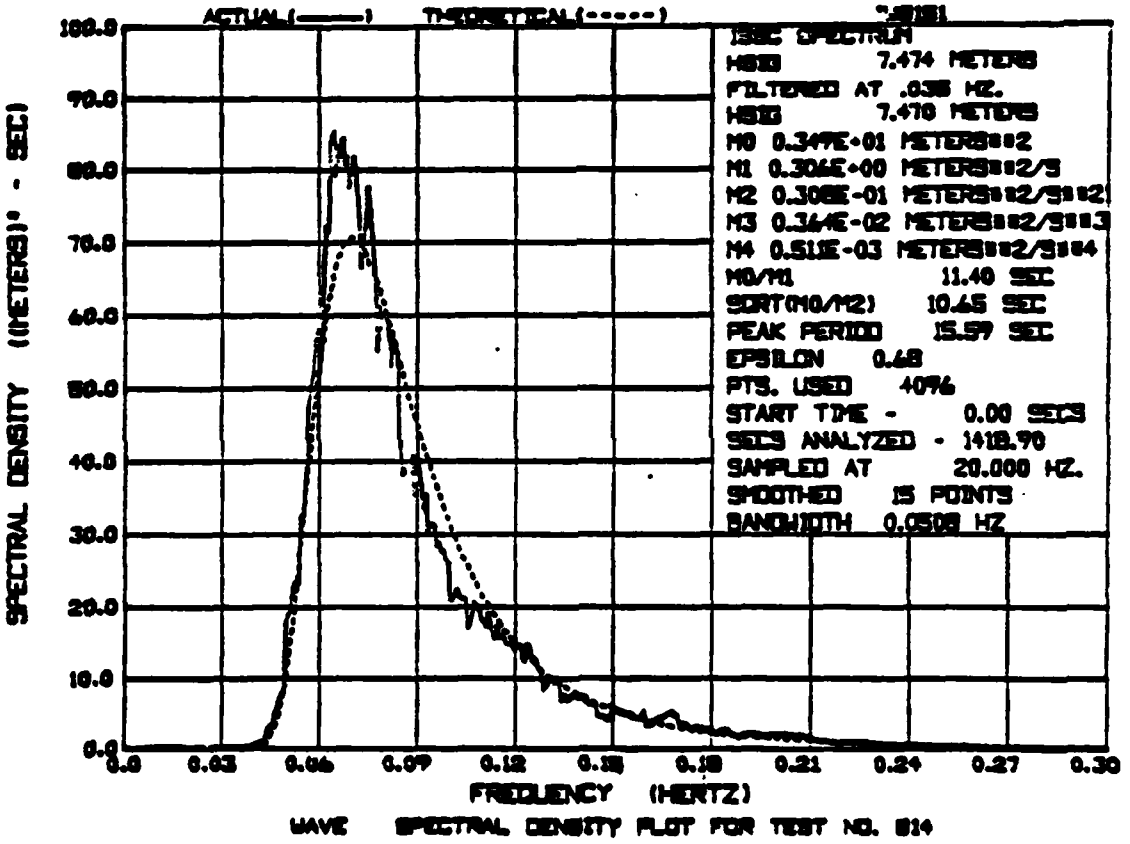

WAVE SPECTRAL DENSITY PLOT FOR TEST NO. 814

Figure 3.2A

Average time between successive positive zero crossings,

$$\overline{T}_o = \left(\frac{M_o}{M_2}\right)^{1/2}$$

Average mean period,

$$\overline{T}_1 = \frac{M_o}{M_1}$$

Skewness,

$$\nu = M_3 / (M_2)^{3/2} = \left(\frac{2 - \varepsilon^2}{2}\right)^{1/2}$$

Problems with record length are generally handled in one of two ways. Records that are too short (less than a power of 2) can be extended to a power of 2 by appending zeros to the record. Records that are too long can be analyzed by simply "skipping points", i.e. reducing the effective sampling rate by using every 2nd, 3rd or 4th point.

3.3 Frequency Response Function

The complex-valued cross-spectrum Gxy(f) between an input signal x(t) and a response y(t) is computed as a function of the frequency, f, where f is measured in Hertz. The familiar RAO is then the modulus (magnitude) of the transfer function Hxy(f), namely,

$$Hxy(f) = \frac{Gxy(f)}{Gxx(f)}$$

$$RAO(f) = |Hxy(f)|$$

The phase angle $\phi xy(f)$ is the argument of the transfer function, namely,

$$\phi xy(f) = \tan^{-1}\left[\frac{\text{Im } Hxy(f)}{\text{Real } Hxy(f)}\right]$$

This is the same as the argument of the cross-spectrum Gxy(f).

The cross-spectrum described above is generally the preferred method of calculating RAO's and phase angle relationships. It produces the ideal linear transfer function excluding any noise and non-linearities. Care must be taken however to assure that the input signal is measured where it is affecting the output; e.g., the wave probe must be transversely aligned with the model; and should be free of noise. Too, cross-spectrum RAO's may yield misleadingly low values if significant non-linearities are present. This can be detected when values are compared with periodic wave RAO results (which will include noise

and non-linearities), or by computing the coherence of the cross-spectrum.

The coherence function $\gamma^2_{xy}(f)$ is computed by the relation,

$$\gamma^2_{xy}(f) = \frac{|Gxy(f)|^2}{Gxx(f)\ Gyy(f)}$$

using the smoothed estimates of Gxx(f), Gyy(f) and Gxy(f).

The coherence plot is absolutely vital in interpreting the RAO and should be plotted over the RAO. See Figures 3.3A, B. A coherence value of approximately 0.9 indicates that 90% of the response signal at the frequency can be attributed to linear operations on the input signal. It also indicates that 10% of the response signal is due to other unknown causes such as nonlinear operations, extraneous measurement noise, or the possibility that the output signal is due to other inputs besides the measured signal. As a general rule, for well-defined single input/single output problems, the RAO should be ignored at frequencies where the coherence function is less than 0.80. However, this criteria should be examined and changed as may be appropriate for different situations.

Instead of plotting the coherence function versus frequency, one could plot the normalized random error in estimates of the RAO versus frequency. This would be more meaningful than just the coherence plot for now one would be able to state confidence limits for the RAO estimates. To be specific, if the normalized random error $\varepsilon \leq 10\%$, then one would have 95% confidence that the true value of RAO(f) compared to the estimated value, denoted by $\hat{RAO}(f)$, falls in the internal

$$[(1 - 2\varepsilon)\ \hat{RAO}(f) \leq RAO(f) \leq (1 + 2\varepsilon)\ \hat{RAO}(f)]$$

Thus, for $\varepsilon = 10\%$, one would have 95% confidence that the true value falls in the interval

$$[0.80\ \hat{RAO}(f) \leq RAO(f) \leq 1.20\ \hat{RAO}(f)]$$

In some instances the RAO by auto-spectra may however, be the proper method to use. For example, when towing through waves using a stationary wave probe, the cross-spectrums method will yield erroneous results, while the auto-spectrum method will give correct results, without worse phase angle results.

3.4 Up-Crossing Analysis

The upcrossing, or zero-crossing, method is a traditional analysis tool. It yields much the same overall information as a FFT spectral analysis plus many details not available in spectral analysis. Some of these added

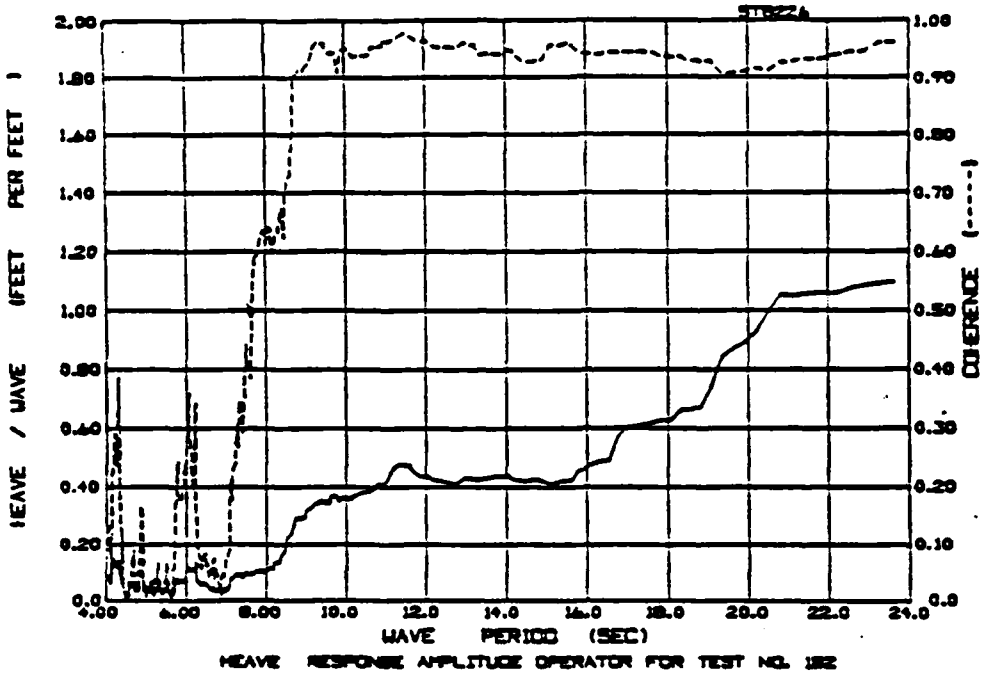

Figure 3.3A

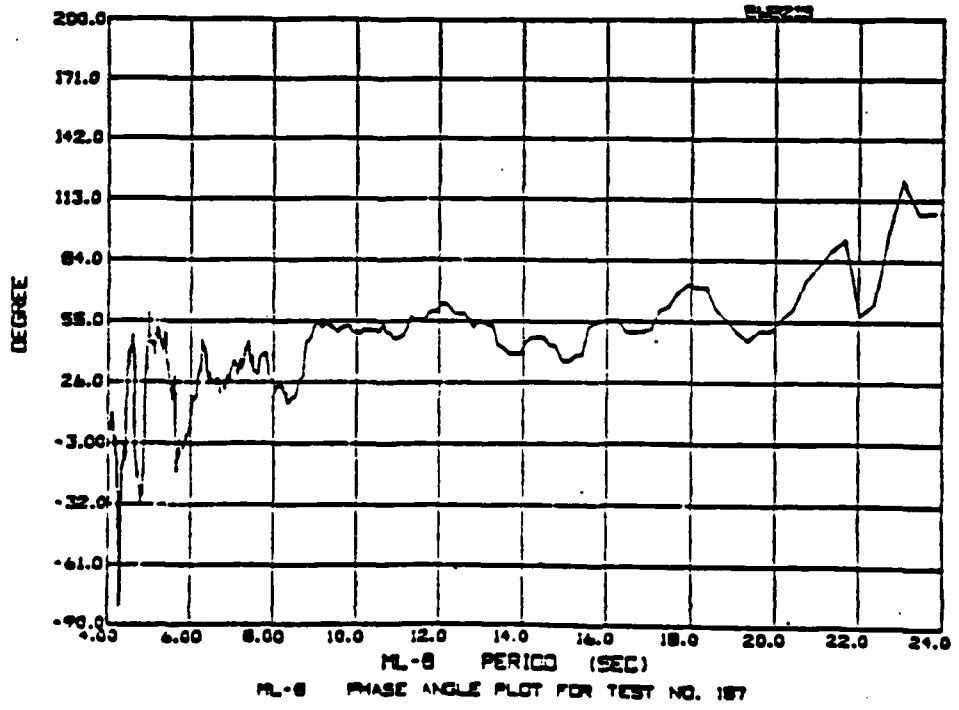

Figure 3.3B

details include:

Maximum wave height (crest to trough)

Distributions of peaks, troughs, periods

Probability prediction of extreme values

Notational convention for the up-crossing analysis is shown in Figure 3.4A. In practice the signal level that defines a "crossing" is usually either zero or the mean value of the data. Once a data channel's analysis is completed the following data should have been obtained for every wave (up-crossing to up-crossing):

$$H^+,\ H^-,\ T_z \qquad \text{and}$$

$$\text{Peak-to-Peak} = H^+ - H^-$$

and statistics on their values can be printed (see Figure 3.4B).

This data can then be processed in several ways. Probably the most common is to simply create a population or cumulative histogram of the distribution of the data values. Figure 3.4C-D show typical histograms. Here we have also elected to plot every point so as to create a relatively smooth curve.

Once the up-crossing analysis has collected and sorted all of this data it is a simple step to compare it with known distributions and extend the test results to longer exposure durations. These methods are described in Section 3.5.

3.5 Prediction of Extreme Values

For many of the parameters measured in the study of ships and offshore structures, it is of considerable design and operational importance to be able to predict the highest value of a parameter that could be expected to occur within a specified time period. Scale model tests typically yield maximum data values for the conditions tested over a relatively short duration. To assure statistically valid results, a test length of at least 30 full-scale minutes is used. Yet the question remains as to whether or not the "maximum" recorded value is indeed the highest that can be expected to occur. Fortunately, a well-founded body of statistics allows us to make predictions of expected extremes in long durations from relatively short data records. Depending on the nature of the data, a 30 minute full-scale test can be used, along with the appropriate statistical method, to predict extreme values at exposure durations of up to 12 hours or more.

It has been well proven that sea wave elevations are well described by a Gaussian probability distribution while the wave peaks are well described by the Rayleigh distribution. For such a narrow bank random process or for a Rayleigh distribution, an extreme amplitude value as a function of time can be predicted from,

CONVENTIONS USED FOR RANDOM SEA ZERO CROSSING ANALYSIS

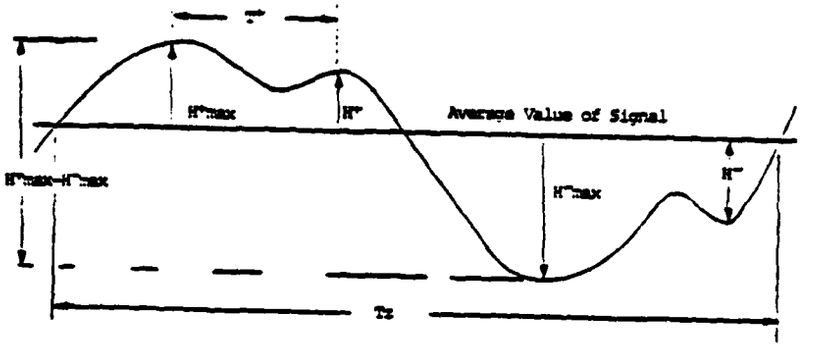

Where: $\bar{T}z$ - Average Zero Crossing Period
$\bar{T}^{+}$ - Average Crest-to-Crest Period
$\bar{H}^{+}max$ - Average Zero Crossing Crest Height
$\bar{H}^{-}max$ - Average Zero Crossing Trough Height
$\sigma(H^{+}max)$ - Standard Deviation of Zero Crossing Crests
$\sigma(H^{-}max)$ - Standard Deviation of Zero Crossing Troughs
$(H^{+}max-H^{-}max)$ - Zero Crossing Crest Heights - Zero Crossing Trough Height

$$\xi = 1-\left(\frac{\bar{T}^{+}}{\bar{T}z}\right)^{2}$$ - Band Width Parameter

Figure 3.4A

Project: NB-128 * * ZERO UPCROSS * * Test Date: 06-JUL-83
Page 1 of 2 * * * STATISTICS * * * Test Time: 13:36:45

TEST: 8401

Wave Height (sig): 6.1 Model Scale: 39.370
Heading: 90.0 deg. Total Duration: 62.75 min.

VARIABLE	UNITS	+H MAX AVG.	+H MAX STDV.	-H MAX AVG.	-H MAX STDV.	TPLUS
PTIN	METER	0.710	2.649	-7.590	2.367	7.276
STBIN	METER	0.113	3.898	-7.465	1.804	9.772

Project: NB-128 * * ZERO UPCROSS * * Test Date: 06-JUL-83
Page 2 of 2 * * * STATISTICS * * * Test Time: 13:36:45

TEST: 8401

VARIABLE	UNITS	P-P AVG.	P-P STDV.	PERIOD AVG.	PERIOD STDV.	EPSILON
PTIN	METER	8.300	4.367	9.827	3.604	0.672
STBIN	METER	7.778	3.091	11.854	3.572	0.566

Figure 3.4B

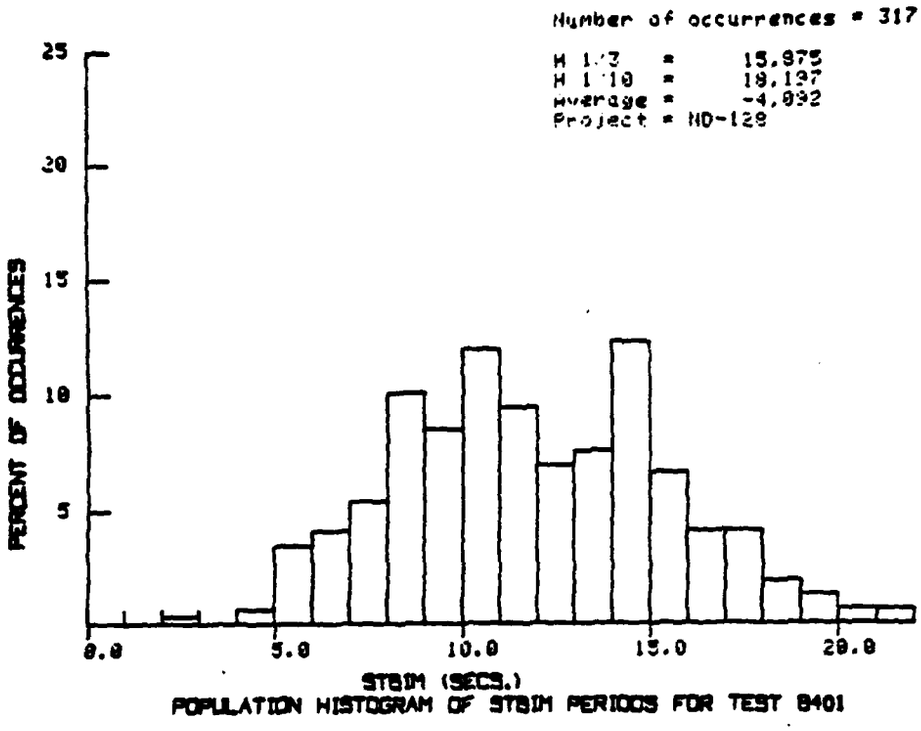

Figure 3.4C

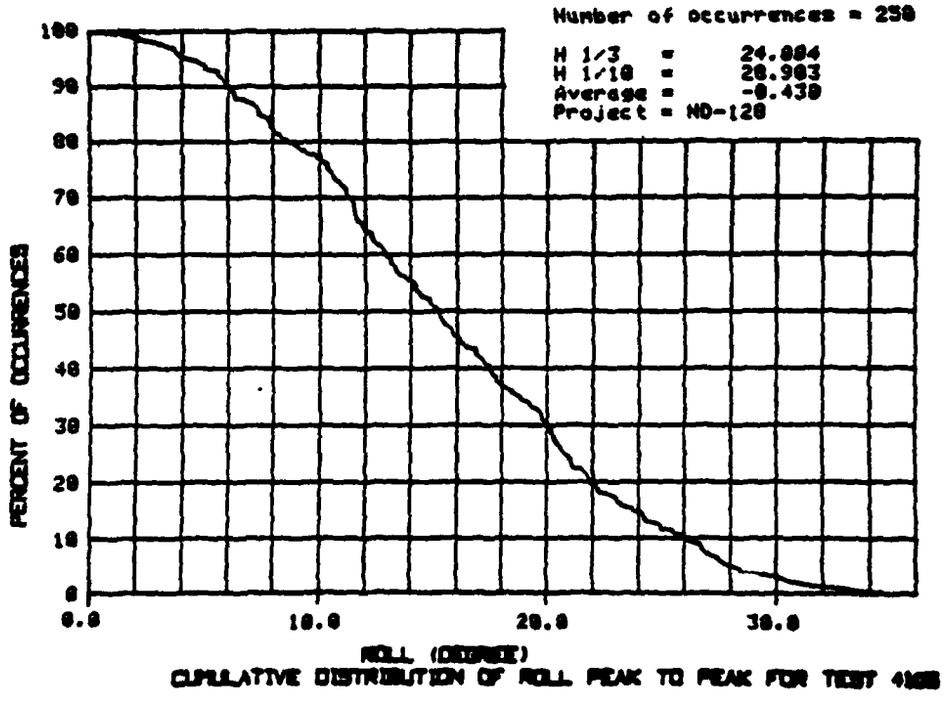

Figure 3.4D

$$\text{extreme amplitude} = \left| 2 \, \text{Ln} \left[\frac{T}{\alpha} \sqrt{\frac{m_2}{m_0}} \right] \right|^{1/2} \sqrt{m_o}$$

for small α. Here α is the probability that the extreme value exceeds a given level during T seconds. The spectral moments are obtained from the energy density spectrum of the random process under consideration.

In this way a series of curves can be plotted to predict extremes of various probabilities for any length of exposure. See Figure 3.5A.

In the prediction of extremes for other types of random data the Rayleigh distribution cannot be assumed. In these cases, statistics based on a Weibull or Gumbel distribution may be required. For instance, the peak hawser load of a tanker attached to a CALM buoy has been shown to follow a Gumbel distribution. Here again, predictions can be made from relatively short data records;

$$P_{\text{extreme value}} = 1 - (1_v - P^{T/t})$$

where P_v was the probability of a given extreme in the record of length t, and $P_{\text{extreme value}}$ is the predicted probability of that extreme occurring during an exposure of length T.

By this method the data points are sorted, assigned probabilities and plotted against the probability distribution to be tested. If the data plot in a straight line then they "fit" that type of distribution and the extreme values can be extended to longer exposure durations. Figures 3.5B to 3.5D show various data plotted against Rayleigh, Weibull and Gumbel distributions. The Weibull plot includes a dashed line that represents a Rayleigh distribution.

The application of such extreme value statistical methods can greatly extend the value and range of scale model test results.

Such techniques have been successfully used to predict such things as the probability of ship slamming, slam loads, jackup leg stresses and the air-gap under the deck of a semi-submersible. In the latter case, instruments to measure the relative wave elevation at the forward and athwartship deck edges were added to the semi. This recorded relative wave elevation data then allowed the creation of a probability plot of the minimum allowable air-gap being exceeded. This allowed limits on operations in given sea states to be set with respect to acceptable levels of the probability of the minimum allowable air-gap being exceeded.

3.6 Filtering

The ability to separate a signal into its components or to eliminate certain components is a highly useful one. Digital filters, their design and implementation is the subject matter of a good many books (Reference 5). Ideal or basic filters commonly used in processing of data are mainly:

Lowpass - passes only information in the frequency range 0 to f_1 H_z.

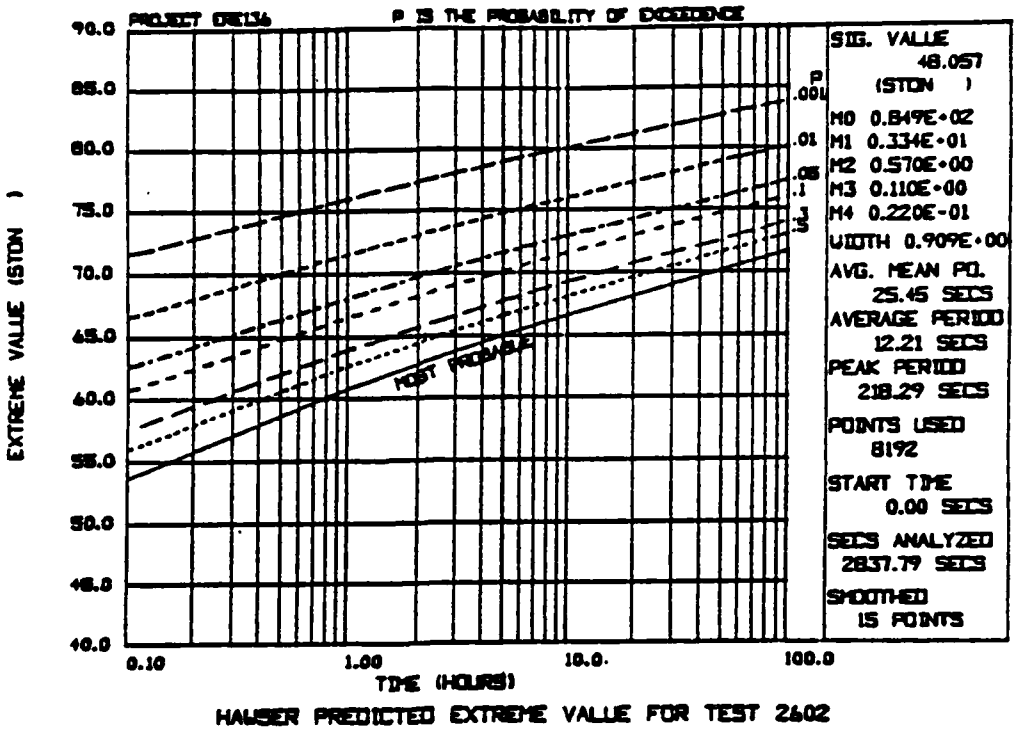

HAUSER PREDICTED EXTREME VALUE FOR TEST 2602

Figure 3.5A

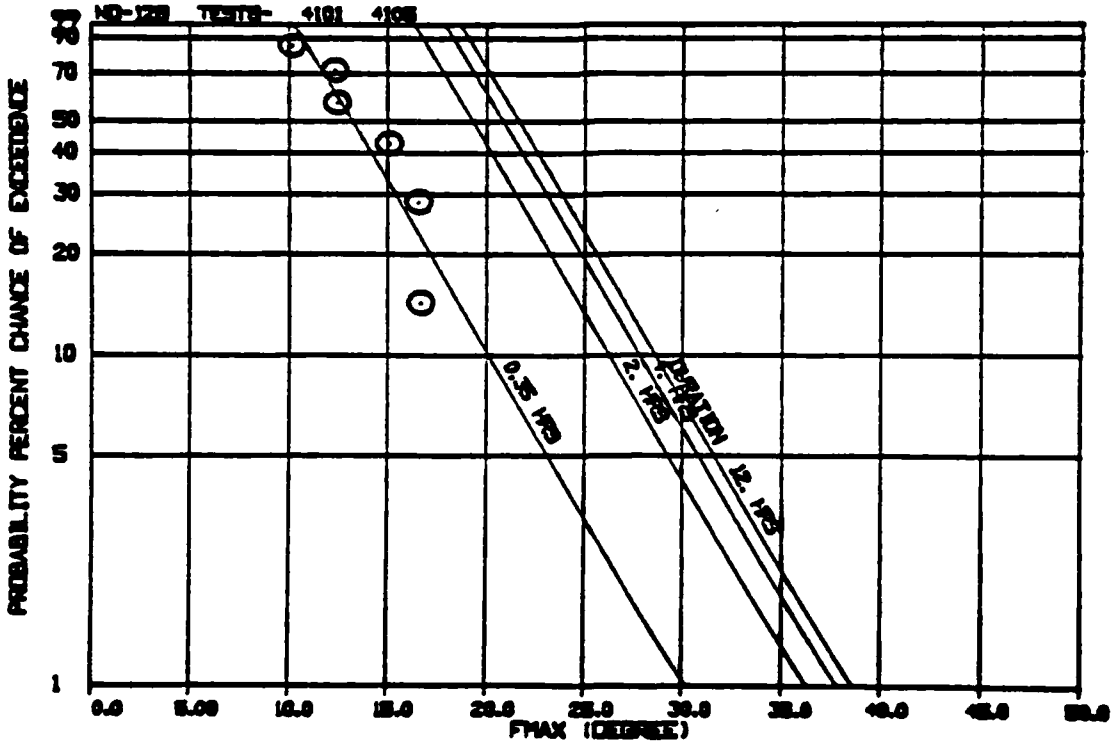

RAYLEIGH DISTRIBUTION PLOT FOR ROLL

Figure 3.5B

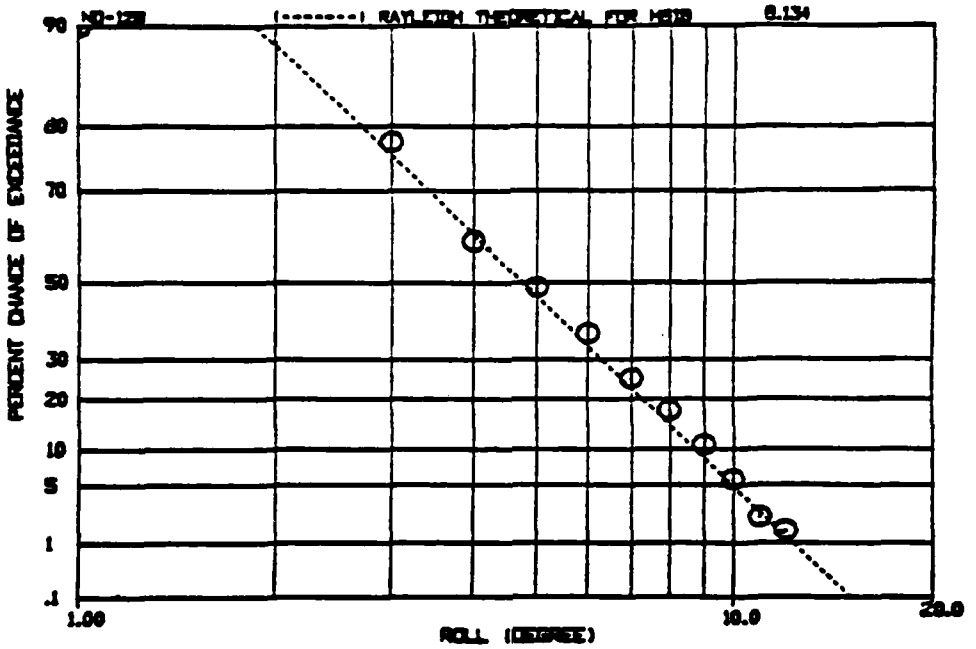

WEIBULL DISTRIBUTION OF ROLL HMAX FOR TEST 4101

Figure 3.5C

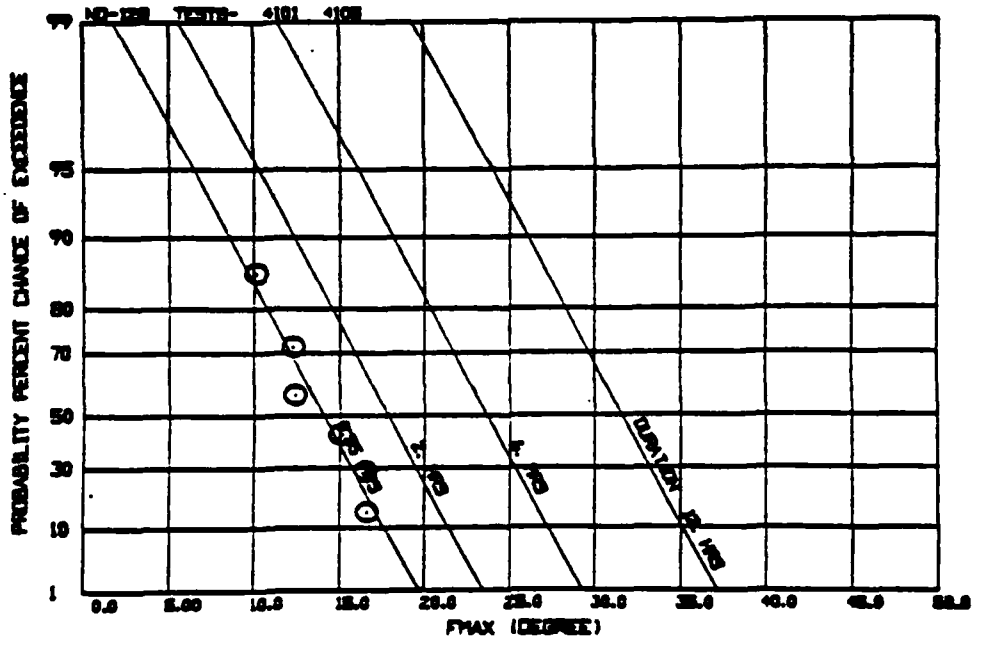

GUMBEL DISTRIBUTION PLOT FOR ROLL

Figure 3.5D

Highpass - passes only information in the frequency range f_1 to ∞ H_z.

Bandpass - passes only information in the range f_1 to f_2 H_z.

Bandreject(notch) - rejects only information in the range of f_1 to f_2 H_z.

Although such ideal filters are desirable, perfect rejection or acceptance is not possible in practice. However, filters can be generated and applied that for all practical purposes conform to the idealized ones. Implementation of digital filters is not always a simple matter, and usually requires that it be "redesigned" each time. Too, questions of noise, distortion, instability and phase shifts must be dealt with.

A second method of filtering that we have found to be easier to use and its accuracy well within practical requirements, is to simply use the Fast Fourier Transform (FFT) to calculate the signal's components and their phase angles, then zero-out the components to be rejected, and then compute the Inverse FFT to create the filtered signal. This method is effectively the exact ideal filter with all phase relationships fully retained. Of course errors still arise simply from the approximate nature of the FFT and the numerical computational capability of the computer. However, no discrepancies have ever been noted in practice. Of course a fairly large FFT (8k or 16k points usually) need to be used, but by using an efficient FFT algorithm, a floating point processor or even an array processor the analysis goes very quickly.

Filtering of a data channel can be very informative during the testing program. The ability to quickly remove extraneous or unwanted signal components can be extremely helpful in identifying sources of excitation for instance. Figure 3.6A shows time-series traces of the bending moment in the leg of a jackup while under tow. The complete signal is, on top (MXBOW), while its low frequency component and high frequency component are each plotted below it. Once filtered and plotted in this manner the damped oscillation (ringing) of the legs is clearly seen. Likewise it is clear that it occurs at the peak of the low frequency cycle which can be correlated to roll extremes and wave impacts.

3.7 Analysis of Low Frequency Responses

There are many type of offshore structures for which the low frequency wave drift forces and the resulting system responses are of considerable importance. Examples are tension leg platforms and softly moored structures in both deep and shallow water. These types of structures may experience a large amplitude low frequency motion in response to the low frequency drift forces. This section illustrates some typical techniques which have been used to analyze these low frequency responses.

It is well known from both theory and experimentation that wave forces exerted on a floating or fixed structure may contain a non-zero average or

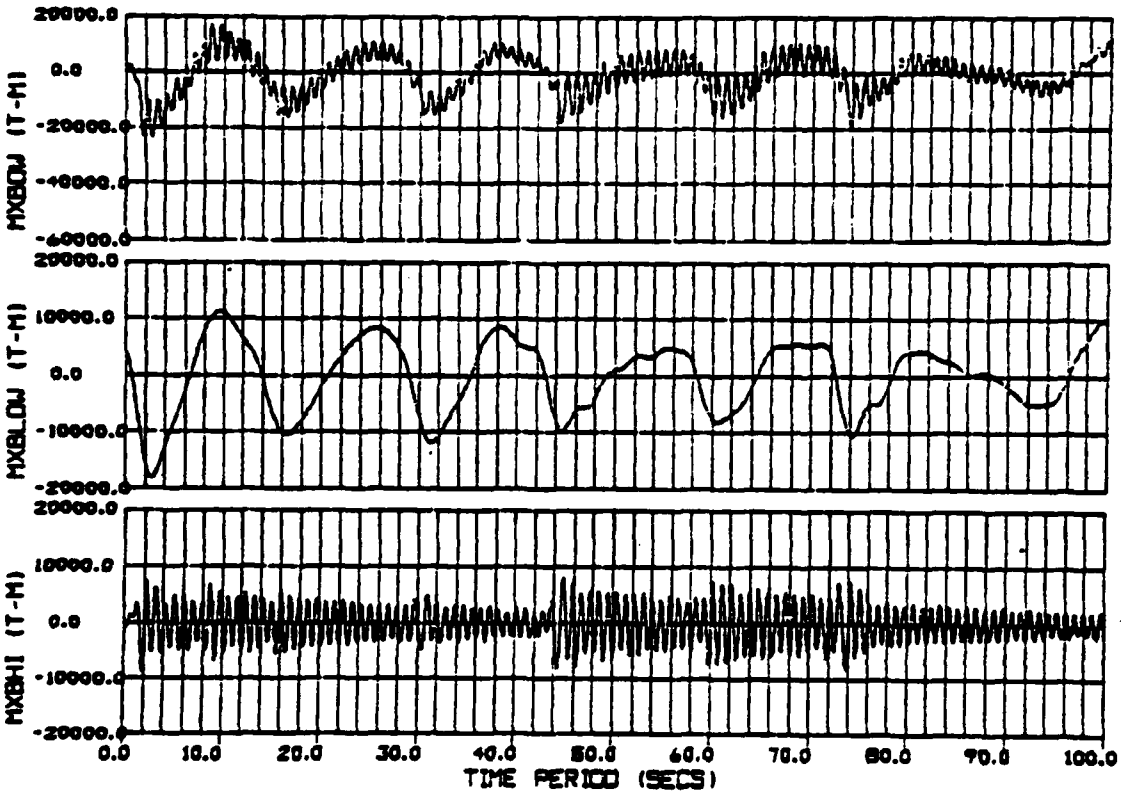
MXBOW (T-M)
20000.0
0.0
-20000.0
-40000.0
MXBLOW (T-M)
20000.0
10000.0
0.0
-10000.0
-20000.0
MXBHI (T-M)
20000.0
10000.0
0.0
-10000.0
-20000.0
0.0
10.0
20.0
30.0
40.0
50.0
60.0
70.0
80.0
90.0
100.0
TIME PERIOD (SECS)
TIME HISTORY PLOT FROM PROJECT NO-12 ... TEST 101

Figure 3.6A

slowly varying component in addition to the wave frequency components. In regular periodic waves this drift force is a steady force which is approximately proportional to the square of the wave height. In irregular waves the drift force may have a slowly varying component which depends on the wave grouping. The filtered time series of the square of the wave height, also known as the smoothed instantaneous wave energy history, or SIWEH, defined by Funke and Mansard [3], [4], is an indicator of low frequency components of the drift force. The SIWEH is defined as:

$$E(t) = \frac{1}{T} \int_{\tau=-T/2}^{T/2} \eta^2(t+\tau) \cdot Q(\tau)\, d\tau$$

where η is the water surface displacement and $Q(\tau)$ is a general smoothing or window function which is zero outside of the rance $-T/2 < \tau < T/2$.

In Reference 3 $Q(\tau)$ was chosen to be a retangular or Bartlett window. The smoothing is performed to isolate the low frequency components of the wave energy which is also proportional to the square of the wave height. Usually the SIWEH is computed as a derived channel. That is, SIWEH is computed and stored as a time series in a format which is compatible with all of the standard data reduction software.

The groupiness of waves may be quantified by a groupiness factor defined by Funke and Mansard [3] as:

$$GF = \sqrt{m_{\varepsilon o}} \Big/ m_o$$

where $m_{\varepsilon o}$ and m_o are the zeroth moments of the SIWEH spectral density and the variance spectral density (auto-spectra) of the wave respectively. The groupiness factor is the standard deviation of the SIWEH about its mean and normalized with respect to this mean.

Figures 3.7A(1) and (2) show a measured wave record and the computed SIWEH. Figures 3.7B(1) and (2) show the measured surge of a softly moored structure and the filtered surge. Inspection of Figures 3.7A and 3.7B suggests that there is a fairly strong coherence between the SIWEH and the filtered surge. The filtering of the surge channel is performed digitally using a double Fourier transform technique. This has the advantage of having a nearly infinite roll-off rate and zero phase shift over the entire frequency range.

The low frequency responses of the system can be quantified using spectral analysis techniques as follows. Figure 3.7C shows the spectral density function of the wave record from Figure 3.7A. Since the drift forces are approximately proportional to the square of the wave height it is useful to create a derived data channel which is the square of the wave height and compute the spectral density function of this channel. This is shown in Figure 3.7D. These figures show two features which are characteristic of this type of analysis. The first is that there is a large amount of energy at frequencies which are twice the frequency of the unsquared wave record. This phenomenon may be easily derived analytically. The second feature is that there is a large amount of energy at low frequencies. This is a result of the

wave grouping and indicates that the wave energy (proportional to the drift force) has some low frequency component.

The effect of the low frequency component of the wave energy on the response of the structure may be seen in the spectral density plot of the surge response which is shown in Figure 3.7E. The variance of the surge displacement of the structure is proportional to the area under the spectral density curve. The numbers in the upper right hand corner of the plot indicate that the significant value of surge (estimated as four times the standard deviation) in the frequency range from zero to 0.035 Hz is about 10 meters. The significant value of surge in the frequency range above 0.035 Hz is about 9 meters. It can therefore be seen from Figure 3.7E that the low frequency variance of the surge is roughly the same as the wave frequency variance in this example. The high frequency energy is centered around approximately 0.07 Hz (15 sec period) and the low frequency drift response has its peak at approximately 0.01 Hz (100 sec period), which happens to correspond approximately with the natural frequency of the system. Note that in this example the vessel responds approximately linearly to the wave frequency exciting forces and quadratically to the low frequency exciting forces. It does not appear to respond at all to the higher harmonics of the wave elevation squared which are represented by all the right-hand peak in Figure 3.7D.

Finally, it is enlightening to compute the transfer function between the surge response and the square of the wave height in the low frequency range. The transfer function (RAO) is shown in Figure 3.7F along with the estimate of the statistical error which is computed from the coherence function. This plot indicates that there is a good coherence (represented by a relatively low percent random error of about 30%) in the range of wave periods longer than about 80 seconds. This is a clear indication that the model is responding coherently to the low frequency variations in the drift force. This transfer function may be used to estimate the amplitude of the low frequency surge response for waves with different grouping.

3.8 Regular Wave Fourier Analysis

This type of analysis is particularly useful when applied to periodic signals such as those resulting from regular wave seakeeping tests of forced oscillation tests. The computer routines which are most often used accept as input one or more time series of periodic signals and produce periodogram plots for each signal and tables of transferfunctions and phases. The procedure consists of the following steps.

* A single record is searched for zero crossings in order to compute the average period which is then used in the subsequent analysis.

* For each data channel an artificial time series is created whose total length is equal to an exact integer multiple of the average period and which contains a number of points which is a power of two. This allows the use of the powerful Fast Fourier Transform on the new time series while eliminating entirely any errors due to "leakage" which would result from transforming an uneven number of cycles. This procedure used in the generation of the new time series is technically refered to as upward decimation and consists of

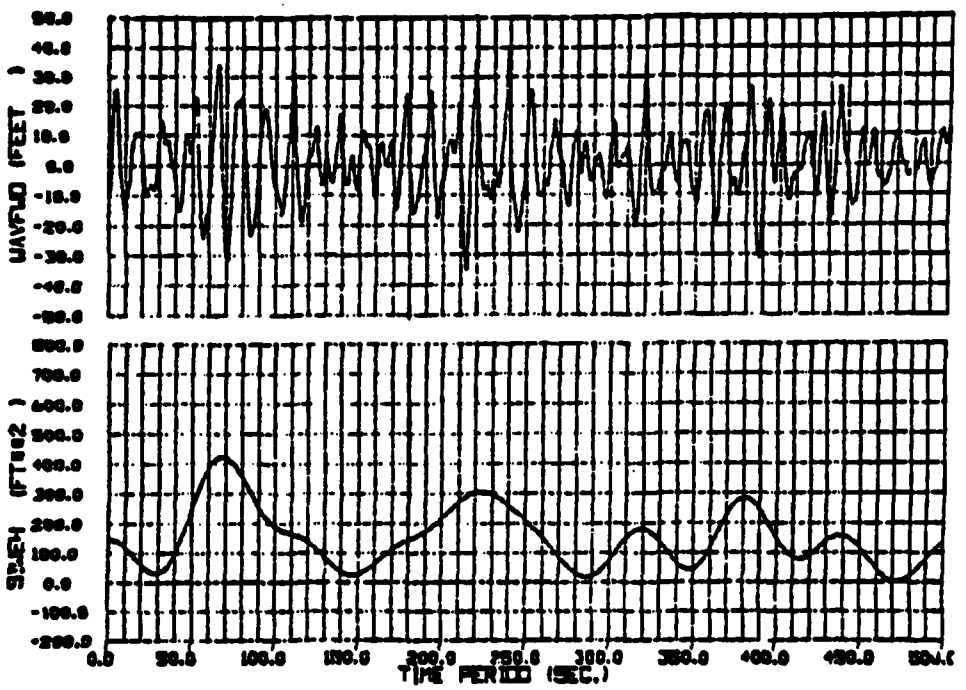

Figure 3.7A Time histories of Wave and SIWEH

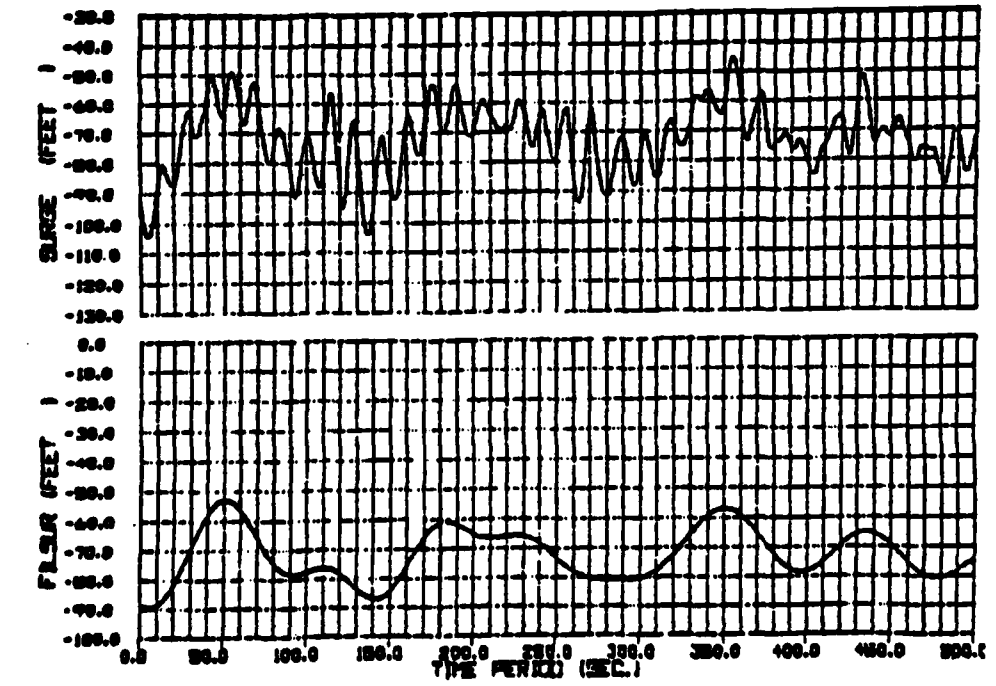

Figure 3.7B Unsmoothed and Smoothed Surge Time Histories

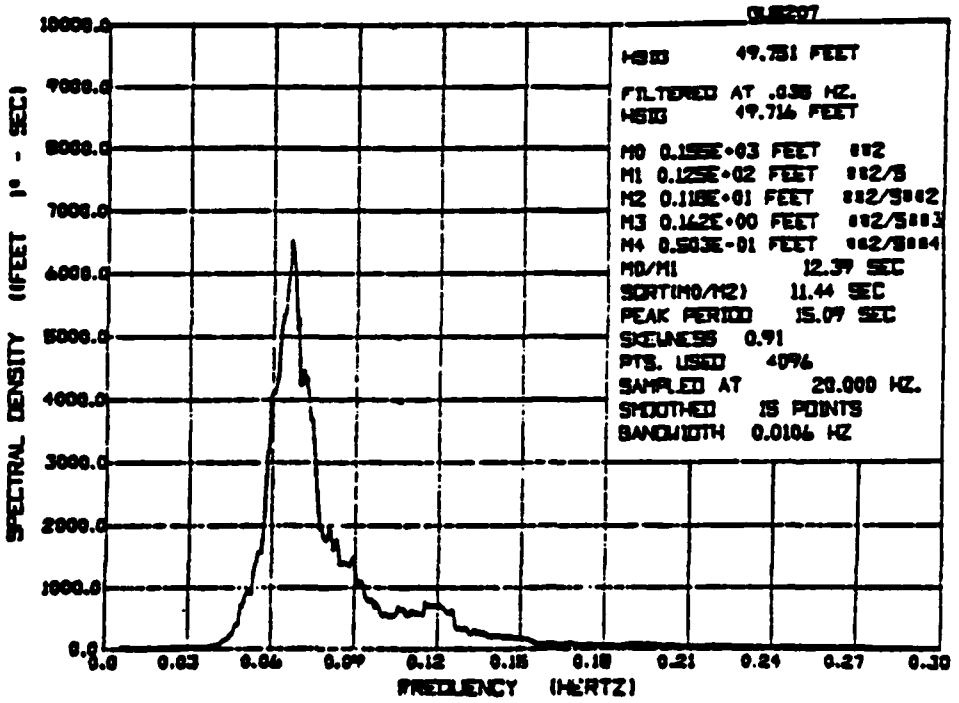

Figure 3.7C Spectral Density of Wave Record in Figure 3

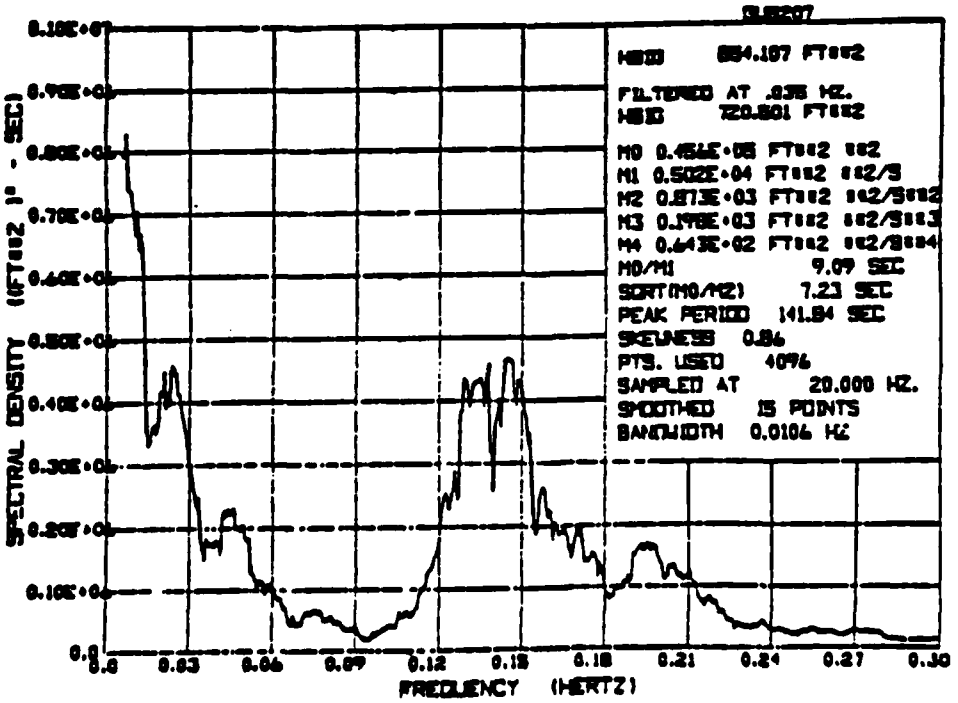

Figure 3.7D Spectral Density of Wave Elevation Squared

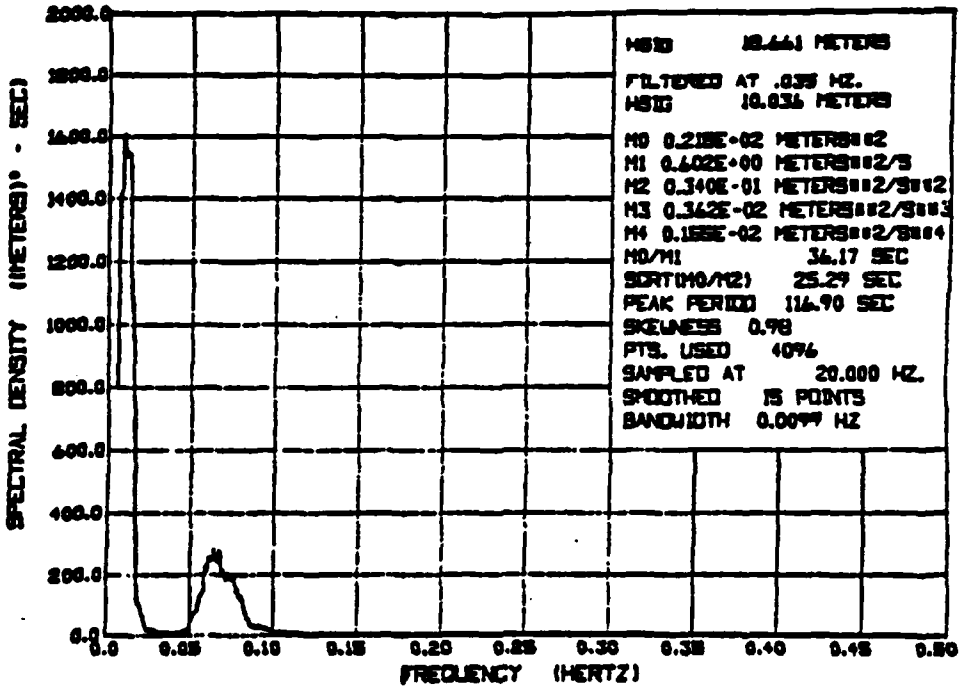

Figure 3.7E Spectral Density of Surge Record in Figure 4

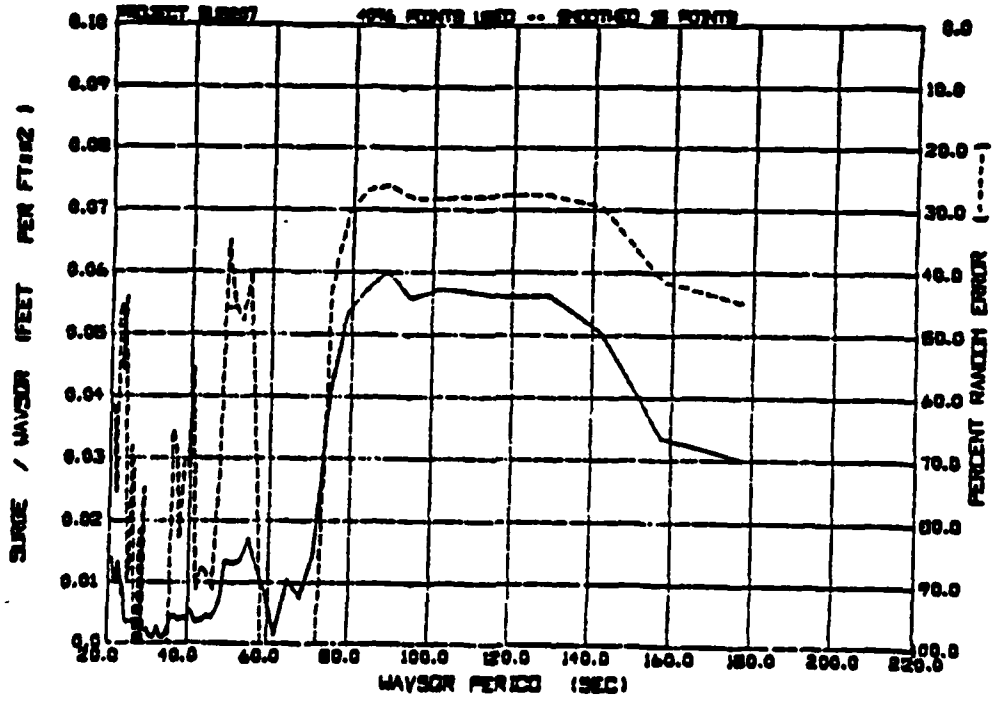

Figure 3.7F Transfer Function Between Surge and Wave Elevation Squared in Low Frequency Range

filling in data points where required by interpolating between existing data points.

* A Fourier transform is performed on each of the new time series and periodogram plots similar to Figure 3.8A are generated if desired.

* The complete amplitudes of the periodograms of different channels are used to compute the transfer functions and phases. Usually, the transfer functions are computed with respect to the wave elevation.

An alternate approach for determining the transfer functions in regular waves was used in the past. This consisted of dividing the average peak-to-peak values of two channels. This had several disadvantages which have been eliminated by the new approach. The old method did not allow the calculation of the phase angles which the Fourier analysis method does. The Fourier analysis method has a built in filtering since it only compares components of the two signals at the same frequencies. Thus it produces very accurate results even when one or more of the signals has noise or wild points. Two examples of the usefulness of the regular wave Fourier analysis method are described below.

Certain types of offshore structures, notably tension leg platforms, may exhibit significant responses at frequencies which are super-harmonics of the wave frequency. The complicated mechanisms which cause this include non-linear horizontal exciting forces at or near the water line which may produce a pitching moment. These non-linear forces may be shown to occur at frequencies which are two or three times the wave frequency even for theoretically perfect sinusoidal waves which do not contain higher harmonic components. In practice it is not possible to generate perfectly sinusoidal waves of finite amplitude. Therefore, when conducting tests to investigate harmonic responses such as this it is imporant to be able to quantify the frequency content of the regular waves. For this purpose the regular wave Fourier analysis is extremely accurate. Figure 3.8A shows a periodogram produced from a measurement of a regular wave. The plot shows distinctly that there are components in the wave at harmonics of the fundamental wave frequency, even though the signal which was used to drive the wave flap was a pure sine wave.

Another application of Fourier analysis is in the determination of added mass and damping coefficients from forced oscillation tests. Consider the forced oscillation of a ship model in heave to determine the heave added mass and damping. If the oscillation is periodic with frequency, ω, the transfer functions may be computed by the Fourier analysis method and are given by:

$$T_R = \left[\frac{\text{Force } (\omega)}{\text{Heave } (\omega)}\right] \cos \varphi \qquad [3.8\text{-}1]$$

$$T_I = \left[\frac{\text{Force } (\omega)}{\text{Heave } (\omega)}\right] \sin \varphi \qquad [3.8\text{-}2]$$

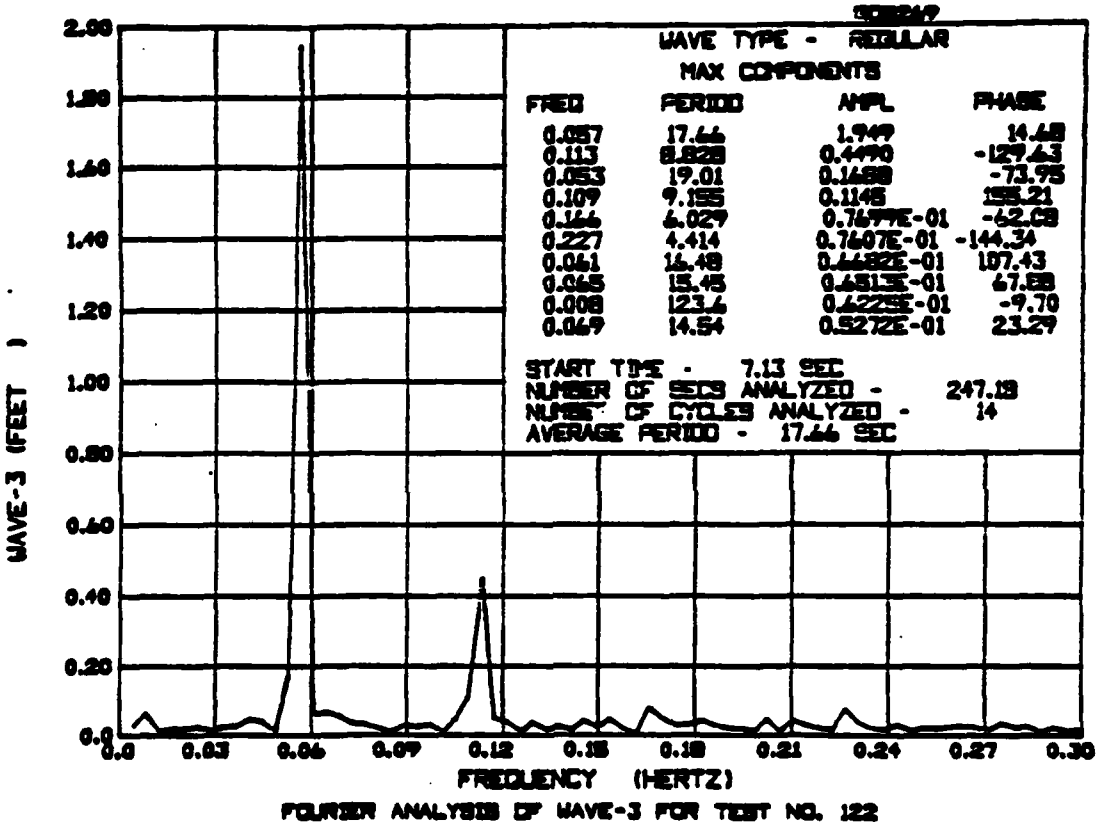
WAVE TYPE - REGULAR
MAX COMPONENTS
FREQ PERIOD AMPL PHASE
0.057 17.66 1.949 14.48
0.113 8.828 0.4490 -129.63
0.053 19.01 0.1688 -73.95
0.109 9.155 0.1145 155.21
0.144 6.929 0.7699E-01 -62.08
0.227 4.414 0.7607E-01 -144.34
0.061 16.48 0.4482E-01 107.43
0.065 15.45 0.4513E-01 67.88
0.008 123.4 0.4225E-01 -9.70
0.069 14.54 0.5272E-01 23.29
START TIME - 7.13 SEC
NUMBER OF SECS ANALYZED - 247.19
NUMBER OF CYCLES ANALYZED - 14
AVERAGE PERIOD - 17.66 SEC
WAVE-3 (FEET)
2.00
1.80
1.60
1.40
1.20
1.00
0.80
0.60
0.40
0.20
0.0
0.0 0.03 0.06 0.09 0.12 0.15 0.18 0.21 0.24 0.27 0.30
FREQUENCY (HERTZ)
FOURIER ANALYSIS OF WAVE-3 FOR TEST NO. 122

Figure 3.8A

where T_R and T_I are the real and imaginary parts of the transfer function between the heave force and the heave displacement. If the effective vertical spring force due to hydrostatic pressure is k then the added virtual mass of the body (mass plus added mass) is given by:

$$M_v = \frac{k - T_R}{\omega} \qquad [3.8\text{-}3]$$

and the damping coefficient is given by:

$$C = T_I \Big/ \omega \qquad [3.8\text{-}4]$$

Difficulties may arise at the very low frequencies since the heave force will be dominated by the hydrostatic spring constant k and the damping force will be relatively small. The ability to determine the damping force depends entirely on the ability to determine the phase angle in expression [3.8-2] accurately. The ability to compute the added mass accurately depends on the ability to determine the magnitude of the transfer function, T_R, since the numerator in expression [3.8-3] will tend towards zero at low frequencies. Both of these potential problems are circumvented to a large extent by the use of the Fourier analysis methods which we have described.

4.0 ERROR ESTIMATION

In interpreting any results it is imperative to have an understanding of the range of error. This includes instrument, digitization, and analysis errors. Instrument and digitization errors were briefly discussed in Section 2.0. Analysis errors will be discussed below. The details of error formulas are best gained from the referenced texts on spectral analyses.

Random error formulas for various spectral quantities are summarized in Table 4.0A. Several important facts for model testing follow from these formulae:

* Auto-spectra (PSD's) must be averaged (smoothed) or 100% random error will result.

* Coherence must be computed along with the cross-spectra (RAO), and used in evaluating the RAO.

* Gain (RAO) random error calculated by auto-spectra is

$$\frac{1}{|\gamma xy(f)|}$$

times the random error by cross-spectra. Therefore, cross-spectra estimates of gain are always more accurate than the auto-spectra methods.

* Gain estimates (RAO's) need at least 20 averages to be used in order to keep its normalized random error under 10%. Figure 4.0B presents this in graphical form.

Sources of random error, low coherence, may be from one or all of the following:

1) Extraneous measurment noise in the transducers, instrumentation or digital calculations.

2) Resolution bias error present in the spectral estimates.

3) Non-linear in the system relating to input and output.

4) The output is in part due to unmeasured inputs and is uncorrelated with the measured input.

Extraneous noise can best be avoided by proper selection of instrumentation, good calibration techniques and accurate analog-to-digital converters. Resolution bias errors can be minimized by good sampling and smoothing techniques. Un-correlated input/output signals is best avoided by assuring that the measured input is as noise free as possible. Since the input signal is usually the wave elevation record this means using an accurate wave probe placed near enough to the model to measure the exciting wave, yet free from any reflections.

TABLE 4.0A

	Quantity	Random Error, ε_r
Autospectra,	$\hat{G}xx(f), \hat{G}yy(f)$	$\frac{1}{\sqrt{n_d}}$
Cross-spectra,	$\lvert\hat{G}xy(f)\rvert$	$\frac{1}{\lvert\gamma xy(f)\rvert\sqrt{n_d}}$
Coherence,	$\hat{\gamma}^2_{xy}(f)$	$\frac{\sqrt{2}[1-\gamma^2 xy(f)]}{\lvert\gamma xy(f)\rvert\sqrt{n_d}}$
Output due to H(f)	$\hat{G}vv(f)=\hat{\gamma}^2 xy(f)\hat{G}yy(f)$	$\frac{[2-\gamma^2 xy(f)]^{1/2}}{\lvert\gamma xy(f)\rvert\sqrt{n_d}}$
Gain by Cross-spectrum, Phase Angle	$\lvert\hat{H}xy(f)\rvert;\hat{\varphi}xy$	$\frac{[1-\gamma^2 xy(f)]^{1/2}}{\lvert\gamma xy(f)\rvert\sqrt{2n_d}}$
Squared Gain by Cross-spectra	$\lvert\hat{H}xy(f)\rvert^2$	$\frac{\sqrt{2}[1-\gamma^2 xy(f)]^{1/2}}{\lvert\gamma xy(f)\rvert\sqrt{n_d}}$
Gain by Auto-spectra	$\lvert\hat{H}xy(f)\rvert_a$	$\frac{[1-\gamma^2 xy(f)]^{1/2}}{\gamma^2 xy(f)\sqrt{2n_d}}$

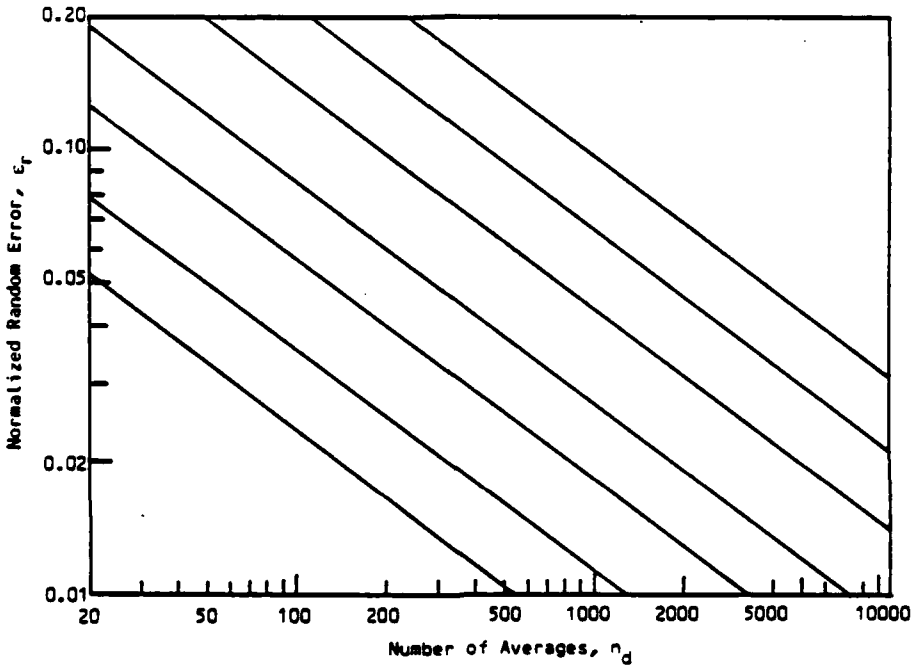

Figure 4.08 Normalized Random Error of Gain Factor Estimates

AD-A144 227 PROCEEDINGS OF THE GENERAL MEETING OF THE AMERICAN TOWING TANK CONFERENCE.. (U) STEVENS INST OF TECH HOBOKEN NJ DAVIDSON LAB D SAVITSKY ET AL. AUG 83 8/8

UNCLASSIFIED SIT-DL-TR-13029-VOL-2 N00167-83-M-4062 F/G 20/4 NL

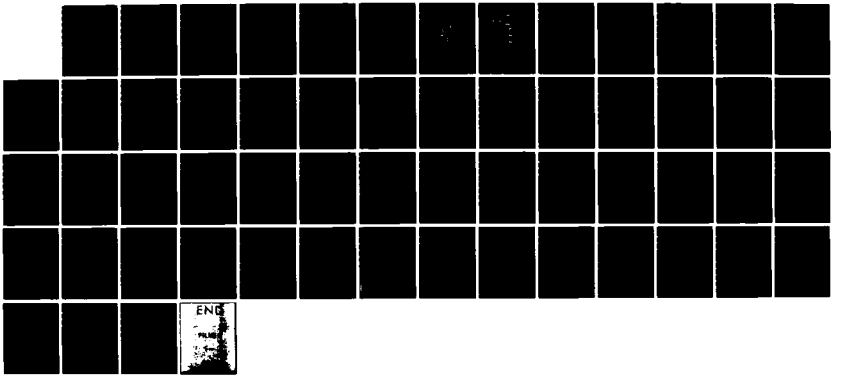

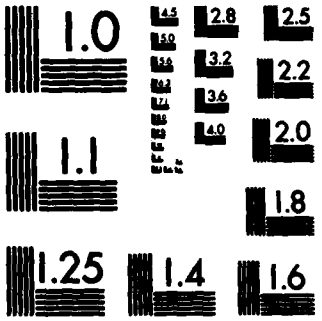

MICROCOPY RESOLUTION TEST CHART
NATIONAL BUREAU OF STANDARDS-1963-A

5.0 EXTENDED AREAS OF ANALYSIS

As hardware and software capabilities increase more and more sophisticated analysis methods will become everyday standards. These analyses are presently in the domain of research or post-test analysis. Several analysis methods that we expect to move into the realm of standard basin analyses are described below.

Non-Linear Systems - One problem we face with present linear spectral analysis methods is that many of motions or loads we are interested in become non-linear at larger magnitudes. The linear RAO reports this non-linear response as noise giving a reduced coherence function. If such non-linear effects are suspected they must now be checked against the results of periodic wave tests. Methods for finite memory square-law systems, consisting of zero memory square-law systems that are preceded or followed by linear systems, have been developed by J.S. Bendat and A. G. Piersol (see reference 7).

Reflected/Incident Wave Analysis - The ability to extract from wave elevation records the incident and reflected wave trains can be of real benefit. We have implemented the analysis method developed by Yoshimi Goda (reference 9). It has proven most useful in determining the actual incident wave spectra in cases where reflected or standing waves were unavoidable.

Multiple Input/Output Systems - Spectral analysis techniques have been developed for systems where more than one input (wave, current, wind ...) exist along with multiple outputs. These methods have been applied and proven in a variety of signal processing applications. We believe many applications exist in the area of model testing that would greatly benefit from their use.

Multi-Directional Seas Analysis - Theoretical descriptions of multi-directional sea spectra have been developed and several test facilities now have the capability of producing such seas. Analysis methods need to be developed and used so as to gain experience with them.

REFERENCES

1) Bendat, J.S. and Piersol, A.G. (1971) Random Data: Analysis and Measurement Procedures, New York, Wiley-Interscience.

2) Bendat, J.S. and Piersol, A.G. (1980) Engineering Applications of Correlation and Spectral Analysis, New York, Wiley-Interscience.

3) Funke, E.R. and Mansard, E.P.D. (1979) On the Synthesis of Realistic Sea States in the Laboratory Flume, National Research Council of Canada, Report LTR-HY-66, Ottawa, Canada.

4) Funke, E.R. and Mansard, E.P.D. (1979) SPLSH, A Program for the Synthesis of Episodic Waves, National Research Council of Canada, Report LTR-HY-65, Ottawa, Canada.

5) Otnes, R. and Enochson, L. (1978) Applied Time Series Analysis, Volume I, Wiley and Sons.

6) Bendat, J.S. (1981) Definitions and Frequency Domain Procedures for Dynamic Data Analysis, International Journal of Vehicle Design, Vol.2, No. 2, p 229-245.

7) Bendat, J.S. and Pierson, A.G. (1982) Spectral Analysis of Non-linear Systems Involving Square-Law Operations, Journal of Sound and Vibration, 81(2),p 199-213.

8) Ludeman, L.C., (1982) Optimum Sampling Times for Spectral Estimation, AFOSR-TR-82-0395.

9) Goda, J. and Suzuki, Y. (1976) Estimation of Incident and Reflected Waves in Random Wave Experiments, Proceedings Coastal Engineering Conference, p 828-845.

10) Michel, W.H., (1967) Sea Spectra Simplified, S.N.A.M.E. Gulf Section, April

BIOGRAPHIES

DR. JEFFREY T. DILLINGHAM - Vice President, Offshore Technology Corporation

Dr. Dillingham originally came to San Diego to enter the graduate program at Scripps Institute of Oceanography after receiving a B.S. degree in mechanical engineering at Cornell University. While at Scripps he worked on several research projects involving underwater acoustics and coastal processes. After receiving his masters degree in oceanography he left Scripps to work at OTC as a project engineer. His continuing interest in offshore engineering prompted him to then continue his graduate studies at the University of California, Berkeley, where he received his Ph.D. degree in naval architecture in 1979. While at Berkeley he conducted experimental and theoretical research in the areas of ship maneuvering, seakeeping, and wave theory. Before returning to work at OTC Dr. Dillingham worked as a consultant for Ship Research, Incorporated, where he was mainly responsible for developing a new method for measuring directional wave spectra using linear programming techniques. Dr. Dillingham's main interests are hydrodynamics and numerical methods. Besides managing model test programs at OTC he is responsible for much of the research and development effort and has been instrumental in implementing new and faster data analysis methods.

MR. JOHN HOSTE - Program Manager, Offshore Technology Corporation

Mr. John Hoste came to OTC over two years ago from General Dynamics Convair where he was the lead engineer in the Composite Structures Stress Group. He brings with him a strong background in structures, including extensive finite-element analysis, computer programming and structural testing experience. He earned a Master's degree in Applied Mechnaics from the University of California at San Diego, and holds two professional engineering licenses in the state of California as a Civil and Mechanical Engineer.

As the director of computer facilities he has managed OTC's installation of state-of-the-art mini-computers for data acquisition and analysis. He was responsible for the design of the new modularized software system and is responsible for its continued development and maintenance. As a program manager he has managed numerous test programs ranging from semi's and jack-up's to CALM's.

APPENDIX A

RECOMMENDATION ON NOTATION AND SPECTRAL DEFINITIONS

The notation used in this paper has become fairly widely accepted as a standard in the offshore industry and in other fields of science and engineering. We recommend that it be used whenever possible. In regard to spectral quantities we have adopted, and strongly recommend the notation of J.S. Bendat. Reference 6 is an excellent description by Bendat of definitions and frequency domain procedures.

APPENDIX B

REVIEW OF A STATE-OF-THE-ART DATA ACQUISITION SYSTEM

The following data acquisition and analysis system was developed at OTC over the last two years. Our desire was to put together a state-of-the-art data acquisition system that was highly flexible in meeting the demands of a wide range of test cases. In addition we required high-speed analysis of the data, immediate printouts and graphics hard copies. The system now meets these goals and is undergoing only minor enhancements to improve processing speed and size.

Physical Description

The complete data acquisition, data processing and software development facilities are basically in two parts. At the test station is a relatively small PDP-11/23 system used for data acquisition and immediate data processing, while in a separate computing facility is a PDP-11/44 used for post-test data processing and software development. See Figures B-1 and B-2.

The data acquisition system is similar to a package now sold by NEFF called System 720. It consists of a PDP 11/23 computer driving a NEFF 620 sixty-four channel stand up analog signal conditioning system and digitizing unit. OTC has two such units in full operation in our deep and shallow water basins (see Figure B-3).

The system equipped with OTC standard software will permit the following:

* Up to 100 channels of data
* Various sample rates among channels
* High sample rates - 1000 Hz/channel
* Data time histories 30 to 90 seconds after each test
* Statistics 30 to 45 seconds after each test
* Long test duration (10 megabyte disc or 125 ips tape drive available for storage)
* Spectral analysis right after test
* Storage media compatible with our 11/44 machine which can transfer data to industry standard magtape for clients' use and can carry out a wide range of post-test spectral, Fourier and statistical analyses

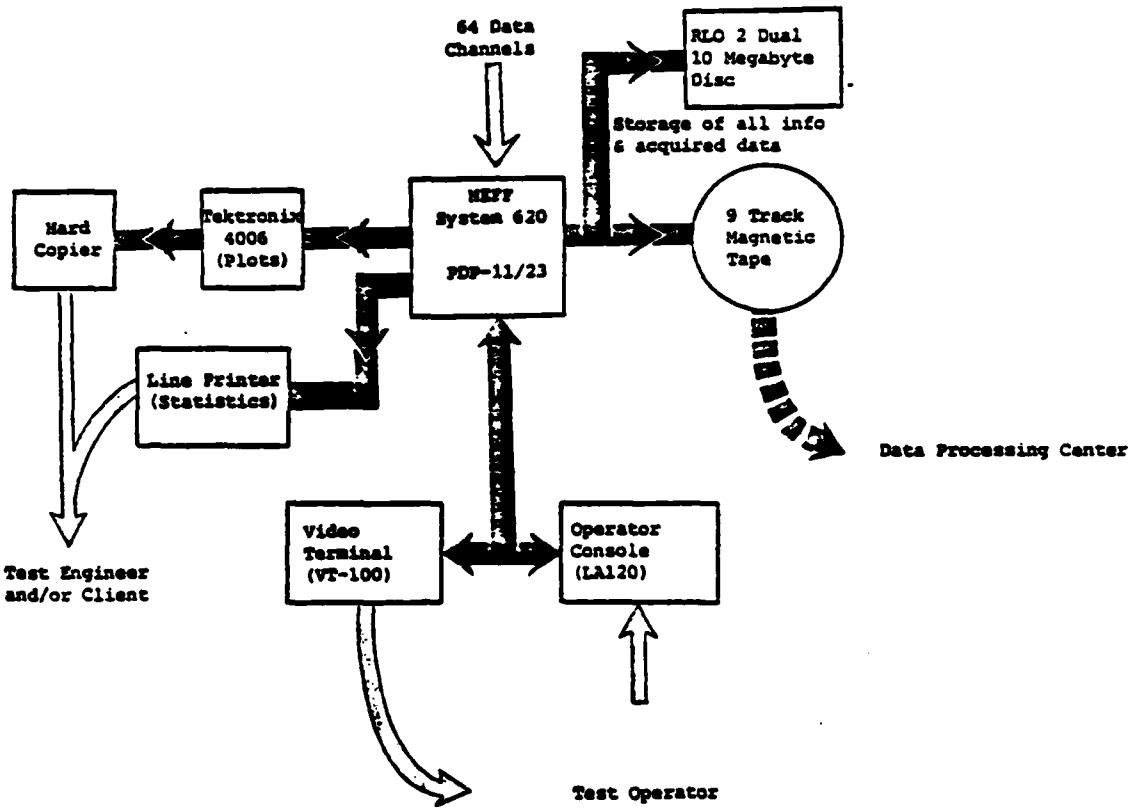

Figure B-1 Typical Data Acquisition Station at Each Test Basin

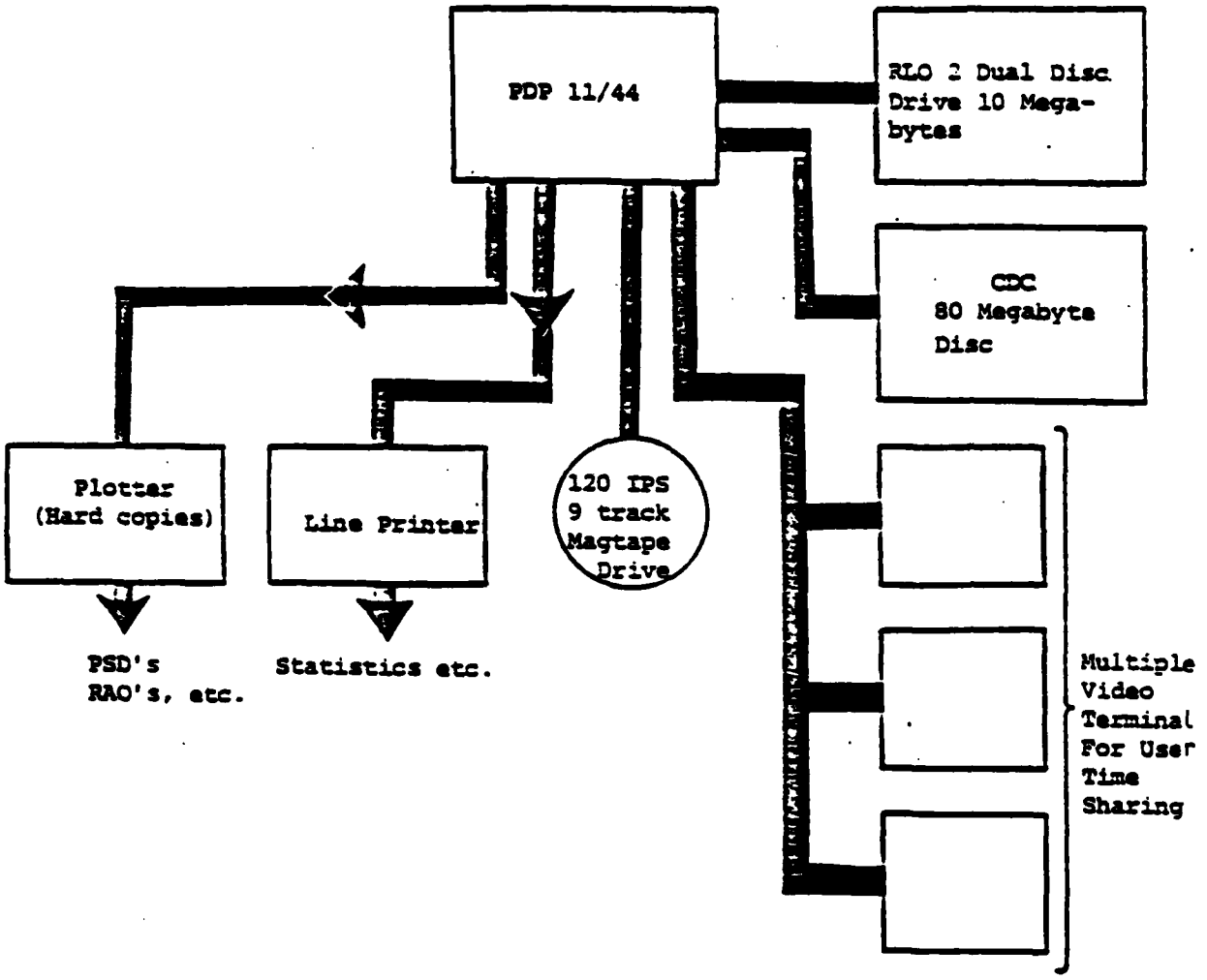

Figure B-2
OTC's Data Reduction and Analysis Computer System

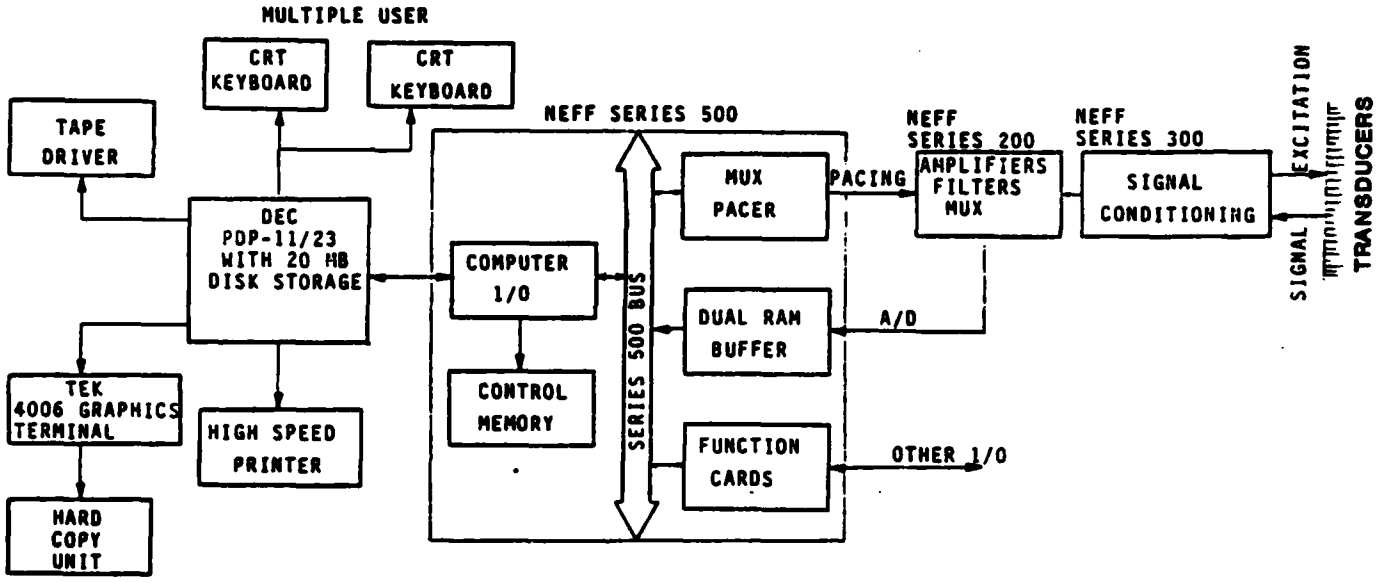

Figure B-3 OTC DEC/NEFF DATA ACQUISITION SYSTEM

The system is capable of a maximum data acquisition rate of 50K samples/second. Analog and digital data can be acquired as well as any TTL input (e.g., switch states). The NEFF can also act as a control device, to activate valve or switches at a specified point during the test.

Capabilities

The PDP-11/NEFF system is an extremely flexible one. Under operator control, via software, any combination of data channels can be sampled, different sampling rates can be assigned to various channels in one test, channel gains can be altered, and tests up to four million samples in size can be easily taken. A typical test might look like that described in Table B-4.

The ability to sample channels at different rates is a real advantage when dealing with constraints of size and processing time. The test in Table B-4 was 1/2 million samples, if it had been necessary to sample all of the channels at 100 Hz (in order to get the few that were required).

This capability does create some challenging software problems however. The original data structure is a bit complex and requires restructuring. Data reduction can be complicated by the fact that an RAO for instance may be wanted between channels sampled at 20 Hz and 100 Hz. This problem is presently handled by effectively reducing the 100 Hz channel to a 20 Hz sampling rate.

TABLE B-4

TYPICAL DATA ACQUISITION PARAMETERS

Data Channel	Cutoff Filter	Sampling Rate
Wave elevation	5 Hz	20 Hz
6 rigid body motions	5 Hz	20 Hz
Angular velocities		
X accelerations		
Y accelerations		
Z accelerations		
°		
°		
°		
Bending Moments (4)	Wide Band	100 Hz
°		
°		
°		
Tie-down Load Cells (9)		100 Hz
°		
°		
°		
°		
34 channels	Total	1720 samples/sec

Test Length = 620 seconds
Test Size = 1,086,400 total samples
Band Width = 0.1 Hz (31 point smoothing)
Random Error = 0.18 Hz (31 point smoothing)

The system's flexibility in testing is best described by brief examples:

* Various Sample Rates, allows a structural vibration data channel (bending of jackup legs, ringing of TLP tendons...) to be sampled at a high rate while wave frequency channels can be sampled at a much lower rate. This greatly reduces total test sample size and data processing time.

* Combined Analog and Switched Signals, as during a jacket upending test it is possible to acquire at one time analog data on the jacket motions and tank levels as well as switched signals (TTL) from the jacket operator's control panel identifying control valve positions. In this way an exact record of the operators commands and the jacket's response is obtained.

* D/A Controlled by Switched Signal, in a test involving the impact of an iceberg and an offshore structure say, data acquisition on perhaps 20+ channels all at 1000 Hz would be triggered by a switched signal (interrupted light beam) a moment before impact. This sort of triggering of the data acquisition assures data is taken at the proper time and minimizes test length.

The Future

The near future holds enhancements to the system largely directed at even faster data processing. These additions include:

* Array Processor - this is an add-on board that would do FFT's in hardware (rather than with software) extremely fast.

* Co-Processor - this might be a second small computer that would have access to all data just as the data acquisition computer would. This second processor would allow the test engineer to analyze the last test's data without interfering in any way with the acquiring of the next test's data.

* Dedicated Pre-Processor - this is a small micro-processor designed and dedicated to preprocessing a few channels prior to sending the data to the main data acquisition computer. In this way instrumentation could be developed whose "special" output would be processed and converted to a meaningful format when the data acquisition computer receives it and stores it.

The long term future is nearly impossible to predict. Advances in computer hardware are occuring at an incredible rate; producing more powerful computers, with more storage at lower effective costs. Future enhancements to data acquisition systems may include:

* 32 Bit computers with several mega-bytes of memory

* Data storage devices storing giga-bytes of data

* Color graphics and color hardcopies.

AD-P003 837

DESIGN OF A DYNAMOMETER FOR TESTING YACHT MODELS

By C.M.J. Gommers* and P. van Oossanen.**

1. INTRODUCTION

Designing a dynamometer for measuring drag and side force on yacht models is a very challenging problem. The designer has to solve the complex interaction between wind, water and gravity forces that exist on the actual yacht. Besides this, the dynamometer must provide the possibility of economic use in the towing tank.

A new wind-force dynamometer was introduced at the Netherlands Ship Model Basin (NSMB). It can be described as an active system because close-loop servo-systems are incorporated in the dynamometer.

In this paper the developed wind-force dynamometer is described, as well as the techniques adopted for test-data analysis and extrapolation of test results to full scale.

2. DESCRIPTION OF DYNAMOMETER SYSTEMS

SYSTEM A

Captive Model Test

A captive model test set-up is often used in model testing and can be described as a test method in which the model is fixed to the towing carriage without any degree of freedom. Between the model and the towing carriage a six-component transducer is installed to measure the forces acting on the model.

---

* Head Instrumentation Department, Netherlands Ship Model Basin

** Head Design Research Department, Netherlands Ship Model Basin

Such a test method is not very suitable for yacht models because of the very complex test procedure which then has to be adopted. The natural balance between the occurring forces, i.e. the hydrodynamic forces on the hull and the simulated wind force, cannot be obtained.

SYSTEM B

Partly-Affixed Model Test

This system is often in use in model yacht testing. The model is fixed to the carriage in such a way that it is free to move in Z, ϕ en θ direction (for definition of symbols see Fig. 1), very similar to the measuring set-up adopted in common resistance and propulsion tests. This approach reduces the number of test runs drastically. The accuracy of the position and direction of the applied towing force is usually not sufficient however (see Fig. 2).

SYSTEM C

Free-Running Model Test

The model is towed with the aid of gimbals placed at a distance from the deck where the wind force is considered to act. The model is free to move in six degrees of freedom. During the test the wind force is assumed to work perpendicular to the mast. To achieve this a servo-system is introduced. A transducer mounted in the mast measures the axial mast force and controls a motor-driven spindle to zero this force by lowering the point of application of the towing force (see Fig. 3). The accuracy of this zero control is such that the axial mast force can be regulated to within about one per cent of the existing towing force.

This set-up was adopted at NSMB in 1980. To set the model at the required drift angle the rudder angle was used. In certain cases, however, the adopted rudder angle is not representative of the full-scale situation. To overcome this problem a variable towing mast position was introduced. The mast position is varied during the beginning of a test run until equilibrium is obtained between the resultant towing force and the resultant hydrodynamic force at the

wanted drift angle. The number of required runs was in this way reduced to a minimum. The drag and side forces are measured in-between the carriage and the gimbals. A description of this system with a fixed towing mast position is given by Murdey [1]*.

SYSTEM D

Free-Running Model Test at a Prescribed Drift Angle

Although System C worked satisfactorily, a slight inconvenience was experienced when the servo-system was set at drift angles of one degree or less. The system became unstable around the zero drift angle because the mast position is the same at equal drift angles over port and starboard. To avoid this the transducer in the mast was modified to also measure the mast torque, thereby allowing the torque to be kept zero. The mast position for zero mast torque is adjusted during a test run at a fixed, prescribed drift angle of the model. The drift angle setting is now very "natural" and the model does not "feel" the setting (see Fig. 4).

A schematic presentation of the 4 systems described above is given in Fig. 5.

3. SERVO SYSTEMS

The servo systems used are very simple (see Fig. 6). The setting for amplification is easy and not critical. The maximum speed of the mast position adjustment and the longitudinal towing force position was approximately 10 cm per second. The electric motors are simple 400 watt DC motors.

4. ANALYSIS AND EXTRAPOLATION OF TEST DATA

During every run with the adopted dynamometer the model attains realistic drift-heel angle attitudes. The corresponding drag and side force measurements represent realistic side and drag forces experienced by the yacht.

---

* References are listed at the end of this paper

For every model speed V_M of interest, a series of tests is carried out at varying drift angles β . For every V_M,β combination, the drag and side forces (R_{T_M} and L_{T_M} respectively) are measured, as are also the heel and trim angles (θ and ϕ respectively).

Also for every V_M,β combination the position of the towing mast, for which the torque in the mast is zero, is recorded. Plots can then be prepared showing L_{T_M}, R_{T_M} and L_{T_M}/R_{T_M} against drift angle for various speeds. In addition, plots can be drawn showing θ, ϕ and mast position as a function of drift angle for each model speed. These plots are useful in a qualitative sense when comparing various yacht designs.

To derive full-scale performance values in relation to the wind velocity, the following procedure can be adopted (for definition of symbols see Fig. 7).

A. The measured side force is scaled up to full scale according to $L_{T_S} = L_{T_M} (\lambda)^3$, where λ = the scale ratio

B. The measured resistance must be decomposed into a part associated with viscous and wave-making drag and a part associated with induced drag. The induced drag can be ascertained from the assumption that the induced drag varies as the square of the measured side force. The total model resistance is set out as a function of side force-squared, to check this assumption. With the induced drag determined and scaled up by multiplying by λ^3 , the remaining part of the resistance is then decomposed in a part dependent on Reynolds number (viscous resistance) and a part dependent on Froude number (wave resistance), which parts can be scaled to full-size using normal towing tank practices.

C. The hydrodynamic or hull drag angle is then calculated from:

$$\varepsilon_H = \tan^{-1}(R_{T_S}/L_{T_S}), \text{ where}$$

R_{T_S} = full-scale resistance

D. The apparent wind angle β_{AW} is determined from:

$\beta_{AW} = \varepsilon_H + \varepsilon_S$ where
ε_S = the aerodynamic or sail-drag angle, defined as
$\varepsilon_S = \tan^{-1}(C_{D_S}/C_{L_S})$ where
C_{D_S} = total sail drag coefficient and
C_{L_S} = total sail lift coefficient

The values of C_{D_S} and C_{L_S} are themselves dependent on the apparent wind angle β_{AW}. To determine β_{AW}, C_{D_S} and C_{L_S}, it is necessary to carry out an iteration process, starting with an estimated value for ε_S as given in step E.

E. Starting with a nominal value for ε_S of 9°, the value of β_{AW} is determined from $\beta_{AW} = \varepsilon_H + \varepsilon_S$.
If β_{AW} is less than 80 degrees, sail coefficients for sailing to windward are used. If β_{AW} is greater than 80 degrees, sail coefficients for sailing downwind are used.
The sail coefficients used at NSMB are those derived by Van Oossanen [2], viz

for $\beta_{AW} < 80°$

$$C_{L_S} = (1.04 + 0.006\,\beta_{AW} + 0.0000125\,\beta_{AW}^2)\left(\frac{GEA}{GEA+MSA}\right) + (0.04113\,\beta_{AW} - 0.0003267\,\beta_{AW}^2)\left(\frac{MSA}{GEA+MSA}\right)$$

$$\text{and } C_{D_S} = 0.044 + \frac{0.089\,C_L^2}{1 - \theta/5000}S$$

where GEA = area of genoa
MSA = mainsail area

For $\beta_{AW} > 80°$

$$C_{D_S} = 1.2\left(\frac{MSA}{MSA+SPA}\right) - (0.3 - 0.0231\beta_{AW} + 0.000088\beta_{AW}^2)\left(\frac{SPA}{SPA+MSA}\right)$$

$$\text{and } C_{L_S} = \frac{C_{D_S}}{\tan(10 + 0.39\beta_{AW})}$$

where SPA = area of spinnaker

F. After the iteration procedure for β_{AW} has resulted in final values for C_{L_S} and C_{D_S}, the resultant sail force coefficient is calculated from:

$$C_{R_S} = \sqrt{C_{L_S}^2 + C_{D_S}^2}$$

and the resultant hydrodynamic force on the hull is calculated from:

$$R_{H_S} = \sqrt{L_{T_S}^2 + R_{T_S}^2}$$

G. Since the resultant sail force equals the resultant hydrodynamic force (for equilibrium), it follows that:

$$R_{H_S} = \tfrac{1}{2}\rho_A \cdot V_{AW}^2 \cdot C_{R_S}(S_s \cos\theta)$$

where ρ_A = mass density of air (1.226 kg/m^3)

V_{AW} = apparent wind speed at the effective centre of effort in m/sec

$S_s\cos\theta$ = effective sail area, where

S_s = total sail area in m^2

θ = heel angle

H. The apparent wind speed is then determined from:

$$V_{AW} = \sqrt{\frac{R_{H_S}^2}{\tfrac{1}{2}\rho_A \cdot C_{R_S} \cdot S_s \cdot \cos\theta}}$$

I. The true wind speed, at the effective centre of effort, then follows from:

$$V_{TW} = \sqrt{V_S^2 + V_{AW}^2 - 2V_S \cdot V_{AW}\cos\beta_{AW}}$$

where $V_S = V_M/\lambda$

J. The true-wind speed angle at the effective centre of effort follows from:

$$\beta_{TW} = \sin^{-1}\left(\frac{V_{AW}\sin\beta_{AW}}{V_{TW}}\right)$$

K. The speed-made-good to windward then follows from:

$$V_{mg} = V_s \cos\beta_{TW}$$

To facilitate step E to be carried out graphically, upwind and downwind sail coefficients are shown in Figs. 8 and 9 for the case GEA = MSA.
Optimum V_{mg} values are found by drawing the tangent to various V_{mg} versus V_{TW} curves, found for each value of V_S.

5. CONCLUSIONS

Servo systems with force and position feedback are very useful in dynamometer design for hydrodynamic research on yachts.

The adopted dynamometer at NSMB allows the number of required test runs to be minimised and the most realistic test set-up to be achieved, resulting in accurate test results.

6. REFERENCES

1. Murdey, D.C.: "Yacht Testing at NRC", Quarterly Bulletin of the Division of Mechanical Engineering, National Research Council Canada, 1978.

2. Oossanen, P. van: "Theoretical Estimation of the Influence of Some Main Design Factors on the Performance of International Twelve Meter Class Yachts", Fourth Chesapeake Sailing Yacht Symposium, Society of Naval Architects and Marine Engineers (Chesapeake Section), 1979.

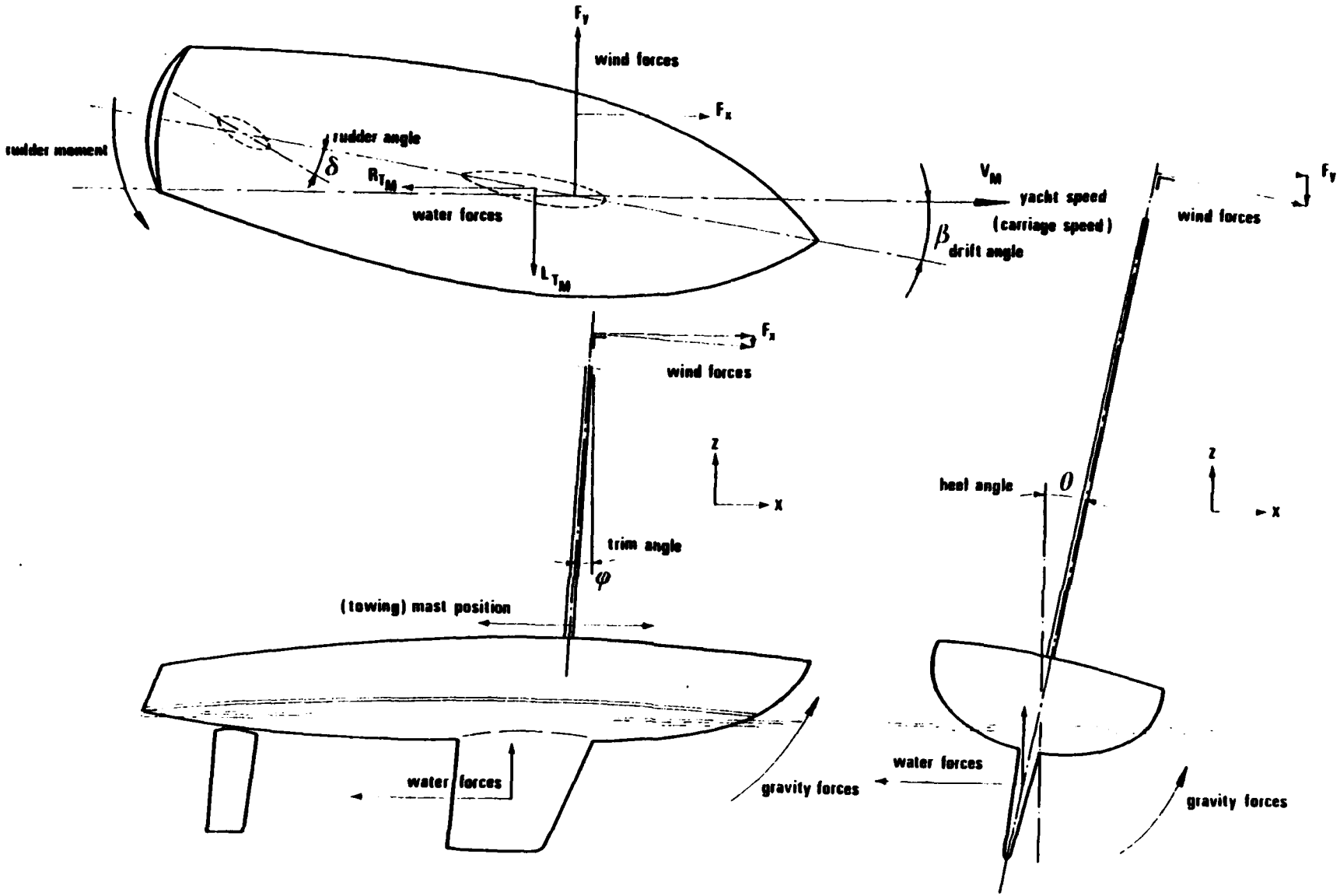

fig.1 DEFINITION OF YACHT FORCES AND VARIABLES

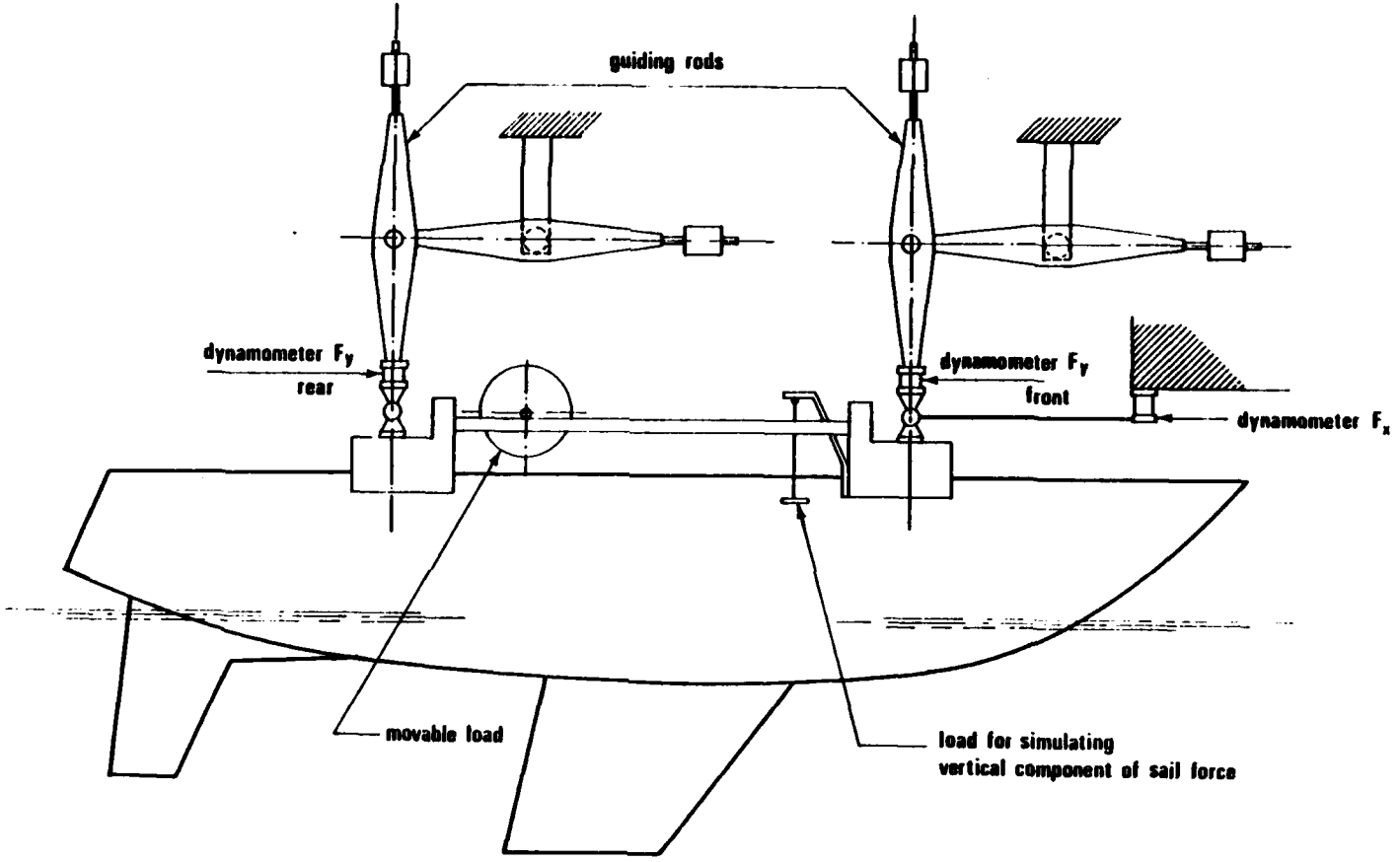

fig. 2 MODEL SET-UP OF DYNAMOMETER SYSTEM B

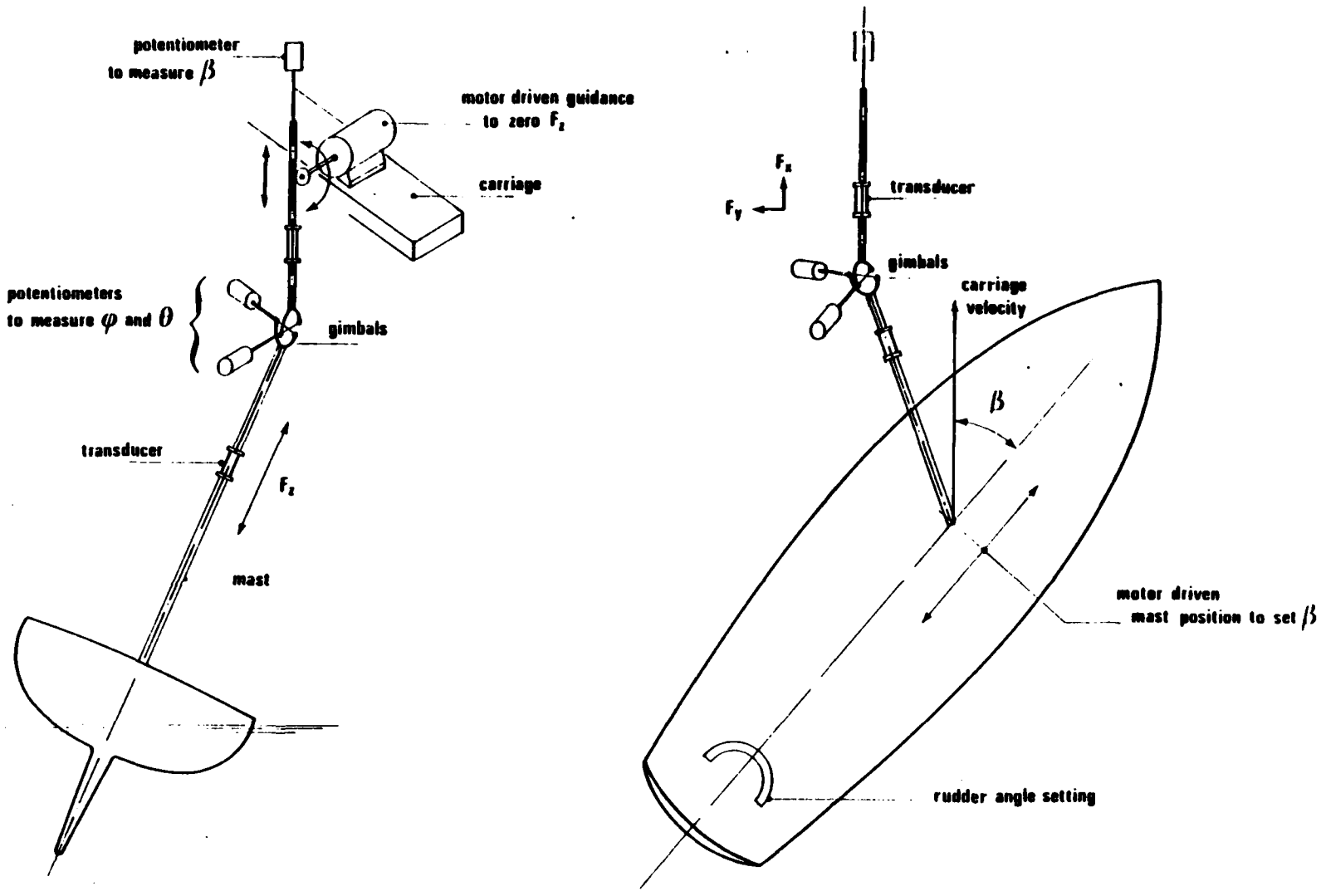

fig. 3 MODEL SET UP OF DYNAMOMETER SYSTEM C

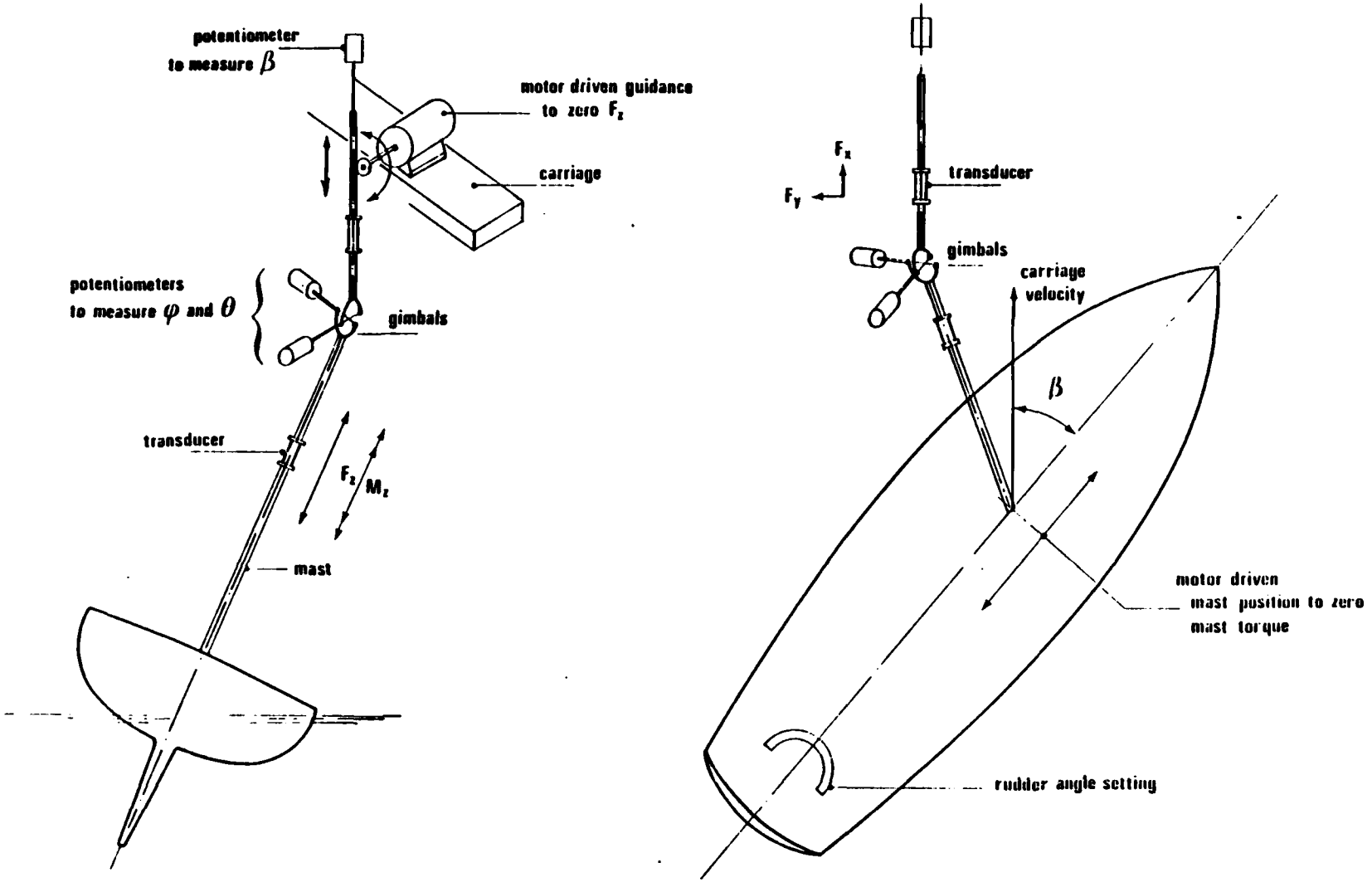

fig. 4 MODEL SET-UP OF DYNAMOMETER SYSTEM D

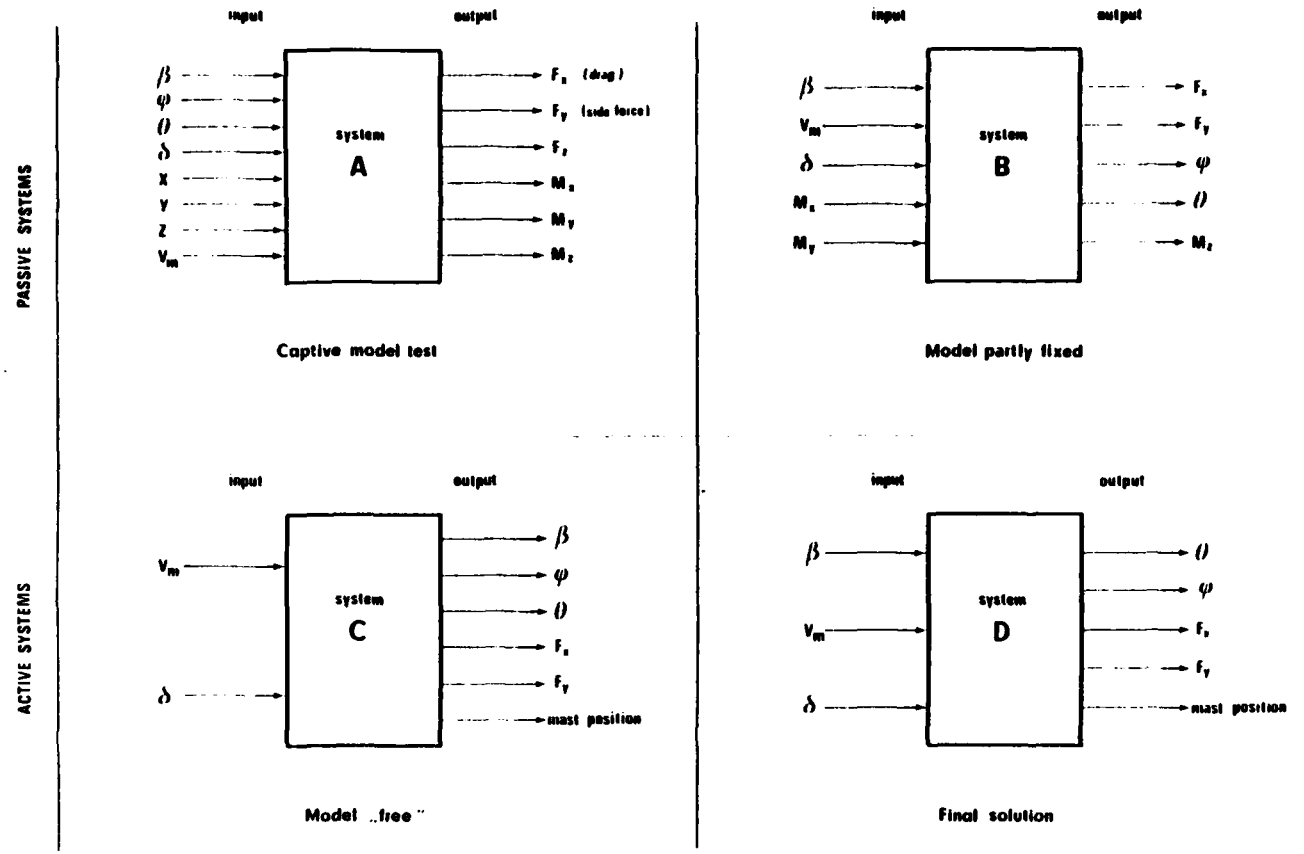

fig. 6 SCHEMATIC PRESENTATION OF POSSIBLE TESTING-SYSTEMS FOR YACHTS

(for meaning of symbols, see fig 1)

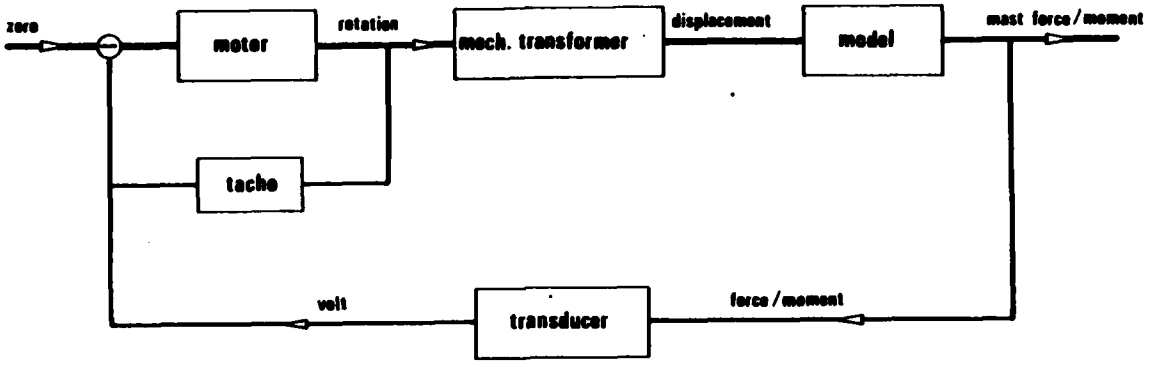

fig.6 PRINCIPLE OF ADOPTED SERVO SYSTEMS

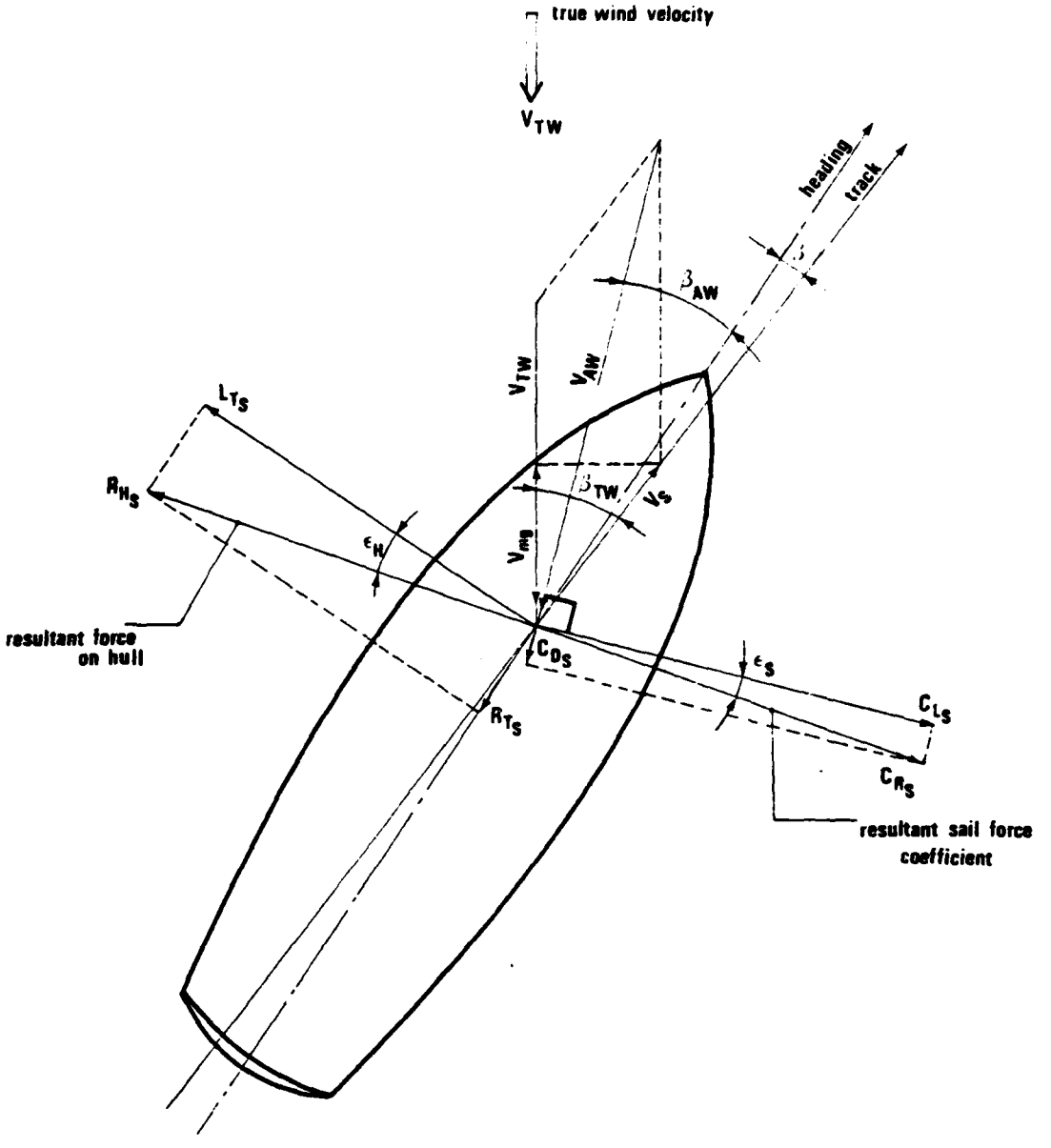

fig. 7 DEFINITION OF VARIABLES USED FOR CALCULATING FULL-SCALE PERFORMANCE.

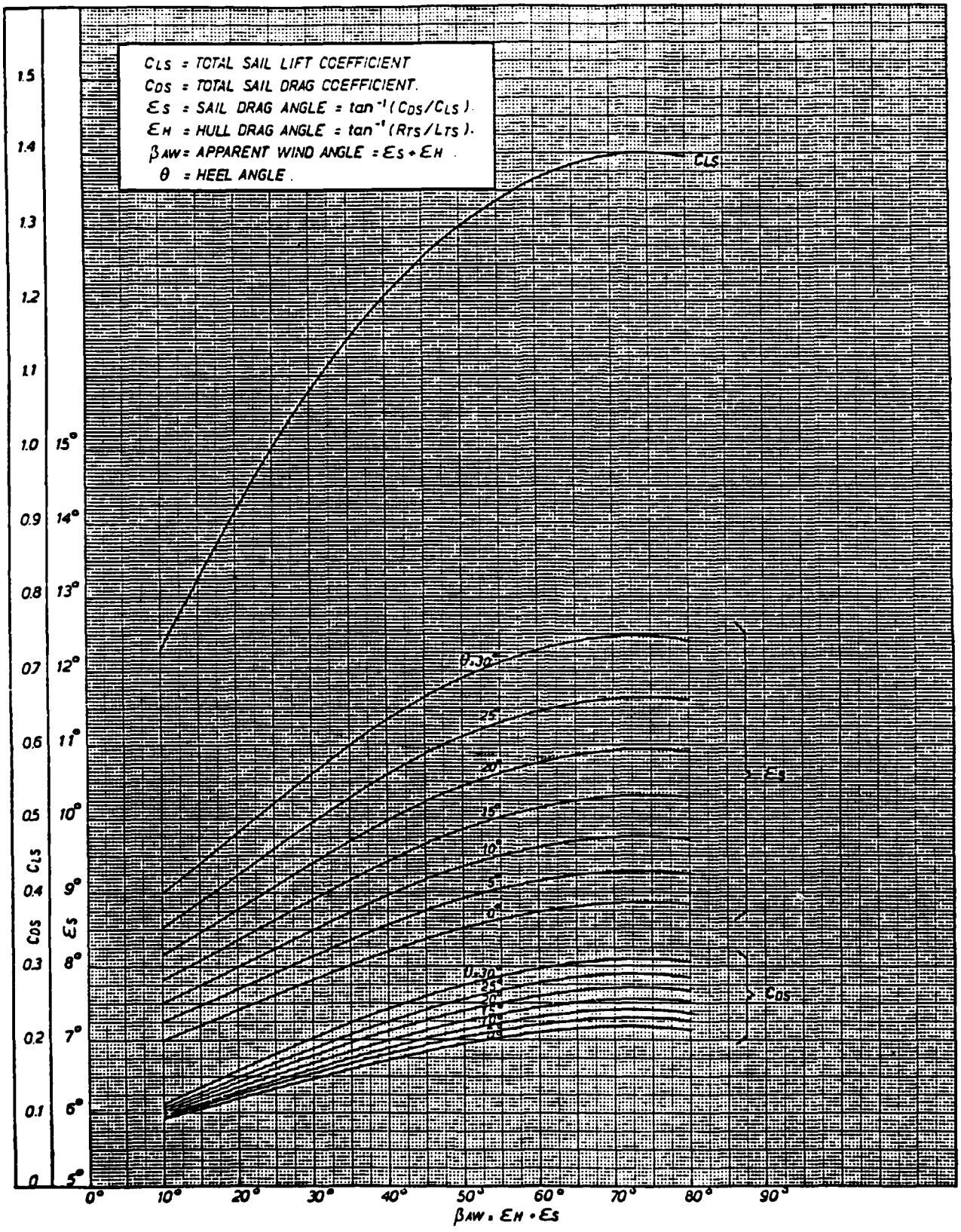

fig. 8 Upwind sail coefficients adopted for V_{mg} and V_{tw} predictions

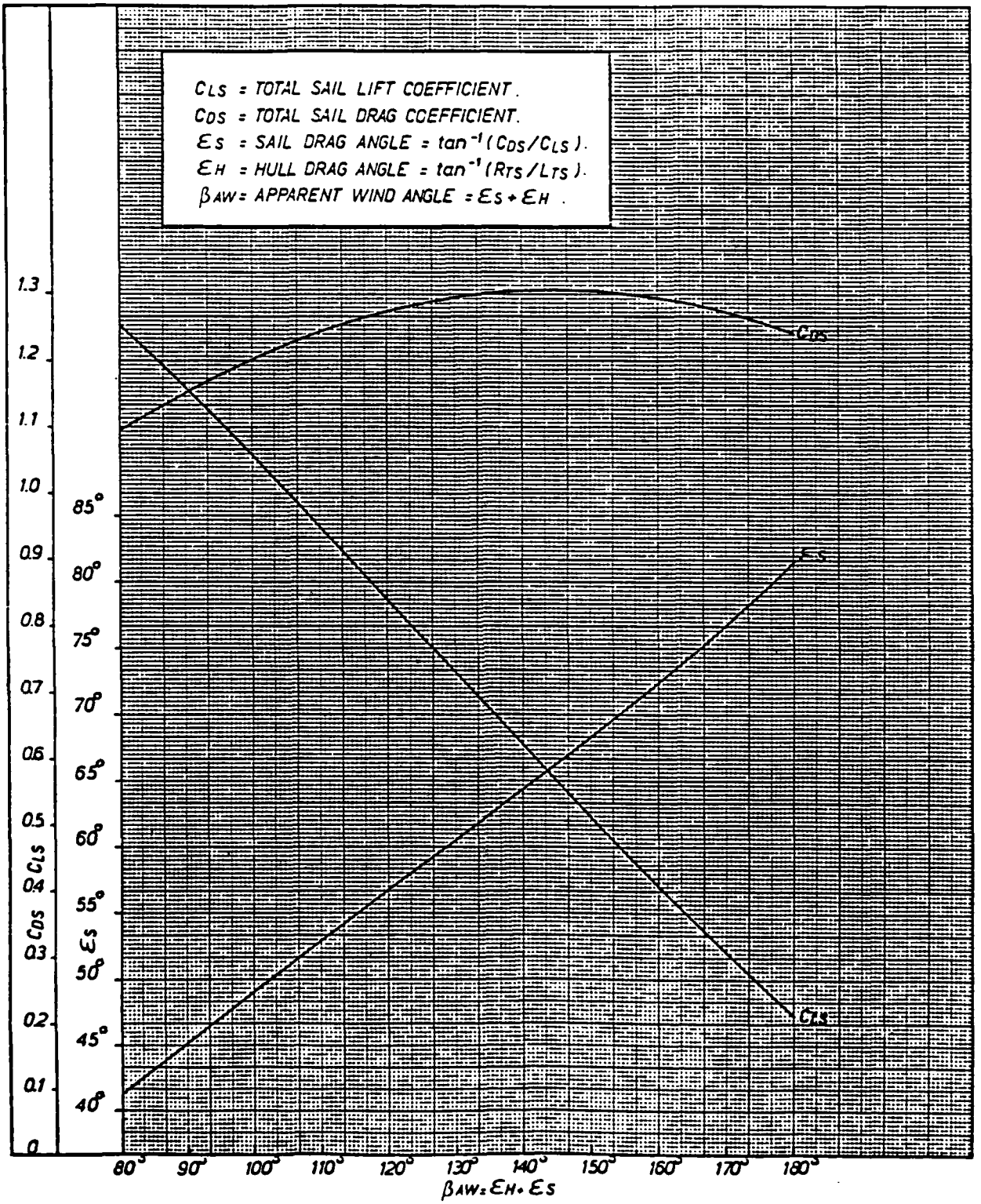

fig. 9 Downwind sail coefficients adopted for V_{mg} and V_{tw} predictions

DISCUSSION

Paul G. Spens
Davidson Laboratory

The original type of yacht dynamometer, devised by K.S.M. Davidson, and used by the Davidson Laboratory and many others, is that classified as 'System B' in the present paper. Instead of applying forces to a mast in the model, forces are applied at or near the waterline. Adjustments are made to weights in the model to allow for the vertical component and bow-down trimming moment of the sail force. Tests are made at fixed speeds and keel angles, varying yaw angle and measuring roll and yaw moments as well as drag and side force.

By calculation and graphical interpolation values of side force, drag and yaw moment are determined for the sailing equilibrium condition of the yacht. This is the condition when the righting moment measured by the dynamometer corresponds to the additional keeling moment in the prototype caused by applying the side force at the sail center of effort (CE) instead of near the waterline. It is easy to include in this calculation the effect of differing model CG and prototype CG and CE positions.

Thus from one set of test data a yacht's performance can be calculated over a range of CG and CE positions. This is a capability that designers often find useful. Furthermore model construction is simplified by the fact that the model CG position can be allowed for in the calculations. It need not correspond to the prototype CG position as is required with the dynamometer described in the paper.

I would like to ask Mr. Gommers whether serious difficulty is encountered in meeting this requirement, which might be particularly onerous in the case of such yachts as 12-meters, where some 70 percent of the displacement is in the lead keel. In this condition it would be of interest to know what size models are used.

In discussion of System B dynamometers it is noted in the paper that "the accuracy of the position and direction of the towing force is usually sufficient". It would be appreciated if Mr. Gommers would expand on this point, as our studies have convinced us that this type of dynamometer gives results corresponding to exactly the same sailing conditions as are represented by applying forces to a mast.

In case no better record is available of the author's reply to discussions, my understanding of Mr. Gommers' replies were:

"Care was necessary in making models."

"Size of model was 5 meters."

"It was thought that the inaccuracy referred to might arise from defects in calculation procedure."

AD-P003 838

University of Michigan - Ship Model Towing Tank Speed Control Upgrade

by

Armin W. Troesch
Department of Naval Architecture and Marine Engineering

Frederick G. Phelps
Integrated Engineering Services Corporation

ABSTRACT

The towing tank at the University of Michigan was constructed in 1904. To remain useful as a research and educational tool periodic overhauls are necessary. This report concentrates on the upgraded speed control installed in 1982. A description of the control hardware is included. Estimates of the level of accuracy of the control along with a calibration procedure are given. Results demonstrate that the new speed control has a maximum relative deviation from calibrated values of under 0.1%.

At the outset of the project to renovate the University's ship model towing carriage, the requirement of a high degree of steady state speed control accuracy and repeatability was stressed as of paramount importance. It was also desired to have separately adjustable acceleration and deceleration rates and up to three adjustable preset speeds, which could be activated during the run. Speed consistency and repeatability was to be demonstrated over a range of .25 fps to 16 fps.

Four synchronous 8.5 hp permanent magnet motors driven by four three-phase full wave regenerative DC controllers were selected for the speed control system. Utilizing the integral tachometer of one motor for the speed feedback, a one master controller - three slave controllers arrangement was adopted. A digital counter feedback system was considered in the early stages of the project; however, because the DC drives accept an analog output many disadvantages with a digital system became apparent. Primary concerns were that an error could be induced by the time base computation required in converting a digital signal to analog and that a slower response of the drive system may result due to the time involved with the conversion process. Three-phase full wave converter units were selected due to cost considerations, quick response, and higher power output. In addition, this application required optimal speed control within the entire speed range for driving and braking in both directions of motor rotation. All these requirements were met by the three-phase converter units.

The following features were incorporated into the design of the upgraded speed control system:

1. Manual Operation - adjustable speed with hand dial in four selectable speed ranges.

2. Automatic operation - selection of three possible adjustable preset speeds during the course of a run.

3. Variable speed units - ft/sec or m/sec for the actual and preset speed displays.

4. Adjustable acceleration and deceleration.

5. Stopping modes - a) selected deceleration by regenerative braking
   b) maximum deceleration by regenerative braking
   c) deceleration by dynamic braking in case of power loss
   d) primary and backup limit switches at tank extremes in both directions
   e) manually applied air brake.

6. Limit Override - ability to position the carriage past safety limit switches at the tank extremes and provide for utilization of maximum tank length.

7. Safety switch for speed range - a keyed selector switch located inside the control panel limits the carriage speed to 16 fps. Higher speeds up to 20 fps are possible, but this requires the repositioning of the tank extreme limit switches and reduces the tank's useable length.

8. Variable input speed signal - a tap into the electronic speed control to facilitate carriage control by an external ±10 volt input signal.

During tryout and acceptance, it was demonstrated that the control exhibited speed variations of less than ±.003 fps and repeatability over a measured distance of ±.001 ft/sec from 0 to 20 fps. Acceleration rates over a range of .09 ft/sec^2 to 3.3 ft/sec^2 and a maximum deceleration of 6.6 ft/sec^2, adjustable downward were provided for.

A contributing factor to the greatly improved speed control is due to the attention given to drive wheel and guide wheel alignment which was performed during the renovation along with the rebuild of those systems. After the elimination of an initial hard start condition the upgraded carriage satisfied all specifications.

When it was established that the speed remained constant over a given segment of the tank, the carriage speed control was calibrated by measuring the elapsed time it took to cover measured distance. A thirty foot segment at mid tank was selected. Optical interrupter modules were installed at each end of the segment. (These are now a permanent fixture in the tank, allowing for immediate spot checks of the speed read out.) The interrupters acted as a start/stop trigger to a HP5304A timer/counter. Dividing the segment length by the elasped time it took to cover the segment gave an average speed. Using the specifications for the interrupter and counter, it was determined that the absolute level of accuracy for the measured speed was under 0.0006 ft/sec over the speed range of interest.

The analog output voltage from the tachometer was digitized at a fixed sample set of 1000 points by the carriage's on board Tektronix 4052 computer. The 12 bit A/D convertor has a resolution of ±0.005 volts. The 1000 samples were averaged to give a mean voltage. Plots of the average carriage speed as functions of the tachometer voltage for the north and southbound directions are shown in Figures 1 and 2 respectively. The actual average of the sampled data points are shown by plus signs. A linear least squares fit is shown by a solid line and a cubic least squares fit by a dashed line. When plotted to the scale shown, both curves seem to be identical. However, when the differences between measured and regressed values are found, the cubic curve gives a higher level of accuracy.

The accuracy of the speed control can be measured in a number of ways. Perhaps the most common is to express the maximum error or degree of linearity as a percentage of the maximum speed. This is often misleading since a small relative error in the high speed range can be of the same order as some of the low speed range settings. For example, if a carriage speed range is from 0.1 to 100 ft/sec and the level of accuracy is given as 0.01% of the full scale reading, the absolute error is 0.01 ft/sec. If this error occurs at 0.1 ft/sec then the relative error at that speed is now 10%. A more useful specification would be to give the percent error in terms of the current given speed. Thus an accuracy level of 0.1% would mean an absolute accuracy of 0.1 ft/sec at 100 ft/sec and 0.001 ft/sec at 1 ft/sec.

Figures 3 and 4 show the actual averaged speed as measured from the optical interrupter modules versus the estimated speed calculated from the voltage and regression coefficients for the north and southbound directions respectively. The solid line is the linear fit and the dashed line is the cubic fit. The largest absolute deviation for the linear curve is approximately 0.011 ft/sec and for the cubic curve approximately 0.003 ft/sec. The more typical level of accuracy over the speed range most commonly used (i.e. 3 ft/sec to 8 ft/sec) is 0.002 ft/sec for the cubic curve.

Figures 5 and 6 show the percent error in the speed estimate for a given actual speed. Again, the solid line represents the linear estimate and the dashed line represents the cubic estimate. For the linear curve, the maximum percent error is near 1.0% at the lowest speed and up to 0.15% in the moderate to high speed range. By using the cubic fit, and maximum percent error is reduced to under 0.15% at the lowest speed and under 0.05% over most of the other speeds.

Either the linear or cubic curve regression coefficients can be stored in the carriage computer. An example of the application of the predicted speed values and the effect of their accuracy in an experiment is demonstrated by considering an EHP test. During a typical EHP test, the error introduced in the total drag coefficient, C_T , due to the incorrect estimate of the speed varies from approximately 0.3% for the linear fit to under 0.1% for the cubic fit. Since the repeatibility margin in the EHP test is in the 1.0% to 1.5% range, it would appear that there are other, more dominate sources of error in that type of test.

In summary, the new speed control has been calibrated to a level of accuracy sufficient for the most demanding research, commercial, or educational projects. The upgraded carriage will improve upon the quality and expand on the capabilities of the University of Michigan Ship Hydrodynamics Laboratory.

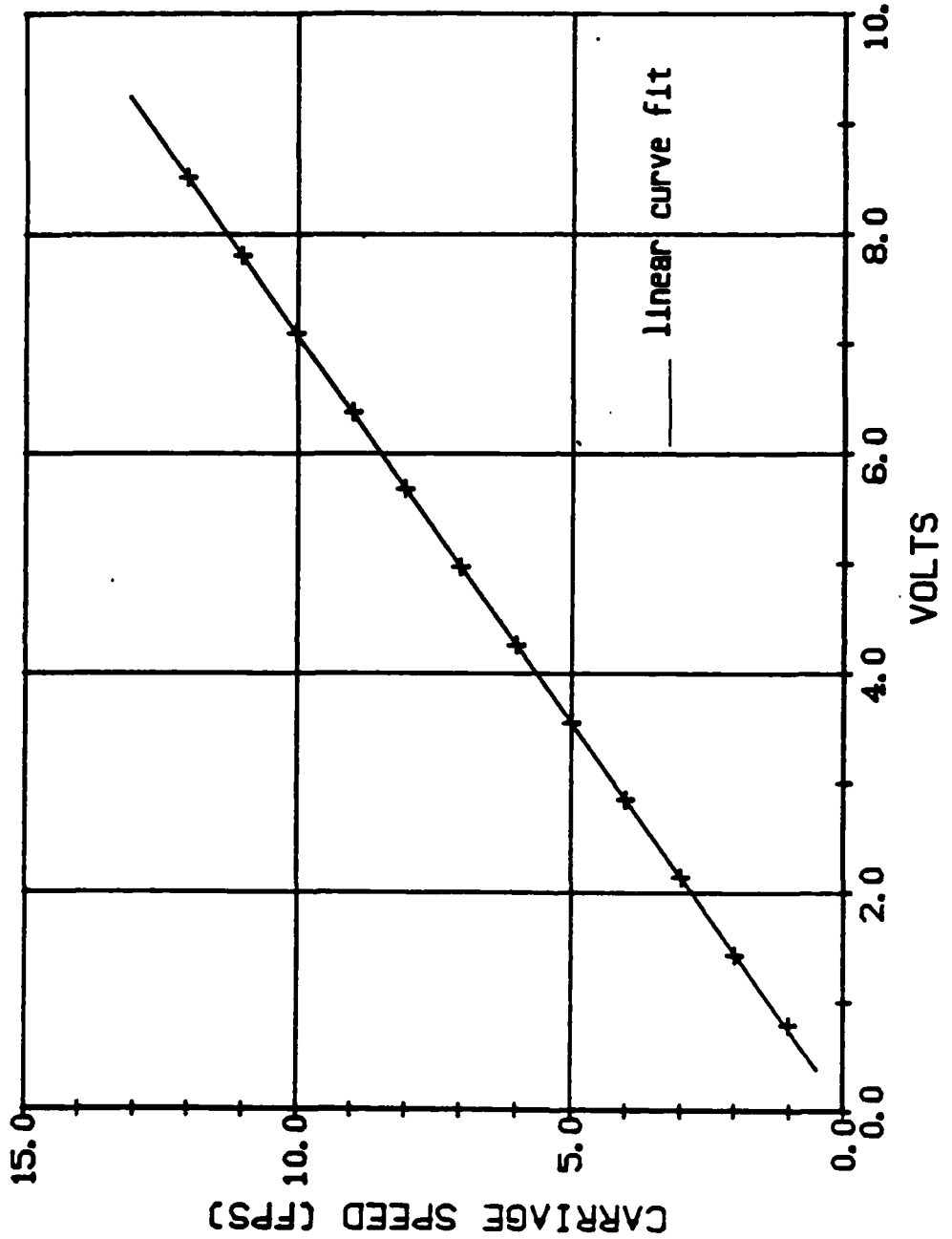

Figure 1: Northbound Carriage Speed vs. Tachometer Voltage

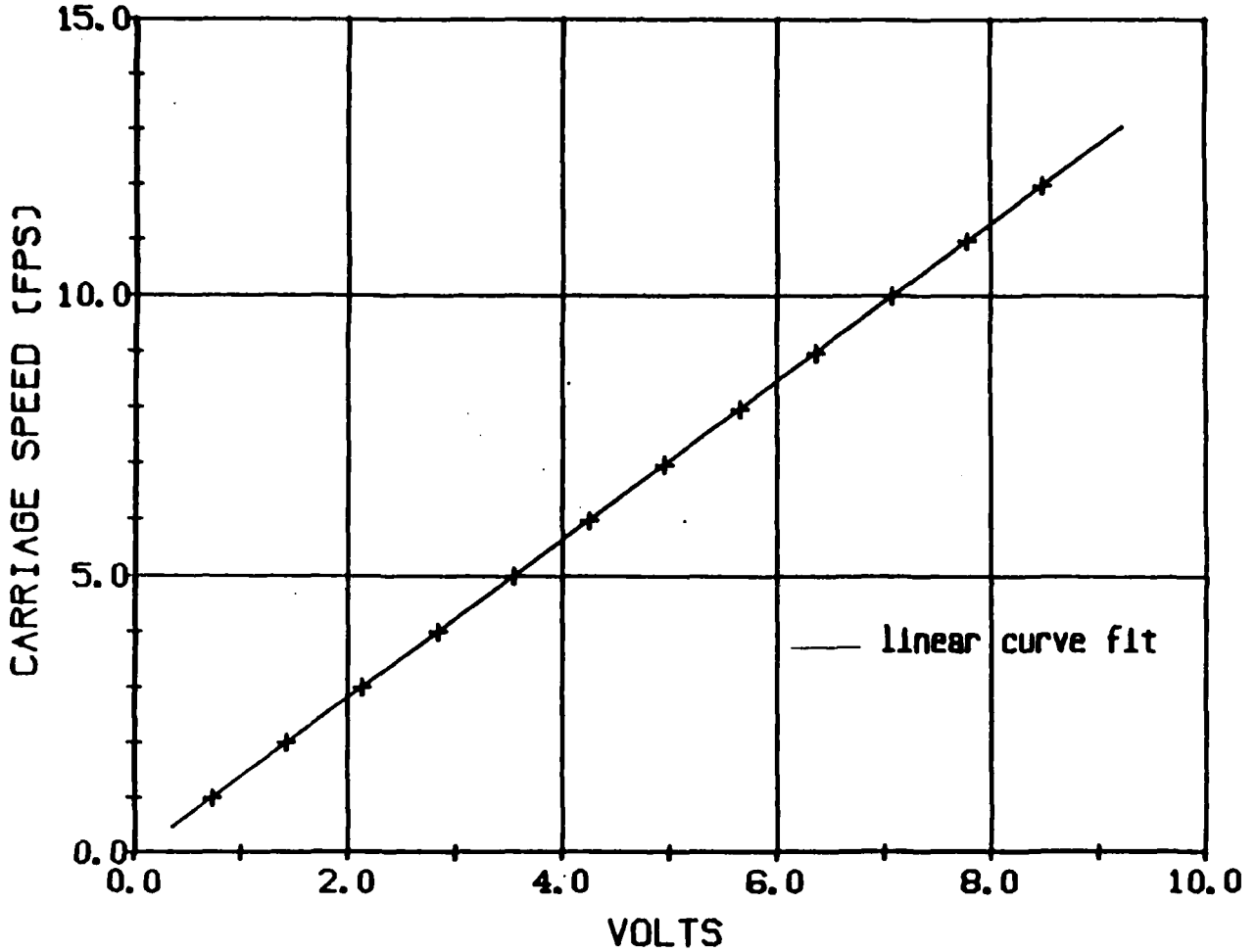

Figure 2: Southbound Carriage Speed vs. Tachometer Voltage

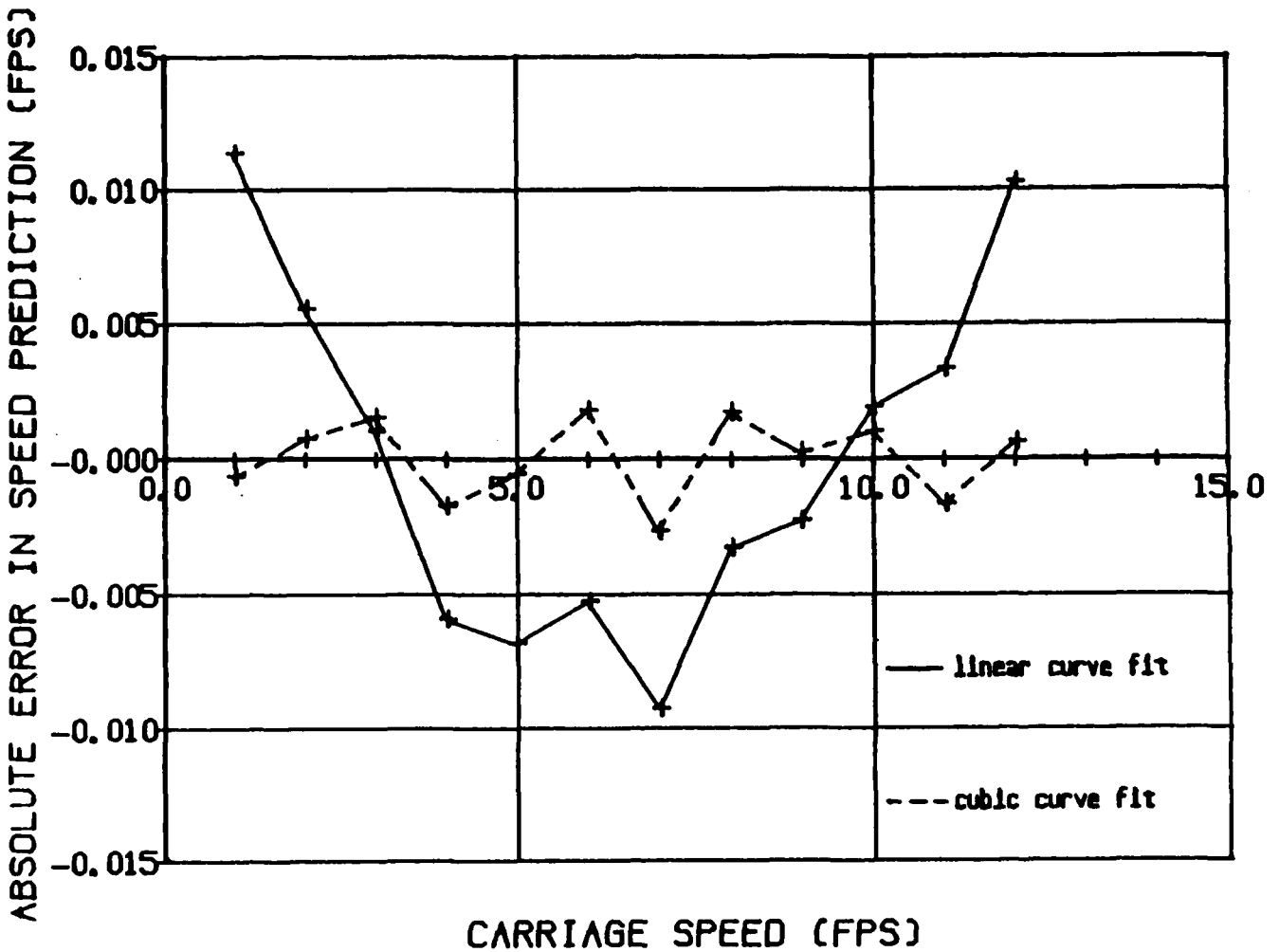

Figure 3: Absolute Error in Speed Prediction vs. Measured Average Speed (Northbound Direction)

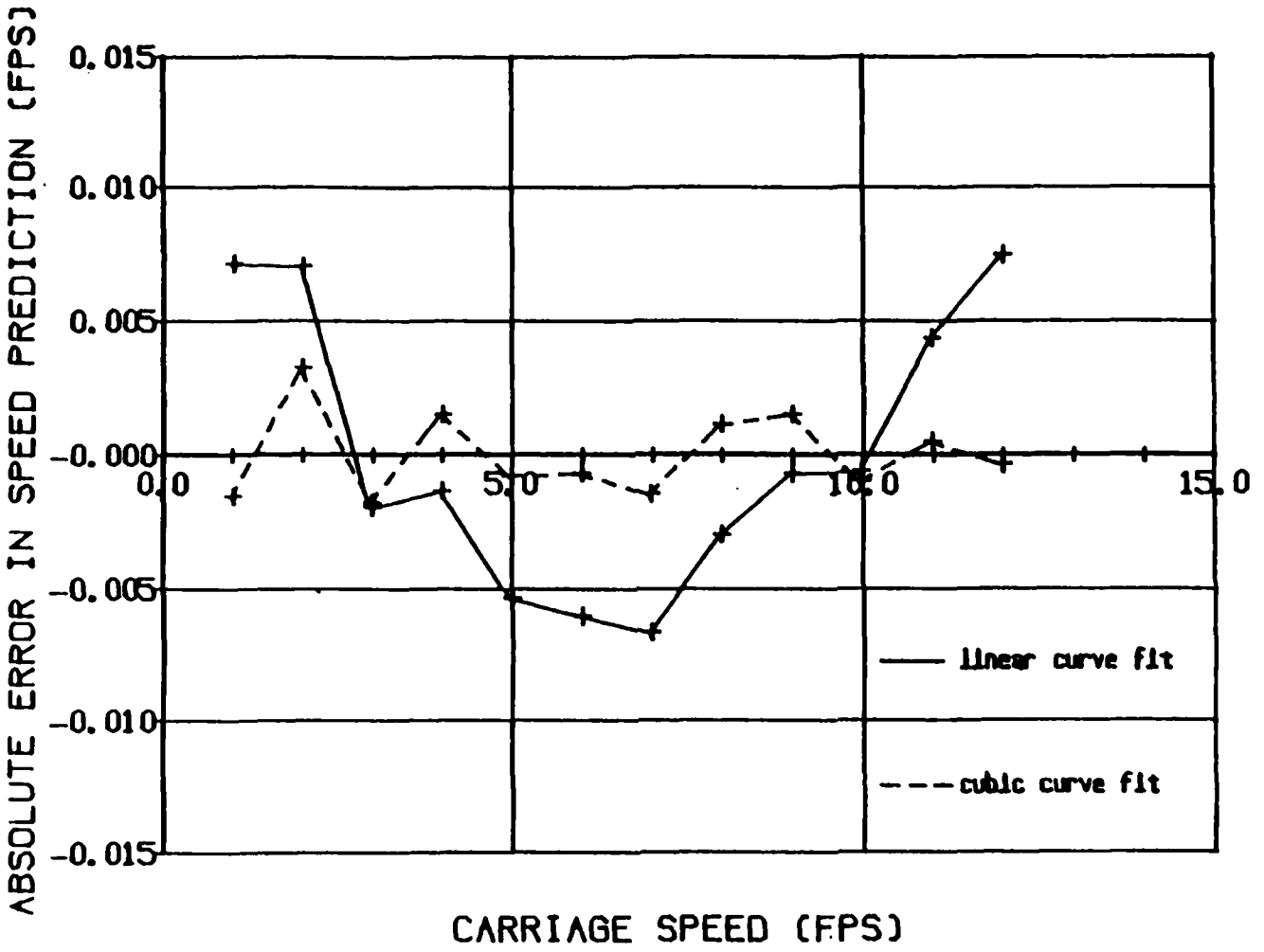

Figure 4: Absolute Error in Speed Prediction vs. Measured Average Speed (Southbound Direction)

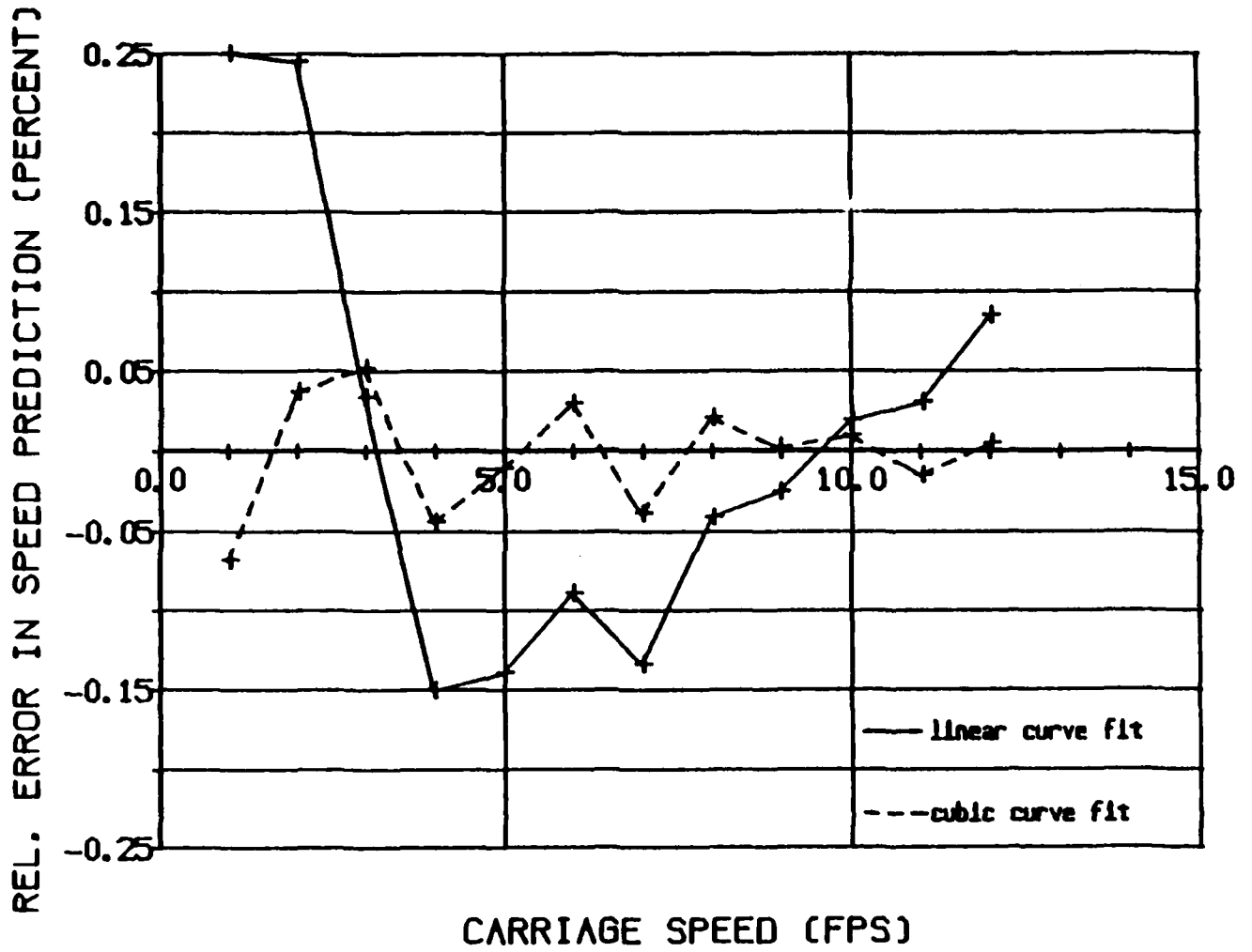

Figure 5: Relative Error in Speed Prediction vs. Measured Average Speed (Northbound Direction)

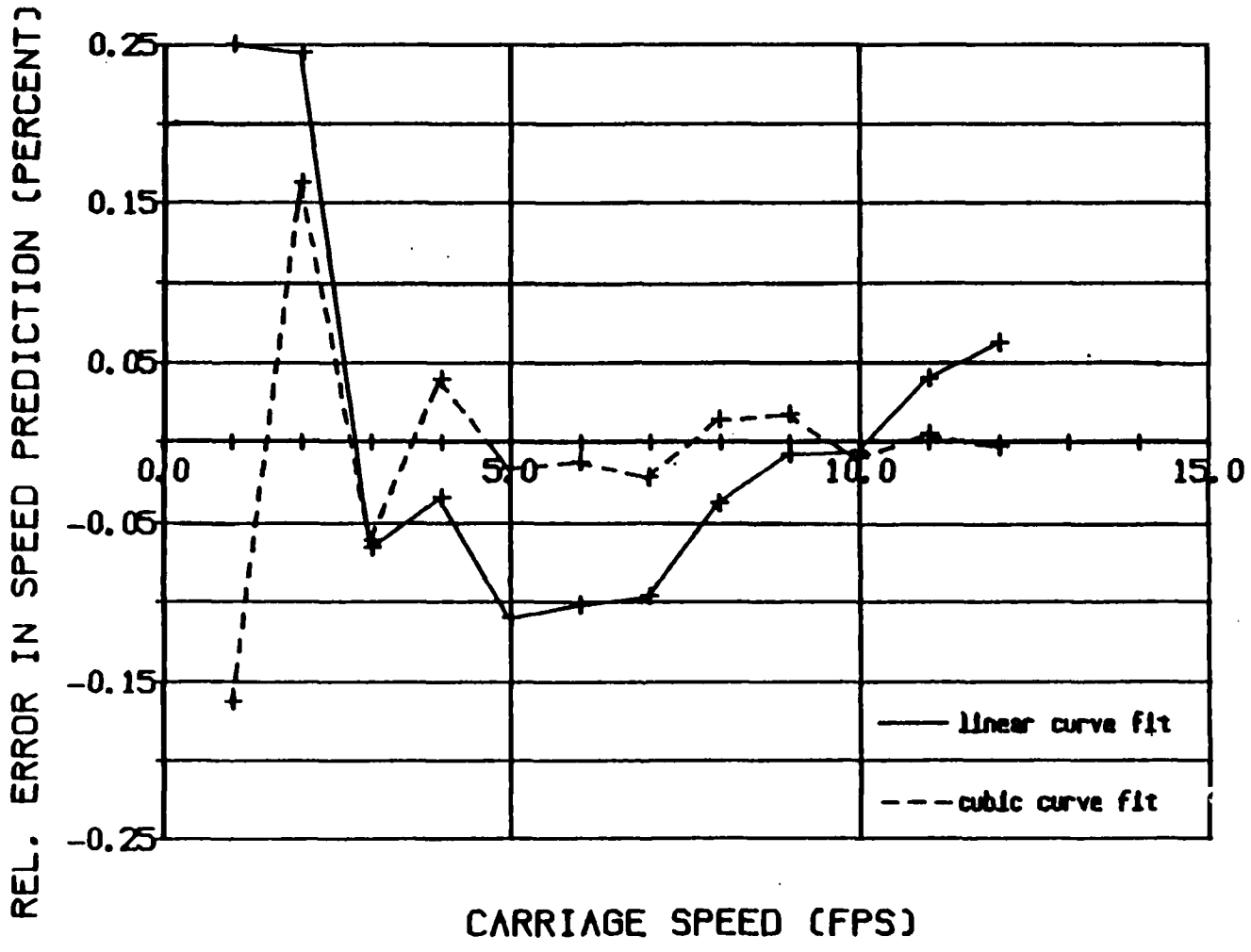

Figure 6: Relative Error in Speed Prediction vs. Measured Average Speed (Southbound Direction)

20TH AMERICAN TOWING TANK CONFERENCE

DAVIDSON LABORATORY
STEVENS INSTITUTE OF TECHNOLOGY

AUGUST 2, 3, 4, 1983

PARTICULARS

DAVIDSON LABORATORY TANK 3 WAVE MACHINE

TYPE: Double Flap/Wetback

COMMISSIONED: 1 September 1982

SYSTEMS RESPONSIBILITY:

MTS Systems Corporation, Minneapolis, MN:

- Waveboards, Linkages and Foundation
- Actuators, Servo Valves, Service Manifold, Power Supply
- Master Control, Feedback Controllers

Davidson Laboratory

- Backbeach and Incidental Mechanical Equipment
- Computer Interface
- Computer and Software

TANK DIMENSIONS:

Length:	295 feet exclusive of dock
Width:	12 feet
Normal Operating Depth:	5.36 feet

WAVEBOARD GEOMETRY:

- Waveboards located 10.5 feet from tank end
- Hinge locations:
  - Lower 0.22 feet from tank bottom
  - Upper 3.95 feet from tank bottom
- At normal operating depth:
  - Lower Waveboard height 3.73 feet
  - Upper Waveboard height 1.40 feet
- Maximum Waveboard angles (mechanical):
  - Lower $\pm 15^{\circ}$
  - Upper $\pm 13.75^{\circ}$ (relative to lower)
- Angle limits set by software, $\pm 13.4^{\circ}$, both waveboards
- Angular velocity limits set by software:
  - Lower ±45 deg/sec
  - Upper ±60 deg/sec

MECHANICAL LINKAGE:

- Stick figure linkage schematic appended as Figure I. There are three fixed hinge points in the system, the lower waveboard hinge, the lower waveboard actuator trunnion, and a third hinge at the top of the vertical link. Extension of the lower flap actuator is magnified three times by the vertical link, which moves the triangular yoke, and ultimately the lower flap through horns at each side. The upper flap actuator is carried by the yoke and is attached directly to the upper flap.
- The nonlinear relationships between actuator extensions and waveboard angles are compensated for in the computer generated actuator extension command signals.

SEALS:

- There are no rubbing seals between the waveboards, or between waveboards and the tank. Various baffle plates are arranged so as to minimize the flow-through area. Width of the resulting cracks is typically 1/8 to 1/4 inches.

SUBMERGED BEARINGS:

- Four submerged journal bearings, two in each hinge line, self lubricating.

BACKBEACH:

- Section, Figure II
- Six layers of wooden grids at about 12^{o} angle are attached to a pile of standard concrete blocks arranged so as to permit flow-through. The various parts are strapped together with stainless steel rods and hooks. Horizontal flow area through concrete blocks is about 35% of frontal area. Slanted grid over the foundation inspection pit required to control splashing.
- Tank sides built up locally about 16 inches
- Design was developed by cut and try with 1/8 scale model.

HYDRAULIC EQUIPMENT:

- Power supply; Variable volume
  40 gpm @ 3000 psi
  Main pump motor, 55KW
- Servo Valves:
  Lower, 2 valves, 15 gpm
  Upper, 2 valves, 5 gpm
- Actuators:
  Lower, 16 inch stroke, 15000 lb force rating
  Upper, 21 inch stroke, 5500 lb force rating

SERVO CONTROLLERS:

- Displacement, velocity, acceleration and delta pressure feedback.
- Limit detectors for all quantities capable of shutting down power supply.
- Offset and span adjustment.

MASTER CONTROL:

- Hydraulics on/off, high/low pressure, run/stop, panic button, interlocks.
- Controls duplicated at dock end of tank.

INTERFACE:

- Isolation amplifiers between computer and rest of system.
- Slow start/stop circuits which ramp signal gain up and down to provide smooth start up and stop, and to prevent computer signals from reaching servo controllers except when in run mode.
- Low pass filters (5 Hz, 6-pole Butterworth) at input to servo controllers.
- Pulse generator to communicate with computer when run/stop mode changed.
- Inclinometers mounted on waveboards, dual digital displays. (To aid in checking net static gains through the system.)

COMPUTER:

- PDP 11/23 System includes:
  LSI 11/23 CPU, memory management
  96 Kb MOS memory
  2 I/O ports
  Boot Strap Prom
  Programmable clock
  4 Channels D/A
  Dual Drive, Double Density
  Floppy System (1mb)
  Hardcopy Terminal

SOFTWARE:

- RT-11 single user operating system and FORTRAN.
- Locally developed calibration and diagnostic utilities.
- Run time Regular Wave generator.
- Irregular Wave Program generator.
  - Modified white noise/fast convolution method
  - 17 hours worth of statistically independent 2 minute samples available
  - Open loop
  - Five spectral forms, ITTC, Neumann, JONSWAP, Voznesenski-Netsvetayev, and "Swell". "Sea plus Swell" simulations possible by combination of above forms.
- Run Time Irregular Wave generator
  - Scales previously stored digital wave programs and runs the machine.
- Software corrections for:
  - Nonlinearity of LVDT actuator displacement transducers
  - Linkage nonlinearity
  - Closed loop servo frequency response
  - Filter frequency response
  - Theoretical wave machine calibration
  - Net deviations between theoretical and experimental calibrations
- Four apportionment schemes:
  - Upper flap only
  - Lower flap only
  - Limited linear regression (USNA method with upper flap only for high frequencies, and in opposed phase operation, upper flap angle limited to value equal to that of lower flap).
  - Main slope (no opposed phase operation, yields a marginally higher wave with slightly less good long wave shape than linear regression).
  - Linear regression apportionment is the standard for normal water depth.

REGULAR WAVE CAPACITY:

- Limiting regular wave capacity indicated in Figure III.

IRREGULAR WAVE CAPACITY:

- Limiting irregular wave (ITTC two parameter) capacity shown in Figure IV

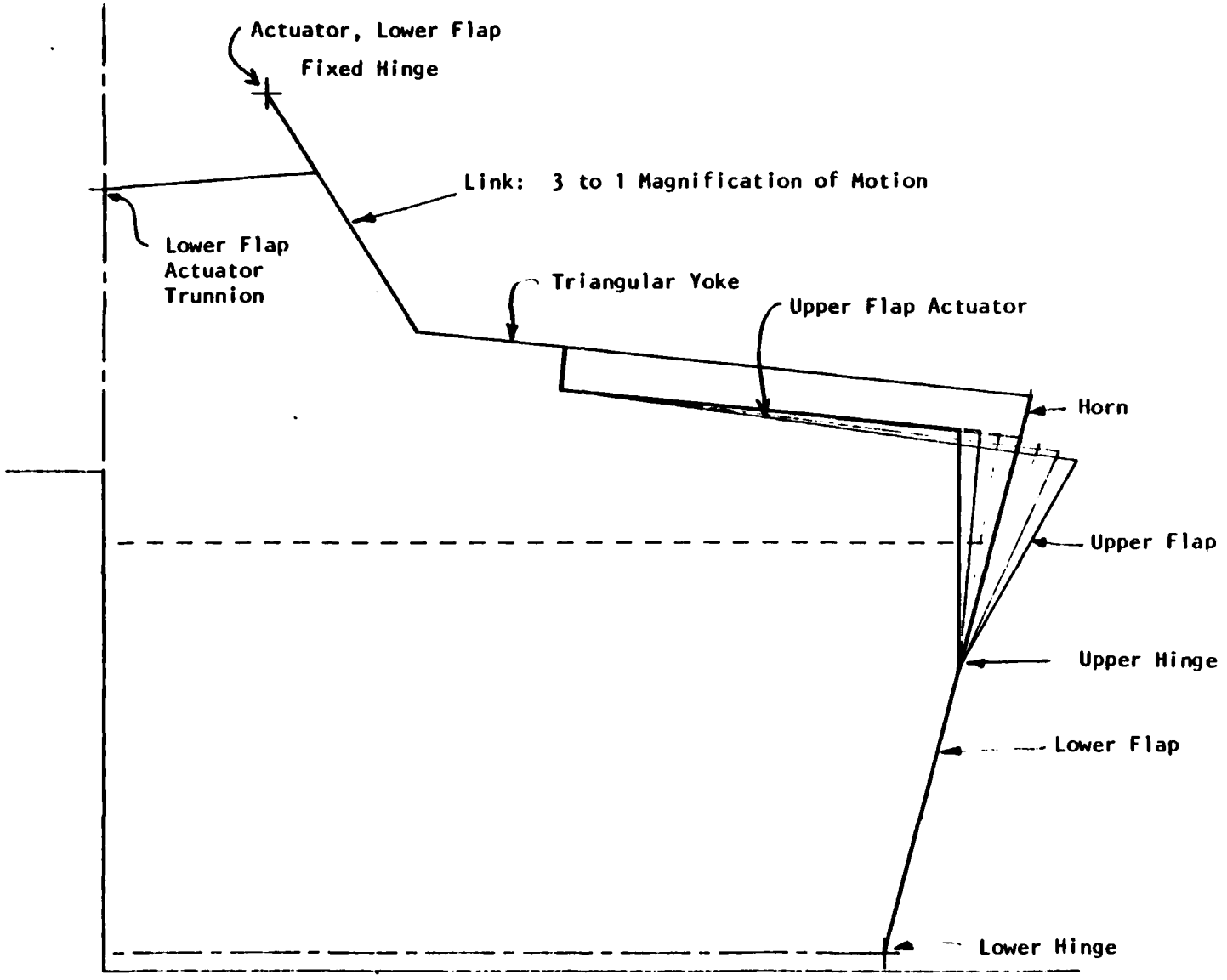

FIGURE I LINKAGE SCHEMATIC

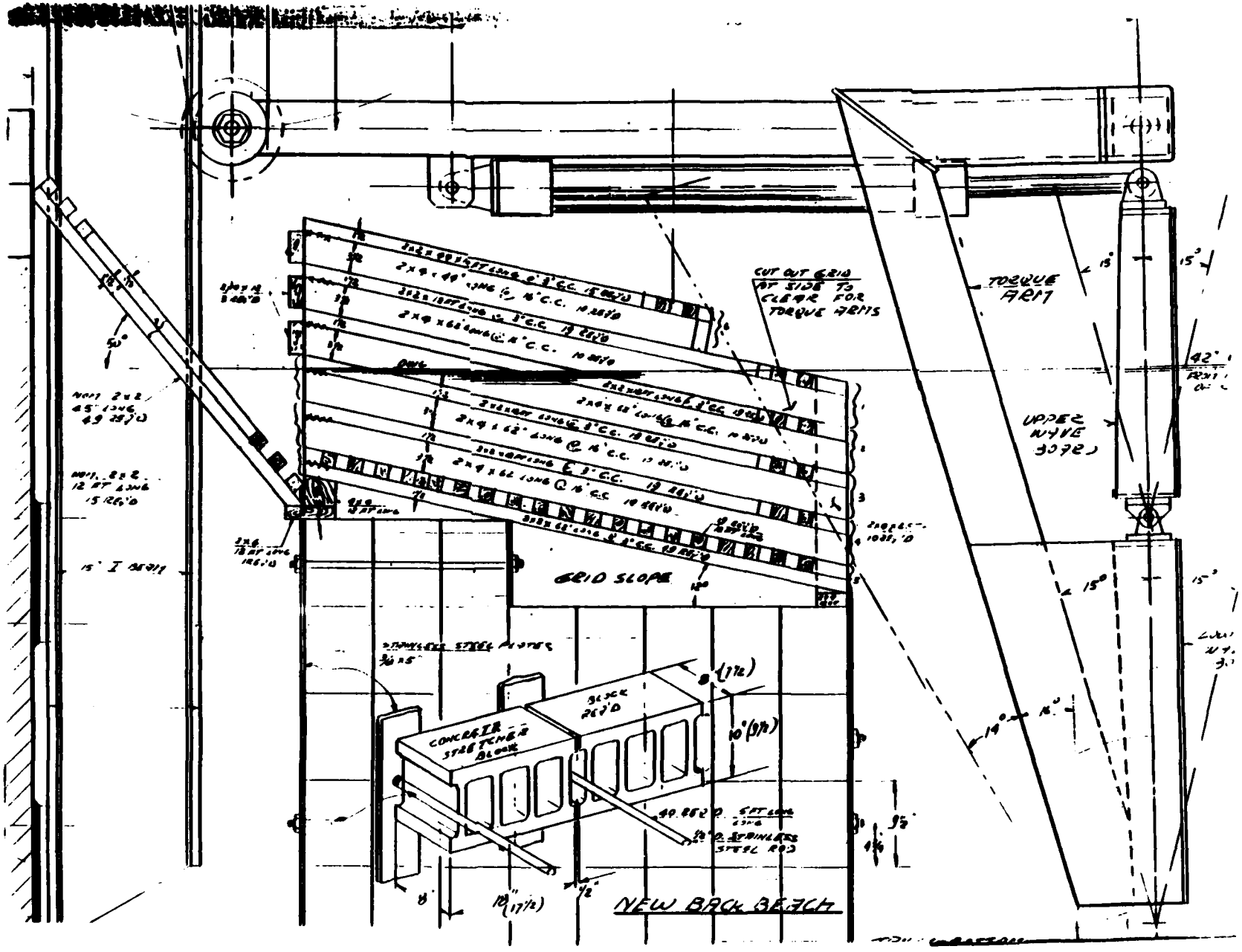

FIGURE II BACKBEACH

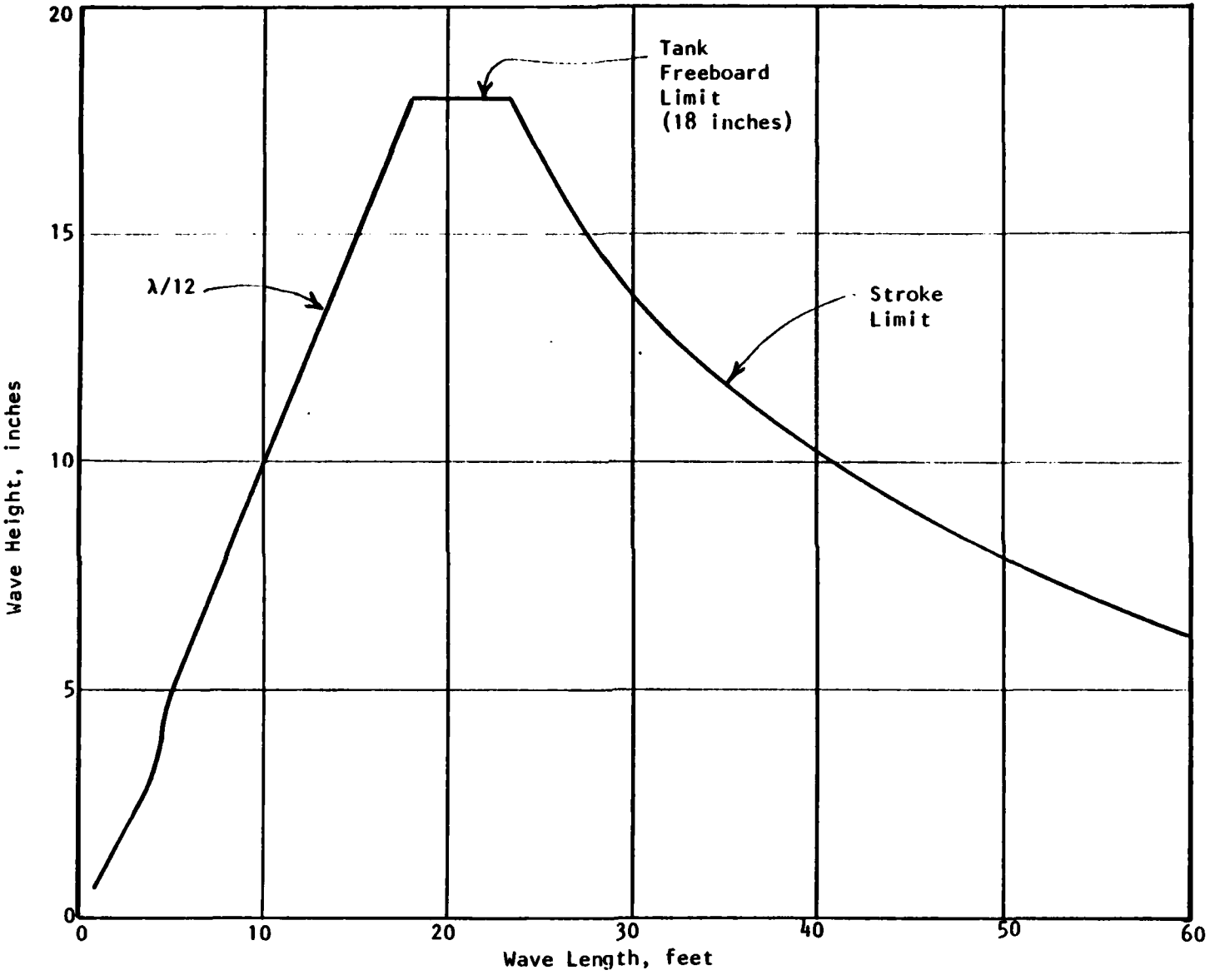

FIGURE III REGULAR WAVE CAPACITY, NORMAL OPERATING DEPTH,
LIMITED LINEAR REGRESSION APPORTIONMENT

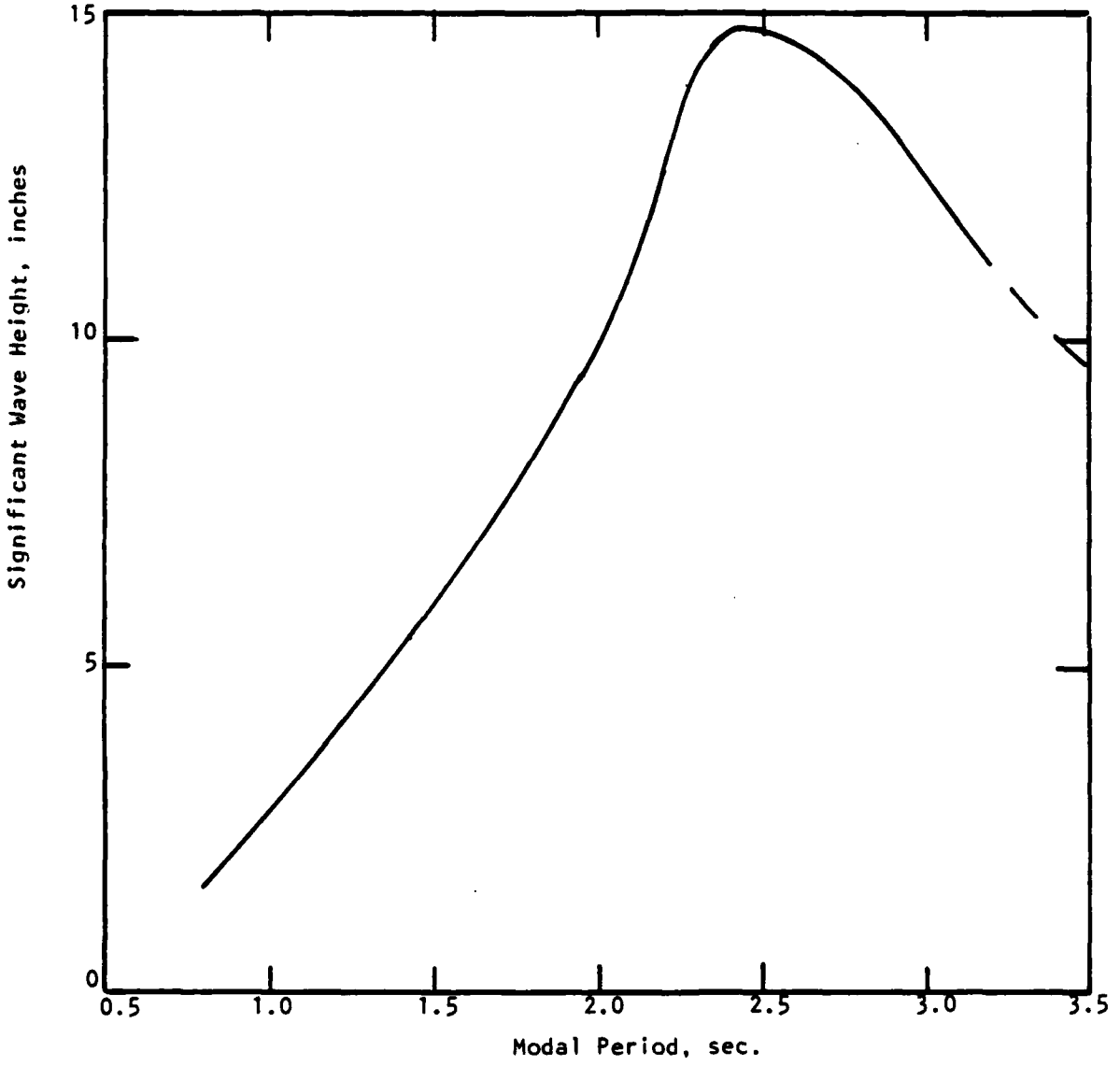

FIGURE IV IRREGULAR WAVE CAPACITY,
ITTC TWO PARAMETER SPECTRUM,
NORMAL OPERATING DEPTH,
PRIMARILY MEAN SLOPE APPORTIONMENT.

GENERAL

REPORT

BUSINESS SESSION

The chairman announced that invitations had been received by the Executive Committee from the David W. Taylor Naval Ship Research and Development Center (DWTNSRDC), the University of New Orleans and the Offshore Technology Corporation of Arctec, Inc. to host the 21st ATTC Conference. We thank these organizations for their generous and enthusiastic offers. After much delibration, it was recommended that the next Conference in 1986 be held at DWTNSRDC. A motion was made, seconded and passed to accept their invitation.

Members of the Conference then undertook the matter of electing the American representative on the ITTC Executive Committee for the term starting in September 1984. Dr. William Morgan of DWTNSRDC was nominated and elected by a unanimous vote. Dr. Morgan thanked delegates for their expressed confidence and stated that he would strive for more active participation of the ATTC in the affairs of the ITTC.

The organization of the ATTC Committees and Conference proceedures were briefly discussed. It was agreed that the ATTC should attempt to establish technical committees which parallel those of the ITTC but that the general "informality" of the ATTC operation be preserved.

Dr. Morgan, who becomes chairman of the 21st ATTC by nature of DWTNSRDC's role of host, will organize a new Executive Committee and plan a schedule of meetings to prepare for the next Conference.

The Conference ended with very gracious expressions of thanks and appreciation to the sponsors, chairmen, committee members, discussors and all who provided the services necessary for organizing the 20th ATTC.

NOTES FOR GUIDANCE

AIMS AND ORGANIZATION OF THE AMERICAN TOWING TANK CONFERENCE

The American Towing Tank Conference is a voluntary association of establishments having a responsibility in the prediction of hydromechanic performance of ships and other waterborne craft and their appendages from tests on scaled models.

The objective of the Conference is to promote exchange of knowledge between tank staffs for the purpose of improving methods and techniques. This includes an exchange of knowledge on the design of facilities, equipment and instrumentation, on experimental and construction techniques, and on scaling laws. As a means to this end, the Conference seeks to correlate testing among the various member establishments in order to facilitate the interpretation of experience, and to issue standards.

The Conference seeks to attain its objective by holding formal meetings triennially and through the encouragement of informal working relationship among the member establishments.

Membership in the Conference is by establishment and is open, upon invitation, to all establishments in the Western Hemisphere. All the member establishments agree to the free and full exchange of all information on the foregoing subjects which is neither proprietary nor of a classified military nature. (To that end mutual agreements on exchange of publications and data of interest will be entered into.)

The members or delegates will be persons holding positions of primary responsibility in Towing Tanks or Water Tunnels, Shipbuilding Research Associations or Departments of Naval Architecture of a University in which prominence is given to the subjects pertaining to the objectives of the Conference. A few delegates can be invited who were not qualified as above but who have rendered services to the aim of the Conference, as well as observers.

The Conference assembles from time to time in different countries of the American Continent. Since 1950 it has assembled at three year intervals.

The details of organization of any particular Conference is the responsibility of the host country.

The Conference is a purely communicative body; it has no authority of financial sponsorship; its membership is voluntary and self-supporting.

Each establishment may be represented by one or more members at triennial formal meetings of the Conference.

Although representation is not limited, it is the intent that it be kept reasonably small so that fruitful discussions can be obtained at the working level. The Conference intends to meet formally at each of the member establishments in rotation, the sequence being decided by the membership.

The scope of the Conference is set by the Executive Committee, based on the recommendations of the previous general meetings.

The Executive Committee shall comprise the nominated representatives of the Institutions at which the last three Conferences were held plus Chairman of the SNAME Hydrodynamics Committee, plus the representative of the Institution at which the next Conference is to be held.

In the event that the Chairman of the Hydrodynamics of SNAME does not serve as a member of the Executive Committee of the ATTC, the Executive Committee may invite another official to serve on the Executive Committee.

If a member of the Executive Committee resigns, a replacement shall be selected by his institution.

In addition the United States of America's representative on the ITTC Standing Committee shall, ex-officio, be a member of the ATTC Executive Committee.

The ATTC membership of the Standing Committee of the ITTC will be rotated. The representative will normally serve through two ITTC Conferences.

The ATTC representative on the ITTC Standing Committee shall:

a. hold a senior position in a model basin;
b. be acquainted with the operation of the ITTC; and
c. have means for financing attendance at an annual meeting of the ITTC Executive Committee

A newly appointed ATTC representative on the ITTC Standing Committee shall take office after the ITTC Conference subsequent to the ATTC Conference at which he is appointed.

The Chairman of the Executive Committee shall be the nominated representative of the Institution at which the next Conference is to be, viz, he is the Chairman of the next Conference.

The Secretary of the ATTC shall be any person so nominated by the Conference Chairman.

The Executive Committee shall appoint Chairmen of such Technical Committees as are felt necessary for the effective conduct of the Conference.

The Chairmen of such Technical Committees will appoint such persons as they consider necessary for the effective conduct of such Committees, and further will be responsible for the production of the State-of-the-Art reports and the soliciting of papers to be presented to the Conference.

The reports accepted by the staff of the Conference are discussed in the Technical Sessions during the meetings, first formally then informally. To this end, those reports are previously forwarded, well in advance of the dates of the Conference, to the Chairmen of the Conference Organizing Committee, who arranges for copies to be transmitted to each member. The same applies to the formal contributions which any member may make to the Conference. If the Chairman of the Technical Committee considers that any contribution is unacceptable in view of the objectives of the Conference, he should reject it.

The Chairman of each Technical Session, in association with the Chairman of the Technical Committee concerned, formulate decisions and recommendations arising from the Session. The decisions and recommendations will then be considered and agreed upon at the concluding Session of the Conference.

The Chairman of the Conference Organizing Committee will arrange for the publication of the Proceedings of the Conference.

The venue of the next Conference is subject to the invitation of an [illegible] such invitation shall be accepted by the Executive Committee after a vote present at the Business Meeting.

PAST MEETINGS OF THE AMERICAN TOWING TANK CONFERENCE

1st	14 - 15 April 1938	Experimental Towing Tank Hoboken, New Jersey
2nd	19 - 20 September 1939	1st day - Receiving Ship Building Navy Yard, Washington 2nd day - David Taylor Model Basin
3rd	14th November 1940	Waldorf Astoria, New York, NY
4th	14th November 1941	Waldorf Astoria, New York, NY
5th	29 - 30 September 1943	David Taylor Model Basin Washington, DC
6th	12 - 13 November 1946	Experimental Towing Tank Hoboken, New Jersey
7th	7 - 8 October 1947	Newport News Shipbuilding & Dry Dock Co. Newport News, Virginia
8th	11 - 13 October 1948	The University of Michigan Ann Arbor, Michigan
9th	11 - 14 September 1950	National Research Council of Canada Ottawa, Canada
10th	4 - 6 May 1953	Massachusetts Institute of Technology Cambridge, Massachusetts
11th	12 - 14 September 1956	David Taylor Model Basin Washington, DC
12th	31 Aug. - 2 Sept. 1959	The University of California Berkeley, California
13th	5 - 7 September 1962	The University of Michigan Ann Arbor, Michigan
14th	9 - 11 September 1965	Webb Institute of Naval Architecture Glen Cove, New York
15th	25 - 28 June 1968	National Research Council of Canada Ottawa, Canada
16th	9 - 13 August 1971	Instituto de Pesquisas Tecnologicas Sao Paulo, Brazil
17th	18 - 20 June 1974	California Institute of Technology Naval Undersea Center Pasadena, California
18th	23 - 25 August 1977	U.S. Naval Academy Annapolis, Maryland
19th	9 - 11 July 1980	The University of Michigan Ann Arbor, Michigan
20th	2 - 4 August 1983	Davidson Laboratory Hoboken, New Jersey

END

FILMED

9-84

DTIC